The role of science, engineering and risk identification in catastrophic disaster preparedness and response

Tony Pearce

Emergency Management Australia

Abstract

Severe natural hazard events are an inherent risk within the Australian environment. Disasters in Australia have resulted in significant loss of life and property, stifled development and resulted in physical, economic, social and psychological costs, placing pressures on communities. The emergency management context and the nature of risks in a changing environment presents developing challenges. The challenge for emergency managers is to improve mitigation and prevention measures, preparedness, response capability, and recovery arrangements.

Science and engineering can make a significant contribution to these processes in a range of ways. Community resilience can be increased by furnishing a better understanding of natural hazard risks and impacts on communities. Severity of disaster impact can be reduced through mitigation. Scenario modeling can supply credible consequence against which capability can be measured and deficiencies identified. At the tactical and operational levels improved impact consequence prediction can facilitate informed warnings, evacuation arrangements, resource deployment, and build important credibility. Expeditious and accurate damage assessments can reduce disruption and misdirection of resources.

A forward vision for advancing prevention, mitigation, preparedness, response and recovery through partnerships between emergency management, science and engineering is presented.

Lessons from Cyclone Larry in co-ordinated earthquake post-disaster surveys

Edwards, M.R. and Corby, N.A.

Geoscience Australia

Abstract

Natural disasters provide an invaluable opportunity to capture data for improving our understanding of risk. Observed damage types and their predominance provide useful insights into the factors contributing to building vulnerability and consequential community risk. They also facilitate the appraisal of mitigation measures directed at reducing that risk where it is found to be high. Survey activities that followed the impact of Tropical Cyclone Larry have highlighted the benefits of a co-ordinated survey response to natural hazard impacts. The response to this event involved liaison with local emergency management and the broad participation of recognised wind engineering experts. Survey techniques were refined to achieve a more efficient and comprehensive approach that ensured consistency, utility and transferability of the data for all collaborators. The refined approach proved very successful and may provide a useful model for similar post-disaster exercises directed at earthquake damage. The sudden nature by which earthquakes inflict damage without warning points to having arrangements already established beforehand for the best survey outcomes. Proposals for advancing such preplanning are presented.

Introduction

The risk natural hazards pose to Australian communities is not precisely known. The review of natural disaster management presented to the Council of Australian Governments (COAG 2002) included recommendations on improving this understanding of natural hazard risk. The subsequently funded Disaster Mitigation Australia Package (DMAP) is directed at addressing these recommendations to COAG and requires an improved understanding of infrastructure vulnerability. Initial wind risk studies of selected Australian communities (Nadimpalli et al, 2006) have highlighted the significant wind risk posed by tropical cyclones to coastal North Queensland. Consequently efforts have been expended to better understand the vulnerability of the infrastructure in the associated communities as a key component of any improved understanding of this risk. Post-disaster surveys are an important part of advancing this work and the response to Cyclone Larry's impact on North Queensland constituted a major effort to advance this work. In a relatively short time a team of 14 comprised of both specialists and experts was mobilised leading to the capture of a substantial infrastructure damage dataset. Many aspects of this approach are transferable to equivalent surveys of earthquake damage. These are identified for consideration in developing a parallel approach to earthquake damage surveys.

Background

The effective development of vulnerability models involves the engagement of recognised experts in the respective hazard areas. Two wind risk related workshops were organised by Geoscience Australia and funded by DOTARS to engage researchers in the wind field. The first of these was held in Canberra on the 1st Dec 2005 (JDH Consulting 2006). It was entitled "Severe Wind Risk Research Workshop" and the content was equally divided between the assessment of wind hazard and the quantification of wind risk. Of the 10 recommendations advanced by the expert group, two were directed at improved post-disaster activity:-

- A clear strategy for damage surveys after a severe wind event should be prepared. This should involve non-GA personnel.

- Damage surveys should be conducted and reported jointly.

This was followed by a subsequent workshop on the 14th and 15th March 2006 which focussed on wind vulnerability alone and was hosted by the Cyclone Testing Station at James Cook University's Townsville campus (TimberEd 2006). The import of post-disaster surveys also featured prominently in the discussions. The workshop further recommended to:-

- Develop a damage report template for use in wind damage assessment. This would include estimation of local wind speeds in the damaged area.
- Form a team of experts and an engagement process for immediately assessing wind damage from both major and minor events, for calibration of models.

Representatives from key New Zealand research agencies attended both workshops with a view to trans-Tasman participation in severe wind event surveys.

In summary, both workshops identified the need for co-ordinated post-disaster surveys in which field observations were consistently recorded. The opportunity to implement these presented itself much sooner than anticipated when Tropical Cyclone Larry crossed the Queensland coast just five days after the close of the second workshop, impacting Innisfail and several neighbouring communities.

Tropical Cyclone Larry

Tropical Cyclone Larry crossed the North Queensland coast at 7:10 am on the 20th March 2006. While of a devastating Category V intensity close to landfall, the cyclone lost intensity close to the coast and crossed as a mid Category IV (Figure 1). Post-impact survey activities gave evidence of this loss of intensity. Road signage damage was the subject of detailed study and suggested that the local wind speeds as observed at a 10 m elevation in level open country were in the range 50 to 65 m/s. These speeds indicate that the event was more severe that Cyclone Winifred (1986) and that the wind speeds were marginally lower than the design wind speeds for ordinary structures.

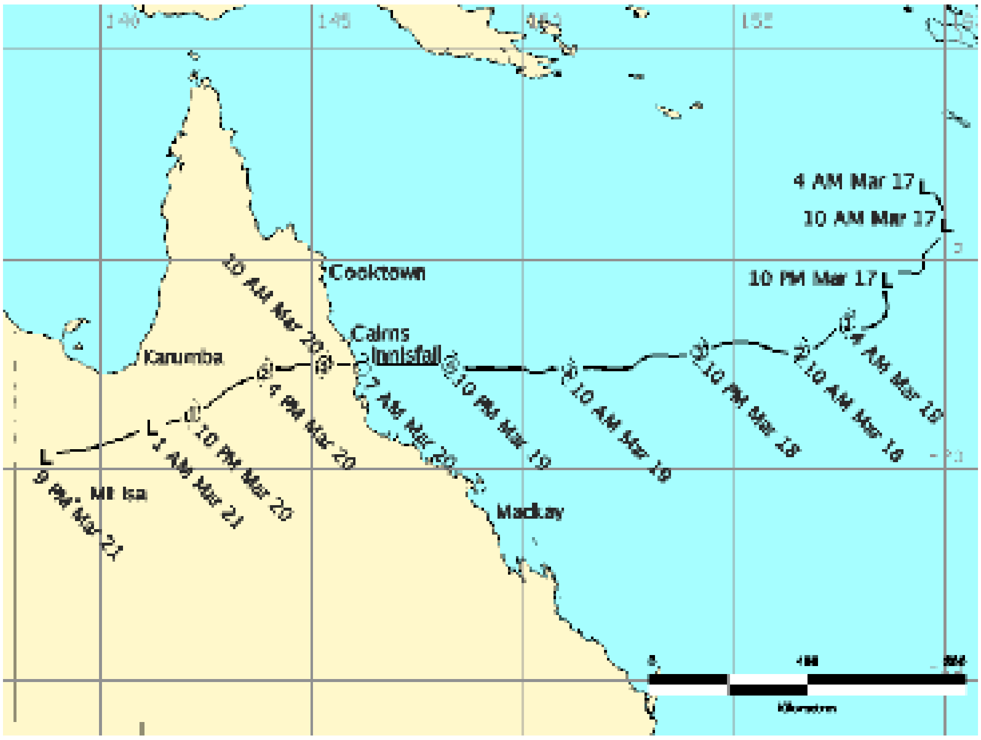

Figure 1: Tropical Cyclone Larry track (Bureau of Meteorology, 2006)

Survey activities

Protocols

Any activity in an area of severe impact needs to be conducted with the approval and co-ordination of emergency services. The existing protocols GA has with Australian emergency management were used in which the duty officer of EMA was contacted who then made contact with the State Emergency Services (SES). The local emergency managers then provided a contact person in the SES for co-ordination of activities. Once in the area the local emergency co-ordination centre in Innisfail was visited to advise of the team's arrival in the area and to be briefed by the SES on any matters that may affect the survey activity.

In parallel with this, previously identified key wind researchers were contacted and a survey team assembled. In the limited time prior to mobilisation efforts were also made to align the survey templates for consistent logging of data. A simple 10 point damage scale was used by all collaborators while GA used in addition a detailed damage logging template on hand-held computers which was refined prior to departure through survey team review.

Team composition

Within 48 hours a forward reconnaissance party departed for Innisfail with the main survey party joining them 3 days later. The combined team comprised:-

Cyclone Testing Station, James Cook University	3
Australian Building Codes Board	1
TimberEd Services	2
JDH Consulting (John Holmes)	1
Risk Frontiers, Macquarie University	1
Geoscience Australia	6
	14

Collaborative field work also took place between GA and the Bureau of Meteorology in the assessment of wind speeds in standard conditions. Both hazard specialists and wind engineers were included in the team as damage severity is meaningless if it cannot be associated with a degree of hazard exposure.

Infrastructure scope

The combined team surveyed in a systematic way almost 2,700 buildings. The composition of the surveyed building stock is summarised in Table 1. Separately Geoscience Australia carried out a non-comprehensive study of critical infrastructure. This included power transmission and distribution along with State Rail radio communication tower assets.

Tools and techniques

Historically post-disaster surveys have tended to focus on damaged infrastructure and their failure types. Novel structural behaviour has been the subject of keen interest as it may give insight into building vulnerabilities and aid the identification of building code deficiencies requiring address. Predominance in the population is approximately considered and the cost of repair is not addressed in detail. Population surveys of all structures (including undamaged) is needed for surveyed damage to be used in a risk process. Further, the level of damage detail captured needs to be greater for reparation costs to be reliably assessed to each structure. Both approaches are needed and were used in the Cyclone Larry survey process.

The building population surveys were undertaken on selected suburbs and communities. GA made use of hand-held computers, GPS equipment and digital cameras whereas the balance of the team surveyed using paper templates. The advantage of the hand-held computers was the ability to control data entry quality through customised predetermined dropdown menus, using aerial imagery, street locality maps as a backdrop and the straightforward input of address and cadastre information from the national database Geocoded National Address File (PSMA 2006 G-NAF). Disadvantages are associated with the cost of the equipment ($2500 per unit), the time involved in overnight data download/upload and the need for some basic training. The equipment utilised is pictured in Figure 2 and the data fields captured are shown in a Geographic Information System (GIS) Figure 3. Assessed overall levels of damage for several suburbs/communities are summarised in Figure 4. The damage to modern residential structures was found to be half that of the older building stock built prior to 1986.

Table 1:- Composition of surveyed building stock following Tropical Cyclone Larry

Building Type	Age	Number Surveyed
Commercial and Industrial	All	177
Government, Community, Education and Other	All	44
Residential	1914 to 1945	413
	1946 to 1959	368
	1960 to 1979	844
	1980 to 1989	239
	1990 to 2006	601
	Total	2,686

Data gathering and collation extended after the field activity. Building portfolio information was obtained from the Queensland Department of Housing which provided data on when their homes were built and roofs were replaced. Building permit data was obtained from the Local Government Authority (LGA) and the high resolution satellite images of the surveyed structures were foot-printed to obtain floor areas. Repair cost modules have been developed for seven building types through a quantity surveying consultancy (Turner and Townsend Rawlinsons, 2006) and are being implemented to turn damage observations into repair cost. Claim data is presently being sought from collaboratiing insurance companies. As a final phase, arrangements are being put in place to survey the residents of surveyed homes to refine and supplement information on retrofitting, building age, window breakage and degree of water ingress.

Figure 2: Field survey equipment used for detailed damage survey activity

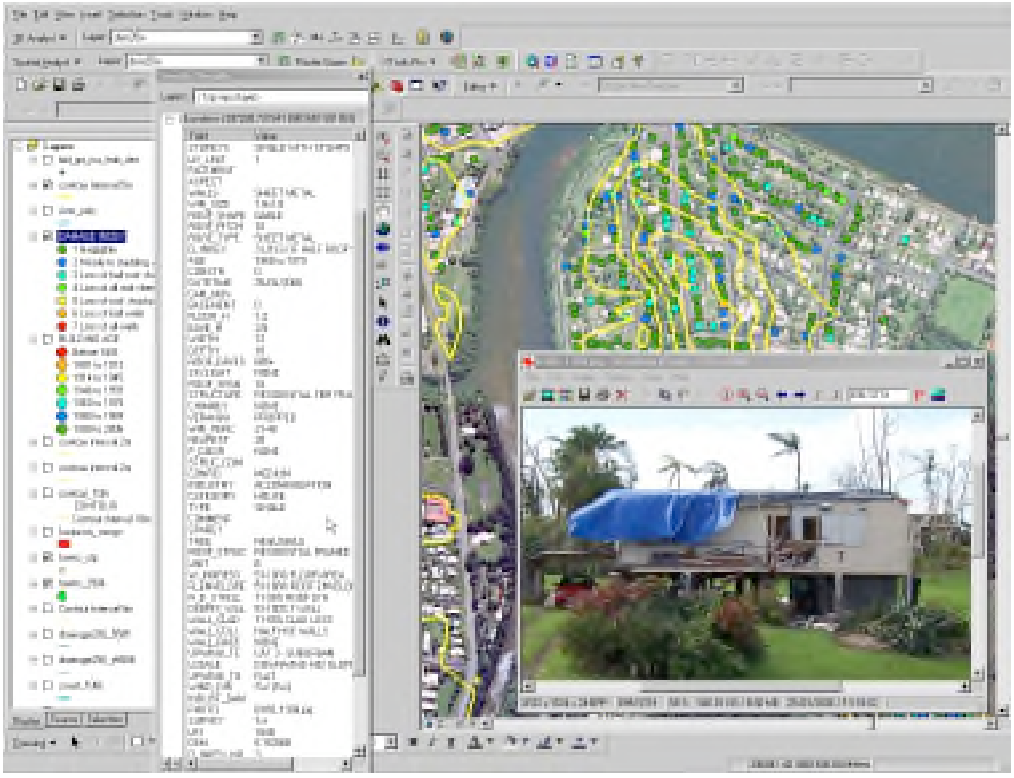

Figure 3: Sample of data captured using field survey equipment in a GIS

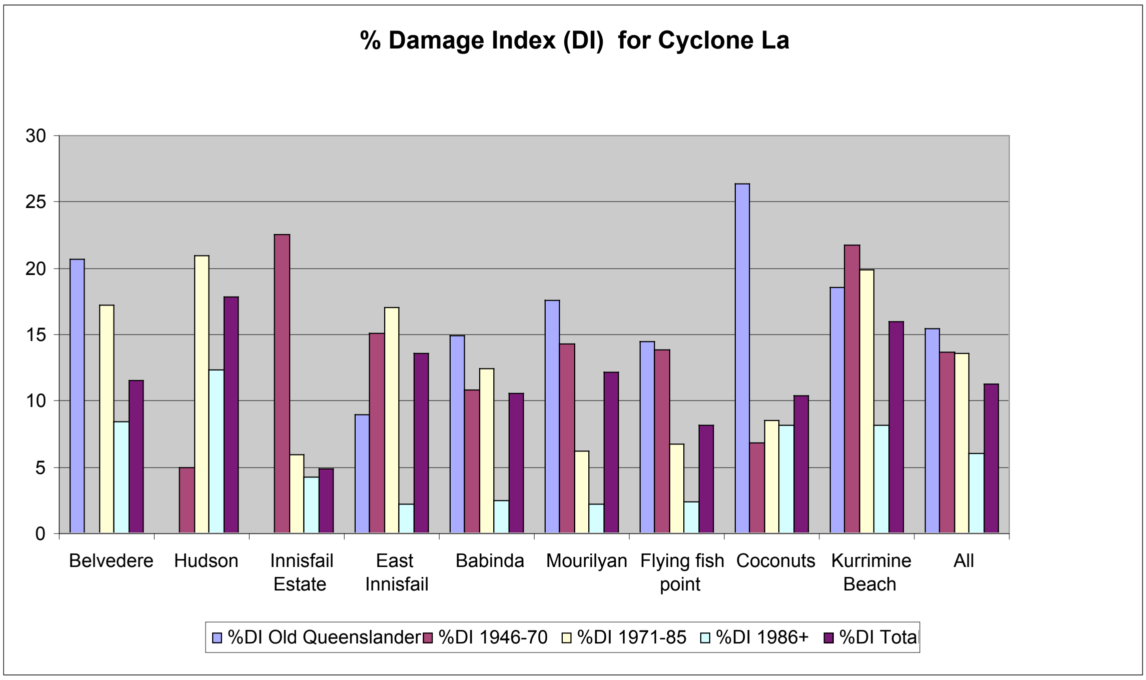

Figure 4: Damage sustained by residential structures for surveyed suburbs and communities separated by age and expressed as a proportion of the cost of complete house rebuild.

Future survey developments

Survey templates for wind damage will be reviewed and refined as part of a third wind workshop scheduled for late February 2007. Geoscience Australia has also acquired field equipment that will permit overall damage as observed from the street to be captured using multiple roof mounted cameras.

Tranferable elements

In the context of equivalent activities the following transferable elements have been identified:-

- The need to seek the input of key specialists in earthquake hazard and vulnerability to resolve the best approach to post-disaster surveys. Workshop activities were found to be an effective way of advancing this for severe wind.
- The value of a regional approach which includes New Zealand researchers. Great value would be derived from participating in damage surveys of both countries infrastructure.
- The establishment of clear protocols with Australian (and New Zealand?) emergency management to permit efficient mobilisation with limited disruption to the first priority management of the immediate event consequences.
- The development of an agreed survey template that captures the data interests of all collaborators. If hand-held computer / GPS data capture is to be used some basic training of all potential collaborators is needed. This could be carried out in conjunction with a workshop activity.
- The inclusion of a broader range of infrastructure. Critical infrastructure needs systematic and comprehensive surveyed.
- The value of early mobilisation. Damage cleanup that quickly follows an event can lead to a corresponding loss on survey information.
- The systematic sourcing of supplementary datasets following an event.

Summary

This survey activity has been the largest and most extensive damage survey undertaken by GA and its other collaborators. It has also drawn upon the broadest group of wind experts ranging from the hazard specialist through to those with a detailed knowledge of structural behaviour. Research outcomes from this activity are expected to become available over the coming months that will permit a better assignment for vulnerability to the North Queensland building stock. Many wind damage survey elements transferable to earthquake damage surveys have been identified which could effectively be incorporated into a coordinated response to the next damaging earthquake in the region.

References

Bureau of Meteorology (2006) Tropical Cyclone Larry, www.bom.gov.au/weather/qld/cyclone/tc_larry

COAG (2002) "Natural Disasters in Australia : Reforming mitigation, relief and recovery arrangements", A Report to the Council of Australian Governments by a high level officials' group, August.

Institution of Engineers, Australia (1990), "Newcastle Earthquake Study", Barton, ACT, 1990

JDH (2006) "Severe Wind Risk Research Workshop : 1st December 2005", Geoscience Australia, Canberra, Report #JDH 06/1, JDH Consulting

Nadimpalli K. , Edwards M. , Cechet B. , Driessen, M. and Forghani, A. (2006) "First steps towards a national assessment of Australian wind risk", GA Record, Geoscience Australia.

PSMA (2006) Australian Geocoded National Address File (G-NAF), www.g-naf.com.au

TimberEd (2006) "Report on Wind Vulnerability Research Workshop: 15th and 15th March 2006", James Cook University, Townsville, Report #2130-02, TimberEd

Turner and Townsend Rawlinson (2006) "Wind Damage Cost Module Development: For North Queensland Building Types", Consultancy Report to Geoscience Australia, 15th September 2006.

Protecting life and reducing damage in earthquakes and terrorist attacks

Colin Gurley

Abstract

Images of structural collapse crowd our globalised television screens; from wars, from terrorist bombs and from earthquakes. The outcomes often look quite similar, but what are the engineering differences?

As engineers, we look for differences relating to collapse mechanisms:

- Earthquake engineering focuses on sway collapse mechanisms in which the building as a whole moves sideways and may collapse under its own weight.
- Explosions may remove one or several load-bearing columns or walls leading to a 'lost support' vertical collapse which may be:
    - localised to the lost support perhaps extending over just a few stories or
    - 'disproportionate' or 'progressive', extending over much of the floor area and, perhaps, the full height of the building.

Records of earthquake damage show that earthquakes can also remove supports, often corner columns, precipitating a vertical collapse which may, again, be 'progressive' and 'disproportionate'. It seems logical and appropriate, in terms of the expertise and technology involved, to regard 'robust' design for 'lost column' events as an extension of earthquake engineering and so to merge earthquake engineering with design against 'disproportionate' collapse.

A further motive for this merger arises when considering the quality and details of ductile detailing to be provided in regions of low earthquake risk such as Australia.

Introduction

Structural thinking has developed in response to the 1968 Ronan Point accidental gas explosion, the 1995 terrorist bomb attack on the Murrah Federal Building in Oklahoma City and the 2001 attack on the World Trade Centre. It now seems evident that there is potential for two areas of engineering to merge in the development of robust standards.

The drafts of AS 1170.4 Earthquake actions and AS 3600 Concrete Structures already cover many of the issues relating to 'lost column' events.

Some matters may require review. One such issue is that:

- these two draft codes permit three different standards of ductile detailing:
    - 'ordinary', 'intermediate' and 'special' and
- they do not discourage 'ordinary' detailing indeed
- they rather encourage 'ordinary' detailing in the sense that the only advantage of 'intermediate' and 'special' detailing apparent from these drafts is a lower design earthquake load. Even this 'advantage' will be ineffectual if the earthquake design load effect is, anyway, less significant than the wind design load effect as it often is, particularly for taller buildings in Australia.

This article takes the view that the minimum standards of ductile detailing should be related to the Importance Level of the building as defined in BCA. The rationale for this view relates both to earthquake performance and also to performance following removal of a support by any event.

The calculation of earthquake design load can then take advantage of the standard of ductility actually provided but a higher earthquake design load should not be used to justify 'ordinary' detailing for important buildings.

The concept of ductile detailing involves a whole basket of design rules but the most obvious, perhaps the most crucial, issue has to do with the continuity of bottom rebars through columns and other intermediate supports. Other important issues relate to secondary reinforcement for shear strength, for confinement and for buckling restraint of compression rebars.

Bottom rebar at columns and other intermediate supports

The Draft of AS 3600 c8.1.10.4 has not changed from earlier editions:

- At an intermediate support "… not less than 25% of the total positive reinforcement required at mid-span shall continue past the near face of the support." No distance is specified so it could be as little, say, as 50 mm.

The 25% required can have negligible anchorage at the column face so the bending strength for any positive moments there will that of an un-reinforced beam hence brittle under cyclic load.

Australian 'ordinary' detailing is somewhat inferior to American 'ordinary' detailing. In ACI 318-05:

- c12.11.1 requires the same 25% but is explicit that it extend 150 minimum into the support while:
- c12.11.2 further requires that:
    - "When a flexural member is part of a primary lateral load resisting system, positive moment reinforcement required to be extended into the support by 12.11.1 shall be anchored to develop f_y in tension at the face of the support."

The ACI Commentary explains that this "… anchorage is required to ensure ductility of response in the event of serious overstress such as from blast or earthquake." Indeed it is although it would be better to make bottom rebars continuous through columns.

Support bottom rebars with wind

The worst design positive (tension bottom) bending moment at a support will be the signed sum of:

- A negative (tension top) moment caused by the minimum long-term gravity loads offset by
- A positive (tension bottom) moment caused by the ultimate (say 500 or 1000 year) wind loads.

If the negative gravity load moment exceeds the ultimate wind moment, even slightly, then a nett positive moment never occurs and 'ordinary' detailing to AS 3600 does not require any effective bottom rebars at the column.

What if an abnormal wind load occurs? Calculation from AS1170.2 Table 3.1 shows that the ratio of wind pressures from 10,000 year return to 500 year return varies from 1.3 to about 1.5 in some cyclone areas. If one neglects global warming then there seems to be an upper limit on wind pressures such that, even at 10,000 years return the pressure, hence bending moment, from wind is, at most, 50% larger than the 500 year value.

This is not quite an acceptable answer. It does imply that:

- If the moment due to 500 year wind is exactly balanced by minimum gravity loads then
- Under the 10,000 year wind the beam will experience a nett positive (tension bottom) curvature equal to half of the gravity load value at a position with no bottom rebars.

This is not just a 50% overstress on steel rebar under extreme conditions, which would be acceptable. Rather it relies on the tensile strength of concrete for a load which is not cyclic but certainly erratic and pulsating. Nevertheless our code writers have accepted it and there may be reasons not least, in that, whatever happens to an individual beam is not likely to happen to the building as a whole so long as the 'overload' is just 50%.

Support bottom rebars with earthquake

The position with earthquake is a good deal worse than with wind for 2 reasons:

- Earthquake loads are not limited with increasing return period to anything like the extent that wind loads are so limited and
- this is compounded by the combined ductility factor of Draft AS1170.4 Table 6.2.

In terms of the ratios of 'Probability Factors':

- Draft AS 1170.4 Table 3.1 shows a ratio of earthquake loads 2500 years/500 years at 1.8 and
- NZS1170.5 shows the same value, 1.8 for 2500/500 years but
- NZS1170.5 Commentary Fig C3.3 shows ratios up to 2.9 for 10,000/500 years (at Dunedin)

In terms of ductility factor, the design earthquake load with just 'ordinary' detailing will have been reduced to just 38% (1/2.6) of the value for an elastically responding structure.

The effect of this is that:

- The 10,000 year response is not just 50% greater than design load response as with wind
- It may be greater by a factor 2.6 x 2.9 = 7.5 and
- The load will be cyclic

If the positive moment curvature at an intermediate column under the design earthquake load is just sufficient to counterbalance the opposite curvature due to minimum long-term gravity load then:

- AS3600 'ordinary' detailing permits zero effective bottom rebars at the column but
- The nett curvature at that un-reinforced section under the 10,000 year event may be 6.5 (=7.5 – 1) times the gravity load curvature.

One normally assumes that ductility provides the basis for reduced return periods and reduced design loads but this does seem to be increasingly questionable when the notion relies on beams with no effective bottom rebars at columns.

This does apply to important buildings including tall buildings and all facilities at BCA Importance Levels 3 and 4 including hospitals, police, ambulance and fire stations and chemical factories producing hazardous materials.

Support bottom rebars after loss of column

If a column in storey x is removed by any means (explosion or earthquake) then the effect is that:

- every floor structural element supported by that column over the full-height above storey x,
- will experience a sudden doubling of its span but,
- with 'ordinary' detailing,
- will have zero sagging strength at what will now become a critical mid-span region.

The total free-span moment strength at a typical floor will have been reduced by about one third in each new half-span. More importantly, a flexural failure at the new mid-span will be brittle so the span, as a whole, may be unable to develop its full plastic mechanism strength.

Floors cannot 'hang' from higher levels unless there is some non-typical stronger structure (or lower gravity loads) at those higher levels. If the total strength over the height of the building is inadequate for the total loads then a progressive collapse will follow.

Note that the better 'ordinary' detailing of ACI 318-05 c12.11.2 does not really cover the 'lost column' situation either. The bottom rebars do need to be continuous through the column.

Design gravity loads under these circumstances are discussed below in the paragraph on GSA 2003.

Britain & Ronan Point

In 1968, at Ronan Point in England, a 20-storey apartment building, of precast concrete construction, was destroyed by an accidental explosion in a domestic kitchen gas stove. After a judicial enquiry, the British Government adopted the 'Ronan Point Rules' for building design, of which the current version is Approved Document A3 2004 *Disproportionate Collapse* downloadable at www.odpm.gov.uk.

Precast concrete construction has moved on since to the extent that New Zealand and California now both have specialised codes for precast construction in regions of high earthquake risk.

Britain has been subject to terrorist bomb attacks for several decades and yet the 'Guidance' documents at the UK website make it clear that, while the writers were aware of terrorist threats, they were (2004) nevertheless primarily focused on accidents: gas explosions and vehicle impacts.

Australian states adopted some of the 'Ronan Point Rules' a few years after the Ronan Point event and there are still vestiges in BCA and in AS1170.0 s6 *Structural Robustness*. These guides are general and not at all specific.

The basic Requirement of British Document A3 is that:

- *"The building shall be so constructed so that in the event of any accident the building will not suffer collapse to an extent disproportionate to the cause.*
- *Subject to the "Limits of Application*
- *"Requirement A3 applies only to a building of 5 or more stories"* counting basements but not roof space if pitch < 70 degrees.

There are still 3 distinct groups of provisions in the British provisions:

- Design of structural elements for blast pressures
- Tie every element to every adjacent element
- Alternative load-path analysis

This list, identified almost 4 decades ago, still covers the important issues arising in 'lost support' events.

Ronan Point 'ties'

The British emphasis is on 'ties' rather than 'ductile detailing'. From an earthquake engineering view:

- Ductile detailing is always important while
- Ties are vital but not often important because they are anyway, in many/most cases, provided by an in-situ floor-slab as diaphragm, and by continuous vertical rebars or by splices of steel columns.

In in-situ concrete-framed buildings, floor rebars will be passed through, or close to, the rebar cages of concrete columns. In steel-framed buildings, rebars will flank 'I' and 'H' columns close on all 4 sides.

One situation that does require care is that of a façade steel column placed close to or outside the edge of the floor-diaphragm. This is already covered by AS4100 c6.6 and c5.4.3;

- a horizontal buckling restraint force of 2.5% of column axial load
- or 2.5% of flange forces if there are also substantial column moments and
- the crucial 'ties' must prevent detachment of the column from the floor-slab as diaphragm.

If the buckling restraint force cannot be supplied by rebar then it must be supplied by steel-to-steel connections (bolts or welds). Construction sequence also needs to be considered; what loads are on the column before the floor-slab is 7 days old?

Ronan Point design of structural elements for blast pressures

is one of the 3 areas covered by the Ronan Point Rules. My guess is that this is/will be a specialist activity for those who design embassies, defense establishments and similar where car/truck bombs can be kept at a distance.

The British document A3 mentions a design blast pressure of 34 kPa (710 psf). FEMA 227/ASCE 1996: The Oklahoma City Bombing calculates a blast pressure of 10,000 psi (69 MPa = 69,000 kPa) at mid-height (smaller pressure above, bigger below) of the crucial 2-storey transfer column located 5 metres from the centre of the bomb.

It is difficult to believe that blast-pressure design can save such a column.

Ronan Point alternative load-path (removed support) analysis

is another of the 3 areas of the Ronan Point Rules and an area that AEES can and should address.

Load-bearing elements are:

- Individual columns or
- Any length of load-bearing wall of length between piers but ≤ 2.25 H (H = clear storey height) or
- Transfer structures supporting 2 or more columns

Any such element not designed for a blast pressure of 34 kPa must be removable without causing 'disproportionate' collapse exceeding:

- 15% of floor area or 70 sq metres (700 sq feet) whichever is less
- On each of, at most, 2 adjacent floors

GSA 2003 (see below) now also covers this area and has requirements for new (US) Federal Buildings involving the notional removal of edge, corner or interior columns or load-bearing walls in the bottom storey only.

The Murrah Federal Building in Oklahoma City

did have concrete transfer beams on the long north facade at 2 stories above ground doubling the façade spans from 6 to 12 metres.

From detailed analysis FEMA 227/ASCE 1996 concludes that:

- Blast pressure directly failed less than 10% of the total floor area. Floor-slabs are normally detailed only for downward loads and one would expect that these floor-slabs were not reinforced for upward loads; hence no mid-span top rebars and no continuous bottom rebars through supports. The failed areas were presumably close enough to the bomb that upward blast pressure exceeded slab self-weight and tensile strength.

- Blast pressure 'brisance' removed north façade column G20 supporting the transfer beam and resulting, momentarily, in a 24 metre span from G16 to G24.
- Columns G16 and G24 then failed in shear under the blast pressure,
- resulting in a 48 metre total span with no effective mid-span bottom rebars thereby progressively bringing down 50% of the occupiable floor area over the full height of the building.
- *"… up to 90% of the (168) fatalities were the result of crushing caused by falling debris"* as distinct from the bomb explosion and the blast pressure.
- The collapse started 2 seconds after the explosion and took a further 3 seconds.
- *"Column G20 would be likely to have been destroyed by brisance even if detailed as a Special Moment Frame."*
- *"If the more recently developed detailing for Special Moment Frames had been present at the time of the blast, Columns G16 and G24 would have had enough shear resistance to develop a mechanism without failure."*

It is clear from FEMA 227/ASCE 1996 (and not surprising) that the 1974 design did not comply with the 2005 edition of ACI 318-05 c12.11.2 on anchorage of bottom bars from a column face. Perhaps there was no corresponding clause in ACI 318-71 and/or perhaps the north façade was not considered to be *part of a primary lateral load resisting system* given that there was a shear core near the centre of the south façade and 4 large vertical (apparently structural concrete?) air-ducts at the 4 corners of the building.

The overview findings from FEMA 227/ASCE 1996 were that:

"It is noted that the loss of 3 columns and portions of some floors by direct effects of the blast accounted for only a small proportion of the damage. Most of the damage was caused by progressive collapse following loss of the columns.

"There is no evidence to suggest any significant lateral or torsional displacements of a global nature..

"The type of damage that occurred and the resulting collapse of nearly half the building is what would have been expected for an Ordinary Moment Frame Building of the type and detailing available in the mid-1970s when subject to the blast from the large bomb that was detonated.

"Special Moment Frame design would provide (presumably bottom) reinforcement in the transfer girder at the third floor that would greatly increase the possibility that the slabs above would not collapse" and "… it is estimated that losses would be reduced by as much as 80%." Note that American third floor = Australian second floor.

"The engineering analysis performed on the Murrah Building suggests that the higher lateral force levels required for seismic design in areas of high seismic risk are not required for blast mitigation in regions of low seismic activity; only the detailing requirements need be followed" and

"Investigations to determine the cost of using Special Moment Frames rather than Ordinary Moment Frames were conducted by the Building Seismic Safety Council. These investigations along with more recent changes in designs, suggest that increase in cost is in the range 1% to 2% of the total construction cost of the building."

The Murrah Federal Building was a 9 storey (35 metres) high building with an area of 1400 sq metres per floor total 12,600 sq metres in a region with no earthquake design requirements at the time of construction. An identical building in Australia would barely qualify as BCA Importance Level 3.

America now

In America there is ongoing debate in the light of the attack on the World Trade Centre 2001 and the 1995 attack in Oklahoma City. There are initiatives on the US East Coast to amplify and adopt the Ronan Point Rules in more voluminous detail.

The British writers of Document A3 have written what they have in the context of a country that has a lower level of earthquake risk (than Australia, New Zealand and America) and a lower level of awareness in the general population and in the home building industry. There are British firms of consulting engineers practicing internationally who are expert at earthquake engineering but they are not the typical home readership of Document A3. Australian consulting engineers often have experience in neighbouring Asian countries where earthquake risk is high.

There is a danger in writing separate codes for 'lost support' terrorist events and for 'progressive collapse' that ignore but largely overlap earthquake codes in earthquake-aware countries thereby adding to the un-necessary length and complexity of codes and to the risk of mis-interpretation.

The American debate is also concerned to protect emergency responders and there are suggestions that some buildings be designed to survive 'burn-out' of contents after active fire suppression systems fail. 'Intermediate' or 'special' ductile detailing might also contribute to this worthwhile objective.

GSA 2003 Progressive Collapse Analysis and Design Guidelines for New Federal Office Buildings

This US Federal document provides extensive direction on the details of lost support /double-span mechanisms.

It recognizes blast-pressure design as a specialist activity and seems to accept that it may only be useful when unauthorized vehicles can be kept outside a 'defended stand-off distance'.

It has some helpful illustrations of double-span mechanisms in concrete and in structural steel.

It provides the first American version of the British rules for *alternative load-path analysis*:

- Supports may be lost only in the lowest storey at about ground level
- Any single perimeter column may be lost
- Any single 9 metre (30 feet) length of perimeter load-bearing wall may be lost
- Any single interior column or any single 9 metre length of interior load-bearing wall may be lost if there is uncontrolled parking beneath the building
- Any corner column may be lost
- Any double-legged (equal angle shaped) portion of load-bearing wall at a corner may be lost for 4.5 metre (15 feet) along each façade or at any interior support if uncontrolled parking
- Under these circumstances collapse should be limited to the immediately adjacent bays of the floor immediately above the removed support but not more than 1800 sq feet (180 sq metres) at a perimeter support or 3600 sq feet (360 sq metres) at an interior support.

This is quite a useful document but it does seem somewhat focused on car/truck bombs. GSA Figure 4.7 shows strengthening at floors 2 and 3 which would be effective if a bottom storey column was lost but not if some column above level 3 was lost. (American floor 3 = Australian floor 2)

Higher level columns might be lost by earthquake or to a terrorist attack using weapons other than car/truck bombs. To accommodate all such unforeseeable possibilities it would seem best to place any special strengthening elements as high in the building as reasonably possible.

GSA 2003 requires double design gravity load but permits doubled strength:

- For static analysis: Gravity Load = 2 * (DL + 0.25 * LL) ; GSA Equation (4.1) and
- Doubled strength: DCR = Demand / Capacity Ratio ≤ 2 for "typical structural configurations"; GSA Equation (4.2)

These appear to be offsetting factors but it is not quite as simple as that:

- In GSA Equation (4.1):
    - The factor 2 is, presumably, an impact factor to account for the sudden removal of a lost support. It seems about right.
    - 0.25 seems to be a reasonable estimate for the long-term (earthquake) component of live-load. It is slightly lower than the figure of 0.30 in the Draft AS1170.4 Earthquake actions. The figure in AS1170.0:2002 *General principles* is still 0.40.
- The DCR = Design to Capacity ratio is also set at 2 for "typical structural configurations". In this regard, GSA 2003 refers to FEMA 356 *Prestandard and Commentary for the Seismic Rehabilitation of* (Existing) *Buildings*

The earthquake literature and FEMA 356 contains extensive material on the over-strength and strain-hardening of steels and this accounts for much of the DCR up to, say, DCR = 1.5 which is the GSA value for "atypical structural configurations".

The value DCR = 2 from FEMA 356 assumes elastic (not plastic) analysis and so also includes an allowance for plastic redistribution. To use this value with capacity calculated from a plastic analysis may involve some double counting.

In any case, one can understand that code-writers, such as the writers of FEMA 356, might reasonably be somewhat optimistic about the strength of existing buildings particularly those that are also heritage buildings. This would be within the public policy domain of code-writers because a value that was not somewhat optimistic would tend to pick up numerous existing buildings that are only marginally under-strength. Should one be just as optimistic in the design of new buildings for abnormal load?

Australia

Records of earthquake damage often give the impression that the quality of ductile detailing is more important to performance in actual earthquakes than the value of earthquake design load.

This does seem to be true for regions designed for high earthquake loads such as New Zealand and California. Perhaps it is even more true for regions designed for low earthquake loads such as Oklahoma City and most of Australia. Earthquake events may far exceed code predictions, especially in areas of low seismic risk as at Newcastle (NSW) 1989, but a ductile building will always fare much better than an otherwise-identical brittle building.

And ductile detailing for bomb attacks is pretty much the same as it is for earthquakes if not always for the same reasons. This is an area that AEES can and should progress.

And we have the opinion from (US) Building Seismic Safety Council that the extra cost of high-quality ductile detailing (as distinct from higher lateral design loads) is so small as to be barely quantifiable. This does make for a strong cost/benefit argument!

There seems to be nothing in the drafts of AS1170.4 or AS 3600 which relate the minimum quality of ductile detailing to the scale and importance of the building. The distinction between 'ordinary', 'intermediate' and 'special' merely results in a lower ductility factor hence more design earthquake load on 'ordinary' frames. If the earthquake load anyway happens to be a low, non-critical load condition compared to wind then there is nothing to encourage the use of 'intermediate' or 'special' ductile detailing. This could apply to tall buildings and to any and all facilities at BCA Importance Levels 3 and 4 such as hospitals, police, ambulance and fire stations and chemical factories producing hazardous materials.

What then about AS 4100 *Steel Structures*? One normally assumes that steel structures are inherently ductile. But it is common practice to design many steel beams for gravity loads with ‘pin’ supports. If ‘pin’ connections really do behave as such when a column is lost then those steel beams may be in a worse predicament than concrete beams with zero bottom rebars. Some of the American research following the Northridge Earthquake of 1994 suggests that some, not all, ‘pin’ connections are better than that and can develop significant moments so long as both flanges have, at least, cleats to the supporting columns or girders.

Conclusion / Recommendation

Earthquake engineering, as a field of professional expertise should be extended to include ‘lost column’ events whether caused by earthquakes, accidental explosions or terrorist bombs.

Relevant Australian Standards should be reviewed so as to:

- consider ductility under ‘lost support’ events whether by explosions or earthquakes
- relate the minimum standards of ductile detailing to the Importance Levels of BCA

In particular, the draft of AS3600 Clause A12 *Moment Resisting Frame Systems* should be urgently revised to require ‘intermediate’ and/or ‘special’ detailing as minimum standards for buildings at BCA Importance Levels 3 and 4 particularly for tall buildings and for emergency response facilities such as hospitals, ambulance, fire and police stations and utility services.

One has to ask whether Australians would find it acceptable, in the light of what we now know and in the current geopolitical climate, for a newly built building in Australia:

- comparable in size and importance to the Murrah Federal Building in Oklahoma City
- to suffer the same degree of loss of life and collapse
- as the result of a truck bomb placed by a group of 3 terrorists and
- as a now foreseeable consequence of ‘ordinary’ detailing?

Particularly when the marginal cost of a much improved ‘intermediate’ or ‘special’ performance is so low as to be barely quantifiable (1% to 2% of total cost).

These issues also need to be addressed in AS 4100 *Steel Structures*. Many steel buildings are designed with ‘simple pin’ connections for beams. These may also be brittle under ‘lost support’ events.

In the longer term, we should, with our colleagues around the world, start to develop a systematic understanding of the collapse mechanisms associated with the loss of supports (columns, load-bearing walls and transfer systems) comparable to our understanding of the sway mechanisms more usually associated with earthquake.

A collaborative approach is likely to achieve more robust solutions and more cohesive structural codes, reducing the complexity of regulatory documentation and improving outcomes for engineers and for the community.

References

ACI 318-71 Building Code Requirements for Reinforced Concrete 1971, American Concrete Institute, Detroit, Michigan, USA

ACI 318-05 Building Code Requirements for Structural Concrete and Commentary, American Concrete Institute, Farmington Hills, MI 483312, USA

Approved Document A3 2004 Disproportionate Collapse; The Building Regulations 2000, Office of the Deputy Prime Minister, London downloadable from www.odpm.gov.uk

AS1170.2: 2002 Structural design actions Part 2: wind actions, Standards Australia, Homebush NSW 2140

AS1170.0: 2002 Structural design actions Part 0: General Principles, Standards Australia, Homebush NSW 2140

AS 4100: 1998 Steel Structures, Standards Australia, Homebush NSW 2140

BCA Building Code of Australia, Australian Building Codes Board, Canberra

Draft for Public Comment DR 04303 2004: Revision of AS1170.4: 1993 Structural Design Actions Part4: Earthquake Actions in Australia; Standards Australia, Homebush NSW 2140

Draft for Public Comment: Revision of AS 3600: 2001 Concrete Structures, Standards Australia, Homebush NSW 2140

FEMA 222A / Building Seismic Safety Council 1994/5 NEHRP Recommended Provisions for Seismic Regulations for New Buildings, Washington, DC

FEMA 227/ASCE August 1996: The Oklahoma City Bombing: Improving Building Performance Through Multi-Hazard Mitigation. Federal Emergency Management Agency, Washington

FEMA 356 Prestandard and Commentary for the Seismic Rehabilitation of Buildings, Federal Emergency Management Agency, Washington

FEMA 403/ASCE May 2002: World Trade Center Building Performance Study. Federal Emergency Management Agency, Washington

GSA June 2003 Progressive Collapse Analysis and Design Guidelines for New Federal Office Buildings, General Services Administration, Office of the Chief Architect, Washington

NZS 1170.5: 2004 Structural Design Actions Part 5: Earthquake Actions – New Zealand; Standards New Zealand, Private Bag 2439, Wellington 6020.

NZS 1170.5 Supp1: 2004 Structural Design Actions Part 5: Earthquake Actions – New Zealand - Commentary; Standards New Zealand, Private Bag 2439, Wellington 6020

Reconciling neotectonic and seismic recurrence rates in SW WA

Mark Leonard and Dan Clark

Geoscience Australia

Introduction

The seismicity of the southwest corner of Western Australia has long been thought to be unusual. Everingham (1968) and Everingham and Tilbury (1972) undertook an analysis of the historical earthquake catalogue for south-western Australia, and concluded that the catalogue is complete above magnitude 4.5 since 1900, and probably since 1878. Michael-Leiba (1987) concluded that there was a sudden increase in seismicity around 1949. The geomorphology of the area (eg. the generally flat landscape) is not consistent with the seismicity rate for the last 40 years, which includes three scarp forming earthquakes, being typical of the seismicity over the Quaternary.

The new sources of data becoming available, such as DEMs and Optically Stimulated Luminescence (OSL) dating, (Clark 2005, Clark et al. 2004, Estrada et al. 2006) are enabling scientists to learn and suggest hypotheses about the nature of the seismicity of Australia, and possibly other areas of stable continental crust, which was not possible until now. This paper compares the number of expected M7.0-7.5 earthquakes estimated from seismic recurrence rates derived from several earthquake catalogues and the number of paleo fault-scarps which have been identified in the area - mostly from DEMs.

Data and method

The availability of high resolution digital elevation model (DEM) data has lead to the identification of over 50 features that are likely to be scarps of surface rupturing earthquakes (Clark 2006 & 2005). Few of these fault scarps have been fully studied but of the 20 which have been the subject of field work all are thought to be fault scarps. Using the fault length and displacement as proxies for magnitude and in some cases identifying multiple events, these scarps have been used to generate a neotectonic earthquake catalogue. The area used in this study is the subset of that covered by the WA Department of land Information (DLI) and Shuttle Radar Tomography Mission (SRTM) DEMs, which has an average rainfall of less than 400mm/yr. A wetter environment would result in more extensive tree coverage which makes identifying scarps more difficult and likely results in much higher erosion rates. This makes estimating magnitude completeness even more difficult and so the data from wetter areas has been excluded.

Estimating the magnitude completeness periods of neotectonic data is very difficult. The higher resolution DLI data is estimated to be complete above M7 for the last 100ka. The lower resolution SRTM is likely less comprehensive and M7.2 for the last 100ka is the completeness period estimated. All earthquakes above magnitude 7.0 are assumed to result in a significant fault scarp for the full length of the rupture area. Smaller earthquakes will not necessarily result in a scarp at all, let alone a full length scarp. Of those scarps formed by these smaller earthquakes their smaller size makes them more difficult to identify and they will have shorter periods of exposure. For these reasons, completeness periods for earthquake with magnitudes <M7 have not been included in this study.

Two sources of earthquake data are used in this study. The first is a catalogue of earthquakes in global stable continental crust (SCC) compiled by the Geological Survey of Canada (GSC) (Fenton et al. 2006, Adams 2005). This has been used to estimate global and Australian recurrence rates. The other is the recently compiled catalogue of Australian earthquakes (Leonard 2006), which has been used to estimate recurrence relations for all of Australia and the SW of WA (Figure 1). The software used is based on the program betaplot developed by the seismology group of the GSC. It uses the method of Weichart (1980), which includes multiple completeness periods, maximum magnitude (Mmax) and the option to fix β.

This software has been applied to the four catalogues discussed using an Mmax of 7.6 The choice of Mmax in SCC remains contentious. Johnston (1994) argues that M7.0 in areas of non-extended continental crust. Others (Somerville P. and Campbell K. Per. Com.) prefer values in the M7.2-7.5 range.

Results

Figures 2, 3, 4 and 5 show the recurrence results for the SWSZ, Australian Shield, Australian Continent and World Shield respectively. So as to be consistent with the output of the betaplot program, the neotectonic derived recurrence rates have been rescaled according to the area of each region and to a per annum basis. These results are given in Table 1. The neotectonic derived catalogue would appear to be complete for ≥M6.9. This is the magnitude where a curve with a slope of 1 (b = 1.0) is tangential to the data. A slope of 1 is chosen as the break point between the slope of the curves at small to medium magnitude (0.6-0.95) and the slope at higher magnitudes (>2). Below M6.8 the number of earthquakes rapidly decreases with 20-25% of the expected number of M6.7 earthquakes and 3% of M6.6 earthquakes being identified via neotectonic methods. This is likely a combination of the lower likelihood of the earthquakes causing a surface rupture and the smaller rupture more rapidly reducing in size to below the detection threshold. All earthquakes of ≥M7.0 appear to produce fault scarps. Scarps formed by earthquakes of ≥M7.3 appear over represented with M7.4-7.5 earthquakes being overrepresented by a factor of perhaps 4-6. This could be explained by the longer preservation age of these earthquakes.

In all the recurrence analyses an Mmax of 7.6 has been used. Several of the fault scarps identified on the DEMs in SW WA consistent with M7.4-7.5 earthquakes. The long period of time (100ka or more) for which it is likely that the neotectonic catalogue is complete for earthquakes >M7 makes it likely that there have been several earthquakes close to Mmax. The Australian instrumental catalogue is complete for M7 earthquakes for around 100yrs. As the study area covers approximately 1/20 of the continent, the likelihood of the neotectonic catalogue having a Mmax earthquake is about 50 times that of the instrumental catalogue. Assuming global shield (N.A., S.A., Africa & Australia) catalogues are also complete for >M7 for 100 years, the Neotectonics catalogue is about 11 times more likely to have recorded an Mmax earthquake (Table 2). The lower rate of Global Shield seismicity compared to Australia suggests that this factor of 11 is possibly an underestimate. The three M7.5 and three M7.4 earthquakes suggest that an Mmax of 7.5 or 7.6 is reasonable. In the regressions M7.6 is used so that the recurrence curve included M7.5.

For the SWSZ the neotectonic derived recurrence rate is an order of magnitude below the seismic recurrence rate (Table 2). This is suggestive that the activity in the SWSZ over the last 50 years is higher than its long term (>10ka) rate. For the Australian shield the neotectonic recurrence rate is about twice the contemporary seismic recurrence rate. Given the uncertainties involved in these estimates this is a close correlation, and supports the hypothesis that seismicity in Australia is not stationary and varies spatially and temporally. In which case, the contemporary activity in the SWSZ is just one of several recent episodes of heightened seismicity, along with notable examples such as Tennant Creek and Simpson Desert. This is consistent with a model of episodic seismicity in Australia as suggested by several authors in recent times (Leonard 2006, Clark 2005, Crone et al. 2003, Crone et al. 1997).

For the whole of Australia the neotectonic and contemporary recurrence rates are approximately the same (Table 2). As the seismic includes data from the Flinders Ranges and SE Australia which are thought to have different tectonic environments to shield areas it is difficult to draw conclusions about this correlation. For the world shield earthquakes the situation reverses with the neotectonic rate being higher than the seismic rate and for the world excluding Australia the neotectonic data over estimates the number of large earthquakes by an order of magnitude. Fenton et al. (2006) model the world shield data with an Mmax of 7.0 which has a slightly better fit to the data than when using Mmax of 7.6. Whether an Mmax of ≥M7.4 to all regions of SCC is statistically consistent with contemporary seismicity is a question for the future.

Conclusions

When combined with the Australian and global earthquake databases a catalogue derived from the recently identified neotectonic fault scarps has the potential to provide significant insights into the seismicity of Australia and possibly the seismicity of other areas of stable continental crust. At present only about _ of the features of have had field investigation. All those inferred scarps that were checked in the field were verified to be actual earthquake scarps. This suggests the method of identifying scarps from DEMs is valid.

This study suggests that:

Under the right geological and climatological conditions fault scarps can be preserved for 100ka or more for scarps from ≥M7.3 earthquakes.
Mmax in stable continental crust is perhaps more like M7.5 than M7.0-7.2.
The recurrence rate for the neotectonic catalogue and historical earthquakes in the SCC of Australia are similar.
The contemporary level of seismicty in SW WA is an order of magnitude higher than that needed to generate the scarps.
Approximately 20% of M6.8 and 100% 7.0 earthquakes are expected to form scarps.

References

Adams J. (2005) On the probable rate of Magnitude >6 earthquakes close to a Swedish site during a glacial cycle. Appendix 5 in Expert Panel elicitation of Seismicity following Glaciation in Sweden. Eds. Hora S and Jensen M. SSI

Clark D., 2005. A preliminary seismicity model for southwest Western Australia based upon neotectonic data. Proceedings of the Australian Earthquake Engineering Society 2005 meeting, Albury Australia. Paper 22, 1-6.

Clark D., 2006. A seismic source zone model based on Neotectonics data. This volume

Clark D.J., Cupper M., Sandiford M., AND Kieknan K., 2004, Style and timing of late Quaternary faulting on the Lake Edgar Fault, southwest Tasmania, Australia: implications for hazard assessment in intracratonic areas. Geological Society of America Special Publication, in press.

Crone A J, Machette M N, AND Bowman J R, 1997, Episodic nature of earthquake activity in stable continental regions revealed by palaeoseismicity studies of Australian and North American Quaternary faults. Australian Journal of Earth Sciences, 44, 203-214.

Crone A J, DE Martini P M, Machette M N, Okumura K, AND Prescott J R, 2003, Paleoseismicity of aseismic Quaternary faults in Australia Implications for fault behaviour in stable continental regions. Bulletin of the Seismological Society of America, 93, 1913-1934.

Estrada B., Clark, D., Wyrwoll K.-H. & Dentith M., 2006. Palaeoseismic investigation of a recently identified Quaternary fault in Western Australia: the Dumbleyung Fault. this volume.

Everingham, I.B. and Tilbury, L. (1972) Information on Western Australian earthquakes 1849-1960. Royal Society of Western Australia. Journal 55, 90-96.

Everingham, I. (1968) Seismicity of Western Australia. BMR report

Fenton, C. H., Adams, J. and Halchuk, S., 2006. Seismic hazards assessment for radioactive waste disposal sites in regions of low seismic activity. Geotechnical and Geological Engineering 24: 579–592. DOI 10.1007/s10706-005-1148-4

Johnston Arch C. (1994) The Stable Continental Region Earthquake database. In: Johnston, A.C., Coppersmith, K.J., Kanter, L.R. and Cornell, C.A., (Eds.) The Earthquakes of Stable Continental Regions Volume 1: Assesment of Large Earthquake Potential, pp. 3-1 - 3-80.

Leonard, M. (2006) One hundred years of earthquake recording in Australia. Bulletin of the Seismological Society of America. 97

Michael-Leiba, M.O. (1987) Temporal variation in seismicity of the Southwest Seismic Zone, Western Australia; implications for earthquake risk assessment. BMR Journal of Australian Geology and Geophysics. 10, Pages 133-137.

Weichart (1980) Estimation of earthquakes recurrence parameters for unequal observation period for different magnitudes, Bull. Seismol. Soc. Am. 70, 1337-1346.

Magnitude	Century	SWSZ	Australian Shield	Australian continent	World Shield
6.5	0.10900	0.059690	0.90833	2.38762	10.17333
6.6	0.10800	0.059143	0.90000	2.36571	10.08000
6.7	0.10700	0.058595	0.89167	2.34381	9.98667
6.8	0.10100	0.055310	0.84167	2.21238	9.42667
6.9	0.08600	0.047095	0.71667	1.88381	8.02667
7.0	0.06400	0.035048	0.53333	1.40190	5.97333
7.1	0.03900	0.021357	0.32500	0.85429	3.64000
7.2	0.01900	0.010405	0.15833	0.41619	1.77333
7.3	0.01300	0.007119	0.10833	0.28476	1.21333
7.4	0.01000	0.005476	0.08333	0.21905	0.93333
7.5	0.00600	0.003286	0.05000	0.13143	0.56000

Table 1 Recurrence rates per century for the Neotectonics catalogue. The recurrence rates have been scaled for area.

Region	SW WA	SWSZ	Australian Shield	Australian continent	World Shield	World ex Aust.
Area 1000 km^2	420	230	3500	9,400	39,200	35700
Mmax likelihood	1	1/2000	1/120	1/45	1/11	1/12
M7 Seis.	-	0.41	1.26	1.72	1.83	0.68
M7 Neot.	0.064	0.035	0.53	1.40	6.0	6.0
Seis. / Neot.	-	12	2.4	1.2	0.3	0.11

Table 2 Summary of recurrence rates and for earthquakes in various regions.

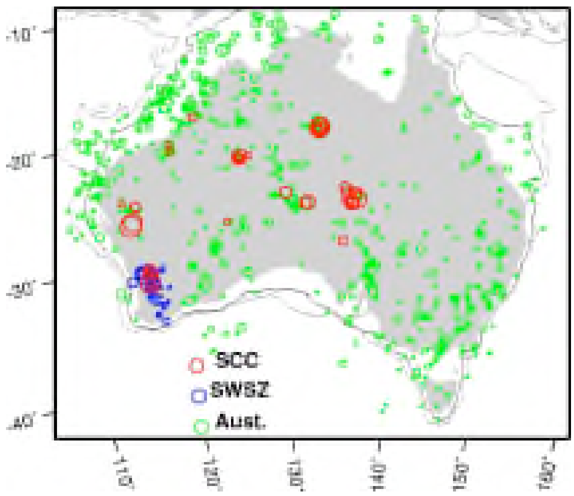

Figure 1 The three catalogues of Australian earthquakes used in this study. The green and blue data are from the GA catalogue and the red data are from the GSC Stable Continental Crust (SCC) database. The two isobaths are at 500m & 2500m.

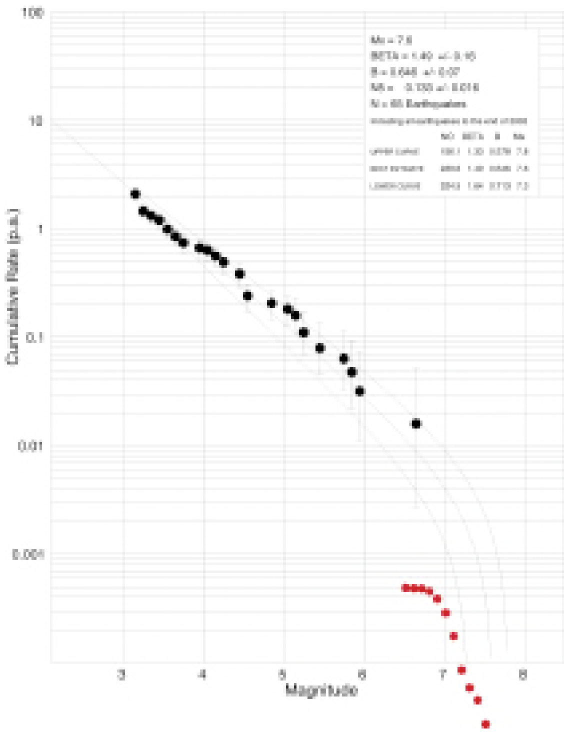

Figure 1 The cumulative recurrence rate of earthquakes in the SWSZ (black) from the GA catalogue and the SW WA neotectonics catalogue (red). The neotectonic catalogue has been scaled for time and area to match the earthquake catalogue.

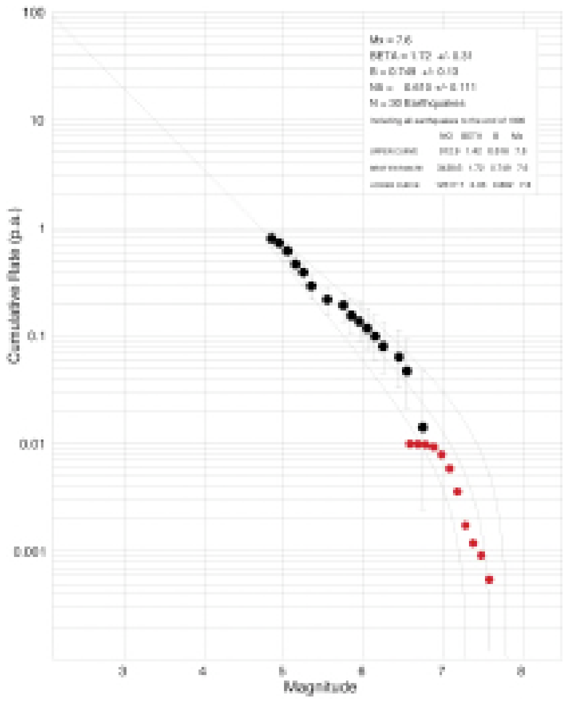

Figure 2 The recurrence rate for the Australian shield, from the world-wide CSS catalogue, and the scaled neotectonic catalogue.

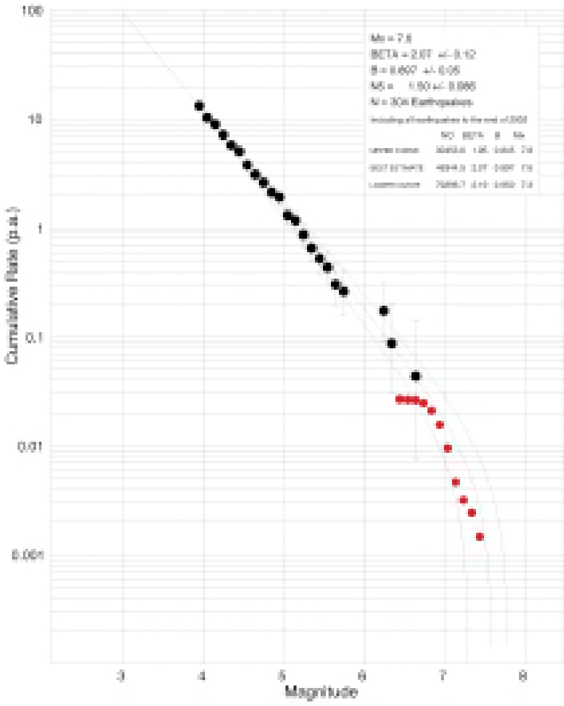

Figure 3 The recurrence rate for the Australian continent and the scaled neotectonic catalogue.

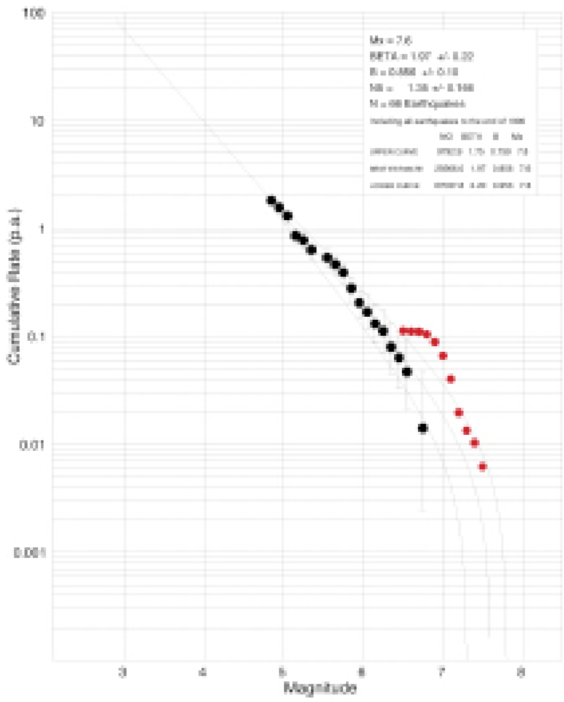

Figure 4 The recurrence rate for the world-wide SCC catalogue and the scaled neotectonic catalogue.

Site classification for earthquake hazard and risk assessment in Australia

Andrew McPherson[1] and Lisa Hall[2]

[1] Geoscience Australia
[2] Macquarie University

Abstract

One of the more important observations from the 1989 Newcastle earthquake was the spatial distribution of earthquake damage, which was strongly related to variability in near-surface regolith properties and their influence on ground-shaking (i.e. site response). This association between ground shaking and sediment distribution is well recognised, but has not previously been investigated for much of Australia.

In an effort to characterise the Australian regolith in terms of its ability to modify earthquake energy, Geoscience Australia, in collaboration with Risk Management Solutions Inc., has developed a national site classification map of Australia for application in broad scale earthquake hazard and risk assessment. Site classes are assigned according to the California-derived classification of Wills et al. (2000), which uses the relationship between geological materials and the shear wave velocity of the upper 30 m (V_s^{30}). Adjustments to the classification scheme are suggested to better account for the occurrence of weathered regolith in bedrock dominated areas. The application of this classification is successfully tested in Australia using borehole data from a variety of Quaternary environments in the Newcastle, Sydney and Perth urban areas.

Introduction

The properties of the regolith material beneath a site can significantly influence the amplitude, frequency and duration of earthquake ground motions, and thereby affect the occurrence and degree of damage to buildings and other structures (Seed & Idriss, 1969; Idriss, 1990). This was demonstrated by the strong spatial correlation between building damage and site conditions observed in the 1989 Newcastle earthquake (Chandler et al., 1991). Previous national scale hazard map products for Australia have not accounted for site effects, and so may significantly underestimate ground motion. As a result, the development and incorporation of a national site classification model and associated amplification factors is essential for the rigorous assessment of earthquake risk in Australia.

This study discusses the development of a broad scale site classification map representing the relative potential response of all major occurrences of surficial geological materials across Australia to earthquake ground shaking. The map has been developed using a number of national and regional scale geological and geotechnical datasets, combined with more detailed local data where available. The site classification scheme applied is that developed by Wills et al. (2000) for California, with modifications made to account for Australian conditions. Amplification factors being developed in association with the site classification map will not be dealt with in this paper.

The map and underlying methodology are validated for Quaternary deposits in the Perth, Sydney and Newcastle urban areas using either measured or calculated shear wave velocity data from previous geotechnical investigations. This analysis demonstrates the influence of grain size and unit age on site classification, as well as the importance of capturing sediment thickness information. It also illustrates the limitations of this type of broad scale investigation, reinforcing the need to collect higher resolution geophysical and geotechnical data when conducting local or site-specific earthquake risk assessments.

Site classification

Local site conditions can significantly alter the amplitude and frequency content of earthquake ground motion, where the regolith material physical properties, such as shear wave velocity (V_s), particle size, density and plasticity, exert a major control on the degree of amplification or attenuation experienced by travelling waves. Three important characteristics of the subsurface material which influence ground motion are impedance, absorption and basin geometry.

A site class represents a group of geological materials that are considered likely to exhibit a similar physical response to a given earthquake ground motion. They are defined by relationships between the physical properties of the regolith materials (such as thickness and particle size) and known responses to ground shaking of materials with similar properties. Correct site class definition is therefore essential for determining the potential response of structures.

As is often the case in broad scale site characterisation, a lack of relevant data makes it almost impossible to assign site classes based on all of the properties influencing site response, including basin geometry. A simpler approach is to consider the ground motion amplification affect of impedance alone (Borcherdt, 1994). In this case, the preferred method for defining site classes is on the basis of the shear wave velocity of the top 30 m below the ground surface (V_s^{30}). This method has become widely accepted as the standard way to characterise site conditions for earthquake site response assessment (Anderson et al., 1996; Wills & Silva, 1998; Wills et al., 2000; Boore, 2004; Choi & Stewart, 2005; Holzer et al., 2005).

Although V_s^{30} is best determined by direct measurement, such data is often not available. As a result, it is necessary to establish a proxy for this parameter. The use of geology as a surrogate for shear wave velocity forms the basis for determining the influence of site conditions in many seismic hazard assessments, and has been tested by numerous workers characterising strong motion sites in the USA, particularly in California (e.g. Fumal & Tinsley, 1985; Park & Elrick, 1998; Wills et al., 2000; Wills & Clahan, 2006).

Site classification in Australia

In Australia our understanding of the relationship between regolith materials and their response to earthquake ground shaking is very poor. This is due to both a paucity of ground motion data and a lack of available geotechnical and geophysical data that could be used to define typical V_s^{30} ranges for different near-surface regolith materials. Accordingly, the site classification we apply in this study is that defined by Wills et al. (2000). This is a version of the National Earthquake Hazard Reduction Program (NEHRP) site classification scheme (Building Seismic Safety Council, 2004) modified to account for the variation in measured V_s^{30} for geological units in California.

Significant areas of the Australian continent are composed of very old bedrock units exhibiting substantial weathering (Chan et al., 1986). The presence of these weathered materials can have a major impact on earthquake site response (Davis, 1995; Steidl et al., 1996), as average acceleration response spectra on weathered rock sites may be up to 20% higher than those at competent rock sites (Idriss & Silva in Rodriguez-Marek et al., 2001).

Table 1. Modified NEHRP site classes, associated V_s^{30} values and general groupings of geologic units associated with each class, based on 556 measured profiles from California (Wills et al 2000).

Site Class	V_s^{30} (m/s)	Geological Materials
B	> 760	Plutonic/metamorphic rocks incl. most volcanics; pre-Tertiary sedimentary units
BC	555 - 1000	Cretaceous fine-grained sediments; serpentine; sheared/weathered crystalline rocks
C	360 - 760	Oligocene – Cretaceous sedimentary rocks; coarse-grained

		younger material
CD	270 - 555	Miocene fine-grained sediments; Plio-Pleistocene alluvium; coarse younger alluvium
D	180 - 360	Holocene alluvium
DE	90 - 270	Fine-grained alluvial/estuarine deposits
E	< 180	Inter-tidal mud

The classification of Wills et al. (2000) does little to account for variations in rock weathering, and therefore an adjustment to the site class definitions is necessary when applying this scheme to weathered bedrock in Australia. A generalised relationship is developed between a recommended rock weathering classification for Australia (Eggleton, 2001) and site class, by relating the typical properties of a material in a given weathering state with available data on Vs and regolith thickness (McPherson and Hall, in prep). An average V_s^{30} estimate and associated site class are assigned to each weathering state based on the limited published information available for Australia (e.g. Awad & Peck, 1976; Herbert, 1979; Henderson, 1981; Hofto, 1990; McNally, 1993; Anand & Paine, 2002; Dhu & Jones, 2002; Nott, 2003; Willey, 2003). Moderately weathered to fresh bedrock is assigned to site class B, highly weathered bedrock is defined as site class BC, and extremely weathered bedrock, with or without residual soil, is typically assigned to site class C.

The relationships between regolith properties and site classes defined for Australia can now be applied on a national scale. The resulting regolith site classification map is shown in Figure 1.

Site class validation

The site classification map and the underlying methodology are validated using a variety of geophysical and geotechnical datasets from the Perth, Sydney and Newcastle urban areas. To test the variation in typical regolith behavior with unit age and texture, composite velocity profiles and associated V_s^{30} statistics (Table 2) are calculated for selected regolith material types in each region.

The Perth metropolitan region is underlain by Pleistocene sands and silts to depths of up to 100 m (McPherson & Jones, 2005). Shear wave velocities measured at 57 SCPT sites around the urban area show a clear correlation between V_s^{30}, sediment texture and age. Medium- to coarse-grained Pleistocene sands and silts have a median V_s^{30} of 302 m/s (class CD-D), while fine- to medium-grained materials of a similar age show consistently slower site conditions, with a median V_s^{30} of 253 m/s (class D-DE). A similar trend is observed in Holocene aged sediments, with sands having a median V_s^{30} of 287 m/s (class CD-D), and fine grained silts and clays a median value of 230 m/s (class D-DE).

Botany Bay contains some of the largest accumulations of Quaternary sands and silts in the Sydney region (Haworth, 2003). No directly measured shear wave velocities are available in this area, however calculated shear wave velocities from SPT blow counts, quantify the variation in shear wave velocity and basement depths for over 300 locations across the basin. Where Quaternary sediment thicknesses exceed 30 m calculated median V_s^{30}ranges from 200-250 m/s, equivalent to site classes D or DE. The underlying Hawkesbury Sandstone has V_s^{30} values in the range of 1200-2500 m/s (class B) depending on the degree and thickness of weathering. Where depth to basement is less than 30 m, V_s^{30} values increase and site classes change accordingly. This illustrates the importance of regolith thickness in determining site class assignments, as observed by Wills & Clahan (2006).

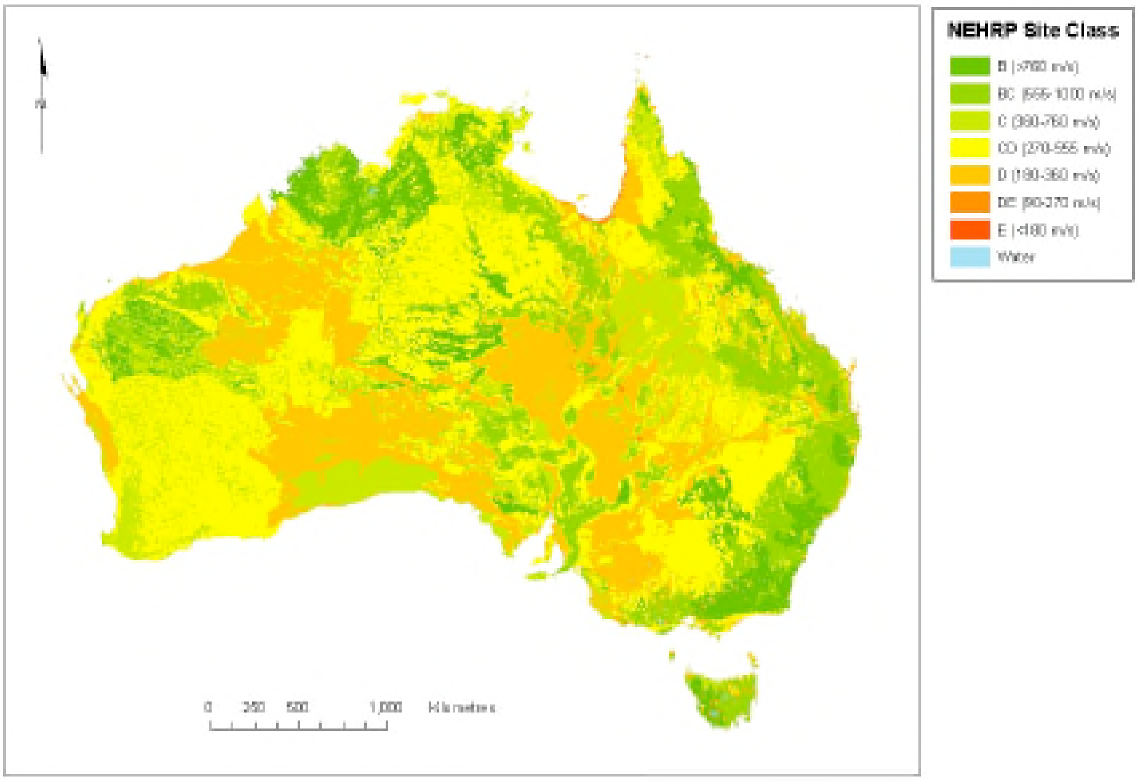

Figure 1. Site classification map of Australia. Over 40 geospatial datasets are incorporated into the site conditions dataset to provide complete country-wide coverage. Input resolution varies depending on population, with all major cities covered by 1:100,000 (or higher) resolution maps.

Table 2. Calculated V_s^{30}statistics for selected rock units in Perth, Sydney and Newcastle regions, where sediment depths > 30 m. V_s^{30}lower and V_s^{30}upper represent 95% and 5% uncertainty bounds.

Region	Age	Material Type	V_s^{30}median	V_s^{30}lower	V_s^{30}upper	No. of Sites
Perth	Holocene	Silts/ clays	230	155	262	5
	Holocene	Mixed sand	287	236	262	4
	Pleistocene	Fine to medium sand	253	215	303	16
	Pleistocene	Medium to course sand	302	228	379	13
Sydney	Holocene	Fill/ peat	269	255	565	7
	Holocene	Fine/ medium sand	284	256	461	214
	Holocene	Course sand	312	194	485	5
Newcastle	Holocene	Silts/ fine sand	200	160	227	6
	Holocene	Fine to medium sand	262	214	336	9

The central Newcastle area is dominated by Holocene fluvial and estuarine sediments associated with the Hunter River. Where sediment thickness exceeds 30 m, median V_s^{30}values decrease from 262 m/s to 200 m/s (effectively transitioning from class D to class DE) as the alluvium thickens and texture becomes finer in proximity to the Hunter River. However, the presence of shallow bedrock (depth to basement < 30 m) causes the V_s^{30}values to increase significantly at sites around the edge of the alluvial deposits.

The measured relationships between regolith properties and Vs30 for selected sites in Australia (Table 2) are consistently grouped by the modified scheme of Wills et al. (2000), demonstrating the suitability of this method for undertaking regional scale site classification in Australia. However, the variability in regolith material type and local basin conditions highlight the difficulty in classifying for site response at higher spatial resolutions, and reinforce the importance of acquiring detailed, directly measured data for local and site-specific studies.

Conclusions

The site classification map presented here is appropriate for application in national to regional scale earthquake hazard and risk assessment in Australia, in conjunction with appropriate amplification factors. Calibration with geotechnical, geophysical and borehole geological data for Quaternary environments indicates that average site conditions are adequately represented at this scale, although local variability in regolith properties means that this product is inappropriate for site-specific assessment. This study suggests that the site classification methodology of Wills et al. (2000) can be successfully applied to other tectonic settings, with modifications to account for bedrock weathering. However, care must be taken to account for sediment thickness, as excluding such information may lead to the misclassification of regolith properties, particularly with respect to their earthquake ground shaking potential (Wills & Clahan, 2006).

Acknowledgements

This work was conducted while Lisa Hall was affiliated with Risk Management Solutions (RMS) Inc., California, USA, and is published with the permission of RMS. Thanks also go to Don Windeler at RMS, Trevor Dhu at GA, and Edida Rajesh and his team at RMSI.

References

Anderson, J.G., Lee, Y.H., Zeng, Y.H. and Day, S., 1996. Control of strong motion by the upper 30 meters. Bulletin of the Seismological Society of America 86, 1749-1759.

Anand, R.R. and Paine, M.D. 2002. Regolith geology of the Yilgarn Craton, Western Australia: implications for exploration. Australian Journal of Earth Sciences 49, 3-162.

Awad, H. and Peck, W. 1976. Tunnel Investigation in the Terrigal Formation of New South Wales. In: Proceedings of the Second Australian Tunnelling Conference - Design and Construction of Tunnels and Shafts. Melbourne, August 1976. AusIMM, Parkville, Victoria. pp. 1-13.

Boore, D.M. 2004. Estimating Vs (30) (or NEHRP Site Classes) from shallow velocity models (Depths < 30 m). Bulletin of the Seismological Society of America 94(2), 591-597.

Borcherdt, R.D. 1994. Estimates of site-dependent response spectra for design (methodology and justification). Earthquake Spectra 10, 617-653.

Building Seismic Safety Council. 2004. NEHRP Recommended Provisions for seismic regulations for new buildings and other structures (FEMA 450). Building Seismic Safety Council, National Institute of Building Sciences. Washington D.C.

Chan, R.A., Craig, M.A., D'Addario, G.W., Gibson, D.L., Ollier, C.D. and Taylor, G., 1986. The Regolith Terrain Map of Australia 1:5,000,000. Bureau of Mineral Resources, Geology and Geophysics Record 1986/27. Bureau of Mineral Resources, Geology and Geophysics, Canberra. 273 p.

Chandler, A.M., Pappin, J.W. and Coburn, A.W. 1991. Vulnerability and seismic risk assessment of buildings following the 1989 Newcastle, Australia earthquake. Bulletin of the New Zealand National Society for Earthquake Engineering 24 (2), 116-138.

Choi, Y. and Stewart, J.P. 2005. Nonlinear site amplification as function of 30 m shear wave velocity. Earthquake Spectra 21(1), 1-30.

Davis, R. O. 1995. Effects of weathering on site response. Earthquake Engineering and Structural Dynamics 24, 301-309.

Dhu, T. and Jones, T. (eds). 2002. Earthquake Risk in Newcastle and Lake Macquarie. Geoscience Australia Record 2002/15, Geoscience Australia, Canberra.

Eggleton, R.A. (ed). 2001. The Regolith Glossary: surficial geology, soils and landscapes. CRC LEME, Floreat Park, WA. 144 p.

Fumal, T.E. and Tinsley, J.C. 1985. Mapping shear-wave velocities of near-surface geologic materials. In: J.I. Ziony (ed.), Evaluating Earthquake Hazards in the Los Angeles Region-An Earth-Science Perspective. U.S. Geological Survey Professional Paper 1360, 101-126.

Haworth, R.J., 2003. The shaping of Sydney by its urban geology. Quaternary International 103, 41-55.

Henderson, G.A.M. 1981. Geology of Canberra, Queanbeyan and environs: notes to accompany the 1980 1:50,000 geological map. Bureau of Mineral Resources, Geology and Geophysics, Canberra. 47 p.

Herbert, C. 1979. The geology and resource potential of the Wianamatta Group. Geological Survey of New South Wales Bulletin No. 25. Department of Mineral Resources and Development, Sydney. 203 p.

Hofto, P.J. 1990. Engineering geology of the Greater Hobart Area; maps 1 & 2. Division of Mines and Mineral Resources, Hobart.

Holzer, T.L., Padovani, A.C., Bennett, M.J., Noce, T.E. and Tinsley III, J.C. 2005. Mapping V_s^{30}site classes. Earthquake Spectra 21(2), 353-370.

Idriss, I.M. 1990. Influence of local site conditions on earthquake ground motions. Proceedings of the Fourth US National Conf. on Earthquake Engineering 1, 55-57.

McNally, G.H. 1993. Effects of weathering on engineering properties of the Terrigal Formation. In: G.H. McNally, M. Knight and R. Smith (eds.), Collected case studies in engineering geology, hydrogeology and environmental geology, 2nd series. pp. 92-102. Geol. Soc. Aus. Inc., Environmental, Engineering and Hydrogeology Specialist Group. Butterfly Books, Springwood, NSW. 134 p.

McPherson, A. and Hall, L. In prep. Development of the Australian National Regolith Site Classification Map. Geoscience Australia Record.

McPherson, A. and Jones, A. 2005. Appendix D: Perth Basin Geology Review and Site Class Assessment. In: Jones, T., Middelmann, M. and Corby, N. (compilers), Natural Hazard Risk in Perth, Western Australia. pp. 313-344. Geoscience Australia, Canberra.

Nott, J.F. 2003. The urban geology of Darwin, Australia. Quaternary International 103, 83-90.

Park, S. and Elrick, S. 1988. Predictions of shear-wave velocities in Southern California using surface geology. Bulletin of the Seismological Society of America 88(3), 677-685.

Rodriguez-Marek, A., Bray, J.D. and Abrahamson, N.A. 2001. An empirical geotechnical seismic site response procedure. Earthquake Spectra 17(1), 65-87.

Seed, H.B. and Idriss, I.M. 1969. Influence of soil conditions on ground motions during earthquakes. Proceedings of the American Society of Civil Engineers, Journal of the Soil Mechanics and Foundations Division 95, 99-137.

Steidl, J.H., Tumarkin, A.G. and Archuleta, R.J. 1996. What is a reference site? Bulletin of the Seismological Society of America 86(6), 1733-1748.

Willey, E.C. 2003. Urban geology of the Toowoomba conurbation, SE Queensland, Australia. Quaternary International 103, 57-74.

Wills, C.J. and Clahan, K.B. 2006. Developing a map of geologically defined site-condition categories for California. Bulletin of the Seismological Society of America 96 (4A), 1483-1501.

Wills, C.J. and Silva, W. 1998. Shear-wave velocity characteristics of geologic units in California. Earthquake Spectra 14(3), 533-556.

Wills, C.J., Petersen, M., Bryant, W.A., Reichle, M., Saucedo, G.J., Tan, S., Taylor, G. and Treiman, J. 2000. A site-condition map for California based on geology and shear-wave velocity. Bulletin of the Seismological Society of America 90 (6B), S187-S208.

Forecasting earthquake ground motions

Gail M. Atkinson

Carleton University Ontario, Canada

Abstract

The "forecasting" of earthquake ground motions involves developing methods to describe the shaking expected at a site as a function of earthquake magnitude and distance (and sometimes other variables). Earthquake ground motion forecasts are the most critical input to seismic hazard analyses, and are also used to develop site-specific simulated earthquake records for design purposes. Advances in this area enable the cost-effective seismic design of engineered structures.

The foundation of ground-motion forecasting is the analysis and interpretation of earthquake source, path and site effects. This agenda may be pursued using empirical regression techniques, applied to large seismological databases. Alternatively, detailed modeling of specific events may be used to elucidate the underlying processes that drive the observed ground motions. Recent research advances in these areas will be overviewed.

Over the last decade, the volume of data available for developing and validating ground-motion forecasting techniques has increased more than tenfold. This offers unprecedented opportunities for furthering our understanding of earthquake processes and improving ground-motion forecast models.

Seismic fragility curves for un-reinforced masonry walls

***Elisa Lumantarna*[1], *Jerry Vaculik*[2], *Mike Griffith*[2], *Nelson Lam*[1] *and John Wilson*[3]**

[1] The University of Melbourne
[2] University of Adelaide
[3] Swinburne University of Technology

Abstract

Quasi-static experiments have been carried out on unreinforced masonry (URM) wall specimens subject to two-way bending and a range of boundary conditions. The hysteretic behaviour so obtained from the experiments have been used to generate fragility curves which define the probability of the wall sustaining minor to severe damage in an earthquake based on different levels of ground motion intensity and boundary conditions of the wall. The calculation for the fragility curves involves the generation of filtered accelerograms which take into account a range of earthquake scenarios, site conditions and building types. The generated accelerograms have been used for input into non-linear time-history analyses for quantifying the amount of drift sustained by the URM walls in order that the level of damage can be ascertained.

Keywords: unreinforced masonry walls, out-of-plane, two-way bending, quasi-static behaviour, seismic.

Introduction

A major experimental program involving quasi-static out-of-plane testing of unreinforced masonry walls subject to two-way bending actions and possessing a range of aspect ratios and boundary conditions were undertaken recently at the University of Adelaide forming part of the collaborative research with University of Melbourne and Swinburne University of Technology. Details of the test results have been reported in the paper by Vaculik et al. (2005) which was presented in the AEES conference at Albury. Classical hysteretic models have been calibrated to match with the behaviour recorded from the quasi-static testings. A large number of non-linear time-history analyses were then undertaken using program RUAUMOKO (Carr, 2003) based on the calibrated models. A total of 1680 floor excitations were employed to simulate the conditions of a Class C and D site and the upper levels of a six-storey building when subject to a multitude of scenarios of both near-field and far-field earthquakes. Fragility curves showing the cumulative probability of damage with increasing peak ground velocity were constructed in accordance with the proportion of cases in which pre-defined displacement limits of the wall (consistent with different damage thresholds) were exceeded by the computed displacement demands.

Hysteretic modelling

Displacement demand on URM walls can be accurately predicted by time history analyses (THA) provided that the analyses incorporate representative hysteretic models. Whilst results from a recent sensitivity study have shown that rigorous parameterisation of the hysteretic behaviour is not justified (Lumantarna et al., 2006), hysteretic modelling should feature "pinching" and strength degradation behaviour as observed from the quasi-static testing of the walls.

The "pinching" behaviour is associated with the self-centering capability of walls which is defined by the unloading part of the force-displacement relationship (refer Figure 1). Walls with perfect self-centering capability revert back to zero displacement at every instant on unloading (as represented by the origin-centered model of Figure 1a). Walls with poor self-centering capability do not recover the inelastic displacement on unloading. The behaviour of walls at unloading can be modelled by the α parameter in the modified Takeda model (Figure 1b).

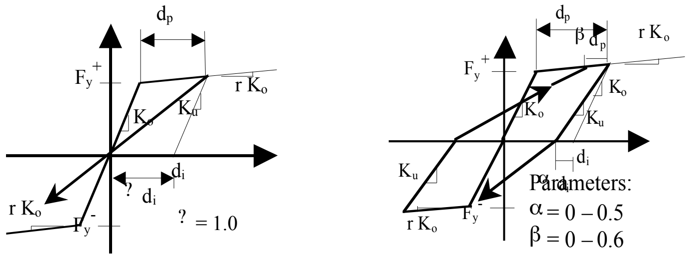

(a) Origin-Centered Model (b) Modified Takeda Model

Figure 1 Hysteretic models

Quasi-static out-of-plane loading tests were performed on eight full-scale unreinforced masonry URM wall specimens to investigate their force-displacement behaviour (Vaculik et al., 2005). The specimens consisted of two long walls without openings (4000 mm x 2500 mm), four long walls with an eccentrically positioned opening (4000 mm x 2500 mm) and two short walls with a symmetrically positioned opening (2500 mm x 2500 mm). All walls were 110 mm thick and subject to vertical pre-compression in the range 0 to 0.1 MPa. The walls were restrained from rotation along the vertical edges and laterally restrained along the top and bottom edges.

The hysteretic models shown in Figure 1 only represent the hysteretic behaviour of the two long walls without openings (walls 1 and 2) which is essentially symmetrical in terms of their "pinching" and strength degradation behaviour (Vaculik et al., 2005). Significant asymmetrical behaviour in the positive and negative displacement direction was observed from the walls with openings. The observed asymmetry has not been taken into account by the hysteretic models considered herein.

In Figures 2 and 3, the face pressure on the walls (ie. lateral loads divided by the surface area) is plotted against their deflection at mid-height. Walls with vertical pre-compression have better self-centering capability than walls without vertical pre-compression (for example, comparing Figures 1 and 2). A reasonable match between the observed hysteretic behaviour of wall 1 and the modified Takeda hysteretic model was obtained by setting the α parameter to 0.5 (Figure 2). The modified Takeda hysteretic model (with value of α parameter equal to 0.5) is shown to underestimate the self-centering capability of wall 2 (Figure 3a). The origin-centered model was used to represent the hysteretic behaviour of the wall (Figure 3b). Although the perfect self-centering capability assumption of the origin-centered model overestimates the wall self-centering capability, the origin-centered model has been shown to provide reasonable predictions of the wall maximum displacement demands (Lumantarna et al., 2006).

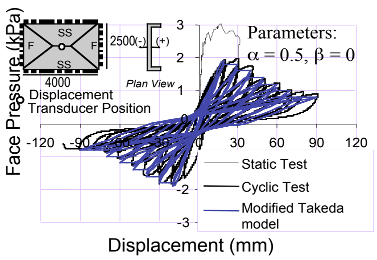

Figure 2 Hysteretic modelling of wall 1

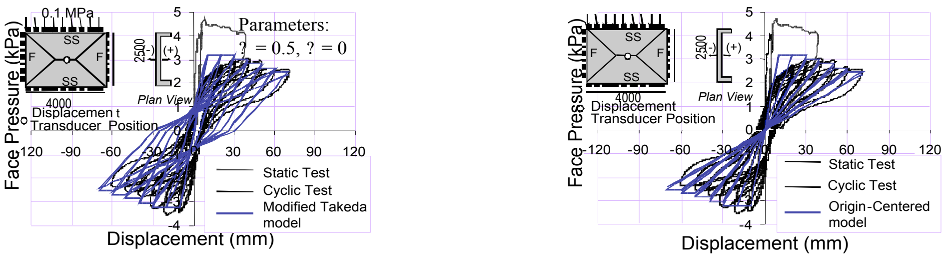

(a) Modified Takeda model (b) Origin-Centered model

Figure 3 Hysteretic modelling of wall 2

For the purposes of time-history analyses, walls can be represented as equivalent single-degree-of-freedom (SDOF) systems assuming rigid body behaviour and a fully cracked wall (Doherty et al., 2002). The effective displacement (Δe) of the equivalent SDOF systems was taken as 2/3 of the maximum displacement of the walls at mid-height. The effective mass (Me) of the wall was taken as 3/4 of its total mass. The initial behaviour of the wall in the uncracked state (ie. in the first half-cycle of the hysteresis loops which was denoted "static test" in Figures 2 and 3) has therefore been ignored. The initial periods (of a fully cracked wall) were 0.2 and 0.1 second for walls 1 and 2 respectively.

Applied excitations

Accelerograms with random phase-angles were generated by stochastic simulations of a seismological model using parameters that are considered appropriate for the attenuation conditions of southeastern Australia (Lam et al., 2000 & 2005). The simulations were based on a range of earthquake scenarios (defined by magnitude-distance combinations) which would produce peak ground velocities on rock sites ranging between 20 mm/sec and 100 mm/sec (refer Table 1). It is noted that the earthquake scenarios considered in the study included both near-field and far-field earthquakes of varying magnitude and distances.

Table 1 Earthquake scenarios with varying magnitude and distance (M-R)

PGV	20 mm/sec	40 mm/sec	60 mm/sec	80 mm/sec	100 mm/sec
M	5.5 6 6.5 7	5.5 6 6.5 7	5.5 6 6.5 7	5.5 6 6.5 7	5.5 6 6.5 7
R (km)	40 75 123 177	24 36 71 124	17 28 40 90	13 22 31 55	11 19 26 40

Accelerograms on Class C and D sites were obtained by non linear shear wave analyses of representative soil column models using program (SHAKE) and the simulated accelerograms for rock conditions as excitation input at the bedrock level (Lam et al., 2005). The shape of the simulated response spectra were generally consistent with the design response spectra stipulated by the new Australian Standard (AS/NZS 1170.4 Doc. D5212-5, 2005). Accelerograms which take into account the filtering behaviour of an unreinforced masonry six-storey building at the upper floor levels (Griffith et al., 2004) have also been obtained. These filtered excitations have been included in the analyses of URM walls to account for the filtering effects of the multi-storey buildings. In summary, a total of 1680 simulated accelerograms representing free field conditions on rock and soil sites and filtered conditions of a six-storey building have been obtained and collated.

Examples of the displacement response spectra calculated from the simulated (and filtered) accelerograms are shown in Figures 4a & 4b to reveal the significance of amplification at the natural period of the site (0.5 second and 1.0 second) and the natural period of the six-storey building (0.3 second). High spectral amplifications resulting from resonance conditions are shown at the fundamental natural period of the building (0.3 second). Exceptionally high amplification resulting from the resonance of the natural period of the building with that of a Class C site has been identified (refer Figure 4a).

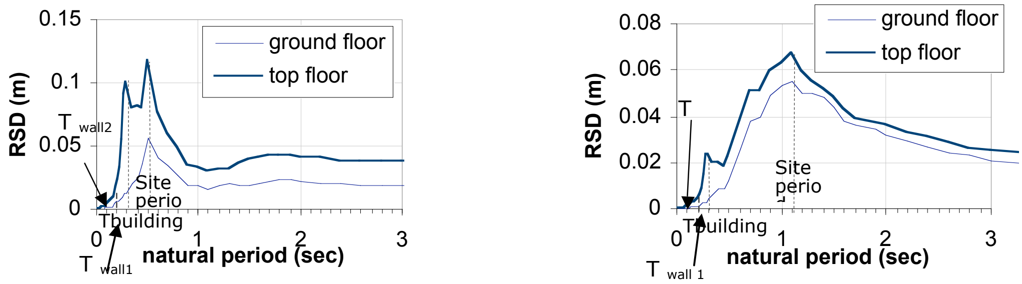

(a) Site Class C (M = 6.5, R = 40 km) (b) Site Class D (M= 6.5, R = 40 km)

Figure 4 Displacement response spectra for the top level of 6 storey building

Fragility curves of unreinforced masonry walls

The SDOF systems with hysteretic models representing URM walls were subject to non-linear time history analyses (THA) using ensembles of simulated accelerograms and computer program RUAUMOKO (Carr, 2003) to predict the wall maximum displacement demands. Load-cycle dependent strength degradation behaviour has been taken into account in the analyses.

Results from the analyses were correlated with the targeted PGV on rock sites for the construction of fragility curves based on the following limit states of damage: "minor damage", "moderate damage" and "collapse". The minor damage limit state was defined at the condition where displacement at mid-height of the wall approaches 5mm, at which the walls are expected to undergo first cracking. The displacement limit at moderate damage was arbitrarily defined at half of the wall thickness (55mm). URM walls subject to displacement exceeding this limit are expected to have a fully developed crack pattern that forms a collapse mechanism. The displacement limit at collapse was defined at the wall thickness of 110mm.

The fragility curves presented in this paper were based on force-displacement relationship of walls 1 and 2 obtained from cyclic test results. The uncertainties in the building modelling were not considered in the generation of filtered accelerograms. The random phase angle of accelerograms was assumed to be the only source of random parameters. Further fragility curves can be developed incorporating variability in material properties and dimensions of walls as well as variability in the modelling of filtering effects in building.

The statistics of the displacement demands as observed from the time-history analyses were analysed to identify the proportion of cases in which the limiting displacements of 5 mm, 55 mm and 110 mm was exceeded. Fragility curves were then constructed to correlate the cumulative probability of exceedance, $F(\nu_i)$, with increasing value of ν_i (or PGV) based on obtaining the best-fitted log-normal distribution function of equation (1) which is defined by the median and standard deviation parameters, c and β respectively.

$$F(v_i) = \Phi\left(\frac{\ln\left(\frac{v_i}{c}\right)}{\beta}\right) \qquad (1)$$

where $\Phi()$ is the cumulative log- normal distribution function

The dual parameters c and β controlling the distribution function were obtained using the well known Maximum Likelihood Method as cited by Shinozuka et al. (2001) which is briefly described in the following. The maximum likelihood parameter L is defined by equation (2).

$$L = \prod_{i=1}^{N} \left[F(v_i)\right]^{x_i} \left[1 - F(v_i)\right]^{1-x_i} \tag{2}$$

where i identifies individual analysis samples, and x_i = 1 or 0 depending on whether the limit state of damage has been exceeded, or not exceeded, in the analysis. The value of c and β was determined for the conditions where the value of L as defined by equation (2) was maximised, using equations (3a) and (3b) respectively.

$$\frac{\partial \ln(L)}{\partial c} = 0 \tag{3a}$$

$$\frac{\partial \ln(L)}{\partial \beta} = 0 \tag{3b}$$

Statistical procedures as described by Shinozuka et al. (2001) have been undertaken to test the goodness of fit of the estimated fragility curves to the results from individual simulations. The analyses have shown that the values of parameters c and β estimated for the construction of fragility curves are the true values under the significance level of 10%.

An example of fragility curves for the minor and moderate damage limit state is shown in Figure 5 for wall no. 1 on a class C site incorporating filtered conditions of a multi-storey building.

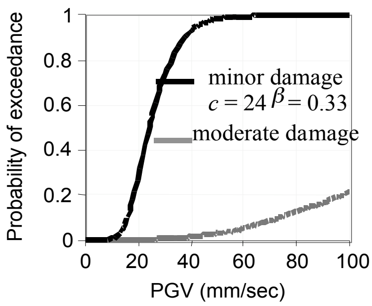

Figure 5 Fragility curves for wall 1 (subject to excitations on site class C)

The development of the fragility curve of Figure 5 had incorporated an equal number of accelerograms simulated for the earthquake scenarios considered in the study (as tabulated in Table 1). It is further shown in Table 2 that the cumulative probability of exceedance, $F(\nu_i)$, as calculated from the individual earthquake scenarios could be very different even though they were associated with a common PGV. It was implicitly assumed in the construction of the fragility curve that there were equal contributions from each of the identified earthquake scenarios for a given PGV. It should be noted that this assumption is contrary to reality as earthquake scenarios of different magnitudes could have different contributions to the potential seismic hazard of an area. The relative weighting of the scenarios cannot be generalised as it is dependent on the nature and configuration of the seismic sources affecting the area.

A de-aggregation plot such as that presented by Koo et al. (2000) in a seismic hazard modelling study for Melbourne can be used to determine the relative contributions of individual earthquake scenarios to the aggregated seismic hazard. The weighting factors inferred from that study were taken and presented in Table 3 as the C(M,R) factors. The weighted aggregated probability of exceedance was then obtained by summing the product of the $F(\nu_i)$ values of Table 2 and the C(M,R) factors of Table 3 for a given value of PGV. The "revised" fragility curve for wall 1 so obtained from this method of calculation is shown in Figure 6. The significance of the "weighting" factors can be seen by comparing Figure 5 and Figure 6a.

Table 2 Probability of exceedance for minor damage based on individual earthquake scenarios

PGV \ M	20 mm/sec		40 mm/sec		60 mm/sec		80 mm/sec		100 mm/sec	
	R (km)	F(ν_i)	R (km)	F(ν_i)	R (km)	F(ν_i)	R (km)	F(ν_i)	R	F(ν_i) (km)
5.5	40	0	24	0.01	17	0.06	13	0.15	11	0.28
6	75	0.01	36	0.04	28	0.1	22	0.17	19	0.25
6.5	123	0	71	0	40	0.03	31	0.1	26	0.21
7	177	0	124	0	90	0	55	0.03	40	0.14

Table 3 Weighting factors defining the relative contributions of the individual earthquake scenarios

PGV \ M	20 mm/sec		40 mm/sec		60 mm/sec		80 mm/sec		100 mm/sec	
	R (km)	C(M,R)	R (km)	C(M,R)	R (km)	C(M,R)	R (km)	C(M,R)	R (km)	C(M,R)
5.5	40	0.56	24	0.47	17	0.53	13	0.6	11	0.56
6	75	0.22	36	0.23	28	0.23	22	0.26	19	0.25
6.5	123	0.11	71	0.19	40	0.12	31	0.07	26	0.13
7	177	0.11	124	0.11	90	0.12	55	0.07	40	0.06

Fragility curves for wall no. 2 which was characterised by a pre-compression of 0.1MPa have also been constructed (Figure 7). Walls without pre-compression (wall 1) are more vulnerable to damage than walls with pre-compression (wall 2) (comparing Figures 6 with 7). Fragility curves constructed for a more onerous site class (Figures 6b and 7b) indicate less damage predicted on walls which are located on the onerous site class.

Further fragility curve has been constructed to show the significance of filtering effects of a multi-storey building (Figure 8). The fragility curve presented in Figure 8 indicates that wall 1 located at the top of a multi-storey building is most vulnerable to damage. This is attributed to the filtering effects of a multi-storey building which is of particular importance as walls without vertical pre-compression (wall 1) are typically located near the top of multi-storey buildings. However, the fragility curve shows that the wall is safe from collapsing under the filtered excitations, assuming the boundary conditions are maintained.

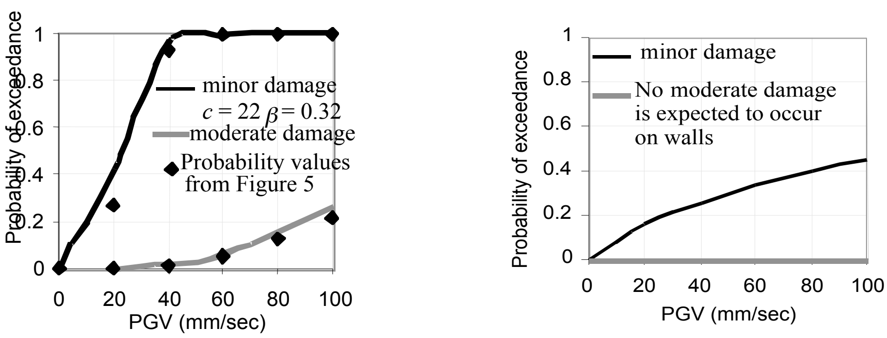

(a) subject to earthquake excitations on class site C (b) subject to earthquake excitations on class site D

Figure 6 Fragility curve for wall 1

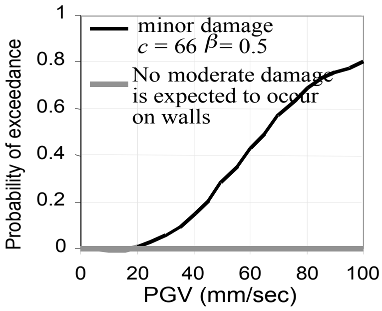

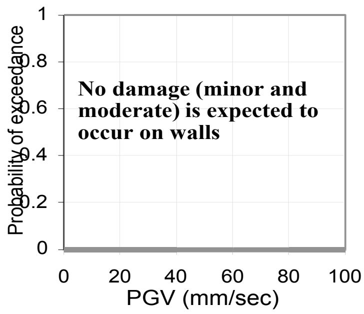

(a) subject to earthquake excitations on class site C (b) subject to earthquake excitations on class site D

Figure 7 Fragility curve for wall 2

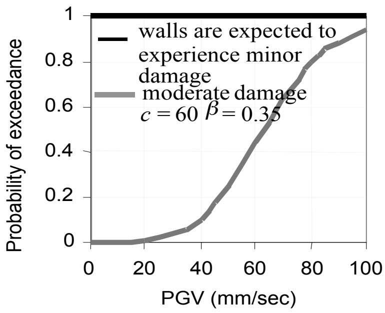

Figure 8 Fragility curve for wall 1 located at the top floor of 6-storey building on class site C

Conclusions

Fragility curves which define the probability of URM walls sustaining minor and moderate damage in an earthquake have been presented. The fragility curves were developed based on the hysteretic behaviour obtained from the quasi-static testing on URM walls. Accelerograms employed in the construction of fragility curves were generated using stochastic simulations taking into account multitude earthquake scenarios representing earthquakes of different levels of intensity, site conditions and building types. Walls without pre-compression located at the top of multi-storey buildings founded on site class C soil were shown to be most vulnerable to damage. However, none of the walls are expected to collapse under an earthquake with level of intensity associated with the seismic hazard of Australia assuming a 500 year return period and that the support conditions are maintained.

References

AS/NZS 1170.4 Draft no.D5212-5.1 (2005). Structural Design Actions – Part 4 Earthquake Actions, sub-committee BS-006-11, Standards Australia

Carr, A. J. (2003) "Ruaumoko, The Maori God of Volcanoes and Earthquakes", University of Canterbury, New Zealand

Doherty, K., Griffith, M. C., Lam, N., Wilson, J. (2002). "Displacement-based seismic analysis for out-of-plane bending of unreinforced masonry walls", Earthquake Engineering and Structural Dynamics, Vol. 31, pp. 883-850

Griffith, M., Lam, N., Wilson, J. (2004). "Displacement-based design of face-loaded masonry walls", 13thWorld Conference on Earthquake Engineering, Paper No. 2463

Koo, R., Brown, A., Lam, N., Wilson, J., Gibson, G. (2000). "A full range response spectrum model for rock sites in the Melbourne Metropolitan Area", Australian Earthquake Engineering Society Proceedings of the 2000 Conference, Paper No. 16

Lam, N., Wilson, J., Hutchinson, G. (2000). "Generation of synthetic earthquake accelerograms using seismological modelling: a review", Journal of Earthquake Engineering, Vol. 4, No. 3, pp. 321-354

Lam, N., Wilson, J., Venkatesan, S. (2005). "Accelerograms for dynamic analysis under the new Australian Standard for earthquake actions", Electronic Journal of Structural Engineering, Vol. 5, pp. 10-35

Lumantarna, E., Lam, N. T. K., Wilson, J., Griffith, M., Vaculik, J. (2006). "The out-of-plane dynamic behaviour of unreinforced masonry walls", The 19th Australasian Conference on the Mechanics of Structures and Materials, In Press

Vaculik, J., Griffith, M., Lam, N., Wilson, J., Lumantarna, E. (2005). "Cyclic response of unreinforced clay brick masonry walls", Australian Earthquake Engineering Society Proceedings of the 2005 Conference, Paper No. 40

Shinozuka, M., Feng, M. Q., Kim, H., Uzawa, T., Ueda, T. (2001) "Statistical analysis of fragility curves", Technical Report MCEER, Department of Civil and Environmental Engineering, University of Southern California, Task Numbers 106-E-7.3.5 and 106-E-7.6

Seismological contributions to earthquake risk mitigation

Gary Gibson

Environmental Systems and Services, Melbourne
Monash University, Melbourne

Abstract

This paper examines the risk mitigation measures (hazard studies, warnings, alarms, predictions, forecasts and alerts) that can be applied to earthquakes, and the seismological contributions required for each.

The observational seismological data used are the records of ground motion as measured by sensitive and strong motion seismic recorders. The variation in the arrival times of seismic waves is used to determine the location of the earthquake. Variation in seismic amplitude with distance (due to geometric spreading, absorption of energy and scattering) is attenuation, and empirical attenuation functions are used to estimate earthquake magnitude (size) and earthquake hazard (effect). Variation of amplitude and direction of motion with both distance and azimuth is used to determine earthquake focal mechanisms. These results are gathered in an earthquake catalogue, which may be used to investigate sources and clustering of earthquakes.

The accuracy and precision that is currently achieved and potentially may be achieved considering both random and systematic uncertainties vary greatly with the seismograph network scale (global, regional, local, mining), especially on the network density. The distance from the earthquake to the nearest seismographs and the number of recording instruments control the accuracy of locations, and whether determination of local attenuation and focal mechanisms is possible. The current and practical limits on this accuracy and precision are discussed, together with their impact on the risk mitigation outcomes.

In Australia there have been some significant improvements in seismograph systems, analysis methods and coverage over the past decade, partially offset by the reduced number of seismologists performing routine analysis. The paper concludes with some suggestions towards developments over the next few years.

Introduction

There is no doubt that the dominant factor in earthquake risk mitigation is improved building standards, and the prevention of structural collapse. Seismology has several contributions to this and other aspects of earthquake risk mitigation.

Seismology tells us much about the earth and its geological structures and processes. Knowledge of earth structure and processes is necessary for earthquake risk mitigation (the basis for much of the funding), but as with any risk mitigation there are several practical things that can also be done.

Seismological contributions to earthquake risk management

Risk mitigation actions can be associated with past, present and future earthquakes.

Past earthquakes

Our knowledge of earthquakes comes from experiences of past events and their effects. This information resides in earthquake catalogues and in publications.

Earthquake hazard studies give the average recurrence interval between the occurrence of earthquakes of a given magnitude within a given source zone, either an area, volume or on a fault, and the primary output is the recurrence of different levels of ground motion at a point. Their use in structural design is to estimate the probability that the design ground motion will be exceeded during the life of the structure. A contour map of ground motion recurrence over a region is often called an earthquake hazard map.

Present earthquakes

The earthquake of most interest to most people is the one that has just happened. In general there are two risk mitigation actions relevant for the current event.

Warnings can be issued if the event has just occurred, but its effects have not yet been felt (rain storms in a catchment allows time for flood warnings downstream, or a large shallow, dip-slip undersea earthquake gives time for a tsunami warning). There is rarely time to give a useful warning for strong earthquake ground motion, but it is attempted in Japan and Mexico.

Alarms are issued after the event has occurred, and after its effects have been felt. The purpose is to optimise the emergency response. They should advise on probable earthquake effects, and assist with emergency response actions. This is particularly important for earthquakes which, being unexpected, are followed by some chaos.

Future earthquakes

Predictions anticipate the event within relatively limited bounds of accuracy, giving the time, place and magnitude, with certainty.

Forecasts anticipate the event within wider bounds of accuracy, giving the time, place and magnitude, with some probability.

Alerts may be given when unusual activity that may be precursory to a larger event has been observed, and it may be wise to check on any preparations.

In summary, the most useful information that seismologists can give at present is in **hazard studies** and **alarms**. In the future, it may be possible to **forecast** events to allow some useful preparation to be undertaken before it occurs.

Seismological inputs to earthquake risk management

Earthquake motion

Seismographs measure the motion that results from an earthquake, usually at a point on the earth's surface, or on a structure such as a building, dam or bridge. In the past, most seismologists used sensitive seismographs to record the three dimensional (east-west, north-south and vertical) motion from distant earthquakes, while engineering seismologists used strong motion accelerographs to record the damaging motion near to large earthquakes. The full dynamic range can be measured by using a six-channel instrument with a sensitive seismometer and a strong motion accelerometer.

The study of earthquake motion is often considered in four stages – source, travel path, site, and structure.

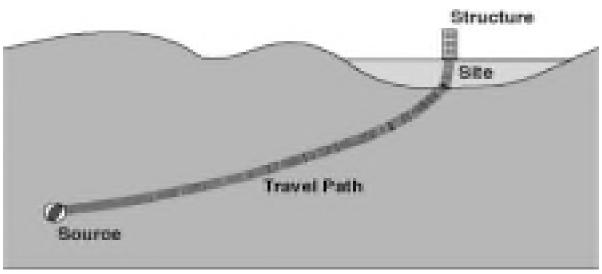

Figure 1: Earthquake motion

The motion recorded by seismographs is affected by at least both source and travel path, and measurements are often affected by site response. Motion recorded on structures is affected by the dynamic response of the structure. To separate the effects of the different stages, almost all seismological analysis is done by comparing motion recorded at different locations.

Earthquakes are located by comparing the arrival times of seismic waves in a surrounding network. Attenuation, and thus magnitudes require comparison of amplitudes with distance. Site response is measured by comparing motion recorded at the surface with motion on nearby bedrock or in a borehole. Structural response is measured by comparing motion recorded on the building with motion at the foundation and with a nearby surface motion reference point. Focal mechanisms inherently require measurements at points that vary in both distance and magnitude.

Determining both attenuation functions and focal mechanisms require measurement of ground motion from a set of earthquakes, each recorded by as many seismographs as possible over a wide range of distances and azimuths, preferably distributed as the logarithm of distance (e.g. 2, 4, 8, 16, 32, 64, 128 km). For each earthquake, the ratio of the greatest distance to the closest distance should be at least one order of magnitude (e.g. 20 to 200 km), ideally more, and preferably two orders of magnitude (e.g. 5 to 500 km).

Seismographs placed around a planned blast or for aftershocks can be arranged in logarithmic distribution with distance, preferably with one or more instruments at considerable distance in each of two orthogonal directions. However, it is not possible to anticipate most earthquake locations to allow a logarithmic distribution. To monitor an earthquake with seismographs ranging in both distance and azimuth it is necessary to have a high density of seismographs.

Earthquake focal mechanisms

The focal mechanism is used to relate the earthquake to local geology, to obtain an estimate of the orientation of the stress field that generated the earthquake, and to refine the estimated seismic wave radiation pattern expected for this earthquake, especially directivity effects near to the fault rupture as required for next-generation earthquake alarm systems and future hazard studies.

When the local stress field is known, as given on the World Stress Map (Figure 2) or locally, faults that are susceptible to failure may be distinguished from those that developed when the stress field was different and are unlikely to reactivate. When other earthquake source parameters are estimated, such as stress drop and rupture dimension, it is possible to characterise local earthquake hazard.

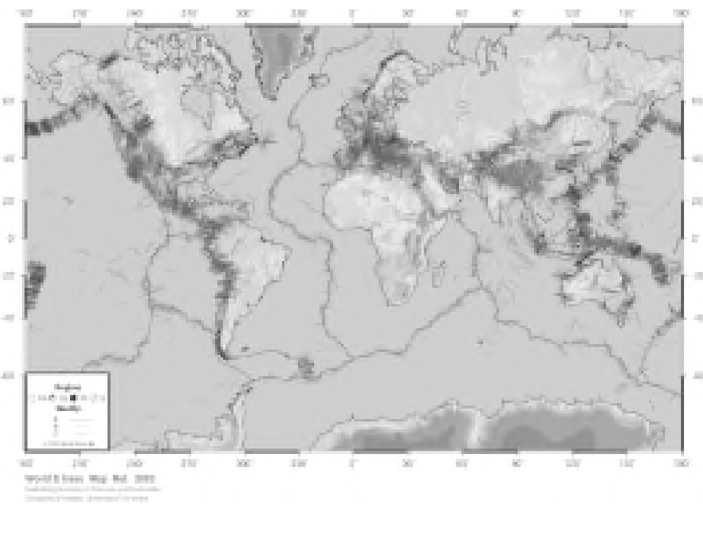

Figure 2: The World Stress Map shows the direction of the maximum horizontal stress, coloured depending on the fault type – blue for reverse faulting, red for normal faulting and green for strike-slip faulting.
Note regional variations; such as extensional normal faulting in Africa, and compressional reverse faulting in Australia, and the dependence on azimuth of normal and strike-slip faulting along oceanic ridges. Such features occur on smaller scales.

Source parameter summary

The limiting factor in the accuracy and precision of earthquake locations is the number of seismographs recording the event, and the distance to the nearest seismographs. Local attenuation functions can only be reliably determined if the event is recorded over a logarithmically distributed range of distances, preferably in orthogonal directions. Earthquake focal mechanisms can only be reliably determined if the event is recorded over a logarithmically distributed range of distances and over a range of azimuths.

To determine all of these parameters to high precision would require a seismograph/ accelerograph network with the same density as is currently installed in Japan, even in places with relatively few earthquakes such as Australia. Rather than installing an observational network that does not work particularly well anywhere, we will probably need to concentrate on populated areas and on more active areas. A very rapidly deployed aftershock network will be highly productive providing very precise location information, and the opportunity to optimise the seismograph network for local attenuation determination and focal mechanism determination.

Earthquake clustering

Clustering must be examined in hazard studies to use independent events for recurrence calculations, and for forecasts.

Earthquakes and geology

The relationship between earthquakes and local geology requires precise locations from a high-resolution network, together with determination of focal mechanisms and estimates of the orientation of the local stress field.

The relationship is bi-directional, in that earthquake data can be used to help decipher the geology, and geological information can be used to explain the earthquakes.

The earthquake seismicity information is limited by the duration of the data available, as only relatively imprecise parameters are available for those few earthquakes before 1960 that were large enough to be reported or recorded. In most parts of the world the seismicity data is still limited by poor precision and accuracy.

Application to earthquake risk mitigation

Earthquake hazard studies

Earthquake hazard studies are based on past earthquakes and their effects. This information is best included in an earthquake catalogue, which includes **locations**, **magnitudes**, **mechanisms**, earthquake **effects**, **clustering** details, any relationship to **geology** (faults or structures), relevant **publications** listed, all with information on accuracy and precision.

Many current generation hazard studies are still computed from simple seismotectonic models based on seismicity alone, and do not incorporate geological information or active faults. Studies range from "flat-earth" models where earthquakes are assumed to occur with equal probability at any location within large regions, resulting in little or no variation in estimated hazard from point to point. The opposite extreme would be where earthquakes are only anticipated on known active faults, resulting in highly variable estimates of hazard with maximum value near to the faults, and very low values elsewhere. Brown (2003) developed a series of models including some active faults, and volume sources tending towards higher resolution in regions where more geological, geophysical and seismicity data was available.

Quantification of earthquake recurrence in areas of low seismicity can be significantly affected by earthquake clustering. The largest earthquake in a cluster sequence will give the strongest and most damaging motion. If other members of the cluster are included in earthquake magnitude studies, these dependent events result in a higher ratio of small to large earthquakes (Gutenberg-Richter b value), and an underestimation of the recurrence of large events. Earthquake catalogues must be declustered for earthquake magnitude recurrence estimates.

One of the most significant limitations on earthquake hazard studies at present is the non-availability of local frequency-dependent ground motion attenuation functions. This affects both the magnitudes being calculated, and the resulting ground motion estimates. Attenuation depends significantly on local geology, with young, soft or hot rocks attenuating motion rapidly with distance, and old, hard, cold rocks giving very low attenuation. In the absence of local measurements, consideration of the geology, particularly the age of rocks in the upper half of the crust, is a very useful guide.

Earthquake alarms

The implementation of an earthquake alarm first requires determination of the earthquake location and magnitude as soon as possible after the event, preferably within minutes. Most alarm systems have an automatic calculation of location and magnitude, which is checked by a seismologist and often modified before the alarm is issued.

Useful alarms require more than just the location, origin time and magnitude of the earthquake (Peck et al, 1996). They need an estimate of the probable effects of the earthquake so that appropriate responses are made. This requires estimation of the ground motion at a number of locations or throughout an area, which needs a local strong motion attenuation function, possibly using site response estimates. The alarm system usually requires estimates of the vulnerability of structures (provided by engineers).

Well-designed emergency response plans should anticipate the actions to be taken, such as inspecting a structure, and taking measurements that will indicate normal or abnormal operation. Communication tasks are the most common, ensuring that all relevant people are informed as soon as possible.

Alarm systems require databases of structure vulnerabilities and responses (actions or tasks to be undertaken) to be prepared in advance, and checked regularly.

First-generation alarm systems estimate ground motions using a simple radially symmetric attenuation function. High precision earthquake locations are not particularly needed for this alarm function, and the existing seismograph system with gaps in coverage filled is adequate. Second generation alarm systems will also estimate ground motions by computation, but will include site response and seismic wave radiation pattern, so will need focal mechanisms and more precise earthquake locations (e.g. as in California). Third generation alarm systems actually measure ground motion over a dense network (e.g. as in Japan).

Earthquake forecasts and alerts

Most earthquakes occur without any indication that it is imminent. A study of earthquake clustering may reveal precursory behaviour.

Precursory activity seems to be more apparent in the stable continental regions, where there are few earthquakes, faults rarely fail, and stress levels reach much higher values than in active areas.

Some earthquakes are preceded by multiple sequences of smaller earthquakes, any one of which is comparable with normal small earthquake sequences that often occur, but together may suggest an oncoming major event.

Two perspectives on seismological monitoring

Seismologists tend to polarise into two groups, depending on the distance between the earthquakes they are studying and the seismographs recording the ground motion.

Global or broadband seismology

Global seismology is concerned with world earthquakes, usually recorded at distances of hundreds of kilometres to thousands of kilometres.

Local or high resolution seismology

Local seismology is concerned with earthquakes within a seismograph network, often covering a country or state, where distances are from hundreds of kilometres down to less than a kilometre. Because seismic wave travel distances are short, travel times are low, and major changes in geological structure are limited. The small area means that large earthquakes are rare, but relatively small earthquakes can be detected and analysed.

However, the strong motion from large nearby earthquakes is one of the most significant aspects when working at this scale because this is what causes earthquake damage. Most of the data used comes from individual networks, but it is very useful to share data between neighbouring networks (local collaboration). Table 1 compares some of the aspects of global and local seismology. It shows that the shorter distances, higher frequency motion, and smaller earthquakes considered on a local scale leads to more precise locations. To emphasise this point the name high-resolution seismology is used instead of local seismology

Global seismology and high resolution seismology

	Global seismology	High resolution seismology
Travel path distances	Hundreds of km to world wide.	Less than 1 km to hundreds of km
Magnitudes	Usually from magnitude 4 to over 9, with some smaller events but rarely less than magnitude 3.	Depending on network size, from ML 0 to 2 and above for earthquakes, or down to magnitude -2 or -3 for events in mines. Strong motion from large nearby earthquakes provides invaluable hazard information.
Minimum frequency motion	From less than 0.01 Hz for very large events, and from 0.05 Hz for magnitudes from Mw 4.0.	From 0.2 Hz for large events, 1 Hz for small earthquakes, and 10 Hz for very small events.
Maximum frequency motion	Typically several hertz for events at thousands of km, up to 10 Hz at hundreds of km.	Tens of hertz for earthquakes at 100 km distance, to 100s or 1000s of hertz closer than 1 km.
Sample Rate (samples per second)	20 to 50 /s.	100 to 200 /s for larger local networks, 500 /s for aftershocks, to 20000 /s or more in mines.
Data per day (compressible for storage and telemetry, all saved for continuous, some for	16 to 39 megabyte	155 to 300 megabyte for local networks to 1.6 gigabyte in mines

	Global seismology	High resolution seismology
triggered)		
Triggered or Continuous	Normally continuous on all channels.	Usually continuous on one or three channels, plus triggered on all channels
Transducers required to detect target bandwidth	Broadband seismometer is ideal for moderate to low frequency motion.	The smaller the network the higher the frequency of motion. Short to moderate period seismometers, geophones and accelerometers cover the range.
Dynamic Range	Significant distances may limit dynamic range requirements.	Wide variation in amplitudes requires large dynamic range. Often requires triaxial seismometer plus a triaxial accelerometer.
Seismometer installation	Expensive vault needed	Vault not needed. Relatively simple weather and security protection is adequate.
Power Requirement	Moderate, often dominated by communications, especially VSAT sites	Low without telemetry (single small solar panel and battery). Moderate when telemetry is used.
Data Collection	Continuous data normally telemetered to observatory, with on site storage used during communication failure.	Can use on site storage manually collected by exchanging discs or memory cards, and/or telemetry of either triggered or continuous data.
Best case earthquake location uncertainty: (many seismographs, and epicentre inside network, and one or more seismographs near epicentre, and simple geology)	Location accuracy usually limited by seismic wave velocity model. Random uncertainty of 2 km, plus systematic uncertainty of several km.	Location accuracy usually limited by the number of seismographs recording each event. Random uncertainty from less than 1 km, plus systematic uncertainty of less than 1 km.
Typical poor quality location uncertainty (few seismographs, or epicentre outside network, or no seismograph near epicentre, or complex geology)	Random uncertainty of ten to hundreds of km, plus systematic uncertainty up to tens of km.	Random uncertainty of ten to hundreds of km, plus systematic uncertainty up to several km.
Cost of each site including installation and operation, excluding analysis (A$, 2006, ±30%)	$50,000 plus $8000 to $12000 per year (assuming alarm reliability needed).	$10,000 plus $3000 to $8000 per year depending on telemetry (assuming no alarm function).
Number of seismographs	Typically tens to hundreds – the current global network (global collaboration).	Depends critically on the local network, plus help from neighbours (local collaboration).
Major contribution to	Global tectonics, nuclear monitoring, tsunami warning, global earthquake hazard and risk.	Local earthquake hazard and risk.

Tennant Creek aftershocks, 1988

Aftershocks of the Tennant Creek earthquakes from January 1988 illustrate the difference between global seismology results and high-resolution seismology. Figure 3 shows earthquakes located using global data. On a map covering Australia or the world, these would all be at almost the same point, but on the scale of this figure, they can be seen to spread over tens of kilometres. Most of the depths are assigned values of 5 or 10 km, so there is no significant depth dimension to the plot. Figure 4 (at the same scale as Figure 3) and the enlarged Figure 5, were produced using results from a local network of 10 to 15 seismographs in a high-resolution network. Despite being before the advent of GPS timing, the typical uncertainties in longitude, latitude and depth were often from one to two kilometres, and the relationship between the earthquakes and the fault is very clear.

A mapped fault is drawn oriented WNW to ESE. This corresponds to the main fault rupture in the earthquake sequence. The southern block was the upthrown block on the south dipping reverse fault. There was also a smaller steeply dipping conjugate fault to the northwest, giving some deeper events that can be seen on Figure 5.

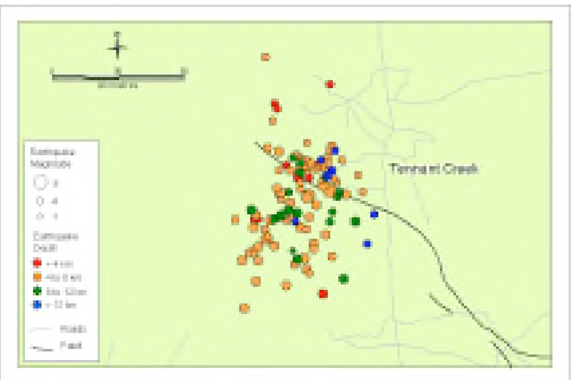

Figure 3: Aftershocks of the 1988 Tennant Creek earthquakes as located by the International Seismological Centre show considerable scatter, with uncertainties of tens of kilometres. There is no obvious relationship between the depths of events and the fault.

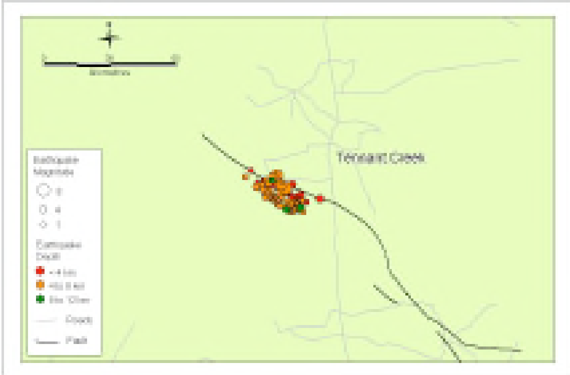

Figure 4: Aftershocks located by a local network have location uncertainties an order of magnitude less, measured in kilometres, and are much more closely related to the fault.

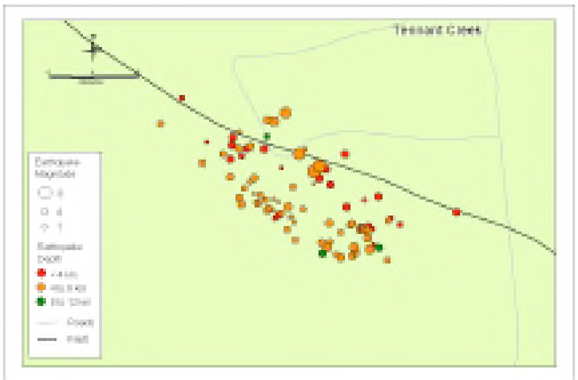

Figure 5: At a larger scale, the aftershocks located by the local network outline the fault rupture, showing the main fault as a south dipping reverse fault, with a smaller conjugate fault dipping to the northwest.

Recent developments in applied earthquake seismology in Australia

Earthquake alarms

When the Newcastle earthquake occurred in 1989, relatively few of the seismographs throughout Australia were telemetered to observatories. Initial locations using data predominantly from the southwest showed the epicentre well inland, but with very high uncertainty because it was well outside the network. It took some hours before the estimates began to indicate a Newcastle location.

This lead to the introduction of automatic telemetered seismograph networks with automatic event detection and automatic preliminary locations at Geoscience Australia in Canberra and the Seismology Research Centre in Melbourne. The other major network in Australia, operated by Primary Industries and Resources South Australia, in Adelaide, also now has an alarm system. The Seismology Research Centre operates independent alarm systems in Brisbane and Melbourne to ensure reliability of the system, especially in the case of an earthquake occurring at either location. The alarm systems operated by Geoscience Australia and PIRSA operate independently but all systems cooperate closely, so automatic locations for most Australian earthquakes are available within minutes of an event, and seismologist revised solutions are usually available within tens of minutes of the event.

Routine earthquake monitoring

The new alarm systems have seen digital recording totally replace analogue recording at most observatories. Most of the analogue drum recorders still operating are only used for educational and public display purposes.

This has been a major change to observational seismology in Australia, and the accuracy and precision of the analysis of larger events has improved. However, it has brought some disadvantages with its advantages. The extensive use of digital recording has meant that many smaller earthquakes remote from seismographs do not trigger the system and are not detected.

Examination of continuous digital data on a screen could be used to manually detect these events, especially in the format with all stations recording in parallel rather than all data from one station on a simulated helical recorder. Correlation between records from different instruments should attract the eye of the observer similar to an automatic multi-channel earthquake trigger. However the resolution of modern computer screens is still not as good as high quality analogue records, and the number of smaller events currently being located per year is about half of that in the past, despite the increase in number of seismographs.

Magnitude and attenuation

Magnitude estimates have always shown inconsistencies. Within a network, calculated magnitudes often vary with recording distance, indicating that the attenuation function used in the calculation is not valid.

Even when magnitudes computed by a given network are consistent, they may vary relative to estimates given by neighbouring networks.

Allen (2004, and related publications) has made steps towards developing attenuation functions that can be used for both:

1. correcting ground motion measurements for distance to calculate earthquake magnitude estimates, and

2. using earthquake magnitudes to estimate the ground motion at a point some distance away, normally for hazard studies.

These functions are empirically determined, and ensure that magnitudes do not vary with distance, and they are related to motion near to the earthquake source rather than at an arbitrary distance, such as 100 km, so magnitudes recorded in areas of high and low attenuation should be equivalent.

Site response

Over recent years, Geoscience Australia and others have placed considerable emphasis on the significance of site response to earthquake hazard. Detailed microzonation maps have been produced that incorporate amplification due to soft surface sediments.

Asten (2005, and earlier papers) has developed the spatial auto-correlation (SPAC) method of determining the shear wave velocity profile at a site using ambient vibrations recorded on a small array. Although not yet being applied extensively, this method shows a considerable advancement over methods using horizontal/vertical motion ratios at a point (Nakamura method).

Seismology and geology

The link between seismicity and geology is best made using high-resolution seismograph networks, especially with earthquake focal mechanisms. Temporary high-resolution networks have been deployed about the Burakin earthquake swarm in Western Australia by Geoscience Australia, and in the Flinders Ranges of South Australia by Geoscience Australia, PIRSA and the ANU. Discussions have been held regarding a temporary high-resolution update on activity in the Tennant Creek region.

Geoscience Australia have developed studies of earthquake geology throughout Australia, and have significantly increased the number of recognised examples of neotectonic activity, particularly in southwest Western Australia (Clark, 2005 and other publications).

Challenges facing us over the next decade

There have been many improvements in seismograph systems and analysis methods over the past two decades. The global scale is now well-covered (apart from oceanic regions) and moderate magnitude earthquakes are usually well located, and have reliable magnitudes and mechanisms. However, resolution remains limited by the velocity or travel time model used, and many earthquake locations have both random uncertainties and systematic uncertainties of tens of kilometres. It is approaching a level that can be regarded as adequate for earthquake alarm systems.

The local scale has many applications for hazard and risk in particular areas. Precise locations of earthquakes delineate faults, recording ground motion over a wide range of logarithmically spaced distances determines attenuation and thus reliable magnitude estimates, and focal mechanisms reveal links between earthquakes and geology. However it is limited by the seismograph/accelerograph network density.

Future routine earthquake monitoring

To improve earthquake locations, magnitudes, and focal mechanism, a high seismograph network density is needed, and the dominant limiting factor in Australia is cost. The challenge is to develop instrumentation with low capital and operating cost that can be deployed widely. The cost of seismograph recorders has significantly reduced over recent years, especially on a local scale.

If trends can be extended to the transducers required (short period and strong motion accelerometers are appropriate for high-resolution monitoring), and costs can be reduced by the economies of larger scale deployment, then much higher seismograph network densities should become economically feasible. It would be a useful and achievable aim to reduce the capital and operating costs by another factor of two.

The current seismograph array in Australia has almost enough instruments telemetering near real-time for earthquake alarm purposes.

If the capital cost plus operating cost of communications is significant (e.g. telephone, mobile telephone, radio modem or VSAT), then remote operation is an option for some or many of the instruments. Modern seismographs have sufficient data storage space for many months of operation, and are sufficiently reliable to allow remote operation with infrequent field visits for data collection.

Despite the increasing deployment of small, relatively low-cost, six-channel instruments, the existing strong motion network in Australia is extremely sparse. Attenuation functions are determined by comparing motion on bedrock sites over a range of distances, so records from a single isolated instrument have limited value.

Very few strong motion instruments are installed on buildings or other structures in Australia, and most of these are on large dams. Give the reductions in cost over the past decade; it is now much easier to instrument a range of typical structures to gather vulnerability data appropriate for earthquake engineering. The multiple locations required to compare motion of the structure, foundation and bedrock could use low-cost wireless connections.

Site response

There is no doubt that earthquake damage is greater on soft surface sediments than on hard rock sites, and that this is due to resonant amplification of the seismic wave motion at the natural frequencies of sites.

Current site response methods, both H/V (Nakamura) methods and SPAC methods, apply to horizontally layered sediments and do not consider three-dimensional structures such as valleys. Site response methods should develop beyond horizontally layered structures, and include valley edge effects.

A challenge that will involve both site response and structural engineering dynamics is to minimise the possibility of multiple resonance. If the natural frequency of a site corresponds to the natural frequency of a structure, the site will first amplify the earthquake motion by some factor, then the structure will further amplify this motion by another factor. This can be avoided by ensuring that the structure does not have the same natural frequency as the site. The natural frequency of the site cannot easily be changed (although it may vary a little with ground-water variations), but the natural frequency of the structure can be varied depending on its mass and stiffness, and particularly on its height. Multiple resonance is not considered in the current version of Australian Standard AS1170.4, although it was considered in the previous SAA Loading Code AS2121-1979.

Seismotectonic models, seismicity and geology

Traditionally, the seismotectonic source models used for earthquake hazard studies were based solely on the limited available seismicity data. This is not a great problem in active areas where the average return period between major earthquakes is of the order of hundreds of years. However, in stable continental regions like Australia, where return periods of large earthquakes may be tens or hundreds of thousands of years, the seismicity record is similar to a jigsaw puzzle with many missing pieces.

These problems can be minimised by the use of geological and geophysical data to provide a framework for the seismotectonic model, use of geological fault slip rates to confirm earthquake magnitude recurrence rates, and using palaeoseismology data to confirm maximum credible magnitude estimates.

Seismotectonic models have traditionally varied between flat-earth models, where the likelihood of earthquakes is uniform over large areas, and the active-fault models, where all future earthquakes are assumed to lie on active faults that have already been delineated. There seems to be little doubt that proximity to an active fault is the major consideration for earthquake hazard, and that future earthquake hazard maps will show more variations at scales of tens of kilometres than the smoothed "fault-less" hazard map used in the current loading code, Australian Standard AS1170.4. The challenge is to identify and quantify all major active faults in Australia.

It is possible that time variant hazard maps will become more apparent in the next decades. The existing AS1170.4 map already includes some time-variant features. The Tennant Creek earthquakes of 1988 have lead to a prolonged period of adjustment activity in the region, and after more than 18 years the region still experiences a significant proportion of Australian earthquake activity. It is possible that more moderate to large events may occur as part of this sequence, and the hazard map reflects this possibility. When this sequence is over, perhaps after about 100 years, the region may experience a long period of quiescence, giving a long-term average fault slip-rate consistent with geological data.

Seismology and geology

Until a dense permanent network of seismographs is installed, temporary deployments of dense networks, either for aftershock sequences or in selected regions, will provide a link between earthquake activity and geology. Aftershock sequences are particularly useful because they occur at a known place, so the seismographs or accelerographs can be deployed with increasing density towards the epicentre.

We are coming up to the 20th anniversary of the Tennant Creek earthquake, and the next major earthquake in Australia may not be very far off. We must be prepared for a very rapid deployment. In the meantime, we should be alert for repeated sequences of small earthquakes that may be precursory events.

Public education

There can be little doubt that one of the best ways to mitigate risk is through a public education program. The program in the Philippines covering geohazards, including earthquakes, volcanoes, tsunamis and landslides, is world leading. It has produced a good level of awareness and sophistication, primarily through its schools program. Seismology can be used as a means of teaching the basics in many school subjects, including physics, geology, geography, mathematics, environment, and social studies.

School seismograph systems have been installed in several regions, and have proved useful, although results are sometimes disappointing and recording systems require too much attention. Development of a reliable school seismograph with adequate long-period response for large distant earthquakes could reduce current limitations. Perhaps this could plug into the USB port of a standard desktop computer with a large LCD screen and appropriate software to handle display, data storage and data exchange. The major problem would be the development of an inexpensive transducer with fair long-period response, a specification that would be appropriate for this application but not adequate for a seismic observatory.

A similar recorder, but with short period and strong motion transducers, could be used by schools and the growing number of amateur seismologists to supplement the local seismograph network.

Conclusion

Both global scale, and high-resolution local monitoring are important. It is easier to fund global monitoring because it deals with larger damaging earthquakes, which occur relatively often about the earth, and is supported by nuclear monitoring and tsunami warning functions.

Permanent monitoring seismicity at high-resolution requires a dense network. A sophisticated network of sites that all have real-time communications, as deployed throughout Japan, is economically unfeasible in Australia. The unit cost (both capital and operating) for seismographs and accelerographs in a dense Australian network will need be minimised. Incorporation of communications by telephone, radio or satellite would be too expensive at many or most sites, and is not necessary for the scientific purposes of the network.

Of the current earthquake risk mitigation measures in Australia, earthquake alarms are approaching a satisfactory level. The large size of Australia means that earthquake hazard studies are limited by the low seismograph network density. Earthquake location precision does not allow fault delineation, and local attenuation functions (and thus magnitudes) and focal mechanisms usually cannot be determined. The high stress drop of many Australian earthquakes suggests that earthquake forecasts or alerts, considering earthquake clusters and possibly other precursors, may have a higher chance of being useful than in more active regions.

The most appropriate extension to current monitoring is to emphasise areas of highest earthquake activity (hazard) and risk (those with high vulnerability and exposure - that is, relatively populated regions), and to be prepared for rapid deployment of instruments for aftershock studies.

References

Allen, Trevor, 2004: *Spectral attenuation and earthquake source parameters from recorded ground motion; implications for earthquake hazard and the crustal stress field of southeastern Australia*, Doctor of Philosophy (Geophysics) thesis, School of Geosciences, Monash University, Melbourne

Asten, Michael, Nelson Lam, Srikanth Venkatesan, Hugh Rutter and John Wilson, 2005: *The importance of shear wave velocity information of a soil site*, Proc AEES 2005 conference, Albury, pages 36-1 to 36-6.

Brown, Amy, 2003: *Towards a geologically based seismotectonic model for use in probabilistic hazard studies in Australia*, Master of Engineering (Geological) Thesis, Dept of Civil and Chemical Engineering, RMIT University.

Clark, Dan, 2005*: A preliminary seismicity model for southwest Western Australia based on neotectonic data*, Proc AEES 2005 conference, Albury, pages 22-1 to 22-6.

International Seismological Centre, web site www.isc.ac.uk.

Peck, Wayne, Gary Gibson and Greg McPherson, 1996: *Earthquake Warning, Alarm and Response Systems*, Proc AEES 1996 conference, Adelaide, pages 14-1 to 14-6.

Standards Australia, 1993: AS1170.4-1993 Minimum design loads on structures, Part 4: Earthquake loads, Standards Australia, ISBN 0 7262 8297 9.

Standards Association of Australia, 1979: AS2121-1979 SAA Earthquake Code, SAA, ISBN 0 7262 1695 X.

World Stress Map: http://www-gpi.physik.uni-karlsruhe.de/wsm/introduction/introduction_frame.html

An approach to response spectrum attenuation modelling for southeastern Australia

G.H. McVerry

GNS Science, Lower Hutt, New Zealand

Abstract

An approach is demonstrated for developing response spectrum attenuation relations that are relevant for southeastern Australia through modifying those from elsewhere. The approach recognises that SE Australia combines features of intraplate regions such as Eastern North America (ENA) and plate-boundary regions such as California. It is in a region of intraplate tectonics, but characterised by sedimentary deposits that produce near-surface attenuation rates (kappa) more typical of plate boundary regions. Also, it is uncertain whether stress drops in earthquakes of about magnitude 5 or greater, being those relevant for earthquake-resistant design, are moderate or high.

The approach starts with a range of attenuation relations that between them account for both moderate and high stress drops, but with high near-surface attenuation, modelled using a high kappa value. This can be provided by selecting a combination of attenuation relations from California (moderate stress-drops, high kappa) and ENA relations (high stress drops, low kappa) modified for high kappa values.

A simple exercise shows that it is possible to generate similar spectra starting from either ENA or Californian attenuation models through the application of kappa-dependent modification factors, although the two sets of relations are very different, with strong high-frequency content in the ENA spectra.

Introduction

South-east Australia (SEA), like many parts of the world, suffers from a sparsity of strong-motion earthquake records for the development of appropriate motions for earthquake-resistant design. The sparsity of data hinders the development of empirical attenuation expressions for modelling the strength of earthquake shaking as a function of the earthquake magnitude and distance from the earthquake source and other parameters such as site conditions and source mechanism of the earthquake.

Adoption of models from other parts of the world is difficult because SEA combines features of intraplate regions such as Eastern North America (ENA) and plate-boundary regions such as California (Lam et al 1998, Somerville et al., 1998). It is in a region of intraplate tectonics, which govern the source effects, but is characterised by sedimentary deposits, which produce moderate near-surface attenuation rates more typical of plate boundaries rather than the low attenuation rates usually found in continental regions.

These issues have been tackled in a detailed way by Lam and Wilson (2003) in their Component Attenuation Model, which they have applied in Australia and elsewhere. The current paper represents a more simplistic approach, demonstrating one of the key factors for SEA. It is based largely on an oral presentation that was made at a workshop on attenuation models for Australia at Geoscience Australia in February 2006.

Important parameters affecting earthquake motions

The spectrum of the earthquake motions expected at distance R from the source of an earthquake of magnitude M as a function of frequency f can be expressed as the product of a number of factors, including the source spectrum, geometric attenuation, anelastic attenuation over the whole path and in the near-surface region, and near-surface amplification resulting from wave-propagation velocity contrasts with the rock at depth, (e.g. Lam et al. 1998, Atkinson and Boore, 1997). Many of these factors depend on the tectonic and geological environment.

Source spectrum and stress drop

The source factor S(M, f) is proportional to the displacement spectrum at the source. Brune (1970) provided a simple commonly-used model for the source function:

$S(M,f) = M_0/(1+(f/f_c)^2)$

The seismic moment M_0, which gives the zero-frequency strength of the source spectrum, is simply related to the moment magnitude M of the earthquake.

The corner frequency f_c determines the frequency band of the high-frequency part of the acceleration spectrum at the source, and the source duration. It depends on the stress drop $\Delta\sigma$, the seismic moment and the shear-wave velocity β at the source

$f_c \propto \beta\ (\Delta\sigma/M_0)^{1/3}$

For a given seismic moment or magnitude, stress drop is a key parameter governing the frequency content and amplitude of the spectrum, and the duration of the motion.

Anelastic attenuation

The spectrum generally decays as the distance increases from the source through geometric and anelastic attenuation. Often the geometric attenuation term D(M,R,f) is taken as simply 1/R, but anelastic attenuation is region-dependent.

The whole-path anelastic attenuation can be modelled by a factor $\exp(-\pi fR/Q(f)\beta)$. The quality factor Q(f) depends on both tectonic and geological factors. High Q leads to rapid attenuation, while motions can persist to large distances in low-Q regions.

Significant attenuation of earthquake motions, especially of their high-frequency content, occurs in the last few kilometres of the source-to-site path, in the near-surface region. This effect can be modelled through the parameter kappa (κ), with the near-surface attenuation factor P(f) given by $\exp(-\pi\kappa f)$.P(f) is strongly dependent on the geological environment, with low κ for strong crystalline rock and much higher κ for weak sedimentary rock or deep soil deposits.

Comparison of tectonic and geological environments

Eastern North America (ENA)

ENA is a stable geological region with strong crustal rock. Strong rock allows earthquakes with high stress drops, low attenuation over both the whole path and near-surface. High stress drops produce spectra with stronger high-frequency components for a given magnitude. Low attenuation maintains strong high-frequency content to large distances.

California

California is a plate boundary region and geologically active. Stress drops are generally lower than in ENA, and attenuation is rapid (low Q and high kappa). As a consequence, spectra lack the strong high-frequency content of ENA.

Southeast Australia (SEA)

South-eastern Australia is within a tectonic plate (i.e. in an intra-plate setting) like ENA rather than at a plate boundary such as in California or New Zealand. However, it is geologically active with sedimentary deposits, so that it does not have the same crustal conditions as stable shield regions such as ENA and western Australia. Consequently, conditions in south-eastern Australia are intermediate between those of ENA and California. It has been found that Q(f) (characterising whole-path attenuation) and kappa values in SEA are more similar to those of California than those of ENA. There is very limited information about stress-drops in south-east Australian earthquakes large enough to be of engineering importance (about magnitude 5 or greater), and it is inconclusive whether the stress-drops are more similar to those in ENA or Californian earthquakes.

Modification of attenuation expressions for SEA

The approach adopted in the case study was to modify a selection of published attenuation models to be more suitable for conditions in SE Australia

Selected attenuation models

Attenuation models were selected from both ENA, characterised by high stress drops, and from California, where stress drops are lower, because of the uncertainty about stress drops in SE Australia at magnitudes important for seismic hazard.

Two models were selected to be representative of ENA models. The two models have different ways of representing source spectra and of modelling attenuation with distance. The ENA models selected for the case study were those of Atkinson & Boore (1995), denoted as AB95, and Toro et al. (1997), both modified as described in the next section to account for the observed upper-crustal attenuation in south-east Australia.

The Sadigh et al. (1997) model was selected to represent recent Californian models. It produces reasonable estimates of earthquake motions in SEA (G.Gibson, pers. comm.).

Modifications to ENA models

Both the Atkinson & Boore and Toro et al. ENA models give sharp short-period spectral peaks from a combination of high stress-drops and low attenuation of high-frequency motions (e.g. Figure 1). The low attenuation of the ENA models is inappropriate for SEA (e.g. Lam et al. 1998). However, it is considered appropriate to retain the possibility of high stress-drops. This has been achieved by selecting the ENA models, which inherently are influenced by high stress drops, but adjusting their kappa values from those appropriate for ENA to values appropriate for California, and, it is believed, SE Australia.

Adjustments for kappa κ

For south-east Australia, kappa has been taken as 0.04s, as given by Lam et al. (1998). Atkinson & Boore (1997, p26) state that the kappa value for ENA equivalent to their modelling is 0.002s. Toro et al. (1997, p43) give a value of 0.006s as an appropriate value typical of ENA for their model. The differences between the kappa values of these models arise from interactions between kappa and other parameters in the modelling.

Adjustment for kappa was performed using a model provided by N. Abrahamson that has been used for studies of the Yucca Mountain Nuclear Waste Repository project in the U.S. The frequency-dependent modification to the response spectra models for a change from kappa=κ_2 for ENA to kappa= κ_1 for SEA is:

$\ln(\text{Scale Factor}(f)) = c_{10}(f) * (\kappa_1 - \kappa_2) + c_{11}(f) * ((\kappa_1-0.025)^2 - (\kappa_2-0.025)^2)$

The coefficients $c_{10}(f)$ and $c_{11}(f)$ are:

Frequency f (Hz)	$c_{10}(f)$	$c_{11}(f)$
0.5	-1.540	-38.64
1.0	-3.156	-24.59
2.0	-6.056	-5.412
5.0	-13.76	26.11
10	-23.37	98.78
≥20	-31.83	378.67
PGA	-18.64	301.22

Examples of original and kappa-modified spectra

Figure 1 compares median 5% damped acceleration response spectra for rock conditions for the Sadigh et al. (1997), Atkinson & Boore (1995) and Toro et al. (1997) models. The two ENA models are unmodified in the left-hand plots and have the kappa modification factors applied in the right-hand plots. The comparisons are shown for horizontal distances from the earthquake source of 10 km (top plot), 30 km (middle plot) and 60 km (bottom plot), for a reverse-faulting magnitude 7.0 earthquake at a focal depth h of 7 km. The Sadigh et al. model includes its reverse fault factor of 1.2. The other models do not contain a reverse fault factor, but it is inherent in them as they have been developed from data from regions where thrusting is likely to be the dominant mechanism.

The two ENA models are plotted with square symbols (■ for Atkinson & Boore and □ for Toro et al.). The very short-period peaks of the unmodified spectra in the left-hand predicted by these two models are apparent at periods of 0.05s and less. This behaviour requires low attenuation at high frequencies, and is thought to be inappropriate for south-eastern Australia. This characteristic has disappeared in the right-hand plots where these models have been modified for higher upper-crustal attenuation (kappa increased to 0.04s, typical of south-eastern Australia and California). With modification for kappa, the two ENA models become similar to the Californian Sadigh et al. model. There has been little modification to the spectra at periods of 0.5s and greater. The right-hand plots are thought to be representative of median spectra for south-eastern Australia for rock conditions. Individual spectra may vary considerably around these median values, with each of the median spectra plotted being associated with a log-normal probability distribution that represents this variability. There is typically a factor of two range between the median spectra for the Sadigh et al. and modified Toro et al. spectra, and up to about a factor of three at long periods when the modified Atkinson & Boore model is included.

Figure 2 shows median attenuation curves for the original and modified forms of the ENA attenuation models, corresponding to the response spectra of Figure 1. Again, the unmodified models are shown on the left and the kappa-modified models on the right. The top plot in each figure is for a period of T=0s, corresponding to peak ground acceleration; the middle plot is for T=0.2s, corresponding to the peak of the spectrum for most cases except for the Atkinson & Boore model; and the bottom plot is for T=1s. The kappa-modified models show considerably reduced accelerations at all distances at short periods (0s and 0.2s). The increased kappa has little effect at 1s period.

Conclusions

From a consideration of tectonic and geological conditions, in southeastern Australia, it was desired to develop spectra with the possibility of high stress drops, as for ENA, but with attenuation characteristic similar to California. It is shown that modifying ENA response spectrum models for near-surface attenuation kappa values appropriate for California largely removes the sharp short-period spectral peaks of the ENA spectra, producing spectra similar to those of Californian models.

References

Atkinson, G. and Boore, D. 1995. New ground motion relations for eastern North America. Bulletin of the Seismological Society of America, 85(1):17-30.

Atkinson, G.M. and Boore, D.M. 1997. Some comparisons between recent ground-motion relations. Seismological Research Letters, 68(1):24-40.

Brune, J. 1970. Tectonic stress and the spectra of seismic shear waves from earthquakes. Journal of Geophysical Research, 75: 4,997-5,009.

Lam, N. Wilson, J. and Hutchison, G. 1998. Development of intraplate response spectra for bedrock in Australia. New Zealand National Society for Earthquake Engineering conference, 137-144. Wairakei, Taupo, New Zealand.

Lam, N.T.K. and Wilson, J.L. 2003. The component attenuation model for low and moderate seismic regions. 2003 Pacific Conference on Earthquake Engineering, Paper Number 099, Christchurch, New Zealand.

Sadigh, K., Chang, C-Y., Egan, J.A., Makdisi, F. and Youngs, R.R. 1997. Attenuation relations for shallow crustal earthquakes based on California strong motion data. Seismological Research Letters, 68(1): 180-189.

Somerville, M., McCue, K. and Sinadinovski, C. 1998. Response spectra recommended for Australia. Australasian Structural Engineering Conference, 439-443.

Toro, G.R., Abrahamson, N.A., Schneider, J.F. 1997. Model of strong ground motions from earthquakes in Central and Eastern North America: best estimates and uncertainties. Seismological Research Letters, 68(1): 41-57.

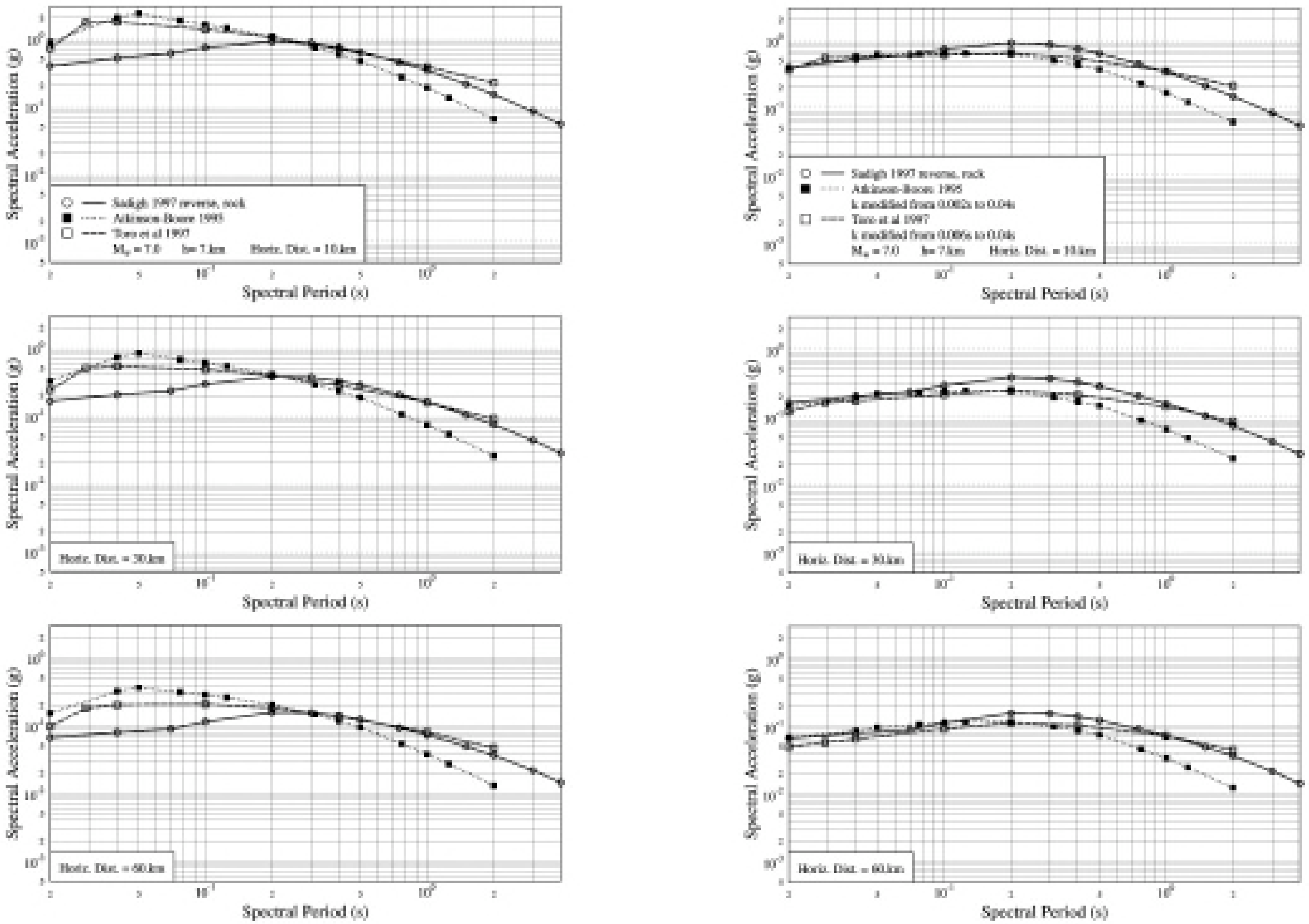

Figure 1 Spectra for magnitude 7 reverse-mechanism earthquakes on rock at horizontal distances of 10, 30 and 70 km. The highly peaked unmodified Atkinson & Boore and Toro et al. spectra (left) become similar to the Sadigh model on application of kappa modification (right).

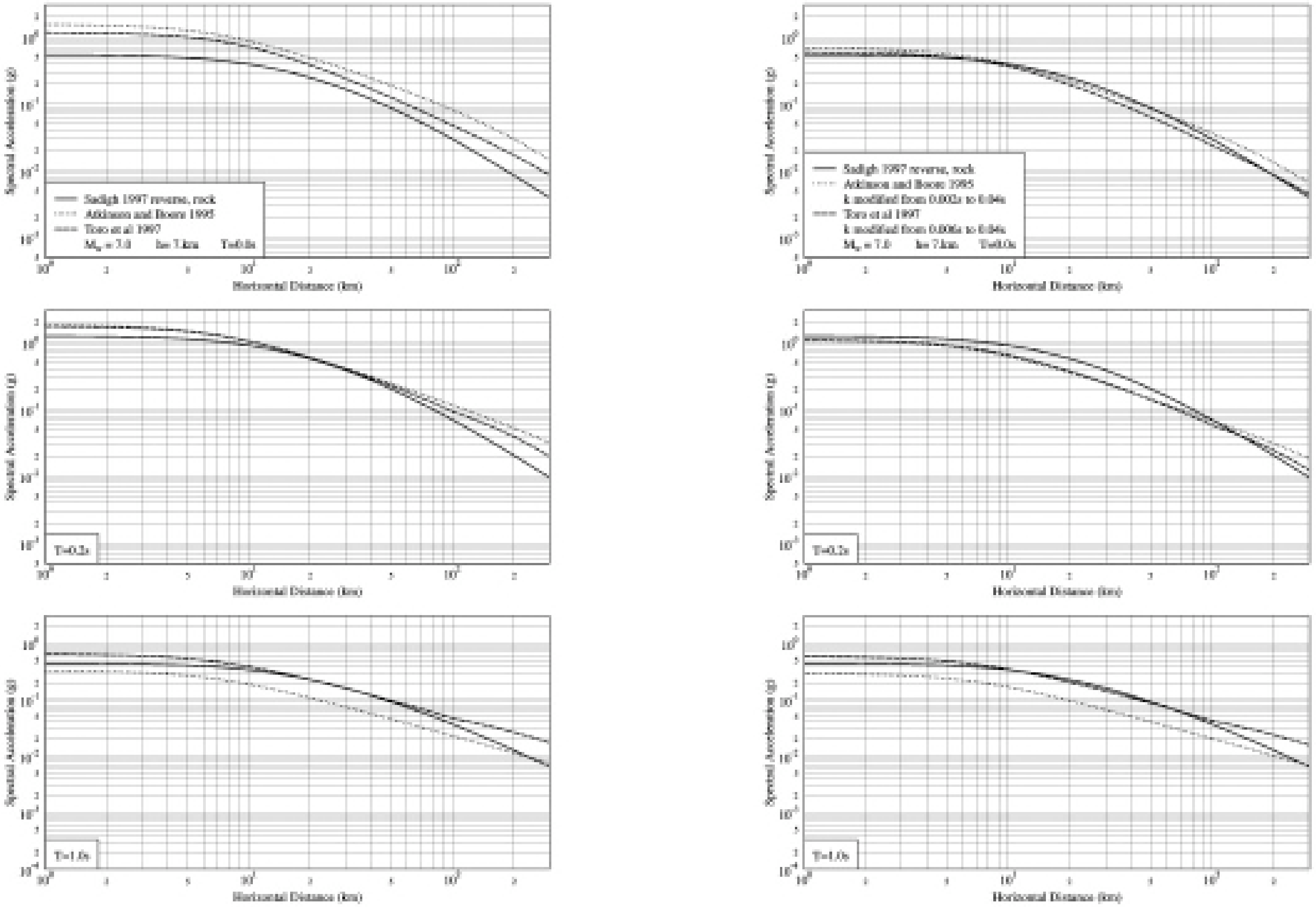

Figure 2 Attenuation curves for periods of 0s (pga), 0.2s and 1.0s, corresponding to the spectra of Figure 1. The short-period (0s and 0.2s) kappa-modified ENA accelerations (right) are much reduced at all distances, but there is little change at 1s period

Comparison of earthquake source spectra and attenuation in southeastern Australia and eastern North America

Trevor Allen[1] and Gail Atkinson[2]

[1] Geoscience Australia
[2] Carleton University, Ottawa, Canada

Abstract

The paucity of ground-motion data in Stable Continental Regions (SCRs) remains a key limitation when developing relations that seek to predict effects of strong ground-shaking from large damaging earthquakes. It is desirable to combine data from more than one SCR in order to increase database size, but this raises questions as to whether the source and attenuation properties of the SCRs are equivalent. We merge recently-compiled spectral-amplitude databases from small-to-moderate events (moment magnitudes $2.0 \leq M \leq 5.0$) in both southeastern Australia and eastern North America in order to compare the key characteristics of ground motion in these two regions. Both are SCRs, but are widely separated, spatially and in tectonic history.

We statistically compare ground motions by plotting mean and standard deviations of spectral amplitudes for data grouped in magnitude and distance bins. These comparisons show that the source and attenuation properties of the two regions are very similar, particularly at shorter hypocentral distances R (i.e. R < 70 km). At larger distances, regional attenuation differences are observed that may be attributed to differences in crustal structure. We conclude that it is valid to combine the Australian and ENA ground-motion datasets in the development of ground-motion relations.

These may serve as generic functions for SCRs around the world.

Introduction

A major shortcoming of all predictive ground-motion models developed for Stable Continental Regions (SCRs) is that they are based on relatively scarce observational data in comparison to ground-motion models derived for more tectonically active regions (e.g. Sadigh et al., 1997; Boore and Atkinson, 2006; Campbell and Bozorgnia, 2006). Stochastic simulation methods are often employed to develop predictive ground-motion equations that describe the ground-motion expected from large earthquakes in SCR regions, to mitigate the lack of strong-motion data. However, the reliability of the stochastic relations depends entirely on the reliability of the assumed source and attenuation models, which must be developed from limited SCR databases. It is therefore important to know whether the assumption of generic source and attenuation models is appropriate for all SCR regions. If so, we may combine data from more than one SCR in order to improve the database on which our models are based.

Bakun and McGarr (2002) used limited intensity and digital data to compare the attenuation properties of ground motion among several SCRs. They concluded that attenuation in the Australian continent is greater than that of eastern North America (ENA), but less than that in interplate regions such as southern California. These comparisons were based upon observations from the MS 6.3, 6.4 and 6.7 earthquakes of the 1988 Tennant Creek, Northern Territory, sequence that occurred in the Proterozoic crust of central Australia (Jones et al., 1991; Bowman and Kennett, 1991). However, it is recognised that attenuation across Australia cannot be captured with a single attenuation model (e.g. Gaull et al., 1990). Rather, it is observed the attenuation of seismic wave energy varies transversely across the continent, with relatively low attenuation in the Archaean and Proterozoic terranes of western and central Australia and higher attenuation in the younger Palaeozoic terranes of eastern Australia (Allen et al., in review). Furthermore, recent analysis of data recorded during the 2001-02 Burakin earthquake swarm (Allen et al., 2006) suggests that attenuation of low-frequency ground-shaking in the Archaean cratons of Western Australia may be lower than that observed in ENA (e.g. Atkinson, 2004) at short hypocentral distances. Consequently, significant uncertainty still surrounds the attenuation behaviour of SCRs and, in particular, whether attenuation models developed for one SCR are applicable to another region for the purposes of earthquake hazard assessment (Bakun and McGarr, 2002). In this study, we compare recorded ground-motion spectral amplitude data from ENA and southeastern Australia (SEA) to examine whether it is applicable to derive a common ground-motion model from the combined dataset.

Ground-motion data & methodology

The data used in the analysis are the vertical-component spectral amplitude databases recently compiled by Atkinson (2004) and Allen et al. (in review) for ENA and SEA, respectively. Figure 1 indicates the magnitude-distance distribution of the datasets. The inclusion of data is limited by the magnitude-distance criterion employed by Atkinson (2004) to eliminate low-amplitude quantisation noise problems. The magnitude of all events is represented by moment magnitude M, as calculated from the spectral amplitudes by Atkinson (2004) and Allen et al. (in review). It is worth noting that much of the data employed from SEA were recorded on short-period weak-motion instruments with natural frequencies at 1.0 or 2.0 Hz. Consequently, the SEA data for frequencies below 2 Hz are less reliable than at higher frequencies.

We compare spectral ground-motion amplitudes for the two regions in a range of magnitude-distance bins: M 2.6 (±0.1), 2.8 (±0.1), etc., sorted by distance bins 0.1 log units wide in hypocentral distance. We calculate the mean and standard deviation of the log spectral amplitudes for each bin, for a range of frequencies from 0.5 to 20 Hz.

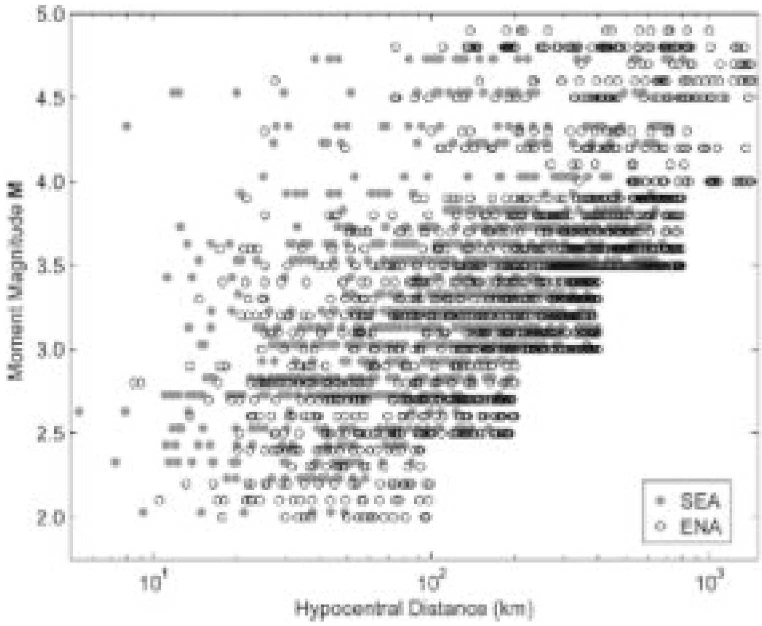

Figure 1. Magnitude-hypocentral distance distribution of the ENA and SEA datasets. Note: a small vertical offset (+0.03) has been applied to the SEA magnitude values for plotting clarity.

Results

Figure 2 compares ENA and SEA spectral amplitudes for a discrete magnitude range (M 2.8) that is well represented in both databases, at frequencies of 1, 2, 5, and 10 Hz. Overall, near-source (approximately R < 30 km) low-frequency (f ≤ 2 Hz) amplitudes match well across the two regions, although this is difficult to see in individual magnitude plots such as Figure 2, due to the limited number of near-source data for any one magnitude. This serves as an important quality check that the moment magnitudes assigned to ENA and SEA earthquakes are consistent between the regions.

In general, there appears to be no statistical difference in source amplitudes or attenuation between the two SCRs for distances out to approximately 100 km. Beyond this distance range, average spectral amplitudes from SEA appear to be consistently lower than the corresponding ENA amplitudes. Furthermore, higher-frequency SEA ground-motions (f ≥ 10 Hz) appear to diverge faster from ENA with increasing distance than do the low-frequency SEA data, indicating a greater contribution of anelastic attenuation in the upper mantle (i.e. lower quality factor Q). This result is consistent with large-scale tomographic studies that demonstrate low Q in the upper mantle beneath Australia (Mitchell et al., 1998).

Figure 4 compares the relative high frequency characteristics of the data in more detail. We plot average ENA and SEA acceleration spectra versus frequency for a few selected magnitude-distance bins. These are selected based on which near-source distance bins (20 ≤ R ≤ 35 km) have the most abundant data for the comparison in both regions. Data are scaled to a hypocentral distance of 20 km by assuming a geometrical attenuation coefficient of $R^{-1.3}$ (e.g. Atkinson, 2004; Allen et al., in review). These spectral comparisons suggest significant differences in high-frequency attenuation (f>10 Hz), indicating that the near-surface effects that control ground-shaking at higher frequencies, as modelled with the coefficient kappa (κ), may be stronger in the upper crust of SEA than in ENA. It is worth noting that in this distance range, we would not expect the spectral amplitudes to be affected significantly by Q.

Consequently, high-frequency effects can be attributed largely to influences from the near-surface geology.

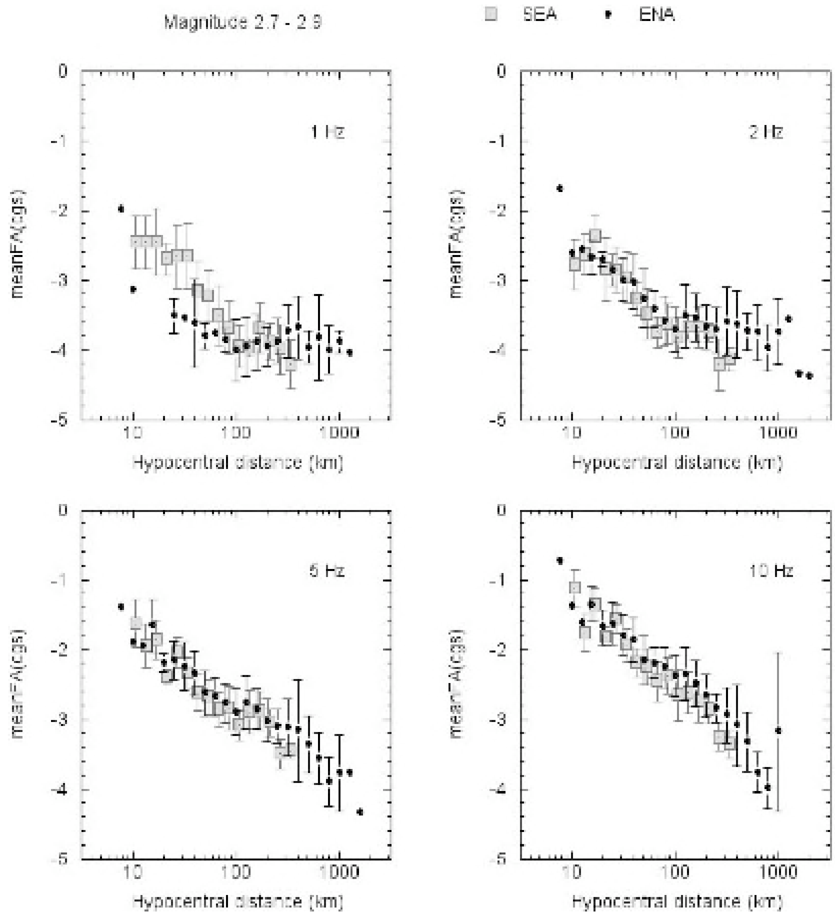

Figure 2. Mean Fourier acceleration spectral amplitudes, binned with distance, for M 2.8 ± 0.1. A small horizontal offset to the SEA distance values has been applied for plotting clarity.

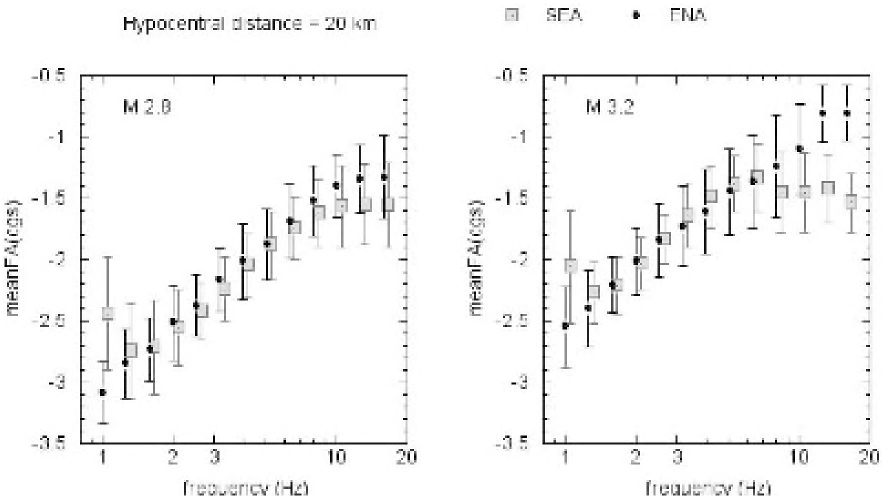

Figure 3. Mean Fourier acceleration spectra for data recorded within a hypocentral distance range of 20 to 35 km. Data are scaled to R = 20 km applying a geometrical spreading coefficient of R-1.3. A small horizontal offset has been applied to the SEA frequency values for plotting clarity.

Discussion

Previous studies suggested that attenuation in ENA is significantly less than that for other SCRs (e.g. Bakun and McGarr, 2002). This conclusion is correct over a large distance range (i.e. out to 1,000 km) when we compare SEA to ENA data. However, if we only consider data for R < 100 km, which is the critical distance range in terms of earthquake hazard and risk, we observe that there is no statistically significant difference in the source and attenuation properties of the respective SCR crusts. These observations are consistent with the studies of Allen et al. (in review) that compare predictive spectral models and demonstrate that ground-motion in ENA and SEA is fundamentally equivalent for sites at distances of R < 70 km for moment magnitudes 2.0 ≤ M ≤ 4.7.

Both regions are characterised by a trilinear attenuation model featuring an initial amplitude decay of $R^{-1.3}$ to a transition zone in which direct waves are joined by postcritical reflections from the Moho. The transition zones appear to take effect near R = 70 km in ENA and R = 90 km in SEA, suggesting differences in regional crustal structure. In these transitional zones, spectral amplitudes decay slowly at high frequencies, and demonstrate a slight increase with distance for low frequencies (Atkinson, 2004; Allen et al., in review). Beyond the transition zone, spectral amplitudes fall off again. Attenuation beyond the second transition distance in SEA appears to be greater than that of ENA. The high attenuation at larger distances is attributed to the well-established velocity gradient in SEA (Collins et al., 2003) that allows dispersion of Lg-wave energy into the upper mantle (e.g. Bowman and Kennett, 1991).

Conclusion

Through this simple statistical analysis, we can conclude that there is no significant difference in source characteristics of ENA and SEA earthquakes. Attenuation differences between the regions are significant, but only for distances greater than 100 km. SEA crust appears to be characterised by slightly larger kappa values (high-frequency attenuation) than ENA crust. Based on these observations, it is reasonable to use ENA and SEA earthquake ground motion data as "analogs" for each other, at least for hypocentral distances less than 100 km and frequencies less than 10 Hz. This is a key result, as it suggests that it is valid to derive a common ground-motion model based on combined data for these two regions. By merging the datasets, we have significantly increased the number of available ground-motion data from which to perform ground-motion studies. This is important in deriving more robust estimates of earthquake source and attenuation parameters for input into stochastic simulations of large damaging earthquakes, and in reducing the epistemic uncertainty associated with such models. It also implies that they may serve as generic predictive ground-motion models for other SCRs around the world.

Acknowledgements

The authors would like to acknowledge the generous contribution of ground-motion data from the members of the Australian National Committee of Large Dams (ANCOLD). We particularly acknowledge the efforts of Phil J. Cummins of ANCOLD, coupled with Wayne Peck and Gary Gibson of Environmental Systems and Services to gain support from Australian dam owners. The ENA ground motion data were provided by the Geological Survey of Canada.

References

Allen, T.I., P.R. Cummins, T. Dhu, and J.F. Schneider (in review). Attenuation of ground-motion spectral amplitudes in southeastern Australia, Bull. Seism. Soc. Am.

Allen, T.I., T. Dhu, P.R. Cummins, and J.F. Schneider (2006). Empirical attenuation of ground-motion spectral amplitudes in southwestern Western Australia, Bull. Seism. Soc. Am. 96, 572-585.

Atkinson, G.M. (2004). Empirical attenuation of ground-motion spectral amplitudes in southeastern Canada and the northeastern United States, Bull. Seism. Soc. Am. 94, 1079-1095.

Bakun, W.H., and A. McGarr (2002). Differences in attenuation among the stable continental regions, Geophys. Res. Lett. 29, DOI 10.1029/2002GL015457

Boore, D.M., and G.M. Atkinson (2006). NGA empirical ground motion model for the average horizontal component of PGA, PGV and SA at spectral periods of 0.1, 0.2, 1, 2, and 3 seconds, Interim Report for USGS Review, 50 pp. (http://peer.berkeley.edu/lifelines/repngamodels.html).

Bowman, J.R. and B.L.N. Kennett (1991). Propagation of Lg waves in the North Australian Craton: Influence of crustal velocity gradients, Bull. Seism. Soc. Am. 81, 592-610.

Campbell, K.W, and Y. Bozorgnia (2006). NGA empirical ground motion model for the average horizontal component of PGA, PGV and SA at selected spectral periods ranging from 0.01–10.0 seconds, Interim Report for USGS Review, 87 pp. (http://peer.berkeley.edu/lifelines/repngamodels.html).

Collins, C.D.N., B.J. Drummond and M.G. Nicoll (2003). Crustal thickness patterns in the Australian continent, in Evolution and Dynamics of the Australian Plate, R.R. Hillis and D. Müller (eds.), Geological Society of Australia Special Publication 22 and Geological Society of America Special Paper 372, 121–128 pp.

Gaull, B.A., M. Michael-Leiba, and J.M.W. Rynn (1990). Probabilistic earthquake risk maps of Australia, Aust. J. Earth Sci. 37, 169-187.

Jones, T.D., G. Gibson, K.F. McCue, D. Denham, P.J. Gregson and J.R. Bowman (1991). Three large intraplate earthquakes near Tennant Creek, Northern Territory, on 22 January 1988, BMR J. Aust. Geol. Geophys. 12, 339-343.

Mitchell. B.J., S. Baqer, A. Akinci, and L. Cong (1998). Lg coda Q in Australia and its relation to crustal structure and evolution, Pure Appl. Geophys., 153, 639-653.

Sadigh, K., C.Y. Chang, J.A Egan, F. Makdisi, and R.R. Youngs (1997). Attenuation relationships for shallow crustal earthquakes based on California strong motion data, Seism. Res. Lett. 68, 180- 189.

A seismic source zone model based on neotectonics data

Dan Clark

Geoscience Australia

Introduction

Australia's rich neotectonic record provides an opportunity to understand the characteristics of intraplate deformation, both at the scale of a single 'active' fault and at the scale of the entire continent. Over the last decade our knowledge of Australian intraplate faults has advanced significantly (e.g. Crone et al., 1997, 2003; Clark & McCue, 2003). Herein, six preliminary seismicity source zones spanning continental Australia, and based upon neotectonics data, are proposed. Each source zone contains active faults that share common recurrence and behavioural characteristics, in a similar way that source zones are defined using the historic record of seismicity. The power of this domain approach lies in the ability to extrapolate characteristic behaviours from well-characterised faults (few) to faults about which little is known (many). This data, and conceptual and numerical models describing the nature of the seismicity in each source zone, has the potential to significantly enhance our understanding of seismic hazard in Australia at a time scale more representative than the snapshot provided by the historic record of seismicity.

Australia's neotectonic record

Herein, an "active fault" is one which has hosted displacement under conditions imposed by the current Australian crustal stress regime, and hence may move again in the future. Similarly, "neotectonic deformation" is defined as deformation under conditions imposed by the current crustal stress regime. Estimates of 10-5 Ma for the establishment of the current crustal stress regime (e.g. Sandiford et al., 2004) are based upon several lines of evidence. A major unconformity related to uplift, gentle folding and reverse faulting of late Miocene strata in all southeastern Australian basins is constrained to the period 10-5 Ma (Dickinson et al., 2002; Sandiford, 2003), and Pliocene and Quaternary strata overlying this unconformity contain structures consistent with the current stress field. This time interval also corresponds to the initiation of the current phase of uplift in the Southern Alps of New Zealand (Sutherland, 1996) and in Papua New Guinea (Hill & Raza, 1999). Hence, neotectonic displacement is defined as faulting that has occurred in the last 10-5 Ma, and an "active" fault one that has hosted displacement since that time. In practice, the footprint of individual seismic events might only be recognisable in the landscape for several tens of thousands of years to a few hundreds of thousands of years. Consequently the vast majority of known active faults have hosted surface breaking earthquakes in the last 100 kyr.

Figure 1 presents the more than 200 instances of potential neotectonic deformation (predominantly active faults) compiled in the Australian Neotectonics Database at Geoscience Australia. The data have been collected as a result of analysis of DEMs, aerial photos, satellite imagery, geological maps and consultation with state survey geologists and a range of other earth scientists. Verifying the features as active faults is an ongoing process, but has thus far had a high success rate (e.g. Sandiford, 2003; Celerier et al., 2005; Clark, 2005; Quigley et al., 2006; Clark et al., in press; Estrada et al., this volume).

The catalogue of active faults varies in completeness as sampling is biased by the available datasets (e.g. DEMs, mine records, state survey records), by the extent of unconsolidated sedimentary cover on the surface, the rate of landscape processes relative to the rate of tectonic processes etc. Large swathes of northern Australia have not yet been examined. The catalogue is most complete in the southwest of Western Australia (Clark, 2005), where it might be expected that most surface ruptures relating to greater than Mw6.5 earthquakes having occurred in the last 100ka are represented. The Mount Lofty Ranges in South Australia is similarly complete, and perhaps also the Nullarbor Plain.

Less than a dozen faults, mainly from southern Australia, have been quantitatively examined to determine source parameters (e.g. timing of events, recurrence, magnitude, Fig. 2). Two important characteristics of Australian intraplate faults are revealed in the extant data:

1. recurrence of surface breaking earthquakes on a single fault is typical (ie. areas hosting active fault scarps are earthquake-prone).
2. temporal clustering of events apparent on some faults (ie. large earthquake recurrence in 'active' phases might be much less than during 'inactive' phases).

This is not the sum total of our knowledge as slip rates on faults can be estimated from offset units of known age without knowing about specific seismic events (e.g. Sandiford et al., 2003). Furthermore, if the data in Fig. 2 is combined with information such as the total displacement across faults in the current stress regime, fault length and distribution, relationship to contemporary seismicity, and to topography and landscape etc, the analysis can be taken further by grouping faults sharing common traits into domains.

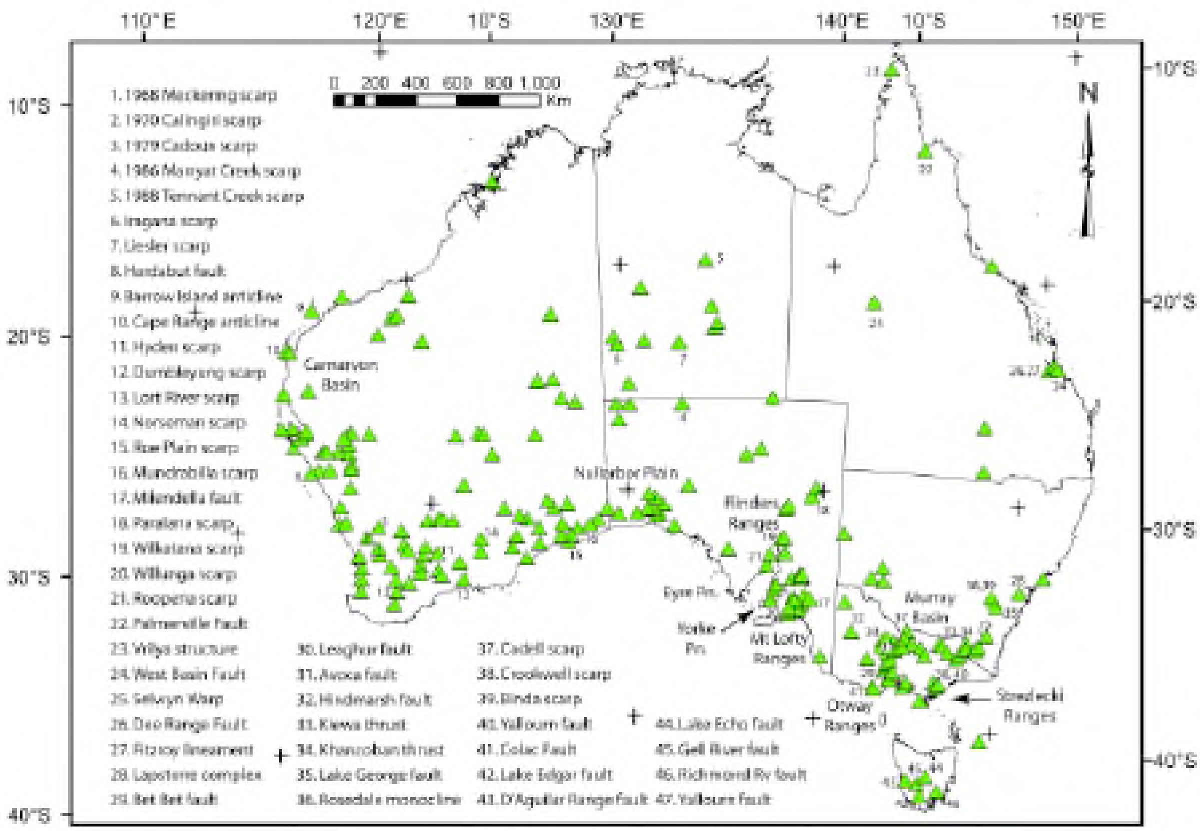

Figure 1. Location of neotectonic features from the GA Australian Neotectonics Database. A selection of the better known scarps have been named.

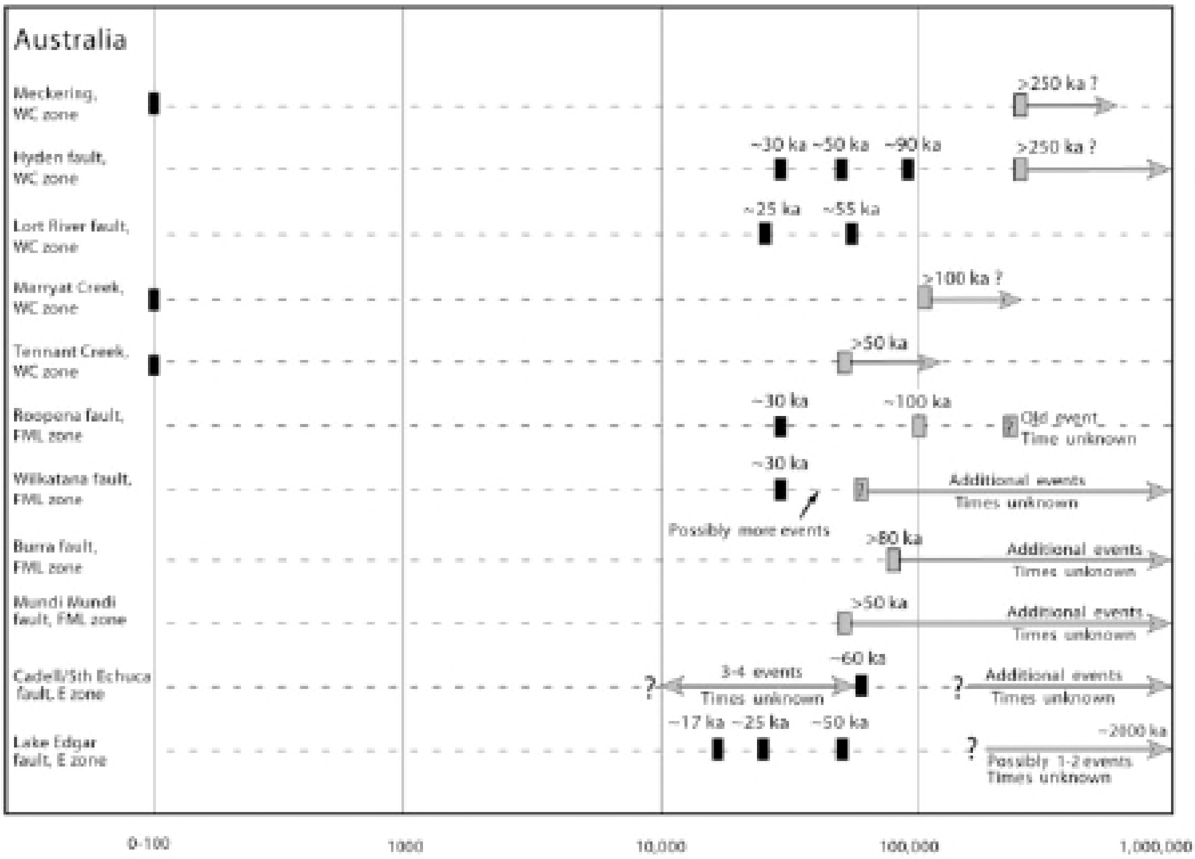

Figure 2. Recurrence data for Australian faults. WC=Western and Central domain, FML=Flinders/Mt Lofty Ranges domain, E=Eastern domain.

Preliminary Seismicity Source Domains based upon neotectonic data

A cursory examination of the landscape and faults in Western Australia and South Australia reveals a marked disparity in the crustal response to imposed stresses (Fig. 3). For example, active faults in Western Australia are typically widely spaced, are not associated with historic seismicity and displace a low undulating landscape by less than 10 m (Fig. 3a). In contrast, faults in the Mt Lofty Ranges are closely spaced, are commonly associated with historic seismicity, and host neotectonic displacements of up to a couple of hundred metres (Fig. 3b).

A summary of the fault characteristics data from across Australia is presented in Table 1. The primary thesis of this study is that Australia may be divided into a number of domains which are distinguished by differing active fault characteristics (Fig. 4). To a large degree the differing active fault characteristics may be related to gross geologic setting (e.g. Archaean craton cf. Proterozoic mobile belt cf. Palaeozoic/Mesozoic arc complex). A consequence of this is that data from a Western Australian fault may not necessarily be directly applied to understand the rupture behaviour of an eastern Australian fault.

In general, known active fault density is low in the Western and Central and Nullarbor domains, high in the Flinders/Mt Lofty Ranges Domain, and intermediate in the Eastern Australia Domain. Neotectonic displacements on individual active faults are typically in the order of ten metres or less in the Western and Central Domain, less than a few tens of metres in the Nullarbor Domain, and up to a couple of hundred metres in the Flinders/Mt Lofty and Eastern Australia domains. A belt of faults with anomalously large displacements for the Western and Central Domain (several tens of metres) occurs in the Carnarvon Basin. These faults fringe the Archaean Yilgarn and Pilbara cratons which may focus strain in this belt. Active fault length is variable within domains and is not diagnostic between domains. Faults longer than 50 km occur in each domain, suggesting that earthquakes of greater than Mw7.0 are possible Australia wide.

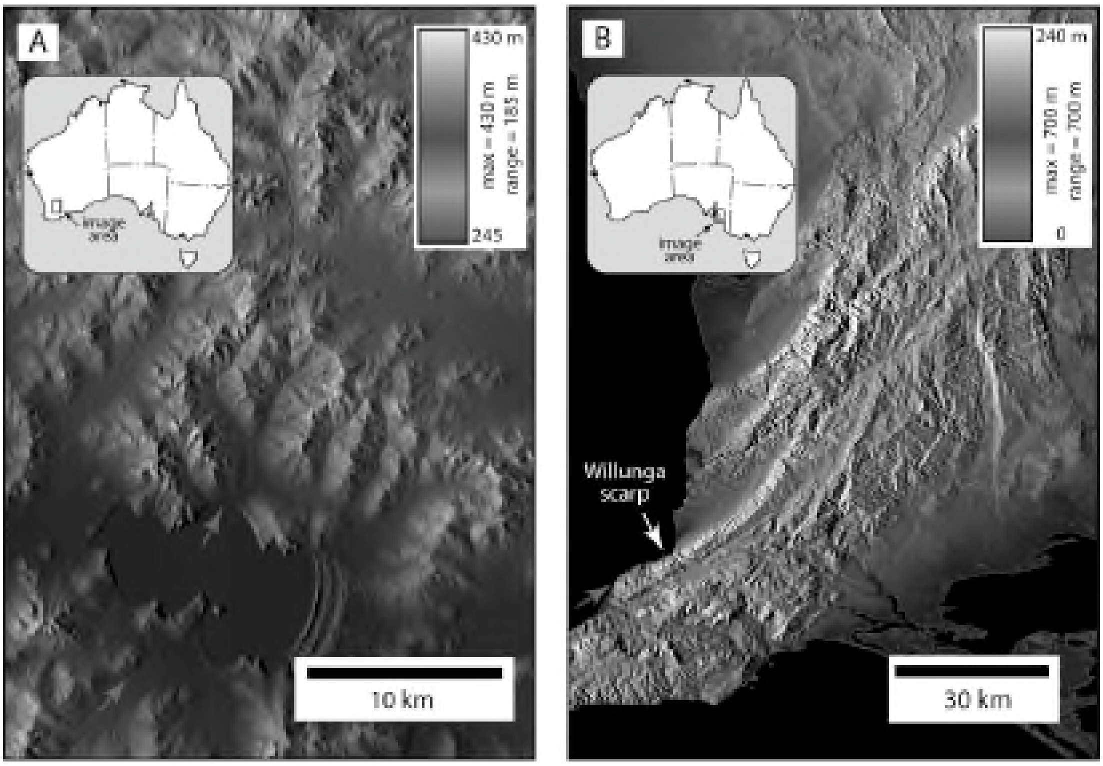

Figure 3. Colour draped shuttle radar 90 m digital elevation model images. (A) Dumbleyung Fault scarp, wheatbelt southwest Western Australia. (B) the Willunga Fault scarp, western range front of the Mt Lofty Ranges, South Australia.

Earthquake recurrence appears to be highly temporally clustered in the Western and Central domain, with events in active periods being separated by several tens of thousands of years, and intervening quiescent periods lasting hundreds of thousands to millions of years. Temporal clustering of events also seems likely for faults on the western margin of the Flinders/Mt Lofty Ranges Domain, but recurrence may be more regular for the faults associated with the greatest uplift in the domain (e.g. Wilkatana Fault, Quigley et al., 2006). The one fault for which data is available in the Eastern Australia domain, the Cadell Fault, demonstrates very marked temporal clustering of events. Three periods of activity since the mid Eocene are imaged in seismic data, each building several tens of metres of relief. The last (current?) period of activity generated 15 m of relief in the last 60 ka, indicating a slip rate for periods of activity at least two orders of magnitude greater than the long term slip rate. Only in the Flinders/Mt Lofty Ranges Domain is there compelling evidence for significant relief relating to active faulting (ie. range building). This domain also bears the clearest relationship between contemporary seismicity and active faulting (with the exception of the five historic surface ruptures in the Western and Central Domain). In most domains, the bulk of active faults are not associated with contemporary seismicity. The Queensland Domain is too poorly known to meaningfully characterise at present.

Table 1 Characteristic of active faults and their relationship to the record of seismicity in the five domains.

Neotectonic region	Western and central Australia[§]	Nullarbor	Flinders/Mt Lofty Ranges	Queensland	Eastern Australia	Tasmania[#]
Completeness of active fault dataset	high in SW, low elsewhere	moderate	high in Mt Lofty and northern Flinders Ranges, moderate elsewhere	low	moderate to high in victoria, moderate to low elsewhere	low
Number of known active faults[*]	~80-100	5-15	20-30 (a dozen more occur on the Eyre and Yorke peninsulas)	<5	~50-70[^]	~5
Relative density of known active faults	low to moderately high	low	moderate to high	very low	low to high	moderate
Relationship between active faults to building of ranges	no relation between active faults and large-scale topography, except perhaps in the Carnarvon Basin	no relation between active faults and subdued large-scale topography	ranges bound by active faults	no relation between active faults and large-scale topography	typically no relation between active faults and large-scale topography, but locally some active faults do bound ranges	typically no relation between active faults and large-scale topography, but locally some active faults do bound ranges
Relative historic seismicity rate	moderate to high in SW, low elsewhere	very low	high	very low	moderate	moderate
Relationship of historic seismicity to known active faults	concentrated where there have been historic surface ruptures, rarely associated with pre-historic fault scarps	no association with pre-historic scarps	well defined belt of high seismicity, locally associated with pre-historic fault scarps	no association with pre-historic scarps	no clear association with pre-historic fault scarps	no clear association with pre-historic fault scarps
Post ca. 9 Ma displacement on known active faults	10 m or less	10 m or less	many with displacements up to ~100 m	less than 10 m ?	many less than 10 m, some up to 100 m	some less than 10 m, some up to 100 m
Number of post ca.10 Ma ruptures on an individual fault	<4	no data	many	no data	few to many	few to many
Examples	Hyden, Meckering, Lort River	Roe Plain, Mundrabilla	Wilkatana, Roopena	Palmerville	Khancoban, Cadell, Lake George	Lake Edgar, D'Aguilar Range

[*] most regions are under explored, and the level of study is not homogeneous within and between regions. For example, large areas of NW Western Australia are shown as having no active faults. This may largely be a consequence of the area having not been studied.
[#] subset of eastern Australia neotectonic region
[§] relationships based upon the better-studied SW portion of this region
[^] several features in Victoria are based upon subsurface mine records of faulted Late Tertiary (10-3 Ma) basalts, where faulting has no surface expression. Further records associate concentrations of small earthquakes with large scarps.

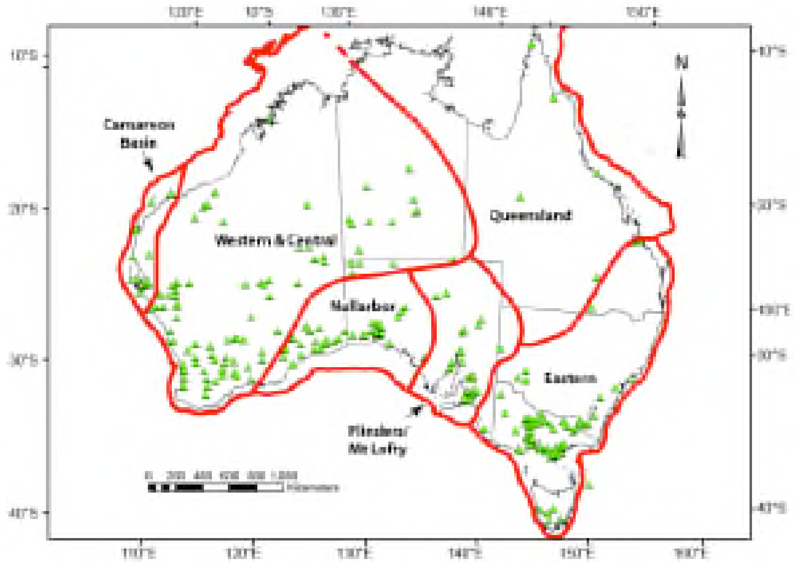

Figure 4. Preliminary neotectonic source domains. Outer boundary is the 200 m isobath. Future refinements will concentrate on refining the basis for the domains with additional neotectonic information. For example, the Queensland domain is almost completely unquantified. The eastern coast of this domain is similar in landscape character to parts of the Eastern domain. Similarly the central Australian orogenic belts (Arunta, Musgrave, Strangways) are of similar geologic character to the seismogenic basement beneath the Nullarbor domain, potentially requiring a redefinition of boundaries.

Discussion: Applications to seismic hazard assessment

In general, Australia is under-explored in terms of its neotectonic record. As a consequence, important conclusions regarding the seismic activity of a region and the characteristics of faults within a region are necessarily based upon incomplete data. However, neotectonic data, and the neotectonic source domains proposed above, has the potential to contribute to seismic hazard assessment in a number of important ways.

1. Improved source parameters for seismicity-based source zones, and a neotectonics-based seismicity source zone map

Neotectonics data provides information about the larger infrequent earthquakes that dominate the moment release budget. Consideration of active fault scarp height and length provides robust estimates of Mmax, and palaeoseismological investigations provide recurrence data. Active fault magnitude-recurrence data for the southwest of Western Australia (Clark, 2005) has already been combined with data from the historic record of seismicity to generate a Gutenberg-Richter relationship which extends out to magnitude Mw7.5 (Leonard & Clark, this volume). The a and b values derived thereby might be applied to the entire Western and Central Source Domain. A similar exercise might be undertaken in other domains as further neotectonics data becomes available, thereby generating a neotectonics seismicity source map that might be included in a weighted logic tree containing seismicity based source zone models for generation of the next national seismic hazard map. Such neotectonics-based models might be expected to better reflect the long-term pattern of seismicity than those based upon the historic record, and hence are appropriate for consideration when designing or assessing critical infrastructure.

In addition, earthquake prone regions may be defined based upon the presence of active fault scarps upon which recurrence can be demonstrated, potentially affecting the background value of hazard for seismicity-based source zones.

2. Active fault source zones for use in the national hazard map

Faults with well understood activity (e.g. Lake Edgar, Cadell) will be included into the next generation hazard model by defining small source zones around the faults which accommodate the larger (>~M6) earthquakes, surrounded by a general zone which accommodates the smaller earthquakes. Parameters from known faults might be extrapolated to faults within the same neotectonic source zone inferred to be active but lacking in detailed recurrence information. Palaeoseismicity data from a representative suite of faults from each source zone will be required to assess the validity of such extrapolations.

3. Active fault source zones for site specific hazard assessment.

A limited number of rupture scenarios have been run for well-characterised active faults (e.g. Cadell Fault, Echuca; Morwell Fault, La Trobe Valley; Lapstone Fault, western Sydney) in order to assess the impact of a recurrence of an event in the palaeo-record (e.g. Dhu et al., 2006). The results indicate impacts of far greater magnitude than those experienced as a result of events in the historic catalogue (e.g. the 1989 Newcastle event). For example, a simulated rupture of the Cadell Fault, generating a Mw7.2 earthquake has been modelled as causing greater than 50% total loss over a 6800 km2 area.

4. Modelling of hazard based upon neotectonic seismicity models and strain rate data.

An alternative approach, perhaps further from realisation, involves the development of hazard maps largely independent of historic seismicity data by using neotectonics data as constraint on numeric crustal strain models. If each active fault is modelled using a generic (or specific) behaviour model derived from the available palaeoseismological data, then a hazard map for larger events might be constructed using the appropriate neotectonics seismicity model for the domain in which the faults occur (ie. uniform strain distribution at long time frames in the Western and Central Domain, Clark, 2005). For the southwest of Western Australia, a model of uniform fault distribution may be adopted with a fault behaviour model involving temporal clustering of events. Each event would collectively sum to a strain rate estimated from GPS, seismic moment release, or finite element crustal strain modelling, with constraint from the landscape character (ie. mountain ranges are not building). Similar scenarios may be run for the Flinders Ranges neotectonic source zone, based upon the neotectonic seismicity model of Celerier et al. (2005).

Conclusions

The neotectonics source zones proposed in this paper are a first attempt to group active faults of like characteristics. With more paleoseismic data (to capture variability in source behaviour) and refinement of neotectonic source zones, extrapolations may be made from well-known faults to other faults, and models describing the long term seismic behaviour of the Australian crust developed. The potential exists thereby to overcome the limitations of the short historic record of seismicity in Australia, upon which all current hazard assessments are based.

References

Celerier J., Sandiford M., Hansen D.L. and Quigley M., 2005. Modes of active intraplate deformation, Flinders Ranges, Australia. Tectonics 24, doi:10.029/2004&C001679.

Clark D.J. and McCue K., 2003, Australian Palaeoseismology: towards a better basis for seismic hazard estimation: Annales of Geophysics, 46, 1087-1105.

Clark D., 2005. A preliminary seismicity model for southwest Western Australia based upon neotectonic data. Proceedings of the Australian Earthquake Engineering Society 2005 meeting, Albury Australia. Paper 22, 1-6.

Clark D.J., Cupper M., Sandiford M., and Kiernan K., 2004, Style and timing of late Quaternary faulting on the Lake Edgar Fault, southwest Tasmania, Australia: implications for hazard assessment in intracratonic areas: Geological Society of America Special Publication, in press.

Crone A J, Machette M N, and Bowman J R, 1997, Episodic nature of earthquake activity in stable continental regions revealed by palaeoseismicity studies of Australian and North American Quaternary faults.: Australian Journal of Earth Sciences, 44, 203-214.

Crone A J, de Martini P M, Machette M N, Okumura K, and Prescott J R, 2003, Paleoseismicity of aseismic Quaternary faults in Australia Implications for fault behaviour in stable continental regions: Bulletin of the Seismological Society of America, 93, 1913-1934.

Dhu T, Robinson. D., McPherson A. Leonard M., Sinadinovski C., Cummins P. & Schneider, J., 2006. Earthquake Risk in Australia. Proceedings Volume of the Australian Earth Science Convention 2006. Melbourne, Australia. p144.

Dickinson J.A. Wallace M.W., Holdgate G.R., Gallagher S.J. and Thomas L., 2002. Origin and timing of the Miocene–Pliocene unconformity in southeast Australia. Journal of Sedimentary Research, 72, 288-303.

Estrada B., Clark, D., Wyrwoll K.-H. & Dentith M., 2006. Palaeoseismic investigation of a recently identified Quaternary fault in Western Australia: the Dumbleyung Fault, this volume.

Hill K.C. and raza A., 1999. Arc-continent collision in Papua New Guinea: constraints from fission track thermochronology. Tectonics, 18, 950-966.

Leonard. M. & Clark D., 2006. Reconciling neotectonic and seismic recurrence rates in SW WA., this volume.

Quigley, M., Cupper, M., Sandiford, M, 2006. Quaternary faults of southern Australia: palaeoseismicity, slip rates and origin. Australian Journal of Earth Sciences 53, 285-301.

Sandiford M, 2003. Neotectonics of southeastern Australia: linking the Quaternary faulting record with seismicity and in situ stress: In: eds Hillis R.R. & Muller D, Evolution and dynamics of the Australian Plate, Geological Society of Australia Special Publication 22, 101-113.

Sandiford, M., Wallace, N., Coblentz, D, 2004. Origin of the in situ stress field in southeastern Australia, Basin Research 16, 325-338.

Sutherland R., 1996. Transpressional development of the Australia-Pacific plate boundary through southern South Island New Zealand: constraints from Miocene-Pliocene sediments, Waiho-1 borehole, South Westland. New Zealand Journal of Geology and Geophysics 39, 251-264.

Structural condition assessment from recorded earthquake response data

Wirtu L. Bayissa[1], Nicholas Haritos[1] and Sven Thelandersson[2]

[1] The University of Melbourne
[2] Lund University, Sweden

Abstract

Monitoring of changes in vibration response has been widely used for assessment of structural integrity, performance and safety. In particular, on-line health monitoring and diagnostic assessment of critical infrastructure becomes vital after the occurrence of extreme events such as earthquakes and blast loads. However, it is found difficult, if not impossible, to characterize structural condition and detect time-varying, non-stationary spectral characteristics using the traditional frequency spectrum analysis method. In this paper, a wavelet signal analysis technique is implemented for post-earthquake damage assessment directly from recorded response data. The results obtained from numerical simulations and real response data from moderate to severe earthquakes indicate that wavelet analysis is a powerful tool that can be used to identify hidden transient characteristics and high energy bursts that may occur due to progressive structural stiffness degradation and/or pounding between structural components. The appearance of multiple closely spaced transient peaks in the details of the wavelet decomposition coefficients is used for the assessment of the occurrence of progressive damage in the structural system. Finally, the structural response behavior during earthquake excitation is characterized from a critical investigation of the details of the local high frequency signal energy variations in the time-frequency domain.

Introduction

The occurrence of high dynamic loading events such as earthquakes and blast loading may cause damage to civil engineering structures, including microcracking, flexural cracking, shear and bond slippage, crushing of concrete and yielding of reinforcement. Visual inspection of these types of damage may not be reliable to establish condition states of structural integrity and safety. In the last few decades, vibration-based non-destructive damage identification and health monitoring techniques have been widely used in the areas of aerospace, automotive, civil and mechanical engineering (Doebling et al, 1996). The majority of these techniques are based on common simplifying assumptions regarding structural linearity and response stationarity and require two sets of measurements, one from each of the undamaged and possible damaged states in order to achieve the desired results. However, for cases involving time-varying processes and nonlinear damage mechanisms, such as breathing cracks, sudden loss of stiffness and damage in composites, traditional fast Fourier transform (FFT) based damage identification methods are no longer effective.

In this application oriented paper, the use of a wavelet analysis approach is proposed for post-earthquake damage condition assessment and response characterization directly from acceleration response records. Wavelet analysis is a novel signal analysis tool which has been widely used in numerous fields of study (earth science systems, engineering geophysics, medical physics, astronomy, remote sensing) for signal processing, pattern recognition and image compression. In the past, wavelet analysis has been extensively applied for characterization of a non-stationary signal, denoising, nonlinear system identification and detection of transients (Brenner, 2003; Basu and Gupta, 1997; Gurely and Kareem, 1999); machine condition monitoring and fault diagnostics (Peng and Chu, 2004); structural damage detection and long-term health monitoring (Hou et al, 2000; Kim and Melhem, 2003; Moyo and Brownjohn, 2005). These studies demonstrate the strong promise that wavelets offer to a wide range of studies. However, their application to practical problems such as post-earthquake condition assessment is not yet fully exploited. In this regard, this paper demonstrates the application of wavelet analysis on simulated data and earthquake records, in particular.

The wavelet transforms

Signal analysis using wavelet transforms involves decomposition of a one-dimensional time series signal into two-dimensional time-frequency space by using a series of basis functions of the translated (shifted) and dilated (stretched) analyzing (or mother) wavelets. Detailed information regarding the theoretical treatment of wavelets is given in Daubechies (1992). In general, wavelet transforms can be applied in two ways: the continuous wavelet transform (CWT) or the discrete wavelet transform (DWT). The CWT is defined as the sum over all time of the signal multiplied by a scaled, shifted version of the wavelet function, as follows:

$$Q(\alpha,\beta) = \frac{1}{\sqrt{\alpha}} \int_{-\infty}^{\infty} y(t)\psi^*\left(\frac{t-\beta}{\alpha}\right)dt \qquad (1)$$

where wavelet coefficients, Q, represent a regression of the signal $y(t)$ on the wavelet. α and β are the scale index (dilation factor) and the translation factor (or time shifting), respectively. ψ^* is the complex conjugate of the mother wavelet. Similarly, DWT can be defined mathematically using the discrete wavelet function and the associated scaling function.

Finally, wavelet transforms-based features that have significant areas of application, such as wavelet power spectrum (WPS), wavelet cross power spectrum (WCS) and wavelet coherence (WCO), can be defined as follows (Torrence and Compo, 1998):

$$WPS(\alpha) = \left|Q(\alpha,\beta)\right|^2 \qquad WCS(\alpha) = \left|Q(\alpha,\beta)^X\, Q^{Y*}(\alpha,\beta)\right|$$
$$WCO(\alpha) = \frac{\left(s\alpha^{-1}WCS(\alpha)\right)^2}{s\left(\alpha^{-1}WPS^X(\alpha)\right).s\left(\alpha^{-1}WPS^Y(\alpha)\right)} \qquad (2)$$

where WPS finds regions of high power in the time-frequency domain; WCS reveals areas of high common power and phase relationship of two processes; WCO provides normalized correlation and phase locked behavior of two processes; and s is a smoothing operator.

Simulation studies

Identification of breathing crack condition in a SDOF system

In this section, the merit of using wavelet transforms over FFT based methods is demonstrated with respect to localization of breathing cracks and their associated

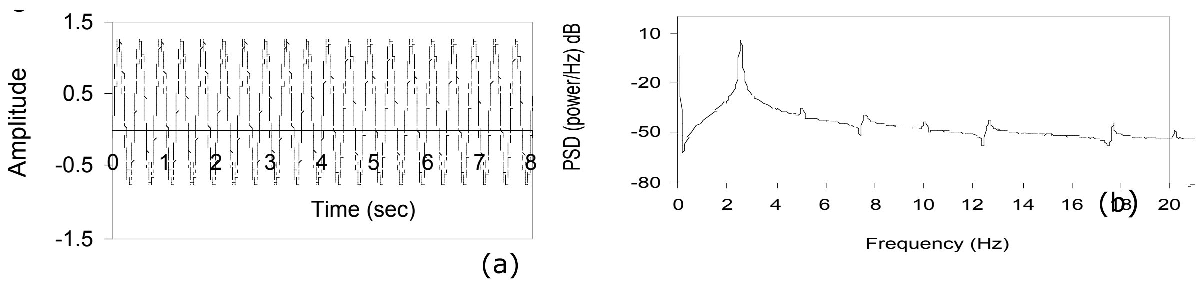

Figure 1 Free vibration response analysis of undamped SDOF bilinear system: (a) piece-wise linear time record; (b) power spectral density in decibel scale.

frequencies. The simulation of the breathing crack condition is conducted using a piecewise linear time record based on a bilinear stiffness model in a single degree of freedom (SDOF) system. The response time series and its spectral density are presented in Figure 1. The occurrence of high frequency harmonics at integer multiples of the fundamental frequency is attributed to nonlinearity caused by the breathing crack. However, this result does not give any indication of location of these harmonics in time space. Therefore, further investigation is conducted using DWT and CWT (see Figure 2).

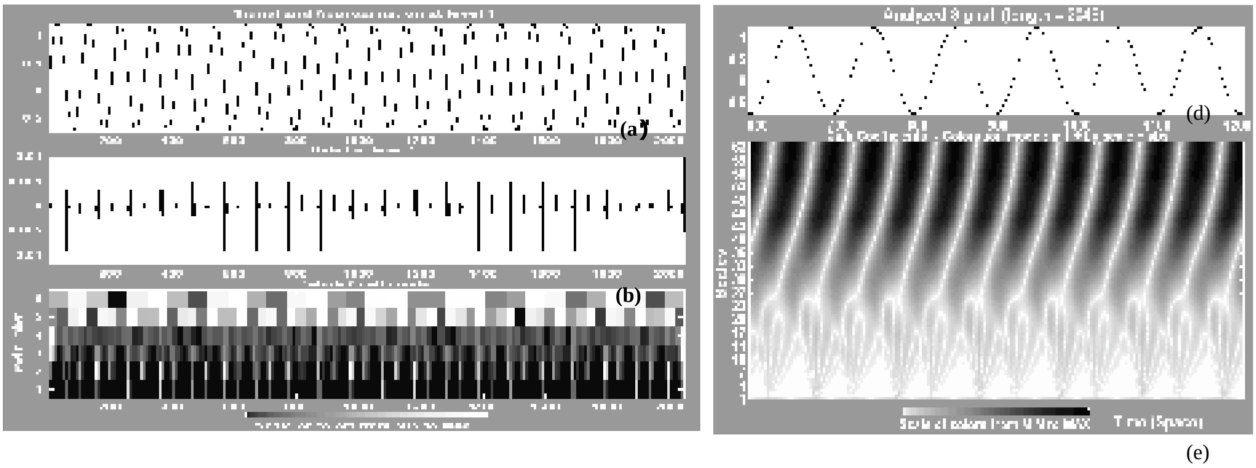

Figure 2 (i) DWT: (a) time series; (b) details at level 1; (c) details coefficients; and (ii) CWT (zoomed view): (d) time series; (e) CWT coefficients.

The details at level 1 of DWT conducted using Daubechies wavelet (db8) at level 6 show a series of spikes at the exact locations of the discontinuities; which is attributed to high frequency impulsive events at the crack interface due to the breathing crack condition (Figure 2 (b)). Moreover, the detail coefficients at the highest octave (level 1) provide the locations of the spikes and the consistent reduction in the ridge widths from higher to lower levels indicate the harmonics are the integer multiples of the fundamental frequency (Figure 2 (c)). Moreover, the CWT coefficients determined using db8 show a single ridge at higher scales (or lower frequencies) and multiple ridges at lower scales (or higher frequencies) which indicates the occurrence of higher harmonics breathing crack (Figure 2 (e)).

Identification of stiffness degradation in SDOF system

In this section, DWT is conducted on acceleration response data to detect and localize progressive stiffness degradation. First, inelastic dynamic analysis is performed on a SDOF system subjected to cyclic loading using a modified Takeda degrading stiffness hysteresis model (Figure 3 (a)). Second, DWT is conducted on the acceleration data using db8 at level 4 which clearly shows a series of spikes at level 1 details (Figure 3(b)). The locations of these spikes in time space are found to be in a close agreement with the stiffness history curve (Figure 3(c)).

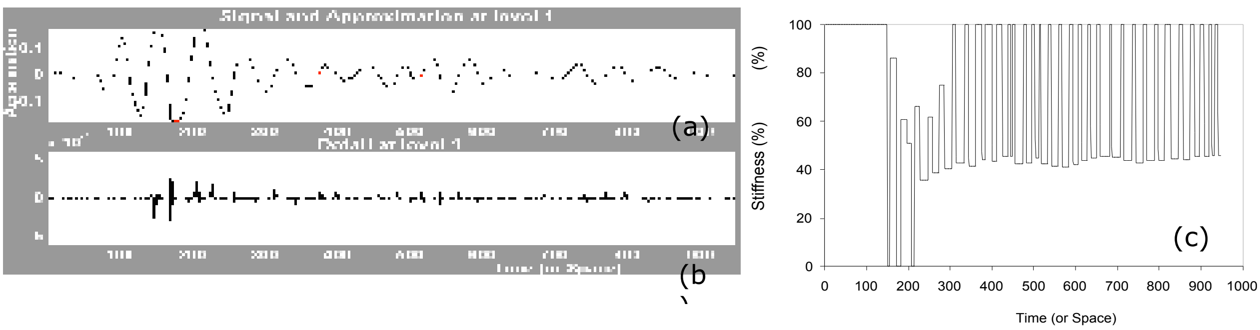

Figure 3 DWT of the acceleration response: (a) acceleration response; (b) details at level 1; (c) stiffness time-history.

Case studies using earthquake records

Los Angeles 54-story building (LA54) subjected to 1994 Northridge earthquake

This study uses acceleration response records at 20 measurement points with a sampling interval of 0.01sec and a sampling length of 180 sec to produce 18001 data points per record as shown in Figure 4 (Ventura et al, 2001). First, modal parameters are extracted for the first 8 modes using the Enhanced Frequency Domain Decomposition (EFDD) option of the ARTeMIS Extractor® software (Table 1). Second, structural damage condition assessment is conducted using DWT of the acceleration record at the top of the building (ART) (Figure 5). The DWT tree for the 50 Hz signal is given in Table 2. Third, to look for any sign of nonstationarity for signal power and period with time and height of the building, the CWT is conducted using the Morlet wavelet on the acceleration record at the base of the building (ARB) and ART. Consequently, the WPS for both ARB and ART and the WCS and WCO between the ARB and ART were computed and presented in the time-period domain in Figure 6 and Figure 7, respectively.

(i) *Discussion on DWT Analysis*: The DWT details coefficients at level 1 of Figure 5 (b) show closely spaced short lived spikes which correspond to the higher frequency octaves. These observations clearly indicate impulsive and/or major rocking events that may have occurred during the early stage of the earthquake. Moreover, the detail coefficients in Figure 5 (c) reveal variations of the dominant modes for different frequency bands as shown by the dark color. At the early stage of the ground motion, transients and the clamped nature of the signal power were observed. This indicates that at early stage of the ground motion, the vibration response is mainly due to the higher frequency modes. However, the lower frequency components in levels 8 to 9 were largely stationary for most of the duration.

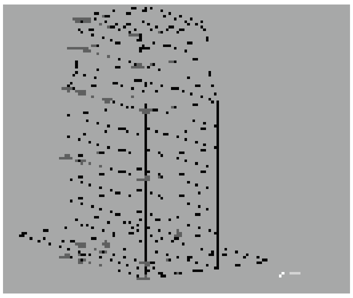

Figure 4 Building geometry and positions of transducers.

Table 1 Modal parameters of LA54 building

Mode No.	Frequency (Hz)	Period (sec)	Mode No.	Frequency (Hz)	Period (sec)
1	0.167	5.988	5	0.537	1.862
2	0.197	5.076	6	0.821	1.218
3	0.361	2.770	7	1.167	0.857
4	0.498	2.008	8	1.475	0.678

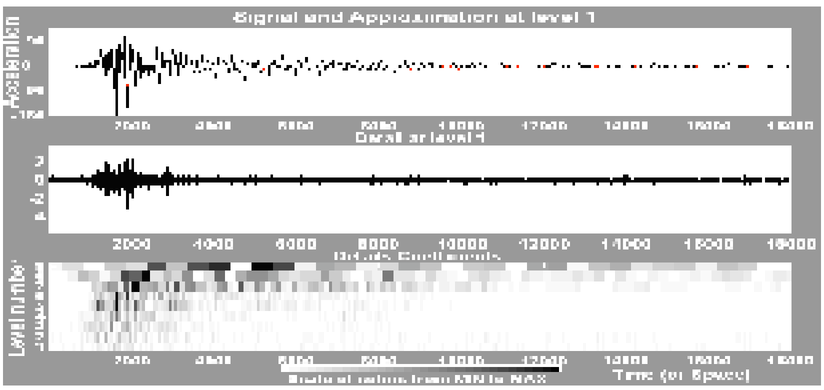

Figure 5 DWT of the Northridge Earthquake ART: (a) time series; (b) details at level 1; (c) details coefficients for different frequency bandwidths.

Table 2 DWT tree for 50 Hz

Level No.	Frequency bandwidth (Hz)
1	25-50
2	12.5-25
3	6.25-12.5
4	3.125-6.25
5	1.5625-3.125
6	0.781-1.5625
7	0.391-0.781
8	0.195-0.391
9	0.098-0.195

(ii) *Discussion on CWT Analysis*: The cone of influence shown by the parabolic curve in Figures 6 and 7 demarcate the boundary for edge effects, where any results below the curve are considered dubious. The dark grey color (or reddish in color format) enclosed with black contour lines represents the dominant power of the processes with 95% confidence level while the light grey color (or yellowish in color format) outside the contour line indicates moderate power and the rest show low power. Figure 6 (a) and (b) show common features as well as significant differences between the two power spectra in terms of the variations of high power with time and amplitude modulation across the height of the building. Figure 6 (b) indicates that during the intensive stage of the earthquake, the building response was mainly dominated by the higher frequency vibration modes and following the intensive shaking, the lower modes controlled the response of the structure. These results have significance in the context of wider application. For example, in the case of natural input experimental modal analysis, the assumption that the excitation is stationary is not so reasonable. Moreover, the appearance of time-varying signal power for ART has influence on the design of structures since earthquake excitation causes variations in response amplitudes and frequencies both within the time and space domains.

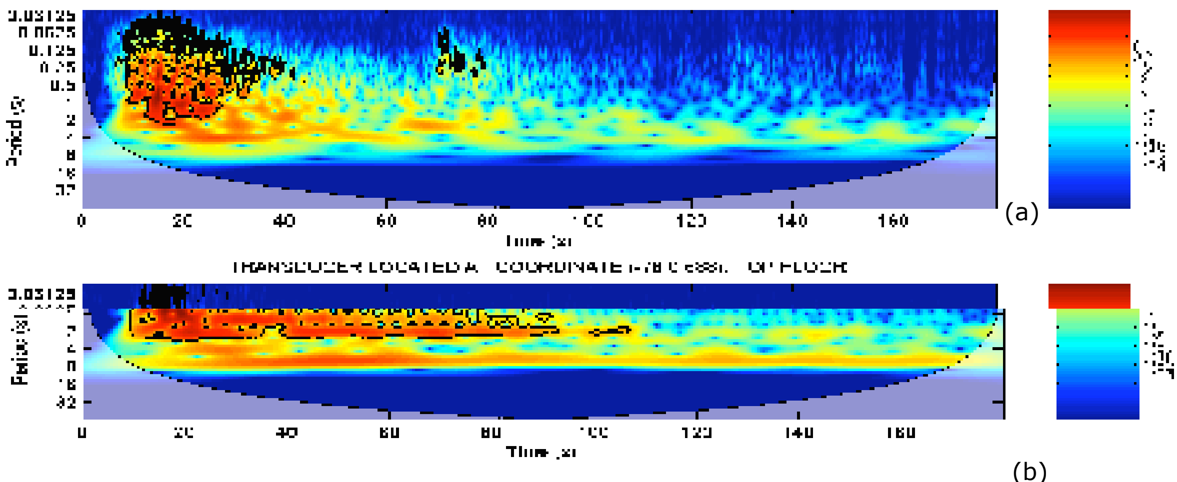

Figure 6 Contour plots of WPS: (a) ARB; (b) ART.

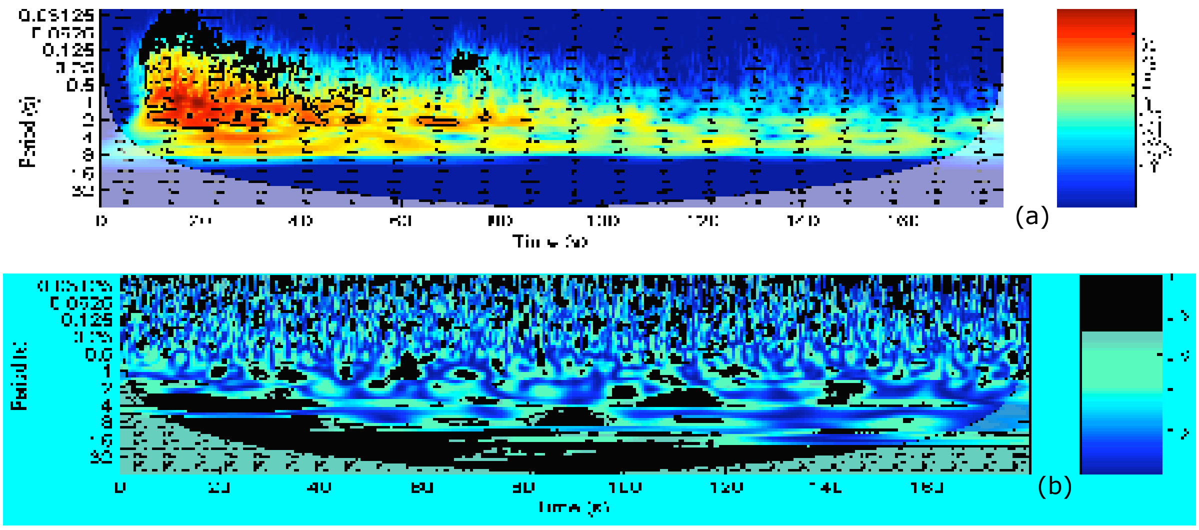

Figure 7 Contour plots of (a) WCS of the vibration data on the ground floor level against the top floor; (b) WCO between the vibration data on the ground floor level and top floor.

On the other hand, the WCS and WCO of ARB and ART are presented in Figure 7 (a) and (b), respectively. The relative phase relationship between the two processes is shown using arrows (where in-phase is pointing right, anti-phase is pointing left, ART leading ARB by 900 is pointing straight down). In Figure 7 (a) and (b), the light grey color (red in colored format) enclosed with black contour lines show areas of high common power and high coherence of the two processes at the 95% confidence level, respectively. While the WCS shows high common power at lower period bands of 0.125 to 2.75 seconds and at the early stage of the ground motion, WCO indicates negligible degree of correlation of the two processes at these locations. Instead, a significant coherence is observed for regions outside the area with significant common power and in the period bands of 1 to 8 seconds (Figure 7 (b)).

DWT of the ground motion records: Friuli earthquake M (6.4) and Imperial Valley earthquake in the 1940 at El Centro M (7)

The DWT of the Friuli and El Centro ground motion records are presented in Figure 8 (i) and (ii), respectively. The DWT results of the Friuli earthquake reveal the occurrence of stationary Gaussian white noise at high frequency band (Figure 8 (b) and (c)). This is evident from the property of the time trace at level 1 details, where the energy variation with time at level 1 of the detail coefficients is largely uniform (Figure 8 (c)). This shows that there is no sign of damage at this particular location during the Friuli earthquake. On the other hand, the DWT details of the El Centro ground motion record at level 1 show a series multiple spikes during the early stage of the ground motion (Figure 8 (e)). Figure 8 (f) also shows that these spikes correspond to the high frequency bandwidths or lower level details coefficients. Therefore, it can be concluded that there is enough indication to suggest progressive damage and/or that high energy impulsive events have occurred during the earthquake concerned.

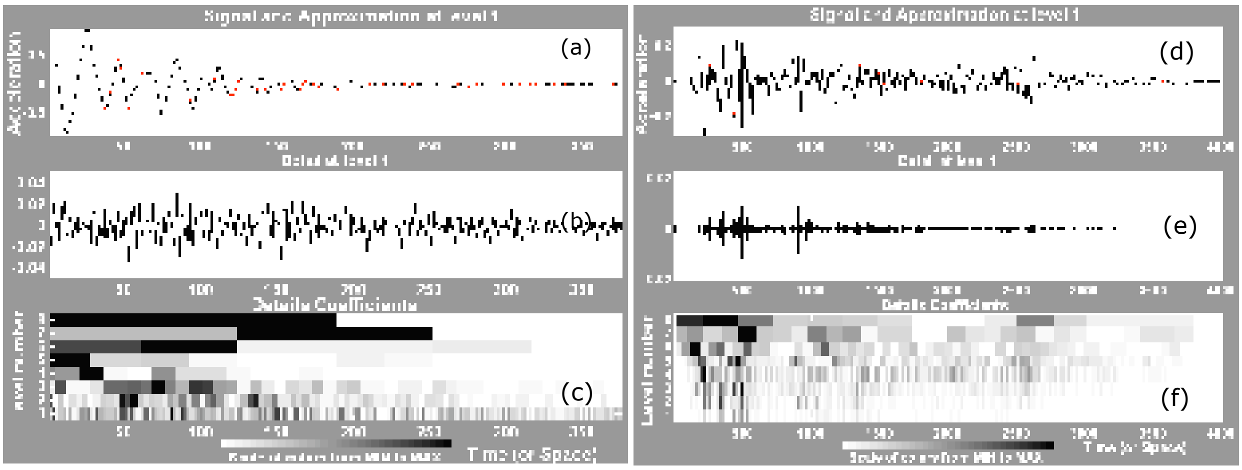

Figure 8 DWT of (i) Friuli earthquake: (a) time series; (b) details at level 1; (c) details coefficients; (ii) Imperial Valley earthquake at El Centro: (d) time series; (e) details at level 1; (f) details coefficients.

Conclusions

This paper presents wavelet analyses for condition assessment/damage detection after occurrence of extreme events by using earthquake ground motion records, directly. Unlike the Fourier transform, the wavelet analysis schemes adopted provide the capability to examine localized features of a larger signal through multiple levels of details and approximations of the original signal to determine the instantaneous changes in a real-time manner, including detection of sudden loss of stiffness, impulsive events due to breathing crack conditions, assessment of progressive cracking in structural mechanisms and differentiation of impulsive events from random noise. Moreover, features extracted from wavelet transforms were used to characterize the dominant modes of variations of power and frequency with time and space, including areas of significant high common power; phase relationship; and degree of correlation of the earthquake records at the base and top of a building.

Finally, the results and techniques presented in this study may contribute to development of post-earthquake integrity assessment strategy for in-service structures and for understanding structural response behavior when structures are subjected to nonstationary random processes.

Acknowledgement

The principal author wishes to acknowledge support from The University of Melbourne (sponsoring institution) and Lund University, Sweden, (host institution) under the Solander Travel Award program, which helped initiate the work performed towards this paper. The authors would also like to acknowledge: Professor Carlos Ventura, University of British Colombia (Canada), for providing the measurement data from LA54; C. Torrence and G. Compo for the Matlab software used to perform WCS and WCO; Elisa Lumantarna, the University of Melbourne, for providing data from the nonlinear dynamic analysis.

References

ARTeMIS Extractor 3.5 User's Manual, Structural Vibration Solutions A/S, Denmark.

Basu, B.B. and Gupta, V.K. (1997) Non-stationary seismic response of MDOF systems by wavelet transform, *Earthquake Engineering and Structural Dynamics*, Vol 26, pp 1243-1258.

Brenner, M.J. (2003) Non-stationary dynamics data analysis with wavelet-SVD filtering, *Mechanical Systems and Signal Processing*, Vol 17, pp 765-786.

Daubechies, I. (1992) Ten Lectures on wavelets, Society for Industrial and applied mathematics.

Doebling, S.W. Farrar, C.L. Prime, M.B. and Shevitz, D.W. (1996) Damage identification and health monitoring of structural and mechanical systems from changes in their vibration characteristics: A literature review, Los Alamos National Lab. Report, LA-13070-MS.

Gurely, K. and Kareem, A. (1999) Application of wavelet transform in earthquake, wind and ocean engineering, *Engineering Structures*, Vol 21, pp 149-167

Hou, Z., Noori, M. and Amand, R.St. (2000) Wavelet-based approach for structural damage detection, *Journal of Engineering Mechanics*, Vol 126, pp 677-683.

Kim, H. and Melhem, H. (2003) Fourier and wavelet analysis for fatigue assessment of concrete beams, *Experimental Mechanics* Vol 43, pp 131-140.

Moyo, P. and Brownjohn, J.M.W. (2005) Long term bridge health monitoring using wavelet analysis, *Proceedings of 1st International Conference on Structural Condition Assessment and Improvement*, Perth, Australia, pp. 275-282.

Peng, Z.K. and Chu, F.L. (2004) Application of the wavelet transform in machine conditioning monitoring and fault diagnostics: a review with bibliography, *Mechanical Systems and Signal Processing*, Vol 18, pp 199-221.

Torrence, C. and Compo, G.P. (1998) A Practical guide to wavelet analysis. *Bulletin of the American Meteorological Society*, Vol 79, pp 61-78.

Ventura, C.E, Laverick, B., Brincker, R., Andersen, P. (2003) Comparison of dynamic characteristics of two instrumented tall buildings, *Proceedings of 21st International Modal Analysis Conference (IMAC)*, Kissimmee, Florida.

Bounds on the distribution of amplitudes in ground motion prediction models

Jeff Fisher[1], Paul Somerville[1], John Zhao[2] and Jian Zhang[2]

[1] Risk Frontiers
[2] GNS Science

Abstract

In current ground motion models, the uncertainty in predicted ground motion is modelled with a lognormal distribution. One consequence of this is that predicted ground motions do not have an upper limit. In reality, there probably exist physical conditions that limit the ground motion. Use of unbounded models in probabilistic seismic hazard analysis leads to ground motion estimates that may be unrealistically large, especially at the low annual probabilities considered for important structures, such as dams or nuclear reactors. Due to the limited size of earlier strong motion data sets, statistical analysis of the distribution of earthquake ground motion amplitudes was unable to provide a clear point at which to truncate the lognormal distribution.

Recently, very large data sets of strong motion recordings have become available, making statistical analysis more viable. We have analysed very large strong motion data sets from the K-net and Kik-net strong motion networks in Japan. Preliminary analyses by us and other investigators using normal probability plots show departures from lognormal behaviour at about 2.5 standard deviations above the median. Our basic approach is to calculate residuals of the recorded data from the ground motion model developed for Japan by Zhao et al. (2006) using the K-net and Kik-net data. These residuals are then used to construct normal probability plots, and the significance of departures of the residuals from lognormal distributions is quantified. The significance of departures is assessed in light of earthquake source, wave propagation, and site response effects that may be present in the data but not taken into account in the ground motion model of Zhao et al. (2006) that form the basis for measurement of residuals.

Introduction

Due to the limited size of strong motion data sets, statistical analysis of the distribution of earthquake ground motion amplitudes has, to date, been unable to provide a clear indication that the distribution has an upper limit. Recently, very large data sets of strong motion recordings have become available, making statistical analysis more viable (Bommer et al., 2004). The three crustal earthquake data sets analyzed by these authors using normal probability plots all show departures from lognormal behaviour at about 2 standard deviations above the median, tending toward shorter upper tails. However, the Japanese K-net data sets that were analyzed contain ground motion values almost 5 standard deviations above the median. We anticipate that these very high values may be due to data errors or to extreme site effects.

Data analysis

Strasser and Bommer (2005) analysed the intra-event variability of ground motion amplitudes in sets of K-net recordings of individual crustal earthquakes in Japan using K-net data. They noted data quality issues in the strong motion recordings, but did not attempt to correct them. They used site corrections derived from extrapolation of shallow shear wave velocity measurements to 20 metre depth, but found them not to have a large impact on their measurements of ground motion variability. They concluded that the distribution of ground motion amplitudes is consistent with the lognormal distribution up to the 2.5 sigma level.

The methods used by Zhao et al. (2006 a,b) in deriving their ground motion model may provide a more reliable basis for the evaluation of ground motion variability, because of the approaches taken for strong motion data processing and the classification of recording sites. In Zhao et al. (2006 a,b), strong motion recordings from Japanese earthquakes recorded on strong motion stations of the K-net and Kik-net networks were gathered and processed using a high-pass filter to eliminate the long period ground motions with frequency less than the corner frequency of the filter determined for each record. Among the total of 4518 Japanese records from 249 earthquakes, 1285 are from crustal events, 1508 are from interface events and 1725 are from slab events.

The magnitude and source distance distribution for earthquakes with focal depths of up to 162 km is shown in Figure 1(a) for the Japanese strong-motion data set used by Zhao et al. (2006). In order to eliminate the bias that could be introduced by untriggered instruments, data for the modelling were selected from a much larger data set by exclusion of data at distances larger than a specified value for a given magnitude. For subduction slab events, the maximum source distance was set to 300km. Earthquake locations, especially focal depths, determined by JMA were not consistent with those determined by other seismological organizations, and so the relocated ISC locations and depths were used. The moment magnitudes from the Harvard catalogue were used unless moment magnitude from a special study was available. In addition to the crustal earthquake category analysed by Strasser and Bommer (2005), our analysis includes subduction interface earthquakes and intra-slab earthquakes, which have larger magnitudes and much larger numbers of recordings than the crustal earthquakes. Our analysis also looks at the full variability in the ground shaking, both the intra-event variability and the inter-event variability.

The standard deviations used are those of the Zhao et al. (2006) models, which are independent of magnitude. For subduction and slab events, these standard deviations are much lower than those of the widely used subduction zone model of Youngs et al. (1997), especially for periods longer than 0.2 seconds. This is an important feature of the Zhao et al. (2006) model, because in probabilistic seismic hazard analysis, the variability of ground motion about the median value is often just as important as the median value itself.

Since many of the K-net stations have shear wave velocities that extend to depths of only 10 and some to 20 meters, Zhao et al. (2006) devised an alternative method for categorising their site conditions, based on response spectral ratios of horizontal to vertical ground motions. They used H/V ratios for records from K-net sites having adequate shear-wave velocity measurements to establish a site classification index using the mean spectral ratios over a wide range of spectral period, to assign sites to the long-established Japanese classes (Molas and Yamazaki 1995) that correlate approximately with the US NEHRP classes as indicated in Table 1. Using the index, they were able to classify both K-net stations with soil layers thicker than 20m and other strong-motion stations in Japan. The peak period of the H/V spectral ratio was also used to identify soft soil sites.

Results

Our basic approach is to calculate residuals of the recorded data from the ground motion model of Zhao et al. (2006) using the site classifications developed by Zhao et al. (2006). The significance of departures of the residuals from lognormal distributions has been quantified. These significance of departures will be assessed in light of earthquake source, wave propagation, and site response effects that may be present in the data but not taken into account in the ground motion models of Zhao et al. (2006 a, b) that form the basis for measurement of residuals.

Figure 2 shows the distribution of the residuals after they have been normalised. It is apparent that the lognormal distribution fits the bulk of the data very well. However, this relationship is well established and it is the tail ends of the distribution that is of interest, particularly the upper tail, although the lower tail is also important. What happens in the tail is best described with a normal plot, as shown in Figure 3. In this figure, a lognormal probability distribution is indicated by a straight diagonal line. The change of the slope of the data points for residuals between 2 and 2.5 log units above the median indicates departure from the lognormal distribution through a shortening of the tail of the distribution, consistent with the idea that physical bounds do indeed limit the upper tail of the distribution. However, there are still two points that lie outside this limit, indicating that more extreme values are possible. These outliers pose a significant problem. If they are legitimate recordings, i.e. not caused by data or recording errors, then any truncation point should lie outside these values.

We examined the two records with the largest positive deviations from the median value to see if there was anything unusual about them. We found that each has a single isolated spike in acceleration whose amplitude is considerably higher than the next highest peak. The fact that one of the sites produced this spike in just one earthquake and not in ten others suggests that the site response is dependent on the azimuth and/or incidence angle of the incoming ground motion, possibly due to departures from flat lying ground structure near the site. The other station has only one record so we are unable to determine whether it characteristically has such a spike.

We also examined the spectral acceleration curves of each of these records to determine if there is a single period that is extremely high or if this is consistent across all periods. They both had an extremely elevated peak between 0 seconds and 0.3 seconds and after this they died away very rapidly. At longer periods, 1 and 3 seconds, the residuals for both recordings had dropped back to between 0.9 and 1.6. While these numbers are still higher than those predicted by the attenuation relations, they are well within the bounds of the proposed truncation point of 2.4. As such we felt that these data points were not sufficiently problematic to warrant extending the truncation point so as to include them, since it is the longer spectral periods that are most important for a typical seismic hazard analysis.

Conclusions

Current ground motion prediction models assume an unbounded lognormal distribution of random variability in ground motion level. In reality, there probably exist physical conditions that limit the ground motion distribution. Use of unbounded models in probabilistic seismic hazard analysis leads to ground motion estimates that may be unrealistically large, especially at low annual probabilities. The probabilistic seismic hazard map of Australia uses ground motion models that are assumed to be truncated at three standard deviations above the median value. Given that the standard deviation in the attenuation model is of the order of 0.7 log units for most spectral periods, it is likely that truncating 2.1 log units above the mean is probably slightly underestimating the uncertainty. The current study indicates that a more appropriate cutoff point would be 2.0 – 2.5 log units beyond the median. Truncating the distribution in this fashion would serve to reduce the hazard at long return periods.

References

Berge-Thierry, C., Cotton, F., Scotti, O., Griot-Pommera, D.A. and Fukushima, Y., 2003. New empirical response spectral attenuation laws for moderate European earthquakes, Journal of Earthquake Engineering, 7: 193-222.

Bommer, J.J., Abrahamson, N.A., Strasser, F.O., Pecker, A., Bard, P.Y., Bungun, H., Cotton, F., Fäh, D., Sabetta, F., Scherbaum, F. and Studer, J., 2004. The challenge of determining upper limits on earthquake ground motions, Seism. Res. Lett., 75: 82-95.

Chang, T.Y., Cotton, F. and Angelier, J., 2001. Seismic attenuation and peak ground acceleration in Taiwan, Bull Seism. Soc Am, 91: 1229-1246.

Lussou, P., Fukushima, Y., Bard, P.Y. and Cotton, F., 2001. Seismic design regulation codes: contribution of Knet data to site effect evaluation, Journal of Earthquake Engineering, 5(1): 13-33.

Molas, G.L. and Yamazaki, F. (1995), Attenuation of earthquake ground motion in Japan including deep focus events, Bulletin of the Seismological Society of America, Vol. 85, No. 5, pp. 1343-1358

Strasser, F.O., and J.J. Bommer (2005). Analysis of intra-event ground-motion residuals from K-NET and KiK-NET data. Research Report No. 05-003-SM, Imperial College, London, U.K.

Youngs, R.R., Chiou, S.-J., Silva, W.J. and Humphrey, J.R. (1997), Strong ground motion attenuation relationships for subduction zone earthquakes, Seismological Research Letters, Vol. 68, pp. 94-127

Zhao, J.X., J. Zhang, A. Asano, Y. Ohno, T. Oouchi, T. Takahashi, H. Ogawa, K. Irikura, H.K. Thio, P.G. Somerville, Yasuhiro Fukushima, and Yoshimitsu Fukushima. (2006a). Attenuation relations of strong ground motion in Japan using site classification based on predominant period. Bull. Seism. Soc. Am., 96, 898-913.

Zhao, J.X., Irikura, K., Zhang, J., Fukushima, Y., Somerville, P.G., Asano, A., Ohno, Y., Oouchi, T., Takahashi, t. and Ogawa, H. (2006b). An empirical site classification method for strong motion stations in Japan using H/V response spectrum ratio. Bull. Seism. Soc. Am., 96, 914-925.

Table 1. Site class definitions used by Zhao et al. (2004; 2005) and the approximately corresponding NEHRP site classes (BSSC 2000)

Site class	Description	Natural period	V_{30} calculated from site period	NEHRP site classes
SC I	Rock	T < 0.2s	V_{30} > 600	A+B
SC II	Hard soil	0.2 = T < 0.4s	300 < V_{30} = 600	C
SC III	Medium soil	0.4 = T < 0.6s	200 < V_{30} = 300	D
SC IV	Soft soil	T ≥ 0.6s	V_{30} ≤ 200	E+F

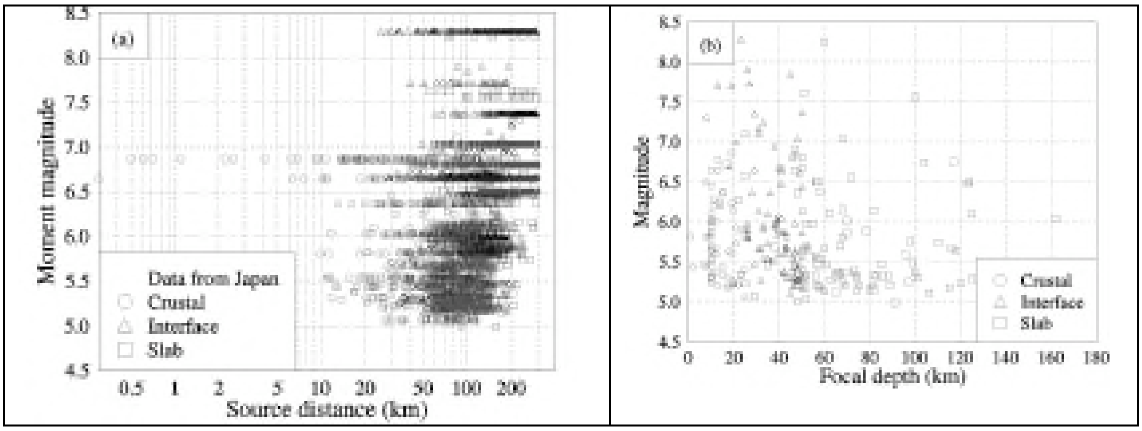

Figure 1 Magnitude-distance distribution for (a) data from Japan; and (b) magnitude-focal depth distribution of Japanese data. Source: Zhao et al. (2006)a.

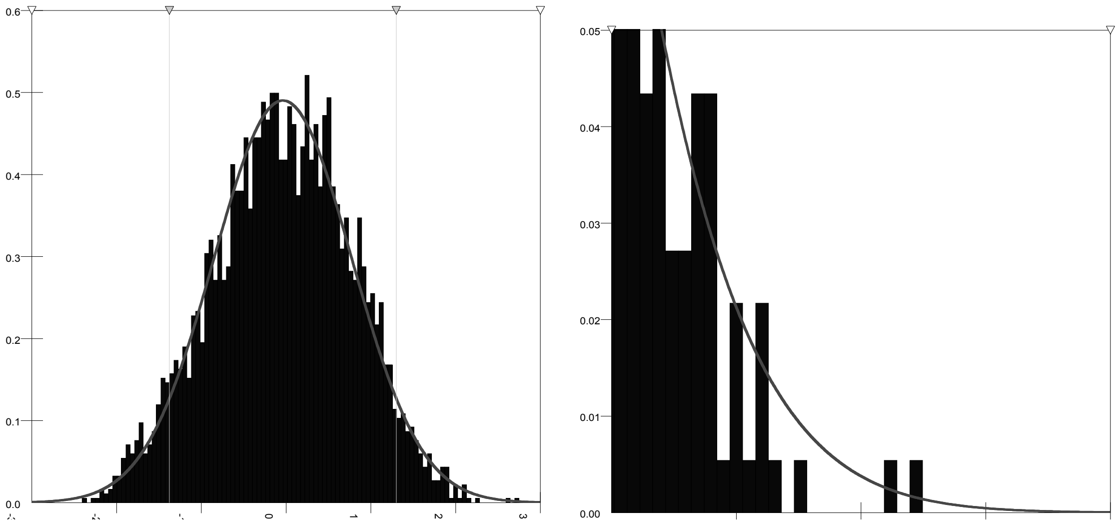

Figure 2 a. Full distributions of the residuals. b. The upper tail of the distribution.

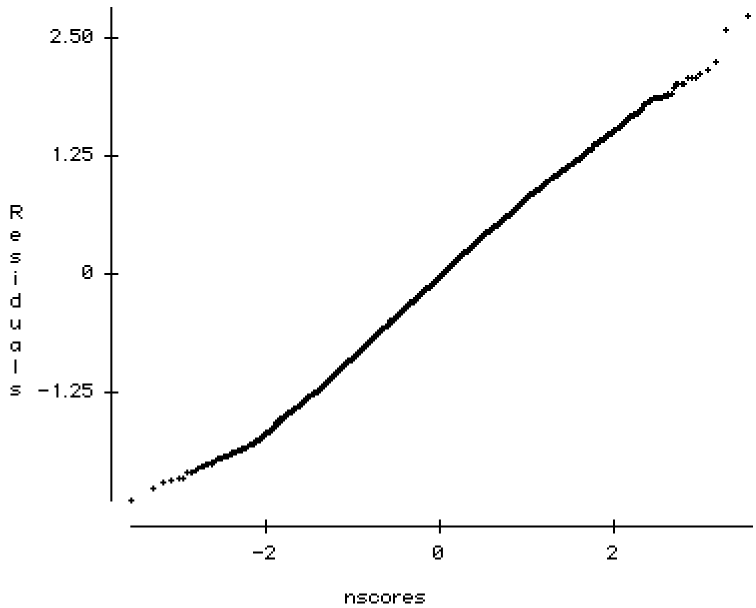

Figure 3 Normal probability plot of the ground motion residuals against their n-scores.

Seismic fragility curves for soft-storey buildings

Kittipoom Rodsin[1], Nelson Lam[1], John Wilson[2] and Helen Goldsworthy[1]

[1] The University of Melbourne
[2] Swinburne University of Technology

Abstract

Buildings with a soft-storey are notoriously vulnerable to collapse under strong earthquake shaking. However, a building subject to a small or moderate magnitude earthquake has a fair chance of survival depending on the drift demand on the soft-storey. This paper presents fragility curves which define the probability of collapse of a soft-storey column when subject to a pre-defined drift demand. The calculation for the fragility curves is based on the estimated shear (frictional) resistance to slip along a major diagonal shear crack (which is the plane of weakness for collapse to occur). The fragility curves presented can be shown to provide a more realistic representation of the seismic vulnerability of the building than the conventional approach based simply on the degradation in the horizontal resistance of the column.

Keywords: soft storey, collapse, fragility curves, column, seismic

1. Introduction

The research described in this paper forms part of a long-term program to assess and reduce the seismic risk and rationalizes the seismic design procedures and practices in Australia. Soft-storey buildings are considered to be particularly vulnerable because the rigid block at the upper levels has limited energy absorption and displacement capacity, thus leaving the columns in the soft-storey to deflect and absorb the inelastic energy. Collapse of the building is imminent when the energy absorption capacity or displacement capacity of the soft-storey columns is exceeded by the energy demand or the displacement demand.

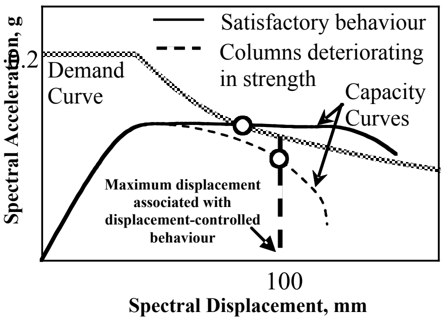

Figure 1 Schematic view of acceleration-displacement response spectrum diagram

This concept is illustrated using the 'Capacity Spectrum Method' shown in Figure 1 where the seismic demand is represented in the form of an acceleration-displacement response spectrum (ADRS diagram) and the structural capacity is estimated from a non-linear push-over analysis expressed in an acceleration-displacement relationship (as illustrated in Wilson & Lam 2003). The structure is considered to survive the design earthquake if the capacity curve intersects the demand curve and collapse if the curves do not intersect.

The current force-based design guidelines are founded on the concept of trading-off strength with ductility to ensure the structure has sufficient energy absorbing capacity. The limitation of this approach in lower seismic regions has been examined in Lam & Chandler (2005) in which the phenomenon of displacement-controlled behaviour was first introduced. By displacement-controlled behaviour, the peak displacement demand on the structure is well constrained around a definitive upper limit. Structures with seismic displacement capacity in excess of the seismic demand could be deemed seismically safe irrespective of the horizontal strength capacity or energy absorption capacity. Consequently, the authors have defined the ultimate drift capacity of a soft-storey building to be associated with the condition whereby the column can no longer resist gravity load. This definition is in contrast to the more conservative approach used in high seismic regions where failure is deemed to occur when the lateral load resistance degrades by 20%.

The horizontal force-displacement behaviour of a soft-storey building can be modeled using classical approach of integrating curvature along the column. Contributions from deformation due to flexure, shear, yield penetration and joint rotation are then aggregated to calculate the horizontal displacement of the column. Pilot studies have been undertaken recently by the authors (Rodsin et al. 2004, 2005 and 2006) to predict displacement at the limit of collapse. For a column failing in flexure, collapse occurs soon after the rapid loss of the lateral strength capacity, in which case the displacement capacity at collapse could be predicted reasonably accurately using existing deformation models. In contrast, a column with widely spaced stirrups and with low aspect-ratios (hence failing in shear or flexure-shear) shows an early degradation in lateral strength. The rate of degradation is so gradual that a 2 - 3 % drift (at axial load ratio of approximately 0.2) could be sustained without the gravity load carrying capacity being compromised (Rodsin et al. 2004). This surprisingly high value of limiting drift is attributed partly to the widening of the major shear cracks. This additional drift capacity is given the notation: δ_{add}. Collapse is imminent when resistance to slip at one of the cracks has been exceeded.

This paper presents a new model for predicting the limiting drifts of non-ductile columns which pertain to fail in shear or flexure-shear due to their low aspect-ratios and wide stirrup spacings. The model is then extensively used to construct fragility curves based on the estimated shear resistance to slip along a major diagonal shear crack in Section 5.

2. Column shear failure

The ultimate behaviour of a column with low aspect-ratio and poor confinement is likely to be controlled by shear at the ultimate stage. The brittle shear failure (shear-dominated) of a column occurs before the flexural strength has been reached while ductile shear failure (flexural shear-dominated) occurs after plastic hinge in a column has been developed. The limit deformation at the onset of shear failure of a column failing in brittle shear could be accurately predicted once the column shear strength (V_{ini}) is known as shown in Figure 2 (curve 4).

For a ductile shear failure column, the shear strength of the column has been degraded as the ductility increases. The shear strength has degraded due to crushing of the compression strut of concrete in the compression zone and widening of the flexural shear crack which reduces the capacity of shear transfer by aggregate interlock. The well-known shear strength degradation as a function of ductility is shown in Figure 2.

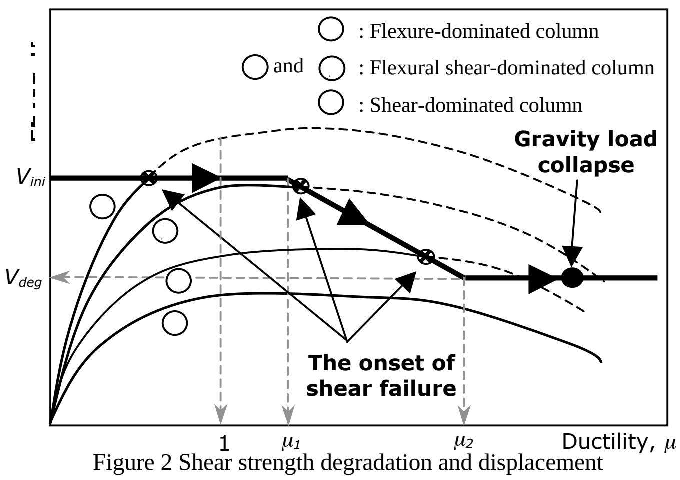

Figure 2 Shear strength degradation and displacement ductility

The onset of shear failure of a flexural shear-dominated column is predicted when degraded shear force capacity of the column intersects with the shear force demand as shown in curve 2 and 3. The "ductility dependent shear strength" relationships of columns have been proposed by many researchers (ie. Priestley et al. 1994 and Sezen & Moehle 2004).

Whilst the predicted shear strength V_{ini} using these models are agreed in general, these models provide significantly different results in predicting ductility dependent shear strength relationships. This is because the degraded concrete or the stirrup contributions to the total shear strength cannot be directly measured or defined from the test with confidence (ie. the shear strength of a column cannot be measured when it does not fail in brittle shear). Consequently, the models developed empirically based on the test results provide only an approximate value which cannot be reliably used to estimate the degraded shear strength (V_{deg}) and the deformation at the onset of shear failure.

The model estimates degraded shear strength (V_{deg}) based on the equilibrium condition along the failure surface of a flexure-shear damage column has been developed by the authors and is presented in Section 3. In this study, the shear strength is assumed to linearly decrease with an increase in the displacement ductility. The values of μ_1 and μ_2 are conservatively assumed to be 2 and 3 respectively. The initial shear strength V_{ini} can be calculated using the predictive model suggested by ATC-40 1996.

The ductility dependent residual shear strength as shown in Figure 2 can be constructed when V_{ini}, V_{deg}, μ_1 and μ_2 are known. The onset of shear failure is predicted at the intersection between the degraded shear force capacity and demand as shown in Figure 2. The shear force demand relationship (inferred from the force-displacement relationship of the column) can be calculated using the deformation model proposed by Rodsin et al. (2005, 2006). From this force-displacement relationship, the yield displacement (δ_{yu}) which is corresponding to a ductility of one (μ = 1) can be determined by extrapolating the displacement at the first yield (δ_y) by the moment ratio (Priestley 1996) as shown in Equation 1.

$$\delta_{yu} = \frac{M_n}{M_y}\delta_y \qquad (1)$$

where M_n = the theoretical flexural strength of the column and M_y = the flexural strength corresponding to first yield of longitudinal bar.

At the onset of shear failure, the column may show some degradation of the lateral strength but without the axial load carrying capacity being compromised. It was observed from the recent experimental investigations that if no slippage occurs along the shear failure surface, then the column may rotate by a small angle α about the compression edge causing the crack to open slightly as shown in Figure 3a and increasing the lateral displacement capacity of the columns. This additional drift (δ_{add}) capacity after the onset of shear failure is of particular interest and is discussed further in Section 3. The total deformation at gravitational load collapse can be calculated from the summation of the deformation at the onset of shear failure and δ_{add}.

3. Limiting drift of a column failing in shear

The model presented herein is aimed at simplifying the mechanism of shear collapse in order that the column drift capacity (or limiting drift) could be conveniently estimated. The model for modeling collapse is shown schematically in Figure 3b. Collapse of the column is deemed imminent when the shear resistance along the crack interface (V_{ci}) (attributed to aggregate interlock) is exceeded by the shear force demand along the crack interface (V^*_{ci}). This shear force demand V^*_{ci} is often dominated by the axial load component resolved in the direction of slip. The procedure to calculate V^*_{ci}, V_{ci} and δ_{add} are presented in the following sections.

3.1 Calculation of shear force demand along the crack interface V^*_{ci}

The shear force applied along the crack interface V^*_{ci} can be calculated by equating the gravity load component and forces in the stirrups resolved in the direction along the shear failure surface as shown by Equation 2.

$$V^*_{ci} = P\cos\theta - F_{vy}\frac{h_c}{S}\cos\theta - F_{sc}\cos\theta + F_{st}\cos\theta + V_{\deg}\sin\theta \qquad (2a)$$

where P = the gravity load; θ = the angle defining the orientation of the crack; F_{vy} = the stirrup yield strength; h_c is the width of the concrete core; and S = the stirrup spacing; F_{sc} = forces in the longitudinal reinforcement under compression F_{st} = forces in the longitudinal reinforcement under tension; and V_{deg} = the degraded shear force.

The angle θ can be estimated using the Modified Compression Field Theory (MCFT) or alternatively, a conservative value of 30 degree may be assumed for typical columns with shear span-to-depth ratio of between 2 and 3.

Forces in the longitudinal reinforcement under compression (F_{sc}) and tension (F_{st}) can be estimated using Equation 2 which is based on the assumption that the longitudinal reinforcements have buckled.

$$F_{sc} = 0.2 \cdot f_y A_{sc} \quad \text{and} \quad F_{st} = 0.2 \cdot f_y A_{st} \qquad (2)$$

where f_y = the yield strength of the longitudinal reinforcement, A_{sc} = the total area of the longitudinal reinforcement under compression and A_{st} = the total area of the longitudinal reinforcement under tension.

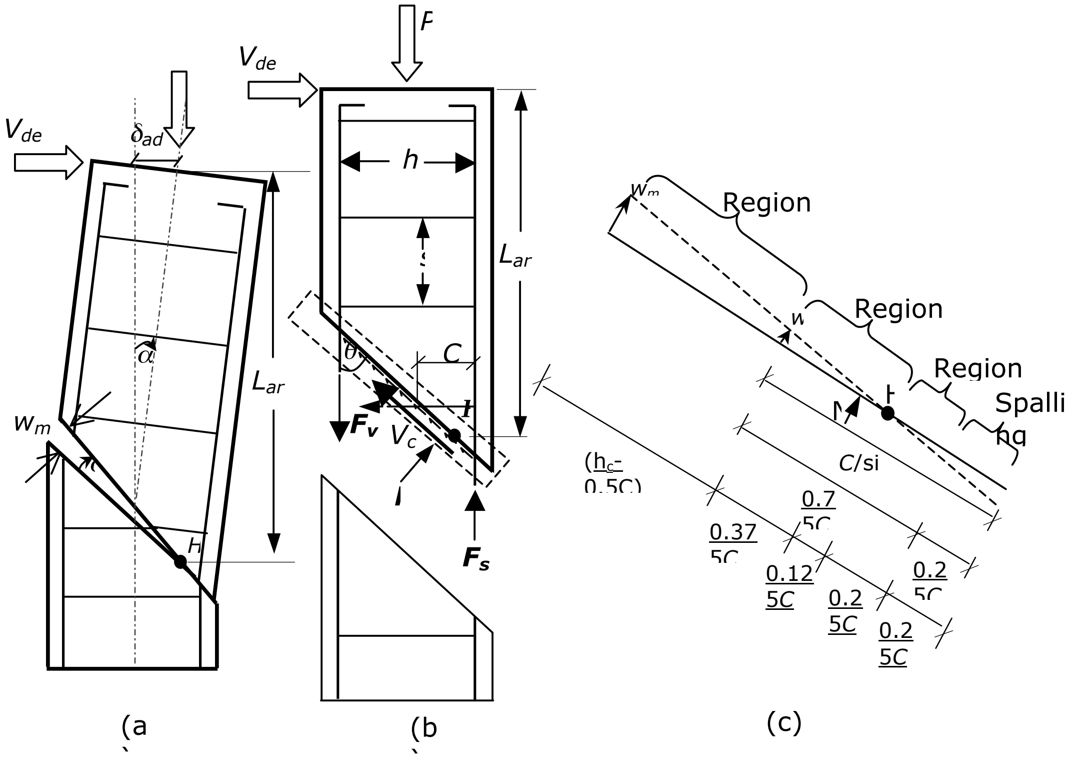

Figure 3 (a) additional displacement due to rotation at critical crack, (b) free body diagram of forces at the onset of shear failure and (c) geometry of the crack at the crack interface.

The unknown degraded shear strength (V_{deg}) and the force applied normal to the shear failure surface (N) can be calculated by solving Equations 3 and 4. Equation 3 is based on taking moment about point H (assumed to be at middle of the compression zone) as shown in Figure 3b. The assumption of plane strains remaining plane associated with bending deformation enables the depth of the compression block (C) (as shown in Figures 3b and 3c) to be estimated conveniently.

$$V_{\deg} = \frac{1}{L_{arm}}[0.5P \cdot (h_c - C) + F_{st} \cdot (h_c - 0.5C) + F_{sc} \cdot 0.5C - 0.125N \cdot \frac{C}{\sin\theta} + 0.5\frac{F_{vy}h_c}{\tan^2\theta \cdot S} \cdot (h_c - C)] \qquad (3)$$

The equilibrium condition of forces in the direction normal to the shear failure surface is shown in Equation 4.

$$N = P\sin\theta + \frac{F_{vy}h_c}{S\tan\theta}\cdot\cos\theta + F_{st}\sin\theta - F_{sc}\sin\theta - V_{\deg}\cos\theta \tag{4}$$

3.2 Calculation of shear resistance of concrete along the crack interface V_{ci}

It is assumed that after the onset of shear failure shear forces are transferred across the crack only by aggregate interlock. The limit of shear force V_{ci} transferred by such a mechanism is a function of both crack width (w_{cr}) and the normal stress on the crack surface (σ). It is shown in Figure 4a that the crack width is not constant along the crack interface. Therefore, the crack interface is divided into 3 regions in order that the average normal stress and the average crack width in each region could be calculated and used to estimate shear resistance in regions I to III. The shear resistance V_{ci} from the 3 regions can be calculated using Equation 5.

$$V_{ci} = \sum_{n=I}^{n=III} v_{cin}A_{crn} = V_{ciI} + V_{cicII} + V_{cicIII} \tag{5}$$

where ν_{cin} = the shear stress transfer across the crack in region n; A_{crn} = the area of crack interface in region n; V_{ciI}, V_{ciII} and V_{ciIII} = the shear resistance in region I, II and III respectively.

The shear stress ν_{ci} in each region can be calculated in accordance with the relationship between shear transmitted across the crack, the normal stress on the crack and the crack width suggested by Vecchio & Collins (1986) as shown by Equations 6a and 6b.

$$v_{cin} = v_{ci\max n}\left(0.18 + 1.83\frac{\sigma_n}{v_{ci\max n}} - 1.01\left(\frac{\sigma_n}{v_{ci\max n}}\right)^2\right) \le v_{ci\max n} \tag{6a}$$

$$v_{ci\max n} = \frac{\sqrt{f_c^{/}}}{0.3 + \dfrac{24w_{avgn}}{a+16}} \qquad \text{MPa, mm} \tag{6b}$$

where $\nu_{ci\ max\ n}$ = the maximum shear stress parameter in region n; σ_n = the normal stress on the shear failure surface in region n; w_{avgn} = the average crack width in region n.

3.3 Calculation of additional displacement δ_{add}

The average crack width in each region w_{avgI}, w_{avgII} and w_{avgIII} calculated based on the geometry of the crack (as shown in Figure 3c) is shown in Equation 7.

$$w_{avgI} = w_{\max}\frac{0.5h_c}{h_c - 0.5C},\ w_{avgII} = w_{\max}\frac{0.25C}{h_c - 0.5C} \text{ and } w_{avgIII} = 0 \tag{7}$$

In the model, it is assumed that the normal force N is applied to regions II and III and 25% of concrete in the compression zone has spalled as shown in Figure 3c. The normal stress in each region σI, σII and σIII can be calculated using Equation 8.

$$\sigma_I = 0,\quad \sigma_{II} = \frac{N\sin\theta}{0.75C\cdot b} \quad \text{and} \quad \sigma_{III} = \sigma_{II} \tag{8}$$

where b = the width of the column section

The crack width w_{max} at axial load collapse can be obtained iteratively by matching value of V_{ci} (as calculated from Equations 5 – 8) with the value of V^*_{ci} (as calculated from Equation 2).

It was observed from recent experimental investigations by the authors that if slippage does not occur along the failure surface of the shear crack, then the part of the column above the crack may rotate by a small angle α (which is approximately equivalent to additional drift) resulting in a small crack opening as shown in Figure 3a. The additional column deformation (δ_{add}) associated with this limiting crack opening can be calculated by substituting the maximum crack width w_{max} into Equations 9 and 10.

$$\alpha = \frac{w_{\max} \sin\theta}{h_c} \qquad (9) \qquad\qquad \delta_{add} = \alpha \cdot L_{arm} = w_{\max} \cdot \frac{\sin\theta}{h_c} L_{arm} \qquad (10)$$

where L_{arm} is the distance between the tip of the column and the rotation point H.

The calculated column deflection at the point of collapse may include the additional displacement δ_{add} associated with the limiting crack opening. It is noted that although the limiting angle of crack opening (α) at the threshold of collapse is generally very small, the associated increase in the displacement capacity of the column can be significant depending on the column geometry.

4. Experimental results

Half-scaled cantilever reinforced concrete column specimens with a similar cross-section of 160×200 mm and aspect ratios of 2.75 (S1) and 2.25 (S2) were tested to study their cyclic force-deformation behaviour under high shear force demand. The gravitational load carrying capacity of the column and mechanism of failure at collapse were studied. The innovative Vision Metrology System (VMS) was used to measure deformation of the columns including deformation of the area surrounding the shear cracks. The 3D displacement of the VMS targets attached to the surface of the columns was monitored throughout the test. Full details of the test can be found in Rodsin et al. (2004).

To validate the proposed model described in Section 3, data from the VMS targets located near the major shear crack have been analysed. The limiting angle of crack opening (α) and the additional displacement (δ_{add}) at the threshold of collapse were recorded for comparison with estimates obtained from the model (refer Table 1). The comparisons show general agreement between the experimental measurements and the analytical estimates. It should be noted that at this threshold of collapse, two displacement cycles have been applied to ascertain that the columns can sustain the cyclic loading without axial load carrying capacity being compromised.

Table 1 Comparison of experimental versus predicted crack rotation along the major crack plane, additional displacement (δ_{add}) and total displacement at incipient collapse.

Column	Length	Crack rotation (α)		Additional disp. (δ_{add})		Total disp. (δ)	
	mm	Radian (x10^{-3})		mm (%drift)		mm (%drift)	
		Exp.	Model	Exp.	Model	Exp.	Model
S1	550	5.8	6.6	2.9(0.5)	3.3(0.6)	21.0(3.8)	17.0(3.1)
S2	450	7.0	5.2	2.8(0.62)	2.1(0.47)	11.0(2.4)	9.3(2.1)

5. Fragility curve of soft-storey column failing in shear

The major uncertainties associated with additional displacement calculation are material properties, load conditions, the shear crack angle (θ) and the shear resistance along the crack surface. For the test column specimens, the first three parameters can be accurately measured with small variations so that they do not significantly affect the accuracy of the test results. In contrast, the mechanism of shear transfer across the crack is more complicated and the experimental data often show some degrees of scatter (as shown in Figure 4). Therefore, the fragility curves for a soft-storey column in this study are constructed based on the uncertainties associated with shear resistance to slip along a major diagonal shear crack. Fragility curves presented in this paper was based on laboratory controlled condition in which the values of ν_{cimax} and σ are predetermined.

These fragility curves could be further developed to incorporate variability in material properties, workmanship and load conditions encountered in practice.

The relationship between the measured shear stress transmitted across the crack and the compressive stress on the crack is shown in Figure 4. A non-linear regression analysis has been used to estimate the shear stress resistance v_{ci} from Equation 6. The standard error (S.E.) was found to be 0.06. Although there is a limited number of data generated for each $\frac{\sigma}{v_{ci\max}}$, a considerable number of data covers a wide range of $\frac{\sigma}{v_{ci\max}}$ values. The statistical parameters in a regression analysis could be reliably estimated when there are sufficient data within the range of interest.

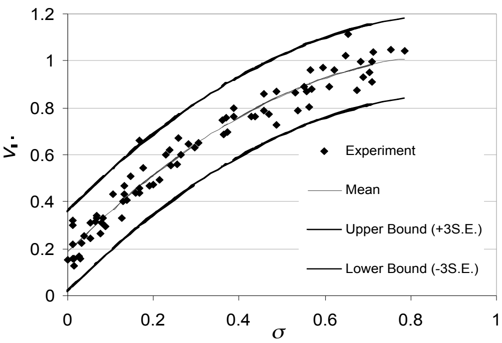

Figure 4 Relationships between normalized shear stress transmitted across crack (v_{ci}/v_{cimax}) and normalized compressive stress on crack (σ/v_{cimax}) (Vecchio and Collins, 1986).

A probability distribution of test data associated with crushing and spalling of materials usually follows a Gumbel distribution. However, under low $\frac{\sigma}{v_{ci\max}}$, only slippage along the crack interface (without material crushing) is expected. Therefore, a Gumbel distribution may not be applicable for modeling probability distribution for the whole range of data. For the sake of simplicity, it is assumed that the errors are normally distributed and there are about 2 chances in 3 that the data lies within the forecast equation (Equation 6) plus and minus one standard error. Therefore, the upper and lower bound (plus and minus 3 S.E.) plotted in Figure 4 show that there are 99.75% of data points lying within these two limits.

The fragility curve in Figure 5a is defined as a probability of gravity load collapse of shear damage columns when subject to a pre-defined additional displacement (δ_{add}) or a percentage drift. The probability of failure is calculated using a deterministic equation (Equation 6) to determine crack opening angle (α) (approximately equal to additional drift angle) at 50% chance of failure. A series of standard errors (S.E.) have been used to modify Equation 6 in order that other α values at a different probability of failure could be estimated. (ie. +1S.E. and -1S.E. associated with 83% and 17% probability of failure respectively).

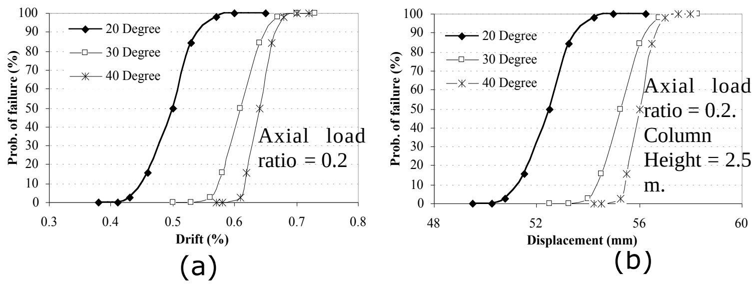

Figure 5 Fragility curves of (a) additional drift (crack opening angle) and (b) pre-defined displacement for different shear crack angles.

The fragility curves of a soft-storey building subject to a pre-defined displacement demand are shown in Figure 5b. To construct these fragility curves, the total drift is calculated by simply adding the drift at the onset of shear failure (the method of predicting drift at the onset of shear failure was suggested in Section 2) to the additional drift calculated in Figure 5a. This total drift is subsequently used to calculate the total displacement of a soft-storey column based on a given column height.

It was assumed that load conditions and geometry of an example column supporting soft-storey are similar to those of the column S2. The height of the first storey column is assumed to be 2.5 m (shear span = 1.25m). Therefore, the column specimen S2 was scaled from the corresponding prototype using a geometric scale factor of approximately 0.4 (0.45/1.25).

The displacement demand in Figure 5b is then presented in form of the peak ground velocity (PGV) as shown in Figures 6a-6c. The simplified response spectrum model for rock site in Australia as proposed by Wilson and Lam (2003) was used to estimate a displacement demand from a given PGV. Subsequently, the displacement demand was amplified using soil amplification factors S of 1.3, 1.8 and 3.0 for soil class B, C and D sites respectively. The corner period T2 is conservatively assumed to be 1.5 secs.

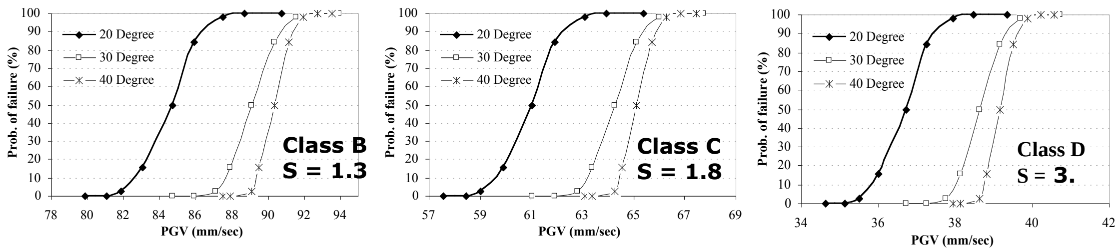

(a) (b) (c)

Figure 6 Fragility curves of a soft-storey column (the first storey height = 2.5m) for different shear crack angles under axial load ratio = 0.2.

From Figures 6a-6c, the soft-storey building founded on rock (class B) and shallow soil (class C) sites seems to be seismically safe (a notional PGV = 60 mm/sec). However, on the soft soil site (class D), this building may collapse when the PGV is greater than 40 mm/sec and is seismically safe when the PGV is lower than 35 mm/sec.

6. Conclusions

The concept of displacement-controlled behaviour has been introduced in this paper whereby the ultimate drift limit is based on the condition when gravity loading can no longer be supported by the damaged column. A model for predicting the deformation behaviour of a column at the limit of collapse has been presented. The model is intended for columns with low aspect-ratio and hence failing in shear or flexure-shear. The predictions calculated from the proposed models show good agreement with experimental results obtained from tests performed by the authors. The model has been further used to construct fragility curves which define the probability of collapse of a soft-storey column when subject to a pre-defined drift demand and a peak ground velocity based on different soil sites. The development of the gravity-collapse model for estimating the displacement capacity of soft-storey columns forms an important part of the displacement-based methodology for assessing the seismic performance of building structures in regions of low and moderate seismicity.

7. References

ATC40. 1996. Seismic evaluation and retrofitting of concrete buildings, Applied Technology Council, USA.

Lam, N.T.K. & Chandler, A.M. 2005. Peak displacement demand in stable continental regions, Earthquake Engineering and Structural Dynamics 34: 1047-1072.

Priestley, M.J.N., Verma, R. & Xiao, Y. 1995. Seismic shear strength of reinforced concrete columns, Journal of Structural Engineering 120(8): 2310-2329.

Rodsin, K., Lam, N.T.K., Wilson, J.L. & Goldsworthy, H. 2004. Shear controlled ultimate behaviour of non-ductile reinforced concrete columns, Procs. Conference of the Australian Earthquake Engineering Soc. 17. Mount Gambier: Australia.

Rodsin, K., Lam, N.T.K., Wilson, J.L. & Goldsworthy, H. 2005. Displacement limits for building collapse, Procs. Conference of the Australian Earthquake Engineering Soc. 33. Albury: Australia.

Rodsin, K., Lam, N.T.K., Wilson, J.L. & Goldsworthy, H. 2006. Collapse behaviour of columns with low aspect ratios, 19th Australasian Biennial Conference on the Mechanics of Structures and Materials, University of Canterbury, Christchurch, New Zealand to be published in 2006.

Sezen, H. & Moehle, J.P. 2004. Shear strength model for lightly reinforced concrete columns, Journal of Structural Engineering 130(11): 1692-1703.

Vecchio, F.J. & Collins, M. 1986. The modified compression field theory for reinforced concrete elements subjected to Shear, ACI Structural Journal 83(2): 219-231.

Recent developments in the research and practice of earthquake engineering in Australia

JL Wilson[1] and NTK Lam[2]

[1] Swinburne University of Technology
[2] The University of Melbourne

Abstract

This paper presents multi-disciplinary facets of earthquake engineering research and developments in Australia over the past decade. Past and current research into seismic activity modelling and the associated challenges is first described. The Component Attenuation model (CAM) that provides estimates for the seismic displacement demand in regions lacking strong motion data is then introduced along with other models developed by conventional methods. Research into the seismic performances of typical Australian construction which incorporates the use of unreinforced masonry, steel and concrete has been summarized together with a brief report on current activities with risk modelling and the earthquake loading standard. A new two-tier displacement based approach for assessing the seismic performance of structures is presented along with future trends in earthquake engineering.

Introduction

Over the past 100 years, Australia has been subject to, on average, one earthquake event exceeding M5 every year and one event exceeding M6 every five years (McCue et al, 1995). Most of these earthquake events did not cause casualties but there has been noticeable damage to infrastructure including railway lines and gas mains (eg. earthquake at Meckering, Western Australia and at Tennant Creek, Northern Territory). The location of historical earthquakes obtained from archive sources has been central to the modelling of seismic hazard across the continent.

The first seismic design Standard (AS2121) was introduced in Australia in 1979. Every aspect of seismic design provisions ranging from the definition of the spatial distribution of seismic hazard, loading requirements and rules for design and detailing was covered in one document. However, because most cities were located in zone zero there was little impact from this standard on the engineering profession.

An earthquake event of mere M5.6 which occurred at Newcastle, New South Wales (some 100km northeast of Sydney) in December 1989, cost 11 lives and resulted in widespread damage to unreinforced masonry walls (Melchers, 1990). This was by far the most significant earthquake event in Australian history. Ironically, Newcastle was designated seismic zone zero in AS2121(1979).

Earthquake engineering research in Australia was limited to seismic activity modelling and seismological monitoring until the late 1980s when research into the response behaviour of structures in seismic conditions was first undertaken at the University of Melbourne. The current Australian Earthquake Loading Standard AS1170.4, which was introduced in 1993, was essentially based on the 1991 version of the Uniform Building Code (UBC, 1991) of the United States.

The 1989 Newcastle earthquake prompted intensive multi-disciplinary research on earthquake engineering, with Geoscience Australia (then Bureau of Mineral Resources) being the major centre of investigation into the seismological aspects, and the University of Melbourne into the structural engineering aspects. Investigations into the seismic performances of unreinforced masonry walls have primarily been based at the University of Adelaide. With strong and sustained collaborations between these three centres along with numerous other groups across the country, studies targeted initially at Australian conditions, have been developed into generic studies for worldwide applications in regions of low and moderate seismicity. The formation of the Australian Earthquake Engineering Society in 1990 and the introduction of an annual technical conference provided an opportunity to exchange information and collate research findings. Strong links between these centres and other international centres on mainstream earthquake engineering research in New Zealand, Canada and USA have been established. Importantly, strong international research collaborations have also been formed with overseas institutions from regions with similar levels of seismicity, namely South China, Italy and Singapore.

This paper presents an overview of Australian earthquake engineering research activities and their outcomes.

Seismic activity modelling

In Australia, little is known of the rate of seismic activity of individual faults. Consequently, earthquake sources have been modelled as "polygonal areal source zones" in the seismic hazard analysis procedure (Gaull 1990). The size and geometry of these source zones have been delineated in accordance with information of localizing geological structures or "groups of faults" that have the potential of generating future earthquakes. Many of the decisions in delineating the zone boundaries were dictated by subjective judgement. The location of historical earthquakes is strongly reflected in the developed zonation model due to infrequent occurrence of earthquakes of engineering significance and the very limited time-window in the historical events database. Consequently, many "bulls-eye" type contours which coincide in location with recorded earthquake epicentres are displayed on the seismic hazard maps of the country (refer hazard maps in AS1170.4, 1993).

The Kernel method which expresses seismic activity density as a continuous function in space (eg. Woo 1996) has been applied recently to Australia (Stock 2002a&b). This new approach is in contrast to the traditional approach of modeling seismic activities as discrete polygonal sources which have distinct boundaries. A Kernel function is used to "smear" a historical epicentre into the surrounding area. This smoothing process will suppress, if not completely eliminate, the "bulls-eye" effects mentioned previously.

Another important shortcoming with the historical database is the very limited number of recorded large magnitude events. Consequently, the recurrence behaviour of large magnitude earthquakes has been predicted by extrapolating observations from the smaller magnitude events. The paucity of seismicity data can be compensated by using relevant information gained from on-going studies in the area of paleoseismology (or seismic geomorphology) which is the branch of science devoted to studying pre-historical earthquake activity based on making observations from landforms. In Australia, there is a wealth of geomorphic evidence associated with seismic activities, but there have been very few detailed investigations. Information on the orientation of stress fields from oil exploration investigations undertaken by Denham also provides useful information on the failure susceptibility of known faults. The study of seismic activities is not limited to investigating faulting activities and slip-rates. Landform evolution on a much larger scale (eg. mountain building) has been studied to gain insight into the underlying tectonic processes which drive seismic activities. Evidence for mountain building could come from extensive geophysical data that measures radioactivity and magnetic fields of exposed soil and rock. Rocks of different ages and types display different levels of radioactivity and magnetic properties. Faults and uplift which bring older rocks to the surface or bury younger strata can be detected through such measurements. Intense mountain building in southeastern Australia over the past 10 million years has been detected from such an approach (Sandiford et al, 2003).

Recently, high resolution digital elevation models (DEM) have emerged as important tools for finding and characterizing earthquake related geomorphology and particularly fault scarps (Clark 2005). The method is advantageous for locating fault scarps over large or remote areas and can provide a basis for imposing restraints on seismicity models. The mapping of geophysical quantities such as gravity fields, magnetic fields and heat flows have also provided very relevant information on the underlying tectonic processes which drive intraplate seismic activities (Brown 2003).

Numerous modelling approaches involving input from a range of disciplines have been described. The spatial distribution of seismic activity within Australia as inferred from seismological observations and from geo-morphological and paleo-seismological studies are based on events of different magnitude range. Thus, comparative studies need to be undertaken to identify major anomalies. Overall, the challenge is in reconciling differences between contributions from different modelling approaches and integrating them into a robust seismic model that is representative for the Australian continent.

Attenuation modelling

Intensity attenuation relationships were first developed for different parts of Australia by Gaull (1990) using iso-seismal maps. Such valuable information on intensity has been translated into approximate peak ground velocity (PGV) information using the well known transformation of Newmark (1971). The current seismic hazard maps for Australia (in AS1170.4, 1993) are based on those established benchmarks. However, intensity data only provides overall indication in the intensity of the ground shaking and not its frequency properties which characterize the shape of the response spectrum. The potential for an earthquake to displace a structure and cause damage and instability, depends on both the PGV and the frequency properties of the ground shaking. The PGV parameter alone is not fully indicative of the potential seismic hazard in engineering terms since the displacement demand of an earthquake increases with earthquake magnitude for a constant PGV. The potential hazard of an area can be characterized more effectively using design earthquake scenarios expressed in terms of magnitude-distance combinations. For this reason, the realistic modelling of the seismic hazard depends on the accurate representation of the seismicity of moderate and large magnitude events as well as the frequency dependent (response spectrum) attenuation behaviour of the earthquake.

During the 1990s, the Australian Geological Survey Organisation (AGSO, now renamed Geoscience Australia) undertook a detailed study of 13 accelerograms measured at rock sites from reverse thrust fault events with magnitude ranging from 5.4-6.6 (Somerville, 1998). Records were normalised to a PGV of 50mm/sec, and the normalised design response spectrum (NDRS) model proposed from this study has been illustrated in tri-partite form. However, Somerville's model did not directly account for the variation in the regional geological conditions across the Australian continent as described by Dowrick (1995). The Component Attenuation Model (CAM) was soon developed to allow for variations in regional conditions. CAM was developed initially in Australia and was first published internationally in Lam (2000a-c). In CAM, response spectrum is defined as a product of factors representing various source, path and site effects. CAM has now been developed into a generic tool for international applications (refer review by Chandler 2001; Hutchinson 2003; Lam 2003 and 2004). CAM is essentially a tool by which information obtained from local seismological monitoring studies is utilized to construct a representative response spectrum for direct engineering applications. Through the CAM framework, contributions from Australian seismological research (eg. Allen 2003; McCue 2003; Wilkie 1995; Gaull 1990) can be translated into valuable information for response spectrum modelling for the country.

Remarkable consistencies between the Intensity Model of Gaull, the empirical intraplate model of AGSO and CAM have been demonstrated recently (Lam 2003). Meanwhile, shortcomings of employing overseas attenuation models (eg. Toro 1997) for applications in different regions within Australia have been highlighted. A response spectrum model recommended for Australia by Somerville 1998 and Wilson and Lam 2003 (based on CAM) has been incorporated into the draft for the new Australian Standard for earthquake actions.

Site response modelling and microzonation

The significance of site effects was confirmed by observations from the 1989 Newcastle earthquake in which the most severe damage was found in areas covered by soft soil sediments (Institution of Engineers report, edited by Melchers 1990). Research into site effects can be divided into two main streams, namely (i) site classification and micro-zonation and (ii) soil amplification.

Studies on site classification and micro-zonation were based either on (i) identifying regolith properties and their potential response behaviour using information obtained from seismic cone penetrometer tests (eg. Dhu 2002) or (ii) identifying site natural period using borehole information (eg. Lam 1999) or the well known Nakamura technique (eg. Turnbull 2003). These conventional modelling techniques were applied to numerous cities around Australia including Newcastle and Lake Macquarie in New South Wales; and Bundaberg and Hervey Bay in Queensland.

A more advanced site identification technique was developed recently by Asten who makes use of background noises generated by meteorological and cultural sources, with machinery and vehicle traffic being the principal sources at periods of interest. This seismic energy propagates primarily as surface waves which are then analysed by what is known as the Spatial Autocorrelation (SPAC) method (Asten 2002; Asten, 2003). The shear wave velocity profile of the site could be determined using the SPAC method down to a depth which is comparable to the diameter of the geophone array (typically in the order of 50-100m but could be increased as desired). The SPAC technique, which is still in the early stage of its development as a practical engineering tool, has been put into test in a recent study undertaken in Perth (Asten 2003).

Studies on soil amplification were undertaken as part of the research into the regolith identification procedure described above (Venkatesan 2002, 2003 and 2004). The analyses employed either the stochastic equivalent-linear methodology (Electric Power Research Institute, 1993) or the non-linear one-dimensional shear wave analysis methodology using the well known program SHAKE (Idriss 1991). A significant development in the study of soil amplification is the modelling of displacement demand in conditions where seismic waves entering flexible soil layers are trapped between the soil surface and the high impedance contrast interface with the underlying bedrock. When conditions pertaining to resonance behaviour are developed, the displacement demand of the earthquake is particularly amplified at the "period of resonance" which is often well correlated with the natural period of the site. Structures with an initial (elastic) period lower than the site period are potentially at risk given that the natural period of a structure tends to lengthen as a result of deterioration in the structural strength and stiffness during the earthquake. The displacement demand on a flexible soil site can be particularly sensitive to the magnitude-distance combination of the earthquake due to the changes in frequency content and duration of the rock motion. The modelling of this high amplification phenomenon has been described in international research literature and incorporated into the CAM framework (refer Lam 2001; Chandler 2002; Lam and Wilson, 2004).

Structural response research

This section provides a brief overview of a number of research studies that have been undertaken in Australia. The majority of the studies focus on the post-elastic performance and the response of Australian structures which typically have been designed for gravity and wind loading without consideration of seismic excitation. Research has been focussed on assessing the overstrength, failure patterns, displacement ductility and more recently the displacement capacity of different structural members, sub-assemblages and systems using both experimental and analytical techniques.

Buildings with soft storeys are well known to be particularly vulnerable to collapse and severe damage under earthquake excitation. Despite this, buildings possessing soft storey features are commonly found in low to moderate seismic countries such as Australia. A research program has been undertaken to assess the axial load, lateral force and displacement capacity of reinforced concrete soft storey buildings. The displacement model accounts for the effects of axial compression, flexure, shear, column end rotation, foundation flexibility and plastic hinge formation. An experimental program to evaluate the accuracy and reliability of the analytical model is currently in progress (Rodsin 2003). The studies indicated that many buildings with soft storeys failed with limited ductility in flexure (rather than brittle shear failure) with storey drift capacities in the order of 2%. A comparison of the displacement capacity with the seismic displacement demand suggested that many soft storey buildings on rock and shallow soil sites would survive earthquakes with return periods in the order of 500 years.

Griffith (2003) has developed an innovative retrofit technique for improving the drift capacity of soft storey structures. The technique involves attaching steel or FRP plates to the flexural faces of columns using bolts. Tests have indicated that retrofitted columns develop drift capacities in excess of 2.5% with numerical models suggesting that 10% drift capacities could be possible.

An extensive experimental and analytical research program has been undertaken investigating the seismic performance of reinforced concrete wide band beam structures (Stehle 2001; Abdouka 2002). The sub-assemblage testing research indicated that such structures designed for gravity loading using the minimum detailing requirements in Australia had drift capacities in the order of 2.5% before the lateral strength capacity is reduced. An innovative method of de-bonding the continuous top reinforcement in the band beam adjacent to the column demonstrated that the damage levels associated with large drifts could be significantly reduced.

The performance of concentrically braced steel frames (CBF) designed for elastic wind loads with no consideration of seismic loading was investigated (Wallace 2002). In particular the connections between the diagonal braces and the columns were studied to investigate the failure mechanism and overstrength. The research findings indicated that the connections were typically weaker than the members with an overstrength factor of the welded connections in the order of 1.5. Failure was typically initiated by low cycle fatigue cracking in the weld resulting in limited displacement capacity of the CBF system. A cost-effective retrofit measure to improve the ductility and drift capacity was briefly investigated and showed some potential. The retrofit measure involved introducing a structural fuse into the brace by a deliberate localised weakening of the member away from the connection to encourage local yielding rather than brittle fracture of the weld connection.

An innovative connection has been developed by Goldsworthy for connecting steel beams to concrete filled steel tube columns (CFT) using blind bolts (Yao 2005). The cyclic behaviour of this connection is the subject of an on-going industry funded research project that involves extensive laboratory testing and non-linear finite element modeling.

The behaviour of low rise precast concrete load bearing panel structures was investigated by Robinson (1999). These precast structures which are very common and popular for apartment buildings are characterised by having connections much weaker than the precast panel members. A study of this form of construction concluded that the better detailed connections allowed a limited ductile mechanism to develop resulting in the in-plane rotations of the panel members and a drift capacity in the range of 1-3% depending on the depth of connection embedment in the floor slab.

The behaviour of domestic structures (plasterboard lining with brick veneer external cladding) to lateral loads has been extensively investigated by Gad (1999). The studies indicated that the non-structural plasterboard contributes significant lateral strength to the overall system. In contrast, the brick veneer contributes negligibly to the lateral strength and is vulnerable to collapse from out-of-plane shaking depending on the condition of the brick ties. This study has been recently extended to investigate the damage thresholds of such construction under low level blast vibrations (Gad 2004).

An innovative displacement based technique for assessing the out-of-plane response of masonry construction has recently been developed by Griffith and the authors (Doherty 2002, Lam 2003 and Griffith 2004, 2005). The traditional force based methods are shown to be overly conservative and unreliable in predicting the failure of masonry walls. The displacement based procedure uses a tri-linear relationship to characterise the real non-linear force-displacement behaviour of a masonry wall and has been substantiated from an extensive experimental and complementary analytical program.

An investigation into the behaviour of adobe mud-brick construction has been undertaken by Dowling using extensive shaking table testing (Dowling 2004). The annual rate of fatalities and injuries from earthquake events is dominated by people living in adobe construction. The project focuses on low cost and low technology improvements for developing countries such as reinforcing the corners and mid-spans of walls with bamboo and other materials and the provision of a ring beam at roof level.

The response of tall reinforced concrete chimneys to earthquake excitation was investigated by Wilson (2002, 2003). These structures were historically very conservatively designed on the assumption that highly tuned dynamically sensitive cantilevers were inherently brittle. The experimental tests and analytical studies indicated that chimneys possess some ductility if designed appropriately. Such structures were best designed using modal analysis techniques and the elastic loads could be reduced by a structural response factor of R=2 to allow for inelastic response, with significant cost savings.

Several analytical studies investigating the overall behaviour of structural systems have been undertaken. These studies have investigated: the ductility reduction factor in the seismic design of buildings (Lam 1998), equivalent damping ratios in reinforced concrete frame buildings for incorporation into the substitute structure method for seismic displacement response predictions (Edwards 2003) and the inelastic torsion response of buildings using a displacement based approach (Lumantarna 2003).

Risk modelling

Geoscience Australia has undertaken an extensive all-hazards risk study for selected Australian cities using GIS in a project termed 'Cities'. The earthquake aspects of the study involved field surveys to document the vulnerability characteristics of a representative sample of buildings and site studies to evaluate the soil conditions. Australian damage models based on the capacity spectrum method were then developed from heuristic studies of 'experts' and economic losses estimated using the HAZUS framework and the results displayed using the GIS model. Monte Carlo simulations were undertaken to consider the various combinations of magnitude, location, attenuation, soil amplification and building damage curves. The city of Newcastle, which experienced the M 5.6 in 1989, was the initial city studied and the results showed that the annualised loss was in the order of 0.04% or around $12 million per annum (Dhu 2002).

Reinsurance purchased by Australian companies is dominated by the need to protect against catastrophic loss from property damage caused by earthquakes. In excess of $100 million is paid annually to reinsurance companies to cover earthquake losses. The amount of reinsurance purchased is based on earthquake risk modelling and currently there are significant differences in the models being used. Walker (2003) recommends that a national consensus is required to develop the best assumption for modelling earthquake occurrence, attenuation, soil amplification and damage curves. Such information would have direct benefits to the insurance industry and Government agencies involved in emergency management and building regulations.

Earthquake loading standard

The current Earthquake Loading Standard (AS1170.4) was released in 1993 and the updated version is due for release in 2006. Originally the updated version was to be a joint and harmonised Standard with New Zealand, however severe difficulties developed during the drafting process. The largest challenge was how to combine the existing New Zealand Standard developed for a high seismic country with that of Australia where the design practices were quite different and the Standard reflected that of a low to moderate seismic country. In addition, some cities in each country had similar levels of seismicity (eg. Auckland has a seismicity level similar to Melbourne and Sydney). After much deliberation it was decided in 2003 to develop separate Earthquake Loading Standards but to use similar notation where possible.

The 2006 Australian Earthquake Loading Standard is similar in layout to the 1993 edition but has been significantly simplified and updated. Most structures will now have to be designed for some earthquake actions to ensure minimum levels of robustness. The structural response factors (R_f factors) have been standardised (refer Table 1) and the designer is able to use a non-linear push-over curve to provide a better estimate where required (refer Section 8). The material standards have also been updated over the past decade with improvements to the base level of detailing particularly concrete structures to improve inherent robustness and toughness.

System	Ductility (μ)	Over-strength (Ω)	$R_f = \mu \times \Omega$
URM	1.25	1.3	1.6
Limited Ductile	2	1.3	2.6
Moderate ductile	3	1.5	4.5
Ductile	4	1.5	6

Table 1: Revised ductility and over-strength factors in AS1170.4 (2006)

The design response spectra have also been significantly updated with a better estimate of the response acceleration, velocity and importantly displacement for a given location and site (Wilson and Lam 2003). The design response spectra have been reproduced in Figure 1 in the form of an ADRS plot (acceleration-displacement response spectrum which has the advantage of simultaneously indicating the acceleration (force) and displacement (drift) demand) for a zone factor (or acceleration coefficient) of Z=0.08 (or PGV=60 mm/sec) which applies to major cities in southeastern Australia including Sydney, Melbourne and Canberra. The velocity and displacement demand parameters: RSV_{max} and RSD_{max} (or PDD) estimated for different return periods and site classes have also been listed in Tables 2a and 2b for Z=0.08 and Z=0.08x1.8=0.14. The site factors listed in Column 2 of the table were inferred from the response spectra stipulated in AS1170.4 (2006). The demand parameter values for the 2500 year R.P. were obtained by multiplying the 500 year R.P. estimated demand values by a factor of 1.8 as recommended in AS1170.4 (2006).

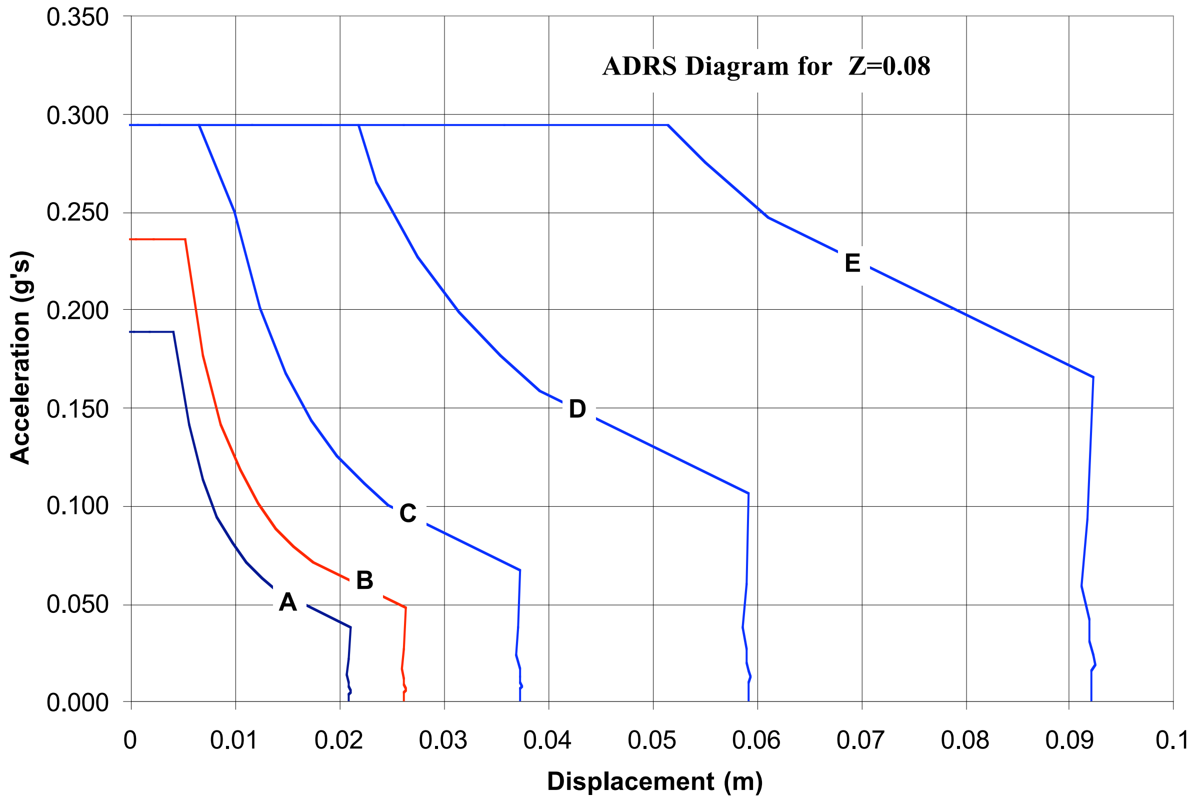

Figure 1: Design response spectra for Z=0.08 plotted in ADRS format

Soil Class	Site factor	Demand Parameters	
		RSV_{max}	PDD
A	0.80	85 mm/sec	20 mm
B	1.00	110 mm/sec	25 mm
C	1.40	150 mm/sec	35 mm
D	2.25	245 mm/sec	60 mm
E	3.50	380 mm/sec	90 mm

(a) 500 year return period, Z=0.08g

Soil Class	Site factor	Demand Parameters	
		RSV_{max}	PDD
A	0.80	155 mm/sec	35 mm
B	1.00	200 mm/sec	45 mm
C	1.40	270 mm/sec	65 mm
D	2.25	440 mm/sec	110 mm
E	3.50	685 mm/sec	160 mm

(b) 2500 year return period, Z=0.14

Table 2: Velocity and Displacement Demand for Australia (Wilson and Lam 2005)

The stipulated response spectra and the values of PDD, which are based on a "corner period" of 1.5 seconds (Wilson and Lam 2003), are considered reasonable and conservative, although the phenomenon of site resonance phenomenon and magnitude dependence has not been explicitly accounted for in the provisions.

Displacement based design

Over the past decade, in recognition of the fact that damage is directly related to drift and material strains (as opposed to induced inertia forces), the displacement-based (DB) design approach has been developed (refer review by Priestley 2000). The DB method is simpler in concept to apply and has great advantages for checking the performance of structures in low to moderate seismic regions at the ultimate limit state (ULS). In such regions, the serviceability earthquake which is associated with a return period in the order of 75 years (50% probability of exceedance in 50 years; abbreviated as 50/50), is typically small and does not need to be considered. In Australia, the ULS earthquake event is typically associated with a return period of between 500 and 2500 years (10/50 – 2/50) and structures should be designed to ensure that collapse is prevented.

The DB method summarised in this paper provides an elegant and simple means of checking performance at the ULS and is considered a major advancement on the more indirect FB method using overstrength and ductility factor (or structural response factor). The DB method requires the structure to be represented as a single degree of freedom structure and the seismic performance is assessed by comparing the displacement demand with the estimated structural displacement capacity. The DB approach, in which demand and capacity are defined in terms of displacement, can be used conveniently to illustrate the importance of magnitude dependence and the phenomenon of soil resonance as highlighted earlier in the paper. A more comprehensive description of the DB method is provided in Wilson and Lam (2005).

The displacement capacity (Δ_c) is obtained from a non-linear push-over analysis where the designer calculates the displacement as a function of increasing horizontal force until the structure is deemed to have failed. In this context, "failure" is assumed to have occurred when the overall structure ceases to be able to support the gravitational loads and collapse follows. There is an important distinction between this definition of failure (in terms of ensuring sustained gravitational load carrying capacity) with the traditional definition of failure used in high seismic regions for ensuring that horizontal resistance capacity is at least 80% of the nominal capacity (NZS1170.5:2004).

The resultant force-displacement plot is commonly known as the "push-over" (or capacity) curve which indicates the capacity of the structure to deform, and can be transformed into a acceleration-displacement curve by normalizing the base shear with respect to the mass of the building. Calculations in developing the transformed capacity curve are material dependent but should include effects such as the elastic and inelastic deflections of the structure together with deflection contributions from foundation flexibility and P-delta effects.

The performance of the building can be simply assessed using a "first tier" approach by comparing the peak displacement demand (PDD) with the displacement capacity (Δ_c). If PDD is less than Δ_c, then the structure is deemed satisfactory in terms of its ultimate performance.

If PDD is greater than Δ_c, it is recommended that the "second tier" capacity spectrum method (CSM as outlined in ATC40 1996, and Freeman 1998) be used to assess the seismic performance. The transformed capacity curve (as described above) is superimposed onto the demand diagram as shown in Figure 2. If the capacity curve intersects the demand diagram, the structure is deemed satisfactory. The intersection of the capacity and demand curves is defined as the "performance point" and provides a conservative estimate of the actual maximum displacement and acceleration demand on the building. The use of 5% damping is considered as a reasonable representation of real structural behaviour, given that recent research by the authors on the seismic performance of typical Australian structures revealed that effective damping is unlikely to exceed 10% (Edwards 2003).

If an intersection point cannot be obtained, there is a further option for the designer to adopt a refined procedure which involves modifying the demand line for different damping ratios (reflected by the inelastic energy absorptions by the structure). For example, point "2" in Figure 2 indicates that the performance is satisfactory with the updated (higher) damping value. It should be noted that the refinement going from 5% to 10% damping will only decrease the displacement demand by a small amount.

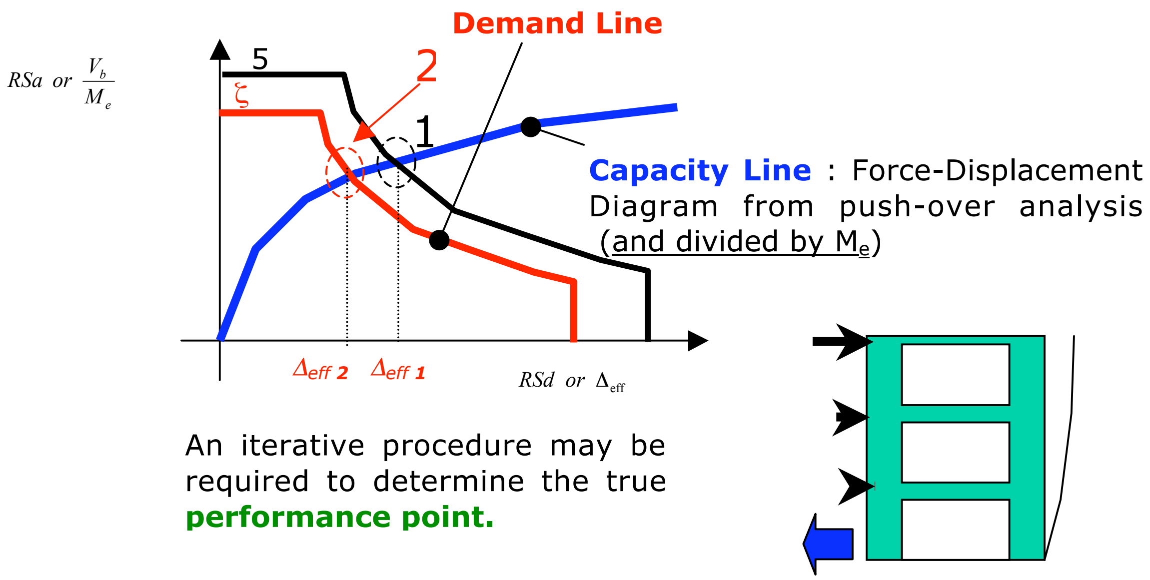

Figure 2: Capacity Spectra with Different Damping Ratios (Wilson and Lam 2005)

This two level Design Based (DB) check of structures has considerable advantages for regions of low to moderate seismicity. The PDD values presented in Table 2 can be converted to estimates of maximum drift demand using the following simplified equations for one storey and multi-storey buildings:

One storey: Max drift = PDD / h_1 (1a)
Multi storey: Max drift = [PDD / $n.h_1$].$PF_1.\gamma_{max}$ (1b)
Multi storey: Max drift = 3 [PDD / $n.h_1$] (1c)

where PDD is the Peak displacement demand of SDOF system, h_1 is the storey height, n is the number of stories, PF_1 is the Participation factor and γ_{max} is the Amplification factor to convert average linear drift to peak drift at any storey. For typical regular structures, the participation factor is around PF_1=1.5 and the amplification factor γ_{max} = 2 (Lam 2005) results in a maximum drift demand given by equation (1c).

Equations (1a) and (1c) have been used to estimate the maximum drift demands of 1, 5 and 10 storey regular buildings (assuming a constant storey height of h_1=4m) for different soil conditions and return periods of RP=500 and RP=2500 years, as listed in Table 3. The maximum drift demands have been calculated for a zone factor (or acceleration co-efficient of 0.08), corresponding to a 500 year return period event for Melbourne or Sydney. In addition, the value of "n" in Table 3 may be taken to be equal to 1 for the assessment of soft-storey structures where all the drift is assumed to be accumulated in one storey.

Return period	500 yr				2500 yr			
Site Classification	PDD	n=1	n=5	n=10	PDD	n=1	n=5	n=10
	mm	Drift (%)	Drift (%)	Drift (%)	mm	Drift (%)	Drift (%)	Drift (%)
A	20	0.5	0.3	0.2	40	1.0	0.6	0.3
B	25	0.7	0.4	0.2	50	1.2	0.7	0.4
C	35	0.9	0.6	0.3	65	1.7	1.0	0.5
D	60	1.5	0.9	0.4	105	2.7	1.6	0.8
E	90	2.3	1.4	0.7	165	4.1	2.5	1.2

Table 3: Drift Demand Ratios of Regular Multi-Storey Buildings (Wilson and Lam 2005)

The maximum drift demand values presented in Table 3 may be amplified further if the structure is torsionally irregular or reduced if the effects of foundation compliance are significant. The maximum drift demand associated with the 500 year return period event are clearly modest for site classes A, B and C, whilst more demanding for the soft site classes D and E where the PDDs are magnified. Structures considered at most risk in the Australian context with these drift demands are unreinforced masonry, tall buildings with a soft storey configuration, single storey tilt-up construction and some façade systems.

Future trends

The DB method approach described in Section 8 is deterministic in nature but can be converted to a probabilistic approach for use in risk modeling through the development of representative fragility curves. The intersection of the demand and capacity curve on the capacity spectrum diagram shown in Figure 2 creates a deterministic performance point associated with a level of damage. However, if probabilistic distributions (normal or log-normal) are included in each of these curves to represent the actual variability of capacity and ground motion then the resulting performance can be represented by a log-normal cumulative probability density function, known as a 'fragility curve'. Sample fragility curves developed for damage states of pre-yield, repairable damage, irreparable damage, incipient collapse and collapse are shown in Figure 3.

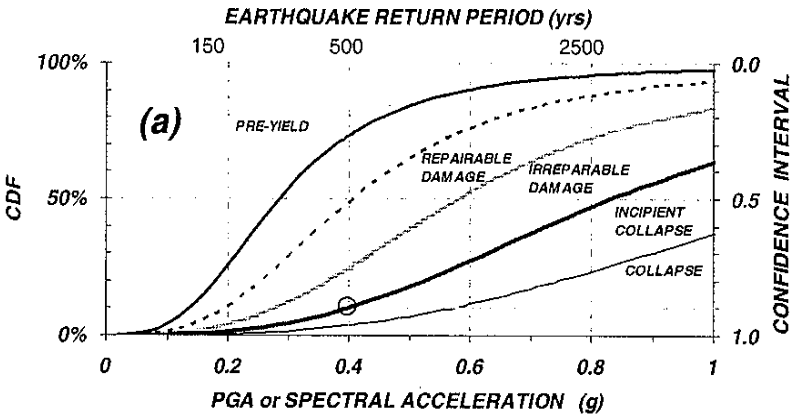

Figure 3: Classical example of fragility curves (after Mander 2004)

The development of representative fragility curves for different structural systems is considered the next challenge in Australian earthquake engineering to assist in risk modelling. Fragility curves can be used to screen code revisions and assess the need for seismic retrofitting. This probabilistic approach has been used in the low-moderate seismic regions of the United States to assist in decision making using a risk-benefit based framework. The method allows a structured framework for assessing public safety and economic losses from damage/failure to public infrastructure and has the potential to assess the effectiveness of various risk mitigation strategies in terms of risk reduction as a proportion of money invested (Ellingwood 2005). The concept of risk is defined in terms of the earthquake hazard, structural vulnerability, consequence of damage and collapse and the context or frame of reference of the risk assessment which varies amongst different stakeholders.

An on-going challenge in Australia is the level of funding invested in earthquake engineering research, which has steadily fallen over the past decade as the memories of the 1989 Newcastle earthquake fade. This is an international challenge for those researchers investigating areas that can be considered low probability/high consequence events and can be demonstrated by the considerable funding that was suddenly made available after the devastating 2004 Boxing Day tsunami that killed some 300,000 people. A study undertaken by Dr Neil Swan for the Geological Survey of Canada (Swan 1999 and reported by Griffith in the AEES newsletter 3/2003) has particular relevance for

Australia. Swan undertook a cost/benefit analysis on the level of funding invested in earthquake engineering research in Canada and concluded that the benefits outweighed the investment by around 10 to 1. A similar study in Australia is needed to demonstrate the importance and benefits derived from a recurrent investment in seismic monitoring, data collection and earthquake engineering research.

Summary and concluding remarks

- Numerous approaches utilizing information developed in the field of seismology, geophysics, geomorphology and neo-tectonics have been applied to Australia for the modelling of its seismic activity, particularly the recurrence behaviour of potential moderate and large magnitude events. The challenge is in reconciling differences between contributions from different modelling approaches and integrating them into a robust model that best reflects the state of the developing knowledge.
- Attenuation relationships have been recommended for different regions within Australia based on different approaches including the Component Attenuation Model (CAM) approach which has now been developed into international applications. Good consistencies between the different approaches have been demonstrated.
- Site classification has been based on identification of the regolith types and site natural period.
- Displacement amplification on flexible soil sites associated with conditions pertaining to soil resonance behaviour has been incorporated into CAM.
- Research into the seismic performances of typical Australian construction which incorporates the use of unreinforced masonry, steel and concrete has been summarised.
- A brief report on current activities with risk modelling and Standards development has been given.
- A displacement based procedure (DB) as an alternative to the traditional force based procedure (FB) has been outlined and is considered a more direct and elegant approach for assessing the seismic performance of structures.
- The future trends in earthquake engineering will be to translate the research outcomes into a probabilistic framework that can be used to provide improved risk-benefit-based design decisions for a range of stakeholders.

Acknowledgements

Much material presented in this paper was developed from research projects funded by the Australian Research Council (Discovery Grants and Large Grants) over the past ten years. Invaluable contributions and support over the years by Prof. Graham Hutchinson and other colleagues at the University of Melbourne and by other research collaborators in Australia namely A/Prof. Mike Griffith of the University of Adelaide, Prof. Michael Asten of Monash University, Gary Gibson of the Seismology Research Centre and Kevin McCue are gratefully acknowledged. Contributions by international research collaborators including colleagues from New Zealand, Prof Adrian Chandler of the University of Hong Kong, Prof. T Balendra of The National University of Singapore and Prof. Andrew Whittaker of University of Buffalo (State University of New York) are also gratefully acknowledged. The authors also acknowledge the reviewers comments which have added clarity to the paper.

References

Abdouka, K. and Goldsworthy, H.M. (2002). "Shear force - unbalanced moment transfer at reinforced concrete exterior wide band beam connection", Australian Journal of structural Engineering, Vol. 4 No. 2

Allen, T., Gibson, G., and Cull, J. (2003). "Comparative study of average response spectra from Australian and New Zealand Earthquakes", Procs. of the Annual Technical Conference of the Australian Earthquake Engineering Society, Melbourne, paper no.10.

AS1170.4 (1993) Standards Association of Australia. Minimum design loads on structures : Part 4: Earthquake Loads - AS1170.4 and Commentary, 1993.

AS2121 (1979) Standards Association of Australia. SAA Earthquake Code.

Asten, M. (2003). "Lessons from alternative array design used for high frequency microtremor array studies", Procs. of the Annual Technical Conference of the Australian Earthquake Engineering Society, Melbourne, paper no.14.

Asten, M. and Dhu, T. (2003). "Comparison of shear-velocities measured from microtremor array studies and SCPT data acquired for earthquake site hazard site hazard classification in the northern suburbs of Perth W.A.", Procs. of the Annual Technical Conference of the Australian Earthquake Engineering Society, Melbourne, paper no.12.

Asten, M. and Dhu, T. (2002). "Enhanced interpretation of microtremor spectral ratios in seismic hazard zonation using multimode Rayleigh-wave particle motion computations". Proc. Aus. Earthquake Eng. Soc. Conf., Adelaide, 2002.

Asten, M., Lam, N.T.K., Gibson, G. and Wilson, J.L. (2002). "Microtremor survey design optimized for application to site amplification and resonance modeling". Procs. Australian Earthquake Eng. Soc. Conf., Adelaide, 2002.

ATC-40 (1996) Seismic evaluation and retrofit of concrete buildings, Vols.1&2. Redwood City, CA: Applied Technology Council, 1996.

Brown, A. and Gibson, G. (2003). "Earthquake Hazard in Australia Using a Multi-Tiered Source Model", Procs. of the Annual Technical Conference of the Australian Earthquake Engineering Society, Melbourne, paper no.20.

Chandler, A.M., Lam, N.T.K. and Sheikh, M.N. (2002). "Response spectrum predictions for potential near-field and far-field earthquakes affecting Hong Kong: soil sites". Journal of Soil Dynamics & Earthquake Engineering 2002:Vol.22, pp.419-440.

Chandler, A.M. and Lam, N.T.K. (2001): "Performance-based design in earthquake engineering: A multi-disciplinary review", Journal of Engineering Structures: Civil Zone Review. 23, 1525-1543.

Clark D, (2005), "A preliminary seismicity model for south-western Australia based on neo-tectonic data", Proceedings Australian Earthquake Engineering Society Conference, Albury 2005, Paper No. 22.

Dhu, T., Jones, A., Fityus, S., Jones, T., Robinson, D. and Schneider, J. (2002). "Site response analysis in Newcastle and Lake Macquarie", Procs. of the Annual Technical Conference of the Australian Earthquake Engineering Society, Adeladie, paper no. 18.

Dhu, T. and Jones, T. (eds), (2002). "Earthquake risk in Newcastle and Lake Macquarie", Geoscience Australia Record 2002/15, Geoscience Australia, Canberra

Doherty, K., Griffith, M.C., Lam, N.T.K. and Wilson, J.L. (2002). "Displacement-Based Analysis for Out-of-Plane Bending of Seismically Loaded Unreinforced Masonry Walls" Earthquake Engineering and Structural Dynamics, Vol 31 No. 4 pp 833-850

Dowling DM, Samali B, Li J, (2004), "Shake table testing of un-reinforced and lightly reinforced 'U' shaped adobe mud brick wall units", Proceedings of Australian Earthquake Engineering Society 2004 Conference, Paper No. 23.

Dowrick D.J., Gibson G. and McCue K. (1995). "Seismic Hazard in Australia and New Zealand", Bulletin of the New Zealand National Society for Earthquake Engineering.1995: Vol.28(4), pp.279-287.

Edwards, M., Wilson, J.L. and Lam N.T.K. (2003). "Seismic Displacement Response Predictions Using a Calibrated Substitute Structure Approach", Procs. of the Sixth

Pacific Conference of Earthquake Engineering, University of Canterbury, Christchurch, New Zealand, March, Paper no.110.

Electric Power Research Institute (1993). Vol.2 : "Appendices for ground motion estimation" in Guidelines for determining design basis ground motions – EPRI TR-102293, California, USA.

Ellingwood BR, Wen YK, 2005, "Risk benefit based design decisions for low-probability high consequence events in mid-America", Proceedings Structural Engineering and Materials, Vol 7, pp 57-70.

Freeman, S.A. (1998). "Development and use of capacity spectrum method". Proceedings of the 6th US National Conference on Earthquake Engineering, Seattle (USA), 1998.

Gad, E.F., Wilson, J.L., Moore, A.J. and Richards, A.B. (2004). "Effects of mine blasting on residential structures" ASCE Journal of Constructed Facilities, (in press)

Gad, E.F., Chandler, A.M., Duffield, C.F. and Hutchinson, G.L. (1999). "Earthquake ductility and overstrength in domestic structures", Journal of Structural Engineering and Mechanics, Vol. 8, Number 4, October, pp 361-382.

Gaull, B.A., Michael-Leiba, M.O. and Rynn, J.M.W. (1990). "Probabilistic earthquake risk maps of Australia". Australian Journal of Earth Sciences, 1990: Vol.37, pp.169-187.

Hutchinson, G.L., Lam, N.T.K. and Wilson, J.L (2003) "Determination of earthquake loading and seismic performance in intraplate regions", Progress in Structural Engineering and Materials, 2003. John Wiley & Sons Ltd., Vol.5:181-194.

Griffith, M.C., Lam, N.T.K., Wilson, J.L. and Doherty, K. (2004). "Experimental investigation of unreinforced masonry walls in flexure" Structural Journal of the American Society of Civil Engineers, Vol.130(3), pp.423-432.

Griffith, M.C., Wu, Y. and Oehlers D. (2003), "Steel plated seismic retrofit for RC columns in soft storey frames" ", Procs. of the Australian Earthquake Engineering Society Annual Conference, Melbourne, November. Paper no.9.

Griffith MC, Wilson JL, Lam NTKL, (2005), "Displacement based assessment of the seismic capacity of un-reinforced masonry walls in bending" Australian Journal of Structural Engineering, Vol 6 No 2, pp 119-1131.

IBC, (2000). International Code Council. International Building Code, USA.

Idriss, I.M. and Sun, J.I. (1991). User's manual for SHAKE-91, sponsored by National Institute of Standards and Technology, Maryland, U.S.A. and Department of Civil & Environmental Engineering, University of California, Davis, U.S.A., 1992.

Lam NTK, Chandler A, 2005, "Peak displacenment demand in stable continental regions", Earthquake engineering and Structural dynamics, Vol 34, pp 1047-1072.

Lam, N.T.K. and Wilson, J.L. (2004). Displacement Modelling of Intraplate Earthquakes, International Seismology and Earthquake Technology Journal (special issue on Performance Based Seismic Design). Indian Institute of Technology. Accepted for publication and in press)

Lam, N.T.K. and Wilson, J.L. (2003). "The Component Attenuation Model for Low and Moderate Seismic Regions", Procs. of the 2003 Pacific Conference on Earthquake Engineering, Christchurch, New Zealand. Paper no.99.

Lam, N.T.K., Sinadinovski, C., Koo, R.C.K. and Wilson, J.L. (2003), "Peak Ground Velocity Modelling for Australian Earthquakes". International Journal of Seismology and Earthquake Engineering, Vol.5(2), pp.11-22

Lam, N.T.K., Griffith, M.C., Wilson, J.L. and Doherty, K. (2003), 'Time-history analysis of URM walls in out-of-plane flexure" Journal of Engineering Structures, Vol. 25, pp. 743-754.

Lam, N.T.K., Wilson, J.L. and Chandler, A.M. (2001), "Seismic displacement response spectrum estimated from the frame analogy soil amplification model". Journal of Engineering Structures 2001; Vol.23(11), pp.1437-1452.

Lam, N.T.K., Wilson J.L., Chandler, A.M. and Hutchinson, G.L. (2000a). "Response spectral relationships for rock sites derived from the component attenuation model". Journal of Earthquake Engineering & Structural Dynamics 2000; Vol.29, pp.1457-1489.

Lam, N.T.K., Wilson, J.L., Chandler, A.M. and Hutchinson, G.L. (2000b). "Response spectrum modelling for rock sites in low and moderate seismicity regions combining velocity, displacement and acceleration predictions". Journal of Earthquake Engineering & Structural Dynamics 2000; Vol.29, pp.1491-1525.

Lam, N.T.K., Wilson, J.L. and Hutchinson, G.L. (2000c). "Generation of synthetic earthquake accelerograms using seismological modeling: a review". Journal of Earthquake Engineering 2000; Vol. 4(3), pp.321-354.

Lam, N.T.K. and Wilson, J.L. (1999). "Estimation of the Site Natural Period from borehole records", Australian Journal of Structural Engineering, 1999 : Vol.SE1(3), pp.179-199.

Lam, N.T.K., Wilson, J.L. and Hutchinson, G.L., (1998). "The ductility reduction factor in the seismic design of buildings", Earthquake Engineering and Structural Dynamics, Vol. 27, pp 749-769.

Lumantarna, E., Lam, N.T.K. and Wilson, J.L. (2003). "A displacement approach to the analysis for seismically induced torsion in buildings", Procs. of the Australian Earthquake Engineering Society Annual Conference, Melbourne, November. Paper no.15.

Mander JB, 2004, "Beyond ductility: the quest goes on", Bulletin NZSEE, Vol 37 No 1, pp35-44

Melchers, R.E. (ed.) (1990). Newcastle Earthquake Study. The Institution of Engineers, Australia.

McCue, K.F. and Sinadinovski, C. (2003). "Earthquakes in dissimiliar tectonic regimes – comparison study of two shallow events with similar magnitude", Procs. of the Annual Technical Conference of the Australian Earthquake Engineering Society, Melbourne, paper no.13.

McCue, K.F., Dent, V. and Jones, T. (1995). "The Characteristics of Australian Strong Ground Motion". Procs. of the fifth Pacific Conference of Earthquake Engineering, Melbourne.

Newmark, N.M. and Rosenblueth, E. (1971) Fundamentals of earthquake engineering. Prentice-Hall, New Jersey, 1971.

Priestley MJN, 2000, "Performance based seismic design", Proceedings 12th World Conference of Earthquake Engineering, Auckland, 2000, Keynote paper no. 2831.

Robinson, A., Sanders, P. and Wilson, J.L. (1999). "Lateral loading behaviour and earthquake response factors of precast concrete load-bearing panel structures", Proceedings Concrete Institute of Australia 19th Biennial Conference, Sydney, Paper no. 92.

Rodsin, K., Lam, N.T.K., Wilson, J.L. and Goldsworthy, H.M. (2003). "The seismic assessment of soft-storey buildings in Melbourne", Procs. of the Australian Earthquake Engineering Society Annual Conference, Melbourne, November, Paper no.17.

Sandiford, M., Leonard, M. and Coblentz, D. (2003). "Geological constraints on active seismicity in southeast Australia", keynote presentation given to the Australian Earthquake Engineering Society Annual Conference, Melbourne, November 2003, paper no. 1.

Somerville, M., McCue, K. and Sinadinovski, C. (1998). "Reponse Spectra Recommended for Australia", Australian Structural Engineering Conference, Auckland, pp.439-444.

Stehle, J.S., Goldsworthy, H.M. and Mendis, P. (2001). "An experimental study of reinforced concrete wide band beams under earthquake loading", American Concrete Institute Structural Journal, Vol. 98, No. 3, pp 270-279.

Stock, C. and Smith, E.G.C. (2002a). "Adaptive Kernel Estimation and Continuous Probability Representation of Historical Earthquake Catalogs". Bulletin of the Seismological Society of America : 92(3):904-912.

Stock, C. and Smith, E.G.C.(2002b) "Comparison of Seismicity Models Generated by Different Kernel Estimations", Bulletin of the Seismological Society of America : 92(3):904-912.

Swan N, 1999, “Benefits from expenditure on earthquake research at Natural Resources Canada” Geological Survey of Canada Open File 3764, http://earthquakescanada.nrcan.gc.ca/hazard/OF3764/OF3764abs.php

Toro, G.R., Abrahamson, N.A. and Schneider, J.F. (1997). “Model of strong ground motions from earthquakes in Central and Eastern North America: best estimates and uncertainties”. Seismological Research Letters 1997; Vol.68(1), pp.41-57.

Turnbull, M and Fichera, J. (2003). “A relative seismic vulnerability analyses of Hervey Bay City, Queensland”, Procs. of the Australian Earthquake Engineering Society Annual Conference, November 2003, paper no. 7.

Uniform Building Code (UBC), (1991). International Conference of Building Officials, Whittier, California, USA.

Venkatesan, S. (2004). Departmental Report : Component Factors for Site Resonance, Department of Civil & Environmental Engineering, University of Melbourne, 2004.

Venkatesan, S., Dhu, T., Lam, N.T.K. and Wilson, J.L. (2003). “The Effect of Rock Motions on Soil Amplification Factors for Australian Conditions”. Procs. of the Australian Earthquake Engineering Society Annual Conference, Melbourne, November 2003, paper no. 16.

Venkatesan, S., Dhu, T., Robinson, D., Lam, N.T.K., Wilson, J.L. and Jones, A. (2002). “Site response analysis – a comparison of methods and scales”. Procs. of the Australian Earthquake Engineering Society Annual Conference, Adelaide, November 2002, paper no. 14.

Walker, G. (2003). "Earthquake risk in Australia and insurance", Procs. of the Australian Earthquake Engineering Society Annual Conference, Melbourne, November, Paper no.25

Wallace, D.G., Goldsworthy, H.M., Wilson, J.L. (2002). ”Seismic performance of steel concentrically braced frames in Australia” Australian Journal of Structural Engineering, Vol. 4 No. 1, pp. 51-61

Wilkie, J. and Gibson, G. (1995). “Estimation of seismic quality factor Q for Victoria, Australia”. AGSO Journal of Geology & Geophysics 1995; Vol.15(4), pp.511-517.

Wilson, J.L. and Lam, N.T.K. (2003). “A recommended earthquake response spectrum model for Australia”, Australian Journal of Structural Engineering. Institution of Engineers Australia, 5(1), pp.17-27.

Wilson, J.L. (2003). “Earthquake response of tall reinforced concrete chimneys” Journal of Engineering Structures, Vol. 25 No. 1, pp. 11-24

Wilson, J.L. (2002). “Code recommendations for the aseismic design of tall reinforced concrete chimneys” ACI Structural Journal, Vol.99 No. 5, pp. 622-630

Wilson JL, Lam NTKL, 2005, “Earthquake design of buildings in Australia using velocity and displacement principles” Australian Journal of Structural Engineering, Vol 6 No 2, pp 103-118

Woo, G. (1996). “Estimation Methods for Seismic Hazard Area Source Modelling”. Bulletin of the Seismological Society of America. 86(2):353-362.

Yao H, Goldsworthy H, Gad E, (2005), “Finite element modeling of blind bolted ‘T’ stub connections to CFT columns”, Proceedings of Australian Earthquake Engineering Society 2005 Conference, Albury, Paper No. 16.

Preliminary test of the EEPAS long term earthquake forecast model in Australia

Paul Somerville[1,] Jeff Fisher[1,] David Rhoades[2] and Mark Leonard[3]

[1] Risk Frontiers
[2] GNS Science
[3] Geoscience Australia

Abstract

EEPAS is a long term earthquake forecasting procedure (Every Earthquake a Precursor According to Scale) developed by Evison and Rhoades. To date, the EEPAS procedure has been successfully tested in the tectonically active regions of New Zealand, Japan and California, but has not been tested in tectonically stable regions like Australia. We have made a preliminary test of the EEPAS procedure in Australia, beginning our analysis by applying it in a retrospective fitting mode to four regions of Australia, identified by Leonard (2005), that have relatively high levels of seismic activity and catalogue completeness. These include Southeast Australia, South Australia, Southwest Australia, and Northwest Australia. It appears from our preliminary analysis that the EEPAS procedure is applicable to the tectonically stable region of Australia. In Southeastern Australia, the data are sufficiently complete above M2.0 to use M2.0 as a minimum magnitude, with a target set of M>4.25 for the time period of 1975 – 2003. The optimal EEPAS parameters are similar to those obtained in tectonically active regions, except for a high value of 0.5 for the failure rate. The information gain per earthquake of EEPAS over a simpler model (PPE, i.e. Proximity to Past Earthquakes) is 0.64 for SE Australia, which is roughly the same as in other applications, but we note that this only a retrospective fitting exercise. We have tested the procedure in a prospective mode to the 1989 Newcastle earthquake. EEPAS did not indicate a large likelihood gain before the Newcastle earthquake, but the magnitude 5.3 Ellalong earthquake of 1994, together with the magnitude 5.5 Newcastle earthquake of 1989, give rise to increased probability of a larger earthquake in this region.

Introduction

At present, there is no generally recognised capability for earthquake prediction, which seismologists define as specifying the time of occurrence, location and size of an earthquake within reasonably narrow uncertainty bands. However, it has long been recognized that there are periodicities in earthquake occurrence, and recently it has become clear that earthquake forecasting based on the preceding sequence of earthquakes in a region is feasible. One kind of forecasting relates mainly to the occurrence of aftershocks in the very short term (hours and days) following a mainshock. Another kind of forecasting, which relates to the long term (years to decades) forecasting of mainshocks (which we define here as potentially damaging earthquakes), is based on decades of prior seismicity.

To date, the most successful long term earthquake forecasting method is the EEPAS procedure (Every Earthquake a Precursor According to Scale) developed by Evison and Rhoades (2004) and Rhoades and Evison (2004). These authors have shown that a mainshock is preceded by an increase in the rate of occurrence of smaller earthquakes in the surrounding region. These smaller earthquakes appear to herald the reloading of the region to a level of stress that locally exceeds the strength of the crust. Equations have been developed that relate the magnitude M of the impending earthquake to the duration of precursory seismicity and the size of the region in which it occurs. These equations provide the means to forecast the time-varying level of seismic activity throughout a region based on its preceding seismicity. This method does not predict specific earthquakes, but in hindsight specific earthquakes are found to have occurred in regions with high forecast levels of activity.

To date, the EEPAS procedure has been successfully tested in the tectonically active regions of New Zealand (Rhoades and Evison, 2004), California (Rhoades and Evison, 2004), Japan (Rhoades and Evison, 2005, 2006) and Greece (Console et al., in press). In this paper, we show that it is expected to be also effective in the tectonically stable region of Australia.

This development has important implications for the evaluation of seismic hazards. At present, seismic hazard analyses usually assume that earthquakes occur randomly in time (Poisson model). However, the accelerated seismicity model described above provides a much more accurate forecast of seismicity than the Poisson model. The use of a time-dependent method of analysis based on this model would potentially provide much more accurate estimates of earthquake loss in a given region during a given year. In a particular year, damaging earthquakes, if they occur at all, are likely to occur in locations that are identified as having an increased level of activity.

Analysis

We applied the EEPAS earthquake forecasting methodology in a retrospective fitting mode to the Southeastern Australia region. This is one of the four regions of Australia, identified by Leonard (2005), that have relatively high levels of seismic activity and catalogue completeness. The earthquake catalog that we have used is that described by Leonard (2005). In the Southeastern Australia zone, the seismicity data are sufficiently complete above M2.0 to use M2.0 as a minimum magnitude, with a target set of M>4.25 for the time period of 1975 – 2003. The optimal EEPAS parameters are found to be similar to those obtained in tectonically active regions, except for a high value of 0.5 for the failure rate. However, the uncertainty in the parameter estimates is large because of the small number of earthquakes (22) in the target set. The information gain per earthquake of EEPAS over a simpler model (PPE, i.e. Proximity to Past Earthquakes) is 0.64 for SE Australia, which is roughly the same as in other applications, but we note that this is only a retrospective fitting exercise.

Test against the 1989 Newcastle earthquake

We tested the EEPAS procedure against the 1989 Newcastle earthquake (McCue et al, 1990), because this is the largest earthquake to have occurred in Southeastern Australia in recent years. The magnitude of this earthquake in the catalog described by Leonard (2005), which we used for consistency, but note that McCue et al. (1990) prefer a magnitude of 5.6. The EEPAS precursory scale increase parameters for the 1989 Newcastle earthquake are shown in Figure 1. The epicenter of the earthquake is at about Latitude -33.0, Longitude 151.75. The average magnitude of the three largest precursory earthquakes MP is 3.5, the time interval over which the precursory activity occurred TP is 4144 days (over 11 years), and the area over which the precursory activity occurred AP is 518 km^2. Compared with many other examples of the precursory scale increase phenomenon (Evison and Rhoades, 2004), the Newcastle precursory increase of seismicity is typical, but TP is much longer than expected for an Mm 5.5 earthquake.

The EEPAS forecast is shown spatially in the form of rate density of earthquakes of a specified magnitude (Figure 2). The units shown in this figure are RTR units, which is a comparison with a reference density in which there is an expectation of 1 earthquake per year exceeding any magnitude M in an area of 10m km^2. With this normalization, the average rate density in a region in RTR units is approximately constant over all magnitudes. In more seismically active plate boundary regions such as New Zealand and California, the average RTR value is about 1. In SE Australia the average RTR value is about 0.015.

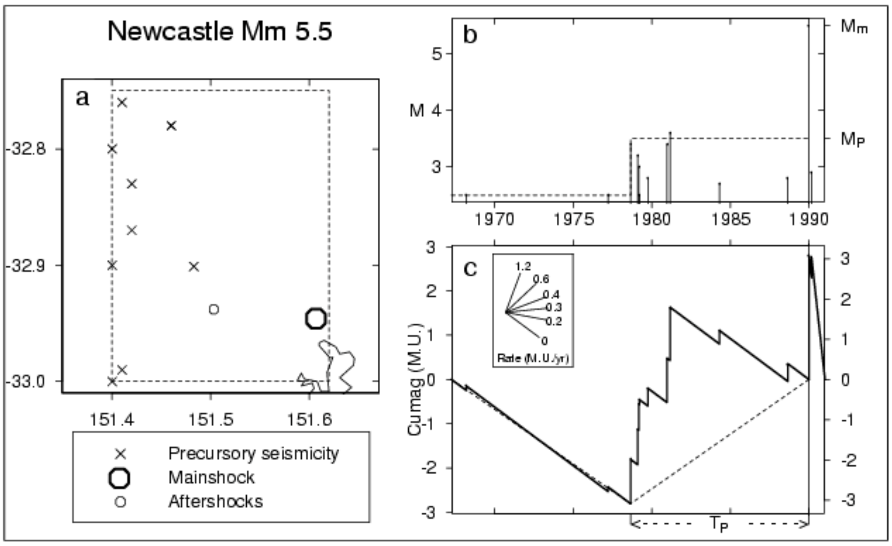

Figure 1. Precursory scale increase for Newcastle Mm 5.5 earthquake of 1989/12/27. MP = 3.5, TP = 4144 days, AP = 518 km^2. (a) Epicentres of precursory earthquakes, mainshock and aftershocks. Dashed lines enclose the precursory area AP. (b) Magnitudes versus time of prior and precursory earthquakes, also mainshock and aftershocks. Dashed lines show precursory increase in magnitude level. Mm is mainshock magnitude; MP is precursor magnitude. (c) Cumulative magnitude anomaly (Cumag) versus time. Dashed lines show precursory increase in seismicity rate. Protractor translates cumag slope into seismicity rate in magnitude units per year (M.U./yr), for times before the mainshock. Cumag values at the right hand ordinate refer to times beginning with the mainshock.

Figure 2 shows the earthquake forecast in Southeastern Australia just before the 1989 Newcastle earthquake. The RTR in the epicentral region of Boolaroo just west of Newcastle has a value of about 0.05 (yellow colour in Figure 2). Thus the EEPAS procedure indicated a moderate likelihood gain before the Newcastle earthquake.

The M5.3 Ellalong earthquake of 1994, together with the M5.5 Newcastle earthquake of 1989, have since given rise to increased probability of a larger earthquake in this region, as shown in Figures 3 through 6. The likelihood as of 2004/1/1 of an M5.5 earthquake has not changed, as shown in Figure 3, and becomes larger in relative terms (compared with other locations) for increasingly large earthquakes, as shown for M7 in Figure 4. Although the absolute likelihood of an earthquake in a given region of fixed area does not increase with magnitude, the RTR values in the Newcastle area increase up to M7 because the probability increase is centered on magnitudes 1 - 2 units higher than those of the earthquakes generating it (i.e., 5.5 and 5.3). The increased probability at around M7 would have arisen gradually over the preceding decade and will subside gradually over the next 1 – 2 decades, unless reinforced by the occurrence of further earthquakes of magnitude 5 – 6 in the same vicinity.

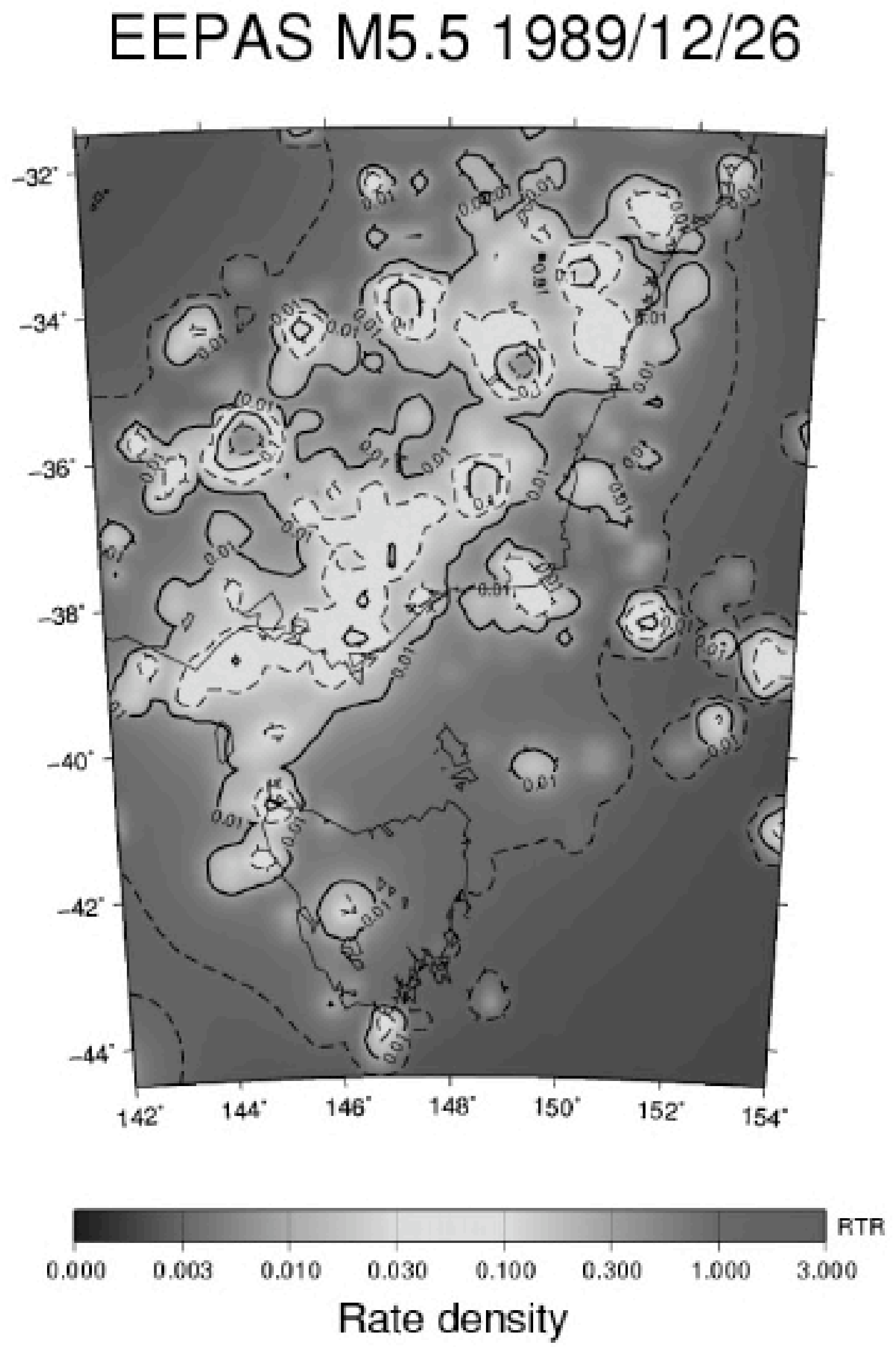

Figure 2. EEPAS rate density of earthquake occurrence in Southeastern Australia as at 1989 Dec 26, just before the Newcastle earthquake for M5.5 in RTR units, i.e. relative to a reference density in which there is an expectation of 1 earthquake per year exceeding any magnitude m in an area of 10m km^2. Seismicity data to 26 December 1989.

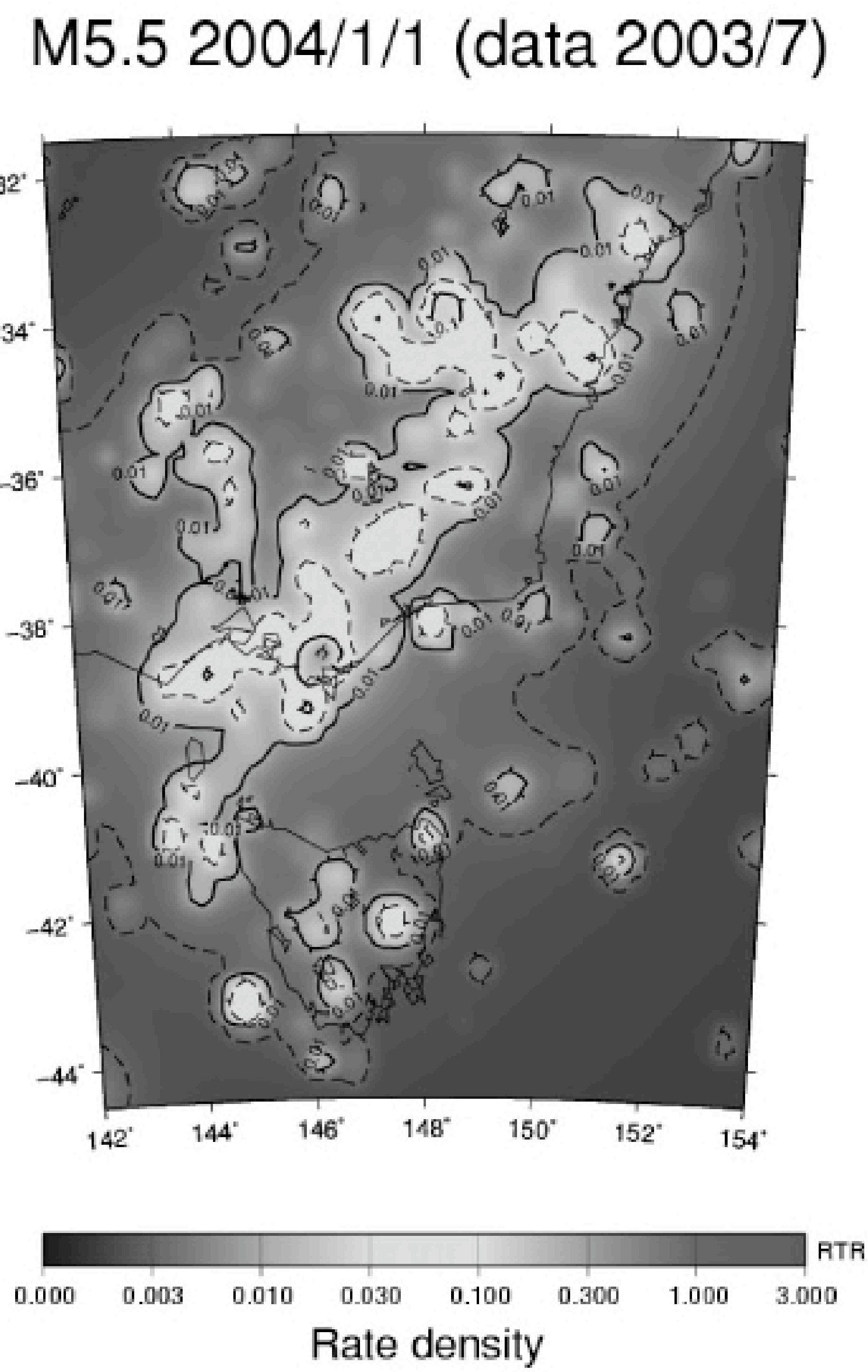

Figure 3. EEPAS rate density of earthquake occurrence in Southeastern Australia as at 2004 Jan 1 for M5.5 in RTR units, i.e. relative to a reference density in which there is an expectation of 1 earthquake per year exceeding any magnitude m in an area of 10m km^2. Data to July 2003.

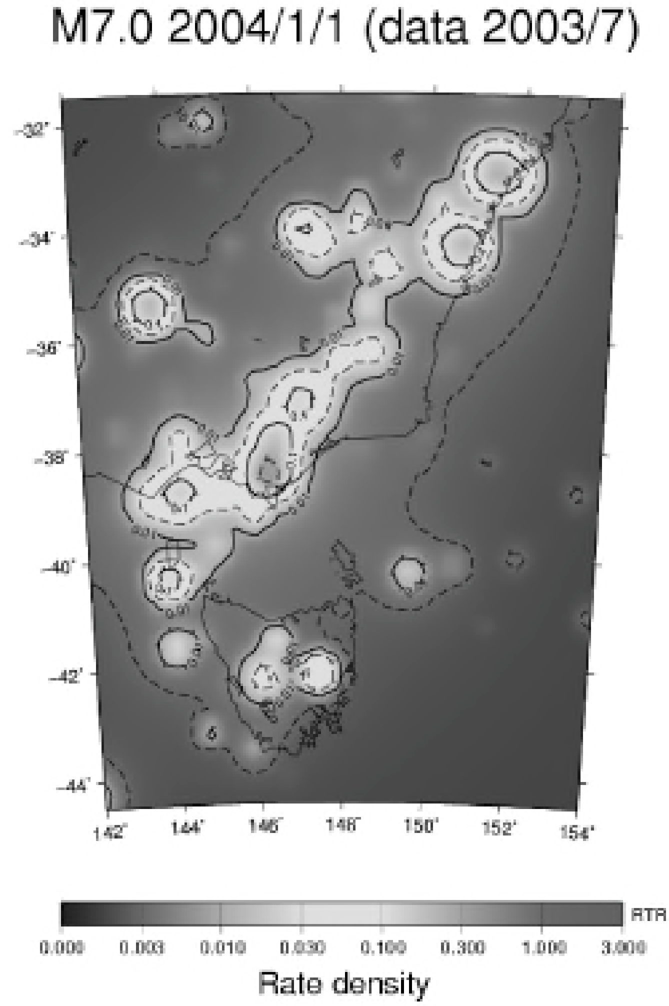

Figure 4. EEPAS rate density of earthquake occurrence in Southeastern Australia as at 2004 Jan 1 for M7.0 in RTR units, i.e. relative to a reference density in which there is an expectation of 1 earthquake per year exceeding any magnitude m in an area of 10m km^2. Data to July 2003.

References

Evison, F.F. and D.A. Rhoades (2004). Demarcation and scaling of long-term seismogenesis. Pure and Applied Geophysics 161, 21-45.

Leonard, M. (2005). One hundred years of earthquake recording in Australia. Bull. Seism. Soc. Am., 96, in press..

Console, R., Rhoades, D.A., Evison, F.F., Murru, M., Papadimitriou, E.E., and V.G. Karakostas, (in press). Comparative performance of time-invariant, long-term and short-term forecasting models on the earthquake catalogue of Greece. Journal of Geophysical Research.

McCue, K.F., Wesson, V., & Gibson, G. (1990). The Newcastle New South Wales, earthquake of 28 December 1989. BMR Journal of Australian Geology & Geophysics, 11, 4, 559-568.

Rhoades, D.A. and F.F. Evison (2004). Long-range earthquake forecasting with every earthquake a precursor according to scale. Pure and Applied Geophysics 161, 47-72.

Rhoades, D.A. and F.F. Evison (2005). Test of the EEPAS forecasting model on the Japan earthquake catalogue. Pure and Applied Geophysics 162, 1271-1290.

Rhoades, D.A. and F.F. Evison (2006). The EEPAS forecasting model and the probability of moderate to large earthquakes in central Japan. Tectonophysics 417, 119-130.

Ground displacement at the North Shore Pier of the Narrows Bridge during the Meckering earthquake

Geoffrey Cocks & Michael Hillman

Coffey Geotechnics Pty Ltd

Abstract

The original Narrows Bridge in Perth, Western Australia was constructed in the 1950s. The Northern shoreline comprised dredged sand fill, placed over a deep sequence of soft and compressible estuarine sediments. During the placement of the fill, the existing soft sediments were deliberately displaced by constructing a sand embankment until a slip occurred. The displacement was only partially successful and a wedge of alluvium of non-uniform thickness was left in place below the sand fill. The retention of this wedge of soft alluvium, and the presence of very loose zones within the sand fill lead to concerns about ongoing lateral creep and horizontal loads on piles. Main Roads Western Australia (the State Road Authority) established a number of survey monitoring points on the North Shore to measure displacement in the X, Y (horizontal) and Z (vertical) directions. These points were monitored regularly until the 1970s and the monitoring data spans the time of the 1968 Meckering Earthquake. When plotted with time on a log scale, the survey displacement data is approximately linear and shows distinct "steps" both vertically and horizontally, corresponding to the time interval in which the Meckering Earthquake occurred. Displacements inferred from the "steps" were in the range of 5mm to 18mm vertically and 10mm to 16mm horizontally. The horizontal movement is consistent with that calculated using the Youd et al (2002).

Introduction

The Narrows Bridge connects Perth to South Perth across a narrow part of the Swan River estuary. During the last Ice Age, the sea level off the coast of Western Australia was much lower and the Swan River flowed in a paleochannel about 20 m to 30m lower than the current elevation. As the sea level rose, the paleochannel was filled with soft marine and estuarine deposits. When it was decided to construct a bridge across the "Narrows" an attempt was made to improve the soil profile. The attempt required the displacement of the soft "mud" at the north shore by rapidly constructing a sand embankment to induce a slope failure. The sand was also required for engineering fill purposes, to raise ground surface elevations well above Swan River flood levels. This work commenced in May 1955 (Marsh 1993). Marsh (1961) provides more information on the reclamation process.

The attempt at displacement was only partly successful and a wedge of soft soil remained in place. There was concern that consolidation of the non-uniform thickness of soft alluvium would result in horizontal movement at the north shore pier of the Narrows Bridge. As a result of this concern, the North Shore pier of the bridge was constructed using a caisson pile system with the load bearing pile located within a larger diameter hollow steel tube driven into stable subsoil conditions some 20m below river level. The outer hollow steel pile was free to move horizontally (with the moving soil) without imposing lateral loads on the inner load bearing piles. The load bearing pile was placed eccentrically inside the outer steel tube, with the large gap (on the north side) to be taken up by movement of the soil and outer tube towards the south. Main Roads established a set of survey monitoring points on the north shore to measure the lateral and vertical movement of the outer steel tube. Survey monitoring spanned the period when the 1968 Meckering Earthquake occurred (Magnitude 6.9).

The Meckering earthquake

The Meckering earthquake occurred on 14 October 1968. The magnitude was approximately 6.9 and the duration was about 40 seconds. The fault line was about 37km long with a maximum vertical displacement of about 2m. The epicentre was approximately 120km east of the Narrows Bridge site.

Observed displacements at the Narrows Bridge North Shore

Vertical (Z) and horizontal (Y) movement of the monitoring point at the north shore of the Narrows Bridge site were plotted by Marsh (1993) from which the following displacements associated with the Meckering earthquake, can be estimated:

Table 1 North Shore Displacements Associated with the Meckering Earthquake

Direction	Location	Displacement (mm)
Vertical	East End	18
Vertical	West End	5
Horizontal	East End	10
Horizontal	West end	16

A sample plot using data scaled from Marsh's (1993) report is presented as Figure 1.

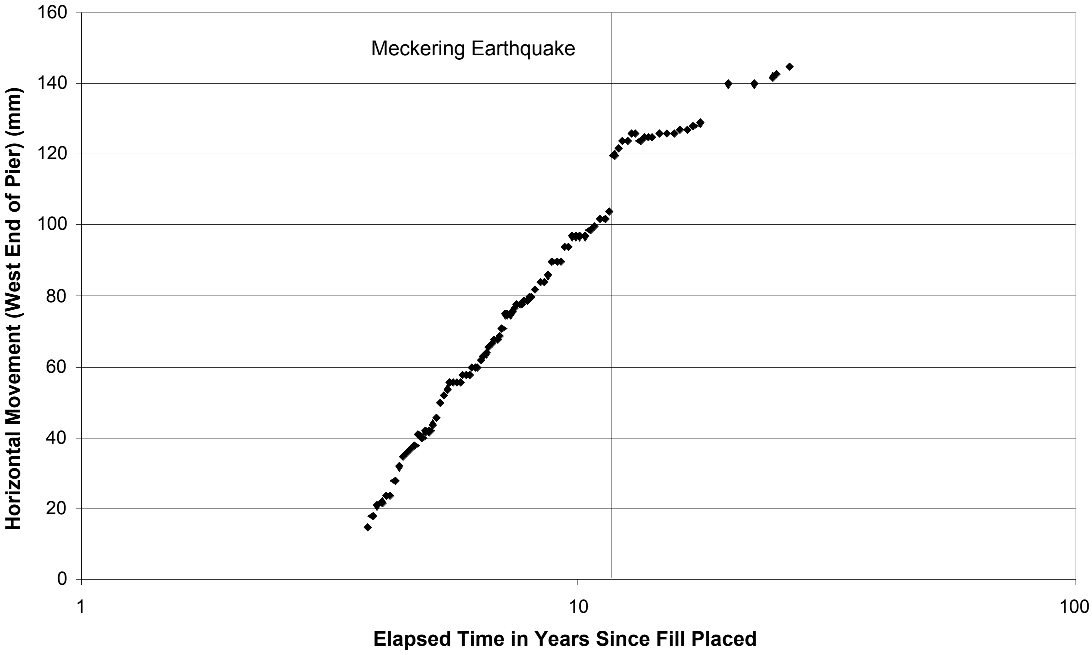

Figure 1 Horizontal Movement at North Shore Narrows Bridge

Marsh's (1993) report only included the displacement in the Y direction (towards the river in the direction of the bridge span). It is understood that displacement in the X direction has been much smaller than for the Y direction.

Recent investigations

In 1998 Main Roads Western Australia commissioned BHP Engineering to carry out geotechnical borehole drilling and laboratory testing for the proposed duplication of the road bridge over the Swan River at the Narrows. Bore Hole BHPE_03 (NSP) indicated very loose to loose sand with Standard Penetration Test (SPT) blow counts (N) of 4 at 2.5m, 3 at 5.5m and 4 at 8.5m depth. There was a total of about 20m thickness of sand with a SPT of less than 15. The ground water level was not measured but is estimated to have been at about 1m deep based on the ground level and proximity to the Swan River.

In 2003 Coffey undertook geotechnical studies at the Narrows Bridge site as part of the design for a third bridge (to carry the Perth Mandurah Rail) that would be located between the original road bridge and the recently completed duplicate road bridge.

Displacement analysis for the Meckering earthquake

As part of the design of the piled foundations for the new rail bridge, consideration was given to any lateral displacement that may be caused by earthquake liquefaction of the loose sand at the North Shore pier.

Youd et al (2002) proposed an empirical equation for assessing lateral spread adjacent a free face slope, based on multilinear regression:

$$\text{Log } D_H = -16.713 + 1.532M - 1.406\text{Log } R^* - 0.012R + 0.592\text{LogW} + 0.540\text{Log } T_{15} + 3.413\text{Log } (100-F_{15}) - 0.795\text{Log } (D50_{(15)} + 0.1)$$

where

- D_H is lateral ground movement in mm
- M is earthquake magnitude (6.9 for the Meckering earthquake)
- R is the mapped distance to the earthquake (approximately 115km)
- R* is the modified source distance (refer to Youd et al 2002)
- W is the free face ratio (approximately 20% for the Narrows Bridge site)
- T_{15} is the thickness of sand with an SPT of less than 15
- F_{15} is the average fines content (1% for The Narrows Bridge site)
- $D50_{(15)}$ is the average grain size for sand in the zone with SPT <15 (0.45 mm)

Applying these parameters to the North Shore of the Narrows Bridge site, the predicted lateral spread associated with the Meckering earthquake is 10 mm. This is reasonably close to the average measured horizontal movement of 13 mm (refer to Table 1).

Discussion

The method of Youd et al (2002) for estimating lateral spread from liquefaction gave a reasonable fit with the measured displacement at the North Shore of the Narrows Bridge site, corresponding to the time of the Meckering earthquake. It must however be recognised that this does not provide proof that liquefaction occurred. There are other possible explanations of the lateral movement including remobilisation of the original slip.

A number of possible causes of lateral load on the piles were investigated in the design of the rail bridge at the Narrows site. Lateral spread under earthquake shaking was one of the sources of movement included in the design.

Acknowledgements

The approval from Main Roads Western Australia to reproduce the displacement data from the Narrows Bridge site is gratefully acknowledged.

References:

Marsh J G (1961) Reclamation for Narrows Bridge, Perth WA. Jnl IEAust Vol 33 No 7-8

Marsh J G (1993) Narrows Interchange And Section Of Kwinana Freeway On South Perth Foreshore, Implications Of Construction History. Main Roads Western Australia, Materials Report

Youd T L, Hansen C M, & Bartlett S F (2002) Revised Multilinear Regression Equations for Prediction of Lateral Spread Displacement. Jnl of Geotech & GeoEnv, Engng, Vol 128 , No 12 ASCE

Validation of using Gumbel probability plotting to estimate Gutenberg-Richter seismicity parameters

Mike Turnbull[1] and Dion Weatherley[2]

[1] Central Queensland University
[2] Queensland University

Abstract:

The Gumbel Type I statistics of extreme events have been successfully used in the past to forecast various natural events such as annual exceedence of design flood level, and hail fall. Some attempts have been made to determine seismicity parameters using the annual maximum magnitude events in historic records. The results from these determinations have invariably been criticized for various reasons, including the perception that the methodology ignores important data, and that the method has no verification basis. This paper addresses both topics by discussing the principles of the Gumbel Type I statistical method, and verifying that the method is capable of reliably deducing the Gutenberg-Richter seismicity parameters of complete synthetic earthquake calendars, using only the annual maxima.

Introduction

It is common to characterize temporal and quantitative earthquake seismicity of a region by respectively specifying values for the a and b parameters of the Gutenberg-Richter seismicity model (the G-R model). Estimations of these parameters can be derived from a number of statistical processes. In situations where a comprehensively complete catalogue of earthquake events is not available, methods provided by the statistics of extreme events (the so-called extreme value theory (EVT)) have been applied, using reduced variate probability plotting.

The generalized EVT cumulative distribution function (cdf) reduces to one of three specific Fisher Tippett distributions (Fisher & Tippett, 1928), depending on the value chosen for its three parameters, ξ, $\theta(> 0)$, and $k(>0)$. These three distributions are summarized below (Johnson et al, 1995).

Fisher Tippett Type 1:

$\Pr[X \le x] = \exp\{-\exp\{-1/\theta(x - \xi)\}\}$ … Eq. 1

Fisher Tippett Type 2:

$\Pr[X \le x] = 0,$ where $x < \xi$ … Eq. 2

$= \exp\{-\exp\{-(1/\theta(x - \xi))k\}\},$ where $x \ge \xi$

Fisher Tippett Type 3:

$\Pr[X \le x] = \{-\exp\{-(1/\theta(\xi - x))k\}\},$ where $x \le \xi$ … Eq. 3

$= 1,$ where $x > \xi$

The Type 2 distribution is often referred to as the Fréchet distribution. The Type 3 distribution is often referred to as the Weibull distribution. The Type 1 distribution is mostly referred to as the Gumbel distribution, but is sometimes referred to as the log-Weibull distribution. In this paper it will be referred to as the Gumbel distribution.

There are two common criticisms made, arguing that the probability plotting method of analysing extreme events to estimate regional seismicity is of little value to practical seismology. These criticisms are that:

1. The extreme value methods only assess the few maximum value events and ignore the many other important smaller events.
2. The various methods of determining the plotting positions used to calculate the reduced variate are arbitrary in nature. Therefore the choice of plotting position algorithm can be used to manipulate the results.

This paper addresses these two criticisms via counter-arguments and a demonstration that the reduced variate probability plotting method in conjunction with Gumbel statistics of extreme events can reproduce accurate estimates of a priori seismicity parameters used to generate synthetic earthquake calendars. Our analysis consists of two parts. Firstly we demonstrate that the probability plotting method estimates to within 2% accuracy, the Gumbel parameters of a synthetic dataset constructed with a priori values of these parameters. Secondly we apply the Gumbel method to analyse synthetic seismicity calendars generated from a Gutenberg-Richter distribution with prescribed a- and b-values. Our results testify that the Gumbel method accurately estimates the a and b values of the underlying G-R source distribution, via statistical analysis of only the extreme values of the synthetic catalogues.

Are important data being ignored?

Statistical analysis aims to provide an accurate model for a given set of observations, using some assumptions about the underlying process giving rise to the observations. In the case of regional seismicity, one assumes the underlying process gives rise to a Gutenberg-Richter frequency-magnitude distribution: a two-parameter model determining the average rate of seismicity (a value) and the scaling of recurrence intervals with given earthquake magnitude (b value). For a particular region, one aims to estimate the values for these two parameters via curve fitting of the observed historical seismicity. Since the dataset of observations is invariably only a small subset (or sampling) of the seismic history and the observations may contain errors (e.g. imprecise magnitude determination or poor detection level) one cannot expect to obtain an arbitrarily accurate estimation of the model parameters.

It is well-known that estimated values for the model parameters may be significantly skewed when using a dataset which does not provide a sample a data set containing adequate samples of the full range of observable values. Seismicity particularly suffers from this limitation as historical seismic catalogues are typically complete for large magnitudes (the extreme values of the G-R distribution) but incomplete or non-existent for smaller magnitudes. Historical catalogues are biased towards extreme values.

The Fisher-Tippett probability distributions are specifically formulated to model the extreme data values that are invariably found in samples extracted from underlying source distributions. EV distributions provide a parameterisation for the extreme values that is related to the parameters of the source distribution, while taking into account the inherent bias towards extreme values in the dataset under analysis. It was Fisher and Tippet (1928) who proved that no matter what source probability distribution data is derived from, the distribution of extreme data values will necessarily converge to one of the three forms Eq. 1, 2 or 3.

The perception that extreme value methods ignore important small value data is false. EV methods are designed to model the distribution of extreme values accurately, not the distribution of non-extreme values. Including these latter values in the analysis would be erroneous. Since the dataset of extreme values is complete, one does not suffer from the finite sampling issues when estimating the parameters of the EV distribution. It must be emphasised that EV methods make allowance for the bias towards extreme values in the original dataset. This is codified in the relationship between EV model parameters and those of the source distribution. Thus it is possible, by analysing a catalogue of extreme values, to accurately estimate the parameters of the source distribution. Given the indisputable bias towards large magnitudes in seismic catalogues, EV methods are well-suited for modelling regional seismicity.

The probability integral transformation theorem

The theorem of probability integral transformation states that any cumulative distribution function, considered as a function of its random variable X, is itself a uniform random variable on the closed interval (0,1) (Bury, 1999, p 25).

$F(X; \theta) = U$ … (Eq. 4)

where θ represents parameters, either known or not yet determined.

A consequence of this theorem is that all possible values of X are equally likely. So that any sample variate $F(x_i; \theta)$ derived from the parent distribution $F(X; \theta)$ can be expressed in the form:

$F(x_i; \theta) = u_i$ … (Eq. 5)

where u_i is a value in the closed interval (0, 1), and where all values of u_i are equally likely.

A corollary of the probability integral transformation theorem is that:

$x_i = F\text{-}1(u_i; \theta)$ (Eq. 6).

This corollary has two important applications in practice – simulated random observations, and probability plotting.

Simulating random variates

The corollary of the probability integral transformation theorem provides a means of simulating random variates from any known probability distribution. By substituting random numbers u_i from the closed (0, 1) interval into the inverse of the distribution's cumulative distribution function, independent identically distributed random variates can be generated.

For example (Bury, 1999, p 268), the cdf of the Gumbel distribution may be expressed in the form

$F(x; \mu, \sigma) = \exp\{-\exp\{-1/ \sigma (x - \mu)\}\} = u$ (say). (Eq. 7)

By inversion

$x = \mu - \sigma\ln(-\ln(u))$ (Eq.8)

Therefore, simulated random variates x_i from the Gumbel distribution can be generated using the following formula, where u_i is a random number on the closed interval (0, 1).

$x_i = \mu - \sigma\ln(-\ln(u_i))$ (Eq.9)

Probability plotting

Manipulation of Eq. 9 produces the following linear relation.

$-\ln(-\ln(p_i)) = 1/\sigma (x_i - \mu)$ (Eq.10)

where the u notation has been replaced by a p, for reasons that will become clear below.

This relation provides a potential means of testing whether a set of n experimental observations $\{x_i\}n$ is a sample from a Gumbel distribution. If the reduced variates $\{-\ln(-\ln(p_i))\}n$ are plotted against the experimental observations $\{x_i\}n$, and a straight line graph results, then the postulated Gumbel parent distribution is confirmed, and ordinary linear regression can be used to estimate the parameters σ and μ from the slope and intercept. There is one difficulty in accomplishing this task. In any real experimental situation the observations $\{x_i\}n$ are known, but the n reduced variates $\{-\ln(-\ln(p_i))\}n$ cannot be calculated exactly because the plotting positions $\{p_i\}n$ are unknown.

The only things that can be assumed regarding the p_i values is that they are in the closed interval (0, 1), and that each value has equal likelihood of presence. This information suggests a widely used, but controversial, method for producing artificial plotting positions that can be substituted for the actual ones. The method used to determine the substitute plotting positions can be described as follows.

The n observations are first ordered and ranked according to their relative values. Depending on the requirements of the particular situation this ranking may be in ascending or descending order. The examples described here will use ascending order. The ordered observations are notated as

$\{x_i\}*n$ _ $\{x_1 \leq x_2 \leq x_3 \leq \ldots \leq x_{n-2} \leq x_{n-1} \leq x_n\}$

where x_1 is the smallest valued variate, x_n is the largest valued variate, and the subscript values are the variate ranks.

The next step is the controversial part of the method. The rank value of the mth ordered variate is used to determine an artificial plotting position quantile p_m for that variate. There is no single definitive formula or equation for doing this. However, there are guidelines for doing so.

Gumbel (1958) expressed the following five conditions as requirements that substitute plotting positions should necessarily fulfil.

1. The plotting position should be such that all observations can be plotted.
2. The plotting position should lie between the observed frequencies (m – 1)/n and m/n and should be universally applicable, i.e., it should be distribution-free. This excludes the probabilities of the mean, median, and modal mth value which differ for different distributions.
3. The return period of a value equal to or larger than the largest observation, and the return period of a value smaller than the smallest observation, should approach n, the number of observations. This condition need not be fulfilled by the choice of the mean and median mth value.
4. The observations should be equally spaced on the frequency scale, i.e., the difference between the plotting positions of the (m + 1)th and the mth observation should be a function of n only, and independent of m. This condition … need not be fulfilled for the probabilities at the mean, median, or modal mth values.
5. The plotting position should have an intuitive meaning, and ought to be analytically simple. The probabilities at the mean, modal, or median mth value have an intuitive meaning. However, the numerical work involved is prohibitive [at the time of writing. Current computing capabilities now make these calculations routine].

The simplest approach is to assume that the value of the plotting position quantile is equal to its fractional position in the ranked list, m/n. This would assign the quantile 1/n to the smallest plotting position and n/n = 1 to the largest. This is unsatisfactory because it leaves no room at the upper end for values greater than the largest variate observed thus far.

Most plotting position formulae are ratios of the form (m ± a)/(n ± b) where the addends and subtrahends are chosen to improve estimates in the extreme tails of the postulated distribution.

Gumbel (ibid) recommended the following quantile formulation, which calculates the mean frequency of the mth variate.

$$p_m = m / (n + 1) \quad \ldots \quad \text{(Eq. 11)}$$

This formulation ensures that any plotting position is as near to the subsequent one as it is to the previous. It also produces a symmetrical sample cdf in the sense that the same plotting positions will result from the data regardless of whether they are assembled in ascending or descending order.

A more sophisticated formulation is

$$p_m = (m - 0.3) / (n + 0.4) \quad \ldots \quad \text{(Eq. 12)}$$

This formulation approximates the median of the distribution free estimate of the sample variate to about 0.1% and, even for small values of n, produces parameter estimations comparable to the results obtained by maximum likelihood estimations (Bury, 1999, p 43).

Using the Gumbel distribution to model extreme earthquakes

Cinna Lomnitz (1974) showed that if an homogeneous earthquake process with cumulative magnitude distribution

$F(m; \beta) = 1 - e^{-\beta m}; \quad m \geq 0$ (Eq. 13)

is assumed (compare with Eq. 24), where β is the inverse of the average magnitude of earthquakes in the region under consideration; and α is the average number of earthquakes per year above magnitude 0.0; then y, the maximum annual earthquake magnitude, will be distributed according to the following Gumbel cdf.

$G(y; \alpha, \beta) = \exp(-\alpha \exp(-\beta y)); \quad y \geq 0$ ... (Eq. 14)

Using the probability integral transformation theorem, simulated maximum yearly earthquakes can be generated using the following inversion formula.

$y_i = -(1/\beta) \ln((1/\alpha) \ln(1/u_i))$ ... (Eq. 15)

The conversion factors to transform Eq. 4 and 6 to Eq. 11 and 12 are as follows.

$\alpha = \exp(\mu / \sigma)$ ... (Eq. 16)
$\beta = 1 / \sigma$ ... (Eq. 17)

Conversely:

$\sigma = 1 / \beta$ ... (Eq. 18)
$\mu = (1/\beta) \ln(\alpha)$ ... (Eq. 19)

Manipulation of Eq. 15 produces the following linear relation.

$-\ln(-\ln(p_i)) = \beta y_i - \ln(\alpha)$ ... (Eq. 20)

where p represents the plotting position, and the left hand expression is the reduced variate that can be used to plot data that is postulated as being drawn from a Gumbel distribution.

Demonstration of Gumbel probability plotting

Eq. 15 was used to generate ten random, one thousand year catalogues of synthetic annual extreme earthquake magnitudes, using the input parameters α = 48, and β = 1.37. Each set of data was analysed by plotting Eq. 20, with the plotting positions determined using both Eq. 11 and 12. Figures 1a and 1b show one of the ten resulting graphical plots obtained using each plotting method. The dotted lines in Figure 1 are the ordinary linear regression approximations. The linear approximation equations and coefficients of linear determination (r^2) are shown at the top right hand corner of each graph. The visual interpretation of the graph is that, for the majority of the lower magnitude data, the Gumbel distribution is appropriate; but, for magnitudes above about

Figure 1(a): Gumbel Probability Plot using i/(n+1)

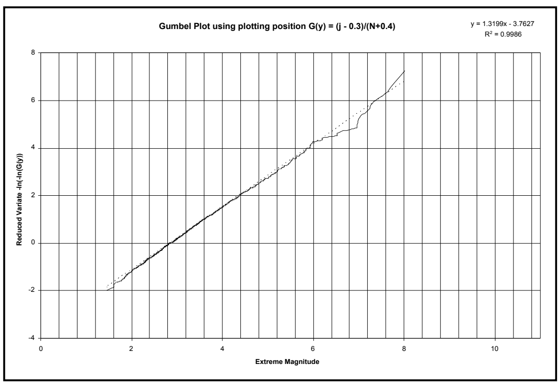

Figure 1(b): Gumbel Probability Plot using (i-0.3)/(n+0.4)

6.0 (i.e. for the extreme of the extreme values), the assumption of a Gumbel distribution may be suspect (in fact, a Weibull analysis may be more appropriate for those data).

Estimations of α and β were made using ordinary linear regression of each set of data. Table 1 summarises the resulting approximations, as well as showing the average and standard deviations of the estimated parameters.

Table 1: Parameter estimations using Gumbel Probability Plotting

Parameter estimation	_		_	
	pi=i/(n+1)	pi=(i-0.3) /(n+0.4)	pi=i/(n+1)	pi=(i-0.3) /(n+0.4)
Data Set 1	42.17857	43.06256	1.313218	1.319945
Data Set 2	44.00797	45.03307	1.328423	1.335858
Data Set 3	44.30699	45.27417	1.338465	1.345506
Data Set 4	51.20298	52.48388	1.409218	1.417366
Data Set 5	41.95601	42.79609	1.317657	1.324136
Data Set 6	49.80841	50.87322	1.374311	1.381216
Data Set 7	47.47786	48.46969	1.362259	1.369031
Data Set 8	50.64748	51.86245	1.382438	1.390142
Data Set 9	42.62512	43.62954	1.33023	1.337812
Data Set 10	43.24977	44.15485	1.348617	1.355476
Average	45.75	46.76	1.35	1.36
Std Dev	3.49	3.60	0.03	0.03
Std Error	1.10	1.14	0.0095	0.0095
Rel Error	2.4%	2.4%	0.7%	0.7%
Exact Value	48.00	48.00	1.37	1.37

It is evident that both plotting methods can estimate α and β within standard relative errors of 2.4% and 0.7% respectively, if sufficient trials are made. It is expected that trials with a larger number of data sets would improve the relative errors.

In real situations it may only be possible to extract a single useful data set from the earthquake history. This will limit the precision of parameter estimation in practice. For single estimations, there is a 95% confidence that α and β can be estimated within two standard deviations of the averages quoted in Table 1. That is, within 15% and 5% respectively.

It is clear from this demonstration that the fundamental method of probability plotting is scientifically sound in that it can reproduce accurate approximations of underlying process model parameters (at least for the two plotting position formulations used in this demonstration).

It is pointed out that the forgoing error analysis pertains to the method itself. Other errors in the inferred results of particular analyses may be introduced by faulty data. In particular incorrect determination of earthquake magnitudes may adversely affect inferred results.

Demonstration of Gutenberg-Richter parameter estimation using the Gumbel distribution

Background Theory

The Gutenberg-Richter (G-R) seismicity relation of earthquake frequency versus magnitude may be expressed as:

$$N(m \geq M) = 10^{(a - b\,m)} \qquad \ldots \qquad \text{(Eq. 21)}$$

where $N(m \geq M)$ is the number of earthquakes observed having magnitudes greater than or equal to M; and a and b are parameters specific to the observed data set. As a pragmatic mathematical and practical choice, the lower limit of M, M_0 is usually assigned the value zero. In that formulation the parameter a represents the logarithm to the base 10 of the number of independent earthquakes in the observation period with magnitude greater than or equal to zero.

$$a = \log_{10} N(m \geq M_0) \Rightarrow N(m \geq M_0) = 10^a \qquad \ldots \qquad \text{(Eq. 22)}$$

If it is assumed that all earthquake included in the data set are independent, and that each event has equal probability of occurring, then Eq. 21 can be normalised to produce a frequency relation as follows,

$$Pr(m \geq M) = N(m \geq M)/ N(m \geq M_0) = 10^{(a - b\,m)}\, 10^{-a} = 10^{-b\,m} \quad \text{...(Eq. 23)}$$

It can be seen from Eq. 23 that the value of the parameter b determines the propensity for lower or higher magnitude earthquakes. Smaller values of b model a system that has a greater propensity for larger magnitude earthquakes. It also demonstrates that magnitude of the earthquakes is not dependent on the a parameter. The cdf formulation is as follows.

$$Pr(m \leq M) = 1 - 10^{-b\,m} \quad \text{... (Eq. 24)}$$

Using the probability integral transformation theorem, Eq. 24 can be inverted to produce a random magnitude generator

$$m = -1/b \log_{10}(1 - u) \quad \text{... (Eq. 25)}$$

where u is a random number in the closed (0, 1) interval. Eq 25 also provides the reduced variate for conducting a G-R plot to test whether a data set is drawn from a G-R distribution.

If it is further assumed that the timing of the earthquake events is a Poisson process, then a random event generator can be devised (c.f. Bury, 1999, p 104).

$$t = -10^{-a} \ln(v) \quad \text{... (Eq. 26)}$$

where t is a random time interval between events, v is a random number in the closed (0, 1) interval, and 10^{-a} is the average time between events.

From Eqs. 13 and 24, and the fact that α and 10^a specify the average time between events in the Gumbel and G-R formulations respectively, the relationships between the Gumbel parameters α and β and the G-R parameter a and b are seen to be

$$e^{-\beta} = 10^{-b} \quad => \quad b = \beta \log_{10} e \quad \text{... (Eq. 27)}$$
$$\alpha = 10^{a} \quad => \quad a = \log_{10}\alpha \quad \text{... (Eq. 28)}$$

Using the same parameter values that were employed in the demonstration of Gumbel plotting, if α = 48, then a ≈ 1.69; and if β = 1.37, then b ≈ 0.59.

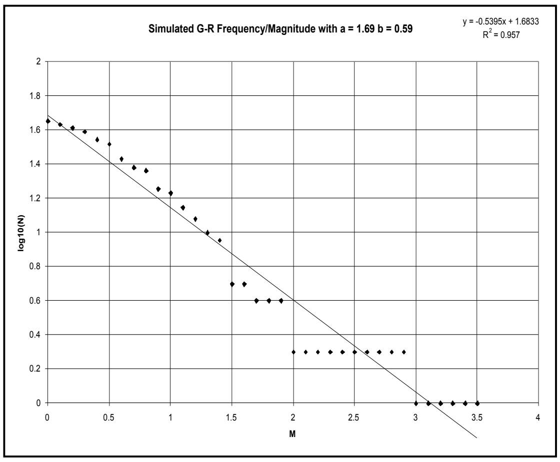

Figure 2(a) : G-R Frequency/Magnitude chart

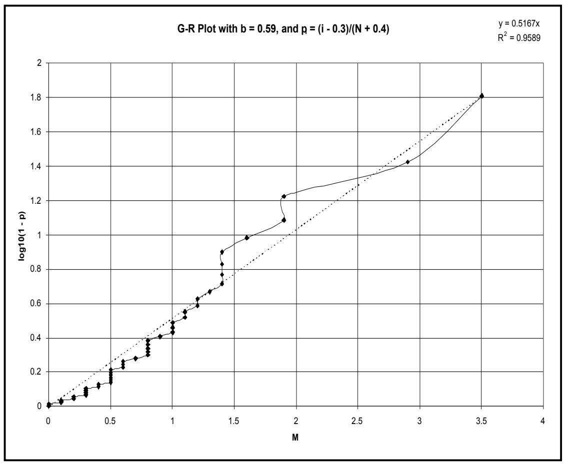

Figure 2(b) : G-R Probability Plot

Simulated G-R catalogues

Using Eqs. 25 and 26, with a = 1.69 and b = 0.59, eleven 131 year catalogues of earthquake events were generated. Figures 2(a) and 2(b) show analysis of one typical year of synthetic earthquakes using the Gutenberg-Richter frequency/magnitude method, and with a Gutenberg-Richter reduced variate plot.

Linear regression of the data used in Figure 1(a) estimates a to be approximately 1.68, and b to be about 0.54: which agrees with the actual input parameters used to generate the data. Similar linear analysis of the data plot in Figure 2(b) estimates the b parameter to be 0.52.

Visual inspection of Figure 2(b) shows that, although it is reasonable to use the G-R relation to analyse the earthquakes with synthetic magnitudes up to 1.3, events above that magnitude should not be so treated in this particular case.

Figures 3(a) and 3(b) show analysis of the same 131 year of synthetic earthquakes using the Gumbel extreme event method, with the full annual extreme data set, and with the extreme of the annual extreme values truncated.

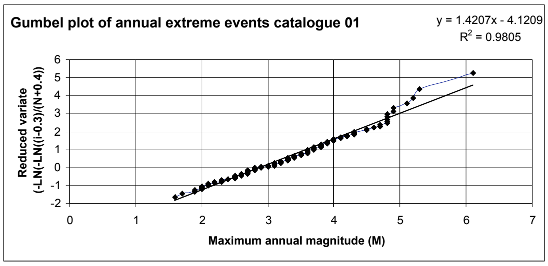

Figure 3(a) : Gumbel analysis full data set

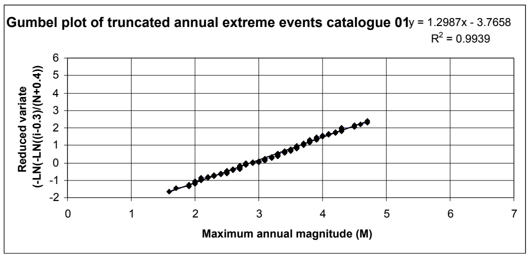

Figure 3(b) : Gumbel analysis truncated data set

Tables 2 and 3 provide a listing of the a and b parameter estimations and averages obtained using the Gumbel extreme value method of analysis, from the full extreme data set, and with the extreme of the extreme values omitted. It can be seen that both methods are capable of recovering the a priori parameter values, and that using the full data set provides the better relative errors.

	Set 1	Set 2	Set 3	Set 4	Set 5	Set 6	Set 7	Set 8	Set 9	Set 10	Set 11	Avg	Rel Err
a	1.79	1.51	1.67	1.71	1.76	1.70	1.89	1.57	1.61	1.63	1.55	1.67	1.8%
b	0.62	0.52	0.56	0.61	0.64	0.59	0.65	0.56	0.56	0.58	0.55	0.59	1.7%

Table 2: Parameter estimations and average using full extreme data set.

	Set 1	Set 2	Set 3	Set 4	Set 5	Set 6	Set 7	Set 8	Set 9	Set 10	Set 11	Avg	Rel Err
a	1.64	1.59	1.62	1.70	2.00	1.71	1.82	1.64	1.69	1.59	1.58	1.69	2.4%
b	0.56	0.54	0.55	0.61	0.72	0.60	0.63	0.59	0.58	0.57	0.55	0.59	3.4%

Table 3: Parameter estimation and averages using truncated data set.

Summary

It has been demonstrated that analysis of multiple synthetic earthquake catalogues, derived from a Gumbel seismicity model, using Gumbel distribution plotting of annual extreme earthquake magnitudes, is capable of estimating the a priori a and b parameters values within a relative error of 2%. There is a 95% confidence that individual estimations of α and β will be within 15% and 5% respectively of the true value.

Acceptable parameter estimates are obtained using either full annual extreme data sets, or truncated data sets with the extreme of the extreme values omitted from the data plot, but the full data set provides smaller relative errors.

References

Bury K. 1999, Statistical Distributions in Engineering, Cambridge University Press, ISBN 0 521 63506 3.

Fisher R.A. & Tippett L.H.C. 1928, Limiting forms of the frequency distribution of the largest or smallest member of a sample, Proc. Cambridge Phil. Soc., 24:180.

Gumbel E.J. 1958, Statistics of Extremes, Dover Publications Edition 2004, ISBN 0 486 43604 7, originally published Colombia University Press, 1958.

Johnson N.L., Kotz, S. & Balakrishnan N. 1995, Continuous Univariate Distributions, Volume 2, 2nd Ed., John Wiley & Sons. ISBN 0 471 58494 0.

Lomnitz C. 1974, Global Tectonics and Earthquake Risk, in Developments in Geotectonics 5, Elsevier Scientific Publishing Company.

Automatic calculation of seismicity rates in eastern Queensland

Russell Cuthbertson

Environmental Systems and Services

Abstract

In the probabilistic approach to seismic hazard analysis, earthquake source zones are assigned seismicity rates with the assumption that seismicity is distributed uniformly within each zone. Defining a seismic source zone and then calculating the seismicity rates of that zone has typically required manual calculations and corrections that are time consuming and which ignore significant proportions of the recorded dataset.

An automatically calculated detection threshold has been shown to adequately represent detectability changes with time (even deteriorating changes) and detectability changes in space. Using this detection threshold to correct observed seismicity rates utilises a much larger proportion of the dataset, and produces a linear magnitude-frequency plot over a larger magnitude range, than is possible with existing previous techniques. This in turn provides more accurate estimates of the a and b-values.

The minimal amount of subjective input means the results from one area can be compared directly with the results from another.

Application of the technique to eastern Queensland shows that previous seismicity models have all overestimated the recorded seismicity.

Introduction

Recent attempts to quantify earthquake hazard in Australia have used a probabilistic approach as developed by Cornell (1968) and McGuire (1976). In this approach earthquake source zones are assigned seismicity rates with the assumption that seismicity is distributed uniformly within each zone. The analysis has typically involved a two-step process of first defining a seismic source zone and then calculating the seismicity rates of that zone.

Calculation of the seismicity rates requires corrections to the recorded dataset for non-uniformity. These corrections have typically been performed manually using a technique that neglects large proportions of the dataset. Australian earthquake databases are not large and discounting any large proportion of the database from analysis will compromise the results.

This paper describes a methodology of automatically processing a major proportion of the recorded seismicity to obtain both seismicity rates and source zones. There is no discussion regarding the validity or otherwise of the concept of source zones with uniform seismicity - we are simply describing a technique that can be used to assist in the analysis.

Data to demonstrate the application of the process to areas of eastern Queensland is taken from the Queensland earthquake catalog maintained by Environmental Systems & Services. This data was declustered using the event code (foreshock, mainshock, aftershock, swarm) that has been subjectively assigned by a seismologist.

Seismicity rates - theory

The power-law relationship between earthquake numbers and magnitude is exhibited in plots of the logarithm of the number of earthquakes (or rate of earthquakes) against magnitude as a straight line that is defined by an “a-value” (the earthquake rate at a defined magnitude) and a “b-value” (the gradient). Energy considerations can be used to show that this log-linear relationship must have an upper magnitude bound. There has been considerable discussion about the effect of this upper bound (and its value) but the simplest approach is to have a simple maximum magnitude above which no earthquakes occur. The effect of this on a cumulative magnitude-rate plot, where the number of earthquakes above a given magnitude is plotted, is to deflect the graph as magnitudes increase to the upper limit until it is asymptotic to the maximum magnitude (see Fig. 1).

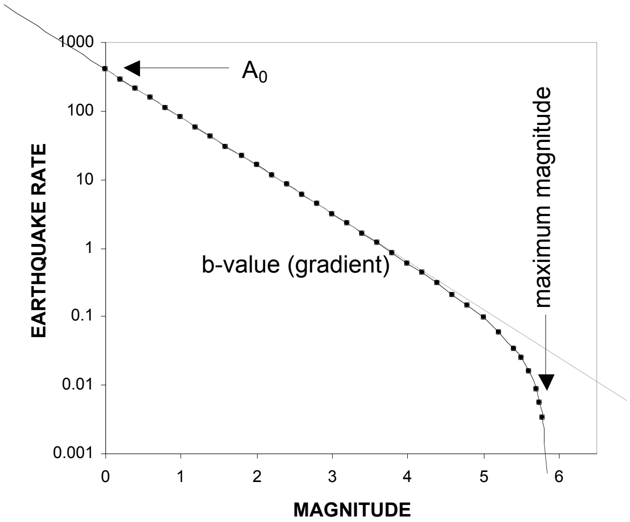

Figure 1: Theoretical cumulative magnitude-rate plot showing A_0, b-value and maximum magnitude.

An improved estimate of the b-value will be obtained if the earthquakes are spread over a large range of magnitudes. A long observation period will provide a larger number of earthquakes which will in turn reduce the uncertainty in the estimate of the rates.

In this paper all rates are expressed in terms of the annual number of earthquakes greater than a particular magnitude in an area 100 km by 100 km, and all a-values are for magnitude 0 (A_0).

Database completeness

The level of completeness of an earthquake catalog can be defined as the minimum magnitude above which all of the earthquakes in a given space-time volume have been recorded. While some earthquakes below the level of completeness may be recorded, not every one will be. This magnitude threshold will vary both in time and in space.

Spatial variation will occur because a seismograph network will only be able to record small earthquakes if they occur close to a seismograph. Earthquakes from outside a network or where the network has a large station spacing will only be recorded if they are of a larger magnitude.

Temporal variation of the magnitude detection level will occur when networks are installed and removed, when instrumentation is changed and even when operating or analysis procedures are altered.

Non-uniformity of dataset

A magnitude threshold that varies in both space and time makes the mapping of source zones and assigning of seismicity rates difficult. Variation of the detection magnitude in space will make identifying a source zone with a constant seismicity level difficult. Variation of the detection magnitude with time will make the determination of seismicity rates difficult.

Note that we are talking about non-uniformity introduced by observation methodology. The database may well contain natural variations in seismicity with time but this is a situation we choose to ignore. It is assumed that the natural variations in space are supposedly taken into account in the choice of source zones (if such a concept is indeed valid!).

A B

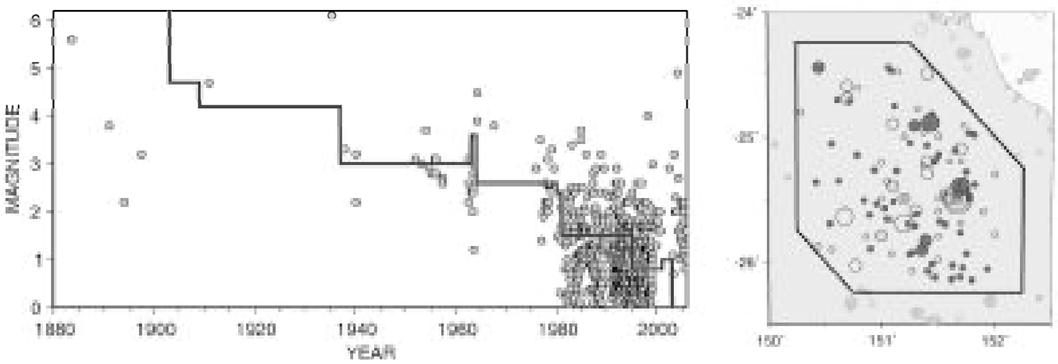

Figure 2: (A) Earthquake date plotted against magnitude for events from database within zone in southeast Queensland (shown in B). Solid line (in A) is calculated detection limit for central point of zone.

Figure 2(A) is a plot of the time of occurrence of earthquakes in a region of southeast Queensland plotted against magnitude. The area is indicated in Figure 2(B). Note that the configuration of the zone was chosen simply as a demonstration of the technique – it is not meant to represent what would be considered a final source zone. The lack of lower magnitude earthquakes in the period 1880 to 1980 indicates that the detection threshold in this region has changed over time.

Also plotted in Figure 2(A) is the theoretical detection threshold for a central point in the zone (see Network Detectability section for a description of the algorithm). The detection threshold theoretically separates a region of "constant" seismicity (in time) (above) from an area where earthquakes are less well recorded or not recorded at all (below). Note that the detection level generally improves with time but that there are instances where it has degraded.

The classical approach to analysing this dataset would be to select a series of horizontal time windows that are entirely above the detection threshold. Rates of recorded earthquakes within each band are then adjusted according to the duration. This simple approach would not include data from periods prior to any increase in the detection threshold magnitude.

A B

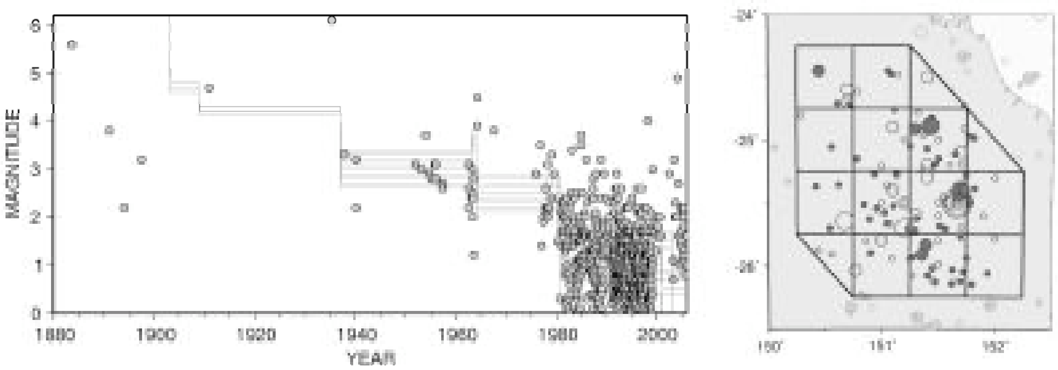

Figure 3: (A) Earthquake date plotted against magnitude for events from database within zone in southeast Queensland (shown in B). Multiple lines (in A) are calculated detection limits for central point of each sub-zone in B.

Figure 3 shows data from the same zone as Figure 2 but with the detection level versus time for a grid of points within that zone. The variation of the detectability across that zone would mean that any simple analysis would have to pick the maximum of all the possible detection curves to ensure a uniform dataset is being analysed.

Australia, and especially Queensland, has low seismicity and a short recording history so the earthquake databases are not large. Discounting any large proportion of the database from analysis will reduce the number of events available to statistically insignificant levels.

Completeness periods

There have been numerous approaches designed to automatically determine completeness periods from the shape of the magnitude-frequency plot (see Woessner and Wiemer, 2005). These techniques require a considerable amount of data and will only provide a detection threshold for a single time period. To obtain a detection threshold over time requires numerous subsets to be analysed – each one having to contain a significant number of events to be statistically useful.

The Stepp Test (Stepp, 1972) has been used in numerous studies to obtain completeness periods from recorded data. This test relies on the statistical property of the Poisson distribution – looking for periods during which the recorded earthquake rate is uniform. Figure 4 shows two Stepp Test plots (for the period up to 1999 and up to 2005) that have been plotted with earthquake rate (number / time) on the vertical axis rather than the more traditional standard deviation (square root of the rate divided by time).

This method of plotting Stepp Test results has two distinct advantages over the more traditional method. Firstly, the fitted lines are horizontal rather than sloping, allowing for easier interpretation. Secondly, the need to artificially adjust the observed rates to get estimated rates is obviated as the rates are read directly from the plot.

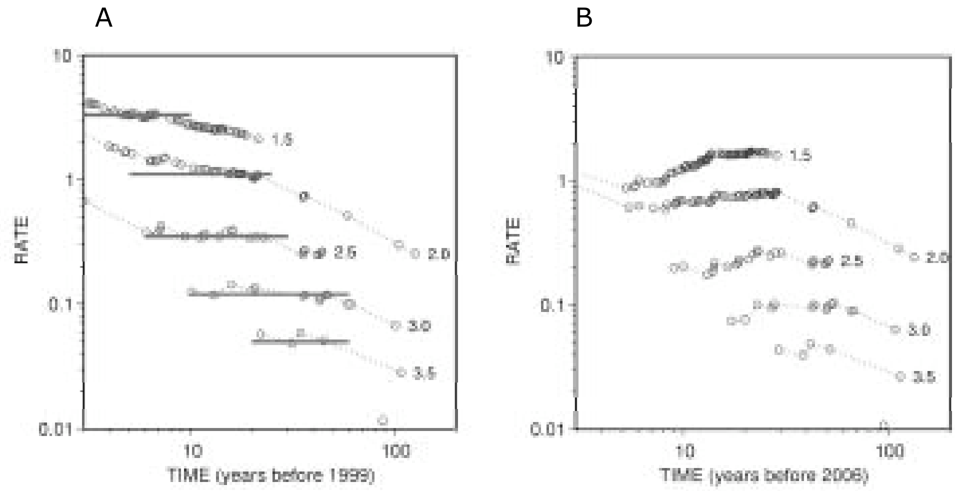

Figure 4: Modified Stepp Test plots for earthquakes in zone depicted in Figures 2 and 3. Base year for calculation is 2000 for A and 2006 for B. Labels are magnitude units. Cumulative seismicity rates (horizontal lines) have been interpreted for A.

Figure 4(A), showing data up until the end of 1999, can be fitted with horizontal lines but the data in Figure 4(B) shows no time periods where horizontal lines can be confidently drawn. During the period 2000-2003 there was a decrease in the detection capability of the network, leading to a reduction in the number of earthquakes recorded. The Stepp Test does not handle this situation at all. The only way to use the Stepp Test would be to only include data up until the end of 1999.

The results of a Stepp Test will also be compromised if there has been any natural variation in seismicity. A Stepp Test would also not be able to discern the effect of detection levels varying across a source zone.

The fitting of lines to each plot in a Stepp Test is a time-consuming process if done manually and prone to gross errors if attempted automatically.

Network detectability

Rather than analysing the recorded data in an effort to obtain detection thresholds, we used a network detection magnitude that was calculated automatically from the network configuration (in space and time), instrumentation type and crustal attenuation. Software was written so that the magnitude detection level at any location and time could be determined from these inputs.

A quality factor was subjectively assigned to each seismic station based on the instrumentation that was installed (seismometer or accelerometer), the noise level at the site and the recording technique (continuous or triggered). While a more sophisticated algorithm could be used the current simple method appears adequate.

The number of stations required to detect an earthquake was an additional parameter that could be varied. For this paper a value of one was used and shown to be suitable - i.e. an earthquake had to be only within detection distance of one station for it to be deemed detected.

For the subsequent analysis, detection levels were calculated for each one-month interval from 1900 to 2006 using the seismograph history. The attenuation function used was that used in Rynn (1987).

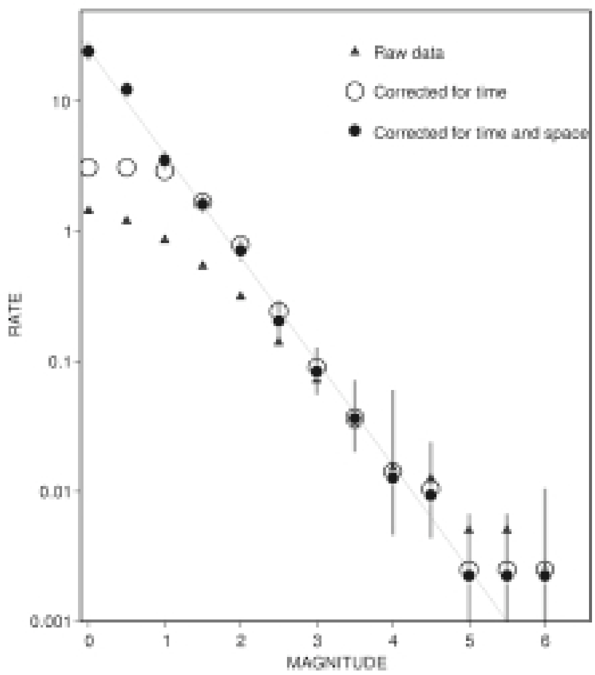

Figure 5: Magnitude-Rate plot for earthquakes in the zone depicted in Figures 2 and 3. Rates are annual numbers of earthquakes above a given magnitude per 10,000 km^2. Reference line has a b-value of 0.8. 90% confidence limits are shown for rates that have been corrected for time and space.

Calculating rates using detectability curve

Once a source zone has been mapped then rates can be calculated by only considering events that occurred above the detection threshold (and correcting for the length of time that the magnitude being considered was above the detection level).

Figure 5 shows the earthquake rates for the same area of southeast Queensland as depicted in Figures 2 and 3. Raw rates from earthquakes within the zone are shown as solid triangles while the rates corrected using the detectability curve for a central point of the zone are shown as solid black circles (The solid circles are described in the following section).

The raw data shows a linear trend for only a small section of the magnitude range but this trend extends down to magnitude ~1.5 for the data that has been corrected for detectability variations in time. The correction has also caused a marked steepening of the curve – an increase in the b-value to ~0.8 (see reference line).

Improving estimates by adding results

The process described in the previous section accounts for the variability of detection threshold with time but it does not take into account variability in space. As shown in Figure 3 there is a significant variation in detection level across the zone. This variation can be handled by dividing the source zone into multiple sub-zones (as in Figure 3) such that there is essentially no variation in detectability across each sub-zone. The same analysis as described above is then performed on each sub-zone.

Various sizes of square were chosen but the optimal trade-off (between spatial resolution and number of earthquakes) was for a square measuring ~50 x 50 km. Results from the individual sub-zones have large errors (due to the small number of events) but if they are added together (using weights based on the period of time above the detection threshold) then the errors are significantly reduced.

The results of subdividing the source zone in Figure 2(B) into 15 sub-zones (as shown in Figure 3(B)) and then summing the results are shown in Figure 5 as the solid circles (along with 90% confidence limits). The range over which a linear trend is observed is now extended down to magnitude 0.

Comparison with model estimates

Three models for the seismicity in eastern Queensland have been produced; Rynn (1987), QUAKES (Cuthbertson and Jaumé, 1996), and AUS5 (Brown and Gibson, 2000). The seismicity predicted from these models along with the results of the technique presented in this paper are shown in Figure 6(a).

As in Figure 5 there are three rates depicted, taken from; raw, recorded data with no correction for detection threshold; data corrected for detectability (but only for detectability at a single point in the centre of the region); and data corrected for detectability at every 0.5 degree within the region. While the linear trend for the data corrected for detection variability in time extends over several magnitude increments, the trend is extended all the way to magnitude 0 when the data is corrected for detection variability in space.

To accentuate the differences between the calculated rates and those predicated from the models Figure 6(B) shows exactly the same data but reduced assuming a b-value of 0.8. The Rynn and AUS5 models have b-values that do not fit the data. The b-value used in the QUAKES model appears to be more consistent with the data but all three models seriously overestimate the seismicity rates (a-values). Future hazard calculations in Queensland should ensure that there is a closer match between the corrected rates and those predicted from the source zone model.

To gain a better understanding of the distribution of seismicity the information from the multiple sub-zones can be plotted on a map. Figure 7 shows the average A_0 rate for each 0.5 degree square that have been smoothed with adjacent grid points and contoured. Only areas for which data is available are shaded and contoured. While the results are for A_0 the map is based on data from all magnitudes recorded (with the appropriate corrections).

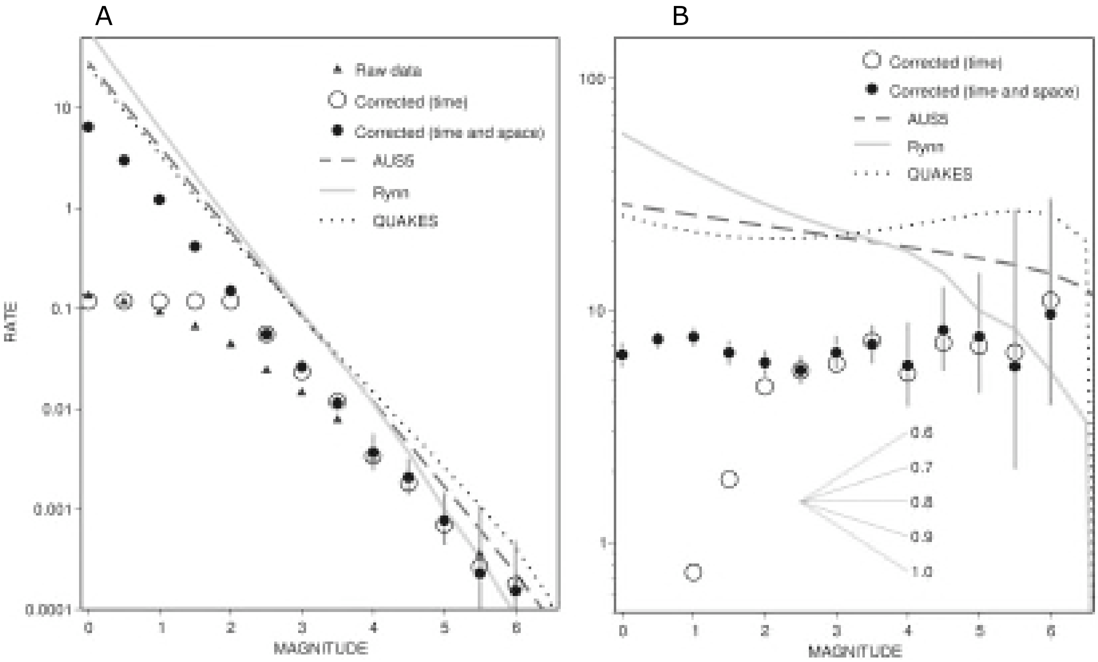

Figure 6: Magnitude-Rate plot for earthquakes in eastern Queensland together with rates predicted from seismicity models. Rates are annual numbers of earthquakes above a given magnitude per 10,000km^2. Data in Figure B has been reduced using a b-value of 0.8. Representative b-values shown for reference. 90% confidence limits are shown for the rates corrected for time and space.

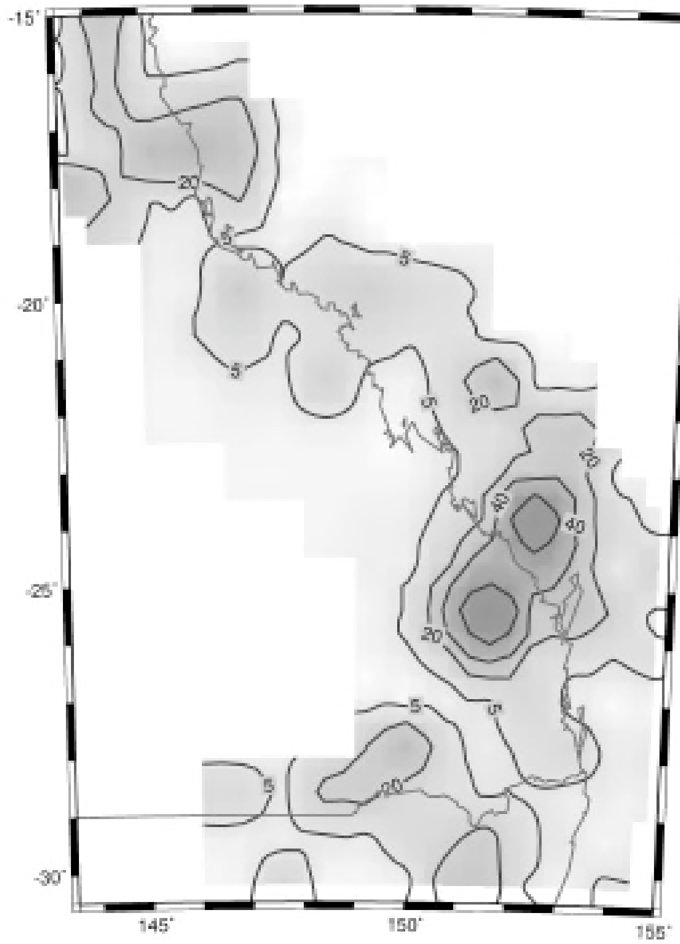

Figure 7: Map of A_0 values for eastern Queensland calculated on a 0.5 degree grid.

This map could be used as a simple, visual aid in deciding how source zones may be mapped. This would be much easier than the approach of: deciding on a zone, calculating a rate and then perhaps having to redraw the zone based on the results. It would also be much better than simply using the larger magnitude earthquakes to decide zone boundaries as it would use data from a much larger range of magnitudes.

Conclusion

An automatically calculated detection threshold has been shown to adequately represent detectability changes with time (even deteriorating changes) and detectability changes in space. Using this detection threshold to correct observed seismicity rates utilises a much larger proportion of the dataset, and produces a linear magnitude-frequency plot over a larger magnitude range, than is possible with existing previous techniques. This in turn provides more accurate estimates of the a and b-values.

The minimal amount of subjective input means the results from one area can be compared directly with the results from another.

While the techniques described in this paper appears to provide useful results, additional work needs to be done on the detection level algorithm and inputs before the technique can be applied universally. In some instances variations in the observed seismicity are not matched by variations in the detection level. This may mean a change is required in the attenuation function, the station quality code or perhaps the number of stations used.

The network history could more closely represent reality by using days instead of months and by including periods when a site was non-operational. The detection algorithm could also be modified to include a “probability of detection” rather than a simple magnitude cut-off. However these added sophistications do not seem to be required as the existing algorithm (once parameters have been properly determined) should provide useful results.

References

Brown, A. and G. Gibson (2000). Reassessment of Earthquake Hazard in Australia, 12th World Conference on Earthquake Engineering, Auckland, paper 751.

Cornell, C. A., (1968). Engineering seismic risk analysis, Bull. Seis. Soc Amer. 58, 1583-1606.

Cuthbertson, R. J. and S. C. Jaumé, (1996): Earthquake hazard in Queensland, in QUAKES Report #1, Section II, 13-39.

McGuire, R. K. (1976). FORTRAN computer program for seismic risk analysis. U. S. Geol. Surv. Open File Report, 303.

Rynn, J. M. W. (1987). Queensland Seismic Risk Study, Queensland Department of Mines, 191 pp.

Stepp, J. C. (1972). Analysis of completeness of the earthquake sample in the Puget Sound area and its effect on statistical estimates of earthquake hazard. 1st Microzonation Conference, Seattle, 1972, 897-909.

Woessner, J. & Wiemer, S. (2005). Accessing the quality of earthquake catalogs: Estimating the magnitude of completeness and its uncertainty. Bull. Seis. Soc Amer. 95, 684-698.

Coulomb stress changes due to Queensland earthquakes and the implications for seismic risk assessment

D. Weatherley

University of Queensland

Abstract

Coulomb stress change analysis has been applied in numerous seismically active regions of the globe. These studies demonstrate categorically that the timing and rates of future earthquakes are affected by the static stress changes due to nearby historical earthquakes. This has significant implications for seismic hazard assessment and earthquake forecasting. Static stress interactions result in significant spatio-temporal variations in seismicity patterns, calling into question the reliability of estimates of long-term seismicity rates based on relatively short historical earthquake catalogues. Furthermore, the probability of earthquakes in some regions may be significantly reduced or enhanced depending on the proximity to earthquakes in the recent past. In Australia there has been much debate as to whether static stress changes should be considered when assessing the seismic hazard within the continent. We examine patterns of static stress change due to past M>4.5 earthquakes in Queensland. Due to insufficient observations to constrain the focal mechanisms, we employ assumptions on the orientations, rupture lengths and average slip associated with each earthquake in order to calculate stress changes. Although preliminary and involving a number of assumptions, the results demonstrate that past M>4.5 earthquakes have occurred in sufficiently close proximity for static stress interactions to occur. We also show that earthquakes along either of a pair of reverse faults bordering uplifted blocks tend to promote the occurrence of subsequent earthquakes along the other reverse fault. One hypothesises that the seismicity of such regions may be dominated by pairs of reverse faulting earthquakes, occurring within a relatively short interval compared with the average recurrence interval of the earthquakes.

Introduction

In recent years significant progress has been made in forecasting the locations of aftershocks and subsequent mainshocks by considering the theoretical stress changes induced by past earthquakes (King et al., 1994). The technique, known as Coulomb stress analysis, assumes that an earthquake may be modelled as a slip dislocation within a uniform elastic half-space. By utilising analytic solutions for the displacement and stress in the surrounding medium and assuming that subsequent earthquakes result from frictional instability along pre-existing faults, one may compute the amount by which faults are brought closer to, or removed further from, brittle failure.

Coulomb stress analysis places firm constraints on the regions most likely to experience aftershocks in the days following a mainshock. Most notably, the analysis predicts an increased probability of so-called "off-fault" aftershocks, occurring some distance from the mainshock hypocentre. These off-fault aftershocks are of considerable concern during relief efforts as these typically occur along fault segments that are already pre-stressed, resulting in larger magnitudes than aftershocks within or near the rupture zone.

Coulomb stress analysis also offers the possibility to calculate the time-evolution of stress within a fault system and to predict the regions with heightened probability of mainshocks in the near future. A classic demonstration of this potential is the successful forecast of the 1999 Izmit, Turkey earthquake (Parsons et al. 2000) and the analysis of Coulomb stress changes due to M>7 earthquakes along the North Anatolian Fault during the 20th Century. Static stress triggering of mainshocks is expected to give rise to time-dependent recurrence statistics. The probability of occurrence of mainshocks of a given magnitude will depend upon the recent seismic history in the surrounding region.

Traditional approaches for estimating recurrence statistics, based upon the Gutenberg-Richter relation do not take account for this time-dependency of earthquake occurrence.

There has been some debate as to whether stress interactions need be considered when estimating the seismic risk of the Australian continent. This paper constitutes a first step towards addressing this issue. We examine the theoretical stress change patterns of past Queensland earthquakes and demonstrate that subsequent seismic activity has occurred within sufficiently close proximity for stress interactions to occur. We also consider the stress changes induced by two hypothetical earthquakes of M=5 occurring on conjugate reverse faults, bordering an uplifted Block in south-east Queensland. The analysis suggests that such earthquakes may be cooperative in the sense that an earthquake on one fault will increase the Coulomb stress within the seismogenic zone of the other fault. A dearth of focal mechanisms and detailed structural information necessitates the use of arguably crude assumptions on the orientation and rake of the modeled earthquakes; however the results clearly demonstrate the potential for static stress interactions between faults in eastern Queensland.

Methodology

The procedure for computing the Coulomb stress changes due to an earthquake is well described by King et al. (1994). The appropriate starting point is to model the earthquake as a slip dislocation on a rectangular fault plane (or planes) representing the earthquake source zone. One may then compute the change in both shear and normal stress caused by the earthquake, utilising the Okada (1992) analytic Green's Function for stress changes due to rectangular dislocations in an uniform, elastic half-space. If one further assumes an orientation for faults in the region surrounding the earthquake, one may compute the net change in Coulomb stress along these surrounding faults. Coulomb stress is defined as the difference between the shear stress (τ) and the normal stress (σ) multiplied by an effective coefficient of friction ($\mu^{(eff)}$), namely:

$$CFS = \tau - \mu^{(eff)}\sigma$$

An increase in Coulomb stress on a fault may thus be interpreted as a loading of the fault towards brittle failure (i.e. earthquake rupture). Conversely, a decrease in Coulomb stress is interpreted as an unloading of a fault, thus inhibiting earthquake rupture. Although earthquakes indisputably result in an overall decrease in the net stress accumulated in a region, the patterns of stress change are such that certain regions surrounding a given earthquake experience an increase in stress. Most notably there is a marked Coulomb stress increase in the zone surrounding the rupture plane (the zone most likely to experience aftershocks) and two or more off-fault lobes where delayed triggering of subsequent mainshocks may occur.

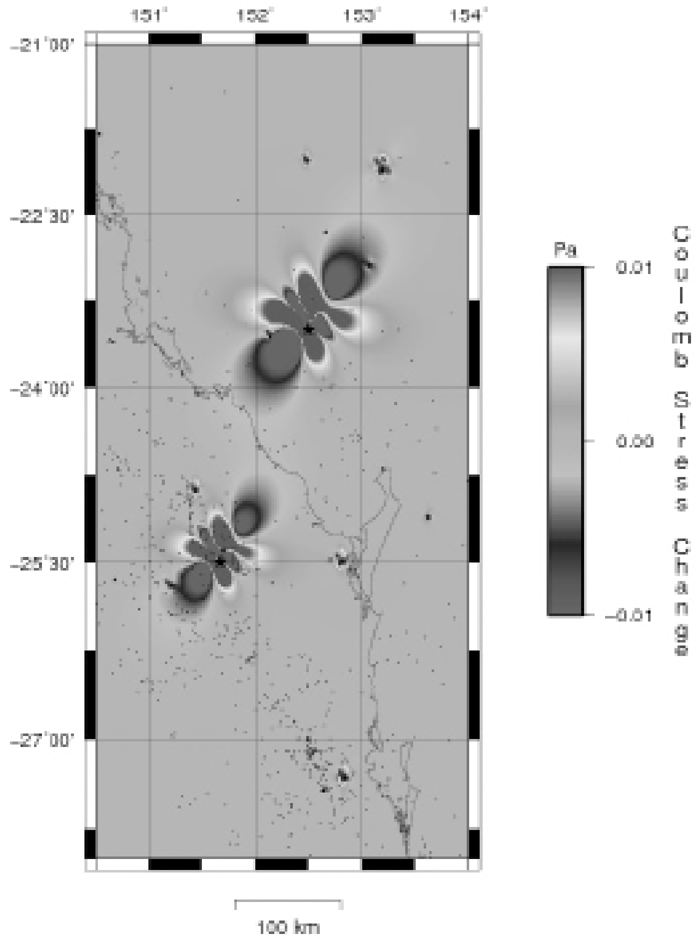

Figure 1: Coulomb stress changes due to M>5 earthquakes in Southern and Central Queensland.

In this work we have employed the 3ddef software to compute stress changes due to modelled earthquakes. This software permits the specification of the earthquake source in terms of a rectangular plane in 3D with a prescribed average slip dislocation across the fault plane. We have selected for analysis all earthquakes of magnitude M>4 in the Queensland earthquake catalogue. The rupture zone of each earthquake is a square of side-length L, extending from a depth of 10km with an average slip (u) across the fault plane. We utilise the following scaling laws (Papadimitriou and Sykes, 2001) to determine the rupture length (L) and average slip (u) for each earthquake:

$$\mathrm{Log}L = 0.51M - 1.85 \qquad \log u = 0.82M - 3.71$$

Due to a lack of focal mechanisms for these earthquakes we are unable to adequately constrain neither the strike and dip angle of the fault planes, nor the rake of the earthquakes. Examination of geological maps for the regions of interest reveals a general trend of N30W striking faults displaying oblique reverse-faulting tendencies. From available transects, the dip angles of faults range between near vertical and up to 45degrees to either the East or West. In south-east Queensland for example, the West Moreton Fault dips towards the east while the North Pine Fault dips towards the west. In the following analysis we assume that all earthquakes strike N30W and model the earthquakes with either pure strike-slip or pure dip slip for a range of easterly and westerly dip angles.

Having specified the source parameters for each earthquake, we compute the static stress changes via 3ddef. From the computed static stress changes we compute the theoretical Coulomb stress change along fault planes oriented parallel to the earthquake source (in the surrounding region). This amounts to calculating the net change in both shear and normal stress along the specified fault planes. We assume here that the effective coefficient of friction of all faults is approximately 0.4. Coulomb stress calculations are relatively insensitive to the choice of effective friction coefficient so this value is considered reasonable (King et al. 1994).

Results

We commence by examining the Coulomb stress changes due to past M>5 earthquakes in South and Central Queensland. To simplify the investigation we have a priori constrained the dip angle of all fault planes to 45 degrees, dipping to the east. We compute the Coulomb stress change along faults oriented at N30W at a depth of 5km. The results are shown in Figure 1, overlain with the epicentres of all past earthquakes in the Queensland seismic catalogue. The 1935 Gayndah earthquake (M=6.1) and the 1918 offshore Gladstone earthquake (M=6.3) dominate in Central Queensland. It is evident that these two largest earthquakes are sufficiently close to form a “stress bridge” across the Queensland coast near Gladstone. Isolated M>5 earthquakes also result in more localised Coulomb stress changes including at least three M>5 earthquakes lying within the stress change lobes of the two M>6 earthquakes. In all cases, a number of recorded earthquakes lie within or near regions of large Coulomb stress change.

There is no question that the assumption of eastward dipping reverse faults is rather crude. A much closer inspection of the local geology and focal mechanisms (where available) is required to accurately model the stress changes due to past earthquakes. The results in Figure 1 simply demonstrate that stress changes of up to 0.01 bar are expected at sufficiently large distance from the rupture planes of past earthquakes that the timing of nearby earthquakes may be altered by static stress interactions.

In many parts of eastern Queensland and other regions in Australia, the structural geology is dominated by pairs of eastward and westward dipping reverse faults, bordering an uplifted block. One such example is the South D'Aguilar Block in south-east Queensland, bordered to the west by the easterly dipping Eastern Border Fault and to the east by the westerly dipping North Pine Fault. Figure 2 is a caricature of the three dimensional fault structure of the region. The 1960 M=5.0 Mt Glorious earthquake is thought to have ruptured a portion of the North Pine Fault.

We shall examine the static stress changes induced by a pair of hypothetical M=5.0 earthquakes rupturing a 5km x 5km patch of the Eastern Border and North Pine Faults (marked as coloured squares in Figure 2). A net slip of 2.4cm is applied across each fault plane with the slip direction selected to promote uplift of the region between the two faults. The rupture planes commence at a depth of 5.25km and extend to almost 10km depth (the assumed depth of the seismogenic zone) dipping at an angle of 30 degrees to vertical. The epicentre of the North Pine earthquake is within 10km of the Mt. Glorious earthquake epicentre.

Figure 3 contains snapshots of the Coulomb stress change induced by these earthquakes for a sequence of horizontal cross-sections of increasing depth. For shallow depths, the two earthquakes induce Coulomb stress increases along parallel faults outside the South D'Aguilar Block, with only a slight Coulomb stress increase within the Block due to slip near the base of the rupture planes. As depth increases, the lobes of increased Coulomb stress migrate into the Block, with positive CFS lobes dominating within the block for depths greater than 7.5km.

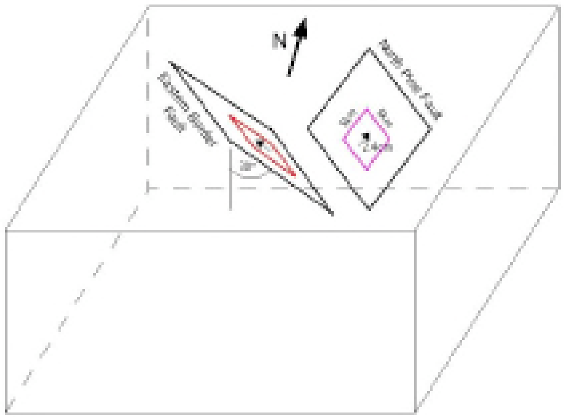

Figure 2: A diagram of the 3D fault structure in the region of the South D'Aguilar Block, SE Queensland.

Conclusions

Two important facts arise from these calculations. Firstly, the static stress changes will promote the occurrence of shallow focus aftershocks outside of the South D'Aguilar Block. Since shallow aftershocks are expected to have a higher damage potential, this is a valuable constraint for post-mainshock mitigation efforts. Secondly, positive Coulomb stress changes at seismogenic depths of between 5 and 10km are focused towards the fault plane on the opposite side of the South D'Aguilar Block. In essence, a reverse faulting earthquake on one side of the Block promotes the occurrence of an earthquake on the other side of the Block and vice versa. While the Coulomb stress increase for a $M=5$ earthquake is very small (less than 0.001bar), a larger magnitude ($M>6$) earthquake may result in between 0.01 and 0.1bar Coulomb stress increases. An increase of this magnitude is comparable with that shown to result in static stress triggering in other seismogenic regions and hence must be considered in seismic hazard assessment, particularly the calculation of recurrence times or probabilities.

Although preliminary in nature, these results highlight the need to consider static stress interactions when estimating the seismic hazard in Eastern Queensland. Past earthquakes have occurred within sufficient proximity of mainshocks for static stress interactions to affect their timing. Furthermore, earthquakes with $M>5$ occurring on conjugate reverse faults promote the occurrence of mainshocks on opposing faults. Further research and modelling is required to quantify the long-term impact of such stress changes. One may hypothesise that seismicity patterns may be dominated by episodic occurrence of “twin” mainshocks rupturing either side of uplifted blocks, separated by relatively long periods of seismic quiescence.

Acknowledgments

D. Weatherley gratefully acknowledges the contributions of R. Cuthbertson and C. Lynam towards this research. Numerical simulations were performed using the Australian Computational Earth Systems Simulator. This research is supported by the Australian Research Council, the Queensland State Government Department of Main Roads and the University of Queensland.

References

King, G.C.P., Stein, R.S., and Lin, J. (1994) "Static Stress changes and the triggering of earthquakes", Bull. Seismol. Soc. Am., 84, pp. 935-953.

Okada, Y. (1992) "Internal deformation due to shear and tensile faults in a half-space", Bull. Seismol. Soc. Am., 82, pp. 1018-1040.

Parsons, T., Toda, S., Stein, R.S., Barka, A. and Dieterich, J.H. (2000) "Heightened odds of large earthquakes near Istanbul: An interaction-based probability calculation", Science, 288, pp. 661-665.

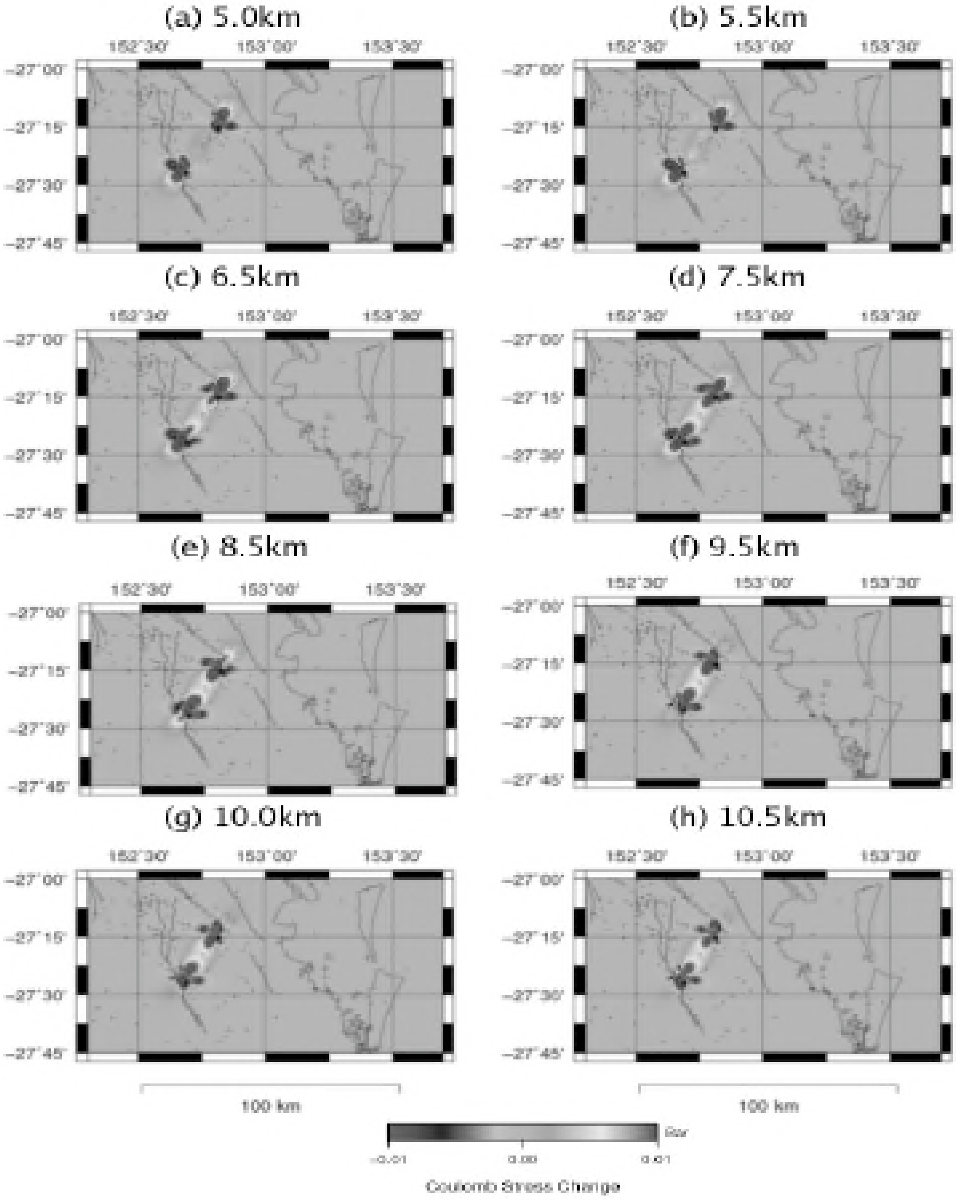

Figure 3: Coulomb stress change within horizontal planes at various depths.

Historical earthquakes: a case study for the Adelaide 1954 earthquake

Cvetan Sinadinovski[1], Stewart Greenhalgh[2] and David Love[3]

[1] Australian National University
[2] Adelaide University
[3] Primary Industries and Resources South Australia

Abstract

The accuracy of a seismic risk assessment is related to the time span of the data base. The longer the seismicity of an area is observed, the better the ability to predict future activity. Historical records of earthquakes stretch back more than four times the period of instrumentally recorded earthquakes, so the value of historical earthquakes and isoseismal maps is of great importance for calibration of ground motion models because the building type is taken into account during assigning of the intensity values and such maps reflect the local geology and soil characteristics.

Of interest to the insurers are also interrelated aspects of risk calculation such as the expected earthquake occurrences, maximum magnitudes and intensities, and anticipated damage. We have used a well-documented case of the Adelaide 1954 earthquake to address these aspects and tried to compare the MM intensities with the damage ratios for the purposes of loss calculation. Our estimates expressed in percentage of the effective loss of the replacement value of insured dwellings in Adelaide are comparable with the results of the recent studies by the insurance industry.

Introduction

Earthquakes have been recorded on Australian seismograph networks only within the last forty years or so (Greenhalgh et al., 1994). Historical records of earthquakes stretch back more than four times the period of instrumentally recorded earthquakes, so the value of historical earthquakes and isoseismal maps is of great importance for research.

Malpas (1991a) presented a list of historical earthquakes in South Australia for the pre-network period 1883-1961 and from 1962-1991. She also reviewed the State's two important events (Warooka 1902 and Adelaide 1954). The general engineering design and construction of buildings was considered in a seismic risk study for South Australia by McCue in 1975 and later in Eastern Australia (McCue, 1977). He gave a series of recommendation regarding the instrumentation, seismic methods and risk calculation.

Of interest to the insurance industry are three interrelated aspects of risk calculation, namely the expected earthquake occurrences, estimates of maximum magnitudes and intensities, and anticipated damage.

Gaull et al. (1990) published the first probabilistic hazard study of earthquakes in Australia and many other studies have since followed. However, the question remains regarding the maximum magnitudes of earthquakes in zones with relatively short seismic history and when the magnitude-frequency relationship is not constrained. The insurance industry has adopted a slightly different approach based on the concept of Probable Maximum Loss (PML) which is a measure of the maximum loss which can be anticipated in a given period (Blong, 1992; Irish, 1992).

While the Loading Standards present the likely ground motion in a region using peak ground acceleration on rock, the insurance industry approach is to use a "design" earthquake to model the expected effects from some likely events. The second approach is dependent on the selected earthquake location and magnitude, as well as a detailed knowledge of the path characteristics, including the local site conditions, which in some cases are difficult to obtain.

The existing isoseismal maps reflect, in addition to the distance from the epicentre and the focal depth of the earthquake, the local geology and the soil characteristics of the area. The actual building response, upon which intensity values are determined, depend not only on the ground motion levels, but also on the building type and height. Each building will have its own natural period of vibration, which may resonate with the earthquake frequency range. After taking account of building type, it is possible to use the isoseismal maps for particular earthquakes to directly calibrate for ground motion models. Microzonation maps exist for the shallow sediments beneath some Australian capital cities (Love, 1996; Jones et al., 2004). When such detailed maps are available, the inclusion of the regolith amplification by using the soil type description and corresponding amplification factors in the earthquake loading standard can be applied in given situations.

Adelaide 1954 earthquake

In the early hours of 1st March 1954, at 3.40am (local time), the city of Adelaide experienced one of the States severest earthquakes, equal only to the events at Beachport 1897 and Warooka 1902 (Malpas, 1991c). From the list of historical earthquakes (McCue, 1975, Malpas, 1991a, Dyster, 1995) it was the first earthquake of such size in the vicinity of the city. The isoseismal map of the earthquake is shown in Fig. 1 (after Kerr-Grant, 1956). The strong shaking woke most residents, cracked walls and loosened plaster from many buildings (Love, 2002). Southern suburbs sustained the worst damage, with fallen chimneys and partial wall collapse of some dwellings. Other hill areas, especially along the Burnside fault, also reported damage, attributed to down-slope slippage of subsoil during the disturbance or perhaps resonance. The maximum intensity of the earthquake has been established as MM VIII.

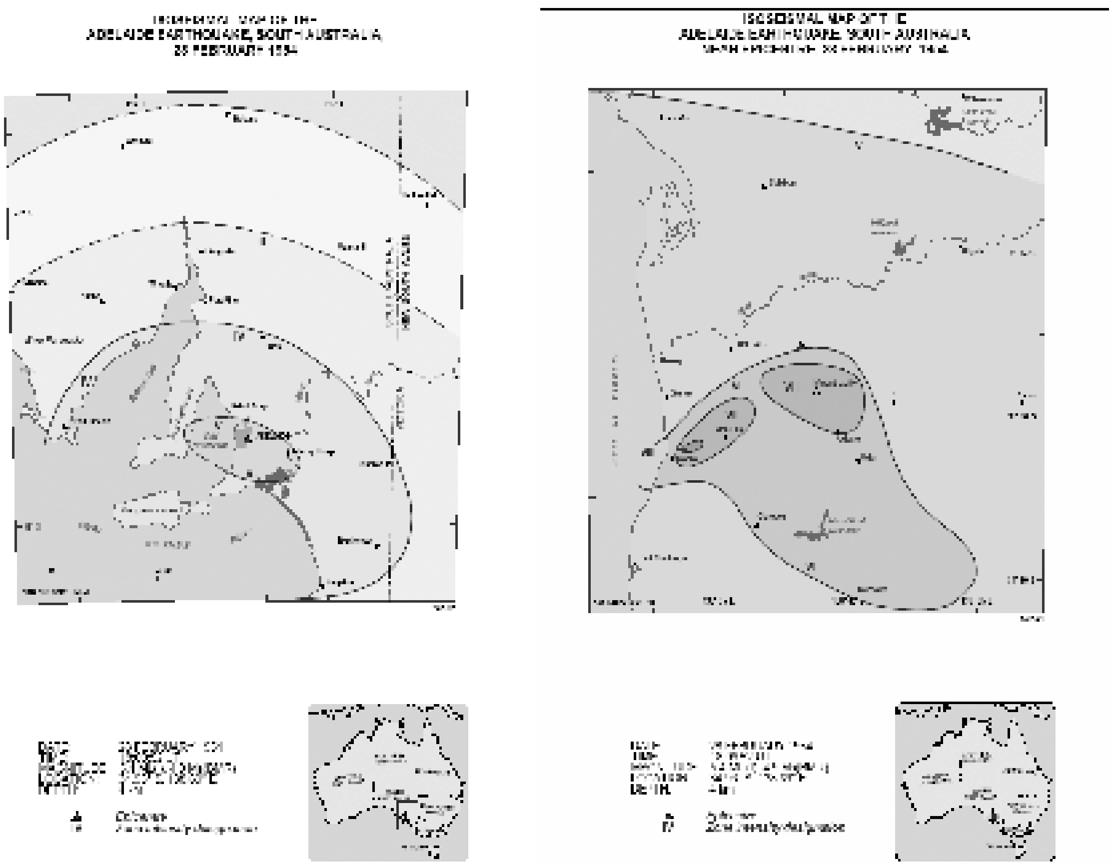

Figure 1: Isoseismal map of Adelaide 1954 earthquake

In view of the importance of the 1954 earthquake, the macroseismic data were reviewed and the isoseismal map redrawn (Fig. 2) based on numerous excerpts from newspaper reports in the Public Library of South Australia and the State Archives (Malpas, 1991b). The new map still retained a maximum intensity of MM VIII, but zones with intensities MM V and MM VI were increased alongside faults.

Seismograms of this earthquake were obtained at Melbourne, Riverview, Perth and Brisbane, though it was not large enough to be recorded in New Zealand nor Manila. Apparently the Adelaide seismograph was still in operation, but had problems with the time marks and was overloaded due to proximity to the epicentre. The initially assigned local magnitude was 5.4 and has been reviewed a few times (Malpas, 1991b, McCue, 1980). In the absence of any instrumental records under a distance of 600km, the isoseismal maps become crucial evidence in deciding the epicentral location. A small aftershock of magnitude 3.2 occurred in the same area the following day at 5.45am local time with a felt radius of around 20km and maximum intensity of MM IV.

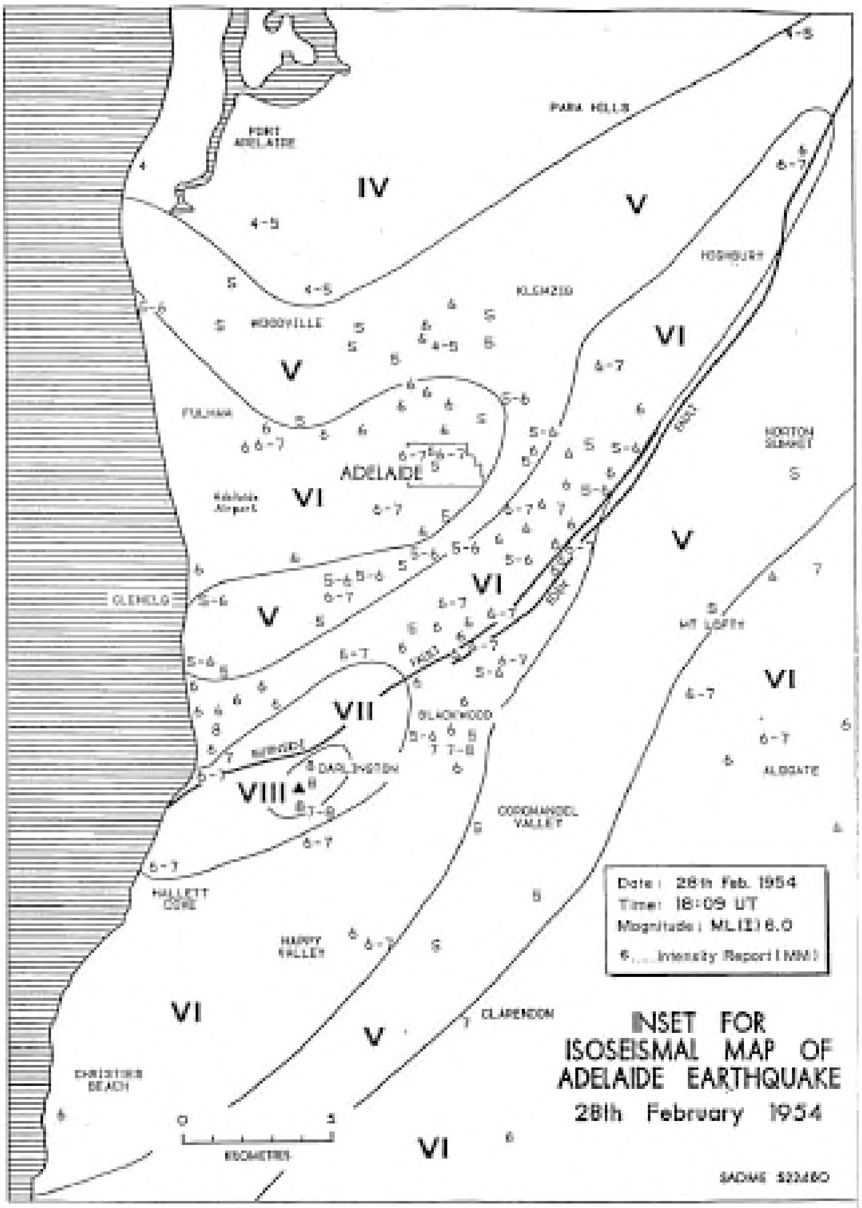

Figure 2: Enlarged isoseismal map of Adelaide 1954 earthquake (after Malpas 1991)

Damage calculation process

Damage ratios which relate MM intensities to building types and loss ratios are relatively recent, and usually not very constrained, because building codes and construction types may vary from area to area. However, there are some general empirical relationships regarding attenuation of seismic waves from given earthquakes in Australia, and the vulnerability of common building structures.

The total damage bill will depend on the maximum intensity of the earthquake and the decay of intensity with distance from the epicentre. The areal distribution of intensity levels depends on the magnitude of the event and its depth, and the attenuation function of seismic waves within the region. Local geological conditions such as soil thickness and type and proximity to faults, can alter the degree of ground shaking and hence the damage pattern. In general, the shallower the earthquake, the greater the maximum reported intensity I_{max}, but the lower the total area affected. From a systematic study of available intensity information for Australian earthquakes, the average relationship between local magnitude ML, maximum observed intensity I_o and radius of perceptibility R_p was determined by Greenhalgh et al., (1989) through the following formulas:

$ML = 1.35(\pm 0.34) + 0.57(\pm 0.06)\ I_o$ and
$ML = 0.35(\pm 0.12)\ (\log R_p)2 + 0.63(\pm 0.41)\ (\log R_p) + 1.87(\pm 0.36)$

The formulas predict that for a shallow earthquake producing a maximum intensity Imax=VIII (comparable to the 1954 Adelaide event), the area shaken at MM intensities VIII, VII and VI would be 250, 900 and 3100 km^2 respectively, though the comparative areas for such an event in Western Australia might have been somewhat different (Sinadinovski and McCue, 2003). Intensity MM VI is generally taken as the engineering threshold for building damage (plaster cracks, chimney damage).

Thus the likely number of insurance claims to be expected following a particular earthquake according to these formulas can be specified with a certain probability depending on the housing density and the size of the epicentral zone.

The average levels of damage for houses of brick construction as a fraction of property value at different Modified Mercalli intensities have been assessed by the Australian Government Actuary as:

MM Intensity	V	VI	VII	VIII	IX	X	XI
Fractional Value of Damage	0.01	0.03	0.09	0.25	0.75	0.95	1

For timber or fibro dwelling (brick chimneys, concrete block etc.) the damage would be less by a factor of 3 at intensity MM VII, and a factor of 5 at intensity MM IX.

In Australian conditions unreinforced masonry (URM) is a common form of building construction. A team from the University of Adelaide has developed a two-step vulnerability assessment procedure for URM buildings that considers both the global in-plane and local out-of-plane URM building response. Data from the Newcastle earthquake were used to verify the accuracy of that approach. Their results showed good correlation with the observed damage on a suburb-by-suburb basis (Brezezniak et al., 2003).

The quantification of the earthquake load (demand) on potential structures in the study region was represented as the earthquake demand curve. Vulnerability was then defined as a response of different buildings types to a given event by finding the displacement corresponding to the intersection of the earthquake demand and the capacity curve. The values typically correspond to the displacement at which the cracking occurs (usually ultimate strength) and the point at which the wall's loss of strength becomes significant. For in-plane wall response, values were expressed on the basis of the storey drift, i.e. dividing lateral displacement by the height. For out-of-plane wall response, the concept of drift was taken as the wall deformation divided by the wall span.

The drift ratios for URM buildings with tile roof and metal roof were considered for low- and mid-rise building heights, i.e. 4.5 and 10.7m. The authors also specified four URM threshold drift ratios for the slight, moderate, extensive and complete damage state. Almost every assessment indicated that out-of-plane damage was significantly more than in-plane damage. The assumptions for the vulnerability part of the model have to account for building degradation, quality of construction, and local out-of-plane failure mechanisms in URM buildings.

Loss results

The Adelaide 1954 earthquake produced intensities of MM VI or greater over an area of about 600km^2, with two areas totalling about 100km^2 experiencing MM VII in the south, and one very small area near Darlington sustained MM VIII. Most of the urban area experienced an intensity of MM V. The majority of the dwellings in Adelaide at the time of the 1954 earthquake were of brick or stone construction and many were vulnerable to damage from an earthquake producing intensities greater than MM VI. The 1954 Census showed the population of Metropolitan Adelaide as 483,500, and a total of less than 137,000 dwellings (Greig Fester report, 1996). Records maintained by the Fire and Accident Underwriters Association of South Australia indicate that by the end of September 1957 a total 30,303 claims had been paid. That suggests that claims were made for 22% of buildings for earthquake damage. Many of the claims paid were for cracks in the walls of houses and some cracks were probably initiated by earlier movements of subsoils and foundations.

In 1954 there was generally no excess applied to earthquake claims. Most claims were relatively minor, with the total payout for all claims around $6 million – an average claim of $200. Unfortunately, no information remains concerning the location of buildings on which claims were paid or the distribution of the claims amounts. However, the number of claims paid by the 63 insurer companies range from 1 to 2622, while the claims paid range from $54 to $352. A February 1955 memo of the Fire and Accident Underwriters' Association of South Australia gave the aggregate statistics of Earthquake Losses compiled from individual returns submitted by all Members of the Association. The total number of claims lodged as at 31st December 1954 was 30,098 with a total value of £2,777,517.

In the 1996 confidential report on historic exposure and loss data for the Adelaide 1954 earthquake by New Zealand's Works Consultancy Services Ltd, the total domestic exposure of houses and flats (owner occupied and rented) was 94,865, with a total replacement value of $606 million. The average construction cost per house was estimated at $5,500 at time of completion (excluding land) and did not in general include carports, fences or other subsequent additions and alternations. Other comparisons suggested that the average replacement value for the metropolitan area is likely to have been closer to $6,000-$6,500 per house.

Historical loss data for the 1954 earthquake were available only for domestic risks, as very few commercial risks were covered by earthquake insurance at the time. Two figures commonly used for the loss are 30,300 insurance claims at an average of $200 per claim, and a total claim of $6.2 million, and a total loss of $8 million which included the insurers outside the group. Also, the losses quoted above included domestic contents losses (generally minor) as well as damage to dwellings, whereas the exposure figure of $606 million includes the value of the dwellings only. Earthquake cover without excess was automatic under the Householders policies applying at the time and many smaller claims were apparently related to re-opening or enlargement of pre-existing cracks.

However, as the insurance policies at the time provided indemnity cover only, the loss figures do not include any betterment. So, allowing the first amount of $6.2 million, the corresponding effective loss would have been 1.02% of the replacement value of insured dwelling in Adelaide at the time. Discussion in the files of the Fire and Accident Underwriters' Association of South Australia suggests that there was general agreement that industry treatment of claims had been generous, but that the industry was interested in avoiding future claims for damage caused by subsidence and soil movement.

Summary and discussion

Here we have used the Adelaide 1954 earthquake to calculate the risk and compared the MM intensities with the damage ratios for the purposes of loss estimation. Our estimates are about 1% of the effective loss of the replacement value of insured dwellings in Adelaide. Earlier results of the Probable Maximum Losses studies (Greig Fester, 1996) based on aggregation of losses for several regions of MMI produced estimates in the range of 1.9 to 4.8% for a shallow earthquake with magnitude 5.6 below postcode 5000, with uncertainties in the results attributed to the modelling of the subsoils and choice of attenuation function.

By 1957 most of Adelaide Plains had been urbanised with expansion of low density housing (about 20 persons per hectare) after World War II with the growth of outer centres at Elizabeth, Salisbury, Tea Tree Gully, Morphett Vale, Noarlunga and southwards along the coast. Dwellings are defined as separate houses, semi-detached row or terrace, townhouses and 1-2 storey blocks of flats. With the southerly development of Adelaide's suburbs (Fig. 3), an event of similar size recurring today might be expected to cause significantly higher loss.

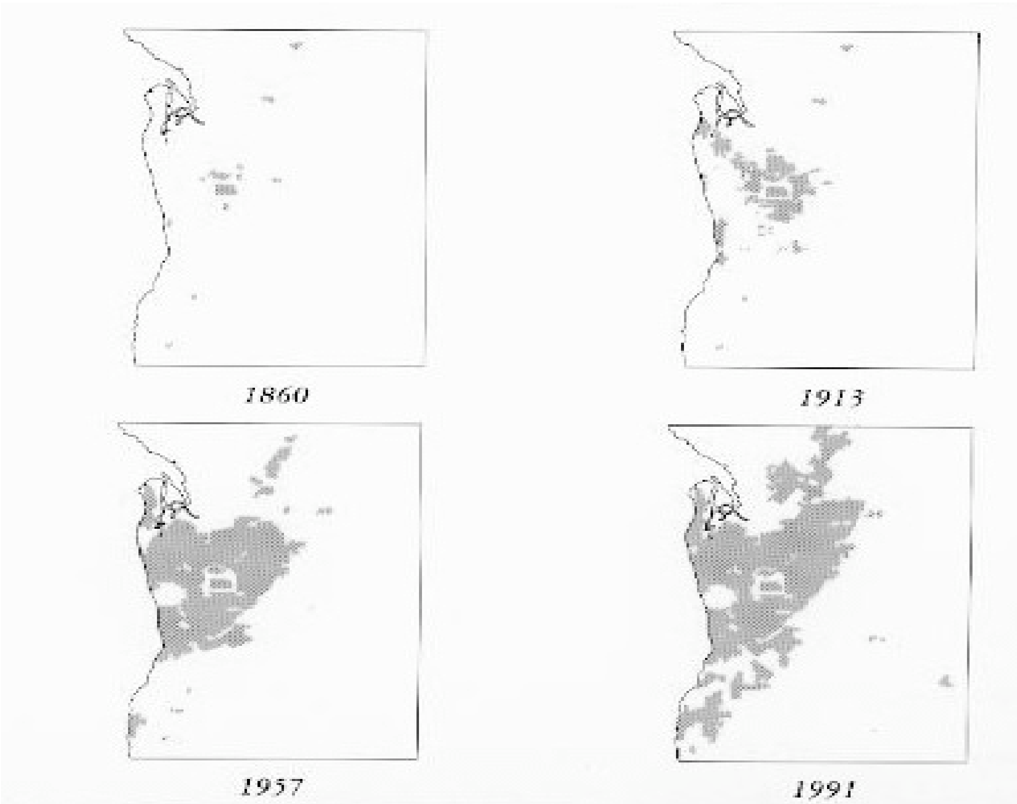

Figure 3: Adelaide and its suburbs

References

Blong, R.J., 1992. Domestic Insured Losses and the Newcastle Earthquake, Earthquake Resistant Design & Insurance in Australia, AEES and Specialist Group on Solid-Earth Geophysics Conference, Sydney.

Brezezniak, N., Lynch, T., Moore, C., Rollison, C., and Griffith, M., 2003. Improved Vulnerability Models for Regional Earthquake Risk Assessment, AEES Conference, paper 23, Melbourne.

Dyster, T., 1995. Strong Shock of Earthquake – The Story of the Four Greatest Earthquakes in the History of South Australia, Mines and Energy South Australia, Report Book 95/47, Adelaide.

Gaull, B.A., Michael-Leiba, M.O., and Rynn, J.M., 1990. Probabilistic Earthquake Risk Maps of Australia, Australian Journal of Earth Sciences, 37, pp 169-187.

Greenhalgh, S.A., Denham, D., McDougall, R. and Rynn, J., 1989. Intensity Relations for Australian Earthquakes, Tectonophysics, pp 166, 255-267.

Greenhalgh, SA, Love, D. and Sinadinovski, C., 1994. Thirty years of seismic network recording in South Australia, Phys.of Earth Plan. Int. 86, pp 277-299.

Greig Fester 1996. Earthquake PML, Household Buildings, Adelaide.

Irish, J.L., 1992. Earthquake Damage Functions for Australian Houses and the Probable Maximum Loss for an Insurance Portfolio, Earthquake Resistant Design & Insurance in Australia, AEES and Specialist Group on Solid-Earth Geophysics Conference, Sydney.

Kerr-Grant., C., 1956. The Adelaide Earthquake of 1st of March 1954. Transactions of the Royal Society of South Australia, 59, pp 177-185.

Jones, T., Middelmann, M., and Corby, N., 2004. Natural Hazards in Perth, Western Australia, Comprehensive report, Geoscience Australia.

Love, D., 1996. Seismic Hazard and Microzonation of the Adelaide Metropolitan Area. Department of Mines and Energy South Australia, Report 27, Adelaide.

Love, D., 2002. Earthquake Photo Collection, Primary Industries and Resources South Australia, CD.

Malpas, K.L., 1991a. Seismic Risk of South Australia, Honours Thesis, Flinders University.

Malpas, K.L., 1991b. Adelaide 1954 earthquake, South Australia, unpublished record, Flinders University.

Malpas, K.L. 1991c. Warooka 1902 Earthquake South Australia, unpublished record, Flinders University.

McCue, K.F., 1975. Seismicity and Seismic Risk in South Australia, ADP 137, The University of Adelaide.

McCue,K.F., 1977. Seismic Risk in Eastern Australia. ADP 153, The University of Adelaide.

McCue, K.F., 1980. Magnitude of Some Early Earthquakes in Southeastern Australia, Search 11, No. 3, pp 78-80.

Sinadinovski, C., and McCue, K.F., 2003. Comparison of Two Earthquakes with Similar Magnitudes in Dissimilar Tectonic Regimes, Proceedings of the European Conference on Earthquake Engineering, Skopje-Ohrid, Macedonia.

Attenuation structure beneath Australia

Agus Abdulah

Australian National University

Abstract

The strategic position of the Australian continent in the middle of seismicity belts which extend from Java to Sumatra and the mid-ocean ridge to the south of the continent provides a wealth of events at suitable distances to be used as probes into the seismic structure of the upper mantle. The extensive deployment of portable broadband seismic stations across the Australian continent and Tasmania since 1993 offers robust seismological data with a dense coverage at distances from 5° to 45°. Over the last two decades, a wide range of studies have been used to gain information on one-dimensional and three-dimensional structure in the mantle which exploits different aspects of seismograms. P and S wave seismic travel times from nearly 4000 three-component seismic datasets from the record have been hand picked. The wave ratio method is then applied to estimate the spectral ratio between shear and compressional waves. Seismic spectra are estimated using the multi-taper method with 512 points in a window range of 30s to 45s and a frequency range of 0.25Hz to 1.00Hz.

Three-dimensional P and S wave speed tomography is conducted by inverting a kernel matrix obtained from a quasi three-dimensional ray tracing which respect to P and S wave seismic travel-time residuals from the ak135 model. The study area from latitude 22° N to 65°S and longitude 78° to 189° and 0-1240km depth is discretised into 11100 cells with a cell size of 3°x3° and depth increments of 35 or 200km. Both P and S-wave speed information from the seismic wave speed tomography are then utilised as data input for 3-D seismic attenuation tomography. In this inversion, it is assumed that $Q_P=2.3Q_S$. The seismic attenuation anisotropy in terms of the ratio between seismic attenuation derived from SV and SH component is also presented.

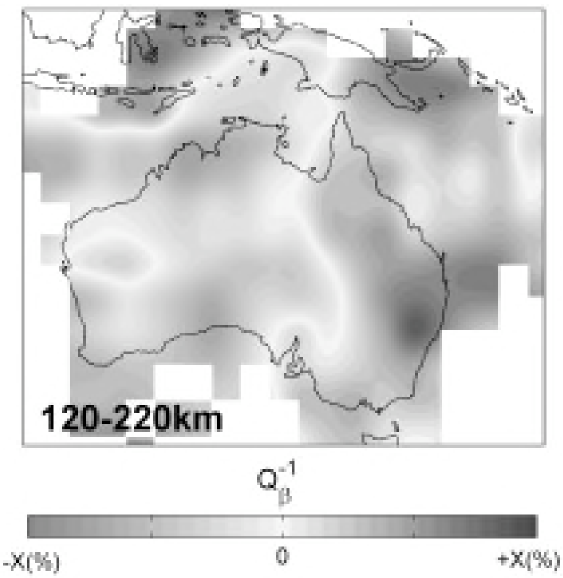

The major feature that is revealed from both the seismic wave and seismic attenuation studies is a strong contrast in deep structure between central Australia and the eastern seaboard (as can be seen in the figure). Further representation of seismic attenuation anisotropy suggests that in the region where seismic coverage is good, the transverse component (S_H) wave is less attenuated than the radial component (S_V). Archaean and Proterozoic rocks in the west and in the middle of the continent point to a high seismic wave speed anomaly and low seismic attenuation, and the Phanerozoic rocks and the presence of recent volcanism and region of high heat flow in the east are associated with low seismic wave speed anomaly and high seismic attenuation.

Seismic fragility curves for damage to building contents

Haider A. Al Abadi, Nelson T.K. Lam and Emad F. Gad

Abstract

Slender free-standing objects in a building could be excited into rigorous rocking and/or sliding motion in an earthquake. Some objects might experience overturning and hence damage when impacting on the floor. Objects which do not overturn might still experience significant damage depending on the severity and nature of the collision with the neighbouring objects and with the floor when excited into motion. This paper presents fragility curves which define the probability of overturning of objects for given object dimensions, dynamic characteristics of the building and location of the object within the building. A method for calculating the level of shock experienced by the object on pounding with the floor is also presented.

1. Introduction

Contemporary codes of practice typically relate the seismic actions on non-structural components and building contents to the maximum acceleration of the floor (eg. Draft AS 1170.4, 2006; AS/NZS 1170.5, 2005). A dynamic amplification factor may be applied depending on whether the component is attached to a flexible mounting. This method of analysis does not accurately take into account the highly non-linear behaviour of the rocking motion in which overturning would occur if the centre of gravity of the object has been displaced past the pivotal position of rocking. For objects that have not overturned, significant level of damage might still be caused by the pounding of the object with the floor and with neighbouring objects. The research described in this paper is aimed at modelling the vulnerability of objects to overturning. Results are presented in the form of fragility (vulnerability) curves in Section 2. A simple method of estimating shock sustained by objects which do not overturn will also be described in Section 3.

2. Vulnerability of objects to overturning

Fragility curves are normally presented to predict the probability of damage to a structure, or component, with increasing intensity of the applied actions. With seismic actions, the intensity is usually represented by the notional peak ground acceleration (PGA), or peak ground velocity (PGV). Similar fragility curves could be used to predict the extent of damage to non-structural components in a building. However, this conventional format of presenting vulnerability to damage is not as effective in providing information on the relative vulnerability for a range of components with different properties, since only one item of interest is represented by each curve. Fragility curves for overturning of objects as presented in this paper are mostly based on correlating the probability of overturning with variations in object height when the thickness and shape of the object is kept constant (eg. Figure 1). Fragility diagrams presented later in the paper contain multiple fragility curves with each representing objects of a constant thickness but varying height (eg. Figure 2a). Thus, the relative vulnerability to overturning can be shown for objects of varying size and aspect ratio in one diagram.

In this study, the earthquake excitations were based on an ensemble of six artificial accelerograms with random phase-angles generated by program GENQKE (Lam et al, 2000) to simulate the ground shaking of a Class D site in a magnitude 6.5 earthquake at a site-source distance of 45 km. The attenuation of the earthquake with distance was based on the crustal model of south-eastern Australia as adopted in the study of Lam et al (2005). The intensity and frequency content of the simulated motions were consistent with the design response spectrum stipulated by the new Australian Standard for seismic actions for a seismic coefficient of $Z = 0.08$, which is the level of seismic hazard defined for most Australian capital cities on the eastern seaboard including Melbourne, Sydney and Canberra for a return period of 500 years (Draft AS1170.4, 2006).

The objective at this stage of the investigation was to reveal the trend of the vulnerability to overturning. Hence, only one earthquake scenario was considered. Uncertainties associated with the buildings' dynamic properties and objects' dimensions have not been incorporated into the fragility curves, in which the random variability of the applied excitations was only taken into account. These fragility curves can be further developed to incorporate variability in the objects' dimensions and other related parameters.

All the rectangular objects were assumed to be free-standing, resting on a perfectly inelastic surface, and have uniform distribution of mass. The filtering of the floor motions was in accordance with: (i) the fundamental mode of vibration of a ten-storey building with natural period equal to 1 second and a linear deflection profile, and (ii) the first three modes of vibration of a 66-storey building model of height 280 m based on micro-tremor monitoring of the Republican Plaza, Singapore (Brownjohn & Pan, 2001). The fundamental natural period of vibration of the second building model was 5.4 seconds.

When the object thickness (t) was fixed, non-linear time-history analyses that could simulate large displacement (rocking) behaviour were applied to objects with heights varying between h = 0.1 m to 4 m (with 100 mm increments) to determine if the object could overturn. Details of this type of analyses have been presented in Al Abadi et al, 2004 & 2006. The total number of simulations in the construction of a fragility curve was 240 (ie. 6 accelerograms x 40 models of varying height). An example of such a fragility curve is shown in Figure 1 in which the object thickness was kept at t = 100 mm and the floor excitations were subject to filtering of the 10-storey building up at the roof level. The scattered plot shown by the "diamond" symbols in the figure indicate the actual percentage of overturning observed from the 6 analyses undertaken for every increment of object height h. The solid line shown in the figure represents the "best-fit" cumulative log-normal probability density function F{h} which is parameterized by the mean and standard deviation of h (with notation m and s respectively) as shown by equation (1). Statistical analyses have been applied to verify the adopted function form for the fragility curves and to test the "goodness-of-fit" (Shinozuka et al, 2001). It is noted that 240 models were analysed for each object thickness in order that a reliable estimation of the mean and log-standard deviation could be achieved.

The "optimal" values of m and s that achieve the best match of the F{h} function with the observed rate of overturning were calculated using the Maximum Likelihood Theory (Shinozuka et al, 2000) which is briefly described herein. With overturning analyses undertaken on 240 cases (ie. N = 240) the maximum likelihood parameter L is defined by equation (2).

$$F\{h\} = \Phi\left\{\frac{ln(h/\mu)}{\sigma}\right\} \tag{1}$$

$$L = \prod_{i=1}^{N} \left(F\{h_i\}\right)^{x_i} \left(1 - F\{h_i\}\right)^{1-x_i} \tag{2}$$

where i identifies each of the N (=240) no. of cases and x_i = 1 or 0 if overturning is predicted to occur , or not to occur, respectively by the time-history analysis. The values of μ and σwere determined for the conditions where the value of L as defined by equation (2) was maximized, using equations (3a) and (3b) respectively.

$$\frac{\partial \ln(L)}{\partial \mu} = 0 \tag{3a}$$

$$\frac{\partial \ln(L)}{\partial \sigma} = 0 \tag{3b}$$

Figure 1 provides a holistic, and simple, representation of vulnerability of objects to overturning with t = 100 mm and floor excitations as specified. It is shown that with such conditions most objects of height equal to, or exceeding 1 m, would be most likely to overturn (with probability of overturning close to 100 %). The probability is reduced to slightly above 50% for object height equal to half a metre.

Further fragility curves were constructed for different object thicknesses and excitations based on different floor levels within the 10-storey and the 66–storey buildings (refer fragility curves presented in Figure 2).

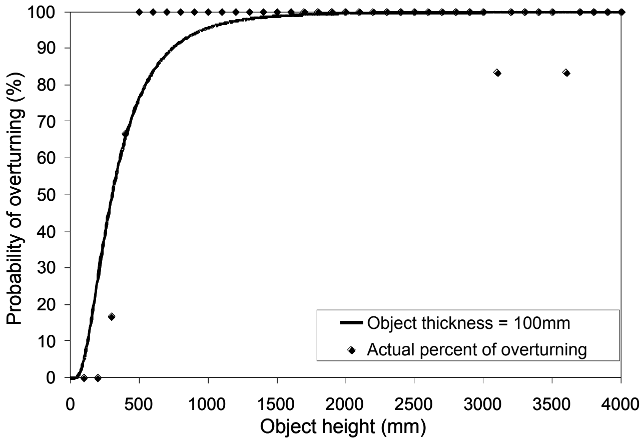

Figure 1: Fragility curve for 100mm thick objects at roof of 10-storey building

It is shown that the fragility curves are very sensitive to the object thickness. For example, the probability of overturning of objects with thickness equal to 500 mm never exceeds 50 %. The floor level within the building and the nature of the building could both be very critical to the object overturning behaviour (Franke et al, 2005). For example, objects in the 66–storey building are much less likely to overturn than in the 10–storey building when other parameters are kept the same. Objects positioned at mid-height of the 66–storey building appear least vulnerable out of all the presented cases.

Fragility curves can also be extended to incorporate multiple earthquake scenarios that have been identified from the de-convolution analysis of the seismic hazard model for an area (in which case vulnerability curves associated with any pre-defined level of PGV could be obtained by aggregating probability of overturning calculated for each contributing earthquake scenario; refer companion paper Lumantarna et al, 2006). Example of such fragility curves is shown in Figure 3 for specific objects of certain dimensions.

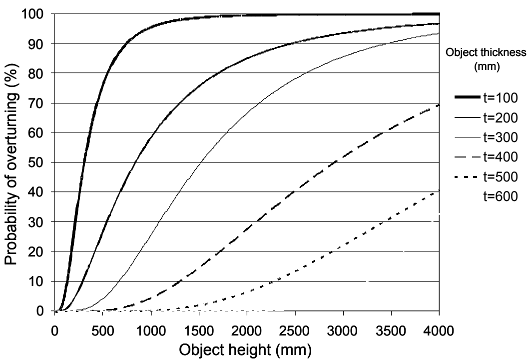

(a) Roof of 10-storey building

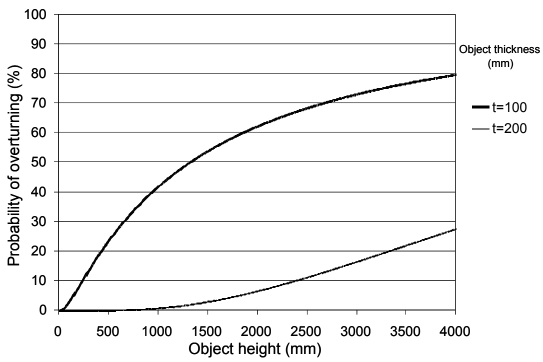

(b) Roof of 66-storey building

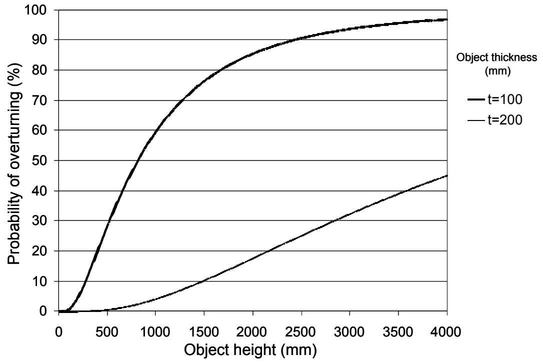

(c) mid-level of 10-storey building

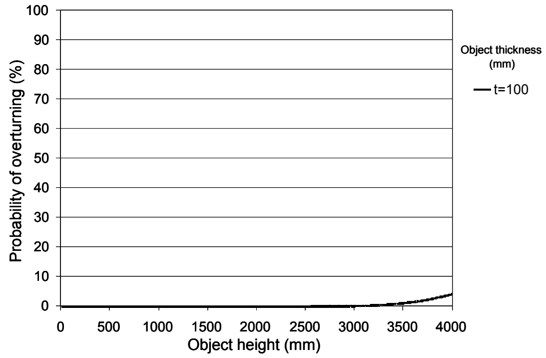

(d) mid-level of 66-storey building

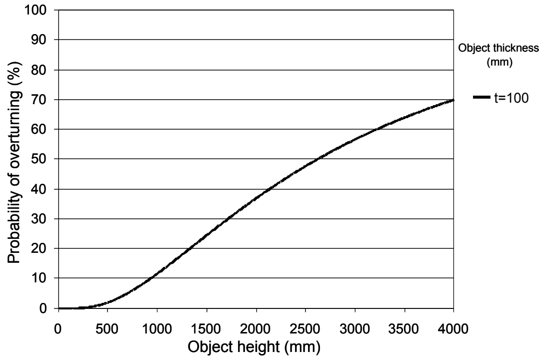

(e) ground level

Figures 2: (a) – (e) Fragility curves at different levels within 10-storey and 66-storey buildings

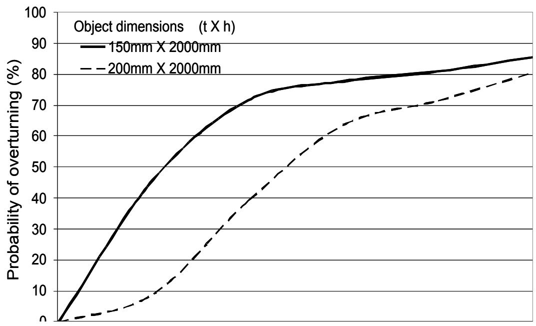

Figure 3: Fragility curves at the rooftop of 10-storey building for two rectangular objects

3. Modeling level of shock on rocking objects

Objects that do not overturn might still be damaged (or have their contents damaged) by shocks sustained at the base of the object when pounding on the floor during the course of rocking. In the worst case (ie. at the threshold of overturning) the centre of gravity (c.g.) of the rectangular object could be displaced by an amount equal to half of the object thickness (ie. t/2). The angle of rotation of a slender object measured from the horizontal is accordingly equal to t/h and its c.g. lifted by the amount defined by equation (4).

The potential energy gained by the lifting of the object as defined by equation (5) will all be converted to kinetic energy which would in turn be dissipated by the impact (it is assumed that the base of the object would not fall flat on the floor but instead only its edge is engaged with the impacting action).

$$\Delta_{c.g.} = \frac{t^2}{2h} \tag{4}$$

$$PE = M.g.\Delta_{c.g.} = \frac{M.g.t^2}{2h} \tag{5}$$

It is the objective of this section to describe the modeling that is required to predict the level of shock experienced on impact. Factors controlling the impacting actions include the amount of kinetic energy to be dissipated, the geometry and stiffness properties of the object, and the stiffness property of the flooring materials and details of the edge of the object which is engaged with the impact. Modeling the impacting action by finite elements may consume a great deal of memory since very fine meshing is required of both the object and the floor surrounding the point of impact. Significantly, the time-step has to be very small given that the impact would only last for a few milliseconds depending on the hardness of the materials that are affected. Given that the computations need to take into account geometrical non-linearity, the dynamic stiffness matrix requires reconstruction at every time-step. Thus, the amount of computational time increases exponentially with the number of degrees of freedom in the finite element model.

The investigation described herein was concerned with a computer server cabinet (which can be modeled as a rectangular body). Small studs were attached to the edges of the cabinet at the base. Thus, the floor surface was in direct contact with the surface of the studs as illustrated in Figure 4. An important feature of the modeling was the simplification of the cabinet into a point mass object model. The size and geometry of the object was to match with that of the studs but the density of the point mass was artificially increased in order that its total mass (M) was made to equate with that of the cabinet as a whole. If the point mass was lifted by the amount defined by equation (4) the potential energy gained by the lifting would then be identical to the potential energy gained by the lifting of the cabinet as defined by equation (5). Given that the force-indentation relationship, or F{δ}, of the base stud of the cabinet into the flooring material has been accurately represented by the point mass model, the force (F) experienced by the floor would also be accurately represented at any instance during the impact.

Figure 4 Rectangular object model and point mass object model

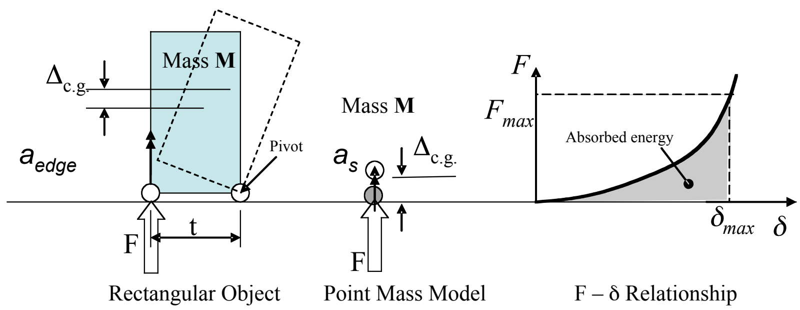

Finite element analysis could be undertaken on the point mass object impacting on the floor for calculating the level of shock (a_s = F/M). This approach to modeling waives the need to model the cabinet as finite elements and hence represents significant savings in computational time. If the stud was spherical, the analysis could be simplified further by employing closed-form solutions (Hertz law) to model the force-indentation relationship of a sphere impacting on the floor (which is modelled as a half-space). In fact, the point mass model could take any geometry which matches with the actual shape of the stud. For example, the geometry of the point mass can take the shape of the rubber stud commonly used for isolating the base of metal cabinets from the floor. If the floor surface was an order of magnitude harder than that of the stud, the force-indentation, or F{δ}, relationship could be based purely on the stiffness behaviour of the stud in isolation, in which case no finite element modeling would be required. No matter which approach is used to obtain the F - δ curve, the maximum impact force (F_{max}), and maximum indentation (δ_{max}), could be identified at the point on the curve where the total amount of absorbed energy equals the amount of potential energy defined by equation (5). This method of calculating the value of F_{max} , and hence as max (= F_{max}/M) is summarized by equations (6a) – (6b).

$$\frac{M.g.t^2}{2h} = \int_{\delta=0}^{\delta_{max}} F\{\delta\} d\delta \tag{6a}$$

$$a_{s\max} = \frac{F\{\delta_{\max}\}}{M} \tag{6b}$$

Equations (6a) and (6b) were based on the worst case of an object being lifted to the limit of overturning. These equations could be modified for calculating the value of as max for any arbitrary lift of the object.

Finally, the level of shock experienced by the cabinet at its edge (a_{edge}) can be related to the calculated value of as max using equations (6c) – (6d) which were derived by taking moment about the pivotal edge of rocking, and by equating the calculated moment to the rate of change of angular momentum immediately following impact.

$$F_{\max}.t = I_o.\ddot{\theta} = \frac{4}{3} MR^2 \frac{a_{edge}}{t} \tag{6c}$$

$$a_{edge} = \frac{3t^2}{4MR^2} a_{s\max} \tag{6d},$$

where R is the length measured from the centre of the object to its corner, Io is the mass moment of inertia of the cabinet around the pivotal edge ($I_o = 4/3M_b R^2$), and $\ddot{\theta}$ is the angular acceleration of the object during impact ($\ddot{\theta} = a_{edge}/t$).

Equation (6d) is based on the assumption that the rocking motion of the rectangular object comes to an abrupt end following the impact of the base stud with the floor. This assumption is generally valid for squat objects but may over-predict the amount of absorbed energy with slender objects. A more accurate expression to predict the value of a_{edge} is defined by equations (6e) – (6f) which takes into account the fact that only part of the kinetic energy is absorbed by the floor (and base stud) as the rocking motion continues due to the angular motion of the object.

$$a_{edge} = \frac{3t^2}{4MR^2} \cdot \frac{1}{\sqrt{1-R_D^2}} a_{s\max} \tag{6e}$$

$$R_D = 1 - 0.375\left(\frac{t}{R}\right)^2 \tag{6f}$$

where R_D is the ratio of the angular velocity immediately after and before the impact.

The accuracy of equations (6a) – (6f) in predicting the level of shock experienced by the edge of the cabinet (a_{edge}) has been evaluated experimentally by comparing the calculated values with the directly measured values (refer Table 1).

Table 1 Comparison of calculated and directly measured values of aedge

Sample no.	$a_{s\ max}$	a_{edge} from equations (6e) – (6f)	a_{edge} from direct measurements
1	7.3	3.3	3.4
2	7.3	3.3	3.45
3	10.4	4.6	4.9
4	10.4	4.6	4.8
5	11.5	5.1	5.3

4. Conclusions

This paper presents unique fragility curves for overturning of objects in buildings when subject to code-compatible earthquakes. These curves predict the probability of overturning for objects with different thicknesses and heights that are located at different levels with two example buildings. In addition, Fragility curves incorporating multiple earthquake scenarios that have been identified from the de-convolution analysis of the seismic hazard model for an area are also presented. Based on these curves critical objects as well as critical building levels can be easily identified. The paper also presents a methodology for estimating the maximum impact shock on objects due to rocking. An equivalent point mass system is proposed to represent solid rectangular objects to simplify the computation's time demand. This method would assist building owners and operators in ensuring continuing operation of critical components after an earthquake event.

References

Al Abadi H., Lam N.T.K., and Gad E. (2006), "A Simple Displacement-Based Model for Predicting Seismically Induced Overturning", Journal of Earthquake Engineering, [Accepted].

Al Abadi, H., Lam N.T.K., Gad E., and Chandler A.M. (2004), " Modelling of Earthquake Induced Overturning of Building Contents", Proceedings of the Australian Earthquake Engineering Society Annual Technical Conference. Mt. Gambier, South Australia, Australia, 5 – 7 October, 2004. Published by AEES. Paper no. 10.

AS/NZS 1170.5 (2004). Standard New Zealand, Structural design actions, Part 5: Earthquake actions. New Zealand Commentary.

Brownjohn J.M.W. and Pan T.C. (2001), "Response of tall buildings to weak long distance earthquakes", Earthquake Engineering & Structural Dynamics, 30(5):709-729.

Draft AS/NZS 1170.4 - 2006. Draft Australian Standard for Structural Design Actions, Part 4: Earthquake Actions in Australia. Document No. D5212-5.1.

Franke D, Lam N.T.K., Gad E., and Chandler A.M (2005), "Seismically Induced Overturning of Objects and Filtering Effects of Buildings", Journal of Seismology and Earthquake Engineering, 7 (2): 95-108.

Lam, N.T.K., Wilson, J.L., and Hutchinson, G.L. (2000), "Generation of Synthetic Earthquake Accelerograms Using Seismological Modeling : A Review ", Journal of Earthquake Engineering , 4(3), 321-354.

Lam, N.T.K., Wilson, J.L., and Venkatesan, S. (2005), "Accelerograms for dynamic analysis under the New Australian Standard for Earthquake Actions", Electronic Journal of Structural Engineering. 5: 10-35.

Lumantarna, E., Vaculik, J., Griffith, M., Lam, N.T.K., and Wilson J.L. (2006), "Seismic Fragility Curves for Unreinforced Masonry Walls", Proceedings of the Australian Earthquake Engineering Society Annual Technical Conference, Canberra.

Shinozuka, M., Feng, M. Q., Kim, H., Uzawa, T., Ueda, T. (2001), "Statistical Analysis of Fragility Curves", Technical REspot MCEER, Department of Civil amd Environmental Engineering, University of Southern California, Task Number 106-E-7.3.5 and 106-E-7.6.

Shinozuka, M., Feng, M. Q., Lee, J. H. and Nagaruma, T. (2000), "Statistical Analysis of Fragility Curves", Proceeding of the Asian-Pacific Symposium on Structural Reliability.

Use of microtremors for site hazard studies in the 2D Tamar rift valley, Launceston, Tasmania

Maxime Claprood and Michael W. Asten

Monash University

Abstract

Analysis of microtremor for risk zonation is conventionally interpreted in terms of sub-horizontal layered geology. This assumption not being valid in some cases, there is a need to take into account the impact of 2D/3D geology for analysis of more complicated models. Bard and Bouchon (1980a, 1980b, 1985) intensively studied SH, SV and P waves motions in sediment-filled valleys. Identification of 2D and 3D effects has been analyzed by Field (1996), Steimen et al (2003), and Roten et al (2006) using spectral amplification and phase behavior. Modeling and interpretation of 2D microtremor data is the next challenge, and several methods have been developed to do so. A finite-difference code was developed by Moczo and Kristek (2002) within the European SESAME project. Tessmer et al (1992) and Faccioli et al (1997) present the basis of a pseudo-spectral approach combined to domain decomposition techniques for modeling of propagating waves. The research group led by Komatitsch and Tromp developed a spectral element code for 2D and 3D seismic wave propagation (Tromp3D), using a combination of finite-elements method with spectral analysis. Assessment of the different methods available for detecting, modeling and interpreting 2D and 3D effects is the main objective of this project, using both H/V and SPAC data. Modeling methods will be compared with microtremor data acquired over a 2D rift valley (the Tamar Valley in Launceston, Tasmania) where there is a history of earthquake damage associated with site effects.

Introduction

Figure 1 shows the location of Launceston in Tasmania, south of the Australian mainland. Even if Launceston is not located in a very seismically active zone, damage has occurred in the past from earthquakes. Epicenters of earthquakes are located in two seismic zones:

- West Tasman Sea Zone,
- Western Tasmanian Zone.

Earthquake damage in Launceston is thought to be caused by site amplification response due to 2D geology effects. Figure 2 presents the results of the microzonation project at Launceston (Michael-Leiba, 1995). Profiles are obtained from a gravity survey (Leaman, 1994). Bedrock is Jurassic dolerite, which presents low seismic risk when outcropping. The survey outlines the presence of at least 2 deep NNW-SSE trending valleys filled with Tertiary and Quaternary sediments:

- along Tamar Valley axis, maximum sediment thickness of 250m,
- along North Esk Valley (floodplain), maximum sediment thickness of 130m.

Microtremor survey has previously been done in Launceston, using the H/V spectrum ratio (Nakamura, 1989) to estimate the natural site period of site amplification at 56 sites, and to create zoning maps of Launceston. Periods calculated present a large range of values from 0.1 to 1.5 sec. These variations in the calculated periods over the 56 sites do not appear to fit known geological depth; hence they may be explained by 2D effects generated by the presence of deep and narrow valleys. More data will be obtained with SPAC processing of array data as well as H/V data, with the aim being to identify and model 2D effects in the Tamar rift valley.

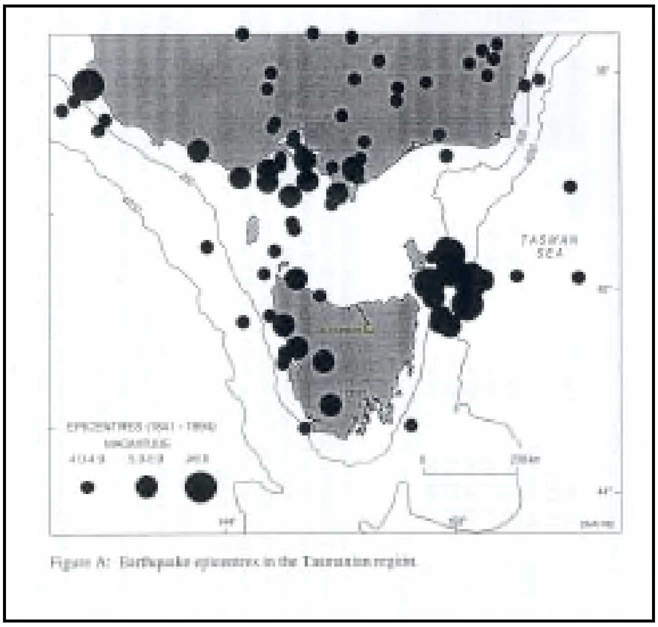

Figure 1. Location of Launceston, Tasmania. Epicenters of earthquakes with Richter magnitudes of 4.0 or more around Tasmania from 1884-1994 (from Michael-Leiba, 1995)

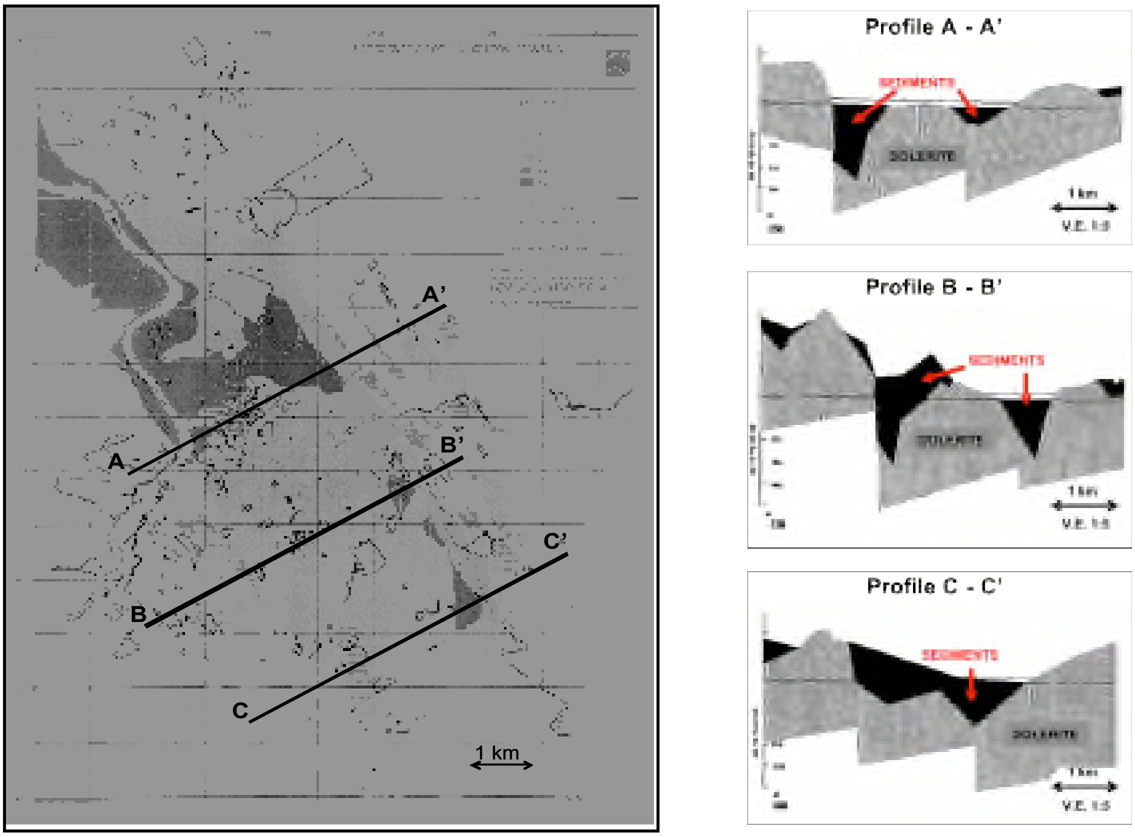

Figure 2. Microzonation of Launceston (Michael-Leiba, 1995). Sites where microtremor data have been obtained with H/V spectrum ratio. Geological profiles obtained from a gravity survey (Leaman, 1994)

Review of the problem

Interpretation of single-station H/V microtremor data has traditionally used the hypothesis of a layered geology, where waves of fundamental modes are assumed to dominate the signal. From Nakamura's technique, natural period of a layered site is calculated as:

$$T = 4H/V,$$

where H is the layer thickness and V is the shear wave velocity in the layer. Developments have been made analyzing variations of H/V spectral ratios and reference site method (RSM) along a profile over a valley to detect and analyze 2D effects.

The SPAC method measures the covariance at different frequencies between the signals observed at different stations. Phase velocities are determined by averaging signal coherency between the different points of observation in an array of receivers. Depending on the components of the signal analyzed, Rayleigh and Love waves can be analyzed to determine a 1D shear velocity depth profile.

Bard and Bouchon (1980a, 1980b and 1985) studied the variation in spectral amplitude of SH, SV and P waves along a profile over 2D geology. Trying to extend the H/V spectrum ratio technique to more complex geology, Field (1996) found that the method did not fit the sediment to bedrock ratio over a 2D geology. He recognized that H/V spectral ratio could be used to detect 2D effects. He observed shifting in the peak frequency along a profile over a valley. Data obtained with SPAC method in Launceston will be of interest to see if the use of H/V ratio and SPAC data simultaneously is of interest to better detect and analyze 2D effects in microtremor data.

Working hypotheses

Measurement of Vs depth profile using array methods will provide quantitative shear velocities to use in models.

H/V spectral ratios are an efficient tool to detect and analyze 2D effect in microtremor data.

Array methods (SPAC) applied over a basin edge will give perturbed microtremor phase velocities; these types of perturbations can be studied using 2D or 3D models.

Information deduced from SPAC data will help improve the detection and interpretation of 2D effects in microtremor data.

Methodology

The first step is to obtain H/V spectral ratio and SPAC microtremor measurements on a profile crossing the Tamar Valley in Launceston. H/V spectral ratio data should then be analyzed using 2D effect developed by Bard and Bouchon (1985) and Roten et al (2006). Modeling should then be used to represent Launceston area, using both 1D and 2D geology models. Comparison between SPAC data modeled from 1D and 2D geology would better assess the type of data recorded at Launceston. Recognition of 2D effects from SPAC data is the final step in the project, using both modeled and field data.

Few programs can be used to model complex geology. Two approaches will be assessed in this study; the spectral element method, and the joint mode-summation and finite-difference method.

Spectral Element Method (SEM)

- Work with Tromp3D program using SEM method (Komatitsch and Tromp, 1999)
- Weak formulation: integral formulation of seismic equations of motion. The weak formulation naturally satisfies the stress-free surface boundary condition.
- Hexahedra elements (quadrangles in 2D)
- Lagrange high-order polynomial representation of elements
- Gauss-Lobatto-Legendre approximation used for integration of equations of motion
- Mass matrix diagonal by construction in SEM: reduces cost of calculations.

Mode-summation and finite-difference modeling

- 3D fourth-order staggered grid finite-difference for modeling seismic motion and seismic wave propagation (Moczo et al, 2002)

- Mode-summation method is used to model wave propagation from source position to local 2D/3D irregularity. Path from source to irregularity is assumed to be flat, homogeneous layers.
- Finite-difference method is used in the laterally heterogeneous part of the model (Tamar rift valley). Spurious effects might be created due to the need to impose artificial boundaries to the model to save on CPU time and memory.

Conclusion

Analysis of microtremor data conventionally assumes a 1D homogeneous geology. This hypothesis does not hold in Launceston, Tasmania, due to the presence of the Tamar rift valley. Amplification of seismic waves is thought to occur at Launceston due to patterns of earthquake damage in historic quakes. 2D site effects are suspected.

The expected pattern in H/V spectrum ratio can be used to identify these 2D effects in the Launceston area. SPAC measurements will be used to complete the study. Microtremor data acquired over Launceston will be used to assess modelling over 2D and 3D effects, using the SEM method and the joint mode-summation and finite-difference method.

References

Bard, P-Y. and Bouchon, M. (1980). The seismic response of sediment-filled valleys. Part 1. The case of incident SH waves, Bull. Seism. Soc. Am., vol.70, no.4, 1263-1286.

Bard, P-Y. and Bouchon, M. (1980). The seismic response of sediment-filled valleys. Part 2. The case of incident P and SV waves, Bull. Seism. Soc. Am., vol.70, no.5, 1921-1941.

Bard, P-Y. and Bouchon, M. (1985). The two-dimensional resonance of sediment-filled valleys, Bull. Seism. Soc. Am., vol.75, no.2, 519-541.

Faccioli, E., Maggio, F., Paolucci, R. and Quarteroni, A. (1997). 2D and 3D elastic wave propagation by a pseudo-spectral domain decomposition method. Journal of Seismology, vol.1, 237-251.

Field, E.H. (1996). Spectral amplification in a sediment-filled valley exhibiting clear basin-edge-induced waves, Bull. Seism. Soc. Am., vol.86, no.4, 991-1005.

Komatitsch, D. and Tromp, J. (1999). Introduction to the spectral element method for three-dimensional seismic wave propagation, Geophysical Journal International, vol.139, 806-822.

Leaman, D.E. (1994). Assessment of gravity survey, city of Launceston. Technical Report for Launceston City Corporation, Seismic Zonation Survey, Leaman Geophysics, Tasmania, Australia.

Michael-Leiba, M. (1995). Microtremor survey and seismic microzonation of Launceston, Tasmania. Technical Report, Australian Geological Survey Organisation, Canberra, Australia.

Moczo, P., Kristek, J., Vavrycuk, V., Archuleta, R.J. and Halada, L. (2002). 3D heterogeneous staggered-grid finite-difference modeling of seismic motion with volume harmonic and arithmetic averaging of elastic moduli and densities, Bull. Seism. Soc. Am., vol.92, no.8, 3042-3066.

Nakamura, Y. (1989). A method for dynamic characteristics estimation of subsurface using microtremor on the ground surface, QR RTRI, vol.30, 25-33.

Roten, D., Fah, D., Cornou, C. and Giardini, D. (2006). Two-dimensional resonances in Alpine valleys identified from ambient vibration wavefields, Geophysical Journal International, vol.165, 889-905.

Steimen, S., Fah, D., Kind, F., Schmid, C. and Giardini, D. (2003). Identifying 2D resonance in microtremor wave field, Bull. Seism. Soc. Am., vol.93, no.2, 583-599.

Tessmer, E., Kessler, D., Kosloff, D. and Behle, A. (1992). Multi-domain Chebyshev-Fourier method for the solution of the equations of motion of dynamic elasticity, Journal of Computational Physics, vol.100, 355-363.

Shear wave velocity measurement at Australian ground motion seismometer sites by the spectral analysis of surface waves (SASW) method

***Clive Collins*[1]*, Robert Kayen*[2]*, Brad Carkin*[2]*, Trevor Allen*[1]*, Phil Cummins*[1] *and Andrew McPherson*[1]**

[1] Geoscience Australia
[2] US Geological Survey

Abstract

Near-surface shear-wave velocity profiles were acquired at eighteen permanent and temporary seismograph sites in Western Australia, South Australia, Victoria and New South Wales. These data were obtained to support ground-motion modelling in Australia by characterising the near-surface response at sites used to record ground-motion from Australian earthquakes. Geoscience Australia contracted the US Geological Survey to obtain shear-velocity data using the Spectral Analysis of Shear-Waves (SASW) technique. Velocity profiles were calculated down to maximum depths between 100-200m. Apart from two sites on alluvium, all sites were located on hard rock at or near the surface. The average velocity to 30m depth (V_{s30}) ranges from 257 m/s for alluvial sites to 1652 m/s for Proterozoic metasediments.

Introduction

Geoscience Australia (GA) has an ongoing program to develop models of ground-motion generated by earthquakes in Australia. Ground-motion models are essential for estimating the risk to buildings and infrastructure from earthquakes and for developing codes for building and engineering design. The potential amplification of the ground motion due to the characteristics of the near-surface rock or soil, particularly the stiffness, has a major influence on the ground-motion. The stiffness can be characterised by the seismic shear-wave velocity, but the paucity of near-surface shear-wave velocity data in Australia makes it difficult to quantify these amplification effects.

With the exception of limited surveys at the Lucas Heights replacement reactor site (Coffey, 1998), and recent site-specific SPAC surveys (Asten and Roberts, 2005), there is little or no data available to characterise near-surface shear wave velocity in bedrock-dominated terranes in Australia. A number of measured shear wave velocity profiles acquired by seismic cone penetrometer testing in two major centres (Newcastle and Perth) are held by GA, but these predominantly characterise unconsolidated near-surface regolith materials to a maximum depth of 30 m.

To address this problem, GA contracted a team from the US Geological Survey (USGS) to acquire near-surface shear-wave velocity data using the Spectral Analysis of Shear-Waves (SASW) technique (Kayen and Carkin, 2006). This non-invasive technique is an inexpensive and efficient means for estimating the stiffness properties of the ground, typically within the upper 10's-to-100 metres. The equipment is highly portable, enabling measurements to be made at remote sites. Other methods, such as direct measurements in boreholes or penetrometer tests are expensive or of limited use in very stiff soils or on rock.

SASW data were acquired at eighteen seismograph sites located in four distinct regions in Western Australia, South Australia, Victoria and New South Wales (Figure 1). These sites are operated by GA, Primary Industry and Resources South Australia (PIRSA) and Environmental Systems and Services (ESS) of Melbourne. In two cases the data were acquired a short way from the seismograph site due to a lack of access, but were located on the same geological unit. Most of these sites have little or no quantitative characterisation of site amplification effects or natural frequency. At all eighteen sites micro-tremor measurements were also made to assess the resonance characteristics of the ground for comparison with the shear wave velocity structure (Nakamura, (1989). These data are not yet processed or analysed and are not presented here.

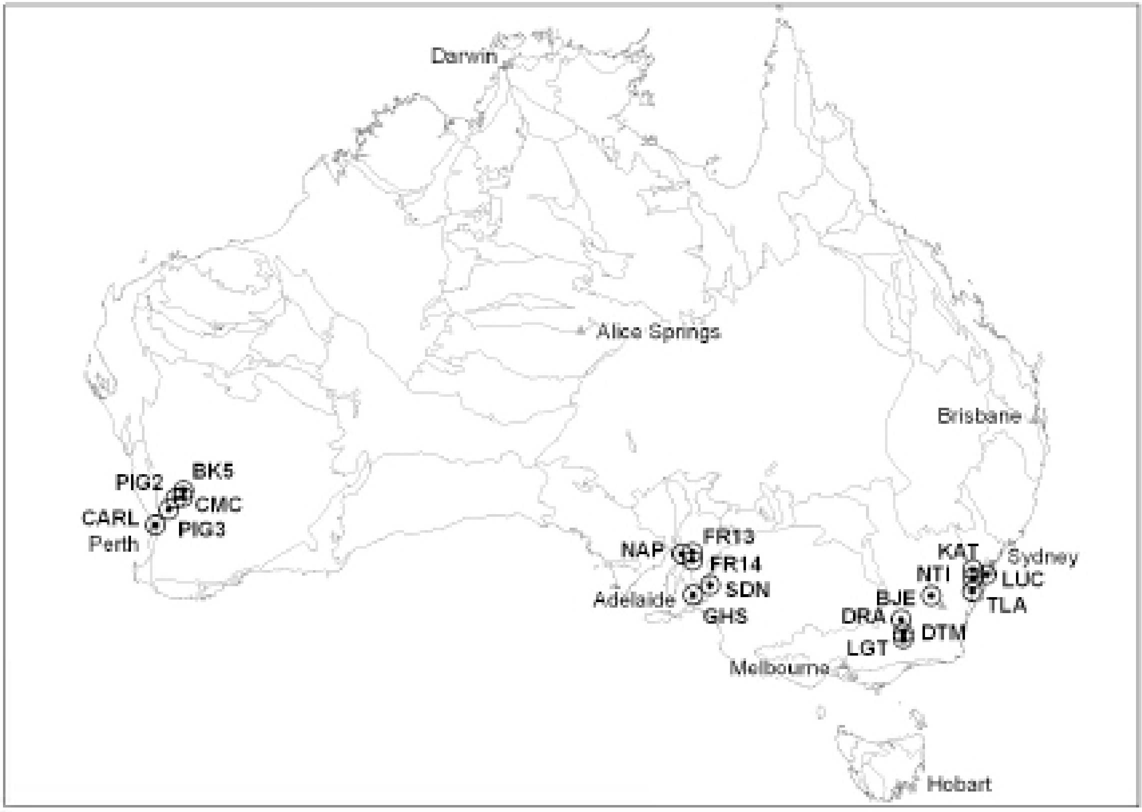

Figure 1. Location of SASW test sites

The SASW method

The field acquisition system comprises two 1-Hz Kinemetrics vertical seismometer receivers, two computer-controlled APS Dynamics Model 400 electro-mechanical harmonic-wave sources (shakers) and their amplifiers, a low frequency spectrum analyser, and a 4.0 kW generator (Figure 2). The spectrum analyser produces a sine wave signal that is split into a parallel circuit, and two separate power amplifiers produce an in-phase continuous harmonic-wave which drives the shakers in vertical motion to excite the ground. A fast Fourier transform (FFT) is performed on each of the receiver signals. In near-real time, the linear spectra, cross power spectra, and coherence are computed. The ability to perform near real-time frequency domain calculations and monitor the progress and quality of the test permits adjustment of various aspects of the test to optimise the capture of the phase data. These aspects include the source-wave generation, frequency step-size between each sine wave burst, number of cycles-per-frequency, total frequency range of all the steps, and receiver spacing.

The dual sources are arrayed orthogonally to the seismometer line. The test steps through a suite of frequencies and, for each frequency, phase computations are made. This method sweeps through a broad range of low frequencies in order to capture the surface wave-dispersion characteristics of the ground. This approach is a modification of the Continuous Sine-wave Source - Spectral Analysis of Surface Waves (CSS-SASW) test presented by Kayen et al. (2004a; 2004b). Spacing of the receivers stepped geometrically from 1 m to 100 m. The two seismometers are separated by a given distance, d, and the source is usually placed at a distance of d from the inner seismometer. Rayleigh wave wavelengths are computed by relating the seismometer spacing and the phase angle (determined from the cross-power spectra) between the seismometers. The Rayleigh wave surface wave velocity is computed as the product of the frequency and its associated wavelength.

The inversion code used to determine the model at each site hunts for the best-fit shear wave velocity profile whose theoretical dispersion curve is the closest match with the averaged field dispersion curve. The term "best-fit" refers to the minimum sum of the squares of residuals from the differences between the theoretical and experimental dispersion curves. The inversion algorithm, WaveEq of OYO Corp. (Hayashi and Kayen, 2003) uses an automated-numerical approach that employs a constrained least-square fit of the theoretical and experimental dispersion curves.

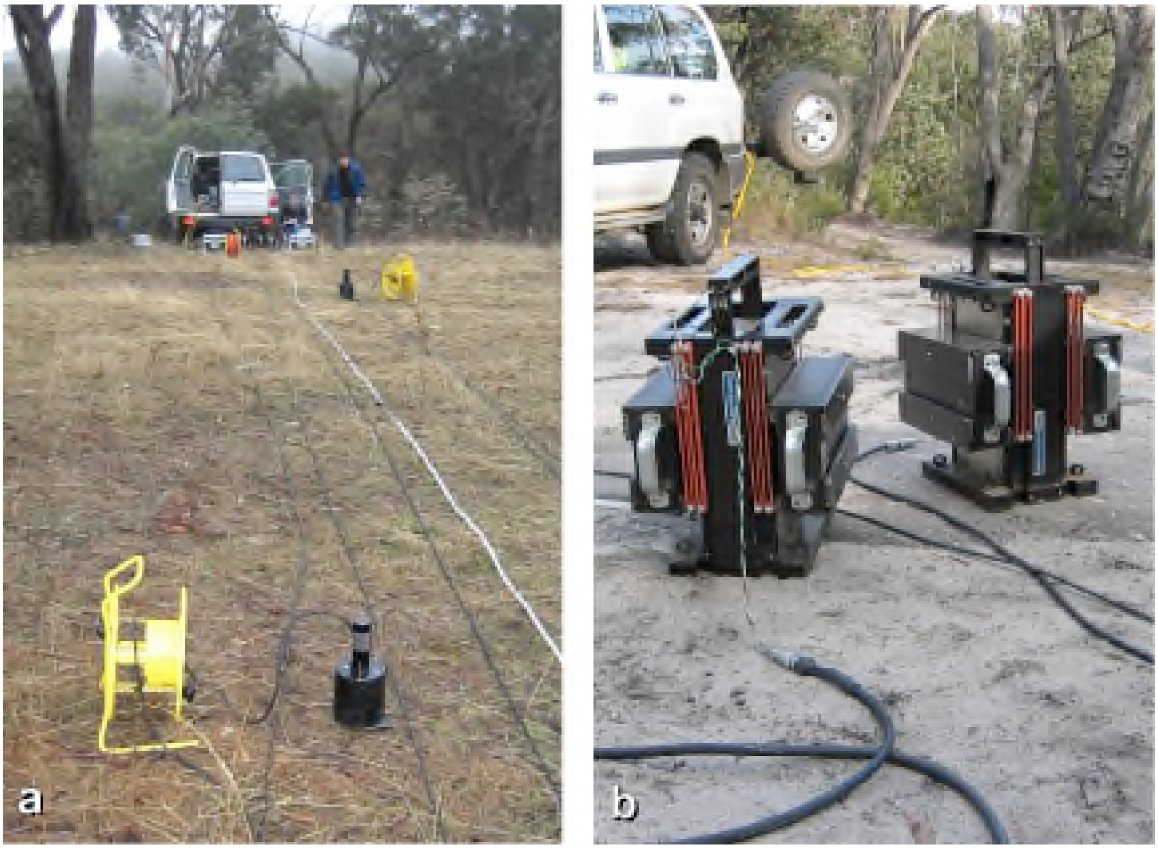

Figure 2. SASW field data acquisition. a) Traverse with two 1 Hz Kinemetrics seismometers, and b) the source array comprising two electro-mechanical shakers

Results

Eighteen sites were occupied in Western Australia, South Australia, Victoria and New South Wales. The shear wave velocity structures for the uppermost 100-200 m of the ground at these sites are presented in Figure 3 and Table 1. Typically, a ten to fifteen layer model was used for the inversion, with layer thicknesses geometrically expanding with depth. The increasing layer thicknesses correspond with decreasing dispersion information in the longer wavelength (deeper) portion of the dispersion curve. The profiles generally increase in stiffness with depth, though low velocity layers are present in several of the profiles.

The simplest way of characterising the overall site condition is to compute the average shear wave velocity in the uppermost 30 m or 100 m of the subsurface (VS_{30} and VS_{100}) from the layer interval velocities. The average V_{S30} velocities ranged from 257 to 1652 m/s, which fall within NEHRP categories "D" through "A". The average VS_{100} velocities ranged from 434 to 2335 m/s.

Most of the Western Australian sites (at temporary seismograph stations CMC, BK5, PIG2, PIG3) are located on Archaean granites, while CARL (a permanent strong-motion station) is located in the city of Perth on soils and alluvium above Perth Basin (Permian to Quaternary) sediments. Two sites in South Australia (at temporary seismograph stations FR13, FR14) are located on Proterozoic metasediments of the Flinders Ranges, and one (at permanent station NAP) on alluvial fan sediments derived from the adjacent Flinders Ranges. The permanent station at SDN is located on Cambrian metasediments of the Mount Lofty Ranges and the permanent strong-motion station GHS is located in Adelaide on alluvium. The sites located in the Lachlan Fold Belt of Victoria and New South Wales (permanent stations DTM, LGT, DRA, BJE) lie on granites, volcanics and metasediments of Devonian to Ordovician age. The sites in the Sydney Basin (permanent stations TLA, NTI, KAT LUC) are all on Hawkesbury Sandstone.

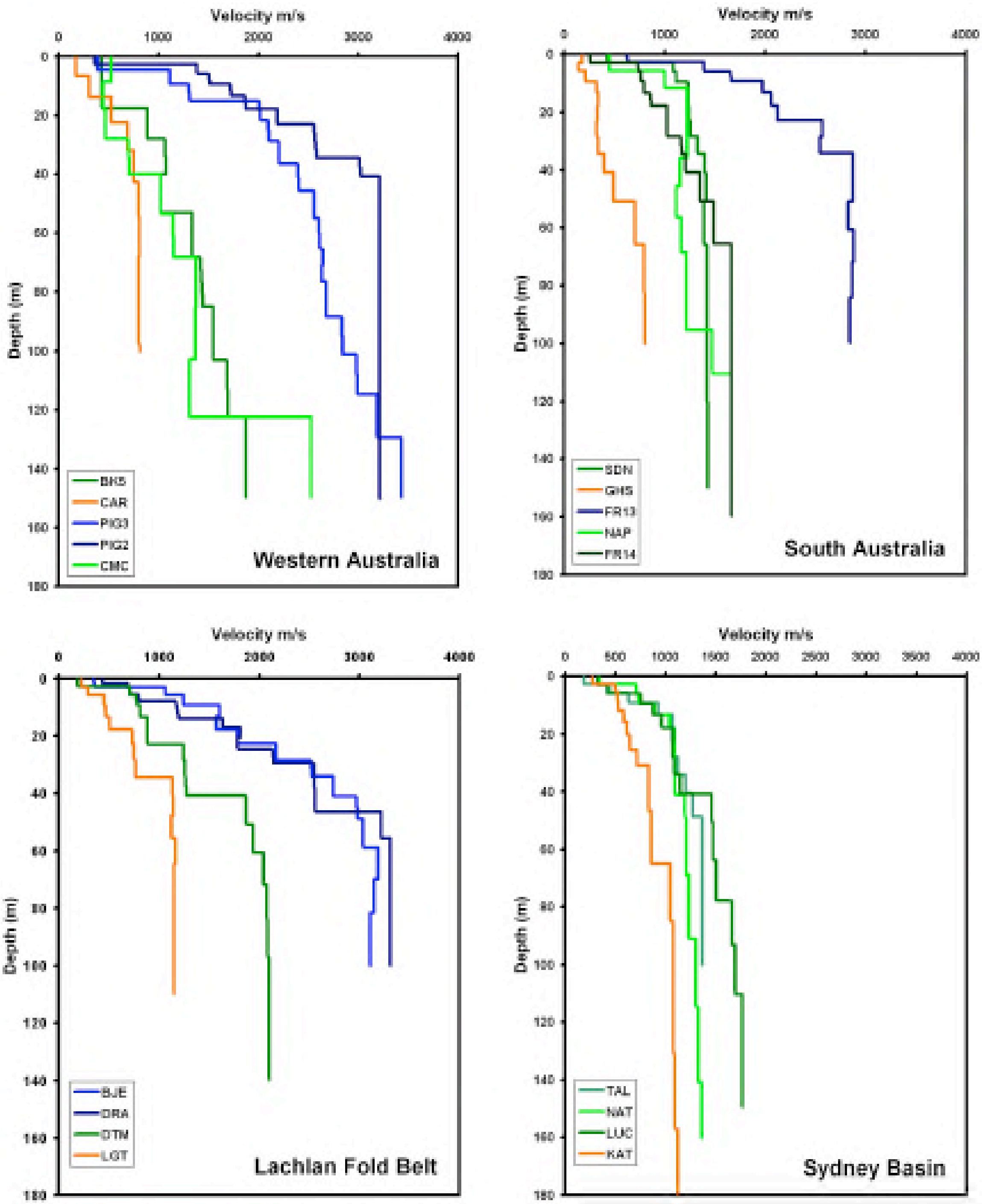

Figure 3. Shear-wave velocity profiles

Table 1. SASW station details with their computed average 30 and 100 metre shear wave velocities and corresponding NEHRP site class.

Site	Geology	Location	V_{S30}	VS_{100}	NEHRP Class
Western Australia					
CMC	Archean Granite	Cadoux, WA	474	785	C
BK5	Archean Granite	Burakin, WA	565	928	C
PIG2	Archean Granite	Macardy Hill, WA	1232	2196	B
PIG3	Archean Granite	Bolgart, WA	1101	1836	B
CARL	Alluvium	Carlisle, WA	338	563	D
South Australia					
SDN	Cambrian Metasediments	Sedan, WA	1026	1267	B
FR14	Proterozoic Sediments	Flinders Ranges, SA	725	1131	B
FR13	Proterozoic Sediments	Flinders Ranges, SA	1652	2335	A
NAP	Proterozoic Sediments	Napperby, SA	893	1087	B
GHS	Alluvium	Adelaide, SA	257	434	D
Eastern Australia (Lachlan Fold Belt)					
DTM	Granite	Dartmouth Dam	659	1194	C
LGT	Ordovician Sst/shale	Lightning Creek, VIC	458	778	C
DRA	Granite	Dora Dora, NSW	1148	2048	B
BJE	Devonian Andesite	Burrinjuck Dam, NSW	1194	2070	B
Eastern Australia (Sydney Basin)					
TLA	Hawkesbury Sst	Tallowa, NSW	643	1001	C
NTI	Hawkesbury Sst	Nattai, NSW	804	1050	B
KAT	Hawkesbury Sst	Katoomba, NSW	536	766	C
LUC	Hawkesbury Sst	Lucas Heights, NSW	728	1121	B

Acknowledgements

The authors wish to thank Owen McConnel (GA), David Love (PIRSA), Wayne Peck, Kirkland Kalder-Bull and Peter Corbett (ESS) for assistance with the field programme. They also wish to gratefully acknowledge the permission granted by the various property owners to undertake this work on their land, and the assistance of ANSTO, NSW National Parks and ESS and their clients in facilitating access to some sites. The GA authors publish with permission of the CEO of Geoscience Australia.

References

Asten, M. and Roberts, J., 2005. Final Report – Microtremor Array Survey of the Burakin Area, WA. Centre for Environmental and Geotechnical Applications of Surface Waves, Monash University

Coffey Partners International Pty Ltd, 1998. Replacement Reactor Site, Lucas Heights, Geophysical Study. Report No. GY617/1-AC, April 1998.

Hayashi, K. and Kayen, R., 2003. Comparative test of three surface wave methods at Williams Street Park in San Jose, USA. Paper S051-009, 2003 Joint Meeting of Japan Earth and Planetary Science, University of Tokyo, Tokyo, Japan 2003 Joint Meeting, May 26-29, 2003.

Kayen, R. and Carkin, B., 2006. Preliminary Report on the Shear Wave Velocity of Australian Strong Motion Seismometer Sites by the Spectral Analysis of Surface Waves Method (SASW) with Parallel-Arrayed Harmonic-Wave Sources and H/V Microtremor Method. United States Geological Survey, Administrative Report 2006-2.

Kayen, R., Seed, R. B., Moss, R.E., Cetin, O., Tanaka, Y., and Tokimatsu, K., 2004. Global Shear Wave Velocity Database for Probabilistic Assessment of the Initiation of Seismic-Soil Liquefaction. Proceedings of the 11th Int'l. Conf. On Soil Dynamics and Earthquake Engineering, January 7-9, 2004, Berkeley, CA, p. 506-512.

Kayen, R., Thompson, E., Minasian, D., Moss, R.E.S., Collins, B.D., Sitar, N., Dreger, D., Carver, G., 2004. Geotechnical Reconnaissance of the November 3, 2002 M7.9 Denali Fault Earthquake, Earthquake Spectra, 20(3) p. 639-667.

Nakamura, Y., 1989. A method for dynamic characteristics estimation of subsurface using micro-tremor on the ground surface, Quarterly Report of RTRI 30, 25–33, Railway Technical Research Institute, Tokyo, Japan.

Structural vulnerability estimation for tsunami loads

***Ken Dale*[1] & *Shaun Flay*[2]**

1 Geoscience Australia
2 James Cook University

Introduction

Structural vulnerability to tsunami is an important component of ongoing work at Geoscience Australia (GA) directed at assessing the risk posed by tsunami hazard to Australian communities. The models currently used are very simple, with probabilities of collapse (for residential structures) based on inundation depth and distance from coast. Damage to non-collapsed structures is calculated using stage-damage curves developed for riverine flooding. This paper describes work currently underway in the Risk Research Group at GA to develop empirically based vulnerability relationships. Also presented here is a proposed method for developing physically based damage curves using an engineering approach. This method is of particular value due to the scarcity of post-event damage data.

The paper has two main sections, a literature review and a section on the engineering approach. The literature review is the basis for the current curve development, with a review of damage reports, curves published to date, and a brief description of the database that will be used in creating empirical damage curves. The engineering approach is viewed as a long-term method for creating tsunami vulnerability curves based on physical models of fluid flow and structural behaviour. This approach also allows the opportunity to investigate mitigation options. The components of this model are discussed in Engineering Model Development.

Literature review

While major tsunami events are a relatively infrequent occurrence at any one location, there have been a number of destructive events globally over the last few decades. Since 1960 there have been three major tsunami events that have propagated across ocean basins to cause high levels of damage at far-field locations. This includes tsunami generated from earthquakes in Chile and Alaska in 1960 and 1964 respectively. These events caused damage not only in the immediate vicinity of their source but also travelled across the Pacific Ocean to cause major damage at other locations such as Japan, Hawaii, and the west coast of the United States. Likewise, the 2004 Indian Ocean tsunami caused significant damage near its source in northern Sumatra, but also propagated across the Indian Ocean to impact the coasts of Thailand, Sri Lanka, India, and several other countries.

Table 1 highlights some notable tsunami events since 1960. While this is by no means a comprehensive list, it does highlight those causing major impacts in terms of casualties and damage to onshore structures (to 2004).

Table 1 Notable tsunami events (1960-2004)

Event	**Date**	**MW**
Chile	22 May 1960	9.5
Prince William Sound, Alaska	28 Mar 1964	9.2
Moro Gulf, Philippines	16 Aug 1976	8.1
Nihonkai-Chubu, Japan	26 May 1983	7.8
Nicaragua	2 Sep 1992	7.6
Flores Island, Indonesia	12 Dec 1992	7.7
Hokkaido Nansei-Oki, Japan	12 Jul 1993	7.8
East Java, Indonesia	2 Jun 1994	7.7
Mindoro, Philippines	14 Nov 1994	7.1
Sulawesi, Indonesia	1 Jan 1996	7.8
Biak Island, Indonesia	17 Feb 1996	8.2
Chimbote, Peru	21 Feb 1996	7.5
Sissano, Papua New Guinea	17 Jul 1998	7.0
Izmit Bay, Turkey	17 Aug 1999	7.6
Vanuatu	26 Nov 1999	7.4
Camaná, Peru	23 June 2001	8.4
Sumatra, Indonesia	26 Dec 2004	9.3

Available curves

A number of tsunami damage curves are available in the literature. Examples include those by Lee et al (1978), Hatori (1984), Shuto (1993), Matsutomi et al (2001), Papadopoulos and Imamura (2001), Peiris and Pomonis (2006), Peiris (2006), and Ruangrassamee et al (2006). For various reasons the published curves are not necessarily applicable for use in risk assessments to Australian communities. Most are based on empirical data from one location and one event. The structures examined are typically dissimilar to those found in Australia. There is a lack of a population focus: undamaged structures are often not included which biases the data to damaged structures, thereby overestimating loss.

It is also difficult to make comparisons between the various curves. Firstly, there is no consistent parameter in use for the hazard, with some studies adopting run-up heights, others inundation height and some the inundation depth at structures. In cases where this parameter is the same it is difficult to standardise the various damage scales used. Several of the studies have highlighted the importance of other parameters in damage estimation including flow velocity (Hatori 1984; Matsutomi et al, 2001), although this parameter is very difficult to estimate post-event.

The most useful curves already published are those by Peiris (2006). These curves are lognormal cumulative distribution functions which provide a probability of being in a particular damage state or worse given an inundation depth. These curves were created using observed data from Sri Lanka following the 2004 Indian Ocean tsunami. The curves are based on damage to unreinforced masonry residential buildings with wall thicknesses of 250mm. The cumulative lognormal distribution is used in earthquake risk modelling at GA and is seen as a good way to describe vulnerability in a probabilistic tsunami risk assessment. There are some problems associated with applying these curves in an Australian context however, they are based on one event at one location and for a structural system not applicable to Australia. The inundation level was also measured as the water depth above ground at the centroid of the census district for each population of structures.

Database creation

Following the literature review of recent historical events a database of damage and flow characteristics was compiled. It consists of damage observations for around 330 individual structures. Figure summarises how each historical event is represented in the database. Clearly, data from the 2004 Indian Ocean tsunami comprises a large portion of the database given both its recent occurrence and the scale of its impact, which has prompted much scientific investigation. Each structure in the database was classified into one of three building classes depending on its construction material; reinforced concrete, unreinforced brick/block, and timber-frame. About half the observations comprise reinforced concrete buildings with the balance equally divided between brick/block and timber-frame type. The damage database will be used in the coming months to derive empirical damage curves for use at GA in the short/medium term. A more recent source of data may be available through the field survey undertaken jointly by GNS and NIWA (New Zealand) in Southern Java in July this year.

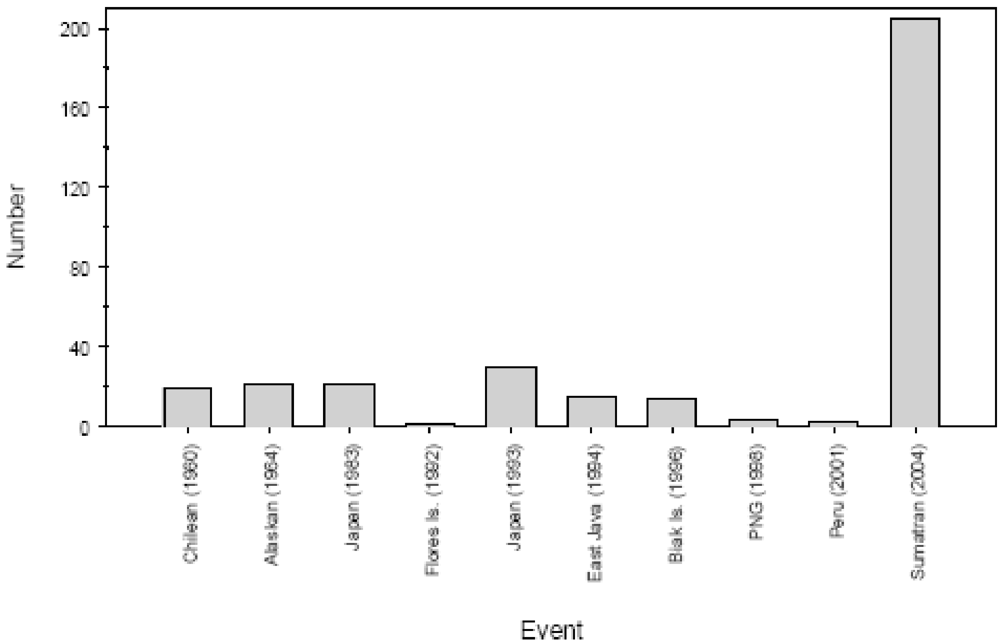

Figure 1: Observations (number of structures) in database by event

Engineering model development

The proposed longer term strategy involves developing an engineering model approach that has a similar framework as the parallel wind vulnerability work being undertaken at GA. The method requires a generalised hazard definition, an engineering model of a particular structure, and a costing module to calculate the real cost of repairs. The initial focus will be Australian residential structures. The components of the model are discussed in greater detail in the following sections.

The engineering model is based on the assumption that connection failure is the primary initiator of structural failure in residential structures (as opposed to say, a beam or wall stud failing in bending). It also assumes that component failures can be aggregated up into overall damage scenarios. The engineering model employs a Monte Carlo simulation approach that allows for the incorporation of variability (in connection strengths, building orientation, opening sizes, and key hazard parameters).

Generalised hazard definition

The generalised hazard definition is a way of generalising the complex behaviour of fluid flow around (and through) a structure and defining the resultant loads on the structure. Forces on a structure due to fluid flow include hydrostatic (horizontal and vertical), wave loads, hydrodynamic loads and debris loads.

A number of design guides exist that contain methods for designing for wave forces (including tsunami). Examples are FEMA 55 (FEMA, 2000), and USACE Technical Note III-29 (USACE, 1990). There are a number of reasons it may be problematic to use these guidelines to estimate wave loads on a structure. They tend to have a design focus and are therefore inherently conservative, while the work proposed at GA requires a mean load estimate. The equations provided in these guides are often impractical for use with a 'real' structure (i.e. wave forces on an infinitely long vertical wall).

Hazard transfer parameters will be chosen to link between hazard modelling and vulnerability. This is analogous to the 3 second gust wind speed at 10m height as used in wind engineering. Water depth and water velocity may be used to describe the hazard at a particular location. These parameters are both outputs of the inundation model used at GA to propagate tsunami waves through shallow water and over land (Nielsen et al, 2005).

Engineering model of structure

Once loads on the structure have been defined an engineering model of a structure can be used to assess damage outcomes (if any). This model requires a knowledge of connection details as well as construction practice and variability. Given this knowledge, probability distribution functions of connection failure can be used. These functions will incorporate variability in connection strengths. The effects of a breach in the building envelope also need to be considered: will the failure of a door allow a sudden inrush of water that may damage the 'back' of the structure? Likely failure modes need to be decided upon, and failure types aggregated into overall damage outcomes. For an example of this type of work, in a wind context, refer to JCU (2005).

An additional consideration for the engineering model is to develop a damage logic that can be programmed as part of the Monte Carlo simulation process. This would relieve the need for continual scenario development on a case by case basis.

The initial engineering model will be based on data collected for two storey houses in Western Sydney (JCU, 2006). The survey involved 45 brick veneer, tiled roof houses at various stages of completeness.

Automated costing module

An automated costing will take the damage outcomes from the engineering model of the structure and cost the repair. This module utilises standard repair rates, which are adjusted for the scale of damage to the component. Internal damage repair costs are also calculated by the module, as are contractor overheads. The module calculates repair costs in a neutral construction industry environment, that is, neither boom nor bust, and with no demand surge as can often follow a natural disaster. The repair costs are those required to reinstate the building to its original state.

Conclusions

This paper describes work being undertaken in the Risk Research Group at Geoscience Australia developing vulnerability curves for Australian structures exposed to tsunami hazard. Curves currently being developed are based on observed damage from a number of tsunami events that have occurred in the past five decades. Future curve development is based on an engineering approach and requires a generalised hazard definition, an engineering model of the structure of interest, and a costing module to convert damage scenarios to restoration costs. This is ongoing work and any feedback is most welcome.

References

FEMA 2000. Coastal Construction Manual – Third Edition: Principles and practices of planning, sitting, designing, constructing, and maintaining residential buildings in coastal areas. Federal Emergency Management Agency, Washington D.C.

Hatori, T. 1984. On the damage to houses due to tsunamis. Bulletin of the Earthquake Research Institute 59(3): 433-439 (in Japanese).

James Cook University 2005. Vulnerability of JCU Group 4 House to cyclonic wind loading, Cyclone Testing Station, CTS Report TS614, James Cook University, Townsville, Queensland.

James Cook University 2006. Survey of Western Sydney Housing, Cyclone Testing Station, CTS Report TS643a, James Cook University, Townsville, Queensland.

Lee, L.T., Chrostowski, J.D. and Eguchi, R.T. 1978. Natural hazards: Storm surge, riverine flooding, tsunami loss models. Report prepared for National Science Foundation, J.H. Wiggins, California, USA.

Matsutomi, H., Shuto, N., Imamura, F. and Takahashi, T. 2001. Field survey of the 1996 Irian Jaya earthquake tsunami in Biak Island. Natural Hazards 24(3): 199-212.

Nielsen, O., Roberts, S. Gray, D., McPherson, A. and Hitchman, A 2005. Hydrodynamic modelling of coastal inundation, MODSIM 2005 International Congress on Modelling and Simulation. Modelling and Simulation Society of Australian and New Zealand, 518-523, URL: http://www.mssanz.org.au/modsim05/papers/nielsen.pdf

Papadopoulos, G.A. and Imamura, F. 2001. A proposal for a new tsunami intensity scale. Proceedings of International Tsunami Symposium 2001, IUGG, pp. 569-577.

Peiris, N. 2006. Vulnerability functions for tsunami loss estimation. First European Conference on Earthquake Engineering and Seismology, Geneva, Switzerland.

Peiris, N. and Pomonis, A. 2006. December 26, 2004 Indian Ocean tsunami: Vulnerability functions for loss estimation in Sri Lanka. In: Chu, J., Phoon, K.K. and Yong, K.Y. (eds.) International Conference on Geotechnical Engineering for Disaster Mitigation and Rehabilitation, World Scientific, pp. 411-416.

Raungrassamee, A., Yanagisawa, H., Foytong, P., Lukkunaprasit, P., Koshimura, S. and Imamura, F. 2006. Investigation of tsunami-induced damage and fragility of buildings in Thailand after the December 2004 Indian Ocean tsunami. Earthquake Spectra 22(S3): 377-401.

Shuto, N. 1993. Tsunami intensity and disasters. In: Tinti, S. (ed.) Tsunamis in the World, Kluwer Academic, Dordrecht, pp. 197-216.

USACE 1990. Wave Forces On A Wall Shoreward Of The Still-Water Line. Coastal Engineering Technical Note – III – 29. USACE Waterways Experiment Station, Mississippi, USA.

A new network of low-cost recorders in WA

Vic Dent[1], Dan Heal[2] & Paul Harris[2]

[1] University of Western Australia
[2] Australian Centre for Geomechanics

A new network of budget seismic recorders has been developed in WA, mainly to service the mining industry in WA, but with spin-off benefits to the monitoring of natural seismicity. Many mines already operate in-house seismic arrays to monitor small events within the mine, but are incapable of locating the occasional larger events which occur outside the immediate mine environment. This project sees a collaborative approach, initiated by the Australian Centre for Geomechanics (ACG), which allows the industry as a whole to better appreciate their tectonic environment.

The new network is based around the low cost digitizer marketed by Larry Cochrane of the Public Seismic Network, California USA (http://quake.psn.net). To this has been added communications software developed by ACG, based at the University of Western Australia in Perth. The basic cost of the hardware, excluding a sensor and a PC, but including a GPS unit, is under $500 US.

Arie Verveer has been using PSN software to operate a high-quality seismic station at the Bickley Astronomical Observatory, just east of Perth, since 1995. Seismograms from his site are posted to www.geosn.com.

The ACG has two networks functioning at present – one in the Kalgoorlie – Kambalda region (8 stations) and another (5 stations) between Perth and Broome, the West Coast Network. The Kambalda-Kalgoorlie network was installed in March 2006. An additional network is planned for installation in the Leinster region (approximately 200 km north of Kalgoorlie) in October 2006.

Data is recorded at 200 s/s, using windows-based software supplied with the digitizer. New software developed at the ACG compresses the data, reduces it to an effective rate of 50 s/s and then sends it via the internet to a node at the ACG in hourly blocks.

The data can be viewed by organisations participating in the project, and accurate phase picking is available. When events of interest are identified, a signal is sent to the remote system and data at the full 200 s/s resolution is downloaded. Automatic phase picking and earthquake location is planned for the future.

In most cases, inexpensive 4.5 Hz, 3-component geophones are used as sensors, but the West Coast network also has a Willmore Mark 1, a Marks products L4C, and a long period Sprengnether, all single component seismometers, in service.

In the event of a break in the internet connection, data is stored on site, and then downloaded in bulk when the connection is re-established.

The geophones are not the best sensors available, but they are inexpensive, and adequate for monitoring nearby events, which is the main interest for the mining companies. Because of the requirements for mains power and an internet connection, it is not often possible to find good seismically quiet sites, and a degree of noise must be tolerated. Calibrating the signal in order to get good magnitude estimates is still a problem to be adequately tackled.

In addition to the hourly downloads of binary signal data, some of the stations of the West Coast Network send data plots in GIF format to UWA several times a day, using FTP. These plots are available for viewing via the internet at http://cyllene.uwa.edu.au/~vdent/SEISMIC

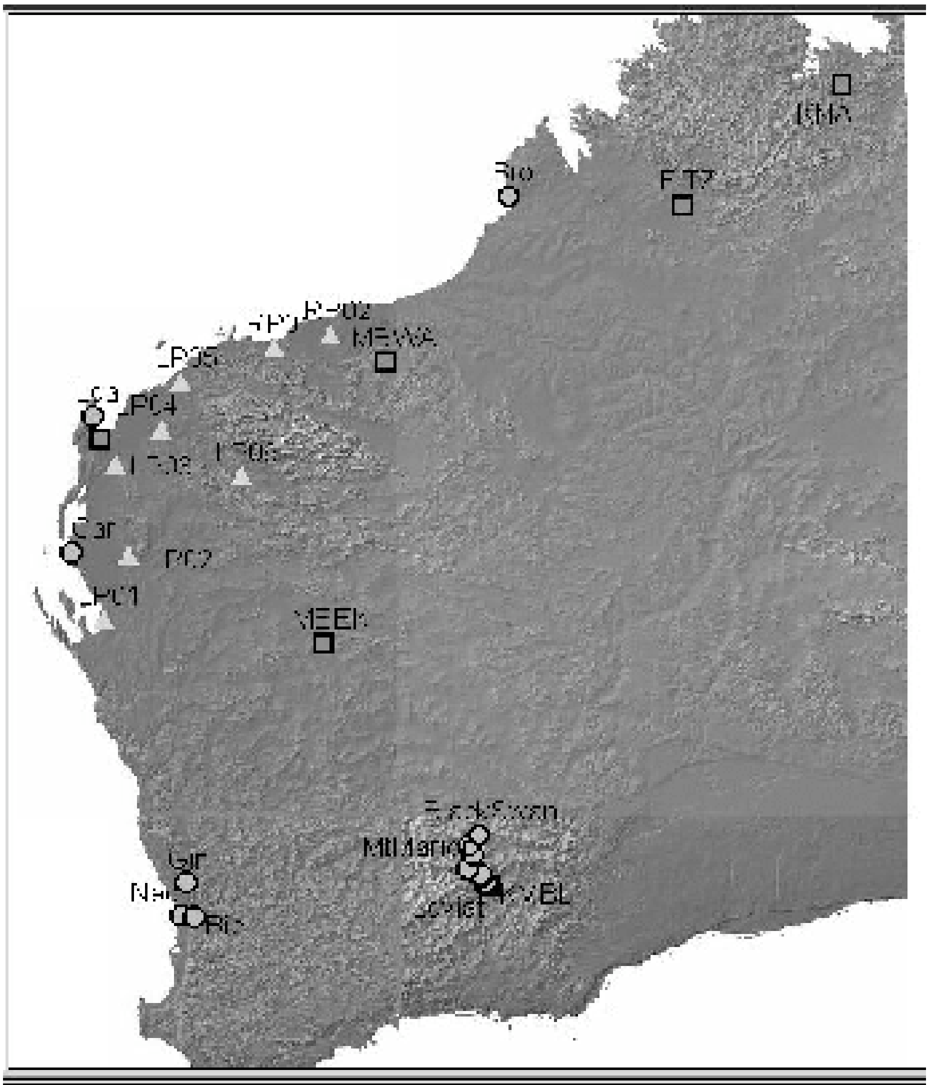

Figure 1 Distribution of new stations in the ACG network (circles); new Reftek stations (triangles), GA stations (squares).

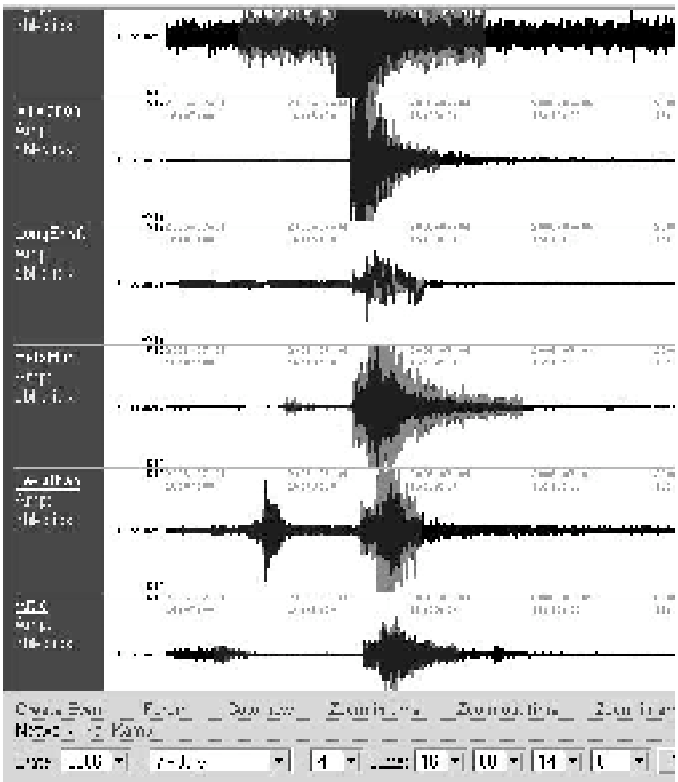

Figure 2 Screen display from the ACG website showing waveforms from a magnitude ML~ 3 Kalgoorlie earthquake on 4 July 2006.

Figure 3 Installing the first ACG recorder at Longshaft Mine

Palaeoseismic investigation of a recently identified Quaternary fault in Western Australia: the Dumbleyung Fault

Beatriz Estrada[1], Dan Clark[2], Karl-Heinz Wyrwol[1] & Mike Dentith[1]

[1] The University of Western Australia
[2] Geoscience Australia

Introduction

Analyses of high resolution Digital Elevation Models (DEM) have led to the discovery of various linear scarps in the southwest of Western Australia, which are apparently related to large surface breaking earthquakes (Clark, 2005). Given the present lack of understanding of palaeoseismicity of this region, investigation of these features will significantly contribute to a better understanding of the seismic hazard.

Detailed analyses of one of these recently recognized scarps, the Dumbleyung Scarp, located 230 km southeast of Perth (Figure 1), revealed this feature to be a prominent and well preserved fault scarp. Field reconnaissance and analyses of DEM, aerial photographs and the associated drainage network indicated the likelihood of significant recent tectonic deformation. Consequently, the Dumbleyung Scarp was selected for detailed palaeoseismological investigations, the preliminary results of which are presented here.

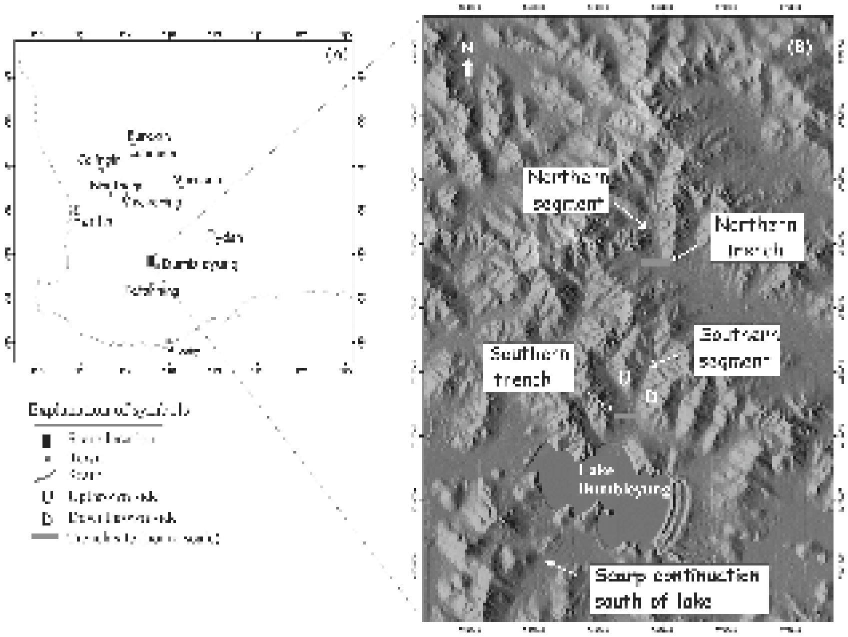

Figure 1. Location of the Dumbleyung Scarp. (A) Location of the scarp in the southwest of Western Australia. (B) Northern and southern segments and location of trenches across the scarp for palaeoseismological investigations

Dumbleyung scarp characteristics

The Dumbleyung Scarp lies within the 'Wheat Belt' of the southwest of Western Australia, on the Western Gneiss Terrain of the Archaean Yilgarn Craton (Gee et al., 1981). Its surrounding area is variably covered by lateritic soils and duricrust formed during the Late Cretaceous and Tertiary (Chin and Brakel, 1986). Regolith materials also include alluvium, colluvium, and reworked sandplain deposits.

The scarp lies within the South West Seismic Zone, SWSZ, (Doyle, 1971). The available seismic record (http://www.ga.gov.au/oracle/quake/quake.online.jsp), indicates that the scarp lies in an area where little instrumental or historical earthquake activity has been recorded (Figure 2).

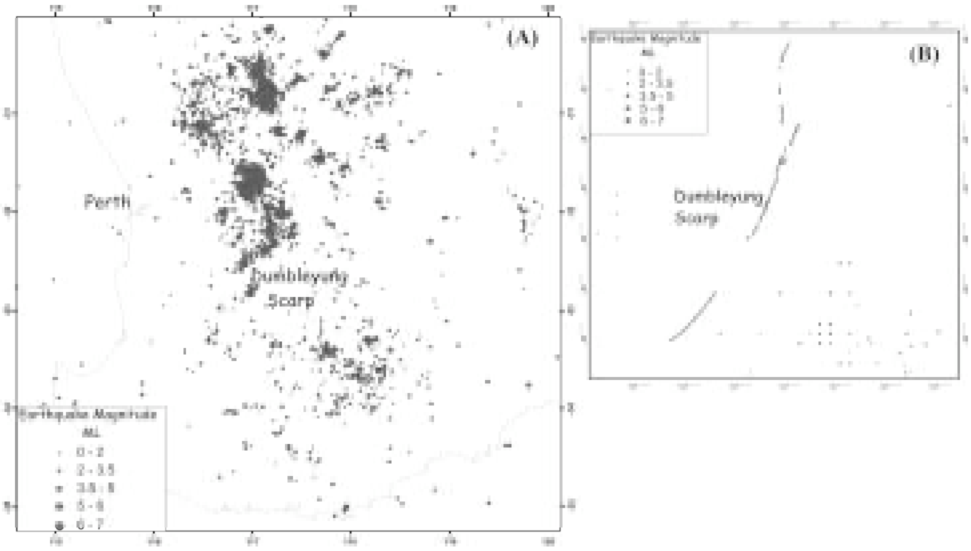

Figure 2. (A) Dumbleyung Scarp location with respect to the SWSZ. (B) Earthquake events recorded close to the scarp.

The Dumbleyung Scarp consists of two segments (Figure 1B). For both segments, uplift occurs in the western side of the fault. The southern segment strikes N20ºE and appears to continue to the south of Lake Dumbleyung, reaching ~24 km in length. The maximum height of this segment is 3 m. The northern segment strikes NS and has a length of approximately 12 km attaining a maximum height of 5 m.

Palaeoseismological investigations of the Dumbleyung Fault scarp: evidence of palaeoearthquakes

Two trenches were excavated across the scarp (Figure 1B) in order to obtain information about the earthquake history of the Dumbleyung Fault. Both trenches revealed that the Dumbleyung Scarp formed as a result of thrust faulting. In the southern trench, an east-facing fault propagation fold in alluvial deposits was exposed. Minor structures within the main zone of deformation in this trench indicate that the fold relates to reverse displacement on a buried west-dipping thrust fault. The northern trench also exposed reverse faulting but of significantly greater amplitude than in the southern trench. Further details of the northern trench are given below.

Northern trench

A trench 27 m long, 4 m deep and 3 m wide was excavated across the northern segment of the Dumbleyung Scarp (Figure 3). The scarp reaches 4 m in height at this site and is developed in a suite of alluvial deposits and younger colluvium. The trench exposed significant deformation largely accommodated by drag-folding and associated disruption of stratigraphic units within a main deformation zone up to 1.5 m wide and dipping 20 to 30º to the west (Figure 3A and 3B). Four discrete reverse faults (F2 to F5, Figure 3) were recognised proximal to the main zone of deformation and a fifth discrete fault (F1 in Figure 3A and 3D) was identified to the eastern margin of the trench, away from the main zone of deformation, apparently displacing sediments of the footwall.

The alluvial units exposed in the hanging wall (west side) of this trench could not be correlated to those exposed in the footwall (east side), indicating significant displacement along the main deformation zone (Figure 3A). The colluvial apron that overlies the main deformation zone (Units 16 and 17, Figure 3) has derived from the scarp that was formed after fault rupturing along the main deformation zone. This colluvial apron may prove to be datable using luminescence techniques and should provide an approximate age of the seismic event that caused the uplift that preceded the formation of the colluvial units.

The eastern end of the trench, on the footwall, Unit 13, (between vertical grid lines 18 and 21, Figure 3A), appears to be controlled by deformation related to F1; Unit 13 thickens across the projection of the F1 fault plane which may correspond to the manifestation of a propagation fold related to F1. Thickening of Unit 13 across F1 suggests that displacement across this fault immediately preceded deposition of the unit. Unfortunately, the superposition of channel Unit 15 (Figure 3) has masked the area where this thickening occurs making it difficult to establish unequivocally if the thickening of Unit 13 reflects relief generation subsequent to another earthquake event. The extent of Unit 13 to the west, close to the main zone of deformation, suggests that relief may have also been generated by displacement across this zone during the event along F1. As Unit 16 colluvium overlies Unit 13, which contains a well-developed palaeosol (Figure 3), it is inferred that Unit 13 was at the ground surface prior to the seismic event that produced the colluvial Unit 16 in the main deformation zone.

Faults F2 to F4 appear to terminate against the base of colluvial Unit 16, and consequently may relate to the main deformation event at the main deformation zone. In contrast, F5 appears to displace colluvium relating to the main deformation event (Unit 16-16′), and therefore may reflect a later, more recent seismic event (MRE). Once luminescence dates become available it may be possible to establish if the base of Unit 16 has indeed been displaced by faulting along F5. The combined evidence suggests the possibility of three discrete seismic events. The oldest event along F1 (and probably also along the main deformation zone) is represented by Unit 13. A second penultimate event (PE) at the main zone of deformation may be indicated by colluvial Units 16 and 17, and as already noted, the possibility of a third event (MRE) is associated with F5 which appears to displace colluvial Unit 16 resulting from the PE .

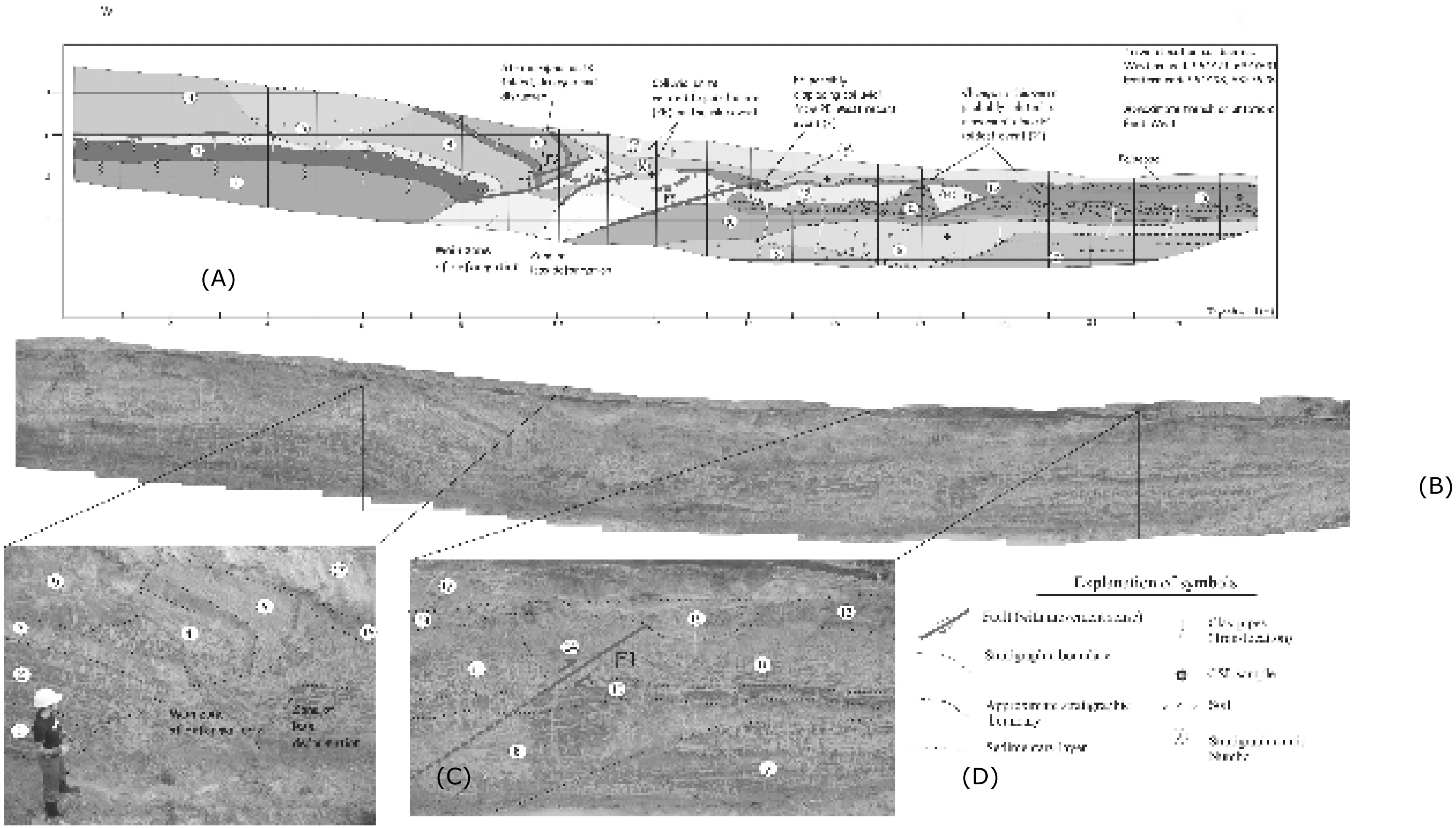

Figure 3. Dumbleyung Scarp Northern trench. (A) Log of the northern trench across the scarp illustrating the different stratigraphic units and their stratigraphic relationships. The main zone of deformation and the faults exposed in the trench are also illustrated. (B) Photographic mosaic of the northern trench. (C) Detail of the main zone of deformation and (D) Detail of fault F1 and Units 11, 13, 14, 15 and 17. Note that Unit 13 thickens in the footwall of F1.

Discussion and conclusions

The Dumbleyung scarp is the surface expression of thrust faulting. The scarp consists of a southern and a northern segment, which together reach 36 km in length. Each segment has different characteristics including strike, vertical displacement and amount of near surface deformation. Luminescence dating results may establish if the northern and southern scarps have ruptured simultaneously during the same earthquake event.

The preliminary evidence presented here suggests the possibility of three earthquake events exposed in the northern trench. However, only one event has been confirmed at this stage (PE), pending the results of the luminescence dating. As indicated above, the three events appear to be represented by the three colluvial deposits inferred (Units 13, 16 & 17). Unit 13 appears to be associated with the relief caused by movement along F1 but its continuation to the west, until the main zone of deformation, suggests that deformation also took place at this zone during this event. A soil profile developed in the upper parts of Unit 13, suggests significant time between its deposition and the deposition of the overlying colluvial units 16, & 17 that formed after a second event (PE). The PE appears to be associated with a large amount of relief generation across the main zone of deformation, and with the significant folding of strata in the hanging wall. Fault F5 appears to displace colluvial Units 13 and 16 and is interpreted as having formed during a more recent seismic event (MRE).

Earthquake magnitude and implications for seismic hazard

The 36 km length of the Dumbleyung Scarp (assuming that the southern and northern segment ruptured together) physically limits the earthquake size that the structure can produce. Empirical equations relating displacement, rupture length and rupture area to earthquake magnitude (Bonilla, 1982, Shimazaki, 1986, Wells and Coppersmith, 1994, Stirling et al, 2002) indicate that a 36 km rupture length may be associated with an earthquake of magnitude Mw 6.9-7.2 and an average vertical displacement of around 2 m. In contrast, a rupture length of about 80 km may be expected for an earthquake large enough to produce 4m of uplift in a single event. A large event implies a large rupture area. However, information from the earthquake records in the southwest of Western Australia and the characteristics of the recent earthquake ruptures such as. Meckering, Cadoux and Calingiri (Gordon, 1971; Denham et al., 1979; Denham et al., 1980; Gordon et al., 1980; Lewis et al., 1981; Langston, 1987; Vogfjord and Landston, 1987); indicate that the seismogenic layer in the region is confined to the top of the crust. Seismic information shows that the seismogenic layer appears to have a maximum thickness of 20 km which in turn restricts the maximum earthquake magnitudes that can be produced in the region.

The height of the scarp (4m) at the northern trench location is therefore best explained as being the result of the whole length of scarp rupturing at least twice. This is consistent with the stratigraphic relationships exposed in the trench profile, which suggest at least one or most probably two major relief-generating earthquake events (oldest and PE), and a third event producing only modest relief (MRE). The smaller displacement across F5 (MRE) may be the result of movement along only the northern segment and not along the whole length of the fault.

Based on the above analysis, at least two events of magnitudes Mw 6.9-7.2 appear to be necessary to produce the scarp relief observed on the northern segment of the Dumbleyung Fault. The northern trench interpretation indicates that these events correspond to the oldest and penultimate events. The earthquake generation dates will help to establish a possible recurrence pattern for this fault, a parameter necessary for seismic hazard assessment.

Although the Dumbleyung Fault appears to be capable of producing earthquakes of Mw 6.9-7.2, the smaller amount of displacement observed along F5 suggest that the fault does not rupture characteristically and may generate earthquakes of lower magnitudes.

A Mw 6.9-7.2 earthquake produced by the Dumbleyung Fault would impact significantly on nearby towns such as Dumbleyung, Wagin and Katanning.

References

Bonilla, M.G., 1982. Evaluation of potential surface faulting and other tectonic deformation. USGS Open-File Report 82-732, Available:http://geopubs.wr.usgs.gov/open-file/of82-732.

Clark, D.J., 2005. Identification of Quaternary faults in southwest and central western Western Australia using DEM-based hill shading. Geoscience Australia Internal Record 2005, 60p.

Chin, R.J. and Brakel, A.T., 1986. Dumbleyung 1:250 000 geological Sheet (SHEET SI/50-07 Internation Index). 1:250 000 geological series - explanatory notes, Geological Survey Western Australia.

Denham, D., Alexander, L.G. and Worotnicki, G., 1979. Stresses in the Australian crust: evidence from earthquakes and in situ stress measurements. BMR Journal of Australian Geology and Geophysics, 4: 289-295.

Denham, D., Alexander, L.G. and Worotnicki, G., 1980. The stress field near the sites of the Meckering (1968) and Calingiri (1970) earthquakes, Western Australia. Tectonophysics, 67(3-4): 283-317.

Doyle, H.A., 1971. Seismicity and structure in Australia. Bulletin of the Royal Society of New Zealand, 9: 149-152.

Gee, R.D., Baxter, J.L., Wilde, S.A. and Williams, I.R., 1981. Crustal development in the Archean Yilgarn Block, Western Australia. Geological Society of Australia, Special Publication, 7: 43-56.

Geoscience Australia online earthquake database, 2006. Available: http://www.ga.gov.au/oracle/quake/quake_online.jsp.

Gordon, F.R., 1971. Faulting during the earthquake at Meckering, Western Australia: 14 October 1968. Bulletin of the Royal Society of New Zealand, 9: 85-93.

Gordon, F.R. and Lewis, J.D., 1980. The Meckering and Calingiri earthquakes October 1968 and March 1970. Geological Society of Australia, Bulletin 162: 213p.

Langston, C.A., 1987. Depth of faulting during the 1968 Meckering, Australia, earthquake sequence determined from waveform analysis of local seismograms. Journal of Geophysical Research, 92(B11): 11561-11574.

Lewis, J.D., Daetwyler, N.A., Bunting, J.A. and Moncrieff, J.S., 1981. The Cadoux earthquake, 2 June 1979. Geological Survey of Western Australia, Report 11: 133p.

Shimazaki, K., 1986. Small and large earthquakes: the effects of the thickness of seismologenic layer and the free surface. Earthquake Source Mechanics, Das. S., Boatwright, J., and Scholz, C (editors). Geophysical Monograph 37. American Geophysical Union: 209-216.

Stirling, M., Rhoades, D. and Berryman, K., 2002. Comparison of earthquake scaling relations derived from data of the instrumental and preinstrumental era. Bulletin of the Seismological Society of America, 92(2): 812-830.

Vogfjord, K.S. and Langston, C.A., 1987. The Meckering earthquake of 14 october 1968: a possible downward propagating rupture. Bulletin of the Seismological Society of America, 44(5): 1558-1578.

Wells, D.L. and Coppersmith, K., J., 1994. New empirical relationships among magnitude, rupture lenght, rupture width, rupture area and surface displacement. Bulletin of the Seismological Society of America, 84(4): 974-1002.

The correlation between physiography and neotectonism in southeast Queensland

Jane H Hodgkinson, Stephen McLoughlin, Malcolm Cox

Queensland University of Technology

Abstract

We tested for correlation between recent earthquake epicentre data and the distribution of major physiographic features, such as escarpments and river channels, in southeast Queensland. Preliminary results indicate that many of the known earthquake epicentres over the past century are distributed in several broad belts, corresponding in location and orientation to major structural discontinuities or narrow sedimentary basins bounded by faults. Other earthquake clusters show broad correlation with linear segments of major river systems where no major faults have been mapped. Several domains dominated by Palaeozoic-Triassic rocks, such as the North and South D'Aguilar blocks, are represented by high terrain flanked by faults that may have been active back to at least the mid-Mesozoic. Reactivation and subsidence along some of these faults may account for the local accumulation of thick sedimentary piles during the Paleogene. Modern earthquake epicentre distributions along the margins of these blocks suggest that recent and on-going tectonism may be enhancing the escarpments flanking the uplands. Unmapped, concealed or deep-seated geological discontinuities may exist where earthquake epicentres correspond to linear physiographic features but not to currently mapped faults or joints. Identification of such concealed geological structures will be important for developing accurate earthquake hazard maps into the future.

Introduction

Tectonism is one of the primary driving forces behind the structural and physiographic modification of land masses. For example, tectonism is largely responsible for terrain uplift and basin subsidence, which allow modification by secondary processes such as weathering and erosion. As tectonics is generally accepted to cause geomorphological change, it is logical to study geomorphological features to identify the influences of tectonics on the landscape (for example Burrato et al., 2003; Vannoli et al., 2004).

The Australian continent is situated within the Indo-Australia Plate. Compared to plate boundary earthquakes, intraplate earthquakes are few and shallow. However, the Global Seismic Hazard Map shows that Australian earthquake activity is moderate to high, relative to other intraplate regions (GSHAP, 1992-1997). The Indo-Australian Plate is presently under compressional stress (Hillis, 1998; Hillis and Reynolds, 2000) and modification of the land will occur in order to accommodate shortening of the continental mass where the stress exceeds the strength of the crust. For example, Neogene-Quaternary reverse faulting and compressional folding has clearly influenced landscape evolution in both central western (for example, Clark, 2005), and southeastern Australia (for example, Sandiford, 2003). Folds, faults, joints, shears and rock fabric alteration, resulting from tectonic movement, have long been known to control the formation of a variety of distinctive land surface features such as scarps and river channels (for example: Hobbs, 1904; Hobbs, 1911; Zernitz, 1932; Strahler, 1960, 1966; Twidale, 1980; Scheidegger, 1998, 2002; Ericson et al., 2005; Hodgkinson et al., in press). The relationship between Australia's geology and its earthquakes is poorly understood and many earthquakes cannot be assigned to known structures (Clark and McCue, 2003). Physiographic analysis in conjunction with recent seismic data will assist identifying those landscape features that are likely to be tectonically controlled and presently active; such analysis has the potential to refine zones hazardous to the population and infrastructure.

For dipping faults, earthquake epicentres will appear more distant from the surface trace with increasing hypocentral depth. As a consequence, epicentres may not be expected to align precisely with surface features, such as mapped faults, scarps and joint systems. Therefore, broad sectors in which earthquake epicentres are located should be identified to determine potentially active fault zones. Earthquake locations may also be inaccurate, particularly those identified from early records and, therefore, care must be taken when relating them to local physiographic features. Since the calculation of actual earthquake depth is typically inaccurate, this parameter should be treated with caution. Using available data, this study aims to provide evidence of tectonic control upon the landscape of southeast Queensland.

Background

Southeast Queensland's geology is complex and derived from several cycles of compressional and extensional tectonic activity since about 370 Ma. Palaeozoic to modern sedimentary and igneous rocks are interspersed with large belts of metamorphic rocks throughout the region. Many of the geological units (Queensland Government, 2003) are bounded by faults. Extensive regolith, vegetation and infrastructure conceal many of southeast Queensland's geological discontinuities including faults, joints and formation boundaries. Some areas appear to be relatively fault-free and, although this may be the case, the apparent dearth of these features may be attributable to concealment by ground cover or the lack of detailed mapping. Recent core logging in southeast Queensland has revealed discrepancies with the published geological maps (geological map, Queensland Government, 2003; Brisbane City Council, 2006 pers. comm.) and confirmed that faults and joints are common in the region. Fault distributions have been analysed recently (Humphries, 2003) but little has been published regarding age constraints on fault activity. Childs (1991) analysed Landsat images of the northern part of the region and showed that the main ranges and drainage systems are strongly concordant with the bedrock geology, and that faults also correspond with channel orientation. However, Humphries noted that some major faults and a shear zone on geological maps were not identifiable on the Landsat image, and may either lack surface expression or have had unfavourable illumination for Landsat (Childs, 1991). The region's elevation ranges from sea-level to 1360 m a.s.l. and the area can be divided into three general terrains: highlands (>300 m a.s.l.), hills (30-300 m a.s.l.) and lowlands (<30 m a.s.l.) (Fig. 1). The greatest portion of southeast Queensland is situated in the hilly to highland terrains. However, most of the population presently resides within the coastal lowlands, especially within the expanding cities of Brisbane, Ipswich and the Gold Coast. Three artificial reservoirs, Somerset, Wivenhoe and Samsonvale, provide southeast Queensland's main water supply: each is situated in known faulted and seismically active zones.

Earthquake monitoring

In order to compare neotectonism and its geomorphological effects, detailed earthquake data are needed. Earthquake monitoring in Queensland is generally sparse by international standards and has only operated intermittently. Earthquakes have been recorded since the late 1800's. In 1937, Queensland's first international monitoring station was opened in Brisbane, followed by the Charters Towers station in 1957. Subsequently, a seismic monitoring network developed slowly, broadening considerably after 1977, when more detailed instrumental monitoring was implemented around the large dams. Dam-site and other seismographs were integrated into a state-wide network, monitored by The University of Queensland (UQ) from 1993 (the QUAKES Centre) but since 1998, much of the operational instrumentation has been progressively discontinued from service. Monitoring is now restricted to southeast Queensland. Since 2000, 22 Queensland Government seismograph stations continue to collect data under commercial contract to Environmental Systems and Services (ES&S, Victoria,). As well as temporal discontinuities, data completeness is also affected by differences in the resolution of monitoring, spatially.

Methods

Digital topographic data at 25 m intervals (Queensland Government, 2005) (Fig. 1), geological and drainage (Fig. 2) maps for southeast Queensland were obtained from the Department of Natural Resources, Mines and Water (DNRM&W) (Queensland Government, 2003). Using the ArcGIS 9 software, a digital elevation map (DEM) was produced and slope maps (Fig. 3) created from which scarp features were extracted. Earthquake data retrieved from Geoscience Australia (2006) provided information for 100 earthquakes recorded in the region since 1872. Further data were supplied by the Earth Systems Science Computational Centre (ESSCC) at The University of Queensland, increasing the total number of earthquakes recorded in the region to 344 (Figs. 3,4,5). The digital maps were combined with seismic data for identification of concordant patterns of geomorphological lineaments and earthquake epicentres. Where 4 or more earthquake epicentres clustered or were well-aligned within a 12-15 kilometre wide corridor, they have been considered to possibly have a common source and be related to similar zones of seismic activity. Such clusters and alignments are referred to here as 'earthquake corridors'.

Results

Highlands and scarps

The highland areas are situated mainly in the west and north of the study area, and generally trend in a northwest-southeasterly direction. A discrete area of highlands, situated in the central region, is separated from the west by the Brisbane River valley. Some highland terrain is situated in the southeast, associated with the Mount Warning shield volcano. The physiography of the latter highland area does not correspond to the predominant northwest-southeast geological trends in southeast Queensland. Scarps are common across the region (Fig. 3). In places they coincide with the orientation of highlands, geological units, faults and drainage.

Drainage

Channel orientation in the region is predominantly northwest-southeasterly and northeast-southwesterly (Fig 2.). These trends are particularly strong in the Brisbane River system, which may be described as a trellis or rectilinear drainage pattern. Secondary trends occur in an east-west orientation and other trends are evident at a finer scale. Drainage in the southeast is radial, away from the centre of the Mount Warning volcanic complex.

Geological discontinuities

High angle dip-slip faults, joints, thrusts and shear zones have been mapped throughout the region (Queensland Government, 2003), although a large area in the southwest and on the coastal plains in the east appears to have few faults. Fault orientations in the remainder of the region strongly trend in a northwest-southeasterly orientation although various other trends are also evident (Fig. 4).

Seismicity

Earthquakes occur throughout the region on all terrains (Figs. 3,4,5). As depth to focus data are highly uncertain, earthquake epicentres only have been considered in this analysis. Their distribution shows some concurrence with drainage, structural features (Figs. 4,5) and scarp distributions (Fig. 3). The epicentres cluster most prominently within a broad northwest-southeast trend but subsidiary southwest-northeast and roughly east-west trends are also evident (Figs. 3,5)

Discussion

Physical relationships

There is some concurrence between the location and orientation of faults and rivers, especially the Brisbane River system (Fig. 4). The presence of a scarp may be due to surface displacement by faulting, mass wasting or by other surface processes such as fluvial erosion. Some scarps appear to have no correlation with present drainage or mapped faults and may represent features with historical controls such as retreating coastal escarpments. A relationship between drainage system pattern and highland location is present, although such definition would be expected due to normal down-cutting of rivers between resistant rock units. The lowland areas primarily consist of unconsolidated Cenozoic sediments, which may conceal faults or joints.

Seismic and physiographic relationships

Earthquake epicentre and drainage patterns commonly concur throughout the region (Figs. 4,5). North of Brisbane/Toowoomba, this association is also closely aligned with faults. However, south of Brisbane/Toowoomba, virtually no mapped faults coincide with earthquake and river-trends. In the north, this alignment suggests that mapped faults may be active and controlling drainage channel orientation and position. In the south however, where some earthquake zones align with drainage but do not coincide with mapped faults, other faults may be concealed and/or not yet mapped. Several scarps coincide spatially with earthquake-prone zones (Fig. 3) and an apparent alignment between some scarps, faults and drainage channels, suggests that these scarps may be fault and/or river controlled. Some earthquake epicentres cluster in close proximity to mapped faults, such as those flanking much of the South D’Aguilar Block (Figs. 4,7). However, some clusters do not appear to align with currently mapped faults despite their linear spatial distribution. The proximity of earthquake activity to channel location suggests that there may be a relationship requiring further investigation.

Seismic zones lacking physiographic relationships

There are several earthquake-prone zones in the region that are commonly located in flat or gently undulating terrain and free from scarps, large river channels and faults. The earthquake epicentres in these areas may be associated with very deep faults that presently have no surface expression, may be in areas that are poorly mapped due to ground cover or may be beyond the resolution of the DEM. Equally, they may be associated with mapped faults with very shallow angles of dip causing the surface expression to be far enough away from the epicentre to appear unrelated. Data may also inaccurately reflect the position of the epicentre.

General

Deep earth investigation such as drilling, reflection seismography or GPR, together with more accurate measurements of hypocentre depths may assist in identifying the faults with which recent earthquakes are associated. Such work may also identify unmapped faults where surface features and earthquakes suggest there is potential faulting in the vicinity. For example, topography, river orientation and earthquake activity suggests faulting occurs along the southern edge of the South D’Aguilar Block. Many of the rock units throughout the region are bounded by faults implying tectonism is responsible for their current position. Recent earthquake activity in the vicinity of these faults suggests continued or sporadic movement of these units is occurring.

Conclusions

This preliminary study suggests that geomorphological evidence, when combined with geological and earthquake data, may be used to successfully identify zones of current faulting. An important consideration in this study has been the scale of viewing both temporally and spatially. Earthquake corridors suggested in our results may not be apparent if each epicentre was viewed in isolation or at a less broad scale in time and space. Although features such as channels and slopes may be controlled by differential weathering, neotectonism may also be influential and this may pose a greater threat than geohazard maps imply. The most widely used seismic hazard map of southeast Queensland (McCue et al., 1998) is a classic representation of a probabilistic earthquake model (defined by Cornell, 1968). The hazard designations are a product of available data, which may be sparse, temporally and spatially. Equally, the earthquakes may not be probabilistic in nature (Clark and McCue, 2003). Consequently, the map may not fully represent actual hazards in the area. Therefore, more detailed, widespread, long-term monitoring programs would be a valuable addition to future hazard assessment and mitigation, together with deterministic seismic modelling. First motion studies are useful in determining the dip orientation of dip-slip faults and whether normal or reverse. Accurate focal depths would also better constrain fault locations. Broad 'zones' surrounding the implied epicentre positions should be used to relate earthquakes to potential, local, physiographic features, unless absolutely certain of the data accuracy. The most densely populated area in southeast Queensland is situated within the lowlands, which hosts a widespread veneer of unconsolidated Cenozoic sediments that may conceal potentially active faults. Better collection and availability of structural data, in combination with high resolution digital terrain models, would enable more thorough landscape analysis to identify potentially active fault zones, areas of concealed faults and deep sediment zones which are conducive to seismic amplification. Ultimately this would provide a better understanding of both neotectonism and localised seismic hazard zones in southeast Queensland.

Acknowledgements

We wish to thank Dr Dion Weatherly and Col Lynam of ESSCC and QUAKES Group at the ESSC Centre, The University of Queensland, for providing us with the ESSCC Earthquakes Database and other useful references, and for interesting collaborative discussions. We are also grateful for the valuable suggestions and comments from Dan Clark and an anonymous reviewer.

References

Brisbane City Council, 2006. City Design, Ground Engineering, Brisbane, pp. Core logging showing that geology maps incorrect in many parts of Brisbane.

Burrato, P., Ciucci, F., Valensise, G., 2003. An inventory of river anomalies in the Po Plain, Northern Italy: evidence for active blind thrust faulting. Annals of Geophysics 46, 865-882.

Childs, I., 1991. Earthquake risk, Landsat imagery and fault zones in the Bundaberg area of central eastern Queensland. Queensland Geographical Journal, Series 4 6, 59-70.

Clark, D., 2005. Identification of Quaternary faults in southwest and central western Western Australia using DEM-based hill shading. Geoscience Australia Record, 60p.

Clark, D., McCue, K., 2003. Australian paleoseismology: towards a better basis for seismic hazard estimation. Annals of Geophysics 46, 1087-1105.

Cornell, C.H., 1968. Engineering seismic risk analysis. Bulletin of the Seismological Society of America 58, 1583-1606.

Ericson, K., Migon, P., Olvmo, M., 2005. Fractures and drainage in the granite mountainous area: A study from Sierra Nevada, USA. Geomorphology 64, 97-116.

ESSCC, Earth Systems Science Computational Centre, 2006. The University of Queensland.

Geoscience Australia, 2006. http://www.ga.gov.au/oracle/quake/quake_online.jsp.
GSHAP, (Global Seismic Hazard Assessment Program), 1992-1997. Global Seismic Hazard Map, http://www.seismo.ethz.ch/GSHAP/global/.
Hillis, R.R., 1998. The Australian stress map. Exploration Geophysics 29, 420.
Hillis, R.R., Reynolds, S.D., 2000. The Australian Stress Map. Journal of the Geological Society 157, 915-921.
Hobbs, W.H., 1904. Lineaments of the Atlantic border region. Geological Society of America Bulletin 15, 483-506.
Hobbs, W.H., 1911. Repeating patterns in the relief and structure of the land. Geological Society of America Bulletin 22, 123-176.
Hodgkinson, J.H., McLoughlin, S., Cox, M., in press. The influence of geological fabric and scale on drainage pattern analysis in a catchment of metamorphic terrain: Laceys Creek, southeast Queensland, Australia. Geomorphology doi:10.1016/j.geomorph.2006.04.019.
Humphries, D., 2003. An analysis of post-Triassic faulting in southeast Queensland. BSc (Hons) Thesis, University of Queensland, Brisbane, 134 pp.
McCue, K.F., Somerville, M., Sinadinovski, C., 1998. The new Australian earthquake hazard map, Proceedings of the Australasian Structural Engineering Conference, Aukland, NZ, pp. 433-438.
Queensland Government, D.N.R.M., 2005. South East Queensland 25 metre Digital Elevation Model - SEQ_DEM_100K.
Queensland Government, D.N.R.M.W., 2003. Queensland Geological Digital Data.
Sandiford, M., 2003. Neotectonics of southeastern Australia: linking the Quaternary faulting record with seismicity and in situ stress. Geological Society of Australia Special Publication 22, 101-113.
Scheidegger, A.E., 1998. Tectonic predesign of mass movements, with examples from the Chinese Himalaya. Geomorphology 26, 37-46.
Scheidegger, A.E., 2002. Morphometric analysis and its relation to tectonics in Macaronesia. Geomorphology 46, 95-115.
Strahler, A.N., 1960. Physical Geography. John Wiley and Sons, New York.
Strahler, A.N., 1966. The Earth Sciences. Harper International, 681 p.
Twidale, C.R., 1980. Geomorphology. Thomas Nelson, 406 p.
Vannoli, P., Basili, R., Valensise, G., 2004. New geomorphic evidence for anticlinal growth driven by blind-thrust faulting along the northern Marche coastal belt (central Italy). Journal of Seismology 8, 297-312.
Zernitz, E.R., 1932. Drainage patterns and their significance. Journal of Geology 40, 498 - 521.

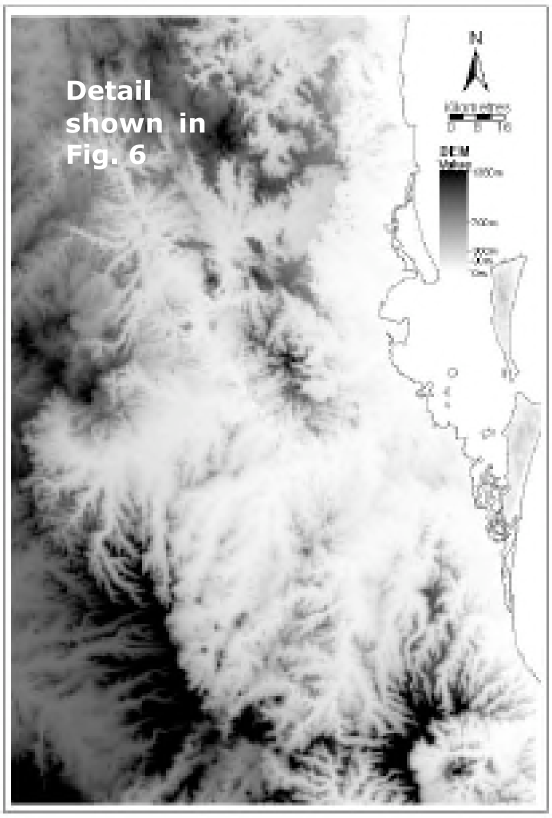

Fig. 1 25m DEM of southeast Queensland

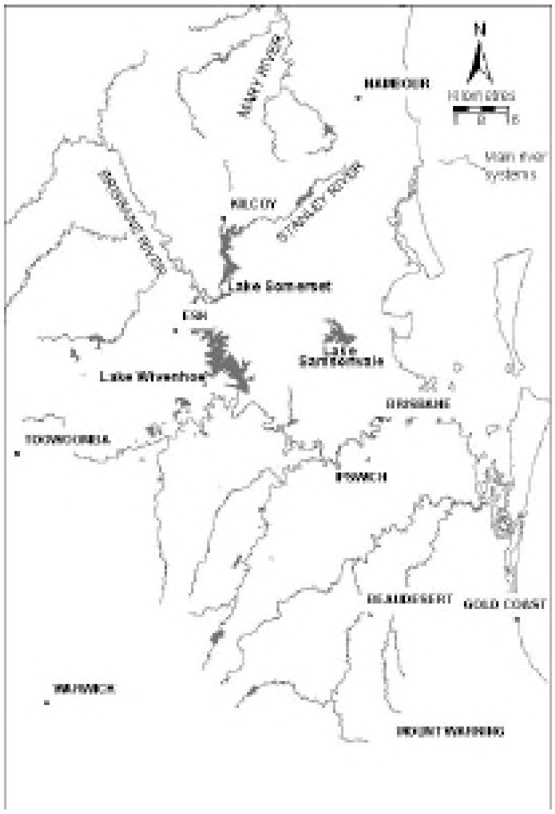

Fig 2 Main drainage systems and locations of southeast Queensland

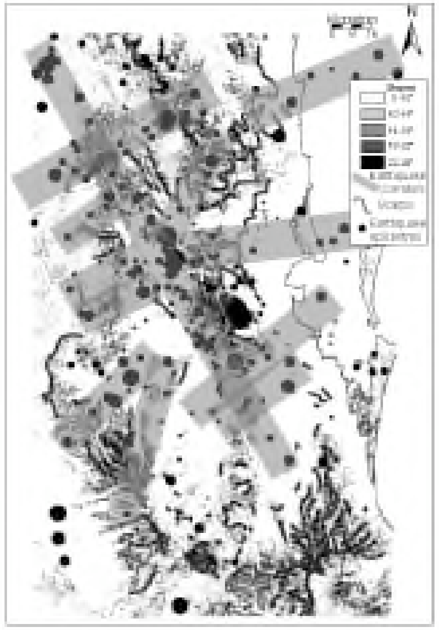

Fig. 3

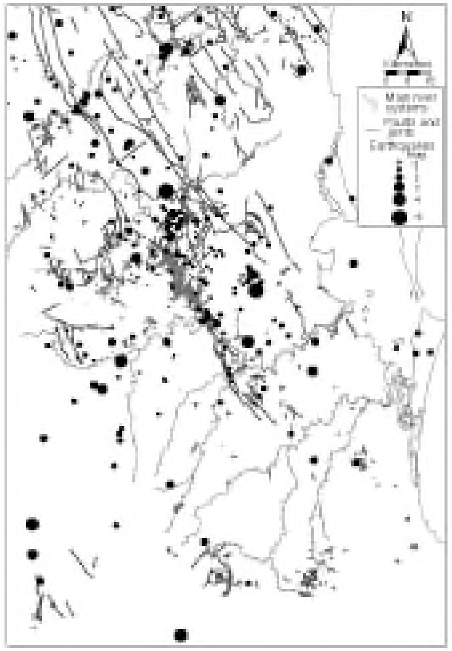

Fig. 4

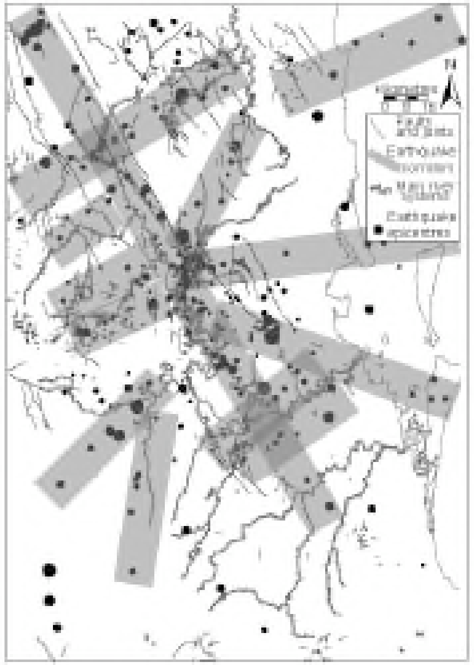

Fig. 5

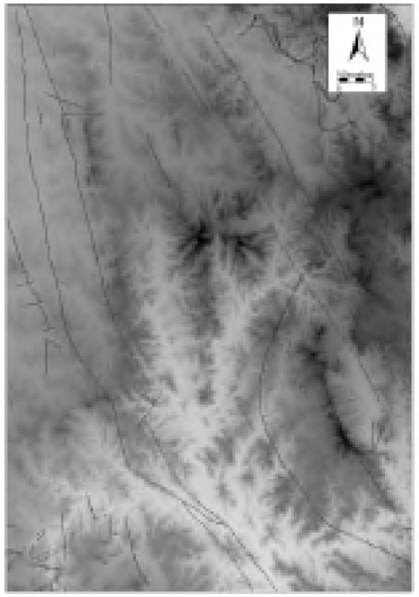

Fig. 6

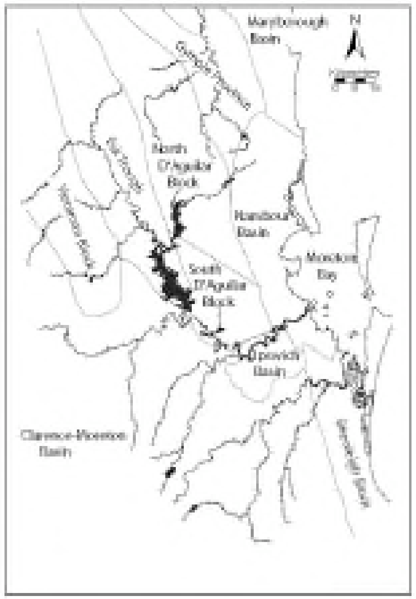

Fig. 7

Fig. 3 Earthquake epicentre corridors superimposed onto slope map. Scarps highlighted in black

Fig. 4 Main drainage, structural features and earthquake epicentres in southeast Queensland

Fig. 5 Data from 'Fig. 4' superimposed with earthquake corridors

Fig. 6 DEM detail (northwest of region) showing linear escarpments with mapped faults superimposed

Fig. 7 Stable geological blocks and basins of southeast Queensland

Seismic hazard assessment through predictive modelling of local stress changes due to hot fractured rock (HFR) geothermal energy operations in the Cooper Basin of South Australia

Hunt, S.P[1]. Morelli, C.[1], Boult P.J.[2], Malavazzos, M.[2], Hill, T.[2], Sinadinovski, C.[3]

[1] The University of Adelaide
[2] Primary Industries and Resources of South Australia
[3] Australian National University

Abstract

This paper reports on a study that has been undertaken in the Cooper Basin region of South Australia where an assessment of seismic hazard has been made to determine stress changes in the region due to HFR geothermal energy operations. The work has considered the basement structural geology and slip tendency for large scale faults, previously interpreted from seismic data. The slip tendency analysis has resulted in a derived factor of safety for all faults of greater than 1. The seismic activity recorded during reservoir stimulation events, at a local geothermal field, has been analysed and incorporated in the probabilistic hazard maps for the region, little change in seismic hazard is evidenced.

The same geothermal field has also been studied using a numerical modelling approach which investigates possible static stress changes and likely interaction of this stress field change with nearby geological structures. The stress field perturbation is small and has an extent which is significantly less than the extent of the field itself. Initial work has been performed in order to investigate the influence of seismic waves on a well bore and numerical well completion models have been developed.

Volcano-tectonic earthquakes and magma reservoirs; their influences on volcanic eruptions in Rabaul caldera

Ima Itikarai, Brian Kennett and Cvetan Sinadinovski

Australian National University

Abstract

Since seismic monitoring began in the late 1960s the seismicity in Rabaul caldera has been marked by intra-caldera high frequency volcano-tectonic earthquakes. The hypocentral distribution of these earthquakes defines an outward-dipping elliptical ring-fault in shallow depths. Before the 1994 eruption other prominent seismicity includes a swarm of earthquakes that occurred in May 1992 away from the caldera in a northeasterly direction.

After the eruption the intra-caldera seismicity decreased significantly. The majority of the locatable events have been located on the southern section of the ring-fault. These events have been overshadowed by a group of earthquakes that occurred northeast of the caldera.

Observations between the ongoing eruptions at Tavurvur and the periodic episodes of northeasterly earthquakes between 1995 and 2005 show interesting correlations. Notable episodes of northeasterly earthquakes have been followed by intensified or renewed eruptive activity. The lead-time between earthquakes and either one of the types of eruptive activity is between few and several months. We speculate that the northeast earthquakes mark episodes of intrusions of a second magma source into the caldera magma reservoir allowing magma mixing to occur, hence resulting in the ongoing eruption at Tavurvur. The tomographic results suggest up to three possible magma reservoirs. The proximity of the northeast earthquakes to the north-northeasterly low velocity anomaly and other information suggests this anomaly is a magma reservoir and is the source of magma injected into the caldera reservoir.

Introduction

Since seismic monitoring began in the late 1960s the seismicity in Rabaul caldera has been marked by intra-caldera high frequency volcano-tectonic earthquakes. Before the 1994 eruption, other prominent seismicity was a swarm of earthquakes in May 1992 that occurred away from the caldera, in a northeasterly direction. The hypocentral locations of the earthquakes define an outward-dipping elliptical ring-fault in shallow depths (Mori and McKee, 1987) (Fig. 1a). After the eruption the intra-caldera seismicity decreased significantly. Most of the locatable intra-events have been located on the southern section of the ring-fault. These events have been overshadowed by a group of earthquakes that are located in a northeasterly direction from the caldera (Fig. 1b). The epicentral distribution of the latter group shows a northeast-southwest trend, however this feature may be an artifact of the location program due to station distribution. Nevertheless, there has been some correlation between the northeast earthquakes and the ongoing eruptions at Tavurvur between 1995 and 2005.

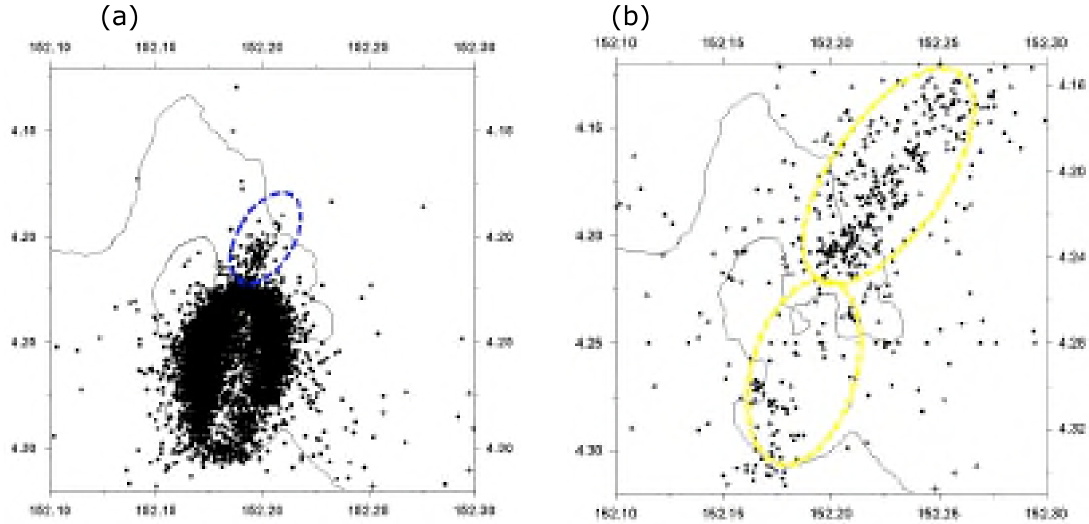

Fig. 1: Seismicity of Rabaul Caldera, (a) before the 1994 eruption, and (b) after the eruption. The pre-eruption northeast earthquakes are marked by the dashed ellipse in (a).

In this study we have attempted P-wave travel-time tomography using the Fast Marching Method, FMM (Rawlinson and Sambridge, 2004) to image the substructure of Rabaul caldera and the surrounding area in order to investigate the existence of low velocity anomalies. Since the region of study is a volcanic region some of these anomalies could be interpreted as magma bodies. Furthermore, the study investigates the proximity of the northeast earthquakes in relation to the low velocity anomalies and attempts to draw meaningful speculations on their influence on the ongoing eruptions at Tavurvur. This information could be useful for forecasting future volcanic eruptions and assist in improving disaster mitigation in Rabaul township and neighboring communities.

Data

Data used in this study include local earthquakes in and near Rabaul caldera and regional earthquakes from the New Britain – New Ireland region of Papua New Guinea (Fig. 2), recorded by the Rabaul Volcano Observatory Seismic Network (inset in Fig.2). The locations for the earthquakes were determined using the Fasthypo program (Herrman, 1979). Magnitudes for the earthquakes range between 1.0 and 7.0. As can be seen in Fig. 2, the majority of the earthquakes are located on the eastern side of the study area. Only earthquakes recorded by 5 or more stations and having horizontal and vertical uncertainties of 1.0 km or less have been used in this study. The total number of earthquakes is 674 which constitutes about 1875 rays paths.

The region of study is bounded by latitudes 3.60°S – 5.60°S and longitudes 151.20°E – 153.20°E. This area has been divided into an 81 x 81 grid, giving a total of 6561 cells with a cell size of 2.7 km. The depth range is shallow - between the surface and 40 km. There are no discontinuities in the model.

For correlation between the ongoing eruptions and occurrences of the northeast earthquakes, all significant episodes of eruptions and northeast earthquakes between the period 1995 and 2005 have been considered.

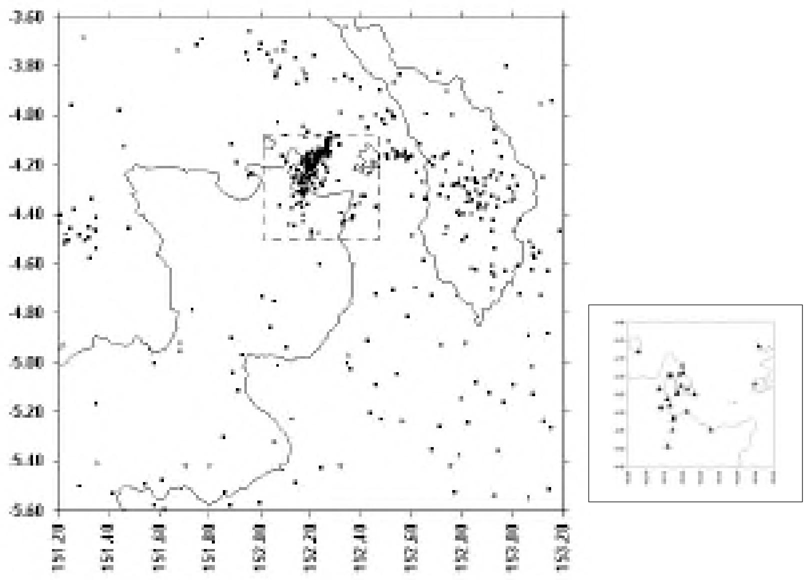

Fig. 2: Distribution of earthquakes used in this study and seismic network (inset).

Methodology

For the P-wave travel-time tomography, the Fast Marching Method (FMM) (Rawlinson and Sambridge, 2004) was utilized. FMM is a grid-based numerical algorithm ideal for wavefront construction from which traveltimes are deduced. It does this by tracking an evolving interface along a narrow band of nodes that are updated by solving the eikonal equation. The eikonal equation, which governs the propagation of seismic waves in the high-frequency limited space is represented by the gradient operator, traveltime, and slowness as a function of position.

FMM deals with problems of discontinuities by enforcing an entropy condition where the wavefront evolves because it can only pass through a point once. The traveltime associated with a particular grid point is updated using a finite difference scheme. The implementation of the scheme requires that the order in which the nodes are updated be consistent with the direction of the flow as time progresses. FMM achieves this by systematically constructing traveltimes ahead of the wavefront from known values behind the wavefront using a narrow-band approach. In the narrow-band concept the grid points are labeled as either alive, close or far, where the alive points lie in front of the wavefront, far points lie behind the wavefront and the close points lie within the narrow band itself. The narrow-band is thus identified with points with minimum traveltime and its shape approximates the first arrival wavefront.

We have applied FMM in a regional model context in this study to produce estimates of P- and S-wave arrival times for source-receiver combinations and compare them with observed times in order to produce tomographic images based on their differences.

Preliminary results

Fig.3 shows tomographic images obtained in this study. All images show relative velocity perturbation. The colour scales are in km/s. We wish to reiterate that these results are deduced from a regional model, hence some of the interpretations may not represent true in-situ structures, as they seem, from a local model context. However, we have used knowledge of the local environment (from the first author) to derive some of these interpretations without introducing bias.

Fig.3 (a-d) shows a subset of horizontal depth slices at 1, 3, 6 and 8 km. The 1 km depth slice shows the general area of Rabaul having a slow travel time anomaly. This could be consistent with a surface geology consisting mainly of soft volcanic deposits. However it fails to pick up the slightly higher velocity zones marking the caldera rim. The 3 km depth slice maintains the low velocity anomaly but is becoming a bit more focused around the caldera area. Other distinct features include two low anomaly lobes fanning out to the northeast and east from the main low anomaly and the high velocity anomalies north and south of the caldera, probably associated with the caldera rim. At 6 km depth the low velocity anomaly at the center of the caldera is still present but it has become more confined to the caldera. Furthermore the low velocity anomaly to the northeast is still maintained, but its connection with the low anomaly to the east presents a complicated picture when associating them with magma reservoirs. At 8 km depth, the low velocity anomaly beneath the caldera is still present. Interestingly the low velocity anomaly to the northeast is also maintained. The high velocity features marking the caldera boundary are also maintained at this depth.

Fig.3e and Fig. 3f are north-south and east-west cross-sections, respectively. The cross-sections are taken at longitude 152.19°E and latitude 4.26°S, respectively, passing through the center of the caldera. Both cross-sections show a low velocity anomaly to about 5 km beneath the caldera. Between 5 km and about 6-7 km the low velocity anomaly becomes patchy like a discontinuity, featuring pockets of high velocity structures, before another low velocity anomaly begins at about 7-8 km depth. The latter feature becomes ambiguous at depths greater than 12 km.

From the above descriptions we infer about three possible low velocity anomalies; the shallow and intermediate depth anomalies in the central part of the caldera and the northeasterly anomaly. The shallow and intermediate depth anomalies appear to be connected as indicated by the patchy features linking the two.

Discussion

This study complements similar studies conducted for Rabaul caldera (Gudmundsson et al., 1999; Finlayson et al., 2003; Bai and Greenhalgh, 2005). Generally, besides the low velocity anomaly in the central part of the caldera at 3-5 km depth, the results of this study are consistent with Bai and Greenhalgh (2005) on the suggestion of a second low velocity anomaly in the same area at slightly greater depths, but quite different. Bai and Greenhalgh (2005) put the top of the second anomaly at about 12 km. Our study puts the top of the second low velocity anomaly at about 8 km. Similarly, like Bai and Greenhalgh (2005), our study suggests that the two bodies are connected, but details of this are complicated. Furthermore, this study agrees with Bai and Greenhalgh (2005) about the suggestion of another low velocity anomaly away from the caldera in a northeasterly direction. Bai and Greenhalgh (2005) have associated this with Tavui caldera, hence the Tavui source. The location of the anomaly determined in this study approximately coincides with the result of Bai and Greenhalgh (2005) (Fig. 13b), but strictly speaking it falls well away from Tavui Caldera. To be more precise it is located slightly south-southeast from Tavui caldera, offshore near Korere-Nodup and approximately coincides with the locations of the so-called northeast earthquakes.

The proximity of the northeasterly source to the basaltic volcanic centers of Kombiu, North and South Daughter, and assuming that eruptives from these volcanoes originated from this source, suggests that the Tavui source is basaltic. To some extent this interpretation is more logical to solve the ambiguity of the source of the basaltic magma, which is a key component in magma mixing in the Rabaul eruptives (Patia et al., 2002; Patia, 2003). Patia et al. (2002) and Patia (2003) alluded to the idea that the basaltic magma is at greater depths beneath the caldera. This is also possible considering the intermediate-depth low velocity anomaly beneath the caldera (Bai and Greenhalgh, 2005 and this study). However, Patia et al., (2002) and Patia (2003) have shown that the eruptives from Vulcan contain no basaltic components whilst eruptives from Tavurvur have abundant basaltic components. The absence of basaltic components in Vulcan eruptives suggest the basaltic source is not within reach from the Vulcan plumbing system, so certainly it is not from the intermediate-depth central magma reservoir. We prefer the easterly source as Roggensack et al., (1995).

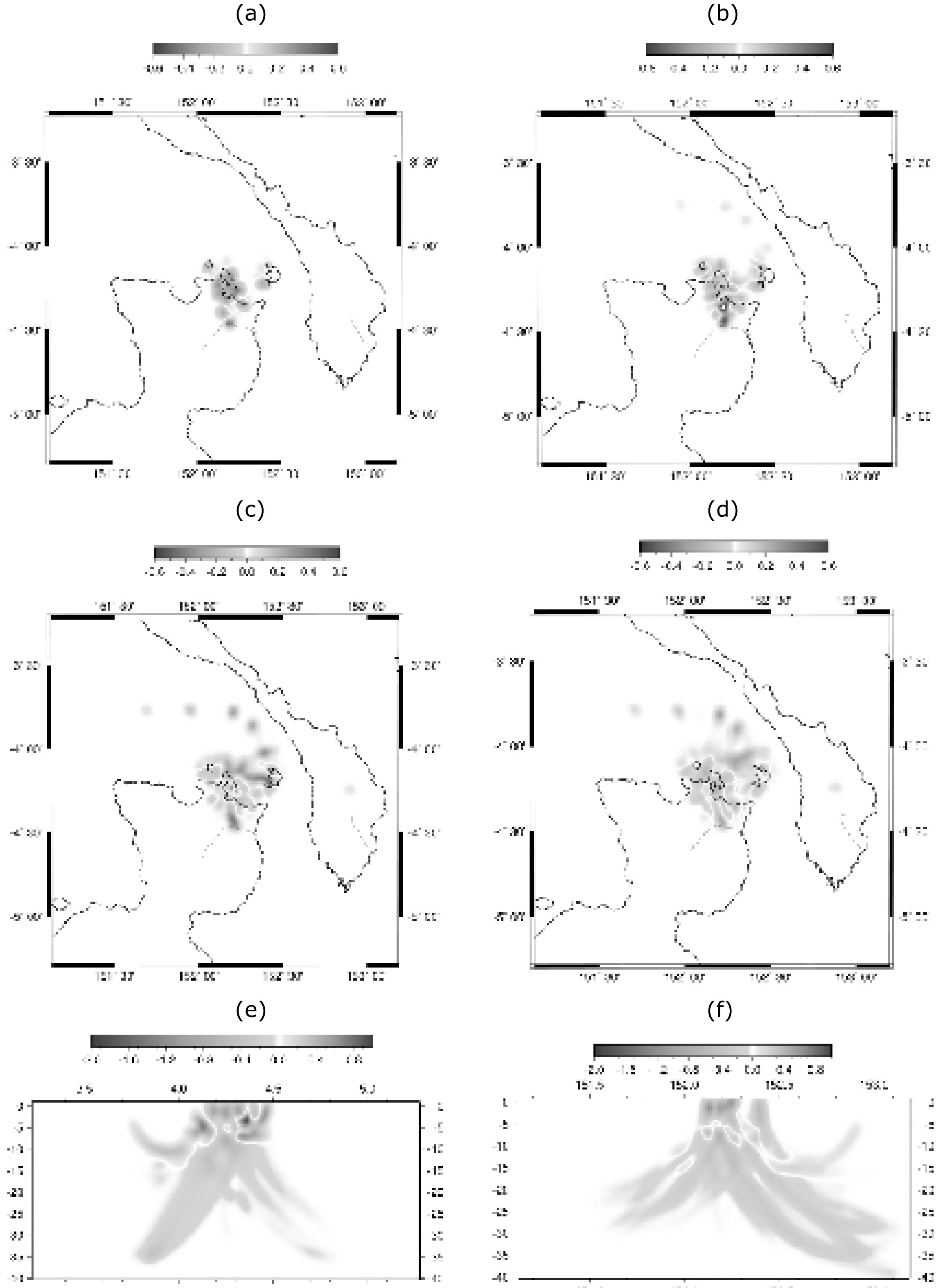

Fig. 3: Preliminary tomographic results showing relative velocity perturbations for 1, 3, 6 and 8 km depth slices (a-d), and north-south and east-west cross-sections (e-f). The north-south cross-section is sliced through longitude 152.18°E and the east-west cross-section through 4.24°S, both of them passing through the center of the caldera.

Magma mixing, in this case involving dacite magma from the caldera source and the basaltic magma from the Tavui area, is considered to be a key process that facilitates the ongoing eruptions at Tavurvur between 1995 and 2005. Petrological analysis on material from the eruptions confirms this (Patia et al., 2002; Patia, 2003). Obviously magma mixing can only occur when basalt magma from the Tavui area injects into the central caldera source. We interpret the northeast earthquakes as an indicator of this activity.

This inference is based on the observed correlation between the occurrence of northeast earthquakes and either intensification of eruptive activity during an ongoing eruption or resumption of eruption (Table 1). The lead-time between the occurrence of earthquakes and either intensified eruptive activity or renewed eruption varies between a few weeks and several months. The shorter response time is associated with an open system and the longer response time is associated with a partially closed system. This suggests that the lead-time will even be longer when the system is completely closed. We demonstrate this by the first-ever swarm of northeast earthquakes in May 1992, followed by the twin eruptions in September 1994. The lead-time was approximately 28 months. In retrospect of the eruption, the eruption in 1994 was preceded by 27 hours of very intense intra-caldera seismicity triggered by two moderate earthquakes. In contrast, before that the caldera system went through a very intense crisis between September 1983 and July 1985 (Mori et al., 1988), marked by high earthquake and inflation rates. An eruption was very eminent but it did not occur. Based on the preceding discussions we form the view that although an eruption was eminent between 1983 and 1985, it did not occur because there was none or no adequate magma mixing to trigger an eruption.

Table 1: Significant cross-correlation between northeast earthquakes and increased summit activity at Tavurvur between 1995 and 2005.

Swarm/EQ dates	*Level of Swarm/EQ activity*	*Type of summit activity*	*Date of Summit activity*	*Lead time between seismicity and summit activity (months)*
Aug 1995	B	ER	Nov 1995	3
Feb 1996	B	IA	May 1996	3
Jul-Aug 1996	A	IA	Oct 1996	2
Feb 2001	C	ER	Sep 2001	7
Jun-Jul 2004	C	ER	Jan 2005	7

Key: IA – Intensified Activity, ER – Eruption Resumption, A –Intense, B – Moderate, C – Low, D – Very low.

These observations suggest that magma mixing is a fundamental process for triggering eruptions in the Rabaul caldera. Furthermore, the northeast earthquakes are possible early indicators for basaltic magma injection and they can be used as precursors for forecasting future volcanic eruptions in the Rabaul caldera. This observation is of crucial importance for disaster mitigation in the township of Rabaul from future eruptions.

Conclusions

The results of this tomographic study are quite consistent with results of similar studies for Rabaul caldera (Finlayson et al., 2003; Bai and Greenhalgh, 2005). Apart from the shallow central caldera low velocity anomaly, this study agrees with Bai and Greenhalgh (2005) on two other low velocity anomalies located at intermediate depth in the central part of the caldera, and northeast from Rabaul caldera near Tavui area. This study suggests the low velocity anomaly near Tavui area is the primary source of the basaltic magma, which is injected into the caldera reservoir allowing magma mixing to occur, as determined by Patia et al. (2002) and Patia (2003).

The occurrence of the northeast earthquakes is indicative of the source near Tavui area being injected into the central caldera magma system. Observations between 1995 and 2005 indicate strong correlation between the northeast earthquakes and eruptions at Tavurvur. In all cases the northeast earthquakes preceded intensified or renewed eruptions with lead-times ranging between few and several months. This outcome could be reliably used as a precursor for forecasting future eruptions in Rabaul caldera and hence help towards disaster mitigation.

In the next phase of this work, another scheme based on Neighborhood Algorithm (Sambridge and Kennett, 2001) will be applied to invert the time differences and thus produce another set of tomographic images.

Acknowledgements

This study is done as part of the Master of Philosophy program for the first author at the Australian National University under an AusAID-funded scholarship. Dr Nicholas Rawlinson has been very helpful on all aspects of the FMM.

References

Bai, C., and Greenhalgh, S., 2005. 3D multi-step travel time tomography: Imaging the local, deep velocity structure of Rabaul volcano, Papua New Guinea. Physics of the Earth and Planetary Interiors, 151, 259-275.

Finlayson, D. M., Gudmundsson, O., Itikarai, I., Nishimura, Y., Shimamura, H., and Johnson, R. W., 2003. Rabaul Volcano, Papua New Guinea: island arc structural architecture and seismic tomography imaging of an active volcanic caldera. J. Volcanol. Geotherm. Res., 124, p153-171.

Gudmundsson, O., Finlayson, D. M., Itikarai, I., Nishimura, Y., Shimamura, H., and Johnson, R. W., 1999. Velocity tomography of shallow structure beneath Rabaul Caldera based on local earthquake and explosion data. IUGG 99, Birmingham.

Hermann R B, (1979). FASTHYPO – a hypocenter location program. Earthquake Notes, v. 50, p. 25-38.

Mori, J., and McKee, C. O., 1987. Outward-dipping ring fault structure at Rabaul caldera as shown by earthquake locations, Science, 235, 193-195.

Mori, J., McKee, C. O., Itikarai, I., Lowenstein, P., de Saint Ours, P., Talai, B., 1988. Earthquakes of the Rabaul seismo-deformational crisis, September 1983 to July 1985: Seismicity in a caldera ring-fault: In – Volcanic Hazards Assessments and Monitoring (Ed. J. H. Latter), Springer – Verlag, p429-462.

Patia, H., Eggins, S., McKee, C. O., and Johnson, R. J., 2002. The 1994 to 2001 eruption at Rabaul, Papua New Guinea: Evidence of repeated basaltic magma influx into a sub-caldera dacitic magma reservoir, 16th Australian Geological Convention, Adelaide, Abstract.

Patia, H., 2003. Petrology and Geochemistry of the recent eruptive history at Rabaul Caldera, Papua New Guinea: implications for magmatic processes and recurring volcanic activity, MPhil. Thesis, Australian National University.

Rawlinson, N., and Sambridge, M., 2004. Wavefront evolution in strongly heterogeneous layered media using the fast marching method, Geophysical Journal International, 156, 631-647.

Roggensack, K., Williams, S. N., Schaefer, S. J., and Parnell Jr., R. A., 1995. Volatiles from the 1994 Eruptions of Rabaul: Understanding large caldera systems, Science, 273, 490-493.

Sambridge, M., and Kennett, B., 2001. Seismic event location: Nonlinear Inversion using Neighbourhood Algorithm, Pure Appl. Geophys., 158, 241-257.

Simulation of strong ground motions with a combined Green's function and stochastic approach

***Zhong Yuan Liang*[1]*, Hong Hao*[1]*, Brian A. Gaull*[2]*, and Cvetan Sinadinovski*[3]**

[1] The University of Western Australia
[2] Guria Consulting
[3] Australian National University

Abstract

A combination of Green's function and stochastic method is developed to generate strong ground motion time histories for engineering applications. This approach is an example of obtaining strong motion data in a region without strong seismicity. Hao and Gaull (2004) proposed a stochastic model based on recorded motion from minor-large magnitude earthquakes on SWWA rock sites. This model is found to be apt to generate moderate-sized earthquake events and below over different epicentral distances. In this study, the strong ground motions from large earthquake events are generated using the Green's function method. The results of this are validated by comparing the Fourier spectrum of the simulated events with the larger magnitude recordings (The M_L 6.2 event in Cadoux in June 1979 and a M_L 5.5 event recorded in Meckering in January 1990).

Introduction

Because there are very few recordings from significant southwest Western Australia (SWWA) earthquakes (M_L 4 or more), it is difficult to derive a reliable strong ground motion attenuation model for this region. Two previously established PGA and PGV attenuation models that are based on local data are Gaull and Michael-Leiba (1987) and Gaull (1988). Gaull (1988) warned of the large uncertainties using his relations due to the limited database. Other models used in SWWA in more recent times are mainly from central and eastern North America (CENA) (Atkinson and Boore 1995, Atkinson and Boore 1997 and Toro et al. 1997). These models are believed to be reliable because both CENA and SWWA are located in the stable continental intraplate region. However, Hao and Gaull (2004) and Kennedy et al. (2005) showed that none of these models yielded very satisfactory prediction of the recorded strong ground motions in SWWA.

Hao and Gaull modified the Atkinson and Boore (1995) model and incorporated SWWA seismological parameters into the model which resulted in a better correlation with the existing SGM data. However, its reliability in representing larger SWWA earthquakes is not known due to the lack of data from events of large magnitude. This means the model could be biased to the ground motion characteristics associated with small events and narrower frequency band biased towards the high frequency region. Furthermore, this cannot be verified because of the lack of such data.

To overcome the problem of paucity of data from large magnitude events, it was decided to use a two-stage approach: 1) Simulating ground motion time histories from minor earthquake events using the stochastic model (Hao and Gaull 2004) and then 2) These time histories will be used to simulate time histories of large magnitude events using empirical Green's Function method. This approach is an example of obtaining strong motion data in a region without strong seismicity. The validity of this approach is verified by comparing the simulated Fourier spectrum with the recorded motions in SWWA from a M_L 6.2 event centred in Cadoux in June 1979 and a M_L 5.5 event in Meckering in January 1990. It should be noted that these are the only two events that are large enough for this validation process.

Simulation of strong ground motion

Methodology

There are two main approaches of simulating strong ground motions. One is stochastic approach (Hanks and McGuire 1981, Boore 1983, Boore and Atkinson 1987, Boore 2003, Hao and Gaull 2004), which is based on a set of assumptions regarding the earthquake source spectrum, propagation path and site conditions. The modified model by Hao and Gaull (2004) was verified yielding reliable prediction of recorded motions in SWWA. However, because most of the recorded motions are from minor earthquakes, this modified model may be biased towards events of this magnitude and may bias the prediction of ground motions for large or greater magnitude earthquakes.

Green's Function method is the other method based on the representation theorem for a kinematic dislocation model. In the empirical Green's function technique of Irikura (1986), the large event has been modelled from the aftershocks that may not be well distributed within the rupture plane. Irikura (1986) divided the mainshock fault plane into subfaults plane to satisfy the scaling law of the source spectral. The size of the mainfault and subfault corresponds to the rupture area of main event and small event respectively. Because the frequency contents of a small event are usually not the same as those of a large event, Irikura et al. (1997) modified an exponential slip function to boost the low-frequency energy in the simulation. Their equation is given as

$$U(t) = \sum_{i=1}^{N} \sum_{j=1}^{N} (r/r_{ij}) \cdot F(t) * (C \cdot u(t)) \tag{1}$$

$$F(t - t_{ij}) = \delta(t - t_{ij}) +$$

$$\left\{ (1/n')\left(1 - \exp(-1)\right) \right\} \sum_{k=1}^{(N-1)n'} \left[\exp\left\{ -(k-1)/(N-1)n' \right\} \times \delta\left\{ t - t_{ij} - (k-1)T/(N-1)n' \right\} \right] \qquad \text{(2) and}$$

$$t_{ij} = \left| r_{ij} - r_0 \right| / V_s + \left(r_{ij} - r_0 \right) / V_r \tag{3}$$

where $*$ means convolution, *U(t)* is the ground motion of large event; *r* the distance between the hypocenter of small event and the receiver; r_{ij} the distance between the subfault(i,j) and the receiver; r_0 the distance between the subfault(i,j) and the hypocenter of large event; *F(t)* the slip-time filtering function; *C* the stress drop ratio; V_s the rupture velocity; V_r the shear wave velocity; *u(t)* the contribution of the jth sub event; $\delta(t- t_{ij})$ the Dirac delta function; t_{ij} the phase delay term. *N* is the scaling law between large and small event, which is derived from the study of Kanamori and Anderson (1975) and Aki (1967) and Brune (1970). *n′* is an appropriate integer to eliminate spurious periodicity. The reader is reminded that small events will be generated by using Hao and Gaull (2004)'s stochastic model and Green's Function will then use these to simulate ground motions from large events.

Case study

Parameter modification

In Figure 1, the predicted FFT spectrum of the ground motion from a M_L 5.5 event by Hao and Gaull (2004)'s model is compared with the recorded motion of the M_L 5.5 Meckering event. It can be seen that the Hao and Gaull (2004) model underestimates the ground motion energy at frequencies lower than 2 Hz. This observation implies that the corner frequency used in the model should be lower in order to more reliably predict motions in SWWA. To achieve this, the source spectrum used in the model is modified as

$$S_a(f) = \frac{k(1-\varepsilon)}{1 + k\left(f/f_a\right)^2} + \frac{k\varepsilon}{1 + k\left(f/f_b\right)^2}, \qquad S_b(f) = 1.0 \tag{4}$$

where k is a modification parameter. It is found that, by trial and error, $k=10$ gives better prediction of the recorded motion. As shown in Figure 1, using the stochastic model and the modified source spectrum yields good prediction of the recorded motion.

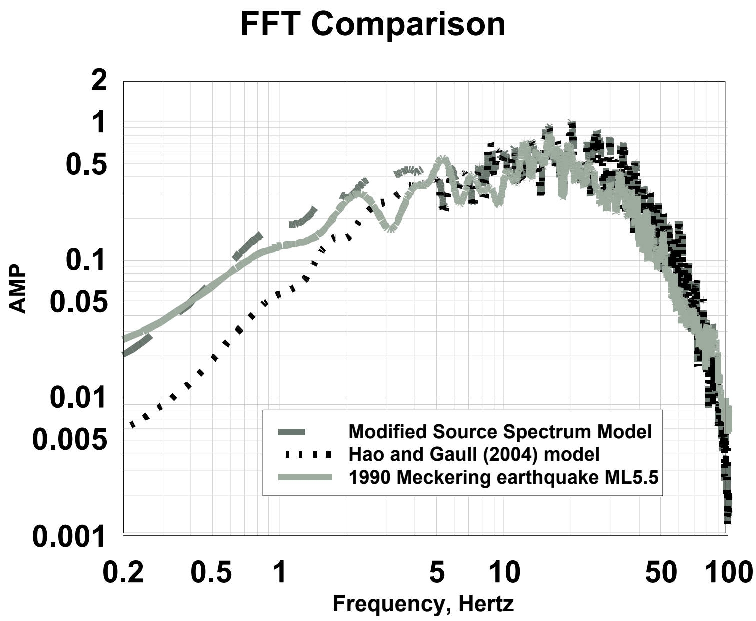

Fig. 1 FFT Comparison of the recorded and simulated M_L 5.5 Meckering earthquake motion

Gaull and Michael-Leiba (1987) used the following relation to estimate the length of fault in accordance with surface-wave magnitude.

$$\log L = 3.2 + 0.5M_s \tag{5}$$

where L is the length of the fault in cm and M_s is the surface-wave magnitude.

Because the earthquake source parameters in SWWA are not well studied and the geophysical conditions of CENA are relatively similar to that of SWWA, many CENA parameters are adopted here. Equation (6) was given by Somerville et al. (2001). It will be used to estimate rupture area.

$$A = 8.9 \times 10^{-16} \times M_0^{\ 2/3} \tag{6}$$

where A is the rupture area in km^2 and M_0 is the seismic moment in dyne-cm.

Boore and Atkinson (1987) indicated that constant-stress model appears to be supported by CENA data. Following this idea, the constant-stress model is used in this work. The shear wave velocity β in SWWA was found around 3.91km/s (Dentith et al. 2000), which is used in this study.

Because no magnitude conversion relation that is specifically for SWWA earthquakes is available, a popularly used conversion relation for CENA earthquakes (Hanks and Kanamori 1979) is used in this study. It has the form

$$Log_{10} M_0 = 1.5M_w + 16.05 \tag{7}$$

where M_0 is the seismic moment and M_w is the moment magnitude. This conversion relation was also used in Hao and Gaull (2004). There is no reliable relation between M_L and M_w for SWWA. For the magnitudes below its saturation point (M_L 6.5), M_L and M_w are almost equivalent. However, more accurate estimation of equivalent M_w and M_L is needed in the future.

The rise time was computed using Equation (8) of Somerville et al. (1993).

$$T = 1.72 \times 10^{-9} \left(M_0\right)^{1/3} \tag{8}$$

where T is rise time in sec.

Simulation

The Green's function method has been cited many times in its application to simulation of large earthquakes from smaller ones, such as Sinadinovski et al. (1996); Frankel (1995); Joyner and Boore (1986), Sinadinovski et al. (2005). For SWWA events, the validity of the method will be verified by comparing the simulated and recorded motions in SWWA. The two events used for the comparison were the 1979 M_L 6.2 Cadoux earthquake that was recorded near Meckering, 96 km distant and the 1990 M_L 5.5 Meckering event that was recorded near Dowerin, some 78 km distant.

Hao and Gaull (2004)'s stochastic model was firstly used to simulate events of M_L 4.5 with the same epicentral distances as those events used for comparison. The Green's Function empirical method with modifications from Irikura et al. (1997) was then used to increase the magnitude of these simulated M_L4.5 events to M_L5.5 and M_L6.2 respectively. Figures 2 compare the FFT spectrum of the simulated with the recorded ground motion time histories. These simulated ground motions agree well with the recorded motions.

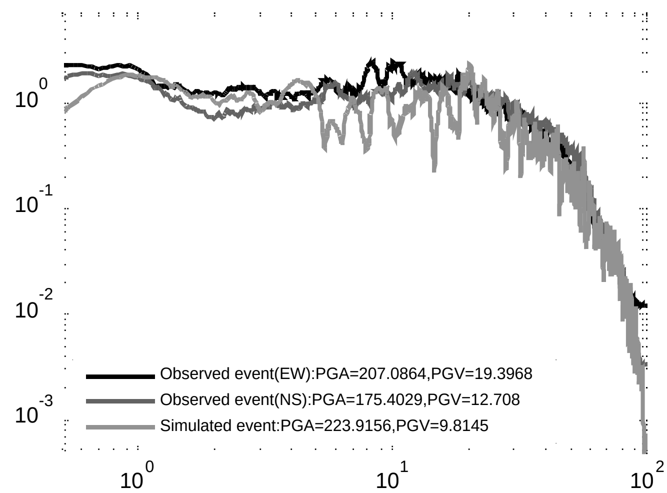

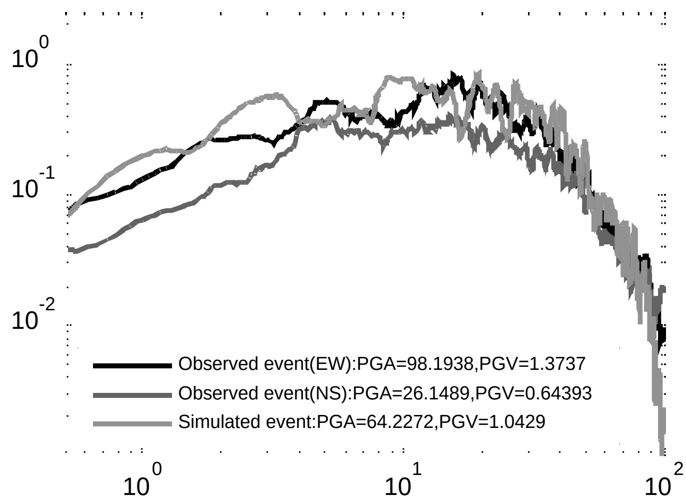

a b

Fig. 2 FFT of the simulated and recorded ground motions (a. M_L 6.2, epicentral distance 96 km, b. M_L 5.5, epicentral distance 78 km)

It should be noted that simply summing small events, as the original Green's function method, with delay time will underestimate low-frequency signal. The modified slip function proposed by Irikura et al. (1997) effectively overcomes this problem. The two simulated motions agree well with the recorded motions in a wide frequency band, as shown in Figures 2.

Table 1. The peak value of the observed record and simulated record

	1979 Cadoux event, M_L 6.2, 96km		1990 Meckering event, M_L 5.5, 78km	
	Observed record	Simulated record	Observed record	Simulated record
PGA (mm/s^2)	191.25	223.92	62.17	64.23
PGV (mm/s)	16.06	9.81	1.38	1.04

The peak values of the observed record and simulated record are shown in Table 1. It should be noted that the substantially larger PGV value of the recorded M_L 6.2 event may be caused by an abnormal low-frequency peak in the recorded time history at about 0.8 Hz, as shown in Figure 3. Because this record was hand digitised, the scope for anomalous low-frequency data is increased.

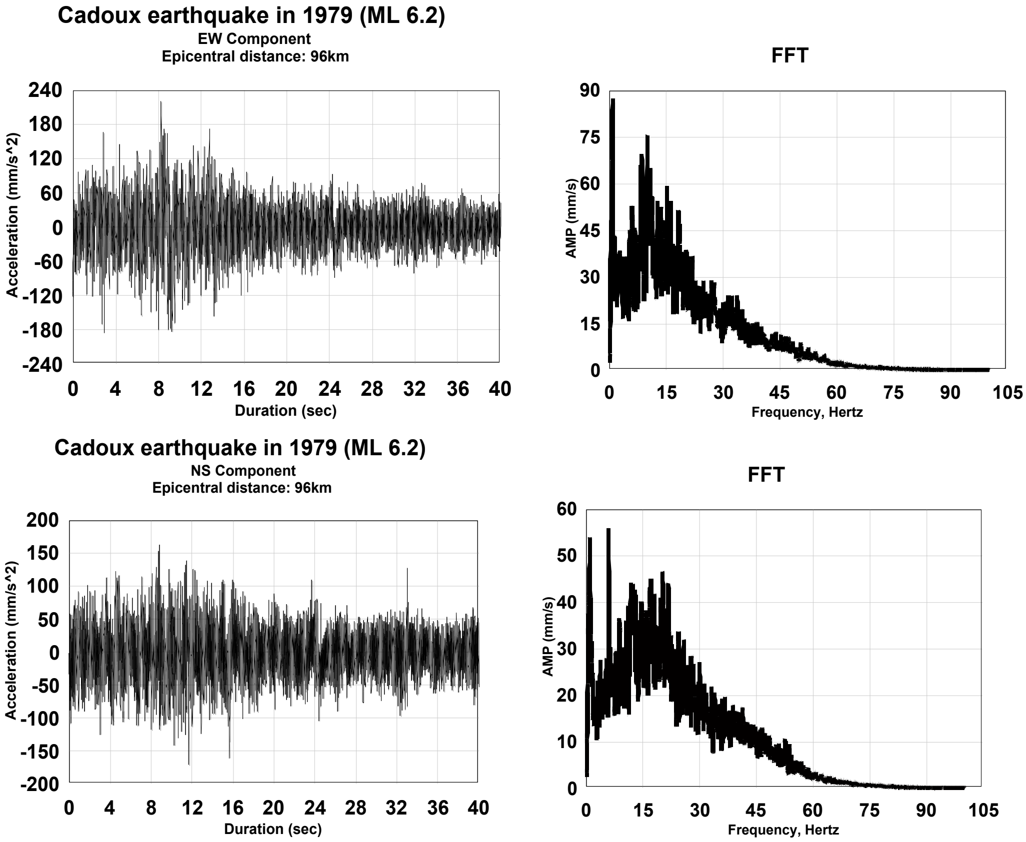

Fig. 3 Time history and FFT of the Cadoux earthquake in 1979

The exact reason why this record has a double peak is not known. It is believed that this low-frequency peak is not the normal free-field ground motion. Other than this significant difference between the simulated and recorded PGV of the M_L 6.2 event, the simulated peak values agree well with the recorded motions. Unfortunately, there is no other record to further verify the validity of the simulation method. This method will be used in further study to simulate ground motions.

Conclusions

This paper presents a method that combines empirical Green's function and stochastic model for strong ground motion simulation. The main conclusions of the study are as follows.

1. By comparing the model with the recorded data of the two earthquake events in SWWA, this method, with the assumption of constant-stress scaling, was proved to be suitable as most of simulated curves fit well against the curves of observed records.

2. Although some parameters referred from ENA data because of limited study of the parameters of the source in SWWA, we still can find satisfaction in the simulation result.

3. Matching the longer periods is also possible if enough data are available for all range of depths. However, there are too few data from large earthquakes in WA to prove that this scaling is correct over the entire magnitude range.

4. It is suggested that this method with these parameters can be used in further study to simulate ground motions that will be added to the SWWA database.

References

Aki, K., Scaling laws of seismic spectrum, J. Geophys. Res., 72, 1217-1231, 1967.

Atkinson, G.M., and D.M. Boore, Ground motion relations for eastern North America, Bulletin of the Seismological Society of America, 85, 17-30, 1995.

Atkinson, G.M., and D.M. Boore, Some Comparisons Between Recent Ground Motion Relations, Seismological Research Letters, 68, 24-40, 1997.

Boore, D.M., Stochastic simulation of high frequency ground motion based on Seismological Models of Radiated Spectra, Bull. Seismol. Soc. Am., 73, 1865-1894, 1983.

Boore, D.M., Simulation of ground motion using the stochastic method., Pure and Applied Geophys., 160, 635-676, 2003.

Boore, D.M., and G.M. Atkinson, Stochastic prediction of ground motion and spectral response parameters at hard-rock sites in Eastern North America, Bull. Seismol. Soc. Am., 77, 440-467, 1987.

Brune, J.N., Tectonic stress and spectra of seismic shear waves from earthquakes, J. Geophys. Res., 75, 4997?009, 1970.

Dentith, M., V. Dent, and B. Drummond, Deep crustal structure in the southwestern Yilgarn Craton, Western Australia, Tectonophysics, 324, 227-255, 2000.

Frankel, A., Simulation strong motions of large earthquakes using recordings of small eathquakes: the Loma Prieta mainshock as a test case, Bull. Seism. Soc. Am., 85, 1144-1160, 1995.

Gaull, B.A., Attenuation of strong ground motion in space and time in southwest Western Australia, in Ninth WCEE, Tokyo-Kyoto, pp. 361-388, Japan, 1988.

Gaull, B.A., and M. Michael-Leiba, Probabilistic earthquake risk maps of southwest Western Australia, BMR Journal of Australian Geology and Geophysics, 10, 145-151, 1987.

Hanks, T.C., and H. Kanamori, A moment magnitude scale, Journal of Geophysical Research, 84 (B5), 2348-2350, 1979.

Hanks, T.C., and R.K. McGuire, The character of high-frequency strong ground motions, Bull. Seis. Soc. Am., 71 (6), 2071-2095, 1981.

Hao, H., and B. Gaull, Prediction of seismic ground motion in Perth Western Australia for engineering application, in Proceedings of the 13th World Conference on Earthquake Engineering, pp. paper no. 1892, Vancouver, Canada, 2004.

Irikura, K., Prediction of strong acceleration motion using empirical Green's function, in Proc. 7th Japan Earthquake Engineering Symposium, pp. 151-156, 1986.

Irikura, K., T. Kagawa, and H. Sekiguchi, Revision of the empirical Green's function method by Irikura (1986), Programme and Abstracts, Seismol. Soc. Jpn., B25., 2, 1997.

Joyner, W.B., and D.M. Boore, On simulating large earthquakes by Green's-function; Addition of smaller earthquakes, 37 Geophysical Monograph of American geophysical union, WashingtonD.C., USA, 1986.

Kanamori, H., and D.L. Anderson, Theoretical basis of some empirical relations in seismology, Bull. Seismol. Soc. Am., 65, 1073-1095, 1975.

Kennedy, J., H. Hao, and B. Gaull, Earthquake Ground Motion Attenuation Relations for SWWA, in AEES, Albury, 2005.

Sinadinovski, C., H. Hao, and B. Gaull, Spectral Response of Recorded and Simulated Strong Ground Motion in Southwest WA, in AEES, Albury, 2005.

Sinadinovski, C., K.F. McCue, M. Somerville, T. Muirhead, and K. Muirhead, Simulation of intra-plate earthquakes in Australia using Green's function Method: Sensitivity Study for Newcastle event, The Australian Earthquake Loading Standard; Proceedings of the Australian Earthquake Engineering Society; Adelaide, Paper No. 11, 1996.

Somerville, P., N. Collins, N. Abrahamson, R. Graves, and C. Saikia, Ground motion attenuation relations for the central and eastern United States, in Final report, the U.S. Geological Survey, 2001.

Somerville, P., K. Irikura, S.Sawada, Y. Iwasaki, M. Tai, and M. Fishimi, Spatial Distribution of Slip on Earthquake Fault, in Proc. 22 JSCA Earthquake Engin. Symp., pp. 291-94(in Japanese), 1993.

Toro, G.R., N.A. Abrahamson, and J.F. Schneider, Model of Strong Ground Motions from Earthquakes in central and Eastern North America: Best estimates and Uncertainties, Seismological Research Letters, 68, 41-57, 1997.

New Adelaide earthquake monitoring network

David Love

Primary Industries and Resources South Australia

Project funding

This project was funded under the National Disaster Mitigation Programme. Funding of $210,000 was received from the Commonwealth, SA Water, SA Dept Premier and Cabinet, and Primary Industries and Resources SA. The network is under construction now, and is expected to be finished by the end of the year.

Objectives

- Provide rapid epicentre and magnitude estimates
- Provide strong motion information
- Collect data for attenuation analysis
- Improve hypocentre accuracy
- Record more seismicity around Adelaide
- Provide amplification information

The network is essentially divided into two parts; the regional sites and the metropolitan sites.

The regional part consists of seven sites being established around Adelaide up to 110 km away from the city (Figure 1). These sites are installed on rock, and transmit data continuously to Adelaide via phone, wireless broadband, mobile phone or radio. Cultural noise, rock and communications are the main determinants in positioning the stations. With seven well positioned stations it is hoped to get good automatic epicentres for any events within or near the network. Five of these sites are new, with ADE (Figure 7) and SDAN being complete upgrades of sites already in use.

The metropolitan part (Figure 2) consists of three recorders which will be installed for one to two years before being moved to another site. These sites may not transmit continuously back to the central office if it is not easy to arrange communications. Security is the main determinant for these stations. It is hoped to record some events to estimate amplification effects at least in the elastic range. The equipment is enclosed in a small cabinet (Figure 6) that is connected to a large paver which is pegged to the ground (Figure 5) to stop it moving in case of a large event. The seismometer is buried alongside or underneath the paver. One site is planned for Lefevre Peninsula, to the north west of the city, which is considered to have the softest and deepest sediments of the metropolitan area, along with much important infrastructure.

The equipment being used consists of Echo recorders from Environmental Systems and Services, each with an internal accelerometer, and recording onto 1Gb Compact Flash cards. There are two Guralp 30 sec (6T) seismometers; one installed at ADE, and the other for the metro area. The remaining seismometers are Guralp 1 sec (6T-1) instruments. Communications equipment being used includes: CDMA 1x modems (which use very low power, and are only moderately expensive to run), Echo internal modems (also low power, but limited to telephone sites), standard short hop wireless radios that are popular on home ADSL connections, and RFI 9265 digital radios for ADE. Wireless broadband is proposed for the site on Yorke Peninsula. The 3G network that Telstra has just opened may improve communication options.

A computer has been set up at the PIRSA / DWLBC office at Glenside. Data from the various sites will be received here. The ADE site will transmit directly by radio to Glenside. The analogue UTT site also transmits to Glenside where it is digitised. A spare equipment set will be installed in a small courtyard in the building. This will ensure that when there is a broadband or internet disruption, data from three stations should still be available. The office is a single storey building of reasonably modern construction, a few kilometres from the city.

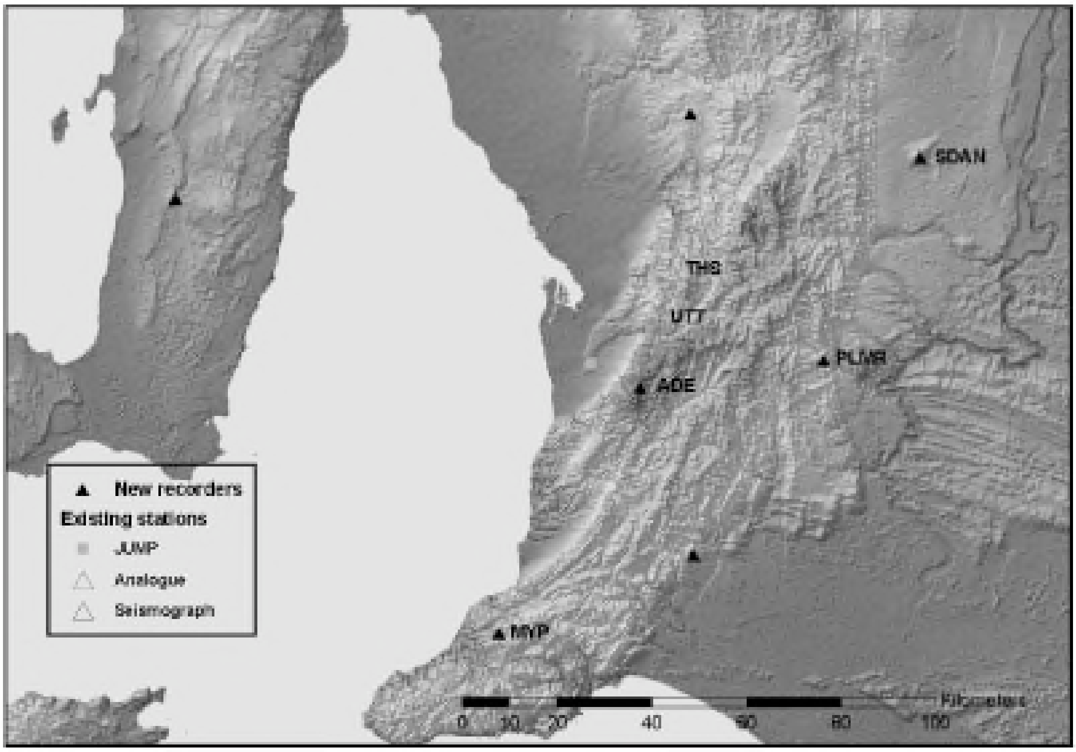

Figure 1 Regional network

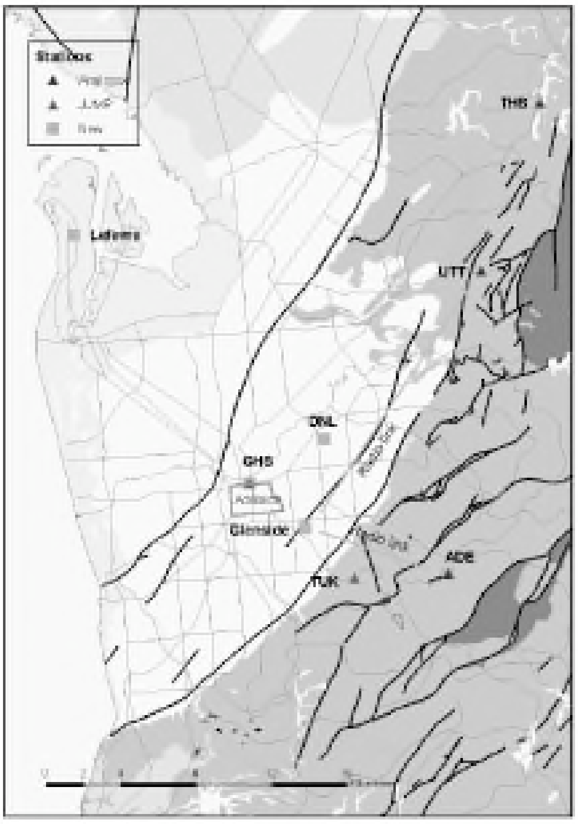

Figure 2 Metropolitan area in detail

Figure 3 Site PLMR

Figure 4 Site MYP

Figure 5 Metropolitan site

Figure 6 Equipment cabinet

Figure 7 Site ADE

Earthquake patterns in the Flinders Ranges - Temporary network 2003-2006, preliminary results

David Love[1], Phil Cummins[2], Natalie Balfour[3]

[1] Primary Industries and Resources South Australia
[2] Geoscience Australia
[3] University of Victoria, Canada

Objectives

The Flinders Ranges region of South Australia is an area of high topographic relief and high seismicity. This, combined with the fact that several faults identified in the Flinders and Mt. Lofty Ranges region have relatively high Quaternary slip rates (Sandiford, 2004), indicates this is a region of pronounced neotectonic activity. However, we have a very poor understanding of what relationship exists, if any, between the earthquakes and faults. Similarly, because the tectonic stress field in this part of Australia is poorly determined (Hillis and Reynolds, 2000), we do not have a clear understanding of the relationship between the stress field and active faults.

The Flinders Ranges region also exhibits high heat flow (Cull, 1982; Neumann et al, 2000), which would suggest a shallow seismogenic crust, and yet earthquake hypocentres, albeit often highly uncertain, indicate that seismicity extends to lower crustal depths. Finally, this high heat flow and the unique crustal structure of the underlying Adelaide Fold Belt may lead to propagation characteristics of earthquake waves that differ from other parts of Australia.

During the period September 2003 – June 2005, a temporary seismograph deployment was established in the Flinders Ranges region, consisting of about 18 stations spaced at roughly 30 km intervals. Among the questions about the Flinders Ranges region which this deployment was intended to address were:

- Which faults are seismically active?
- What is the depth of the seismogenic crust?
- Is the earthquake ground motion similar to other parts of Australia?
- How can the regional stress field be characterised?

It was felt that this area would provide an excellent opportunity to answer such questions, since there were likely to be a sufficient number of earthquakes, plenty of exposed rock for good waveform recording, and easy access to useful recording sites.

Deployment

The equipment was provided by ANSIR, GA and PIRSA. It consisted of:

- Broadband (30sec) 3D Guralp seismometers with Reftek recorders (8)
- 1Hz 3D Guralp seismometers with Kelunji D recorders (4)
- Various 1D and 3D seismometers and accelerometers with Kelunji D and Classic recorders.

It also used data from permanent analogue and digital recorders in the area that are part of PIRSA's permanent seismograph network. Most recording was at 100 samples per second, with a few stations recording at 200sps. All of the temporary stations recorded continuously.

From September 2003 to June 2005 there were up to 18 digital recorders installed from Burra to slightly north of Hawker. It was clear that a considerable number of events were happening at the northern end of this network, so from June 2005 to June 2006 eight recorders were installed further north from Hawker to Blinman. Various equipment problems were encountered and at any one time a number of recorders could be expected to be not running, and in general data return was about 75% (see Figure 1). Data displayed here are up to June 2005.

Preliminary results and interpretation

Over 500 locatable earthquakes were recorded within the network and surrounding areas, with over 250 having 8 or more defining phases. These were located using model SH01 (Shackleford & Sutton, 1981). The largest event was magnitude 3.9, with three others above magnitude 3 within the network. There were very few foreshocks and aftershocks during the recording time. Figure 2 shows the data recorded during the survey in black, with error ellipses (2σ), along with the complete database (1840 – present) in grey. It is clear that many hypocentres, especially when recorded by too few stations, have large errors involved. Using the error ellipses and other calculation data, we removed events that had a large semi-major axis or large areas, significant depth error (or no depth), and a small number of recordings or large angular gap. The remaining 289 better quality locations are plotted with elevation in Figure 3 and with solid geology, mapped and interpreted faults and axial trends in Figure 4.

Closely spaced portable deployments give more accurate data, and more accurate data are more likely to lead to a better understanding of earthquake occurrence. It is clear that the new data exhibit a much tighter pattern of epicentres than has been visible before. There is far less scatter than in the existing database.

There are indications of some earthquake clustering within the area, which are outlined in Figure 4. In the south is a quite strong curvi-linear feature (1), in the north there is a cluster of activity (2), and in between there are indications of curvi-linear features (3). The first feature runs at an angle to the topography (Fig 3) and does not match any mapped fault. The second feature is in an area which is folded and faulted in more than one direction, giving the interesting topographic shape of Wilpena Pound. The final year of data may improve this area. The remaining features are not well defined.

Interestingly, while epicentre patterns are emerging from what was previously a diffuse dataset, there is still no clear match with topography, mapped faults or geology. The recording undertaken is one of the best for local earthquakes that has yet been carried out in the country. The area has been well mapped, and has moderate to excellent geological exposure when compared to other parts of the country. If we cannot find a match in this region then should we be trying to force a direct match between earthquakes and mapped faults in other areas? The answers are likely to be more complex, or related to other data, and perhaps we should not jump to simple conclusions. To date there is no deep seismic reflection line across the region. This would be helpful.

The hypocentres have a range of depths from surface to about 24kms. If this is also the situation nearer Adelaide then it probably has implications for earthquake hazard. There is some indication of the deeper epicentres being nearer the centre of the ranges, with shallower events predominating near the sides of the ranges. This shape has been shown previously, (Greenhalgh & Singh 1988) but earlier depth results could not be relied upon due to the wide separation of permanent stations.

Focal mechanisms and stress inversion

Stresses can be estimated from focal mechanisms, but this requires that enough 1st motion picks are available for each individual event, and using the estimation of uncertainties is problematic. A better approach is to use the 1st motion data directly, because even events with too few first motions to determine a focal mechanism can contribute to the estimation of stress, and the estimation of uncertainties is more straightforward.

We used the MOTSI (Abers & Gephart 2001) stress inversion code which calculates the stress tensor from first motions rather than focal mechanisms. Many stress inversion algorithms use focal mechanisms directly and therefore do not account for mispicked first motions or a number of focal mechanisms for a set of first motions. MOTSI uses the standard Wallace (1951) and Bott (1959) hypothesis that slip on a fault plane occurs in the direction of maximum shear stress and the additional assumption that all motion on faults within a specified volume of crust are due to the same stress tensor. Motsi uses a grid search technique to estimate the four stress parameters; the maximum compressive stress (σ_1), the minimum compressive stress (σ_2), the intermediate compressive stress (σ_3) and the stress ratio (R). It also searches for focal mechanisms that best fit the first motion data and optionally the stress. A search is performed over a grid of fault planes and identifies for each event the focal mechanism that best fits the first motion data and avoids those that are inconsistent with the stress model. Uncertainties in the stress model are dependent on the data distribution and probability of mispicked first motions.

We selected 95 events that fitted our selection criteria, which were that each event have 5 or more clear first motion arrivals and have a reasonable variety of polarities and take-off angles. We weighted the first motions so that the clearly impulsive first motions had a weight of 2 and other first motions had a weight of 1. Nodal picks and emergent arrivals were not included in the inversion. All first motion picks were thoroughly reviewed so that we could minimise the probability of a mispick, as the MOTSI code includes it as a source of error. We used a 10 degree grid search for the stress orientations and a 0.1 increment search of R.

The chosen best solution for the stress inversion shows a predominantly reverse faulting regime as σ_1 is near horizontal and σ_3 is near vertical - the trend and plunge of the σ_1 and σ_3 principal stress directions are 101 and 18 degrees, and 344 and 55 degrees, respectively.

The future

Further detailed analysis and interpretation is required. Location review, and the use of relative relocation techniques such as double-differencing techniques are likely to improve hypocentres so that the validity or otherwise of proposed structures is clearer. Work on attenuation and stress inversion is in progress. It is possible that further focal mechanisms may be produced. There are also data available from teleseismic arrivals for tomographic and receiver function analysis.

It is clear that the survey would have been improved by a greater number of recorders, including extra recorders outside the area of interest, and also a greater density of recorders. When the number of running recorders drops, the reliability and accuracy reduction can quickly make the data of little value for validating features.

References

Abers, G. & Gephart, J., 2001. Direct inversion of earthquake first motions for both the stress tensor and focal mechanisms and application to southern California, J. geophys. Res., 106, 26 523–26 540.

Cowley, W.M., 2006. Solid Geology of South Australia. South Australian Department of Primary Industries and Resources. Mineral Exploration Data Package 15 (version 1.1)

Cull, J., 1982. An appraisal of Australian heat-flow data. Bureau of Mineral Resources Journal of Australian Geology and Geophysics, 7 pp. 11-21.

Greenhalgh, S.A. and Singh, R., 1988. The seismicity of the Adelaide Geosyncline, South Australia. Bull. Seis. Soc. Am. Vol 78, pp 243-263.

Hillis, R., and Reynolds, S. (2000). The Australian stress map, J. Geol. Soc. London, Vol 157, pp 915-921.

Neumann, N., Sandiford, M., and Foden, J., 2000. Regional geochemistry and continental heat flow: implications for the origin of the south Australian heat flow anomaly. Earth and Planetary Science Letters, 183 pp. 107-120.

Sandiford, M. (2002). Neotectonics of south-eastern Australia: linking the Quaternary faulting record with seismicity and in situ stress, Geol. Soc. Australia Special Publication, Evolution and dynamics of the Australian Plate, Vol 22, pp 101-113.

Shackleford, P. R. J., and Sutton, D. J. (1981). A first interpretation of crustal structure in the Adelaide Geosyncline in South Australia using quarry blasts, J. Geol. Soc. Australia, Vol 28, pp 491-500.

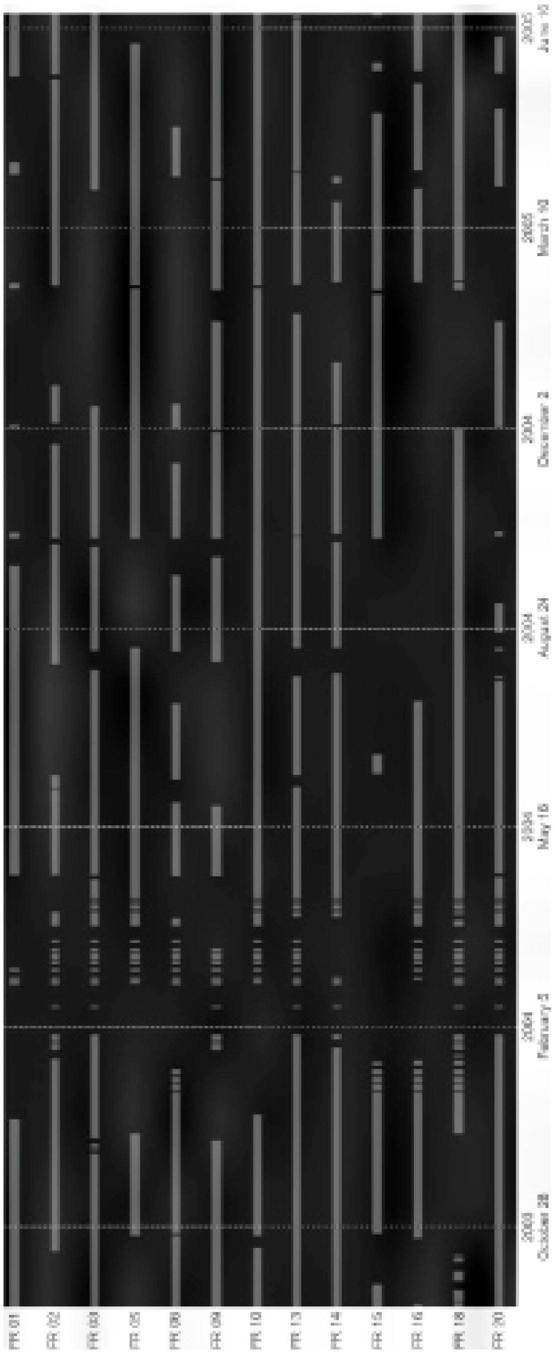

Figure 1 Data completeness

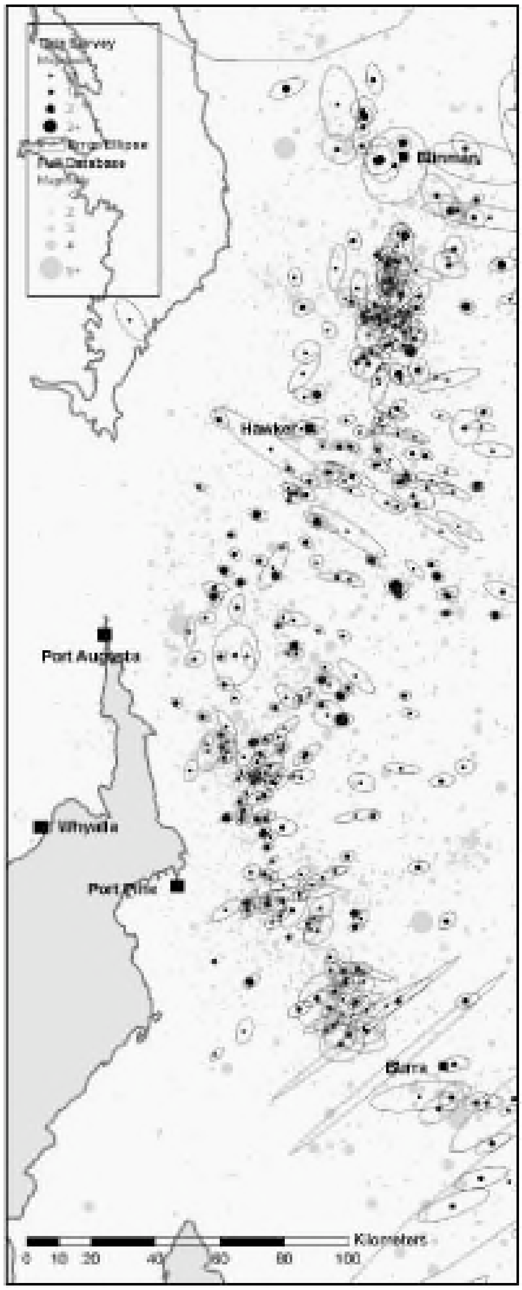

Figure 2 Full database and all data from current survey

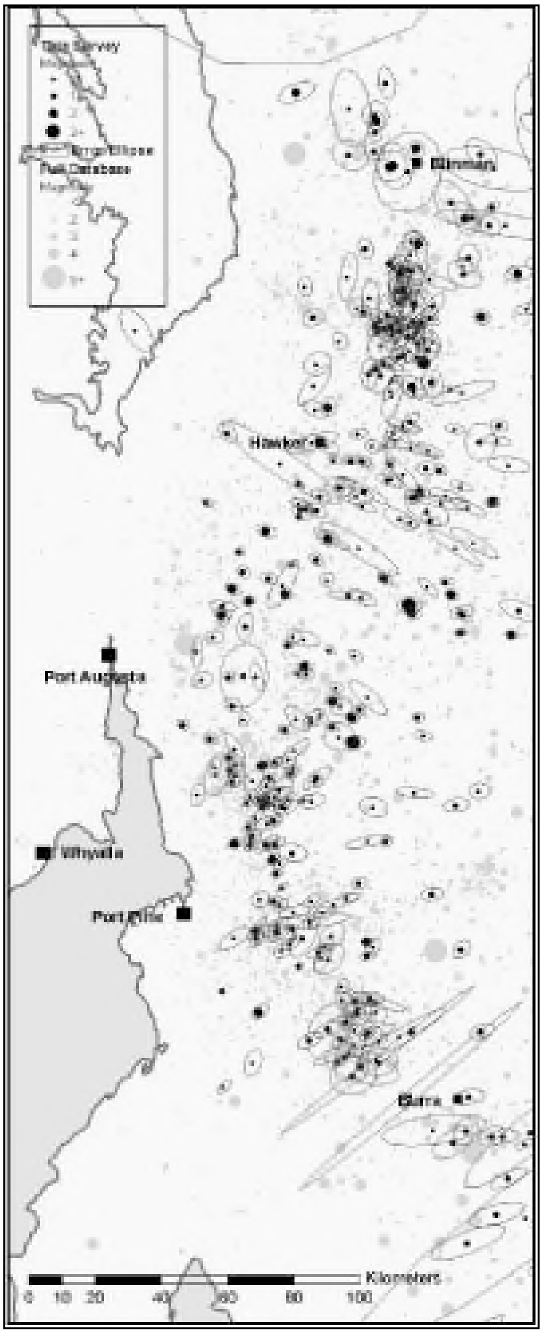

Figure 3 Accurate data from current topography.

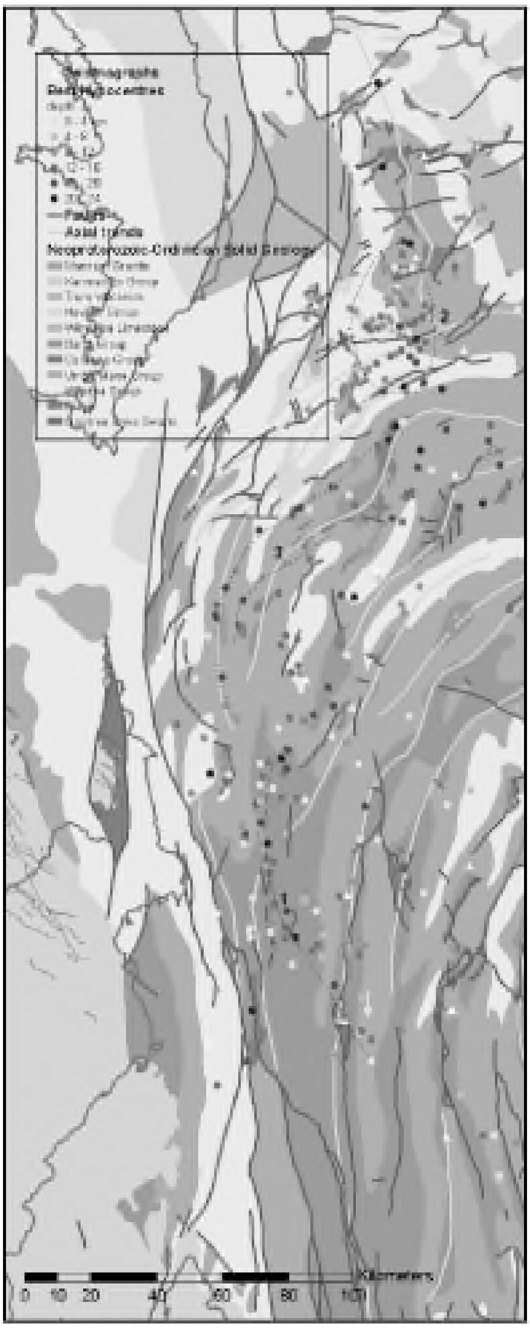

Figure 4 Accurate data from current survey survey with solid geology, trends and faults

Remote triggering of earthquakes in intraplate Australia

Kevin McCue

Australian Seismological Centre

Introduction

As early as the 1960s, Professor Sam Carey, University of Tasmania, had a student investigate the correlation of distant earthquakes with great earthquakes on the then 'Pacific Ring of Fire'. Ambraseys (1970) documented progressive step-by-step faulting on the North Anatolian Fault starting in 1939, each earthquake seemingly triggering the next earthquake to the west. Despite many observations of such occurrences worldwide, there was not general agreement that remote triggering existed (Wikipedia) until the magnitude M 7.3 Landers earthquake struck California on 28 June 1992 (http://www.data.scec.org/chrono_index/landersq.html). Nearby faults experienced triggered earthquakes (up to M 6.4), and minor surface rupture.

Hough and others (2003) report on observations of large earthquakes within North America triggering other earthquakes way beyond the source area out to perhaps 2000 km and within a few hours or days of the triggering event. They suggest that remotely triggered earthquakes occur preferentially in regions of recent and/or future seismic activity and that therefore, faults are at a critical stress state in only some areas.

Analogous observations of triggering in Australia have been observed over the last few decades and are reported here for the first time in response to the paper by Hough and others (2003). They do not always support the possibility suggested by Hough and others (2003) that the triggered events may be limited to areas of past or future seismic activity.

The 2004 Great Sumatran earthquake caused remarkable gravitational changes (tectonic movements) throughout the world detected for the first time by satellites of the Gravity Recovery and Climate Experiment, or Grace.

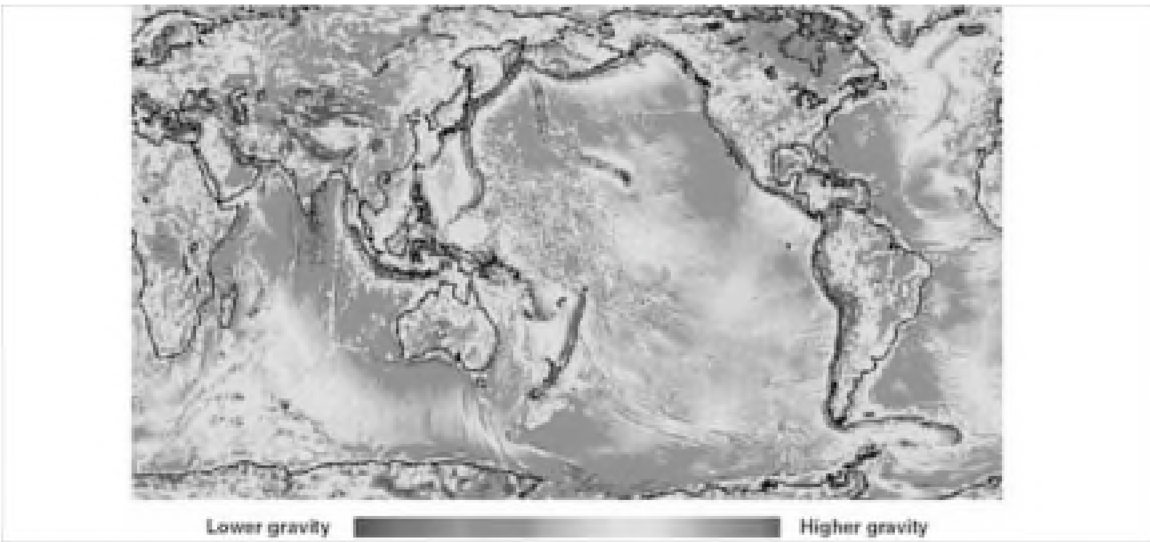

Gravity fluctuations (less than one-thousandth percent of the Earth's total gravity) detected by Grace and published by Kenneth Chang in Science.

The Australian experience

Observations have been made over the last four decades of remote triggering of earthquakes in Australia by some large intraplate earthquakes and great earthquakes on the Australian Plate boundary though never published. Here are two:

- The 1988 Tennant Creek earthquake sequence consisted of three large earthquakes in a 12 hour period on 22 January 1988. Their magnitudes were Mw 6.3, 6.4 and 6.7, equivalent in energy release to one Mw 6.8 event and together they produced a 35 km long surface fault (Jones and others, 1991). Hardly 5 days had passed when three earthquakes between magnitude ML 4.6 and 5.0 occurred near Marble Bar WA about 1300 km to the west of Tennant Creek. Another week later a magnitude ML 5.7 earthquake occurred in WA at Doubtful Bay about 1000 km NW of Tennant Creek. On 10 March an ML 4.3 earthquake occurred near Katherine NT about 600 km to the north, all the while a prolific sequence of aftershocks was shaking Tennant Creek.
- On 23 May 1989 a great magnitude Mw 8.2 earthquake fractured the Macquarie Ridge along the Pacific/Australian plate boundary. This earthquake was felt 2000 km away at Hobart, Tasmania in southeast Australia. Reports of the shaking were still being phoned in from Tasmania as the pen on an analogue short-period seismograph in Canberra traced out the coda of 20s period surface waves, when seismologists had an unexpected call from southern Queensland that an earthquake (presumed to be the earthquake) had been felt in the pub in Hungerford, 3000 km from Macquarie Island. It turned out that a magnitude ML 4.0 earthquake had occurred near the town whilst the surface waves were still passing through. Within five days a magnitude Ms 5.7 earthquake struck Katajuta in the Northern Territory and aftershocks at Tennant Creek NT intensified starting with a magnitude ML 5 earthquake on 11 June. On 26 June a magnitude 4.4 earthquake occurred in the Flinders Ranges SA.

On their own these events would not have rated a mention but taken together and shortly after a significant earthquake, one intraplate (b in table 1) , the other interplate (a in table 1) it seems clear that they were triggered in some way by the earlier event. An example of a great earthquake that did not trigger intraplate earthquakes (c in table 1) is also tabulated below.

Table 1 Triggering and triggered earthquakes in Australia

Date	Origin Time	Lat º	Longº	M	Distance	P%	Place
Tennant Ck earthquake (a)							
1988 01 22	0036	-19.81	133.98	6.3			Tennant Creek NT
1988 01 22	0357	-19.83	133.98	6.4			Tennant Creek NT
1988 01 22 T	1205	-19.84	133.99	6.7			Tennant Creek NT
1988 01 28	0146	-21.05	119.60	4.8	1510		Marble Bar WA
1988 01 28	0149	-21.05	119.60	4.6	1510		Marble Bar WA
1988 01 28	0156	-21.05	119.60	5.0	1510	2	Marble Bar WA
1988 02 06	0523	-16.18	124.51	5.7	1085	<1	Doubtful Bay WA
1988 03 10	1415	-14.64	130.71	4.3	675	12	Katherine NT
Macquarie Is earthquake (b)							
1989 05 23T	1054	-52.34	160.57	8.3			Macquarie Island
1989 05 23	1208	-28.84	143.98	4.0	2950	7	Hungerford Qld
1989 05 28	0255	-25.25	130.65	5.7	3920	<1	Katajuta NT
1989 06 11	1452	-19.86	133.94	5.0	4280	10	Tennant Creek NT
1989 06 26	1118	-31.48	138.58	4.4	2925	>70	Flinders Ranges SA
Balleny Islands earthquake (c)							
1998 03 25	0312	-62.88	149.71	8.0			Balleny Is

T is the triggering event. M is magnitude, either Mw or ML. P is the probability (%) based on logNc/yr = 5.3 – M (McCue, 1993) that an event of this magnitude would (a) happen in the time period since the triggering event within this distance from Tennant Creek or (b) that it would occur anywhere in Australia in the time period after the Macquarie Island event. Case (c) no triggered events were observed.

Discussion

Analogous observations of triggering in Australia have been observed over the last few decades and are reported here for the first time in response to the paper by Hough and others (2003). Only one of the thirteen large plate-boundary earthquakes in the Australian region triggered earthquakes in intraplate Australia. No large earthquakes have since occurred in the triggered–event region, nor have smaller earthquakes been limited to those areas. Triggered earthquakes in Australia do not support the possibility suggested by Hough and others (2003) that the triggered events may be limited to areas of past or near future seismic activity and that therefore, faults are at a critical stress state in only some areas. The triggered events at Tennant Ck were as she would have predicted.

References

Ambraseys, N.N., 1970 — Some characteristic features of the North Anatolian fault zone. Tectonophysics, 9, 143 – 165.

(http://en.wikipedia.org/wiki/Remotely_triggered_earthquakes)

http://projects.crustal.ucsb.edu/NAF-SAF-2006/DIRistanbul/abstract_Hough.pdf#search=%22remote%20triggered%20earthquakes%22

Hough, S.E., Seeber, L., and Armbruster J.G., 2003 - Intraplate Triggered Earthquakes: Observations and Interpretation. Bulletin of the Seismological Society of America, Vol. 93, No. 5, pp. 2212–2221.

Jones, T. McCue, K.F. Denham, D. Gregson, P. Bowman, R., & Gibson, G. 1991 — Three large intraplate earthquakes near Tennant Creek, Northern Territory on 22 January 1988. BMR Journal of Australian Geology & Geophysics, 12, 4, 339 – 344.

McCue, 1993 — Seismicity and Earthquake Hazard in Australia. in Wilson & van Doorn (Eds.) Earthquake Engineering and Disaster Reduction, AEES Conference, Melbourne 1993 pp 9-14.

Appendix: Great earthquakes in the Australian region since 1980

Source	Year	Mo/Day	Time	Lat	Long	Depth	Ms	M Msource
PDE	1980	07 17	194223.20	-12.525	165.916	33 N	7.9	8.0 UKBRK
PDE	1989	05 23	105446.32	-52.341	160.568	10 G	8.2	8.0 MSBRK
PDE	1995	04 07	220656.89	-15.199	-173.529	21 G	8.0	8.1 MSBRK
PDE	1996	02 17	055930.55	-0.891	136.952	33 N	8.1	8.2 MwHRV
PDE	1998	03 25	031225.07	-62.877	149.527	10 G	8.0	8.8 MeGS
PDE	1998	11 29	141031.96	-2.071	124.891	33 N	7.7	8.3 MeGS
PDE	2000	06 04	162826.17	-4.721	102.087	33 N	8.0	8.3 MeGS
PDE	2000	06 18	144413.31	-13.802	97.453	10 G	7.8	8.0 MeGS
PDE	2000	11 16	045456.74	-3.980	152.169	33 N	8.2	8.2 MSBRK
PDE	2000	11 17	210156.49	-5.496	151.781	33 N	8.0	8.2 MSBRK
PDE	2004	12 23	145904.41	-49.312	161.345	10 G	7.7	8.1 MwHRV
PDE	2004	12 26	005853.45	3.295	95.982	30 G	8.8	9.0 MwHRV
PDE	2005	03 28	160936.53	2.085	97.108	30 G	8.4	8.6 MwHRV

An ongoing role for intensity data in Australia

Kevin McCue

Australian Seismological Centre

Abstract

Some may think that with an extensive network of seismographs and a slowly expanding number of accelerographs, there is no longer any reason to investigate the felt effects of earthquakes past or present in Australia. Limited evidence presented here of past and recent earthquakes demonstrates that felt reports and intensity data are still useful for hazard studies in Australia.

An early earthquake?

On 22 January 1988 between local noon and midnight a series of three large earthquakes shook residents of the small town of Tennant Creek in the Northern Territory. Most buildings in the town, including the local hospital, suffered considerable non-structural damage but remarkably little real damage considering the size and proximity of the three events, rated Mw6.3, 6.4 and 6.7. A 35km long, 2m high fault scarp was formed during the earthquakes.

Have such earthquakes happened near Tennant Creek before? What does the historical record tell us? Extensive study of the 19th century pre-seismograph record continues slowly but surely in Australia, mainly through the examination of old newspapers. One contemporary report has provided the following table:

27 August 1883, earthquake at ~10 am local time		
Place	*Distance*	*Effects*
Daly Waters	390km N Tennant Ck	Explosion like blasting and vibration
Alice Springs	450km S Tennant Ck	two distinct explosions
Sheep camp (9miles W Alice Springs)	15km W Alice Springs	ditto
Undoolya	15km E Alice Springs	ditto

The authors of this report of Committee No 1 of the Australasian Association for the Advancement of Science included eminent scientists Biggs, Ellery, Russell, Todd and Hogben. They assigned the terse felt reports Rossi-Forel Intensity 3 which is equivalent to Modified Mercalli (MM) intensity 3. Given the time of day this assigned intensity may be on the low side.

Daly Waters and Alice Springs are almost equidistant north and south of Tennant Creek so an earthquake midway between them could have caused the effects. The authors mention that Daly Waters was struck by another earthquake at about midnight the previous day, sufficient to wake the sleepers (McCue, 2001).

The date however seemed familiar. Rynn et al. (1987) report on a large Queensland earthquake on 29 August 1883 (local date) and mentioned the eruption of the volcano Krakatoa in Indonesia, disavowing any connection as postulated in the media at the time. Wikipedia says: The volcano began erupting around 19 June. At about 1pm (local time) on 26 August, the volcano went into its paroxysmal phase. On 27 August, the volcano entered the final cataclysmic stage of its eruption. Four enormous explosions took place at 5:30 a.m., 6:42 a.m., 8:20 a.m., and 10:02 a.m. The worst and loudest of these was the last explosion. Wikipedia also reports that: the explosion was heard in Perth, WA.

It seems safe to conclude that the widespread felt effects in the Northern Territory in this case were associated with the Krakatoa eruption and not a local earthquake as previously postulated (McCue, 2001).

Sites of known large earthquakes, such as Tennant Creek, have been assigned higher hazard in the Australian Loading Code (AS1170.4) than those where there is no evidence of current or previous seismicity. We should still be cautious of accepting the alternative suggestion that sites of large recent earthquakes are relatively less hazardous.

A detective study unveils an aftershock

The following reports were published in an undated contemporary Newspaper (possibly the Adelaide Advertiser). This extract of the relevant page was provided by the SES coordinator for Mt Gambier, Greg Malseed, during AEES2004 in Mt Gambier.

> EARTH TREMORS AT MOUNT GAMBIER – An earth tremor, which, in certain parts of the town, appears to have been of greater severity than in others, occurred at Mt Gambier at about half past ten on Thursday evening. Bottles, window frames, etc, rattled considerably, while in one or two cases small articles were thrown down, and the tremor was accompanied by a rumbling noise. Another tremor is reported at half-past twelve on Friday night, and three hours later, at half past three, a further shock, slight but unmistakable, was experienced, there being perceptible oscillating motion of the ground as well as the peculiar rumbling noise previously noted. Tremors were also felt at Burrungull, Millicent, Beachport, Lucindale, Kingston and Robe, and at Harrow, across the Victorian border.
>
> MILLICENT
>
> (from our own correspondent) June 7.
>
> On Thursday evening about 10:30 we had a pretty sharp shock of earthquake, which lasted several seconds. The shock awoke several, so from this its force may be estimated. It is reported that another shock was felt on Friday.

As to the date: the year was obtained from other articles in the same newspaper extract describing the coming diamond jubilee of Queen Victoria. She was crowned in 1837 and the diamond anniversary is 60 years. Under one column was the sub-heading Monday June 7, and in 1897 June 7 was indeed a Monday. The local time 10:30 pm, based on longitude, corresponds to about 13:00 UTC (Standard time had not yet been introduced into Australia).

Yet a third article in the newspaper extract may be interpreted as implying that this earthquake was more widely felt in Victoria than just at Harrow (and is interesting because it refers to an earlier undocumented damaging earthquake that ought to be investigated further).

> THE FIRST EARTHQUAKE – An impression has prevailed (says the Hamilton Spectator) that the earthquake recently experienced was the first of any importance remembered in Victoria, but this is altogether erroneous. ….. The oldest colonist Mrs Stephen Henty remembered when residing at Portland, a very similar earthquake occurring there late in February or early in March 1837….. First came a noise like subterranean thunder then followed the rocking motion of the house in which the flooring boards of hardwood were seen to part and the soil from below to protrude through the seams. This was succeeded by a fall-down of plaster ……

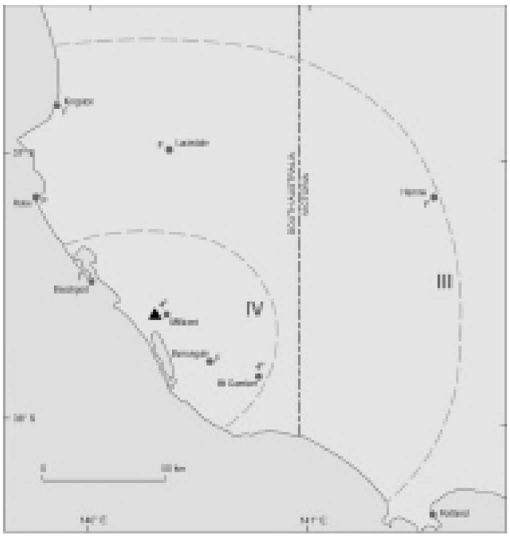

Intensities were assigned from the newspaper reports and plotted in the figure opposite. There are few points on the resultant map, and at most places we only know that the tremor was felt, but the intensities at Mt Gambier and Millicent can be estimated at MM IV to V (people awoken, things fell off shelves). The fact that at least one of the small aftershocks was felt in both Mt Gambier and Millicent supports a location near these towns. That it was felt in western Victoria and along the Limestone Coast of South Australia justifies the empirical magnitude (McCue, 1980) determined from the felt area as ML 4.9, surely an under-estimate!

This earthquake with its own small aftershock sequence turns out to have itself been an aftershock of the large Kingston-Beachport earthquake, magnitude ML ~6.5 on 10th May 1897, for which an isoseismal map was compiled in the early 1970s (McCue, 1975).

A recent micro-earthquake in the ACT - 3 October 2003

Small earthquake stirs suburbs in inner South was the headline of the Sunday Canberra Times on 5 October 2003. The article went on to report: residents of Forrest and Deakin reported hearing loud explosions as an earth tremor shook parts of Canberra yesterday morning.

DATE:	3 OCT 2003
TIME:	22:25:10 UTC
MAGNITUDE:	1.4 ML(I)
LOCATION:	35.326° S, 149.107° E
DEPTH:	3±1 km

Nearly two months passed before the author made a concerted effort by phone and a newspaper appeal to try to outline the felt area since only five reports were emailed to Geoscience Australia. ACT Police did not keep any written records because there was no damage despite the hundreds of calls they received. Confirmation that the source was an earthquake was of more than passing interest to ACT emergency services personnel who were investigating the possibility of an explosion at an embassy or consulate. Most of the diplomatic offices and residencies are concentrated in the inner south suburbs of the National Capital.

Several Deakin residents, retired geologists with BMR, reported that there was a big bang, houses shook and windows rattled violently, dogs stopped barking for a minute and a TV nearly fell on the floor from a cabinet. One reported that small ornaments and tables moved about 10 cm, implying a good intensity MM4. Another Deakin resident and his wife felt a bump and heard a thump and they wondered if a hot-air balloon had landed on the roof. The dishes rattled and they checked the house to make sure the verandah hadn't fallen off! A family member in bed did not feel a thing.

A Garran resident was woken by the loud thump and thought something under the house had fallen down. An ANU Professor of Geophysics and resident of Hughes heard a bang but thought it was thunder, not an earthquake (rated MM2) whilst a former BMR seismologist, recognised that the sharp shock he heard in Griffith was a small earthquake (MM3-).

Another Griffith resident, in bed, heard a loud thump and thought her husband had had a fall in the kitchen (MM2). He, getting breakfast, didn't feel it.

The centre of the isoseismal map is about 3km south of the epicentre computed by Geoscience Australia and under Red Hill in the Canberra Nature Park. This is about 1km from the surface trace of the Deakin Fault mapped by Abell (1991). He identified 5km of sinistral slip with considerable vertical movement but the dip direction is not marked so the earthquake cannot definitely be attributed to movement on the Deakin Fault.

An accelerogram was recorded in the basement of nearby Parliament House (PHB on the map) and a strong Rg phase indicated that the focus was between 1 and 4 km deep. Security staff at Parliament House did not feel the earthquake.

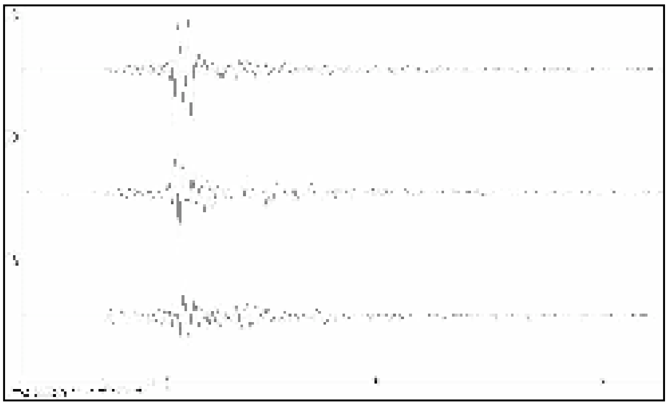

Accelerogram recorded at Parliament House (PHB) Canberra, 3 October 2003

This shallow depth supports the intensity map location rather than the seismograph location which is poor due to the lack of ACT seismographs and the geometry of GA's regional stations (the closest three are co-linear and only one of them within 100 km of Canberra).

Some Australian cities are not well monitored for earthquakes or terrorist explosions. The National Capital unfortunately is one of them as the evidence presented above demonstrates.

Conclusion

Historical felt reports of earthquakes are particularly important in Australia because of the very short instrumental and written record here. The contemporary reports of ground shaking and audible noise in Tennant Creek and South Australia in the 19th century are our only record of possible seismic activity there prior to installation of seismographs. Later research can add value to the earlier interpretations, either by establishing locations and magnitudes of these events, or discounting entirely their seismic origin, as in the case of the 1883 Tennant Creek 'earthquakes'. The more modern example from Canberra convincingly demonstrates that there are circumstances when the best epicentral location can be obtained from felt intensity reports even in this age of digital seismology. Moreover, with few accelerograms available of moderate to large earthquakes, these data are vital for verifying ground motion models. Indeed this is recognised in the US by the US Geological Survey who have invested considerable effort and resources to produce near-real time felt intensity maps on their web site (http://earthquake.usgs.gov/dyfi).

References

Abell, R.S., 1991 Geology of the Canberra 1:100,000 Sheet area. BMR Bulletin 233, page 88.

McCue, K.F., 1975. Seismicity and seismic risk in South Australia. University of Adelaide, Report ADP 137.

McCue, K.F., 1980. Magnitudes of some early earthquakes in south-eastern Australia. Search, 11(3), 78-80.

McCue, K.F., (compiler) 1996. Atlas of isoseismal maps of Australian earthquakes Part 3. AGSO Record 1995/44.

McCue, K.F., 2001. Do large earthquakes recur in Australia? in AEES Newsletter 3/2001 p 7.

Rynn, J.M.W., Denham, D., Greenhalgh, S., Jones, T., Gregson, P.J., McCue, K.F., and Smith, R.S., 1987 Atlas of isoseismal maps of Australian earthquakes Part 2. BMR Bulletin 1987/222.

An improved understanding of earthquake ground-shaking in Australia

Andrew McPherson and Trevor Allen

Geoscience Australia

Abstract

In the past two years, Geoscience Australia has made significant progress in improving our understanding of earthquake ground-shaking in Australia. This research has culminated in the development of two preliminary products - an Australian-specific Ground-Motion Prediction Equation (GMPE) and the first national-scale site classification map of Australia.

Using a scenario based around the 1989 Newcastle earthquake, we demonstrate how these new products can refine our estimates of ground-shaking in Australia compared to what could be achieved in the recent past. In particular, comparisons are drawn against the previous practice of employing GMPEs derived elsewhere (primarily North America) without any detailed consideration of site response.

These models, and in particular, the site classification map, will assist in identifying regions that may be more vulnerable to severe earthquake ground-shaking. These capabilities are important in aiding land use planning and building code development, and, following a large earthquake, the rapid assessment of affected areas for prioritisation of emergency response. The products will also assist risk modellers to produce more reliable loss and damage estimates for scenario events.

Introduction

The devastating 1989 Newcastle earthquake, which claimed 13 lives and caused over $4.3 billion damage (IDRO, 2006), poignantly demonstrated that Australian communities are not immune to the effects of earthquakes. Ironically, our comparatively stable tectonic setting means that, for a given sized event, earthquake impact in Australia has the potential to be greater than in more active regions since both communities and engineered structures are more vulnerable to strong ground-shaking.

Predicting the level of ground-shaking at a given distance from an earthquake rupture is dependent upon three key elements; (1) the magnitude and frequency content of the earthquake source; (2) how earthquake energy attenuates through the crust; and (3) how near-surface regolith modifies the observed ground motions. The first two of these elements are integrated in a Ground-Motion Prediction Equation (GMPE), while the third is represented in a site response model. The combination of these two models provides a fundamental tool for assessing earthquake hazard.

The acquisition of high quality Australian earthquake ground motion data, development of improved numerical simulation techniques and the first national-scale Australian site response model now permits Australian-specific earthquake hazard analyses. Improved prediction of earthquake ground-shaking potential in Australia provides critical decision support information for planners and emergency managers involved in disaster mitigation. It also has potential implications for revisions of Australian Standards and Building Codes.

Ground-motion

A new ground-motion attenuation model has been derived for the southeastern Australian (SEA) crust, obviating or reducing the need to invoke analogues from other settings e.g. eastern North America (ENA). The new model is based on finite-fault stochastic simulations of ground-motion, calibrated by earthquake source and path characteristics from recorded Australian ground motions. These numerical methods have particular utility in stable continental regions such as Australia, where records from larger magnitude earthquakes are not available to develop empirical GMPEs.

The new Australian GMPE is based on recorded data from southeastern Australia, where, due to the development of much of the nation's infrastructure and higher than average seismicity, the seismograph network is well-developed. Inputs to the stochastic simulations employ source and path parameters derived from the empirical studies of Allen et al. (in review). The stochastic finite-fault software package, EXSIM, (Motazedian & Atkinson, 2005) is used to simulate spectral ground-motions for moment magnitudes over a range of M 3.0 to 7.5. The simulated spectra are then regressed to obtain model coefficients (Allen et al., in prep.).

Site response

Regolith, the layer of weathered rock, unconsolidated sediments and/or soils that overlie bedrock, can contribute significantly to the amplification (or de-amplification) of earthquake ground-motions. Modelling the potential impact of earthquakes on the built environment therefore requires an understanding of the behaviour of the regolith when subjected to an input bedrock motion. Significantly, many of Australia's major urban population centres are built on alluvial plains or coastal margins; environments characterised by appreciable thicknesses of regolith. In general such areas can be considered to have a relatively high vulnerability to earthquake ground-shaking when compared to bedrock sites. In these environments where outcropping bedrock does not predominate, earthquake hazard determined as 'hazard on rock' is of limited applicability.

A first generation national scale site classification map based on modified National Earthquake Hazard Reduction Program (NEHRP) site classes (Building Seismic Safety Council, 2004; Wills et al., 2000) has been developed for Australia (McPherson & Hall, 2006) (Fig. 1). The map uses surficial geology and other available geoscientific data at a variety of scales to identify and group regolith materials likely to exhibit a similar response to earthquake ground-shaking. Shear wave velocity in the upper 30 m (Vs30), the key geophysical variable for assessing the response of regolith materials, is inferred from relationships between measured shear wave velocity and geological materials in California (Wills et al., 2000). There is a paucity of data available in Australia to quantify the regolith in three dimensions, particularly with respect to key geophysical properties. Thus mapped Australian geological information is used as a proxy for Vs30, and therefore to approximate the physical behaviour of materials in each site class. Modifiers for the classification have been developed to provide an estimate of the thickness and degree of weathering in bedrock-dominated units and the degree of consolidation in sedimentary deposits.

A series of generic geotechnical profiles from the Next Generation Attenuation Program in the USA (Silva, 2005) are applied to each site class in order to model and generate amplification factors for each site class.

For areas of Australia where local scale regolith information (including geological, geotechnical and geophysical data) are available, more detailed site classification and site response assessment can be achieved. However, in the absence of these more detailed data, the national site classification map now provides a first-pass estimate of site amplification due to site conditions anywhere in Australia.

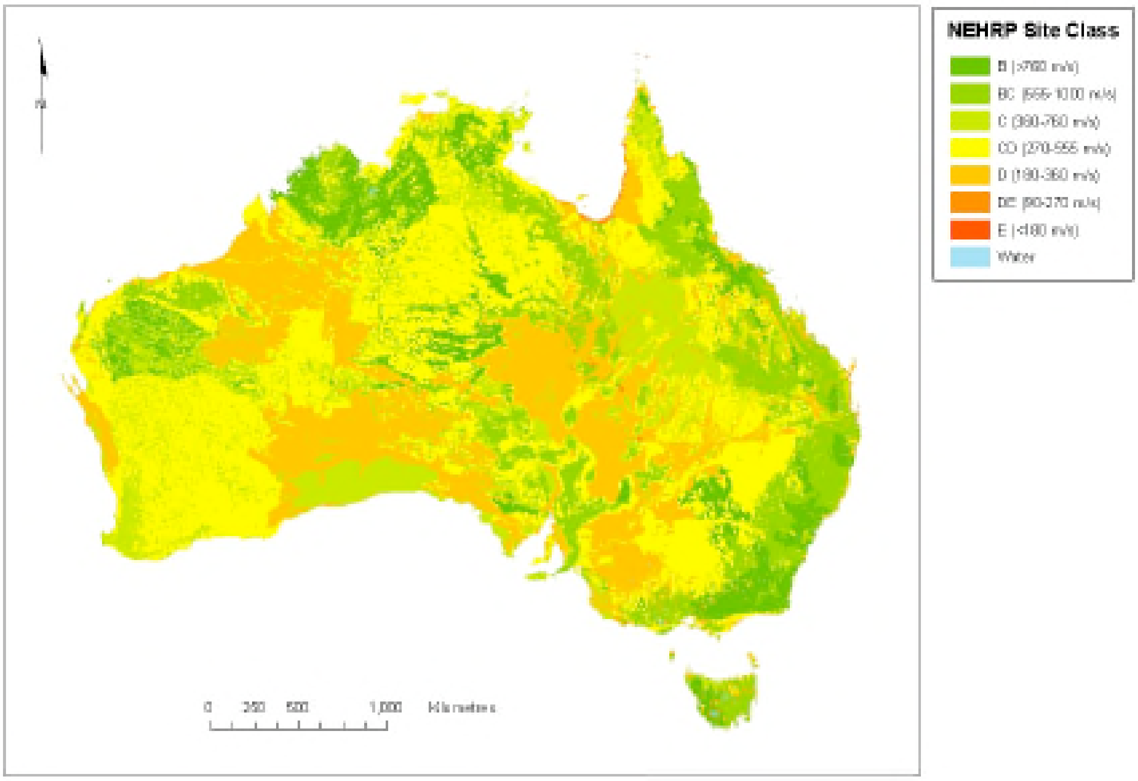

Figure 1. First generation national site classification map of Australia based on modified NEHRP site classes.

Modelling scenario - Newcastle 1989 earthquake

Using the moment magnitude M 5.4† Newcastle 1989 Earthquake as a scenario, we will demonstrate:

- differences in calculated ground-motion between ENA and SEA GMPEs; and
- the significance of modelling earthquake ground-shaking with and without the incorporation of site response information.

† Moment magnitude based on the empirical ML to M relations of AC Johnston (pers. comm. 2000).

Eastern North America (ENA) versus south-eastern Australia (SEA) ground-motion models

Until recently, predicting earthquake ground-motions in Australia relied on the application of GMPEs from elsewhere – principally the United States. Australia's first spectral GMPE (Allen et al., in prep.) has been developed using data from south-eastern Australia, an area previously considered by many to be analogous to the tectonically stable intra-plate setting of eastern North America (e.g. Dhu & Jones, 2002). Recent comparisons of recorded ground-motion data from each of these regions indicate that this assumption may not be so far from reality for short hypocentral distances less than approximately 100 km (Allen & Atkinson, 2006). However, following reinterpretation of ground-motion data from ENA, new ground-motion equations are now predicting lower ground-shaking for sites in this distance range (Atkinson, 2004; Atkinson & Boore, in review). Consequently, hazard and risk modellers should exercise caution when applying first generation ENA GMPEs to the Australian context.

The new SEA model (Allen et al., in prep.) compares favourably against new ENA GMPEs (Atkinson & Boore, in review), demonstrating similar long-period ground-motions at short distances from the earthquake rupture. The SEA model, however, predicts lower levels of short-period motion (and PGA) relative to the new ENA model (Fig. 2) (e.g. Allen & Atkinson, 2006).

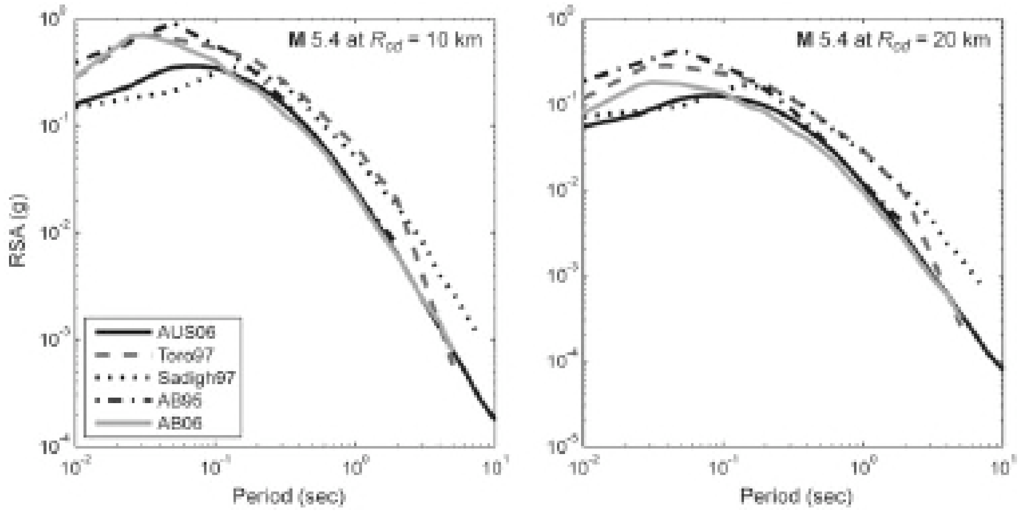

Figure 2. Comparison of the new SEA (AUS06) GMPE against several North American ground-motion attenuation models. The new SEA model demonstrates lower ground-motions over most periods relative to pre-2006 models. The new GMPE compares favourably with the Atkinson & Boore (in review; AB06) model at longer periods, but with lower levels of short-period (and PGA) motion.

Then and now: the current Australian earthquake hazard model

Figure 3 compares modelled earthquake ground-shaking potential employing the ENA ground-motion attenuation model of Toro et al. (1997) (Fig. 3a) against the latest Australian model (Allen et al., in prep) (Fig. 3b) for a scenario earthquake in the

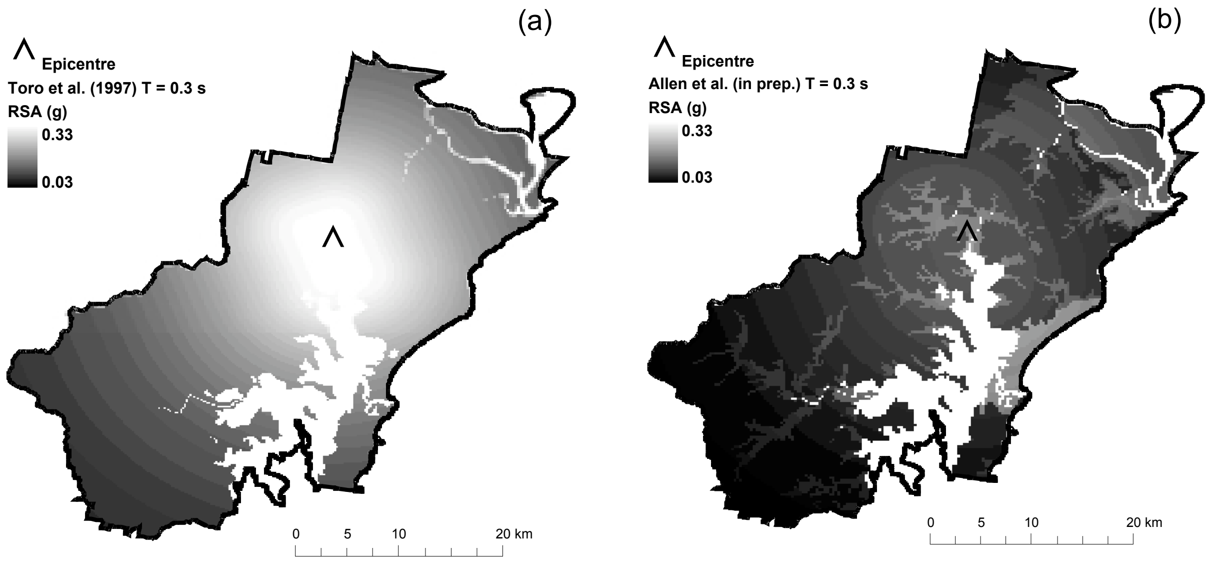

Figure 3. Comparison of earthquake hazard model output for the Newcastle region showing (a) previous capability employing an ENA attenuation model; and (b) present capability for SEA, employing the new southeast Australian ground-motion model in combination with the new national site response model.

Newcastle region. The SEA GMPE underpinning the latter model indicates significantly lower ground-motions relative to the ENA model, but also demonstrates the significance of incorporating regolith site response into earthquake hazard assessment. The addition of modelled site response information significantly enhances our ability to predict spatial variation in strong ground-shaking, a key factor in understanding and modelling the distribution of damage and loss. Despite allowing for increased amplification due to site response we observe lower overall ground-shaking.

Summary

A comparison of SEA and ENA GMPEs clearly demonstrates the importance of recording and modelling Australian-specific earthquake data. We observe that the SEA model predicts significantly lower ground-motions than the first generation of ENA GMPEs (e.g. Toro et al. 1997). Recent revisions of source and site parameters (i.e. stress drop and kappa) may act to increase ground motions between periods of 0.1-0.3 seconds. However, it is expected that levels of PGA will still be lower than predicted by ENA models. The effect of this on hazard is yet to be fully tested. At present the underpinning GMPE is strongly biased towards eastern Australia, and, as such, application of this method to the western and central regions of the continent would be inadvisable based on recent empirical ground-motion studies in Western Australia (Allen et al., 2006). However, the application of a national-scale site response model that can characterise the potential response of the regolith to ground-shaking anywhere in Australia further enhances our estimates of earthquake hazard nationally. In some circumstances invoking models from ‘analogous areas’, such as ENA, may be unavoidable due to a lack of Australian data. However, as demonstrated above, there is inherent risk in applying such models inasmuch as they may not accurately reflect Australian conditions.

We have presented the current methodology for earthquake hazard assessment in Australia. The products developed have particular application to emergency managers and planners for the purposes of disaster planning and potential implications for revision of the Australian Building Code and earthquake loading standard. They also have significant potential application in decision support tools for the rapid post-event assessment of earthquake-affected areas for prioritisation of emergency response.

References

Allen T. and G. Atkinson (2006). Comparison of earthquake source spectra and attenuation in southeastern Australia and eastern North America. Proceedings of the 2006 Australian Earthquake Engineering Society Conference, 24-26 Nov 2006, Canberra (this volume).

Allen, T.I., T. Dhu, P.R. Cummins, and J.F. Schneider (in prep.). Stochastic ground-motion prediction equations for southeastern Australia.

Allen, T.I., P.R. Cummins, T. Dhu, and J.F. Schneider (in review). Attenuation of ground-motion spectral amplitudes in southeastern Australia, Bulletin of the Seismological Society of America.

Allen, T.I., T. Dhu, P.R. Cummins, and J.F. Schneider (2006). Empirical attenuation of ground-motion spectral amplitudes in southwestern Western Australia. Bulletin of the Seismological Society of America, 96, 572-585.

Atkinson, G.M. (2004). Empirical attenuation of ground-motion spectral amplitudes in southeastern Canada and the northeastern United States. Bulletin of the Seismological Society of America 94, 1079-1095.

Atkinson, G. and D. Boore (in review). Earthquake Ground-Motion Prediction Equations for Eastern North America. Bulletin of the Seismological Society of America.

Building Seismic Safety Council (2004). National Earthquake Hazards Reduction Program (NEHRP) recommended provisions for seismic regulations for new buildings and other structures. Part 1: Provisions. prepared by the Building Seismic Safety Council for the Federal Emergency Management Authority, Washington D.C.

Dhu, T. and T. Jones (eds.) (2002). Earthquake Risk in Newcastle and Lake Macquarie. Geoscience Australia Record 2002/15. Geoscience Australia, Canberra. 271 p.

IDRO (2006). NSW Newcastle Earthquake December 1989. Insurance Disaster Response Organisation, URL: http://www.idro.com.au/disaster_list/default.asp.

Jones, T., M. Middelmann and N. Corby (compilers) (2005). Natural hazard risk in Perth, Western Australia. 2005. Canberra, Geoscience Australia - Australian Government.

McPherson, A.A. and L.S. Hall (2006). Site classification for earthquake hazard and risk assessment in Australia. Proceedings of the 2006 Australian Earthquake Engineering Society Conference, 24-26 Nov 2006, Canberra (this volume).

Motazedian, D. and G.M. Atkinson (2005). Stochastic finite-fault model based on dynamic corner frequency. Bulletin of the Seismological Society of America 95, 995-1010.

Sadigh, K., C.Y. Chang, J.A Egan, F. Makdisi, and R.R. Youngs (1997). Attenuation relationships for shallow crustal earthquakes based on California strong motion data. Seismological Research Letters 68, 180-189.

Silva, W.J. (2005). Site response simulations for the NGA project. Draft report prepared for the Pacific Earthquake Engineering Research Center by Pacific Engineering and Analysis, El Cerrito, CA.

Toro, G.R., N.A. Abrahamson, and J.F. Schneider (1997). Engineering model of strong ground motions from earthquakes in the Central and Eastern United States. Seismological Research Letters 68, 41-57.

Wills, C.J., M. Petersen, W.A. Bryant, M. Reichle, G.J. Saucedo, S. Tan, G. Taylor, and J. Treiman (2000). A site-condition map for California based on geology and shear-wave velocity. Bulletin of the Seismological Society of America 90 (6B), S187-S208.

Developing a seismotectonic model using neotectonic setting and historical seismicity

Application to central New South Wales

Dee Ninis and Gary Gibson

Seismology Research Centre (SRC), Environmental Systems and Services

Abstract

We present the methodology behind the development of a seismotectonic model that attempts to bridge the gap between models derived either from the (limited) historic record of seismicity, or high-resolution neotectonic models that consider only faults that are known to be active.

Detailed information regarding local geology, in particular relating to late Tertiary and Quaternary deformation, in combination with an updated catalogue of historical seismicity, were used to refine the AUS5 seismotectonic model for the central New South Wales region. Nearby major geological faults have been investigated in order to determine whether neotectonic activity is evident. Faults believed to have been active in recent geological time and that are consistent with the current stress regime have been assigned an estimated slip rate. A number of active faults have now been included in the model and several new zones have been introduced.

In comparison with the previous AUS5 model for the central New South Wales region, the resulting earthquake hazard estimates have decreased for sites furthest from faults. For sites close to faults identified as active, earthquake hazard estimates have increased, particularly for faults assigned a significant slip rate.

Introduction

Seismotectonic models are typically used for earthquake hazard assessments, by separating a region into sources of seismicity, commonly areas. These differ in characteristics such as earthquake recurrence rate, the relative number of small to large events, and the maximum credible magnitude earthquake - values based on data from catalogues of historical seismicity (Gutenberg & Richter, 1964; Cornell, 1968). Other models may consider only faults which are known to have been active in recent geological time. Both approaches, when considered independently, have limitations in their application.

As in any region, earthquake catalogues available for southeastern Australia are temporally and spatially limited. Prior to sensitive seismograph networks, earthquake locations were derived from felt reports. Thus, reported events were biased towards large earthquakes or those felt within populated areas. Seismograph networks in Australia now allow for some smaller and more remote earthquakes to be located. However, much of Australia remains poorly covered and network coverage varies with time and locality. Another concern is the period captured by current historic records, which is much shorter than the return period of moderate and large earthquakes in Australia, while emphasising the (misleading) effects of earthquake clustering. Consequently, historical earthquake seismicity is not necessarily a good indicator of earthquake hazard.

Neotectonic models consider those faults that are known to have been active in recent geological time, in particular the late Tertiary and Quaternary. These models aim to consider fault activity over the period of the present tectonic stress field, usually the last few million years, giving a more realistic indication of long-term seismicity, especially in regions of low seismicity such as Australia. Faults are normally deemed active if they exhibit a geomorphic expression, such as a scarp. However, modification of surface expressions over time, through ongoing geological processes such as erosion, may conceal a surface rupture or yield a scarp of non-tectonic origin. Also, many active faults can be blind faults that do not rupture the surface.

The AUS5 seismotectonic model defined by Brown and Gibson (2000, 2004) provided a national model over those models previously developed for Australia, particularly in southeastern Australia. The AUS5 model divides Australia into zones based on seismic activity and major geological boundaries, however the model for central New South Wales was based almost entirely on historical seismicity and included no active faults.

This paper outlines the process leading to the modifications to the AUS5 model for the central New South Wales region (Figure 1), using geological data and historical earthquake records in order to identify active faults as earthquake sources, and to improve the surrounding area sources accordingly.

Figure 1: Area of interest

Geological and seismic evidence of neotectonic activity

Initial investigations of neotectonic activity were based on previous geological and geophysical studies of the central New South Wales region. Published geological maps (eg. Raymond & Pogson, 1998; Morgan et al., 1999) indicate that a number of faults cross the central New South Wales region, many of which developed during deformation events of the Palaeozoic and Mesozoic (Scheibner & Basden, 1996). Of particular interest to this investigation were those major faults which align approximately north-south, consistent with the current east-west compressional stress experienced by central New South Wales (Hillis et al 1999; Clark & Leonard, 2002; Reynolds et al., 2002). Gravity and aeromagnetic geophysical data were also examined to identify any similarly oriented lineaments which may not be obvious in the outcrop geology.

The historic record of seismicity for the region was compared with the information obtained from published geological and geophysical investigations. Of relevance were zones of seismicity aligned approximately north-south, consistent with the current stress regime of central New South Wales. It was observed that a number of faults identified in the structural geology were, perhaps not surprisingly, associated with areas of high seismicity (relative to surrounding areas) with activity occurring under the up-thrown block of the fault, as expected with reverse faulting.

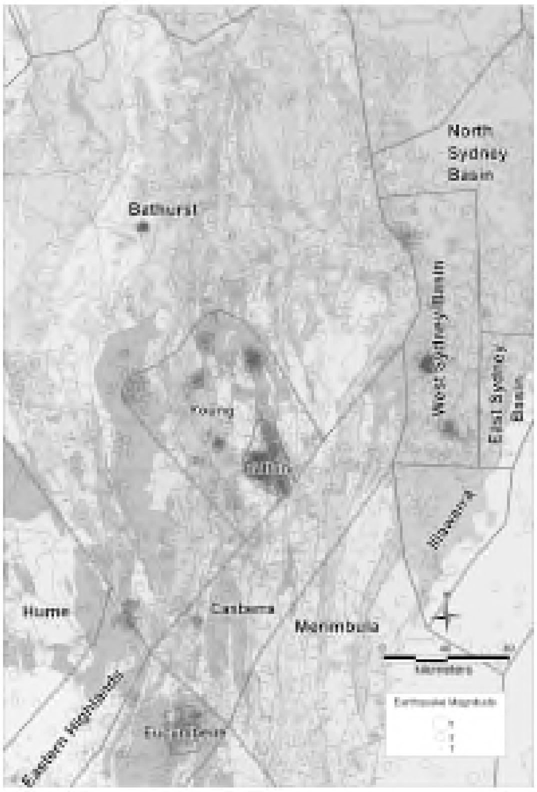

Figure 2: AUS5 model for central New South Wales – original.

A field investigation was conducted at a number of geological and geophysical lineaments in search of geomorphic features which may provide evidence of neotectonic activity. The ages of displaced geological units were used to interpret when these structures may have most recently been active. Given that the current stress field is assumed to have developed from about the late-Miocene (Sandiford et. al., 2004) any activity over the past 15 million years is significant.

It has been assumed that the current long-term rate of activity is best represented by deformation in the past one million years, during the Quaternary. Faults exhibiting evidence of neotectonic movement were assigned an average rate of slip (in metres per million years) based on vertical displacement estimated to have occurred during this time.

Faults that exhibited geomorphic evidence of seismic activity, such as vertical displacement visible as a scarp, were assigned a higher slip rate. Faults whose neotectonic activity could not be supported by geomorphic markers but which still aligned with higher levels of seismicity were assigned a lower slip rate.

Results, discussion & future work

As a result of this study, a percentage of seismicity previously assigned across the whole seismotectonic zone (Figure 2) has now been assigned to a number of faults within the zone (Figure 3).

The active faults are defined as three-dimensional sources – earthquakes of all magnitudes up to a maximum of M 7.5 can occur anywhere along the fault and to a depth of approximately 20 kilometres. The background seismicity has been reduced, but still incorporates seismic activity not associated with known faults.

Overall, earthquake hazard estimates for a site situated close to an active fault compute a higher hazard than a site far from an active fault.

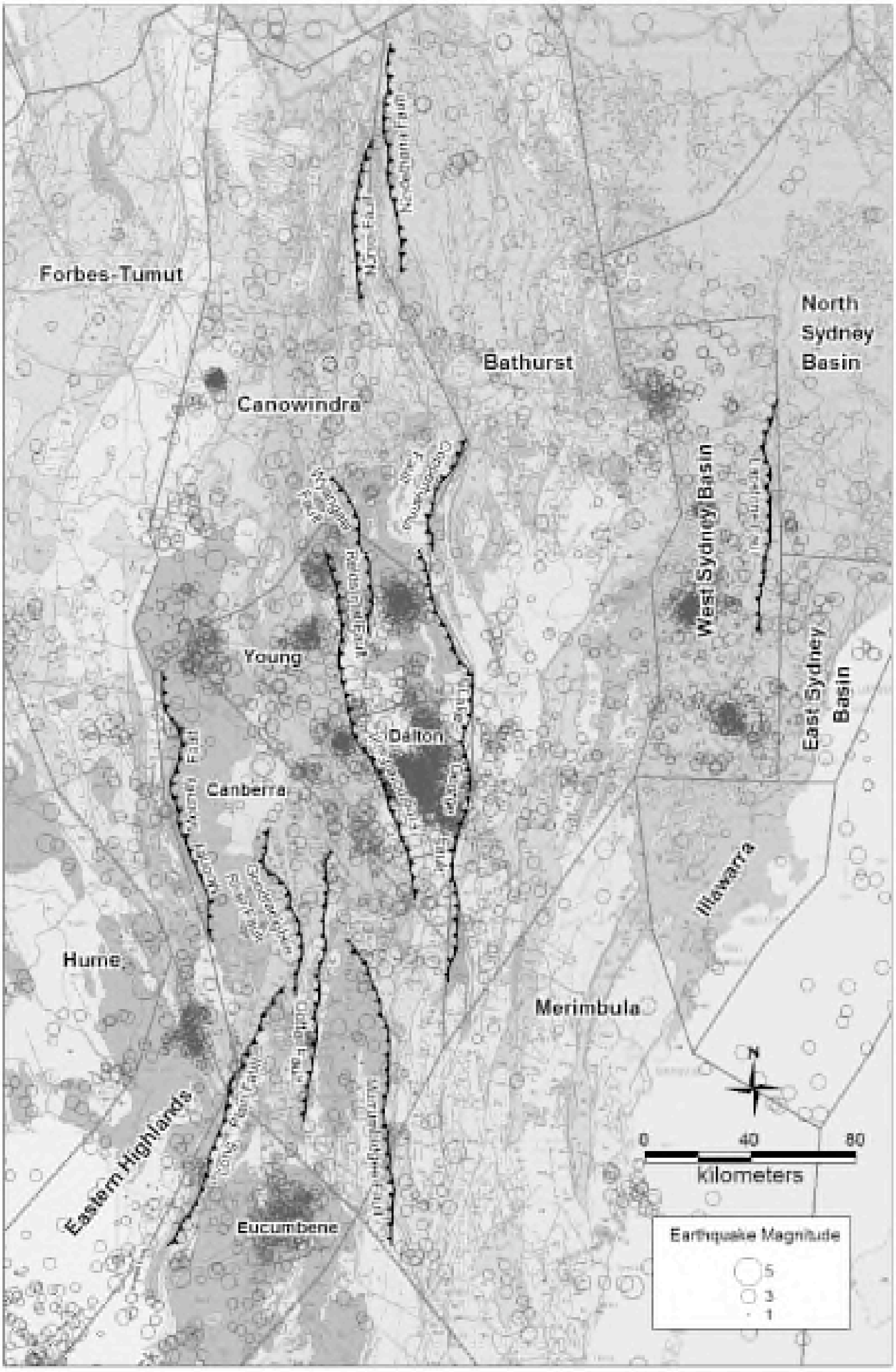

Figure 3: AUS5 model for central New South Wales – refined, showing faults now considered in seismotectonic model. Geology by Scheibner (1997).

Table 1: Faults included in the refined AUS5 seismotectonic model for central New South Wales, showing estimated slip rates.

FAULT	MECHANISM	LENGTH (km)	SLIP RATE (m/million yrs)
Long Plain	West dipping reverse	110	5
Mooney Mooney	East dipping reverse	110	5
Goodradigbee	West dipping reverse	70	5
Cotter	West dipping reverse	105	5
Murrumbidgee	West dipping reverse	122	5
Frogmore North Middle South	East dipping reverse	67 58 15	5 10 5
Wyangala	West dipping reverse	31	5
Reids Flat Thrust	West dipping reverse	35	5
Lake George North Middle South	West dipping reverse	61 59 51	10 15 5
Copperhannia	West dipping reverse	48	5
Nurea	East dipping reverse	63	5
Nindethana	East dipping reverse	90	5
Lapstone	West dipping reverse	92	30

At this stage fault slip rate values presented here (Table 1) are preliminary, influenced by available geological evidence and comparisons with other faults within the region that have better defined slip rates. The further quantification of activity along individual faults requires additional seismic and geological information. Accurately located earthquake hypocentres could be assigned to activity along a specific fault, allowing for magnitude recurrence estimates. Palaeoseismological studies could contribute information such as characteristic earthquake magnitude, frequency of occurrence, and displacement estimates likely to be produced along each fault.

Conclusion

Evidence of neotectonic activity gleaned from geological data has been compared with historical seismicity in order to locate active fault sources and to refine the area sources of the AUS5 model for central New South Wales. The original AUS5 seismotectonic model for this region was based almost entirely on historical seismicity and displayed limited correlation with the local geology.

A number of faults in the region have been assigned an estimated slip rate based on geomorphic evidence. As a percentage of earthquake activity has now been assigned to individual faults, the background seismicity of many zones has been reduced.

Overall, earthquake hazard has increased for sites located close to an active fault, and decreased for sites further from an active fault.

Acknowledgements

This study was funded by the New South Wales State Water Corporation as part of a major earthquake hazard assessment of a number of dams in their portfolio.

For information regarding the local geology we acknowledge the New South Wales Geological Survey, particularly Martin Scott and others at the Orange office. Thanks also to Paul Lennox and Lloyd White at the School of Biological, Earth and Environmental Sciences, University of New South Wales.

Sincere thanks to Trevor Allen and Dan Clarke for comments on the manuscript.

References

Brown, A. and G. Gibson, 2000: Reassessment of Earthquake Hazard in Australia. Twelfth World Conference on Earthquake Engineering, Auckland, New Zealand, February 2000.

Brown, A. and G. Gibson, 2004: A multi-tiered earthquake hazard model for Australia. Tectonophysics 390, 25-43.

Clark, D. and M. Leonard, 2002: Principal stress orientations from multiple focal-plane solutions: new insight into the Australian intraplate stress field. Geological society of Australia Special Publication 22, Chapter 7, 85-99.

Cornell, C.A., 1968: Engineering Seismic Risk Analysis. Bulletin of the Seismological Society of America 58, 5, 1583-1606.

Gutenberg, B. and Richter, C.F., 1964: Frequency of earthquakes in California. Bulletin of the Seismological Society of America 34, 185-188.

Hillis, R.R., J.R. Enever and S.D. Reynolds, 1999: In situ stress field of eastern Australia. Australian Journal of Earth Sciences, Vol. 46, 813-825.

Morgan E.J., R.G. Cameron, G.P. Colquhoun, N.S. Meakin, O.L. Raymond, M.M. Scott, J.J. Watkins, L.M. Barron, G.A.M. Henderson, J.P. Kryen, D.J. Pogson, A.Y.E. Warren, D. Wyborn, E.K. Yoo, R.A. Glen and E.A. Jagodzinski, 1999: Dubbo 1:250 000 Geological Sheet SI/55-4 (Second Edition). Geological Survey of New South Wales, Sydney / Australian Geological Survey Organisation, Canberra.

Raymond, O.L., D.J. Pogson et. al., 1998: Bathurst 1:250 000 Geological Sheet SJ55-8, Second Edition. Australian Geological Survey Organisation, Canberra / Geological Survey of New South Wales, Sydney.

Reynolds, S.D., D.D. Coblentz and R.R. Hillis, 2002: Tectonic forces controlling the regional intraplate stress field in continental Australia: Results from new finite element modeling. Journal of Geophysical Research, 107 (B7), doi: 10.1029/2001JB000408

Sandiford, M., M. Wallace and D. Coblentz, 2004, Origin of the in situ stress field in southeastern Australia, Basin Research 16, 325-338.

Scheibner, E. and H. Basden, Ed., 1996: Geology of New South Wales – Synthesis. Volume 1 Structural Framework. Geological Survey of New South Wales, Memoir. Geology 13 (19).

Scheibner, E., 1997: Stratotectonic map of New South Wales, 1:100,000. Geological Survey of New South Wales, Sydney.

Investigation of near source effects in array-based (SPAC) microtremor surveys

James Roberts and Michael Asten

Monash University

Abstract

Array-based methods for exploiting ambient seismic noise are receiving increasing attention in the literature, particularly for use in providing shear wave velocity profiles to assist with simulation of site-specific earthquake responses. Many of these microtremor methods - such as the spatial autocorrelation technique (SPAC) - operate under the fundamental assumption of plane wave propagation of surface waves. Although the SPAC technique has been successfully applied in urban areas, the effect of near-sources (and thus non-planar Rayleigh wave propagation) has received little attention. This paper explains the use of a simplified geometry-based modelling approach to compare near source effects for 4-station ("triangular") and 7-station ("hexagonal") arrays. Results of theoretical modelling and a field trial show that for near sources (3 array radii from array centre) with limited azimuthal range (1º source arc), the additional stations of the 7-station array mitigate near source effects whereas the SPAC spectrum for the 3-station array produces unreliable results.

Introduction

In recent times, the SPAC technique in particular has seen significant use in urban areas for a range of applications: (Apostolidis et al., 2004; Asten and Dhu, 2004; Asten et al., 2005; Bettig et al., 2001; Chavez-Garcia et al., 2005; Hartzell et al., 2005; Kudo et al., 2002; Roberts and Asten, 2004, 2005; Scherbaum et al., 2003; Wathelet et al., 2005). It is the relatively high level of (high frequency) microtremor energy present in urban areas that makes towns and cities attractive locations for microtremor surveys. In most of the literature, the sources contributing to the microtremor 'wave-field' are considered to be located at significant distance from the array, allowing for the assumption of plane-wave surface wave propagation. Near source effects in microtremor work have received little attention.

The consequences for microtremor measurements resulting from receivers being located close to the microtremor sources can potentially include three distinct effects: non-planar wavefront geometry, dominance of body wave energy rather than surface wave energy, and an increased likelihood for the presence of higher modes in the wave field. The latter two aspects are addressed in many studies associated with the (active) SASW and MASW techniques, eg. Xia et al., 2004, and are not addressed in this paper.

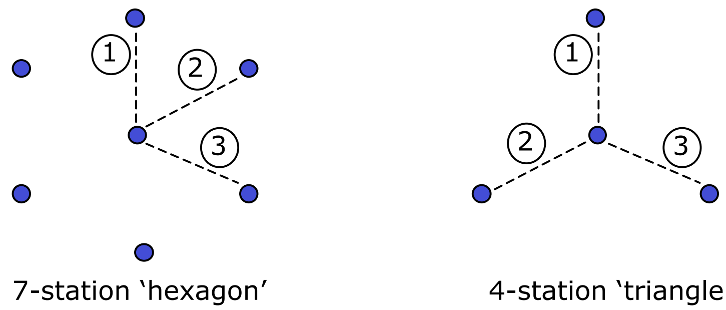

Figure 1: 7-station and 4-station array geometry. Although the 7-station array allows for better statistical averaging of ground motion, it samples only the same azimuths (defined by alignment of station pairs as indicated by the dashed lines) as an equivalent 4-station array.

Recent research by Okada (2006) compared the efficiency of 4-station (triangular) and 7-station (hexagonal) array geometries (Figure 1) for the far-field case. Professor Okada's results showed that the additional stations in the 7-station array configuration did not result in any analytical advantage in minimizing errors associated with only sampling a finite number of azimuths. This paper compares the performance of 4- and 7-station array geometry at a range of source distances.

Geometric modelling of SPAC spectra

The modelling approach adopted here is an extension of that used by Asten (2003; 2006) and Asten et al. (2004) for assessing the performance of differing array geometries in situations where microtremor sources are confined to a fixed range of azimuths. This approach uses a numerical summation of sources, with a single "source" for each 1º of source arc to be analyzed. Thus, continuous source arcs consisting of 1 to 360 sources can be placed in arbitrary positions around the array. For the near source modelling presented here, a further variable is added to the method described by Asten (2003), allowing the sources to be placed at a (finite) fixed distance from the array. This distance is defined in units of array radii (r) measured from the array centre.

The coherency ($\rho_{a,b}$) for a single pair of sensors (a and b) in the presence of an arc of identical sources producing monochromatic waves of wavenumber (k) could be calculated by a simple summation of the differences in phase of each source at each of the sensor positions:

$$\rho_{a,b} = \frac{1}{w_{total}} \sum_{j=1}^{n} w_{f(aj)} w_{f(bj)} e^{i\left(\phi_{a,j} - \phi_{b,j}\right)} \qquad (1)$$

where: ρ is the coherency, ϕ is the phase of waves from each source (j) at each geophone pair, n is the total number of sources, w_f is the weighting factor for each sensor based on distance from the source and w_{total} is the sum of all the weighting factors used inside the summation.

For the far-field case, all sources were considered to contribute equally to the model coherency for a given array configuration (Asten, 2003). Due to the effects of attenuation, for extremely near sources the signal coherency could be biased towards sources that are closer than others. To account for this, weighting factors based on the relative distance of each sensor to the source is added into the summation process (see equation (1)). By repeated application of equation (1), the average model SPAC spectrum ($\overline{\rho}$) for an entire array of sensors can then be calculated by an average of $\rho_{a,b}$ for all of the station pairs in the array.

For surface waves, geometric attenuation of wave energy follows a 1/r relationship with distance from the source, although this rate is for stable far-field propagation. Attenuation of wave energy associated with inelastic losses or absorption is at a rate dependant on frequency and the material properties (specifically the quality factor, Q) of the medium. The weighting factors in equation (1) are calculated using a geometric decay parameter (α) applied to the relative source distance for the station pairs. A value of α=1.0 corresponds to purely geometric decay, with higher values indicating additional attenuation associated with absorption and scattering. A more detailed description of the modelling procedure is given in Roberts and Asten (2006).

Modelling examples

To compare the performance of the 4-station and 7-station array configurations for varying source distances, model SPAC spectra were computed for a range of source distributions, for (dimensionless) source distances of 99r, 6r, 3r and 1.5r, where r corresponds to the array radius. For broad source distributions consisting of more than 90º of sources, the performance of the two array configurations was similar, consistent with the findings of Okada (2006). However, a significant difference is seen for narrow azimuthal distributions of sources under near-source conditions. This is best illustrated for the case of a single (1º) source located as shown in Figure 2. Each plot in the figure compares the model SPAC curve (heavy solid line) compared with the ideal result expected for a halfspace with full (360º) azimuthal coverage – a Bessel function (J_0) shown as a thin solid line. The dashed line is the imaginary component, which is not discussed here.

Comparison of the spectra for the 4-station (triangle) and 7-station (hexagon) arrays at each source distance in Figure 2 reveals a large difference in the performance of the two arrays for a single near source. In the far field case (99r), both arrays yield identical results. In fact, the plot for the 4-station array, far field (99r) case here (Figure 2) is identical (save for use of a linear k.r axis) to that of Figure 1(c) in Okada (2006).

For a source placed at a distance of 6.0r from the array centre (at an azimuth co-linear with a sensor pair) the 7-station array model displays little difference in the real coherency component to the far field case for values of kr up to the first minimum of the J_0 curve (which is the part of the curve most critical to interpretation and inversion of SPAC spectra). In fact, even at source distances of 3.0r and 1.5r, no large deviations from the J_0 'ideal' are observed below approximately kr ≈3. In contrast to the relatively small near source effects for the 7-station (hexagonal) array, the near-source model spectra for the 4-station (triangular) array displays significant deviations from J_0 at kr < 3, beginning with a source distance as large as 6.0r. For the source distances of 3.0 and 1.5r, the deviation from J_0 is very large and extends to kr values as low as 1.

The implications for this difference in behaviour for the 4- and 7-station arrays in the presence of a single (omnidirectional) near-source are two-fold: First, the portion of the coherency curve up to k.r ≈3 can, in principle, be used to produce dispersion curves when only a single near-field source is present provided the geometry of the source is co-linear with any of the sensor pairs in a 7-station array. Second, the performance (and efficiency as described by Okada (2006)) of the relatively sparse 4-station (triangular) array is much more susceptible to near-source effects than a 7-station (hexagonal) array placed with similar source-sensor geometry.

Field validation of array comparison

In order to evaluate the validity of the theoretical near-source effects predicted from the modelling, a field trial was designed with the intention of reproducing some of the model source conditions of Figure 2. A rural location, away from any urban areas, was chosen to minimise the background level of high-frequency microtremor energy. The chosen site was at Laanecoorie, in Victoria Australia, which is known from previous investigations to have predominately horizontal stratigraphy consisting of alluvial sand and clay deposits.

A 10m radius hexagonal array consisting of seven Mark Products L28 seismometers (natural frequency ~5.5 Hz) was used to record a series of 300-second duration files of ground motion. The time domain data were processed using methodology identical to that described by Roberts and Asten (2004; 2005) to produce MMSPAC (Asten et al., 2004) spectra for differing station separations in the hexagonal array. The hexagonal configuration also allows for the processing of the data for two sub-triangles (4-station arrays) to enable comparison of these different array configurations.

For the 10m radius array, files of 300 seconds duration were recorded in the presence of a standard four wheel drive vehicle driving continuously along a circular path at distances of 15m, 20m, 30m and 40m from the array centre. The source path and distances were chosen to mimic the source distribution available in the modelling procedure corresponding to source distances of 1.5r, 2.0r, 3.0r and 4.0r and 360º of azimuthal distribution.

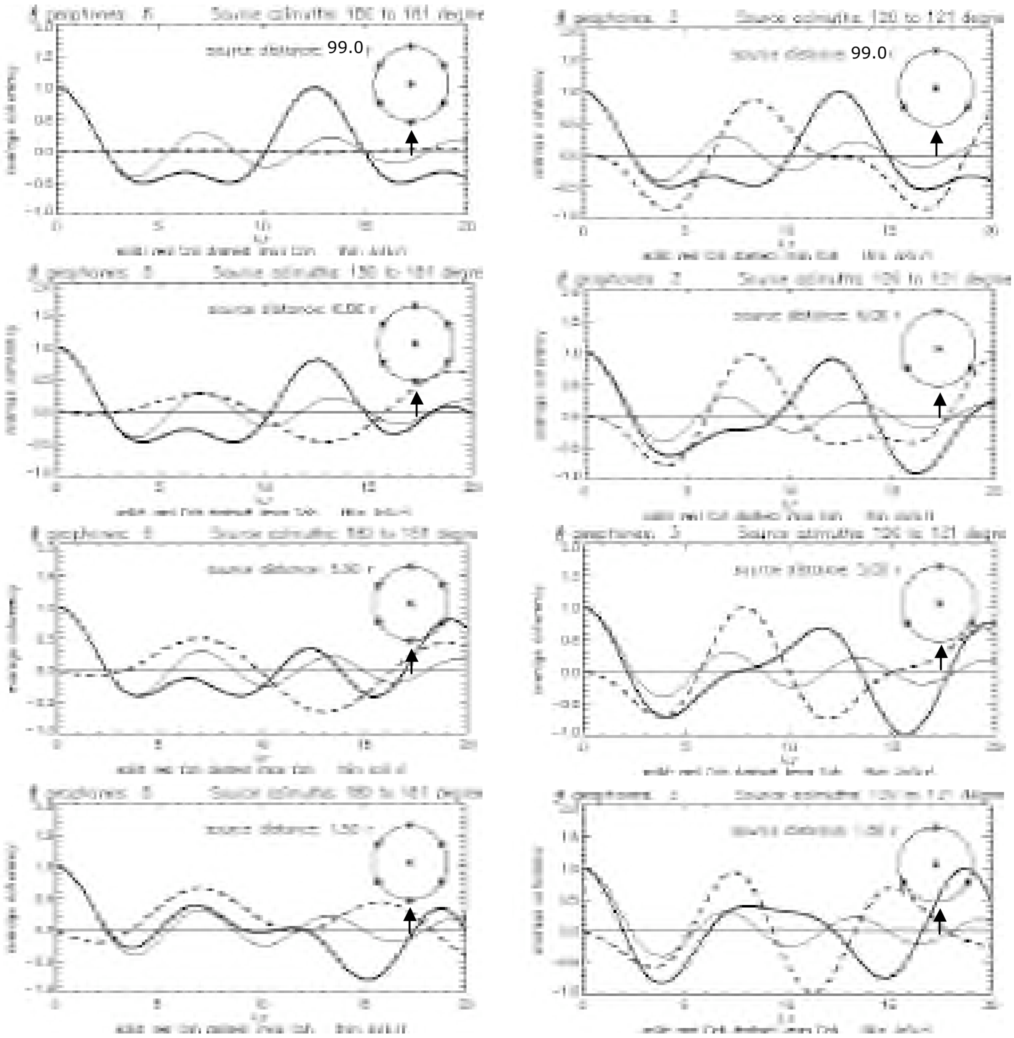

Figure 2: Model SPAC spectra (heavy lines represent the real component; dashed lines represent the imaginary component) compared to J_0 curves (thin lines) for source distances of (top to bottom) 99r, 6.0r, 3.0r and 1. 5r. Models on the left use a 7-station (hexagonal) array; models on the right use a 4-station (triangular) array. All models are the result of 1º of microtremor sources (direction shown by arrow), a geometric decay index (α) of 1.0 and display the average for radial pairs of sensors.

Several files were recorded simulating a 'point' source of microtremor energy (simulated by driving a vehicle backwards and forwards along a radial path outside the array) in various positions relative to the orientation of sensor pairs. Figure 3 shows the SPAC spectrum resulting from a 'point' source located in-line with one of the sensor pairs in a 7-station array (the whole hexagon), along with the two sub arrays consisting of 4-station triangles, each offset 60º in azimuth from the other.

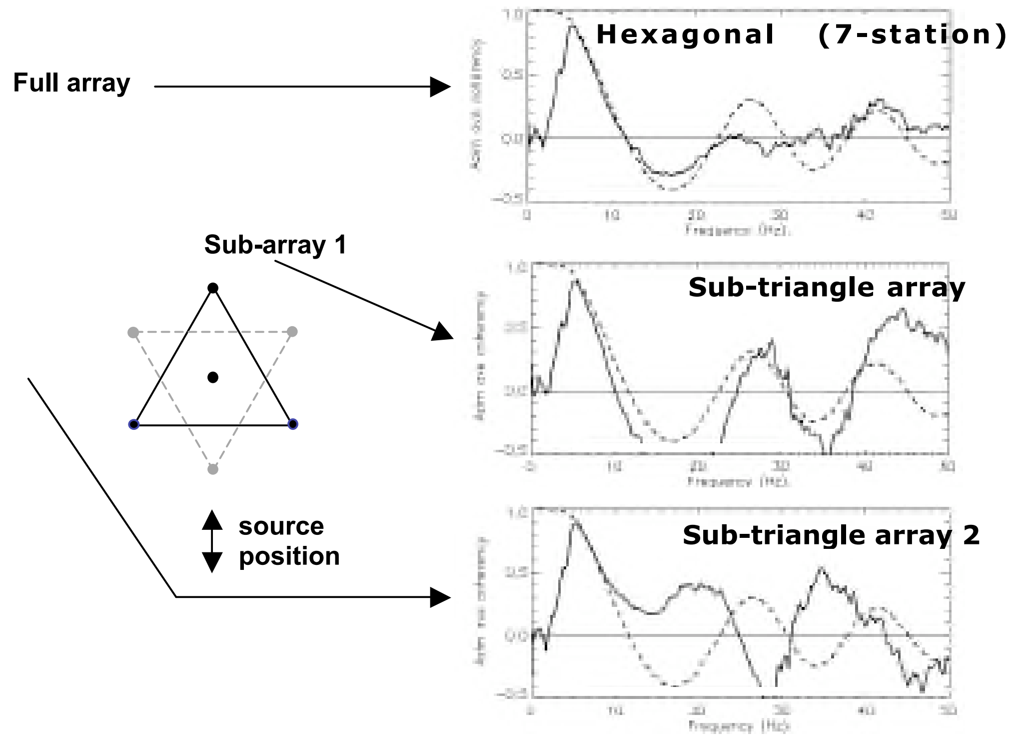

Figure 3: Results for 'point' source located in-line with a sensor pair. Radial averages for the full array (hexagon) and two 4-station (triangular) sub-arrays. Source distance is approximately 30m (3.0r). Thick line is field SPAC; dashed line is reference model SPAC obtained using a 360º source distribution for the 7-station array (same in all three plots).

The plot for the hexagonal array shows that the SPAC curve still fits (up to approximately 25 Hz) the reference model (dashed line) obtained from a 360º distribution of distant (4.0r) sources. However, the two sub-arrays consisting of conjugate 4-station triangles show very large departures from the reference model at all frequencies above approximately 7 Hz. The deviation from the reference model for sub-triangle array 1 is very similar (especially below 25 Hz) to those predicted by the modelling for the triangular arrays in Figure 2.

From these results we can infer that even though Okada (2006) demonstrated the equivalent efficiency for 7-station and 4-station arrays for far-field sources, the 7-station configuration allows for better performance of the array in the presence of near-sources.

Conclusions

Although the modelling procedure presented here makes a number of simplifying assumptions and the source distributions used are highly contrived, the results are useful in providing some indication as to the influence of source distance on the nature of observed SPAC spectra using 7-station and 4-station arrays.

Although 7-station (hexagonal) and 4-station (triangular) arrays sample an identical number of azimuths, the additional stations in the 7-station array make this configuration more reliable under near source conditions. Under near source conditions, the use of the sparser 4-station configuration may lead to significant distortions in the observed SPAC spectra.

This study has also shown that it is possible in both theory and practice to obtain SPAC curves that are reliable up to the first spectral minimum using a single source and a 7-station (hexagonal) array. The reader is directed to Roberts and Asten (2006) for additional results of the near source modelling outlined in this paper.

References

Apostolidis, P., Raptakis, D., Roumelioti, Z. and Pitilakis, K. (2004). Determination of S-wave velocity structure using microtremors and spac method applied in Thessaloniki (Greece). Soil Dynamics and Earthquake engineering 24 (1), 49-67.

Asten, M.W. (2003). Lessons from alternative array design used for high-frequency microtremor array studies: Earthquake Risk Mitigation - Proceedings of the Annual Conference of the Australian Earthquake Engineering Society, Paper 14. AEES Conference, Melbourne, Australia, 27-28 November, 2003.

Asten, M.W. (2006). On bias and noise in passive seismic data from finite circular array data processed using SPAC methods. Geophysics [in press].

Asten, M.W. and Dhu, T. (2004). Site response in the Botany area, Sydney, using microtremor array methods and equivalent linear site response modelling. Australian Earthquake Engineering in the New Millenium - where to from here? Proceedings of the annual conference of the Australian Earthquake Engineering Society, Paper 33. AEES Conference, Mt. Gambier, Australia, 5-7 November, 2004.

Asten, M.W., Dhu, T. and Lam, N. (2004). Optimised array design for microtremor array studies applied to site classification; comparison of results with SCPT logs. 13th Wold Conference on Earthquake Engineering, Paper No. 2903.

Asten, M.W., Stephenson, W.R. and Davenport, P.N. (2005). Shear-wave velocity profile for Holocene sediments measured from microtremor array studies, SCPT, and seismic refraction. Journal of Environmental and Engineering Geophysics 10 (3), 235-242.

Bettig, B., Bard, P.Y., Scherbaum, F., Riepl, J., Cotton, F., Cornou, C. and Hatzfeld, D. (2001). Analysis of dense array noise measurements using the modified spatial auto-correlation method (SPAC): application to the Grenoble area. Bollettino di Geofisica Teorica ed Applicata 42, 281-304.

Chavez-Garcia, F.J., Rodriguez, M. and Stephenson, W.R. (2005). An alternative approach to the SPAC analysis of microtremors: exploiting the stationarity of noise: Bulletin of the Seismological Society of America 95 (1), 277-293.

Hartzell, S., Carver, D., Seiji, T. and Herrmann, R. (2005). Shallow shear-wave velocity measurements in the Santa Clara Valley; comparison of SPAC and FK methods. [extract from] USGS Open File Report 2005-1169.

Kudo, K., Kanno, T., Okada, H., Ozel, O., Erdik, M., Sasatani, T., Higashi, S., Takahashi, M. and Yoshida, K. (2002). Site-specific issues for strong ground motions during the Kocaeli, Turkey, earthquake of 17 August 1999, as inferred from array observations of microtremors and aftershocks. Bulletin of the Seismological Society of America 92 (1), 448-465.

Okada, H. (2006). Theory of efficient array observations of microtremors with special reference to the SPAC method. Exploration Geophysics 37 (1), 73-84.

Roberts, J. and Asten, M. (2004). Resolving a velocity inversion at the geotechnical scale using the microtremor (passive seismic) survey method. Exploration Geophysics 35 (1), 14-18.

Roberts, J. and Asten, M. (2005). Estimating the shear velocity of Quaternary silts using microtremor array (SPAC) measurements. Exploration Geophysics 36 (1), 34-40.

Roberts, J. and Asten, M. (2006). Investigation of near source effects in array-based (SPAC) microtremor surveys. Proceedings of the 3rd International Symposium on the Effects of Surface Geology on Seismic Motion (ESG2006). Vol 1. Grenoble, France, 30 August – 1 September 2006.

Scherbaum, F., Hinzen, K.G. and Ohrnberger, M. (2003). Determination of shallow shear wave velocity profiles in the Cologn, Germany area using ambient vibrations. Geophysical Journal International 152, 597-612.

Wathelet, M., Jongmans, D. and Ohrnberger, M. (2005). Direct inversion of spatial autocorrelation curves with the neighborhood algorithm. Bulletin of the Seismological Society of America 95 (5), 1787-1800.

Xia, J., Miller, R.D., Park, C.B., Ivanov, J.I., Tian, G. and Chen, C. (2004). Utilization of high-frequency Rayleigh waves in near-surface geophysics. The Leading Edge 23 (8), 753-759.

Floor vibrations due to human excitation - damping perspective

***Ibrahim Saidi*[1], *Nick Haritos*[2], *Emad F Gad*[1 2], *John L Wilson*[1]**

[1] Swinburne University of Technology

[2] University of Melbourne

Abstract

High levels of vibrations can occur in floor systems due to excitation from human activities such as walking and aerobics. In building floors, excessive vibrations are generally not a safety concern for building floor systems but a cause of annoyance and discomfort. Excessive vibrations typically occur in: (a) light weight floors; (b) floor systems with low stiffness where the floor dominant natural frequency is close to the excitation frequency; and (c) floors with low damping. While the floor mass and stiffness are normally constant during the life of the structure and can be estimated with a high degree of accuracy, damping is more difficult to predict because it is mostly associated with non-structural components such as partitions, false floors, suspended ceilings and ducts as well as furniture such as filing cabinets and bookshelfs. Current trends in the building industry associated with using lightweight materials, long-span open-plan floors and adoption of the electronic office, give rise to the importance of understanding floor vibrations and specifically damping. This paper provides a summary of factors affecting floor vibrations and discusses available damping systems which can be used to reduce vibration levels in floor systems.

Keywords: Floor vibrations, damping, human excitation, dampers.

Introduction

Annoying levels of floor vibrations due to human movements such as walking and running have become more common during the last two decades. The main factors contributing to this problem are a decrease in the floor mass resulting from the use of high strength building materials and composite systems; decrease in the floor natural frequency due to longer floor spans; an increase in the number of rhythmic human activities such as aerobics; and decrease in damping due to fewer partitions and items of furniture and other contributing factors (Setareh 2006).

Floors in office or apartment buildings are subject to the dynamic forces induced by people when they walk and occasionally, run, jump or dance. The latter three apply especially when an office building contains facilities such as running tracks on roofs, exercise rooms, dance floor or gymnasia. In corridors or long floors, running could be contemplated, but this will only occur in isolated instances (Bachmann et al 1995). Live loads are produced by the use and occupancy of a structure and in general, human live loads are classified into the two broad categories of in situ and moving. Periodic jumping to music, sudden standing of a crowd, and random in-place movements are examples of in situ activities whilst walking, marching, and running are examples of moving activities (Ebrahimpour & Sack 2005).

Human excitation

Occupants excite floors from their activities such as walking, dancing and jumping. Such forces are particularly problematic because they cannot be easily isolated from the structure and they occur frequently (Hanagan & Murray 1997). Walking pedestrians can induce considerable vertical and horizontal rhythmic impulsive dynamic loads that are dominated by the pacing rate. Typical pacing rates for walking are between 1.6 and 2.4 steps per second, i.e. 1.6-2.4 Hz (slow-fast walk) whilst for jogging the pace rate is about 2.5 Hz and running occurs at pace rates up to about 3 Hz (Collette 2004).

Although the load from pedestrians is dominated by the pacing rate, it also includes higher harmonic components caused by the impulsive nature of the load with frequencies corresponding to an integer multiple of the pacing rate. One pedestrian walking at a pacing rate of 2 Hz will therefore load the floor with a force composed of harmonic components at 2 Hz (1st harmonic), 4 Hz (2nd harmonic), 6 Hz (3rd harmonic), etc. A floor may be prone to resonance induced by pedestrian walking, if one or more of its natural frequencies are within the ranges 1.6-2.4 Hz (1st harmonic), 3.2-4.8 Hz (2nd harmonic) and 4.8-7.2 Hz (3rd harmonic). Higher harmonics components for walking seldom induce unacceptable vibrations. Since the annoying vibration amplitudes are caused by a coincidence of the natural frequency (f_n) of the floor with one of the harmonics of the walking excitation, the problem can be avoided by keeping these frequencies away from each other. This strategy is called High Tuning Method (HTM), which for a high damped floor system ($\zeta \geq 5\%$), the lowest f_n of the floor should be above the frequency range of the second harmonic (i.e. above 4.8 Hz) and for a floors with low damping ($\zeta \leq 2\%$), the lowest resonance frequency should be above the third harmonic (i.e. above 7.2 Hz). To allow for some scatter in the accuracy of estimating the parameters, $f_n \geq 7.5$ Hz should be targeted. This HTM is a simple and effective method for design and remedial measures but may be unnecessarily conservative since it does not take account of damping explicitly or the effect of a large participating mass. As a consequence, some floors with a fundamental frequency less than the 7.5 Hz criterion can perform quite satisfactory to walking (Bachmann et al 1995). On the other hand, composite floors with very low damping ($\zeta \leq 2\%$), can experience high levels of vibration even if their first natural frequency is above 7.5Hz (Haritos et al 2005).

The lowest natural frequency can be evaluated using a number of rational methods. AISC Steel Design Guide Series No 11 Chapter 3 details methods for estimating the natural frequency. For a concrete slab supported by simply supported steel joists, the natural frequency can be estimated by calculating the natural frequency for the beam or joist panel mode and for the girder panel mode separately and then combining the two using the Dunkerley relationship given by Equation (1):

$$\frac{1}{f_n^2} = \frac{1}{f_j^2} + \frac{1}{f_g^2} \tag{1}$$

where f_j = beam or joist panel mode frequency and f_g = girder panel mode frequency (Murrary et al 1997).

Acceptance criteria for human comfort

The reaction of people who feel vibration depends very strongly on what they are doing. People in offices or residences are disturbed at peak acceleration of about 0.5% of the acceleration of gravity (g) whereas people taking part in an activity will accept acceleration levels 10 times greater (5% g or more) (Murrary et al 1997). People's perception is also affected by the characteristics of the vibration response including frequency, amplitude and duration (Hanagan & Murray 1997). Figure 1 shows the recommended acceptable peak acceleration for different environments and their variation with frequency. Comfort studies for automobiles and aircraft have found that in the frequency of 5 to 8 Hz humans are especially sensitive to the vibration. This is explained by the fact that many organs in the human body resonate at these frequencies (Alvis 2001) whilst outside this frequency range, people accept higher vibration acceleration levels (Murrary et al 1997).

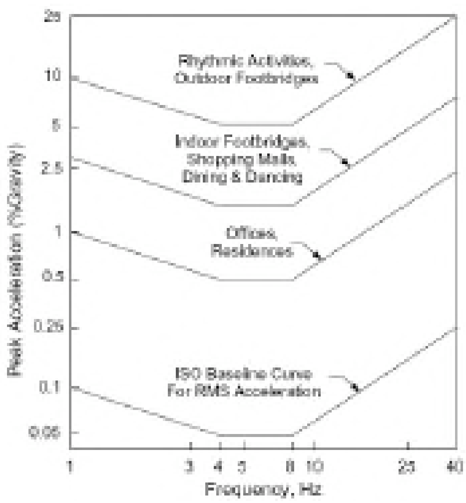

Fig 1: Acceptance Criteria

Determination of damping level

Damping in a vibrating structure is associated with dissipation of mechanical energy, generally by conversion into thermal and sound energy. In most cases, the structural mass and stiffness can be evaluated rather easily, either by simple physical consideration or by generalised expressions. On the other hand, the basic energy-loss mechanism (damping) in practical structures is seldom fully understood; consequently it usually is not feasible to determine the damping coefficient by means of corresponding generalised damping expression. For this reason, the damping in most structural systems must be evaluated directly by experimental methods (Clough & Penzien 1975). There are different methods of estimating the damping ratio using either time or frequency domain analysis. Logarithmic Decrement Analysis (LDA) can be used in the time domain analysis and Half Power Bandwidth (HPB) can be used in the frequency domain analysis.

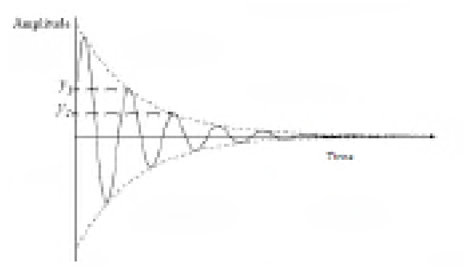

Fig 2: Logarithmic decrement method

In the LDA analysis (see Figure 2), the decay in vibration amplitude (δ) which is defined as the natural log of the ratio of the size of two peaks, m cycles apart, can be estimated using Equation (2)

$$\delta = \frac{1}{m} \ln \frac{y_n}{y_{n+m}} \tag{2}$$

where y_n is the amplitude of nth cycle and y_{n+m} is the amplitude of the n+mth cycle. The damping ration can then be found from Equation (3).

$$\zeta = \frac{\delta}{2\pi} \tag{3}$$

The half-power bandwidth method (see Figure 3) is commonly used in estimating damping in the frequency domain. The dynamic Transfer Function which is defined as $T^2(f)$ is related to the spectrum for force, SF(f), as expressed by Equation (4):

$$T^2(f) = \frac{S_X(f)}{S_F(f)} = \frac{\chi_m^2(f)}{k^2} \tag{4}$$

where χ_m (f) is the structure magnification function and k is the equivalent stiffness. The structure magnification function $\chi_m(f)$ for a single degree of freedom (SDOF) oscillator can be described in terms of the natural frequency f_n and damping ζ via Equation (5):

$$\chi_m^2(f) = \left[(1-(\frac{f}{f_n})^2)^2 + (2\zeta \frac{f}{f_n})^2 \right]^{-1} \tag{5}$$

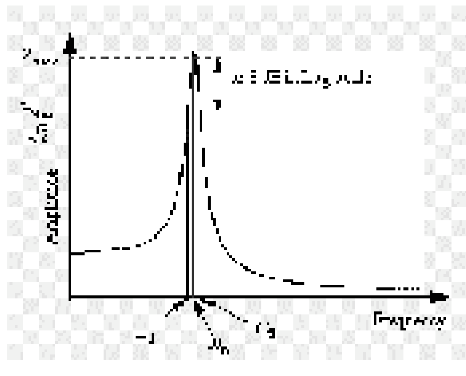

Fig 3: Half power bandwidth method

The half power bandwidth method uses the transfer function (or Frequency Response Function) trace of the structure to estimate the amount of damping for each mode. In this method, the transfer function amplitude of the system is obtained first. Corresponding to each natural frequency, there is normally a peak in the transfer function amplitude as shown in Figure 3 and at the root mean square (RMS) of the peak (ω_n) there are two points corresponding to the half power value (ω_1 and ω_2). The higher the damping, the larger the frequency range between these two points. Half-power bandwidth is defined as the ratio of the frequency range between the two half power points to the natural frequency at this mode. Haritos (1993) investigated an alternative optimised method to obtain the damping level. The "equivalent area" was tested and compared to the "peak value" in the frequency domain and half power bandwidth. The basic concept of the "equivalent area method" is to equate the area under the measured transfer function trace. The reason behind the use of this concept is by conducting such an integration the influence of "noisiness" is minimised because the integration is a form of smoothing operation.

$$\mathrm{A} = \int_0^{\infty} \chi_m^2(f)\,\mathrm{d}f = \frac{\pi\, f_n}{4\zeta}\frac{1-2\zeta}{\sqrt{1-\zeta^2}} \approx \frac{\pi\, f_n\,(1-2\zeta)}{4\,\zeta} \approx \frac{\pi\, f_n}{4\zeta} \tag{6}$$

where A is the area under $\chi^2_m(f)$, $\chi_m(f)$ is the structure magnification function, f_n is the natural frequency and ζ is the damping. For light damped SDOF system the contribution made to the area under $\chi^2_m(f)$ is dominated by A_r, the area associated with the resonance bandwidth (i.e. $f_n/\sqrt{2} < f < \sqrt{2}\, f_n$) so that:

$$\mathrm{A}_r = \int_{f_n/\sqrt{2}}^{\sqrt{2}f_n} \chi_m{}^2\ (\mathrm{f})\mathrm{df} \approx \frac{\pi\, f_n}{4\zeta}\frac{1-2\zeta}{\sqrt{1-\zeta^2}} \tag{7}$$

A_r can be determined by using standard numerical integration such as Simpson's rule. Haritos (1993) used a Monte Carlo style simulation to identify the statistical characteristics of predicted damping levels of a SDOF. The equivalent area method is considered more than satisfactory for determination of damping levels below about 8%.

The accuracy of the estimated level of damping may vary depending on the prediction method. The accuracy is influenced by number of factors in particular the "noisiness" of the data. It is reported that the equivalent area methods produces sufficiently accurate estimates for system with low damping (Haritos 1993).

Dampers

Although structural engineers have some design guideline for evaluating floor vibration before construction, there are still many floors that exhibit excessive vibrations. There are few options available to correct a floor with excessive levels of vibration. The relocation of the vibration source is the cheapest corrective method such as placing the vibration source (eg a gym) on the ground slab or placing sensitive equipment near columns or walls where the vibrations are less severe than at mid-bay (Koo 2003). Increasing the floor stiffness can reduce human induced vibration because it increases the natural frequency of the floor; however, in many instances there is physically not enough space to introduce new structural elements. Adding mass can reduce the vibration level but in most cases it is not practical as it may create overstress in structural members. Adding nonstructural elements such as full-height partitions with the aim of increasing damping and stiffness in most cases is not possible due to architectural requirements (Setareh 2006). Passive, semi active and active dampers can be used effectively to reduce excessive vibrations. Mechanical dampers can be installed more cheaply than structural stiffening and are often the only practical mean of vibration control in existing structures (Webster & Vaicaitis 1992).

Passive Dampers

Tuned Mass Dampers (TMD) and viscoelastic materials represent typical passive dampers. The first use of TMD for floor vibration application was reported by Lenzen who used small TMDs with a total mass of about 2% of the floor mass. The TMDs were made of steel hung by springs from the floor beams and dashpot to provide damping. Lenzen reported floors with annoying vibration characteristics became entirely satisfactory by tuning the TMDs to a natural frequency of about 1.0 Hz less than that of the floor and using a damping ratio of 7.5% (Setareh 2006).

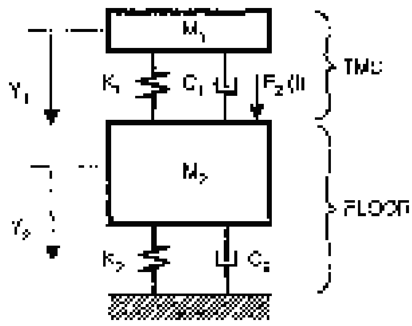

Fig 4: Two DOF (TMD)

Generally, a modern TMD consists of a mass, spring, and dashpot, as shown in Figure 4, and is typically tuned such that when large levels of motion occur, the TMD counteracts the movements of the structural system. The terms M_1, K_1, C_1, Y_1 represent the mass, stiffness, damping and displacement of the TMD, while M_2, K_2, C_2, Y_2 represent the mass, stiffness, damping and displacement of the floor and $F_2(t)$ represents the excitation force. As the two systems move relative to each other, the passive damper is stretched and compressed, reducing the vibrations of the structure by increasing its effective damping. TMD systems are typically effective over a narrow frequency band and must be tuned to a particular natural frequency. They are not effective if the structure has several closely spaced natural frequencies and sometimes they increase the vibration if they are off-tuned (Webster & Vaicaitis 1992). The natural frequency f_n of a TMD and floor can be obtained from Equation (8):

$$\omega_n = 2\pi f_n = \sqrt{(k/m)} \qquad (8)$$

where k = stiffness and m = mass. The optimum damping ratio (ζ_{opt}) of the vibration absorber (TMD) corresponds to

$$\zeta_{\mathrm{opt}} = \sqrt{\frac{3(m_1/m_2)}{8(1+m_1/m_2)^3}} \qquad (9)$$

It should be noted that one TMD can only damp one mode of vibration. If damping of several modes is necessary the arrangement becomes quite complex (Backmann et al 1995).

The Pendulum Tuned Mass Damper (PTMD), as shown in Figure 5, is an innovative new TMD designed and manufactured by ESI Engineering. The mass is provided by steel plates distributed along the PTMD arm. This is done to minimise the PTMD vertical dimension such that it can be installed within the floor plenum. The springs are movable along the PTMD arm, so that the PTMD natural frequency can be fine-tuned and the dampers are attached to the end of the PTMD arm to maximise the damping force. PTMDs are in general tuned to a set of floor dynamic parameters and therefore if these parameters change over time the PTMD can become off-tuned and not be able to reduce the floor vibrations effectively. The main source of off-tuning is variations in the floor mass which is mainly due to the fact that the weight on the floor changes with variation in live loading over time (Setareh 2006).

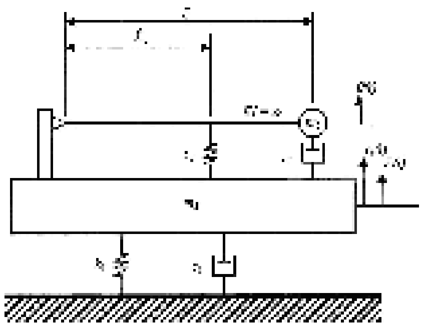

Fig 5: PTMD

Damping using visco-elastic materials: Visco-elastic materials (VEM) offer the advantage of reducing vibrations over a broader range of frequencies compared with TMDs. However, similar to TMDs, visco-elastic damping works optimally only for a specific mode of vibration. Nevertheless use of VEMs is a cheap method of increasing the damping if incorporated during construction (Ljunggren 2002).

An example of visco-elastic damping is the Resotec product which was developed by Arup in collaboration with Richard Lees Steel Decking to provide additional damping to modern composite floor construction. The Resotec system improves the dynamic performance of composite floors by dissipating energy through shearing of the visco-elastic damping layer during low-level vibrations. This product as shown in Figure 6 comprises a thin layer of high-damping visco-elastic material sandwiched between two thin steel plates; the overall thickness of the product is about 3mm. Resotec is placed on top of the top flange of a steel beam for a proportion of the beam near each end. The steel decking is placed normally over the beam (on top of the Resotec) and shear studs are fixed in the central zone of the beam only. The concrete slab is then cast in the usual manner. In the completed floor the visco-elastic layer is effectively sandwiched between the steel beam and the concrete slab to create a constrained layer damping mechanism.

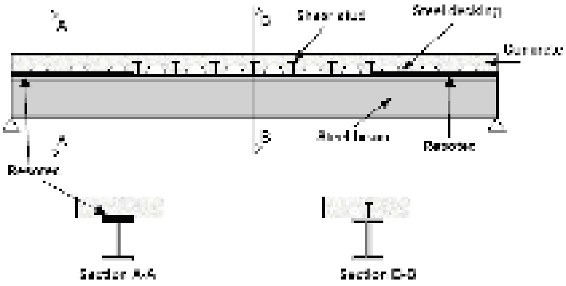

Fig 6: Resotec product installation

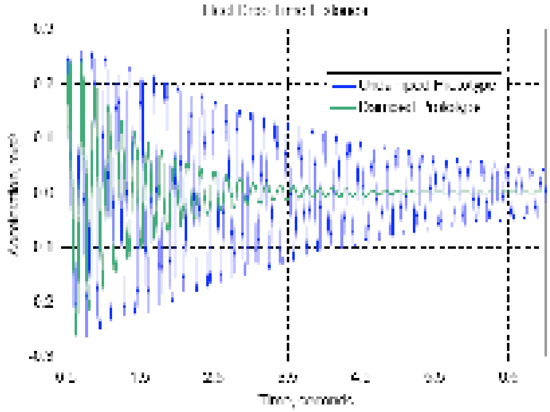

Fig 7: Performance of Resotec product

The steel beam is therefore fully composite with the floor slab only over a portion of its length centred at midspan. The product could be provided over the entire length of the beam (which would develop a large amount of damping), but this would make the entire beam non-composite, which would adversely affect its strength and stiffness. The effectiveness of Resotec is sometimes limited by the floor layout. The system works best for regular layouts where identical secondary beams have the same parallel lines of support. Where the ends of the beams are staggered due to curved or angular edges to the floor, composite and non-composite sections of adjacent beams are positioned next to each other, and constrained layer damping will be less effective. Example acceleration traces (recorded at mid-span) for two prototypes with and without Resotec are shown in Figure 7. It is reported that the damping of a fitted out floor is typically doubled by the incorporation of Resotec (Willford et al 2004). However, this product needs to be incorporated within the floor, during construction.

Semi-active control dampers

During the 1980s, the automotive industry researched, developed and tested various types of semi-active shock absorbers. That research produced a new type of control actuator that has applications in civil, mechanical, and aerospace engineering. The term semi-active describes a system that consists of a variable actuator that requires very little power to operate. The power required for the semi-active dampers (SADs) is that necessary to modulate the valve position and is typically many orders of magnitude less than that required to achieve a similar performance by fully active dampers (FADs).

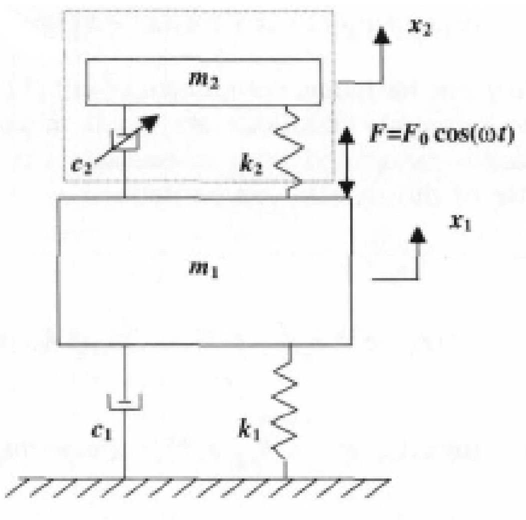

Fig 8: GHTMD

Setareh (2002) and Koo et al (2004) reported the use of a class of semi-active tuned mass dampers called ground-hook tuned mass dampers (GHTMD) as shown in Figure 8 which comprises a TMD with the ground hook semi active damper as a damping element. A magnetically responsive fluid damper can be used for this purpose which is a suspension of micron-sized, magnetizable particles in a carrier fluid. Altering the strength through the application of a magnetic field precisely controls the yield stress of the fluid. The alteration of the inter-particle attraction, by increasing or decreasing the strength of the field, permits continuous control of the fluid's rheological properties. Based on analytical studies, it was demonstrated that the GHTMD is more effective than its equivalent passive counterpart (for the same mass), in reducing the level of displacement when subjected to harmonic force excitation. Specifically, it was found that GHTMD can outperform its equivalent TMD by about 14% (Koo et al 2004).

Active control dampers

Hanagan and Murray (1995) developed an active electro-magnetic actuator that uses a piezoelectric velocity sensor and a feedback loop to generate control forces effectively adding damping to the supporting structure. Significant results were obtained on an office floor and a chemistry laboratory although high initial costs, maintenance, reliability, and the number of actuators needed to effectively reduce vibration levels were issues that were noted with this system. An actively controlled mass provides a larger degree of control compared with a passive device with an equivalent reactive mass. The active system is also less disruptive to the building function than most other repair measures. The active device is compact and can be installed with relative speed and ease in the ceiling cavity available in most commercial buildings. There are also disadvantages to the active control scheme. The cost of the components to provide a single control circuit was reported to be high with the hardware components costing about US$21,000 for a single control circuit. Maintenance and reliability issues also detract from the attractiveness of an active system, however as the technology advances, the cost will reduce (Hanagan & Murray 1997).

Concluding remarks

This paper has presented a summary of factors affecting floor vibrations in buildings with a particular focus on damping. Low damping is one of the primary causes of excessive floor vibrations in buildings. While designers have accurate models and tools to predict strength and stiffness, estimation and calculation of damping can be more difficult.

This paper has also reviewed passive, semi-active and fully-active dampers for floor applications. A passive tuned mass damper (TMD) can be effective in reducing floor vibrations if it is well tuned to the natural frequency of the floor. However, its effectiveness can quickly diminish or even exacerbate the problem if the TMD is "off tuned". As a form of passive damper, visco-elastic materials can be very effective because they can cover a wider range of frequencies compared to TMDs. However, such materials must be incorporated during construction and the floor must be designed to account for the reduced composite action between the slab and beams. Semi-active tuned mass dampers can be more effective than TMDs but an actuator requires power to modulate the fluid flow through the valves. Fully active dampers offer greater flexibility and can be more efficient than the passive and semi active tuned mass dampers, but they require significantly higher initial cost and on going maintenance of their associated electronic and power systems.

There is a demonstrated need for the development of simple passive multi tuned mass dampers for retrofitting applications. By using multi dampers, several modes of vibrations can be treated. Furthermore, having a distributed system would result in the individual units being physically smaller in size. Finally, a multi damper system may be more accommodating if one specific damper is off-tuned due to changes to the floor such as those associated with redistribution of live loads.

References

Alvis S, 2001, "An experimental and analytical investigation of floor vibrations", partial fulfilment of Master thesis submitted to Virginia Polytechnic institute and State University and approved by Thomas Murray et al.

Bachmann H et al, 1995, "Vibration Problems in Structures: Practical Guidelines", Birkhäuser Verlag, Berlin.

Clough R and Penzien J, 1975, Dynamic of Structures, McGraw-Hill.

Collette F, 2004, "Comfort and vibrations on floors due to walking loads", COWI Publications, The Scandinavian Vibration Society (SVIB), Stockholm.

Ebrahimpour A and Sack R, 2005, "A review of vibration serviceability criteria for floor structure", Computers & Structures Vol 83, Issues 28-30; Nov pp 2488-2494.

Hanagan L and Murray T, 1995, "Active control of floor vibration: implementation case studies", Proceedings of the 1995 American Control Conference, 21-23 Jun pp 1911-1915.

Hanagan L and Murray T, 1997 "Active control approach for reducing floor vibrations", Journal of Structural Engineering; Nov pp1497-1505.

Haritos N, 1993, "The 'Equivalent Area' Method for Estimating Damping Levels", Proceedings of the 13th Australasian Conference on the Mechanics of Structures and Materials (ACMSM13), Wollongong; July pp 341-348.

Haritos N, Gad E, Wilson J, 2005, "Evaluating the Dynamic Characteristics of Floor Systems using Dynamic Testing", Proceedings of ACAM2005, Melbourne, Australia, pp 225-230.

Koo J, 2003, "Using Magneto-Rheological Dampers in Semiactive Tuned Vibration Absorbers to Control Structural Vibrations", Dissertation submitted to the Faculty of the Virginia Polytechnic Institute and State University.

Koo J.H et al, 2004, " In Search of suitable control methods for semi-active tuned vibration absorbers", Journal of Vibration and Control Vol 10 No. 2 pp 163-174.

Ljunggren F, 2002, "Development of a new damper to reduce resonant vibrations in lightweight steel joist floors", Doctoral thesis "Floor Vibration-Dynamic properties and subjective perception, Division of Sound and Vibrations, Lulea University of Technology, Sweden.

Murray T et al, 1997, Floor Vibrations Due to Human Activity, AISC Design Guide No. 11.

Setareh M, 2002, "Floor Vibrations Control Using Semi-Active Tuned Damper", Canadian Journal of Civil Engineering Vol 29 No. 1; Feb pp. 76-84.

Setareh M, 2006, "Pendulum Tuned Mass Dampers for Floor Vibration Control", Journal of Performance of Construction Facilities; Feb pp 64-73.

Webster A and Vaicaitis R, 1992, "Application of Tuned Mass Dampers to control vibration of composite floor dampers", Engineering Journal AISC, third quarter, pp 116-124.

Willford M et al, 2006, "A constrained layer damping system for composite floors", The Structural Engineer, Vol 84 issue No. 4; Feb.

Concrete damage assessment for blast load using pressure-impulse diagrams

Zubair I. Syed, Priyan Mendis, Nelson T.K. Lam and Tuan Ngo

University of Melbourne

Abstract

The duration of blast pressure is significantly important along with its magnitude for dynamic response of concrete elements. Pressure-Impulse (P-I) diagrams which include both blast pressure magnitude and duration are often used in concrete damage assessment. Available design guidelines and manuals for protective design are mostly based on the Single degree of freedom (SDOF) approach. Types of resistance function used in SDOF analysis of concrete elements influence the ultimate response and eventually the amount of blast damage. Representation of concrete damage, relating only to the blast pressure magnitude and the over simplification of resistance function, can sometimes be misleading in obtaining the structural responses. This paper explores different methods of obtaining P-I diagrams using SDOF model. Development of nonlinear resistance function using nonlinear material models has also been discussed. Both bilinear and nonlinear resistance functions have been used in SDOF analysis to obtain the P-I diagrams to correlate the blast pressure and the corresponding concrete flexural damage. Realistic combination of pressures and impulses were chosen during analysis to simulate the effect of both the near and far-field blast scenarios. Variation in the post peak response of SDOF models due to use of simplified resistance function has also been presented. Field test result was compared to the analytical result to assess the effectiveness of P-I diagrams in blast damage assessment.

Keywords: SDOF, Pressure-Impulse (P-I) diagrams, Blast load, Concrete damage

Introduction

Single degree of freedom (SDOF) models have been widely used for predicting dynamic response of concrete structures subjected to blast and impact loading. The popularity of the SDOF method in blast-resistant design lies in its simplicity and cost-effective approach that requires limited input data and less computational effort. SDOF model gives reasonable good results if the response mode shape is representative of the real behavior. Accuracy of the dynamic response calculations significantly depends on whether the adopted resistance function resembles the actual hysteretic behavior of the structure. Explosion is an extreme event with a low probability of occurrence, design guidelines and manuals (Task Committee on Blast Resistant Design, 1997, TM 5-1300, 1990, Task Committee, 1999) often use over simplified elastic-perfectly plastic resistance functions to obtain the response of concrete elements. Simplified elastic-perfectly plastic resistance function for concrete elements ignores the nonlinear behavior of concrete. Elastic-plastic-hardening and elastic-plastic-softening resistance functions can model the nonlinear behavior of concrete better than the elastic-perfectly plastic resistance function. The pressure-impulse (P-I) diagrams or isodamage curves are used to correlate the blast load to the corresponding damage where the flexural mode of failure dominates damage of the element. These diagrams incorporate both the magnitude and duration of blast loading to correlate blast load and corresponding damage which can be readily used for quick damage assessment of concrete structures under different blast scenarios.

In this paper different methods of deriving the P-I diagrams for blast damage assessment using the SDOF model are discussed. Comparison between the P-I diagrams obtained using nonlinear resistance functions and elastic-perfectly plastic resistance functions are shown. Use of elastic-plastic-hardening and elastic plastic softening resistance functions in SDOF analysis for obtaining the P-I diagrams is discussed. Post peak response of high ductility concrete elements is also important for blast damage assessment. Variation in post peak response due to the use of simplified resistance functions instead of nonlinear resistance function is presented.

SDOF analysis models for blast design

Protective design manuals (eg.USACE manuals), which are in the public domain, use two common SDOF modeling approaches: the modal method and the equivalent SDOF method. In the modal method, the elastic forced response of a member is approximated by the first mode of free vibration. The natural period of the SDOF model is taken as the period of the first mode of vibration of the element with distributed mass. The main drawback of this method is its lack of versatility as it can only be used with the aid of charts and can not be used for obtaining generalized numerical solutions of SDOF systems involving complex loading histories and resistance functions. In the Equivalent SDOF method, before analyzing the response of a structural element with distributed mass and loading; the mass, resistance and loading are replaced in Newton's equation of motion with the equivalent values for a lumped mass-spring system. The equivalency is based on energy; with the equivalent mass calculated using principles of equal kinetic energy; the equivalent resistance having equal internal strain energy and the equivalent loading having equal external work to the distributed system. The transformation factors that are applied to the distributed values for calculating the equivalent lumped mass values are functions of the distribution of mass and loading over the element and the shape function of the deflected shape (Morision, 2006). The equivalent SDOF method is widely used in protective design practices. This method is also the basis of factors available in Biggs (1964) and TM5-1300 for SDOF calculation for dynamic response. Recent publication "Explosion-Resistant Buildings by Bangash and Bangash also referred to this method for protective design (Bangash and Bangash, 2006).

Resistance functions

The resistance of concrete elements under blast load is highly nonlinear. In practice, an idealised resistance function(R-Δ) is used which is a prediction of the resistance that the element would offer in a quasi-static test. Bilinear elastic-perfectly plastic R-Δ determination ignores some nonlinear effects such as softening due to cracking, tension stiffening effect, initial yielding and strain hardening of reinforcing steel. In the attempt to develop the Nonlinear R-Δ relationship including all these effects, fully nonlinear stress-strain relationship of concrete and steel are used for the analysis. The high strain-rate effect on materials is taken into account by applying DIF factors whilst Bond-slip is considered through the tension stiffening effect. Typical resistance functions are simplified by the bi- or tri-linear curves as show in Fig.1.

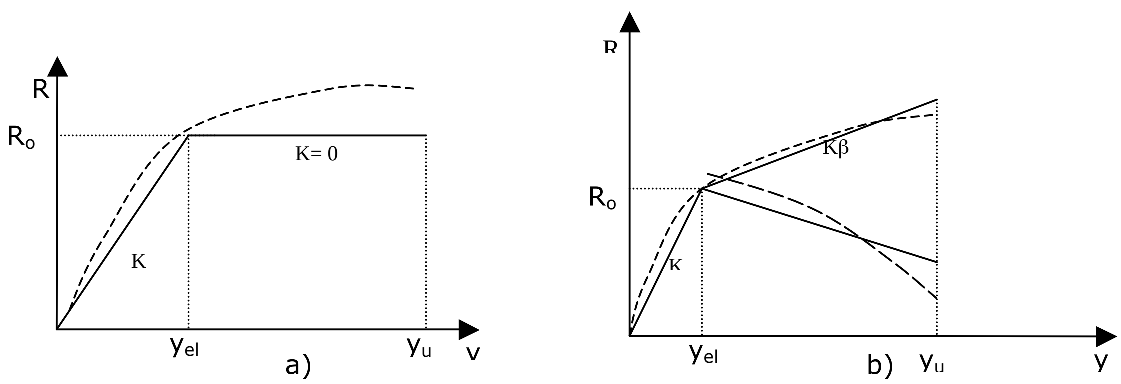

Fig.1 Nonlinear resistance functions and there idealization: a) elastic-perfectly plastic b) elastic-plastic-hardening/softening

Bilinear resistance function

The bilinear elastic-perfectly plastic resistance function has been well-defined in many materials, such as in those by Biggs(1964), Task Committee on Blast Resistant Design(1997). In obtaining bilinear resistance function, resistance, R_o of a structure is chosen as the smaller value of R_b and R_s. Where R_b is the bending resistance and R_s is the shear resistance. The bending resistance behavior of an element can be expressed as a function of the ultimate moment capacity, Mp and the length of the element. The effective stiffness, K_E, is dependent on whether shear deformation is included or not. If only flexural deformation is under considerations, K_E can be calculated as follows for the condition of uniform loading.

$$K_E = \frac{384EI_e}{5L^3} \qquad \text{......(1)}$$

where E is the Young's modulus of concrete, I_e the equivalent moment of inertia, and L is the length of the element.

Krauthammer et al. (1986), from experimental observations, argued that for a SDOF system analysis for blast loading, the flexural and shear effects on the elements can be uncoupled and analysed as independent of each other. When the observed failure mode is the direct shear, sufficient time is not allowed for the specimen to develop any type of flexural response. Similarly, when flexural failures occur, the failure is usually controlled by the fracture of the reinforcing bars which occurs much later than when the slab exhibits significant shear deformation. In the development of the resistance-deflection function presented hereafter, only the flexural effect is considered in the modelling.

The ultimate resistance, R_o of the Elastic-perfectly-plastic model for uniformly distributed blast loading has been calculated from the plastic moment capacity of the concrete section using the following equation.

$$R_o = \frac{8M_{pc}}{L} \qquad \text{.....(2)}$$

where M_{pc} is the plastic moment capacity calculated using modular ratio theory and L is the member length.

Nonlinear resistance function development

The deflection can be obtained by a double integration of the curvature, $\varphi_{(x)}$ along an element as shown by equation (3).

$$\Delta_{(x)} = \iint \varphi_{(x)} dxdx \qquad \text{......(3)}$$

In many cases the variation of curvature cannot be expressed as a continuous relationship (Warner et al., 1998). Hence, the deflection must be calculated from the curvatures using numerical methods. With known material parameters, a theoretical moment-curvature curve model for the section has been derived using fiber sectional method for concrete element. For a given concrete strain in the extreme compression fiber, ε_c, and neutral axis depth, d_n, the steel strains ε_s, and ε'_s was determined from the properties of similar triangles in the strain diagram. The stresses f_s and f'_s, corresponding to the strain ε_s and ε'_s, were obtained from the stress-strain curves. Then, the reinforcing steel forces, T, T', may be calculated from the steel stresses and areas. The distribution of concrete stress, over the compressed and tensioned parts of the cross-section, was obtained from the concrete stress-strain curves. For any given extreme compression fiber concrete strain, ε_c, the resultant concrete compression and tension forces, C and C', were determined by numerically integrating the stresses over their respective areas. In order to do so, the cross-section was divided into rectangular trips along its height. The concrete stress at the middle of each trip was calculated based on considerations of the strain. The stress so obtained was multiplied by the area of the strip to derive the force.

The position of these forces is measured from the extreme compressive fiber. They are calculated by applying the method of geometry with respect to the stress diagram of concrete in the cross-section. The complete moment-curvature relationship was determined by incrementally adjusting the concrete strain, ε_c, at the extreme compression fiber.

Material models and strain-rate effect

The theoretical derivation of moment-curvature relationship was based on the concrete model by Hognestad (1951)and the reinforcement model by Park and Paulay (1975). The formula to calculate elastic modulus of concrete, E_c, specified in ACI 318-95 (1995), is adopted in the study. When carrying out the SDOF system analysis, the effect of high strain-rate is taken into account through the use of the DIF factors as proposed in ASCE task committee report (Task Committee on Blast Resistant Design, 1997). The values of the ultimate and rupture strength of concrete, and the yield and ultimate strength of steel were multiplied by the corresponding DIF factors.

Pressure-impulse diagrams

P-I diagrams are isodamage curves based on the maximum deflection criteria as represented in the space of pressure and impulse of the pulse loading (Li and Meng, 2002a).These curves are equal energy curves which predicts the degree of damage as a function of the physical parameters. These curves are similar to the characteristic curves suggested by Abrahamson and Lindberg (1976). Vaziri et al (1987) produced isoresponse curves which are similar to the characteristics curves. Mays and Smith (1995) and Krauthammer (1998) used P-I diagrams based on elastic SDOF model for damage assessment. P-I diagrams are generally load-shape dependent but Youngdahl (1970) introduced two effective loading parameters in order to omit the load-shape effect on structures of rigid-plastic material and Li and Meng (2002b) extended that work to eliminate pulse load shape effect in both the elastic and elastic-plastic structures. Li and Meng (2002a) also studied P-I diagrams of a SDOF model using dimensional analysis and concluded that P-I diagrams for an elastic system is unique in nature and can be derived from dimensionless parameters as shown equations 4a and b.

$$i = \frac{I}{y_m\sqrt{KM}} \qquad \text{.......(4a)}$$

$$p = \frac{F_m}{Ky_m} \qquad \text{.......(4b)}$$

where, i and p are scaled impulse and scaled pressure. I is the total impulse, y_m maximum structural deflection, K and M are elastic stiffness and lump mass of the SDOF system. F_m is the maximum force on the system.

The calculated value, from equation (4a) for any given elastic SDOF system under a specified blast load, gives the value of the impulsive asymptote on the P-I plot. Similarly, the value calculated from equation (4b) gives the value of the quasi-static asymptote. Using these two values a p-I curve can be plotted for a specific damage level.

In a recent publication, Fallah and Louca (2006) introduced ways of deriving the P-I diagrams using elastic-plastic-hardening and elastic-plastic-softening resistance functions under explosive loading. Some dimensionless parameters to establish the analytical models for elastic-plastic-hardening and elastic-plastic-softening SDOF systems have also been proposed. The following equations to derive quasi-static and impulsive asymptote respectively have been proposed.

Quasi-static asymptote: $$\frac{F_m}{Ky_m} = \alpha(1-\theta\psi^2) + \frac{\theta}{2}(\psi^2 - \theta\alpha^2 + \alpha^2\psi^2) \qquad \text{.......(5a)}$$

Impulsive asymptote: $$\frac{I}{y_m\sqrt{KM}} = \sqrt{2\alpha(1-\theta\psi^2)+\theta(\psi^2-\theta\alpha^2+\alpha^2\psi^2)} \qquad ....(5b)$$

where F_m, K, y_m, and I are as defined when introducing equation (4).

α, ψ and θ are dimensionless parameters, defined as $\alpha = \frac{y_{el}}{y_c}, \psi^2 = \frac{K\beta}{K}$, θ = +1 for elastic-plastic hardening and -1 for elastic-plastic softening

The P-I diagrams of an element subjected to blast loading was established based on certain discrete points. These points are determined by repeated analysis of the equivalent SDOF system. Each point represents the limit state of the structure with respect to the specified damage criterion, which is defined by the ratio of given deflection, Δ, and the span of the element, L. At each point, the time duration td of an idealized triangular blast pressure is firstly determined. Blast pressure is then increased from zero to the ultimate value P, until the maximum response of the equivalent SDOF system reaches the given deflection value, according to the specified damage criterion. Impulse is the area under the pressure-time curve. The time duration td ranges from 5ms to 100ms with 5ms increments. In the present study, quasi-static and impulsive asymptotes were also calculated for elastic-plastic-hardening SDOF model using equations given in Fallah and Louca (2006). Damage criteria for deriving P-I diagrams are based on the damage criteria given in technical manual TM5-1300. Support rotation of simply-supported members has been taken to define damage. Damages have been classified into light, moderate and severe. Support rotation of 2° causes light damage, 5° support rotation causes moderate damage and 12° rotation causes severe damage.

Analysis and results

A normal strength concrete panel and a singly reinforced beam have been used for developing nonlinear and bilinear resistance functions and to obtain the pressure-impulse diagrams for different blast pressure-impulse combinations. The panel, modeled here, was placed under open-air blast trial conducted in Woomera, South Australia in 2004. Details of the panel and other test data can be found in Ngo (2005). Dimensions (in mm) and the properties of the panel and the beam are given in Fig.2 and in Table 1.

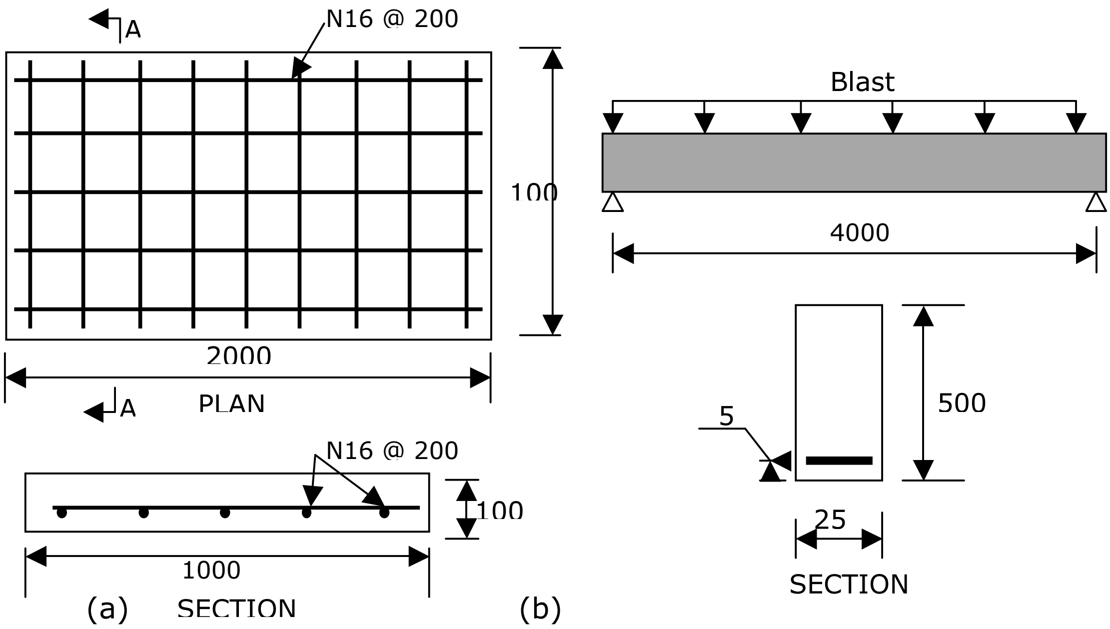

Fig. 2 Geometry and reinforcement details of the a) Panel b) Beam

In the present study both the panel and the beam was analyzed with different reinforcement ratios keeping the physical dimensions the same to obtain resistance functions for different shapes. Different pressure-impulse combinations have also been applied to the panel to get the pressure-impulse points for both the near and far-field conditions. In the present analysis, in-house computer codes have been used for developing the nonlinear resistance function from moment-curvature results by numerical integration techniques. The repeated analysis of equivalent SDOF systems under different combinations of pressure and impulse has also been conducted using the same computer codes. These codes were developed and verified as part of research work at the University of Melbourne (Thuong, 2006).

Table 1- Material properties of the concrete panel and beam

Properties	Notation	Panel material	Beam material
Static compressive strength of concrete	$f_{cs}^{'}$	39.8 MPa	40 MPa
Static tensile strength of concrete	f_t	3.7 MPa	3.5 MPa
Static elastic modulus of concrete	E_{cs}	31.5 GPa	32 GPa
Density of concrete	ρ	2430 kg/m3	2400 kg/m3
Static yield strength of steel	f_y	575 MPa	400 MPa
Elastic modulus of steel reinforcement	E_s	201 GPa	200 GPa

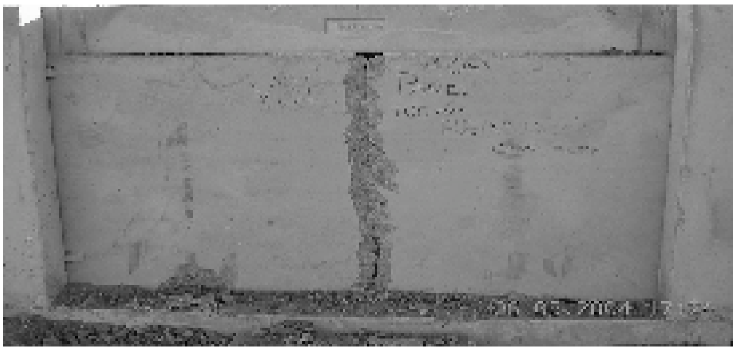

Fig 3. NSC panel after explosion (after Ngo 2005)

The structural response of the panel with different reinforcement ratios and blast loading are shown in Fig.4. Use of bilinear resistance function produces higher panel response under different blast loading. Increased value of the reinforcement ratio reduces the variation in shape of the bilinear and nonlinear functions thus reducing the variation of the peak response of the structural member. Generally, the responses of both the beam and the panel are fairly close in terms of response time. The peak deflection from the nonlinear R-Δ model appears to be smaller than that from the elastic-perfectly plastic R-Δ model. Post-yield behavior of both the beam and the panel under different blast loading was greatly influenced by the shape of the resistance function.

As the R-Δ function influences the peak response of a SDOF system subjected to blast loading, it has a significant effect on the P-I diagram which is related to the maximum response of the system. P-I obtained for different scenarios have been given in Fig.5 to7. The variation in P-I diagrams due to different damage levels are more prominent in the region where damage is dominated by pressure rather than the impulse value.

In the field test, the panel was placed 40m from the ground zero or the centre of blast. The panel experienced a peak reflected pressure of 735kPa with a duration of 33ms. Panel failure due to concrete breach was observed.

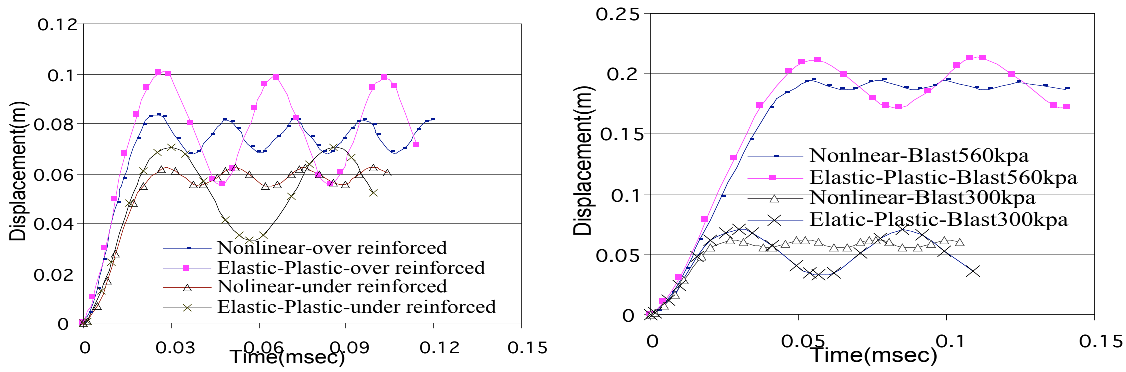

(a) (b)

Fig.4 Time history response of the panel a) with different reinforcement ratios b) under different blast loads.

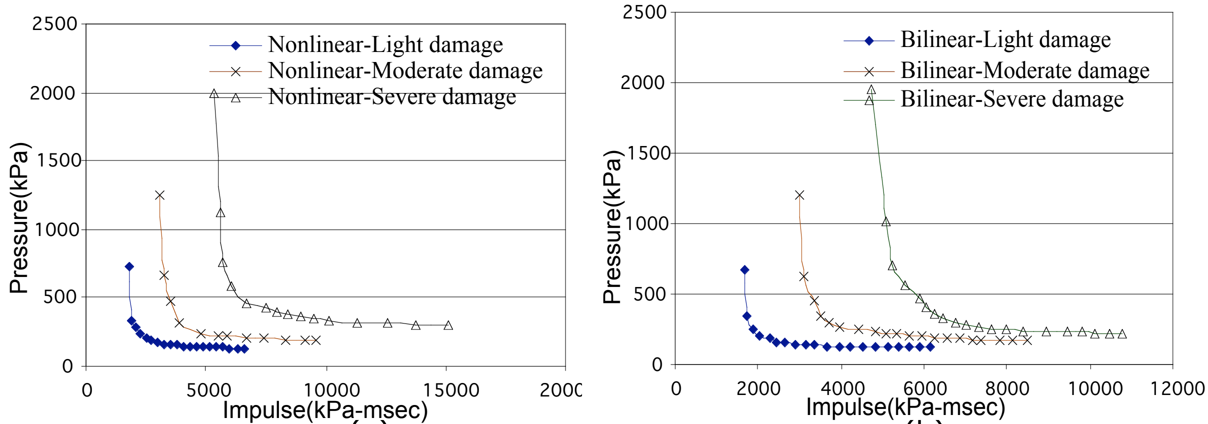

(a) (b)

Fig. 5 P-I diagrams of the panel with 1% reinforcement for different damage levels using a) Nonlinear b) Bilinear resistance functions

FE analysis of the panel under similar pressure-impulse to the blast trial gives a peak inward deflection of 186mm at time t = 28.9msec. In the field test a permanent deformation of 142mm was measured along with an approximately 8-mm wide crack at the mid-span. The failure mode of the panel is shown in Fig.3. From P-I diagrams in Fig.5 shows that the combination of pressure and impulse experienced by the panel in the field trial falls well above and right side of the P-I curve obtained for severe damage condition. So the P-I curve also predicts severe damage of the panel. It also can be seen from the P-I curve that a blast load of same magnitude of 735kPa is not sufficient to cause serious damage if the duration of the pressure is much lower than the field value, i e 10ms. Peak response of concrete panel obtained by SDOF analysis with nonlinear resistance function gives close results to the experiment values. Peak response obtained using nonlinear resistance function gives nearly 10% higher value than that obtained by using bilinear function. The strain energies dissipated into the system are different when the bilinear or nonlinear R-Δ relation is incorporated into the SDOF system. Bilinear R-Δ functions found to have under estimated the capacity of concrete element by exhibiting higher peak response than nonlinear resistance when subjected to the same blast.

Figure 6 shows that the parameters given in equation (5a) and (5b) gives P-I asymptotes close to that obtained using bilinear resistance function. If the response of a structural system under blast pressure is not in the dynamic regime, then the asymptotes (by equation 5a and b) can be used for quick estimate of damage under a given combination of pressure and impulse. Higher amount of reinforcement in concrete member causes stiffer structure and produce close bilinear and nonlinear resistance functions. Fig.7a shows that for stiffer structure whose idealized resistance function is close to the real resistance function, produced less variation in the P-I diagrams.

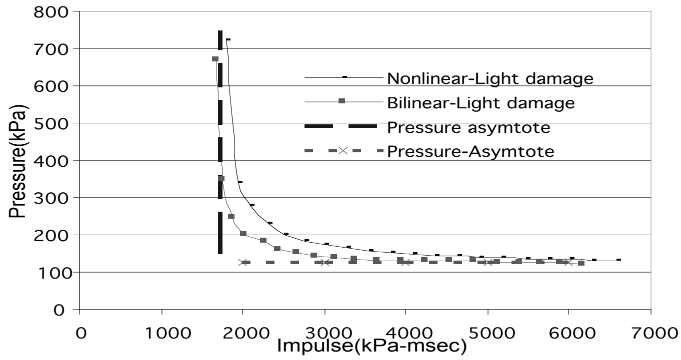

Fig.6 P-I diagrams using nonlinear and bilinear resistance functions along with pressure and impulse asymptotes obtained using method proposed by Fallah and Louca(2006)

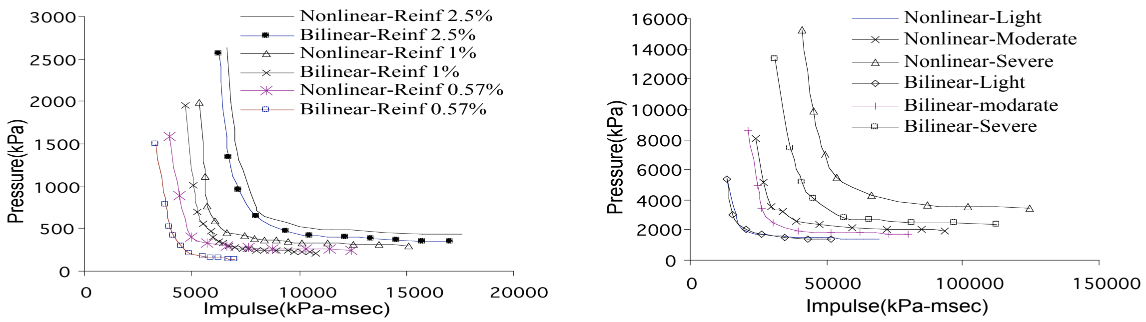

(b)

Fig. 7 P-I diagrams: a) for the panel with different reinforcement ratios for severe damage level b) for the beam for different damage levels

P-I diagrams for light damage are less sensitive to the choice of the nonlinear or idealised resistance functions. Fig.7b shows that variations in P-I diagrams are significantly higher for case of severe damage. For lightly reinforced structures where the plastic part of the response is dominant, the sensitivity to the difference in shape of the nonlinear (or bilinear) resistance functions could be significant. Hence, there is a higher variation in the P-I diagrams.

Conclusion

P-I diagram is a useful tool for the preliminary (or fast-track) damage assessment of concrete elements subjected to blast loading. Steps to develop nonlinear resistance function using nonlinear material models have been discussed. Difference in response of SDOF system to the nonlinear, or bilinear, R-Δ models has been discussed. The post peak response behavior is found to be significantly different when bilinear resistance function is used instead of the full nonlinear resistance function. Use of bilinear resistance function in dynamic analysis of SDOF model found to produce higher peak response which causes variation in the P-I diagrams obtained using those peak responses. Dynamic response of SDOF system also significantly depends on the structural characteristics and loading parameters. For severe damage conditions, the variation in the P-I curves derived using nonlinear and bilinear functions are significantly different. Use of simplified elastic-perfectly plastic model can be misleading in damage estimates when the load is expected to produce severe deformation of the member. The variation in the amount of strain energy level associated with an equivalent bilinear resistance function can cause significant difference in the P-I diagrams. Nonlinear R-Δ model can help establish a better P-I diagram than the common Bilinear R-Δ model, especially in the case of high level damage criterion.

References

Abrahamson, G. R. and Lindberg, H. E. (1976) 'Peak Load-Impulse Characterization of Critical Pulse Loads in Structural Dynamics', Nuclear Engineering and Design, 37, 35-46.

Bangash, M. Y. H. and Bangash, T. (2006) Explosion-Resistant Buildings-Design,Analysis and Case Studies, Springer, Berlin.

Biggs, J. M. (1964) Introduction to Structural Dynamics, McGraw-Hill, New York.

Fallah, A. S. and Louca, L. A. (2006) 'Pressure-impulse diagrams for elastic-plastic-hardening and softening single-degree-of-freedom models subjected to blast loading', International Journal of Impact Engineering.

Hognestad, E. (1951) 'A Study of Combined Bending and Axial Loads in Reinforced Concrete Members',In Bulletin Series No. 399University of Illinois Engineering Experimental Station.

Krauthammer, T. (1998) 'Blast mitigation technologies: developments and numerical considerations for behaviour assessment and design',In Proceedings of International conference on Structures under shock and Impact, Vol. SUSI Computational Mechanics Inc., pp. 3-12.

Krauthammer, T., Bazeos, N. and Holmquist, T. J. (1986) 'Modified SDOF Analysis of R.C Box Type Structures', Journal of Structural Engineering, 112, 726-744.

Li, Q. M. and Meng, H. (2002a) 'Pressure-Impulse Diagram for Blast Loads Based on Dimensional Analysis and Single-Degree-of-Freedom Model', Journal of Engineering Mechanics, 128.

Li, Q. M. and Meng, H. (2002b) 'Pulse loading shape effects on pressure-impulse diagram of an elastic-plastic, single-degree-of-freedom structural model', International Journal of Mechanical Sciences, 44, 1985-1998.

Mays, G. and Smith, P. D. (1995) Blast effects on buildings : design of buildings to optimize resistance to blast loading, T. Telford, London.

Morision, C. M. (2006) 'Dynamic response of walls and slabs by single-degree-of-freedom analysis-a critical review and revision', International journal of Impact Engineering, 32, 1214-1247.

Ngo, T. D. (2005) 'Behaviour of high strength concrete subject to impulsive loading',PhD thesis, In Department of Civil and Environmental Engg The University of Melbourne,

Park, R. and Paulay, T. (1975) Reinforced Concrete Structures, John Wiley & Sons, New York.

Task Committee (1999) 'Structural Design for Physical Security: State of the Practice',In American Society of Civil Engineers.

Task Committee on Blast Resistant Design (1997) 'Design of Blast Resistant Buildings in Petrochemical Facilities',In Petrochemical Committee of the Energy Division, ASCE.

Thuong, V. X. (2006) 'Nonlinear SDOF System Analysis of Elements Sublected to Blast Loading',Maters Thesis, In Dept of Civil and Environmental Engg The University of Melbourne,

TM 5-1300 (1990) 'The Design of Structures to Resist the Effects of Accidental Explosions',In Technical Manual Army TM 5-1300/Navy NAVFAC P-397/Air Force AFR 88-22Department of the Army, Navy, and Air Force, Washington DC.

Vaziri, R., Olson, M. D. and Anderson, D. L. (1987) 'Dynamic Response of Axially Constrained Plastic Beams to Blast Loads', International Journal of Solids and Structures, 23, 153-174.

Warner, R. F., Rangan, B. V., Hall, A. S. and Faulkes, K. A. (1998) Concrete Structures, Addison Wesley Longman Pty Limited, Australia.

Youngdahl, C. K. (1970) 'Correlation Parameters for Eliminating the Effect of Pulse Shape on Dynamic Plastic Deformation', Journal of Applied Mechanics, ASME, 37, 744-752.

Estimation of Gutenberg-Richter seismicity parameters for the Bundaberg region using piecewise extended Gumbel analysis

Mike Turnbull

Central Queensland University

Abstract

The Gumbel statistics of extreme events is used to determine the Gutenberg-Richter seismicity parameters for the Central Queensland region within the ±3° geographical square centred on Bundaberg, based on the annual maximum magnitude events in available historic records from the 1870's through to the present time.

Introduction

It is common to characterize temporal and quantitative earthquake seismicity of a region by respectively specifying values for the a and b parameters of the Guttenberg-Richter seismicity model (the G-R model). Estimations of these parameters can be derived from a number of statistical processes. In situations where a comprehensively complete catalogue of earthquake events is not available, methods provided by the statistics of extreme events (the so-called extreme value theory (EVT)) have been applied, using reduced variate probability plotting.

The generalized EVT cumulative distribution function (cdf) reduces to one of three specific Fisher Tippett distributions (Fisher & Tippett, 1928), depending on the value chosen for its three parameters, ξ, $\theta(> 0)$, and $k(>0)$. These three distributions are summarized below (Johnson et al, 1995).

Fisher Tippett Type 1:

$$\Pr[X \le x] = \exp\{-\exp\{-1/\theta(x - \xi)\}\} \qquad \ldots \qquad \text{Eq. 1}$$

Fisher Tippett Type 2:

$$\Pr[X \le x] = 0, \quad \text{where } x < \xi \qquad \ldots \qquad \text{Eq. 2}$$
$$= \exp\{-\exp\{-(1/\theta(x - \xi))k\}\}, \text{where } x \ge \xi$$

Fisher Tippett Type 3:

$$\Pr[X \le x] = \{-\exp\{-(1/\theta(\xi - x))k\}\}, \quad \text{where } x \le \xi \qquad \ldots \qquad \text{Eq. 3}$$
$$= 1, \quad \text{where } x > \xi$$

The Type 2 distribution is often referred to as the Fréchet distribution. The Type 3 distribution is often referred to as the Weibull distribution. The Type 1 distribution is mostly referred to as the Gumbel distribution, but is sometimes referred to as the log-Weibull distribution. In this paper it will be referred to as the Gumbel distribution.

This paper uses Gumbel plotting of historical annual extreme earthquake magnitudes to estimate the G-R model parameters for the Central Queensland region in the ±3° geographical square centred on Bundaberg.

Using the Gumbel distribution to model extreme earthquakes

Cinna Lomnitz (1974) showed that if an homogeneous earthquake process with cumulative magnitude distribution

$$F(m; \beta) = 1 - e^{-\beta m}; \quad m \ge 0 \qquad \ldots \qquad \text{(Eq. 4)}$$

is assumed (compare with Eq. 24) , where β is the inverse of the average magnitude of earthquakes in the region under consideration; and α is the average number of earthquakes per year above magnitude 0.0; then y, the maximum annual earthquake magnitude, will be distributed according to the following Gumbel cdf.

$$G(y; \alpha, \beta) = \exp(-\alpha \exp(-\beta\, y)); \quad y \geq 0 \quad \ldots \quad \text{(Eq. 5)}$$

Using the probability integral transformation theorem (Bury, 1999, p 268) simulated maximum yearly earthquakes can be generated using the following inversion formula, where u_i is a random value in the (0, 1) closed interval.

$$y_i = -(1/\beta) \ln((1/\alpha) \ln(1/u_i)) \quad \ldots \quad \text{(Eq. 6)}$$

Manipulation of Eq. 6 produces the following linear relation.

$$-\ln(-\ln(p_i)) = \beta\, y_i - \ln(\alpha) \quad \ldots \quad \text{(Eq. 7)}$$

where p represents the probability plotting position, and the left hand expression is the reduced variate that can be used to plot data that is postulated as being drawn from a Gumbel distribution. Eq. 8 has been demonstrated (Turnbull & Weatherly, 2006) to be a suitable formula for determining plotting position values for analysis of extreme magnitude earthquakes, and will be used in this paper.

$$p_m = (m - 0.3) / (n + 0.4) \quad \ldots \quad \text{(Eq. 8)}$$

This formulation approximates the median of the distribution free estimate of the sample variate to about 0.1% and, even for small values of n, produces parameter estimations comparable to the results obtained by maximum likelihood estimations (Bury, 1999, p 43).

It has been demonstrated (Turnbull & Weatherly, 2006) that reduced variate probability plotting using the Gumbel distribution (Gumbel plotting) can be used to estimate α and β parameters from single data set calendars with 95% confidence that the estimated value will be within 15% and 5% respectively of the true value.

The average recurrence period T_y of an earthquake of magnitude y, is given by

$$T_y = 1/N_y \quad \ldots \quad \text{(Eq. 9)}$$

where N_y, the number of expected earthquakes per year exceeding magnitude y is given by

$$N_y = \alpha e^{-\beta y} \quad \ldots \quad \text{(Eq. 10)}$$

giving

$$T_y = (\alpha e^{-\beta y})^{-1} \quad \ldots \quad \text{(Eq. 11)}$$

G-R Parameter estimation using the Gumbel distribution

The Gutenberg-Richter (G-R) seismicity relation of earthquake frequency versus magnitude may be expressed as:

$$N(m \geq M) = 10^{(a - b\, m)} \quad \ldots \quad \text{(Eq. 12)}$$

where $N(m \geq M)$ is the number of earthquakes observed having magnitudes greater than or equal to M; and a and b are parameters specific to the observed data set. As a pragmatic mathematical and practical choice, the lower limit of M, M_0 is usually assigned the value zero. In that formulation the parameter a represents the logarithm to the base 10 of the number of independent earthquakes in the observation period with magnitude greater than or equal to zero.

$$a = \log_{10} N(m \geq M_0) \Rightarrow N(m \geq M_0) = 10^a \quad \ldots \quad \text{(Eq. 13)}$$

If it is assumed that all earthquakes included in the data set are independent, and that each event has equal probability of occurring, then Eq. 12 can be normalised to produce a frequency relation as follows,

$$\Pr(m \geq M) = N(m \geq M)/N(m \geq M_0) = 10^{(a - b\, m)}\, 10^{-a} = 10^{-bm} \quad \text{(Eq. 14)}$$

It can be seen from Eq. 14 that the value of the parameter b determines the propensity for lower or higher magnitude earthquakes. Smaller values of b model a system that has a greater propensity for larger magnitude earthquakes. It also demonstrates that magnitude of the earthquakes is not dependent on the a parameter. The cdf formulation is as follows (compare with Eq. 4).

$$\Pr(m \leq M) = 1 - 10^{-bm} \quad \ldots \quad \text{(Eq. 15)}$$

From Eqs. 4, 5, 13, 15 the relationships between the Gumbel parameters α and β and the G-R parameter a and b are seen to be

$$e^{-\beta} = 10^{-b} \quad \Rightarrow \quad b = \beta \log_{10}e \quad \ldots \quad \text{(Eq. 16)}$$
$$\alpha = 10^{a} \quad \Rightarrow \quad a = \log_{10}\alpha \quad \ldots \quad \text{(Eq. 17)}$$

Methodology

The Gumbel analysis methodology used for this paper is described below.

Basic method

The basic method assumes a complete catalogue. In the earthquake catalogue being analysed, the n annual extreme magnitudes are identified and isolated. The n annual extreme events are then sorted into ascending order, and ranked from 1 to n. Each m ordered event is assigned a plotting position using Eq. 8. From the plotting position value, the reduced variate value for each event is determined (see left hand of Eq. 7). The reduced variates are then plotted against the event magnitudes, using linear scales.

The values for α and β can be estimated from the slope and intercept using Eq. 7.

The values for the G-R a and b parameters can be estimated using Eqs. 16 and 17. Error bounds in a and b can be calculated by applying ±15% to the α estimation, and ±5% to the β estimation, and recalculating (Turnbull& Weatherly, 2006). In a similar manner, the recurrence periods for earthquakes of various magnitudes can be calculated using Eq. 11.

Censoring and imputation of data

Gumbel analysis should only be applied to catalogues, or to subsets of catalogues, that can be considered complete or very nearly so for earthquake magnitudes above a given lower value. For instance, both the Geoscience Australia (GA, 2006) and the Earth Systems Science Computational Centre (ESSCC, 2006) catalogues of earthquakes in the ±3° geographical square centred on Bundaberg have more than 50% of years with no entry. For entries prior to 1975 the lower limit of completeness varies depending on the instrumental coverage and availability of felt reports from time to time. For entries from 1975 to the present the author considers that both catalogues are complete within the area of interest for extreme magnitude 2.0 and above, with only minor absence of data. The author considers the full catalogues to be complete for extreme magnitude 5.5 and above.

Consequently, for Gumbel analysis purposes, two sets of useful data can be obtained: one set covering the years 1975 to 2005, for magnitude 2.0 and above; and a second set covering the years 1872 to 2005 for the ESSCC catalogue, and 1878 to 2005, for the GA catalogue, for magnitude 5.5 and above.

Missing data, or values below the completion magnitude, are imputed to some value less than the completion magnitude (in this case to magnitude zero). The imputed values are included in the ranking and calculation of plotting positions, but censored in the plotting.

Piecewise extension

The formulation used to determining plotting positions in the current study allows for extension of the analysis to include compatible data sets above and below the subset maximum and minimum magnitudes (See Turnbull & Weatherly, 2006, Section 3.2). This allows the two data sets identified in the previous section to be combined in a piecewise fashion, to extend the range of extreme magnitudes considered in the analysis. The lower range data set produces reduced variates from 31 data (including censored and imputed data) from 1975 to 2005. The upper range data set produces reduced variates from 128 and 134 data (including censored and imputed data) from 1878 to 2005 in the GA catalogue and 1872 to 2005 in the ESSCC catalogue respectively. The uncensored reduced variates and magnitudes from both data sets are combined to perform the piecewise extended Gumbel analysis.

Analysis of the Geoscience Australia earthquake catalogue

Figure 1 shows the piecewise extended Gumbel plot of extreme magnitude data extracted from the GA catalogue (GA, 2006).

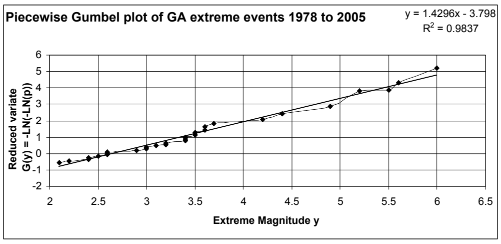

Figure 1: Piecewise extended Gumbel plot of GA extreme events 1878 to 2005

Intercept	-3.80	Error Bounds	
Slope	1.43	Lower	Upper
α	44.61	37.92	51.30
β	1.43	1.36	1.50
a	1.65	1.58	1.71
b	0.62	0.59	0.65

Table 1: Parameter estimation allowing for ±15% and ± 5% error bounds in α and β

Table 1 shows the statistical estimation of parameters, allowing for ±15% and ±5% relative error in the estimation of the Eq. 5 Gumbel α and β parameters respectively (see Turnbull & Weatherly, 2006). This results in an estimation of G-R parameter a within ±4.2%, and b within ±4.8% assuming that the source data is accurate.

Table 2 details the calculated recurrence periods for earthquakes in the magnitude range from 0.0 to 7.0. Extrapolation beyond magnitude 7.0 is not considered prudent until an analysis of the maximum expected magnitude based on the available data has been conducted. In Table 2 year, month and day values have been rounded to the nearest whole number.

	Nominal Parameter Value Expected return period			Lower Parameter Bounds Expected return period			Upper Parameter Bounds Expected return period		
Mag	Years	Months	Days	Years	Months	Days	Years	Months	Days
0.0			3			4			3
0.5			6			7			6
1.0		1	13		4	14		1	12
1.5		2	26		7	27		2	25
2.0		5	53		14	54		5	53
2.5		10	108		27	106		10	112
3.0	2	20		2	54		2	21	
3.5	3	40		3	106		4	45	
4.0	7	82		6	72		8	95	
4.5	14			12			17		
5.0	29			23			35		
5.5	58			46			75		
6.0	119			91			159		
6.5	243			180			337		
7.0	497			355			713		

Table 2: Expected Earthquake Recurrence Periods derived from GA catalogue 1878 to 2005

Figure 2 (below) shows a graph of the recurrence period relationship expressed by Eq.11.

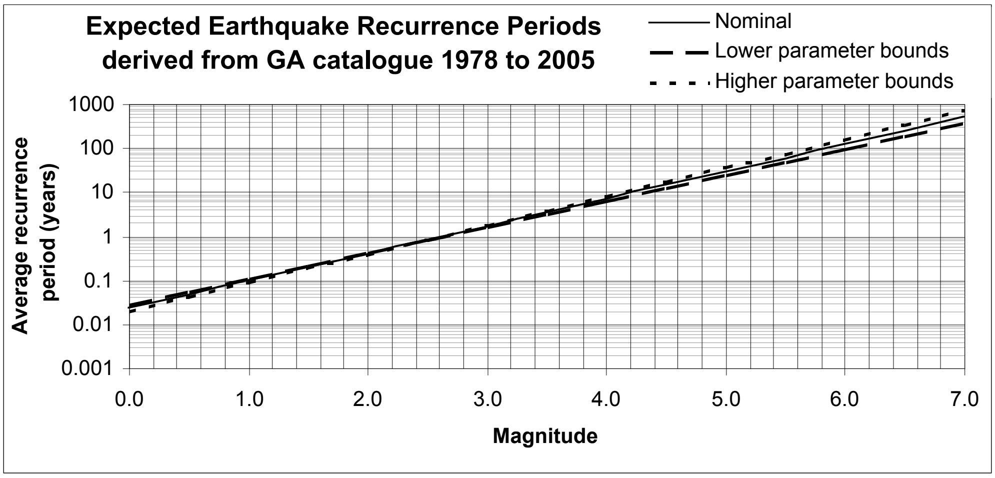

Figure 2: Expected Earthquake Recurrence Periods derived from GA catalogue 1878 to 2005

Analysis of the ESSCC earthquake catalogue

Figure 3 shows the piecewise extended Gumbel plot of extreme magnitude data extracted from the ESSCC catalogue (ESSCC, 2006).

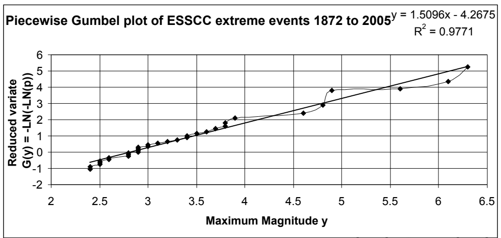

Figure 1 : Piecewise extended Gumbel

Figure 3: Piecewise extended Gumbel plot of ESSCC events 1872 to 2005

Intercept	-4.27	Error Bounds	
Slope	1.51	Lower	Upper
α	71.34	60.64	82.04
β	1.51	1.43	1.59
a	1.85	1.78	1.91
b	0.66	0.62	0.69

Tab

Table 3: Parameter estimations allowing for ±15% and ±5% error bounds in the estimation of α and β respectively

Table 3 shows the statistical estimation of parameters, allowing for ±15% and ±5% relative error in the estimation of the Eq. 5 Gumbel α and β parameters respectively (see Turnbull & Weatherly, 2006). This results in an estimation of G-R parameter a within ±3.8%, and b within ±6.0% assuming that the source data is accurate.

Table 4 details the calculated recurrence periods for earthquakes in the magnitude range 0 to 7.0. Extrapolation beyond magnitude 7.0 is not considered prudent until an analysis of the maximum expected magnitude based on the available data has been conducted. In Table 4 year, month and day values have been rounded to the nearest whole number.

	Nominal Parameter Value Expected return period			Lower Parameter Bounds Expected return period			Upper Parameter Bounds Expected return period		
Mag	Years	Months	Days	Years	Months	Days	Years	Months	Days
0.0			2			2			2
0.5			4			5			4
1.0		1	9		1	9		1	8
1.5		2	18		2	19		2	18
2.0		3	39		3	39		3	39
2.5		7	83		7	80		8	87
3.0	1	16		1	15		1	17	
3.5	3	33		2	30		3	38	
4.0	6	71		5	61		7	83	
4.5	12			10			15		
5.0	27			21			34		
5.5	57			44			74		
6.0	120			90			165		
6.5	256			184			363		
7.0	544			377			803		

Table 4: Expected earthquake recurrence periods from ESSCC catalogue 1872 to 2005

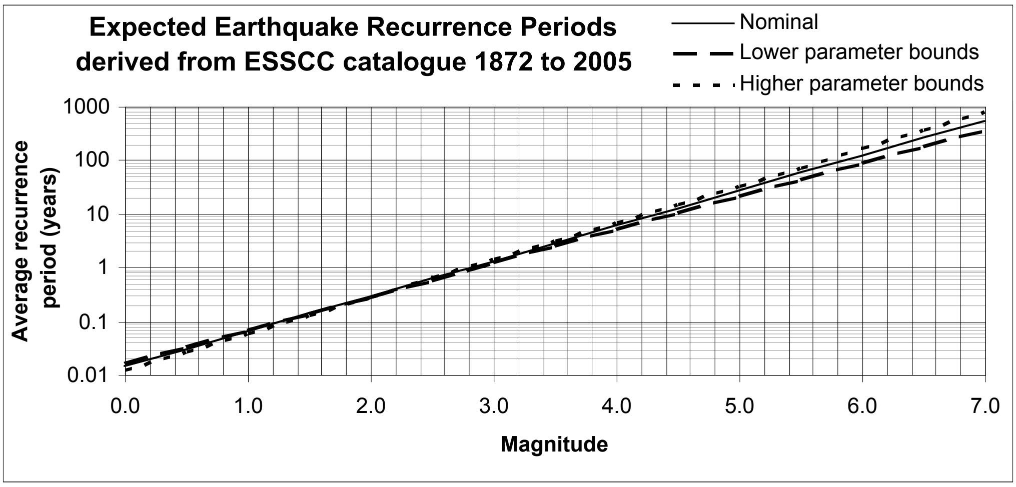

Figure 4 shows a graph of the recurrence period relationship expressed by Eq. 11.

Summary

Piecewise extended Gumbel analysis of the Geoscience Australia and Earth Systems Science Computational Centre catalogues of Australian earthquakes within the ±3° geographical square centred on Bundaberg indicates a Gutenberg-Richter b parameter value of 0.62 to 0.66. The analysis suggests that the region studied can expect on average to exhibit at least one earthquake of magnitude 6.0 or greater in any given 120 year period. This analysis supersedes similar analysis previously carried out by the author (Turnbull, 2001) which calculated a b value of 0.59, and recurrence period of 85 years.

References

Bury K. 1999, Statistical Distributions in Engineering, Cambridge University Press, ISBN 0 521 63506 3.

ESSCC, 2006, Queensland Earthquake Catalogue (1866-2005), the Earth Systems Science Computational Centre, University of Queensland, 2006. Accessed online 7 August 2006 at http://www.esscc.uq.edu.au/Seismology/html/Catalog.html.

Fisher R.A. & Tippett L.H.C. 1928, Limiting forms of the frequency distribution of the largest or smallest member of a sample, Proc. Cambridge Phil. Soc., 24:180.

GA, 2006, Earthquake Online Search Form, Geoscience Australia, 2006. Accessed online 2 August 2006 at http://www.ga.gov.au/oracle/quake/quake_online_input.jsp.

Gumbel E.J. 1958, Statistics of Extremes, Dover Publications Edition 2004, ISBN 0 486 43604 7, originally published Colombia University Press, 1958.

Johnson N.L., Kotz, S. & Balakrishnan N. 1995, Continuour Univariate Distributions, Volume 2, 2nd Ed., John Wiley & Sons. ISBN 0 471 58494 0.

Lomnitz C. 1974, Global Tectonics and Earthquake Risk, in Developments in Geotectonics 5, Elsevier Scientific Publishing Company.

Turnbull M.L. 2001, A Seismic Hazard Assessment and Microzonation of Bundaberg., Central Queensland University, Faculty of Engineering and Physical Systems, Master’s Degree Thesis, April 2001.

Turnbull M.L. & Weatherly D. 2006, Validation of using Gumbel Probability Plotting to estimate Gutenberg-Richter seismicity parameters, Proceedings of the AEES 2006 Conference, Canberra, Australia, November 2006 (in print).

Simple model accounting for the soil resonance phenomenon

Srikanth Venkatesan[1], Nelson Lam[2] and John Wilson[3]

[1] RMIT University
[2] The University of Melbourne
[3] Swinburne University of Technology

Abstract

The site natural period as a parameter for site classification has the attribute of providing an objective, and direct, representation of the risk of a soil site developing resonance behaviour. This parameter has definite advantages over the conventional approach of classifying soil based mainly on description of the sediments close to the ground surface (eg. the upper 30m of the sediment). This is particularly so if the site is characterised by high impedance contrast at the rock-soil interface, and more so in regions of low and moderate seismicity where non-ductile, lightly damped, systems are particularly prone to resonance behaviour. However, site natural period alone will not be able to accurately characterise potential soil amplification behaviour. This paper presents the recently developed Extended Component Attenuation Model (ECAM) which incorporates component factors to account for the effects of the shear wave velocity profile of the soil, damping properties of the soil, impedance contrasts with the bedrock (ie. radiation damping) and the frequency content of the earthquake excitation as transmitted from the bedrock. The presented model, due to its simplicity and generality, could potentially become standard manual calculation procedures that can be codified for widespread practical applications.

Keywords: Soil amplification, site factor, resonance, seismic.

Introduction

The importance of the modification effect of earthquake ground shaking by soft sediments and reclamation fill has been well recognised. The speculation of increased significance of site effects in areas of low and moderate seismicity like Australia is open to different interpretations depending on the perspectives from which research evidences were developed and presented.

The most well known mechanism that is responsible for the soil amplification phenomenon is that of the conservation of energy which causes an increase in amplitude of seismic waves entering from a medium of low impedance (rock or stiff soil sediments) to that of a higher impedance (soft soil) where impedance of the medium is represented by the product of density (r) and shear wave velocity (V). Site factor provisions in major seismic design standards including the current Australian Earthquake Loading Standard (AS 1170.4: 1993) and the International Building Code (IBC, 2000) could be interpreted using the conservation of energy principles to explain the trend.

Another important contribution to site hazards is that of conditions pertaining to resonance behaviour which is particularly important in areas where soft soil sediments are deposited directly on top of the bedrock which has a much higher shear wave velocity. The high impedance contrasts at the soil – rock interface is potentially hazardous in an earthquake due to the containment of energy within the soil medium (seismic waves reflected from the soil surface back down onto the soil – rock interface would be mostly reflected back into the soil medium). Significantly, the periodic reflected waves would superpose with incident waves entering the soil medium. The effects of wave superposition tend to be more pronounced with low intensity shaking as the reflected waves would tend to attenuate at a lower rate in such conditions. The 1985 Mexican earthquake is a notorious example of seismic destruction by soil resonance. The catastrophic destruction of the city was attributed to the long duration ground shaking and resonance between the medium-rise reinforced concrete buildings (typically of about 10 storey) and the deep soft soil deposits of the lake bed which has a natural period of about 2 seconds.

Despite the Mexican earthquake experience, contemporary site factor provisions in major international codes and standards including the International Building Code (IBC, 2000) and the current Australian Earthquake Loading Standard (AS 1170.4, 1993) do not explicitly parameterise the natural period of the site which characterises potential resonance behaviour. The site factors in IBC (2000), based on NEHRP recommendations, were originally developed from regression analyses of recorded ground motion parameters on different site classes. Again, the natural period of the recording stations had not been parameterised in the regression analyses.

The engineering significance of soil resonance has been a subject of debate. The opinion of some investigators is that soil resonance only occurs in the "exceptional" circumstances of the natural period of the structure coinciding with the natural period of the site. Flowing from this argument is the normal recommendation that the natural period of the structure should always be checked to ensure that the condition of resonance would not develop in the first place. This approach is distinguished from the intention of designing a structure which could accommodate the potential effects of high site amplification caused by resonance behaviour. It is also argued, quite rightly, that resonance could be suppressed effectively by energy dissipation in both the soil and the structure during the course of response to strong ground shaking.

Importantly, the capacity of a typical building structure in Australia to dissipate energy must not be assumed to be comparable to that of a code compliant building in a region of high seismicity such as California. The destructive effect of resonance mainly stems from the periodic nature of the waveform causing the amplitude of response of the structure to significantly exceed the amplitude of response of the ground. The amplification is highly selective. Thus, in theory, resonance can be circumvented by ensuring that the natural period of the building is not close to that of the site. However, in reality, the natural period of a building can be very difficult to determine and would often vary with the intensity of the response. For example, a structure with initial natural period significantly lower than the site natural period might risk being subject to the conditions of resonance (as the lateral secant stiffness of the building might deteriorate with increasing displacement amplitude). The reduction in stiffness would cause the natural period of the building to increase and hence its natural period shift closer to the natural period of the site. This period shift phenomenon adds to the scope of structures that are exposed to the risk of resonance behaviour; however, the potential amplification is offset against the non-linear behaviour that intervenes the damping.

In the new Australian Standard for Seismic Actions (DR 04304, 2004), the natural period of the site has been incorporated as a site classification criterion. However, site natural period alone will not be able to accurately characterise potential soil amplification behaviour. This paper presents a recently developed model which accounts for other important factors including shear wave velocity profile of the soil, damping properties of the soil, impedance contrasts with the bedrock (i.e. radiation damping) and the frequency content of the earthquake excitations as transmitted from the bedrock. The presented model, due to its simplicity and generality, could potentially become standard manual calculation procedure that can be codified for widespread practical applications.

Description of the model

A simple site factor predictive model which accounts for the effects of soil resonance has been developed recently at the University of Melbourne based on a parametric study of results obtained from one-dimensional quasi-nonlinear analyses of real borehole records (collected from Melbourne and from international sources) using program SHAKE (Idriss & Sun, 1992). This model, which is given the name the Extended Component Attenuation Model (ECAM), should provide more accurate predictions of the site factor than current code provisions which are mostly based on a prescriptive scheme of soil classification. However, the ability of ECAM to simulate real behaviour in the soil is limited by the capability of one-dimensional quasi-nonlinear analyses (which were employed for the development of the model in the first place). Nevertheless, ECAM is expected to accomplish the intended practical purpose of enabling site factors to be predicted with reasonable accuracy using only manual calculations rather than involving dynamic analysis of the soil column. ECAM is about predicting the soil amplification factor (S) which is defined as the ordinate of the soil response spectrum at the fundamental natural period of the site divided by the respective response spectrum ordinate of the rock outcrop. Since the model is intended to fully account for the effects of soil resonance, the predicted factor is expected to be generally higher than that stipulated by current standards.

In ECAM, the soil amplification Factor (S) is expressed as the product of four component factors as shown by equation 1 (Venkatesan, 2006).

$$S = S\xi . S\lambda . S\psi . S\tau \qquad (1)$$

where, $S\zeta$ represents the effects of hysteretic and viscous damping within the soil medium, and is a function of the intensity of ground shaking as defined by the peak ground velocity of the bedrock (PGV) and the plasticity index (PI); refer Table 1;

$S\lambda$ represents the effects of the impedance contrasts between soil and bedrock which controls the extent of radiation damping, and is mainly a function of the shear wave velocity of the bedrock (half-space); refer Table 2.

$S\psi$ and $S\tau$ both represent the effects of the form of the shear wave velocity profile as illustrated in Tables 3 & 4 respectively.

Table 1: $S\psi$ factor

PGV (mm/sec)	PI-0	PI-15	PI-30	PI-50	PI-100
20	2.6	2.7	3.2	2.9	2.6
40	2.3	2.5	3.0	2.7	2.5
60	2.2	2.5	2.8	2.6	2.4
80	2.1	2.5	2.7	2.5	2.4
100	2.1	2.5	2.6	2.5	2.3

Table 2: $S\lambda$ factor

Bedrock SWV in m/sec (half-space)	Impedance contrast Factor $S\lambda$
750 m/sec	0.96
1000 m/sec	1
1500 m/sec	1.08
2000 m/sec	1.15
2500 m/sec	1.22
≥3000 m/sec	1.3

Table 3: Sψ factor

Lateral spread of SWV → / Generic classification of Soil SWV Profile ↓	S_ψ Lower Bound (consistent with the generic profile within ± 20%) Example: 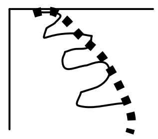	S_ψ Upper Bound (variations in SWV is greater than ± 50%) Example: 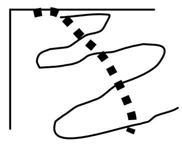
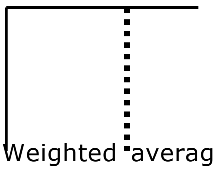 Weighted average uniform profile (reference profile)	1	1
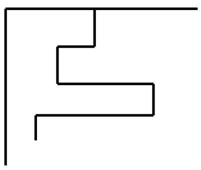 Irregular profile	1.45	1.7
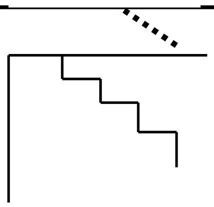 Linear profile	1.55	1.8
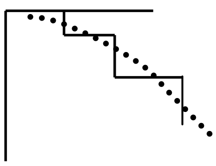 Polynomial profile	1.65	1.95

Table 4: Sτ factor

Soil SWV Profile Modification factor	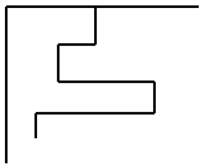 Irregular profile		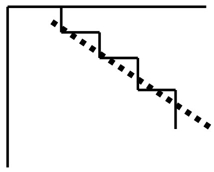 Linear profile		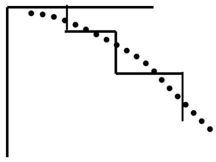 Polynomial profile	
	Sand	Clay	Sand	Clay	Sand	Clay
S_τ	0.	1.1	0.95	1.05	0.85	1.15

Illustration of ECAM by example

The proposed ECAM model is illustrated by the analysis of an example site (denoted herein as "Site – 1") which has the shear wave velocity profile as defined by Figure 1 below.

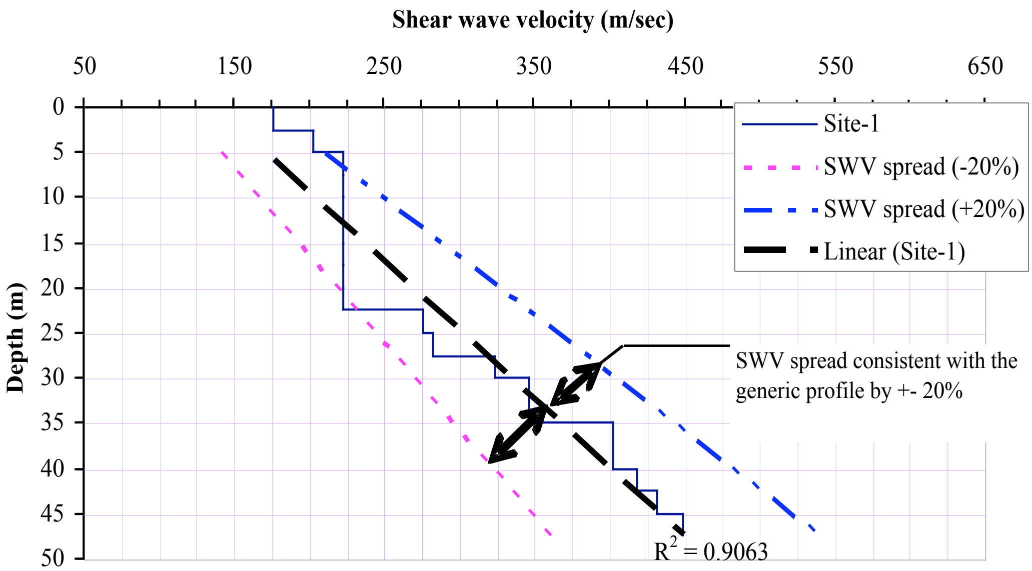

Figure 1 : Shear wave velocity profile for "Site – 1" used in the illustration

Generic classification of SWV profile of site-1 is basically a "linear" profile.

Site – 1 consists mainly of sand (PI=0%) and is subject to a notional peak ground velocity on bedrock of 60 mm/sec approximately.

From Table 1 , $S\zeta$ = 2.2; from Table 2 , $S\lambda$ =1.08 based on a bedrock shear wave velocity of 1500 m/sec ; from Table 3, $S\psi$ =1.55 ; and from Table 4, $S\tau$ = 0.95 for sand.

Finally, from equation (1), the value of S = 2.4 x 1.08 x 1.55 x 0.95 = 3.5

Comparison of ECAM with results from SHAKE analyses

Three additional example sites with shear wave velocity profiles shown by Figure 2 were analysed by both ECAM and SHAKE for comparison. Calculations for the individual component factors for each case are presented in Table 5.

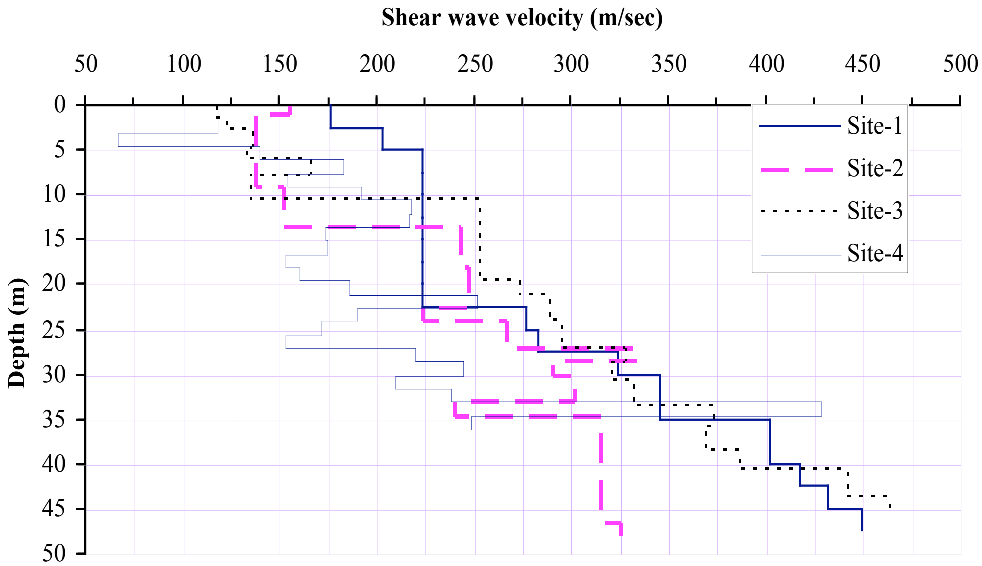

Figure 2: Shear wave velocity profiles for the four example sites

Table 5: Component factors and S value for the four example sites

Site Number	Sξ	Sλ	Sψ	Sτ	"S"
Site-1	2.2	1.08	1.55	0.95	3.5
Site-2	2.5	1.08	1.55	1	4.2
Site-3	2.35	1.08	1.55	1	3.9
Site-4	2.8	1.08	1.55	1.1	5.2

One-dimensional quasi-nonlinear analyses were undertaken on the shear wave velocity models of site 1 - 4 using program SHAKE and bedrock excitations simulated for the earthquake scenario of magnitude (Mw) 7 at 90 km distance which has a peak ground velocity on rock of approximately 60 mm/sec (Lam et al, 2005). The velocity response spectra calculated for each of the soil sites and bedrock are plotted in Figure 3. The site factor for comparison with the ECAM predictions is based on measurement at the natural period of the site (as indicated in the figure).

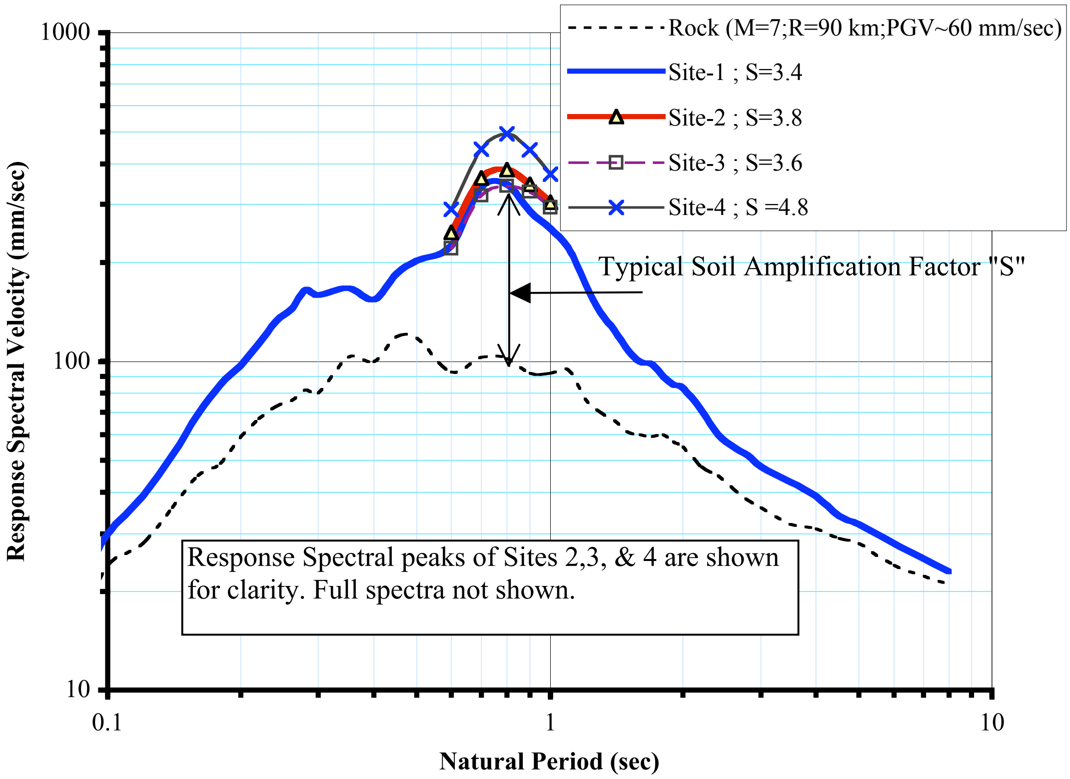

Figure 3: Velocity Response Spectra and soil amplification factors for case study soil sites computed using SHAKE-91

The site factors inferred from Figure 3 (based on SHAKE analyses) are compared with the ECAM predictions in Figure 4 (with the percentage error shown in Figure 5). It is not the intention here to use these four example sites to verify ECAM. Full details of the development of ECAM and a much more extensive verification of the model can be found in Venkatesan (2006).

Closing remarks

A simple manual procedure called ECAM for estimating the soil amplification factor which accounts for the effects of resonance behaviour is presented in the paper. Limited comparisons of ECAM with results obtained from SHAKE analysis revealed that the proposed model provides estimates which were comparable to that obtained from one-dimensional non-linear dynamic analyses of the soil columns.

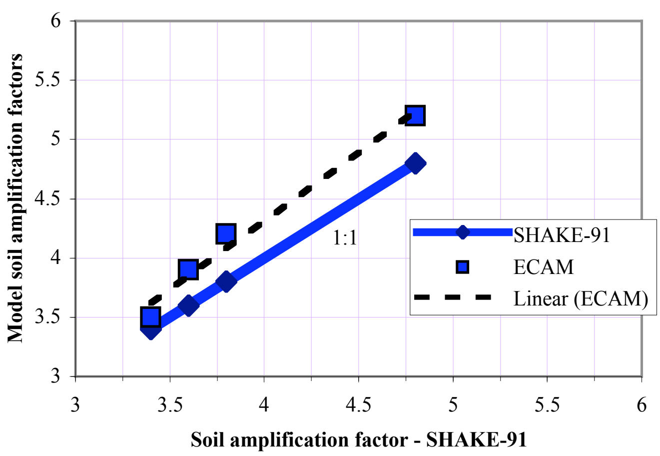

Figure 4: Comparison of soil amplification factor "S" computed using ECAM model with computations using SHAKE-91

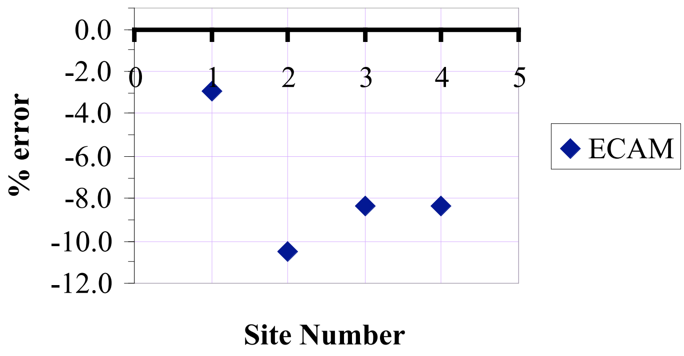

Figure 5. Percent error of soil amplification factor "S" computed using ECAM with computations using SHAKE-91

References

AS1170.4 - 1993. "Standards Association of Australia. Minimum design loads on structures : Part 4: Earthquake Loads - AS1170.4 and Commentary".

DR 04304 (2004). "Draft Australian Standard for Structural Design Actions, Part 4: Earthquake Actions in Australia". Document No. D5212-5.1, Standards Australia, Homebush, Sydney.

Lam, N.T.K., Wilson, J.L. and Venkatesan, S. (2005). "Accelerograms for dynamic analysis under the New Australian Standard for Earthquake Actions", Electronic Jnl of Structural Engineering. Vol.5: pp.10-35. http://www.ejse.org/AuthorsG.htm.

Idriss, I.M. & Sun, J.I. (1992) "Users Manual for SHAKE-91", sponsored by National Institute of Standards and Technology, Maryland USA and Department of Civil and Environmental Engineering, University of California, Davis, USA, 1992.

IBC (2000) "International Code Council. International Building Code, 2000". U.S.A.

Venkatesan, S. (2006). "A soil amplification model for intra-plate seismic regions", PhD thesis, Department of Civil & Environmental Engineering, University of Melbourne.

Simplified component model for curved T-stub connection to concrete-filled steel tube with blind bolts and extensions

Huang Yao, Helen Goldsworthy, Emad Gad

The University of Melbourne

Abstract

This paper describes a simplified component model developed to predict the behaviour of a blind-bolted T-stub connection to a concrete-filled steel tube with or without anchorage extensions within the tube. The components of the connection are considered as springs with certain mechanical properties, such as stiffness and strength. They are assumed to follow a bilinear, trilinear, or non-linear force-displacement relationship. The behaviour of the connection can be predicted by assembling the stiffness of the various components. Comparison of the analytical result with existing experimental data shows good correlation. The proposed model can be easily modified to describe the response of the overall beam-to-column connection coupled with other types of assemblies. The proposed method will efficiently serve practicing engineers in designing appropriate frame connections with blind bolts in regions of low to medium seismicity.

Keywords: Blind-bolted connections, Spring, T-stub, Cog extensions, Concrete-filled steel tube

Introduction

Circular hollow sections (CHS) can be effectively used as columns in multi-storey building construction when combined with one-sided fastening techniques using blind bolts. With concrete filling, CHS provides smaller column footprints than other design solutions and enhances load carrying capacity under fire condition as the infilled concrete acts as a heat sink. A novel blind bolted connection has been developed at the University of Melbourne by adding cogged extensions to the conventional Ajax blind bolts. This type of connection can be used as moment resisting connections in composite steel frame building for regions of low to medium seismicity with great efficiency (Goldsworthy and Gardner 2005 & 2006). A typical blind bolted T-stub connection to the concrete-filled steel tube is shown in Figure 1.

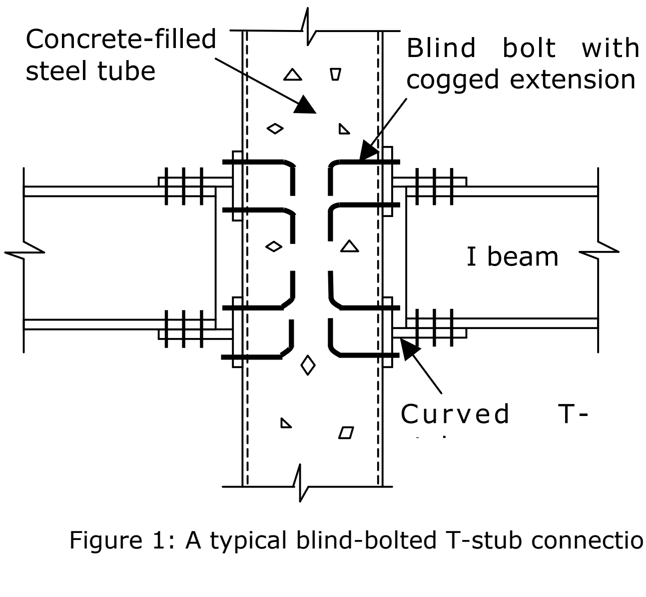

Figure 1: A typical blind-bolted T-stub connection

This paper illustrates a spring-stiffness component model developed to predict the behaviour of blind-bolted T-stub connection between steel beams and concrete-filled circular columns. In the model, the connection components are treated as spring with predefined characteristic such as stiffness and strength. By assembling the characteristics of individual components, the complex response of the joint can be predicted in a reasonably simple way.

Idealisation of blind-bolted T-stub connection

The principal of spring-stiffness (component) models is based on dividing the joint into its basic elements as springs with defined mechanical characteristics (i.e. strength and stiffness). Components of the joint are simulated by individual springs with known stiffnesses which are assumed to follow a predefined force-displacement relationship. For simplicity (see Figure 2), an equivalent single spring stiffness, K_t, is used to represent the stiffness of all components in the tension zone, whilst the compression zone is defined by a separate spring, K_c. The tension zone comprises blind bolt stiffness (K_b), curved endplate stiffness (K_p), cogged extension stiffness (K_x), and membrane stiffness of circular hollow section (K_m). An idealized representation of the T-stub connection joint is shown in Figure 3.

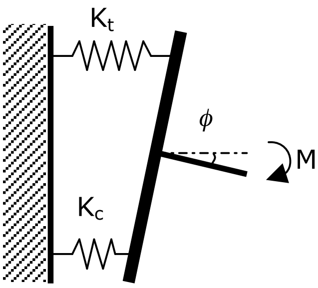

Figure 2: An overall spring model

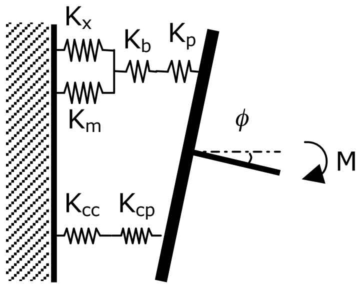

Figure 3: Various spring assembly

Simplified model of the T-stub onnection

Overall joint

The global rotational stiffness, S_j, of the joint can be determined for any given moment based on the assembled stiffness, K_t, of all components acting in the tension zone, and K_c in the compression zone. Therefore, the overall stiffness of the joint can be expressed as:

$$\frac{1}{S_j} = \frac{1}{S_t} + \frac{1}{S_c} \quad (1)$$

$$\frac{1}{S_j} = \frac{1}{K_t \cdot z^2} + \frac{1}{K_c \cdot z^2} \quad (2)$$

where

S_j: global rotational stiffness of the beam-circular column joint
S_t: joint rotational stiffness in the tension zone
S_c: joint rotational stiffness in the compression zone
z: distance from the center of rotation to location of equivalent tension spring

Therefore, the rotation of the joint, at any given moment, M can be expressed as:

$$\phi = \frac{M}{S_j} \quad (3)$$

where

ϕ: rotation of the joint

Equivalent spring in the tension zone and compression zone

The overall stiffness of the components in the tension zone can be expressed as:

$$\frac{1}{K_t} = \frac{1}{K_p} + \frac{1}{K_b} + \frac{1}{K_x + K_m} \qquad (4)$$

In a similar way, the overall stiffness of the components in the compression zone can be expressed as:

$$\frac{1}{K_c} = \frac{1}{K_{cc}} + \frac{1}{K_{cp}} \qquad (5)$$

Behaviour of the connection components

In order to determine the overall stiffness and capacity of the connection, the response of the individual components must be defined.

Blind bolt behaviour

Snug tight condition

The blind bolts are considered to be subjected to direct tensile force in isolation. By applying the principles of Hooke's law, the elastic stiffness of the bolt can be expressed as:

$$K_b = \frac{A_s \cdot E_b}{L_b} \qquad (6)$$

where

A_s: blind bolt shaft area
E_b: modulus of elasticity of blind bolts
L_b: bolt elongation length

The bolt elongation can be obtained from the following relationship.

$$L_b = t_{ep} + t_{tb} + 2 \cdot t_w + t_{bh} \qquad (7)$$

where

t_{ep}: thickness of the curved endplate
t_{tb}: thickness of the tube wall
t_w: thickness of the split washer
t_{bh}: thickness of the blind bolt head

Pretension condition

Until the pretension in the blind bolts is overcome, they are assumed to be infinitely rigid. The stiffness of the preloaded bolts is assumed to be 1000Kb.

Curved endplate behaviour

When load is applied to the joint and the endplate is pulled away from the circular column face, it is assumed that the element is subject to pure bending. The endplate is considered to be a rigid fixed beam subject to a point load. The endplate is restrained against rotation at the horizontal lines of blind bolts. Figure 4 shows the idealisation of the endplate in the tension zone. From simple beam-deflection theory, the endplate stiffness in bending can be expressed as:

$$K_p = 24EI_{ep}/m^3 \tag{8}$$

$$I_{ep} = \frac{\left(R^4 - r^4\right)}{4}\left(\frac{\pi\alpha}{180} + \sin\alpha\cos\alpha\right) - \frac{80\sin^2\alpha(R^3 - r^3)^2}{\pi\alpha(R^2 - r^2)} \tag{9}$$

where

R: radius of external surface of the curved endplate
r: radius of internal surface of the curved endplate
a: angle of endplate from side edge to its centreline
e: distance of bolt row to endplate top and bottom line
m: distance of bolt row to centre of the flange

The stiffness of the endplate is assumed to be elastic until the formation of plastic hinges.

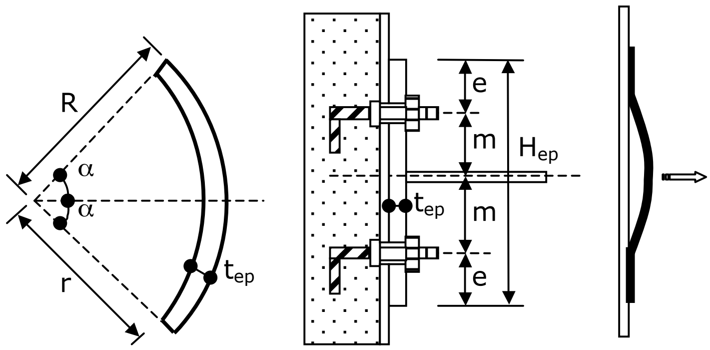

Figure 4: Curved endplate

Cogged extension behaviour

The cogged extensions attached to the blind bolt head provide substantial anchorage to prevent the blind bolts from pulling out, and they also provide considerable stiffness. The performance of cogged bars anchored in concrete filled steel tubes has been studied in great detail by experimental and numerical methods (Yao et al. 2004). The circular hollow section can provide sufficient confinement to the concrete core. As the straight lead-in length is short due to the restriction imposed by the size of the tube and the installation allowance for the blind bolts, its effect on the pullout behaviour is ignored. The pullout resistance of the cog itself can exceed the tensile yield strength of the anchored reinforcing bar. A modified Soroushian model (Soroushian 1988) is proposed to suit the conditions of concrete filled steel tubes instead of reinforced concrete beam-to-column joints.

$$P = \begin{cases} P_1(\delta/\delta_1)^{\lambda} & for\,\delta \le \delta_1 \\ P_1 & for\,\delta_1 < \delta \le \delta_2 \\ P_1 + (P_3 - P_1)\dfrac{\delta - \delta_2}{\delta_3 - \delta_2} \ge P_3 & for\,\delta > \delta_3 \end{cases} \tag{10}$$

where

$\delta_1 = 2.5mm$, $\delta_2 = 7.6mm$, $\delta_3 = 38.1mm$, $\lambda = 0.4$

$P_1 = 271(0.05d_b - 0.25)$, $P_3 = 147(0.05d_b - 0.25)$

d_b: diameter of the reinforcing bar

Thus, the stiffness of the cogged extension can be derived from the above force-displacement relationship.

$$K_x = \frac{P}{\delta} \tag{11}$$

Tube wall membrane behaviour

The bearing of the split-washer on the inside of the tube wall, together with the bearing of the concrete strut from the cogged bend, activates membrane action in the circular tube wall. The load can be shared between the anchorage of the cogged bar and the tube wall membrane action. Initially, the tension load is mainly carried by the cogged bars and the effect of membrane action is small. The membrane action comes into play as the load increases. The ratio of tension load taken by membrane action to the total tension load eventually builds up to 35% of the total load. The membrane action incurred in the tube wall is located at the band of the endplate and adjacent strips to both ends. The stiffness of membrane action in the tube wall can be estimated as:

$$K_m = \frac{1.35 E H_{ep} t_{tb}}{\pi(r + 0.5 t_{ep})} \tag{12}$$

where

E: modulus of elasticity of the steel
Hep: height of the end-plate as shown in Figure 4

Endplate bearing on the tube The stiffness of the T-stub in the compression zone can be estimated by idealising it as a curved plate subject to a uniform compressive force from the beam over the whole depth of the endplate. The stiffness of curved endplate and associated tube wall bearing on the concrete core can be expressed as:

$$K_{cp} = \frac{\pi E \alpha H_{ep} r}{180(t_{ep} + t_{tb})} \tag{13}$$

Infilled concrete subject to compression The compression resistance from the concrete core is based on the assumption that the compression force applied is distributed across the depth of the endplate and the tube wall is assumed to act as a bearing plate on the concrete. The compression force from the endplate is dispersed to the centreline as shown in Figure 5. The stiffness of the concrete in the compression zone can be expressed as:

$$K_{cc} = \frac{\pi E_c \alpha (H_{ep} + 2t_{tb})}{180} \tag{14}$$

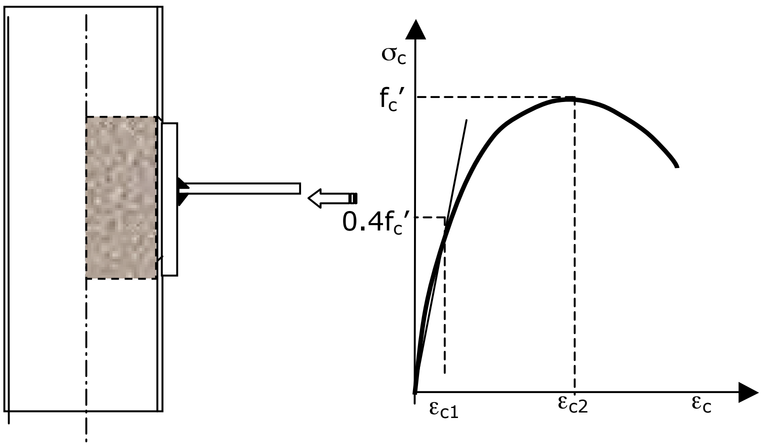

Figure 2: Infilled concrete subject to compression

T-stub tension test

A full scale T-stub connection representing an interior beam-to-column joint has been tested. The specimen consisted of a 323.9 x 6.0 mm circular hollow section of grade 350 with infilled concrete of 45 MPa characteristic compressive strength, two curved endplates (grade 300) of 20 mm thickness, and associated flared flanges (grade 250) of 16 mm thickness. The endplates were fastened to the tube with 16 mm diameter Ajax blind bolts, which had a minimum tensile strength of 800 MPa and yield strength of 640 MPa. Cogged extensions were provided to the head of the blind bolts by using N type reinforcing bars of grade 500 MPa. The specimen achieved a maximum tensile load of 690 kN while it failed due to the weld fracture at the middle bolt of the top T-stub. The load versus displacement is provided in Figure 6.

Validation of the simplified model

Initial stiffness and secant stiffness

Two load cases were modelled at tension loads of 160 KN and 600 KN to obtain the initial stiffness and secant stiffness respectively. The stiffness of the various components is listed in Table 1. The comparison between the experimental result and analytical result for the tension load versus outwards displacement is shown in Figure 6. The proposed model predicts closely the initial stiffness and secant stiffness of the blind-bolted T-stub connection. However, the model is unavoidably approximate because the behaviour of blind-bolted T-stubs is highly nonlinear, which is due to mechanical and geometrical nonlinearity and to complex contact phenomena. Nevertheless, the application of the simplified component model provides satisfactory results.

Table 1: Spring stiffness for various components

	K_b (kN/mm)	K_p (kN/mm)	K_x (kN/mm)	K_m (kN/mm)	K_t (kN/mm)	K_{cc} (kN/mm)	K_{cp} (kN/mm)	K_c (kN/mm)	S_j (kNm/rad)
160kN	913000	13653	411.3	913.7	1206	8252	276948	8013	94341
600kN	913	13653	139	913.7	472	8252	276948	8013	40117

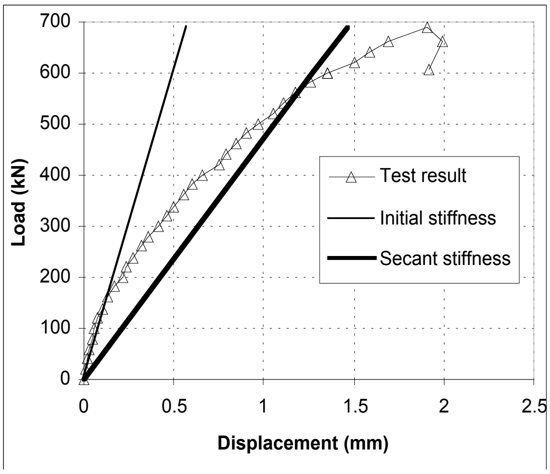

Figure 6: T-stub connection test

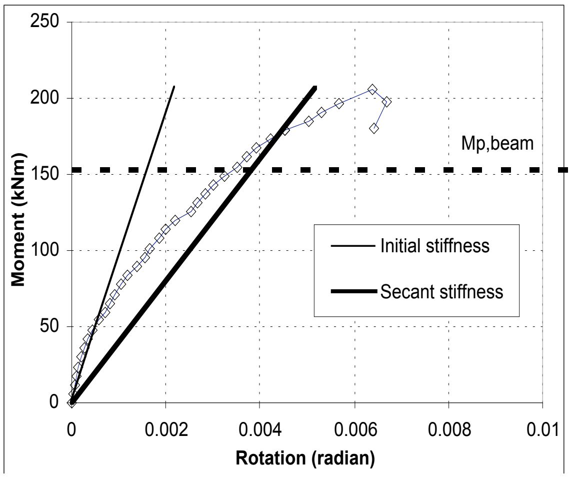

Figure 7: Moment-rotation curve

Moment-rotation curve

Behaviour of a beam-to-column connection can be conveniently represented by a moment-rotation curve (CEN 2005). A moment-rotation relationship has been determined for a concrete-filled circular column with diameter of 323.9 mm and a thickness of 6 mm connected to a steel universal beam of 310UB 40.4kg/m through the double split T connection shown in Figure 7. This represents a moment-resisting connection in a low-rise frame with a beam span of approximately 6 m. The design is based on capacity design principles so that the beam will reach its plastic moment capacity whilst the connection remains strong and stiff.

Conclusions

A simplified spring-stiffness model was presented for modelling the response of a curved T-stub connection with blind bolts and extensions. Joints were modelled by assembling the contributions of individual components. Separation of the joint into its main components allowed different force-displacement response models to be incorporated. The main parameters describing stiffness and capacity of the components were examined. The predicted behaviour of the joint was compared with the observation from the experimental test. There was good agreement between the analytical and the experimental results. The proposed component method can be employed to predict the behaviour of this type of blind-bolted T-stub connection while maintaining a relative ease of practical application.

References

CEN (2005). "Eurocode 3: Design of steel structures, Part 1-8: Design of joints", European Committed for Standardization.

Gardner A. P. and Goldsworthy H. M. (2005). "Experimental investigation of the stiffness of critical components in a moment-resisting composite connection", Journal of Constructional Steel Research, Vol. 61, 709-726.

Goldsworthy, H. and Gardner, A. P. (2006). "Feasibility study for blind-bolted connections to concrete-filled circular steel tubular columns." Structural Engineering and Mechanics: An International Journal, Vol.24, No.4, Nov 2006.

Soroushian P., Obaseki K., Nagi M., and Rojas M. C. (1988). "Pullout behaviour of hooked bars in exterior beam-column connections", ACI Structural Journal, Title no. 85-S28, pp169-276.

Yao H., Goldsworthy H. M., and Gad E. F. (2004). "Anchorage of critical elements in a moment-resisting steel I beam-to-CFT column connection", Proceedings of the 2004 Conference of the Australian Earthquake Engineering Society, Mt. Gambier, paper no.7.

About the authors:

Agus Abdulah is doing his PhD at the seismology group, Research School of Earth Sciences, ANU. He finished his Bachelor and Master degrees at the Department of Geophysical Engineering, Bandung Institute of Technology, Indonesia. He received several awards such as an Australian National University PhD Scholarship funded by an ARC grant, an Australian National University Tuition Scholarship, an ANU APRU DSN Travel Grant, a Postgraduate Scholarship from the Department of Education, Republic of Indonesia.

Haider Al Abadi is a PhD candidate at the University of Melbourne.

Trevor Allen has spent the past 3 years developing ground motion prediction equations for the Australian crust at GA. He is currently working at the USGS in Golden CO on the PAGER (Prompt Assessment of Global Earthquakes for Response) system. PAGER is an automated global alert system being developed to rapidly assess the severity of damage caused by an earthquake to provide an estimate of the impact of any given event.

Michael Asten is a part-time Professorial Fellow at Monash University and founding member of the Centre for Environmental and Geotechnical Applications of Surface Waves (CEGAS). He is also a consulting geophysicist and Partner with Flagstaff Geo-Consultants, Melbourne. He is collaborating with Geoscience Australia, University of Melbourne, the US Geological Survey, Nanyang University Singapore, and the University of Hong Kong in the development of passive seismic methods for geotechnical and site classification tasks.

Gail Atkinson is Professor of Earth Sciences at Carleton University, Ontario, Canada. Her research interests cover earthquake sources, seismic hazard analysis and ground motion studies. Gail is president of a Canadian multi-institutional research venture, which uses 90 portable geophysical laboratories to study the Earth's structure, resources and earthquake hazards.

Natalie Balfour received an MSc from Victoria University in Wellington NZ in 2004, after which she worked at GA for a year. She is now a postgraduate student in geophysics at the University of Victoria, Canada. She has conducted research in earthquake location and stress inversion using earthquake data.

Wirtu Bayissa is a PhD student in Civil Engineering at the University of Melbourne, Victoria 3010, Australia.

Boult P.J. Primary Industries and Resources of South Australia, Adelaide.

Brad Carkin obtained his Bachelor of Science, Geology, in 1982 from Central Washington University, Ellensburg, WA, and a Master of Science, Geology, in 1988 from Western Washington University, Bellingham, WA. He was a Physical Science Technician with the US Geological Survey from 1989 to 1998, and since then has been employed as a Geologist with the USGS.

Dan Clark Earthquake Geologist - Earthquake and Tsunami Hazard Project Geospatial and Earth Monitoring Division Geoscience Australia Joined Geoscience Australia in 2001 as an earthquake geologist in the Earthquake and Tsunami Hazard Project, Geospatial and Earth Monitoring Division after a stint with Connell Wagner following his PhD at the University of NSW in 1999.

Maxime Claprood is enrolled to do his PhD at Monash University after finishing a Masters in Mineral Engineering – Applied Geophysics from the École Polytechnique de Montréal in 2005 and his Bachelor's Degree there in Geological Engineering in 2003. He has worked as a research assistant at the Polytechnique de Montréal and before that at Imperial Oil. Maxime is fluent in French and Spanish as well as English.

Geoffrey Cocks graduated in Engineering from the University of Western Australia in 1971 and completed a Master of Science in Civil Engineering from Purdue University, Indiana in 1975. He has more than 30 years professional experience including more than 20 years in geotechnics. He is currently a Senior Principal with Coffey Geotechnics Pty Ltd and a Fellow of the Institution of Engineers, Australia.

Clive Colllins is a graduate of the Universities of Melbourne and Queensland where he specialised in the use of controlled source seismology for crustal studies. He joined the Bureau of Mineral Resources (now Geoscience Australia) where he has undertaken seismic studies throughout Australia and Papua New Guinea, at scales from crustal and upper mantle structure to shallow high-resolution imaging of palaeoseismic faults. He is project manager of the Earthquake and Tsunami Hazards Project at Geoscience Australia.

Neil Corby is a GIS specialist responsible for post-disaster survey tools and techniques at Geoscience Australia.

Mal Cox is an Associate Professor at QUT and his research areas are largely within groundwater systems and environmental geochemistry. He has worked extensively throughout the Pacific Basin including on geothermal systems and their hydrogeochemistry.

Phil Cummins received a PhD in geophysics in 1988 at the University of California at Berkeley. He has worked at the ANU, U. Tokyo, and Japan Marine Science and Technology Center, before becoming leader of the Earthquake Hazard and Neotectonics Project at GA in 2002. He oversees GA's earthquake monitoring activities and earthquake hazard research.

Russell Cuthbertson has been involved with seismology in Australia for over 30 years. He is currently working out of the Brisbane office of ES&S and is responsible for seismic monitoring stations stretching from Newcastle to Cairns.

Ken Dale has been working in the Risk Research Group at Geoscience Australia since 2003. His research interests there include earthquake, tsunami and flood vulnerability model development. He received his Bachelor's degree in Civil Engineering from Monash University in 1996, and a PhD from the same institution in 2001 before undertaking a post-doctoral fellowship at Sojo University in Kumamoto, Japan, from 2001-2003.

Vic Dent is a geology graduate from the University of Sydney, from where he joined the Bureau of Mineral Resources, and moved into observatory geophysics. After a one year posting at Mawson Station, Antarctica, he was based at the Rabaul Volcanological Observatory for seven years. In 1983 he was posted to the Mundaring Geophysical Observatory, where he worked for 13 years and developed a keen interest in Western Australian seismology. He completed an MSc degree at the University of Western Australia in 1999, and is currently doing more post-graduate work there.

Mike Dentith is Assoc Prof. School of Earth and Geographical Sciences, the University of Western Australia. His research interests include processing and interpretation of potential field data, geophysical signatures of mineral deposits and Australian seismicity.

Mark Edwards leads engineering vulnerability model development at Geoscience Australia.

Beatriz Estrada is a post-graduate student at the School of Earth and Geographical Sciences, The University of Western Australia.

Jeffrey Fisher is a Catastrophe Risk Analyst with Risk Frontiers. He holds a BSc (Advanced Mathematics and Ancient History) from Macquarie University. His research activities include the impact of perceived errors in catastrophe models on reinsurance negotiations, floods and floodplain management and the later Roman emperors.

Emad Gad is an associate professor at Swinburne University of Technology and a senior lecturer at the University of Melbourne. His research interests include structural dynamics, FE modelling and steel connections.

Brian A. Gaull is a Director of Guria Consulting, P.O. Box A112, Australind, Western Australia after many years as an Earth scientist with BMR/AGSO in Perth, Canberra, Papua New Guinea and Antarctica.

Gary Gibson founded the Seismology Research Centre at Phillip Institute of Technology during 1976, and worked at PIT and subsequently at RMIT University until 2001. He now works part-time at the Seismology Research Centre, and is an Honorary Research Fellow at Monash University. Gary is currently the chairman of the Executive Committee of the International Seismological Centre, and is a member of the IASPEI committees on Seismic Risk, Education and Outreach, and the Asian Seismological Commission. His interests are in observational seismology and its practical applications.

Helen Goldsworthy is a senior lecturer in the Department of Civil and Environmental Engineering at The University of Melbourne. She worked as a structural engineer for the firm Skidmore, Owings and Merrill in San Francisco in the early 1980s. On her return to Australia she commenced a Ph.D. under the supervision of Professor L.K.Stevens. In 1987 she was offered a job as a lecturer at the University of Melbourne and has been there ever since.

Stewart Greenhalgh is Professor of Geophysics in the Physics Department at Adelaide University. He is a graduate of Sydney University (B.Sc., M.Sc., D.Sc.) and the University of Minnesota (PhD). Stewart has worked as a professional or consultant in various areas of mining, petroleum and engineering geophysics, as well as having been an academic for over 20 years. Professor Greenhalgh has published widely in both experimental and theoretical geophysics. His primary research interests are in seismic and electrical modelling and inversion. He is a Fellow of the Australian Academy of Technological Sciences and Engineering, a Fellow of the Institute of Physics, UK, and is also a member of AGU, SEG, EAGE and SSA.

Mike Griffith is Associate Professor, Department of Civil & Environmental Engineering, University of Adelaide, SA, Australia. Mike was President of AEES 2002 - 2004.

Colin Gurley teaches Civil Engineering at TAFENSW Sydney Institute Ultimo. He practised as a structural design engineer from 1958 in south-east Australia including 10 years in New Zealand. He was lead structural designer for Centrepoint/Sydney Tower 1967-1971. In 1978, with J. Spencer F. Nicholls FICE, he was awarded the IPENZ Hume Award for work on the earthquake-resistant strengthening of heritage buildings including the Auckland Ferry Building, an 8-storey 1880 building of Sydney (Pyrmont) sandstone. He was a visitor at Auckland University Schools of Civil Engineering and Architecture. He spent April 2006 in Chicago and met members of the ASCE Building Performance Teams after the attacks on the Federal Building in Oklahoma City and the World Trade Centre.

Lisa Hall is at Risk Frontiers, Macquarie University, NSW.

Hong Hao is Professor, School of Civil and Resource Engineering, The University of Western Australia, Australia.

Nicholas Haritos is Assoc. Professor and Reader in Civil Engineering, The University of Melbourne, Australia

Paul Harris is a computing engineer on contract to the Australian Centre for Geomechanics in Perth WA, developing mining-seismicity related software

Dan Heal is an engineer at the Australian Centre for Geomechanics, Perth WA and responsible for projects relating to mine seismicity

Michael Hillman graduated in Engineering from the University of Western Australia in 1973 and completed a Master of Engineering Science there in 1982. He is a Principal with Coffey Geotechnics Pty Ltd and a Fellow of the Institution of Engineers, Australia.

Jane Hodgkinson is in the final stage of her PhD research which is looking at geological influence of landscape morphology at varying scales from small-area catchments through to the whole of southeast Queensland. Jane has a strong background in physical geology, field mapping and modelling approaches using GIS. She has a BSc (Hons) in Geology from Birkbeck University of London, and wide field experience in the UK and western Europe.

Suzanne Hunt is at the Australian School of Petroleum, The University of Adelaide, South Australia.

Ima Itikarai obtained a Bachelor of Science degree from the University of Papua New Guinea in 1983. The following year he commenced work at Rabaul Volcanological Observatory (RVO) as a trainee seismologist and is now the OIC. During his working career he attended various courses in seismology and volcanology, including a postgraduate diploma in seismology at the International Institute of Seismology and Earthquake Engineering in Tsukuba, Japan in 1988. In early 2006 he commenced a two-year Master of Philosophy program at the Research School of Earth sciences, ANU.

Robert Kayen is a senior Research Civil Engineer with the United States Geological Survey in Menlo Park, California and specializes in earthquake geo-engineering. He received a Doctoral degree in Engineering from the University of California at Berkeley. From 2001-2002, he was the RCUSS visiting professor of civil engineering at Kobe University, Japan. Kayen has used surface wave methods to investigate the properties of ground at over one thousand sites on five continents.

Brian Kennett is currently Director and Professor of Seismology at the Research School of Earth Sciences, The Australian National University. He received his Ph.D. in Theoretical Seismology from the University of Cambridge in 1973. He was Interim Director of the School in 1993, and Chair of BIAS and Pro-Vice-Chancellor from 1994-1997. He was President of the International Association of Physics of the Earth and Planetary Interiors (IASPEI) from 1999-2003. His research has covered a wide range of topics in seismology from seismic reflection to the free oscillations of the Earth, and has developed Earth models that are now standard in many applications e.g. earthquake location.

Nelson Lam is an Associate Professor and Reader at The University of Melbourne. His research interests have been on earthquake engineering, impact and collapse behaviour of structures. He is widely consulted in these areas and was awarded the Chapman Medal in 1999 by the Institution of Engineers, Australia. He is a member of the Australian Standard sub-committee responsible for revising the new earthquake loading standard.

Mark Leonard joined GA in 1990 in the Nuclear Monitoring Group and has filled several roles since then, whilst completing his PhD at the ANU.

Zhong Yuan Liang is a PhD student, School of Civil and Resource Engineering, The University of Western Australia.

David Love received a Bachelor of Science with Honours in Geophysics at Adelaide University in 1976. He began work at the SA Department of Mines in 1980, and was involved in exploration, particularly gravity surveys. He has been managing the SA seismograph network since 1986 and been involved in two earthquake loading code committees since 1989. He is an active member of AEES.

Elisa Lumantarna is a PhD student, Dept of Civil and Environmental Engineering, The University of Melbourne, Parkville, VIC 3010, Australia.

Kevin McCue is Director of the Australian Seismological Centre, Adjunct Professor at CQU and a Fellow of IEAust. In 1990 he and Charles Bubb FIEAust co-founded AEES.

Steven McLoughlin is a Senior Lecturer in Geology in the School of Natural Resource Sciences, QUT. He has worked on a broad array of topics spanning the geological and biological sciences but his recent work has focussed on the geological controls on modern fluvial systems and litho- and bio-facies relationships within ancient fluvial deposits.

Andrew McPherson is a research scientist with the Risk Research Group at Geoscience Australia. Andrew was awarded his PhD in Quaternary and Regolith Geology from the Australian National University in 2004. He has worked previously as a professional soil scientist, land use researcher and spatial analyst. He is currently working on the refinement of a national earthquake site response model for Australia.

Graeme McVerry is a Principal Scientist and the senior engineering seismologist at GNS. He has been involved in research and consulting on seismic hazard assessment for about 25 years. He has recently published the attenuation model for response spectrum accelerations in New Zealand earthquakes that he developed with GNS colleagues and international collaborators. Graeme has recommended or reviewed seismic design motions for many major projects in New Zealand, and some in Australia. He drafted the Seismic Hazard Spectra section of the recently published New Zealand Standard NZS1170.5:2004 for earthquake loadings.

Priyan Mendis is Associate Professor and Reader, Dept of Civil and Environmental Engineering, The University of Melbourne, Parkville, VIC 3010, Australia.

C Morelli is at the Australian School of Petroleum, The University of Adelaide, South Australia.

Dee Ninis is an Earthquake Hazard Analyst at the SRC. Prior to her appointment with the SRC she worked at the Victorian Department of Primary Industries in the Minerals & Petroleum Division. Dee has a background in geology and geophysics, and has a keen interest in earthquake geology.

Tony Pearce was appointed Director General - Emergency Management Australia on 14 August 2006. Tony has spent 26 years in the intelligence and emergency management sectors including 9 years in the Royal Australian Air Force (RAAF) as an Intelligence Analyst (imagery). After leaving the RAAF he spent 12 years with Ambulance Service Victoria in senior operations management positions responsible for emergency management and major incident response planning functions and is a qualified paramedic. Two and a half years in the position of Deputy Director of the Victoria State Emergency Service preceded a move to the role of Director Emergency Management and Security in the Office of the Emergency Services Commissioner in July 2003. Tony holds an Associate Diploma of Health Science, a Bachelor of Social Science majoring in Emergency Management, a Graduate Diploma in Management and an Executive Master of Public Administration from Melbourne University and the Australian and New Zealand School of Government. Between 2004 and 2006 he Chaired the National Catastrophic Disasters Emergency Management Capability Review Working Group on behalf of the Australian Emergency Management Committee and in 2005 was also a member of the Prime Ministers Science, Engineering and Innovation Council Tsunami Working Group following the Indian Ocean Tsunami. He is also the National Representative for the International Association of Emergency Managers.

David Rhoades is a Geophysical Statistician at GNS Science, New Zealand.

James Roberts is at the Centre for Environmental and Geotechnical Applications of Surface Waves (CEGAS).

Kittipoom Rodsin is a PhD student, Dept of Civil and Environmental Engineering, The University of Melbourne, Parkville, VIC 3010, Australia.

Ibrahim Saidi graduated from the Faculty of Engineering/Civil Engineering Department, Iraq in 1988. He worked as a site engineer for six years in building construction. He completed a master degree in Construction Management in 1999 at Swinburne University of Technology. Ibrahim worked as a project engineer in Moira Shire Council for five years. Currently he is undertaking a research project in *Floor vibrations due to human excitation*, the objective of the project is to develop dampers to reduce floor vibrations.

Cvetan Sinadinovski is a Research Fellow in Seismology at the Australian National University in Canberra. His PhD in Geophysics was from Flinders University, South Australia. He has worked as a visiting fellow in the USA and Europe, and as a software specialist in Sydney and Adelaide prior to joining GA. He is a Member of AIG, Association of Physicists of Macedonia and AEES.

Paul Somerville Deputy Director of Risk Frontiers, obtained his M.Sc. and Ph.D. in Geophysics at the University of British Columbia in Vancouver, Canada, and spent two years as a Visiting Research Fellow at the Earthquake Research Institute, University of Tokyo. Dr Somerville has been involved in the development of building codes in the United States, and led developments in the engineering characterization of near-fault ground motions. He was a member of the Board of Directors of the Seismological Society of America and the Earthquake Engineering Research Institute, and was Chairman of the EERI panel that wrote the NSF sponsored report entitled *Securing Society against Catastrophic Earthquake Losses*.

Zubair I. Syed is a PhD candidate, Dept of Civil and Environmental Engineering, The University of Melbourne, Parkville, VIC 3010, Australia. He graduated from BUET Bangladesh with a BSc Engg. and MSc.Engg.

Sven Thelandersson is Professor of Structural Engineering, Lund University, Sweden.

Mike Turnbull received his bachelor degree in physics and mathematics from QUT, with distinctions, in 1992. He completed a Master of Applied Science Degree by research and thesis at CQU in 2002. The title of his master's thesis was A Seismic Hazard Assessment and Microzonation of Bundaberg. Mike is an Adjunct Research Fellow at the Bundaberg Campus of CQU. Mike also teaches at the Bundaberg Campus of Central Queensland University (CQU) on a casual basis and is leader of the Central Queensland Seismology Research Group in association with his adjunct appointment.

Jerry Vaculik is a PhD student, Dept of Civil and Environmental Engineering, University of Adelaide, South Australia.

Srikanth Venkatesan is currently a Research fellow at the RMIT University, and has recently obtained his PhD from The University of Melbourne. He has about ten years of experience in consultancy services. His research interests are in modelling the ground motion amplification of deep soil sites for intra-plate seismic regions, modelling the residual service life of public asset buildings and investigating the sustainable performance of concrete bridges exposed to aggressive environments.

Dion Weatherley is a Research Fellow at the Earth Systems Science Computational Centre (formerly QUAKES), University of Queensland. His research interests include the physics of interacting fault systems, numerical simulation of earthquakes and seismic hazard assessment. Dr.Weatherley is a participant in an ARC Linkage Project co-funded by Main Roads Queensland, to develop a capacity for simulation-based seismic hazard assessment for South-East Queensland. Dr. Weatherley is also Project Leader of a Gold Coast City Council Research Contract to monitor seismic activity in the region.

John Wilson is a Professor of Civil Engineering at Swinburne University of Technology in Melbourne. He has a research interest and expertise in structural systems, earthquake engineering, structural dynamics and sustainable structures and is widely consulted in these fields. He was the Victorian Chairman of Engineers Australia in 2002 and is well known to the Australian Earthquake Engineering Society.

Karl-Heinz Wyrwoll is at the School of Earth and Geographical Sciences, The University of WA. His research interests include geomorphology and environmental history.

Huang Yao is a PhD student in the Department of Civil and Environmental Engineering at The University of Melbourne.

Jian Zhang is an earthquake seismologist/engineer at GNS New Zealand with a PhD in structural engineering. He is a member of NZSEE.

John Zhao is a much-published engineering seismologist at GNS Science, New Zealand with a PhD in Civil Engineering (1990). He is a member of NZSEE.

Author index

Page